VIBRIO VIRULENCE REGULATION AND HOST INTERACTIONS

EDITED BY: Lixing Huang, Joanna Brzostek, Yang Fu and Wenxiang Sun
PUBLISHED IN: Frontiers in Cellular and Infection Microbiology

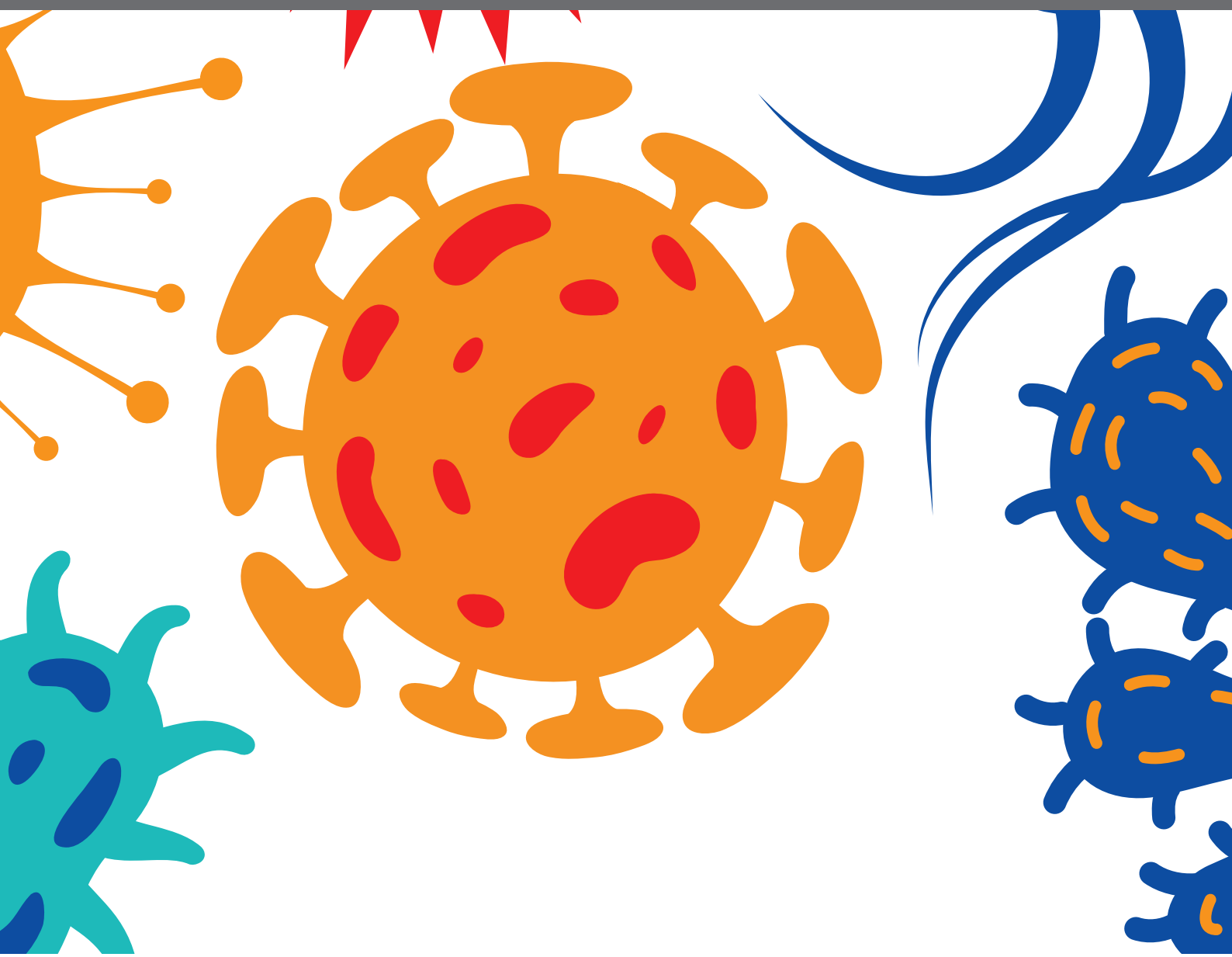

frontiers Research Topics

frontiers

ISSN 1664-8714
ISBN 978-2-88971-919-8
DOI 10.3389/978-2-88971-919-8

About Frontiers

Frontiers is more than just an open-access publisher of scholarly articles: it is a pioneering approach to the world of academia, radically improving the way scholarly research is managed. The grand vision of Frontiers is a world where all people have an equal opportunity to seek, share and generate knowledge. Frontiers provides immediate and permanent online open access to all its publications, but this alone is not enough to realize our grand goals.

Frontiers Journal Series

The Frontiers Journal Series is a multi-tier and interdisciplinary set of open-access, online journals, promising a paradigm shift from the current review, selection and dissemination processes in academic publishing. All Frontiers journals are driven by researchers for researchers; therefore, they constitute a service to the scholarly community. At the same time, the Frontiers Journal Series operates on a revolutionary invention, the tiered publishing system, initially addressing specific communities of scholars, and gradually climbing up to broader public understanding, thus serving the interests of the lay society, too.

Dedication to Quality

Each Frontiers article is a landmark of the highest quality, thanks to genuinely collaborative interactions between authors and review editors, who include some of the world's best academicians. Research must be certified by peers before entering a stream of knowledge that may eventually reach the public - and shape society; therefore, Frontiers only applies the most rigorous and unbiased reviews.
Frontiers revolutionizes research publishing by freely delivering the most outstanding research, evaluated with no bias from both the academic and social point of view. By applying the most advanced information technologies, Frontiers is catapulting scholarly publishing into a new generation.

What are Frontiers Research Topics?

Frontiers Research Topics are very popular trademarks of the Frontiers Journals Series: they are collections of at least ten articles, all centered on a particular subject. With their unique mix of varied contributions from Original Research to Review Articles, Frontiers Research Topics unify the most influential researchers, the latest key findings and historical advances in a hot research area! Find out more on how to host your own Frontiers Research Topic or contribute to one as an author by contacting the Frontiers Editorial Office: frontiersin.org/about/contact

VIBRIO VIRULENCE REGULATION AND HOST INTERACTIONS

Topic Editors:
Lixing Huang, Jimei University, China
Joanna Brzostek, University of Freiburg, Germany
Yang Fu, Southern University of Science and Technology, China
Wenxiang Sun, The University of Utah, United States

Citation: Huang, L., Brzostek, J., Fu, Y., Sun, W., eds. (2021). Vibrio Virulence Regulation and Host Interactions. Lausanne: Frontiers Media SA.
doi: 10.3389/978-2-88971-919-8

Table of Contents

frontiers in Cellular and Infection Microbiology

EDITORIAL
published: 29 October 2021
doi: 10.3389/fcimb.2021.793464

Editorial: Vibrio Virulence Regulation and Host Interactions

Lixing Huang[1], Yang Fu[2], Wenxiang Sun[3] and Joanna Brzostek[4]*

[1] Fisheries College, Fujian Engineering Research Center of Aquatic Breeding and Healthy Aquaculture, Jimei University, Xiamen, China, [2] School of Medicine, Southern University of Science and Technology, Shenzhen, China, [3] Huntsman Cancer Institute and Department of Pathology, School of Medicine, University of Utah, Salt Lake City, UT, United States, [4] Department of Microbiology and Immunology, National University of Singapore, Singapore, Singapore

Keywords: vibrio, virulence, pathogen-host interactions, Research Topic, bacteria

Editorial on the Research Topic

Vibrio Virulence Regulation and Host Interactions

Vibrio is an ubiquitous bacterium that is widely present in various aquatic and marine habitats; among the more than 100 species of *Vibrio* described, about 12 can cause human infections, while other *Vibrio* lead to marine animal infections. *Vibrio cholerae* can cause cholera, a serious diarrheal disease that is life-threatening if left untreated, and usually spread through contaminated water and personal contact. Non-cholera *Vibrio* species cause vibriosis - an infection usually are acquired through contacting with seawater or eating raw or undercooked contaminated seafood. Non-cholera *Vibrio* can cause a variety of clinical manifestations, including self-limiting gastroenteritis, wound infection, sepsis, and death. The incidence of vibriosis is on the rise, partly due to the spread of *Vibrio* spp. favored by climate change and rising sea temperature.

Considering that *Vibrio* is the leading opportunistic pathogen causing serious infections in humans and marine animals, there is an urgent need to better understand the pathogenic mechanism of *Vibrio* infections to guide effective prevention and treatments. Meanwhile, preventing and avoiding *Vibrio* infections and the resulting deaths require a deeper understanding of the mechanisms by which human and animal immune systems recognize and respond to *Vibrio*. To this end and through this Research Topic of 12 articles including original research and comprehensive reviews, we coalesce the latest advances in the current understanding of *Vibrio* virulence regulation and host interactions.

Vibrio cholerae VIRULENCE REGULATION AND HOST INTERACTIONS

V. cholerae is the pathogen causing cholera. It can proliferate in the water environment and infect humans through contaminated food and water. In *V. cholerae*, virulence is a multilocus phenomenon with a large functionally associated network. Ramamurthy et al. extensively summarize the regulation of important virulence factors in *V. cholerae* and the host response in the context of pathogenesis, covering topics such as major toxins produced by *V. cholerae* and their regulation, the control of virulence by the ToxR regulon, the regulation of secretory systems, the host's response to toxins and somatic antigens, as well as the host's inflammatory response. In addition, Kumar et al. evaluate and discuss our current understanding of the different functions of *Vibrio* pathogenicity island-1. In *V. cholerae*, this is related to virulence, important for toxin production, and essential for disease development. Biswas et al. summarize the diguanylate cyclases

OPEN ACCESS

Edited and reviewed by:
John S. Gunn, The Research Institute at Nationwide Children's Hospital, United States

****Correspondence:***
Lixing Huang
lixinghuang@jmu.edu.cn

Specialty section:
This article was submitted to Molecular Bacterial Pathogenesis, a section of the journal Frontiers in Cellular and Infection Microbiology

Received: *12 October 2021*
Accepted: *18 October 2021*
Published: *29 October 2021*

Citation:
Huang L, Fu Y, Sun W and Brzostek J (2021) Editorial: Vibrio Virulence Regulation and Host Interactions. Front. Cell. Infect. Microbiol. 11:793464. doi: 10.3389/fcimb.2021.793464

(DGCs) identified in *V. cholerae* so far, and emphasize the importance of DGCs and their product c-di-GMP in the virulence and lifecycle of *V. cholerae*.

Increased attention is being paid to the fact that the large number of microorganisms residing in human gastrointestinal tract establish a special micro-ecological system, which immediately responds to the invasion of *V. cholera* through the mechanism of "colonization resistance", such as the production of antimicrobial peptides, the competition of nutrients, and maintenance of the intestinal barrier. At the same time, *V. cholerae* can quickly sense these signals and regulate the expression of related genes to avoid stresses during infection, thereby successfully colonizing the surface of small intestinal epithelial cells. The comprehensive review by Qin et al. summarizes the interactions between the gut microbiota and *V. cholerae* in terms of type VI secretion system, quorum sensing, reactive oxygen species/pH stress, and bioactive metabolites.

Vibrio parahaemolyticus VIRULENCE REGULATION AND HOST INTERACTIONS

V. parahaemolyticus is a common pathogenic marine bacteria that can cause gastrointestinal infections and other health complications, posing a life threat to patients with weakened immune functions. In the past two decades, the pathogenicity of environmental *V. parahaemolyticus* has greatly increased. With more frequent studies showing the fast-evolving nature of *V. parahaemolyticus*, in-depth evaluation of its pathogenic ability becomes imperative. In this regard, Liu et al. demonstrate that the difference in pathogenicity of environmental *V. parahaemolyticus* strains is caused by a combination of HGT level, pathogenic elements distribution, and secretory system properties. Therefore, it is necessary to further study the genomic differences between environmental and clinical *V. parahaemolyticus* in order to better understand the pathogenicity of *V. parahaemolyticus*.

An in-depth understanding of the non-classical virulence genes of *V. parahaemolyticus* will help to better understand its pathogenic mechanism. Some manuscripts in this Research Topic reflect this view. For example, Pérez-Reytor et al. identify a gene encoding zonula occludens toxin (Zot) in the genome of highly cytotoxic strains of Chilean *V. parahaemolyticus*, which contributes to the virulence of *V. parahaemolyticus* through disturbance of the actin cytoskeleton. Yang et al. investigate the function of a prophage-related gene named VpaChn25_0724 in *V. parahaemolyticus* CHN25. Their results reveal that VpaChn25_0724 contributes to the cell membrane integrity and growth of *V. parahaemolyticus*.

VIRULENCE REGULATION IN OTHER *Vibrios*

V. harveyi, *V. alginolyticus* and *V. vulnificus* are the chief cause of vibriosis and have led to high mortality of marine animals and severe global economic losses. Understanding the virulence regulatory mechanisms of these *Vibrios* is the key to better development of fish vaccines. To this end, Xu et al. show that chemotactic genes *cheA*, *cheB*, *cheR*, *cheV* and *cheY* can regulate the adhesion ability of *V. harveyi* by affecting motility, and participate in the adjustment of adhesion at different temperatures, salinities and pH. Zeng et al. analyze the succinylome of *V. alginolyticus* for the first time and reveal the possible biological effects of lysine succinylated protein, of which 7.5% is predicted to be a virulence factor so it may provide possible targets for the development of attenuated vaccines. Gong et al. reveal that *V. vulnificus* RpoS regulates TolCV1 expression, thereby affecting the secretion of RtxA1, bile salt tolerance and lethality in mice.

VIRULENCE AND GENE DIVERSITY OF *Vibrio* spp

Vibrios are an abundant and diverse group of bacteria in marine and estuarine environments, and there is evidence of biochemical and genotypic correlations with virulence potential. In this regard, Lydon et al. determine the biochemical characteristics and virulence genotypes of 30 clinical and 39 oyster isolates of *V. vulnificus* based on the types of 16S rRNA gene (*rrn*) and virulence-related gene (*vcg*), which identify a relationship between isolates from the cooler season and systemic virulence potential in *V. vulnificus*. Besides, Wu et al. determine the genomic sequence of T3SS effector-encoding regions from 62 strains of four different species, and clarified the variation of their effector repertoires. In addition, they found a potential novel effector in *V. harveyi* and *V. campbellii* strain, and revealed that differences in T3SS-mediated cytotoxicity not only dependent on variation in the *Vibrio* T3SS effector repertoires, but also initial adhesion ability to host cells.

CONCLUDING REMARKS

The primary articles and reviews featured in this Research Topic are great examples presenting the current state of knowledge in this exciting and fast developing field of *Vibrio* spp. virulence regulation and host interactions. Through each new article, we gain a deeper understanding of the interesting and unique mechanisms controlling *Vibrio* pathogenicity and the pathogen-host interactions. In turn, these studies will contribute to the formulation of vibriosis control strategies and the development of highly effective live attenuated vaccines.

AUTHOR CONTRIBUTIONS

All authors listed have made a substantial, direct and intellectual contribution to the work, and approved it for publication.

FUNDING

This work was supported by grants from the Natural Science Foundation of Fujian Province under contract No. 2019J06020

and the National Natural Science Foundation of China under contract No. 32173016.

Conflict of Interest: The authors declare that the research was conducted in the absence of any commercial or financial relationships that could be construed as a potential conflict of interest.

Publisher's Note: All claims expressed in this article are solely those of the authors and do not necessarily represent those of their affiliated organizations, or those of the publisher, the editors and the reviewers. Any product that may be evaluated in this article, or claim that may be made by its manufacturer, is not guaranteed or endorsed by the publisher.

frontiers in Cellular and Infection Microbiology

ORIGINAL RESEARCH
published: 18 June 2020
doi: 10.3389/fcimb.2020.00301

Type III Secretion 1 Effector Gene Diversity Among *Vibrio* Isolates From Coastal Areas in China

Chao Wu[1], *Zhe Zhao*[1]*, *Yupeng Liu*[1], *Xinyuan Zhu*[1], *Min Liu*[1], *Peng Luo*[2] *and Yan Shi*[1]

[1] *Department of Marine Biology, College of Oceanography, Hohai University, Nanjing, China,* [2] *Key Laboratory of Marine Bio-Resources Sustainable Utilization, Key Laboratory of Applied Marine Biology of Guangdong Province, South China Sea Institute of Oceanology, Chinese Academy of Sciences, Guangzhou, China*

Vibrios, which include more than 120 valid species, are an abundant and diverse group of bacteria in marine and estuarine environments. Some of these bacteria have been recognized as pathogens of both marine animals and humans, and therefore, their virulence mechanisms have attracted increasing attention. The type III secretion system (T3SS) is an important virulence determinant in many gram-negative bacteria, in which this system directly translocates variable effectors into the host cytosol for the manipulation of the cellular responses. In this study, the distribution of the T3SS gene cluster was first examined in 110 *Vibrio* strains of 26 different species, including 98 strains isolated from coastal areas in China. Several T3SS1 genes, but not T3SS2 genes (T3SS2α and T3SS2β), were universally detected in all the strains of four species, *Vibrio parahaemolyticus*, *Vibrio alginolyticus*, *Vibrio harveyi,* and *Vibrio campbellii*. The effector coding regions within the T3SS1 gene clusters from the T3SS1-positive strains were further analyzed, revealing that variations in the effectors of *Vibrio* T3SS1 were observed among the four *Vibrio* species, even between different strains in *V. harveyi*, according to their genetic organization. Importantly, Afp17, a potential novel effector that may exert a similar function as the known effector VopS in T3SS1-induced cell death, based on cytotoxicity assay results, was found in the effector coding region of the T3SS1 in some *V. harveyi* and *V. campbellii* strains. Finally, it was revealed that differences in T3SS1-mediated cytotoxicity were dependent not only on the variations in the effectors of *Vibrio* T3SS1 but also on the initial adhesion ability to host cells, which is another prerequisite condition. Altogether, our results contribute to the clarification of the diversity of T3SS1 effectors and a better understanding of the differences in cytotoxicity among *Vibrio* species.

Keywords: Vibrios, type III secretion system (T3SS), cytotoxicity, effector, bacterial adhesion

OPEN ACCESS

Edited by:
Lixing Huang,
Jimei University, China

Reviewed by:
Qingpi Yan,
Jimei University, China
Xiaohui Zhou,
University of Connecticut, United States
Elsa Irma Quiñones-Ramírez,
Instituto Politécnico Nacional, Mexico
Anastasia D. Gazi,
Institut Pasteur, France

***Correspondence:**
Zhe Zhao
zhezhao@hhu.edu.cn

Specialty section:
This article was submitted to Molecular Bacterial Pathogenesis, a section of the journal Frontiers in Cellular and Infection Microbiology

Received: *02 February 2020*
Accepted: *20 May 2020*
Published: *18 June 2020*

Citation:
Wu C, Zhao Z, Liu Y, Zhu X, Liu M, Luo P and Shi Y (2020) Type III Secretion 1 Effector Gene Diversity Among Vibrio Isolates From Coastal Areas in China. Front. Cell. Infect. Microbiol. 10:301. doi: 10.3389/fcimb.2020.00301

INTRODUCTION

Vibrios are a kind of gram-negative halophilic bacteria widely distributed in marine and estuarine environments (Thompson et al., 2004). To date, more than 120 valid species (https://lpsn.dsmz.de/genus/vibrio) have been identified to be in the genus *Vibrio*, some of which have been recognized as pathogens of marine animals and humans (Austin and Zhang, 2006; Sawabe et al., 2013; Lin et al., 2018). Economic losses and health issues caused by these pathogenic bacteria annually have

become common concerns all around the world. Therefore, research on the pathogenic mechanism of these pathogenic *Vibrio* species has received constant and extensive attention, which has led to the identification of some crucial virulence factors, such as thermostable direct hemolysin (TDH) in *V. parahaemolyticus*, cholera toxin (CTX) in *Vibrio cholerae* and cytolysin in *Vibrio vulnificus* (Klose, 2001; Jones and Oliver, 2009; Broberg et al., 2011). Apparently, different *Vibrio* species employ variable virulence strategies, and even different strains of the same species may not rely solely on a given virulence factor.

The type III secretion system (T3SS) is a conserved supermolecular device located on the surface of many gram-negative bacteria (Coburn et al., 2007). Structurally, the T3SS has a remarkable needle-like appearance, which is composed of three major parts: a needle structure extending into the extracellular space, a basal body spanning the inner and outer membranes of the bacteria, and a cytoplasmic sorting platform essential for effector selection and needle assembly (Hu et al., 2014). Structural proteins of the T3SS machinery are highly conserved and evolutionary connected to bacterial flagellum (Hueck, 1998; Diepold and Armitage, 2015). T3SS pathway is capable of secreting a large number of substrates, with the later ones, the T3SS effectors being delivered directly to the host cell cytoplasm (Wagner et al., 2018). In contrast to structural proteins, these effectors vary considerably between different bacterial systems (Troisfontaines and Cornelis, 2005). Elucidation of the molecular roles of various T3SS effectors could provide important insights into the virulence mechanism of different pathogens.

For *Vibrio* spp., the T3SS was first discovered in *V. parahaemolyticus* (serotype O3:K6, strain RIMD2210633) by genome sequencing in 2003 (Makino et al., 2003). The strain has two different sets of T3SS gene clusters, T3SS1 and T3SS2. T3SS1 directly mediates cytotoxicity in host cells during the infection of cultured cells and is present in almost all clinical and environmental isolates of *V. parahaemolyticus*, whereas T3SS2 is typically associated with enterotoxicity during infection in animal models and found to be unique for Kanagawa phenomenon-positive *V. parahaemolyticus* (Park et al., 2004; Hiyoshi et al., 2010). In addition, T3SS gene clusters (T3SS1 or T3SS2) were also found in some other *Vibrio* species, such as *V. alginolyticus*, *V. harveyi*, *V. campbellii*, *Vibrio tubiashii*, *Vibrio mimicus,* and non-O1/O139 *V. cholerae* (Henke and Bassler, 2004; Park et al., 2004; Dziejman et al., 2005; Okada et al., 2010; Zhao et al., 2010; Liu et al., 2017). Comparative analyses have revealed that most of these clusters are more similar to the T3SS1 of *V. parahaemolyticus* in gene synteny and homology and harbor identical T3SS1 backbones, including all the genes annotated to encode the basal body, the needle-like structure, and the translocator; however, the hypothetical regions (the so-called effector coding regions) located between *vscL* and *vscU* genes of T3SS1, which are supposed to encode the effectors, exhibit many differences in gene content and order among those species (Ono et al., 2006; Zhao et al., 2011; Liu et al., 2017). For example, VopR, an effector encoded by *vp1683* in the *V. parahaemolyticus* strain RIMD2210633, which is involved in the T3SS1-mediated cytotoxicity toward HeLa cells, did not have an ortholog in the T3SS gene cluster of the *V. alginolyticus* strain ZJ51 (Zhao et al., 2010). The T3SS2 was further classified into two clades, T3SS2α and T3SS2β, based on the sequences of the structural genes (Okada et al., 2009). Despite the fact that the T3SS2 was experimentally shown to be functional in only a few *V. cholera and V. parahaemolyticus* strains, effectors in all T3SS2 islands appeared to be pretty variable and performed a wide range of activities (Miller et al., 2019). Moreover, variations in the effectors of T3SS have also been reported in other bacterial systems (Brugirard-Ricaud et al., 2004; Troisfontaines and Cornelis, 2005). Therefore, all these findings prompted us to further characterize the variations in the T3SS effectors among *Vibrio* species and identify the species- or strain-specific effectors.

To this end, we isolated *Vibrio* strains from sea water and marine animals from coastal areas in China and classified those isolates in this study. Subsequently, the distribution of the T3SS gene cluster was examined among the isolated *Vibrio* strains, after which we determined their effector coding regions in the abovementioned T3SS1-postive *Vibrio* strains. Finally, we characterized the variations in the T3SS1 effectors and their ramifications on the cytotoxicity phenotype in fish cells.

MATERIALS AND METHODS

Bacterial Strains and Growth Conditions

Most of the *Vibrio* strains used in this study were isolated from sea water and marine animals collected from coastal areas in South China and the Jiangsu province (**Supplemental Table 1**). Samples were directly plated onto thiosulfate citrate bile salts sucrose (TCBS, BD, U.S.A) agar without the use of enrichment medium. Inoculated TCBS plates were incubated at 30°C for 12–24 h, and well-isolated colonies were re-streaked onto fresh TCBS for further purification. The monoclonal colony was selected based on colony morphology and stored at −80°C until subsequent use. Some standard *Vibrio* strains (**Supplemental Table 1**) were purchased from the ATCC (American Type Culture Collection, U.S.A), BCCM/LMG (Belgian Co-ordinated Collections of Micro-organisms, Belgium), or MCCC (Marine Culture Collection of China, China) and used as references. For routine culture, the bacteria were grown in Luria Bertani Broth (LB, BD, U.S.A) supplemented with 2% (w/v) NaCl or in Difco Marine Broth 2216 medium with shaking (200 r.p.m.) at 30°C.

Common Polymerase Chain Reaction (PCR)

The DNA of all strains in this study was extracted with the MiniBEST Bacteria Genomic DNA Extraction Kit (Takara Bio Inc., Japan). Four conserved genes, the 16S rRNA gene, the glyceraldehyde-3-phosphate dehydrogenase alpha submit (*gapA*) gene, the recombinase alpha subunit (*recA*) gene and the RNA polymerase alpha submit (*rpoA*) gene, were amplified by common PCR using the described primers (Gabriel et al., 2014) and sequenced to identify the isolated *Vibrio* species. The *vcrD*, *vscC*, and *vopB* genes of the T3SS1, as well as the *vscN2*, *vscT2*, and *vscR2* genes of the T3SS2 (T3SS2α and T3SS2β, Okada et al., 2010), were examined using their respective primers (**Supplemental Table 2**) to examine by common PCR

whether T3SS1, T3SS2α, and T3SS2β existed in all strains. PCR amplification was conducted using a Premix Ex Taq™ kit (Takara Bio Inc., Japan) following the manufacturer's instructions; the annealing temperature for each gene was adjusted according to the corresponding primers.

Multilocus Sequence Analysis and Phylogenetic Tree

Multilocus sequence analysis (MLSA) was used to identify the *Vibrio* strains as described previously (Gabriel et al., 2014). Briefly, the gene sequences of the 16S rRNA gene, *gapA*, *recA*, and *rpoA* were combined to produce concatenated sequence in the order of 16S rRNA gene-*gapA*-*recA*-*rpoA*. The concatenated sequences were aligned using ClustalX (version 1.83), after which a phylogenetic tree was constructed using MEGA 7. A maximum likelihood method was selected, and a bootstrap analysis was employed to quantitatively assess the tree.

Long Range PCR and Genome Walking

A pair of degenerate primers located at the intersection of the *vscT*/*vscU* and *vscL*/*vscK* genes of the T3SS1, which flank the effector coding regions (Ono et al., 2006), was designed (**Supplemental Table 2**). Long fragments containing their effector coding regions were amplified from different *Vibrio* strains possessing the T3SS1 using the degenerate primers in long range PCR with LA Taq DNA polymerase (Takara Bio Inc., Japan) as per the manufacturer's recommendations. The sequences were fully determined by using genome walking (Takara Bio Inc., Japan) and subjected to further analysis. Sequence data for the effector coding regions were submitted to the NCBI GenBank and assigned the accession numbers as listed in **Supplemental Table 3**.

Identification and Comparison of T3SS1 Effectors in Vibrios

The obtained sequences were compared to the available *Vibrio* genome assemblies (Whole Genome Shortgun, WGS) in NCBI by sequence alignment using BLASTn with the cutoff E-value of 1e-5. A second iteration using BLASTp (E-value 1e-5) were performed to compare the identified putative T3SS1 effectors against non-redundant (nr) database, aiming to find its orthologs in different *Vibrio* species as many as possible. Further, both the type III secretion signals and the binding site of the chaperones (conserved chaperone binding domain, CCBD) for the identified T3SS1 effectors were predicted by EffectiveDB (Eichinger et al., 2015). The putative functional domain modules were classified by PfamScan v1.6 using Pfam32.0 database (Finn et al., 2016). The *Vibrio* genomes that contain the genomic loci spanning the T3SS1 effectors were inspected and compared by MultiGeneBLAST v1.1.14 with default option (Medema et al., 2013).

Cell Lines and Infection

Epithelioma papulosum cyprini (EPC) cells were cultured in M199 medium supplemented with 10% (v/v) fetal bovine serum (FBS, Gibco, U.S.A) at 28°C. For *Vibrio* infection, EPC cells were seeded into 96-well plates and incubated overnight to 90% confluency. Overnight cultures of *Vibrio* isolates were pelleted by centrifugation at 10,000 × g for 2 min at 4°C. The bacterial pellets were resuspended in serum-free M199 medium, and the bacterial suspensions were added to the cell monolayer at a multiplicity of infection (MOI) of 10.

Lactate Dehydrogenase (LDH) Release Assay

This assay was performed as described previously (Zhao et al., 2018). Briefly, the growth medium of EPC cells in 96-well plates was replaced with 120 μl (per well) of serum-free M199 medium before infection, and the cells were infected with different *Vibrio* strains. At the indicated time point, the 96-well plates were centrifuged at 3,200 × g for 2 min, and 80 μL aliquots of the supernatants were transferred to a new 96-well plate for measuring LDH release by using the Cytotoxicity Detection Kit ^{PLUS} per the manufacturer's instructions (Roche, Switzerland). The background value was measured from the M199 medium only. Maximum LDH release was obtained by total cell lysis using the lysis buffer provided in the kit. Minimum LDH release was obtained from the cell supernatant without infection. Absorbance values from each well were measured at 492 nm by using a microplate spectrophotometer (Spark, Tecan, Switzerland). The results are expressed as a percentage of total cell lysis after subtracting the absorbance value of the background control.

Bacterial Adhesion Assay

For the adhesion assay, EPC cells were seeded into 24-well plates using M199 medium supplemented with 10% (v/v) FBS and incubated overnight to 90% confluency. Overnight cultures of *Vibrio* strains were pelleted by centrifugation at 10,000 × g for 2 min at 4°C. The bacterial pellets were resuspended in serum-free M199 medium and then adjusted to a bacterial concentration of 5×10^7 CFU/mL. Bacterial suspensions (20 μL) were added to the cell monolayer and cultured at 30°C for 60 min. The cells were first washed with sterile PBS (3 times) to remove non-adherent bacteria, after which the surface-attached bacteria were fully resuspended in bacterial culture medium. Bacteria suspensions were diluted in a 10-fold dilution series, and 20 μL of each diluted concentration was plated onto LB agar supplemented with 2% NaCl. The *Vibrio* plates were cultured at 30°C for an appropriate length of time, and the colonies were finally enumerated to determine the number of adherent bacteria.

Statistical Analysis

Statistical analysis was performed with a one-way analysis of variance (ANOVA), and $P < 0.05$ were considered statistically significant. Pairwise comparisons were conducted using a Tukey's multiple comparison test, and the analysis was conducted using the SPSS software (version 22.0).

RESULTS

Identification of *Vibrio* Isolates

In total, 110 *Vibrio* strains were used in this study, including 98 strains isolated from the coastal areas of South China and the Jiangsu Province (**Supplemental Table 1**). The MLSA method was utilized to identify these strains. To assess the accuracy of the identification, 12 known *Vibrio* strains

belonging to 10 different species (**Supplemental Table 1**) were included and randomly put together in our MLSA. Phylogenetic trees constructed using maximum likelihood showed that the 12 known *Vibrio* strains were classified into the right clades as expected (**Supplemental Figure 1**), and the 98 *Vibrio* strains we isolated were sorted into 19 different *Vibrio* species (**Supplemental Table 1**). Among these 19 species, *V. alginolyticus*, *V. parahaemolyticus* and *V. harveyi* were the top three most abundant *Vibrio* species, with 23, 20, and 10 isolates, respectively.

Distribution of the T3SS-Related Genes Among the Examined *Vibrio* Species

To determine the presence of the T3SS genes (T3SS1 and T3SS2) in our *Vibrio* collection, we designed PCR primers targeted to three T3SS1 genes [for the apparatus (VcrD and VscC) and translocon (VopB)] and selected six PCR primer pairs that were used in a previous study for targeting several T3SS2α and T3SS2β genes (*vscN*2, *vscT2,* and *vscR*2). Screening of all *Vibrio* strains revealed that 62 strains exhibited positive signals for the three T3SS1 genes (**Supplemental Table 1**), all of which represented members of *V. parahaemolyticus*, *V. alginolyticus*, *V. harveyi*, and *V. campbellii*. However, the detection of the T3SS2α and T3SS2β genes showed negative signals for almost all *Vibrio* strains, except for *V. parahaemolyticus* strain RIMD2210633 and strain ATCC33847. These two strains were the only T3SS2α-positive strains. These data suggested that the T3SS1, but not the T3SS2, is widely present in all strains of *V. parahaemolyticus*, *V. alginolyticus*, *V. harveyi,* and *V. campbellii* in coastal environments in China.

Genetic Organization of Effector Coding Regions of the T3SS1 in the T3SS1-Positive Strains

To further study variation of the T3SS1 effectors among all T3SS-postive *Vibrio* strains, we determined the nucleotide sequences of the non-conserved regions (here referred to as effector coding regions), which are located between the *vscL* and *vscU* genes of the T3SS1. Sequence analysis showed that the length of their effector coding regions varied obviously among the different *Vibrio* strains, ranging from ∼6.9 to 11.7 Kb. However, the GC content of those sequences only ranged from 43 to 47%, which was also similar to the average GC percentage of the genome sequence of Vibrios. A phylogenetic study was undertaken based on the nucleotide sequences of effector coding regions. The resulting tree showed that these *Vibrio* strains were divided into the four distinct groups: *V. parahaemolyticus*, *V. alginolyticus*, *V. harveyi,* and *V. campbellii* (**Supplemental Figure 2**), and exhibited similar taxonomic status in the harveyi clade of the MLSA tree. These findings suggest that acquisition of the T3SS1-related genes may occur in an ancient evolutionary event.

These sequences were further annotated, and their genetic organizations were compared. Genomic organization of the T3SS1 effector coding region from the *V. parahaemolyticus* strain RIMD2210633, the most studied *Vibrio* T3SS1 by far, was set as a reference, and three known effectors, VP1686 (VopS), VP1683 (VopR), and VP1680 (VopQ), were the primary focus for the comparison analysis. According to gene content and synteny, the organizations of the T3SS1 effector coding regions of 61 strains (except RIMD2210633) were classified into nine different types (**Figure 1**). As expected, certain variations within the effector coding regions among the four *Vibrio* species, even between different strains of the same species were found. As for the three known effectors, their counterparts were found to be present in almost all *V. parahaemolyticus* and *V. alginolyticus* strains, except for two *V. alginolyticus* strains (E401 and A056) belonging to the type Val-I lacking the homologous protein of VopR. However, *V. harveyi* strains exhibited greater variations in their effectors in this region. The type Vh-I harbored all three known effectors, while the types Vh-II and Vh-III only had two (VopQ and VopR) and one (VopQ) of these effectors, respectively. In other words, the latter two types of *V. harveyi* did not harbor the VopS homolog. Interestingly, they both contained *afp17*, a large gene predicted to encode a protein (Afp17) with an ADP-ribosyltransferase domain in its C-terminal according to the PfamScan results. In addition, strong T3SS secretion signals were also found in the amino terminal of Afp17 on the basis of EffectiveDB prediction (**Supplemental Table 4**). For the six *V. campbellii* strains, only one type of gene organization of the T3SS effector coding region was found; these strains not only had homologs of VopS and VopQ but also harbored Afp17. Interestingly, a small gene was found to be located adjacently upstream of *afp17* in certain strains of *V. harveyi* and *V. campbellii* from the present study. Importantly, similar structural linkage between these two genes were also found in several other *Vibrio* species, such as *Vibrio owensii*, *Vibrio tubiashii*, *Vibrio europaeus*, *Vibrio chagasii,* and *Vibrio lentus*, as evidenced by gene cluster comparisons (**Supplemental Figure 3**). The protein encoded by such small gene was considered to be a molecular chaperone for Afp17 since the correct translocation of effectors secreted via the T3SS requires their cognate chaperones for their own stabilization (Akeda and Galan, 2005). Similarly, there were homologs of VP1687, VP1684, and VP1682, serving as the chaperones for VopS, VopR, and VopQ, respectively, in close proximity to their effectors. Four unknown genes in the T3SS1 of the reference strain, *VP1679*, *VP1678*, *VP1677,* and *VP1676*, were also compared, revealing that their homologous genes were only present in *V. parahaemolyticus* VP-I and VP-II. However, some other genes that were annotated to be transcriptional regulators (Lys family, AcrR family, AraC family, and MarR family), transporters (EamA, MFS, and HlyD) and enzymes (N-acetyltransferase, oxidoreductase) were also found in the different types.

Cytotoxicity of Different *Vibrio* Isolates Toward Fish Cells

Considering the variation in the effectors of the T3SS among the different species, especially in *V. harveyi* strains, we measured the cytotoxicity toward fish cells of all *Vibrio* strains that harbored the T3SS and assessed the correlation between the variation and cytotoxicity. The LDH release assays showed that all *V. parahaemolyticus* strains exhibited a similar cytotoxicity as the reference strain RIMD2210633 toward EPC cells, as evidenced by ∼60 and 80% total LDH release at 2 and 3 h post-infection, respectively (**Figure 2A**). Similarly, the LDH levels in

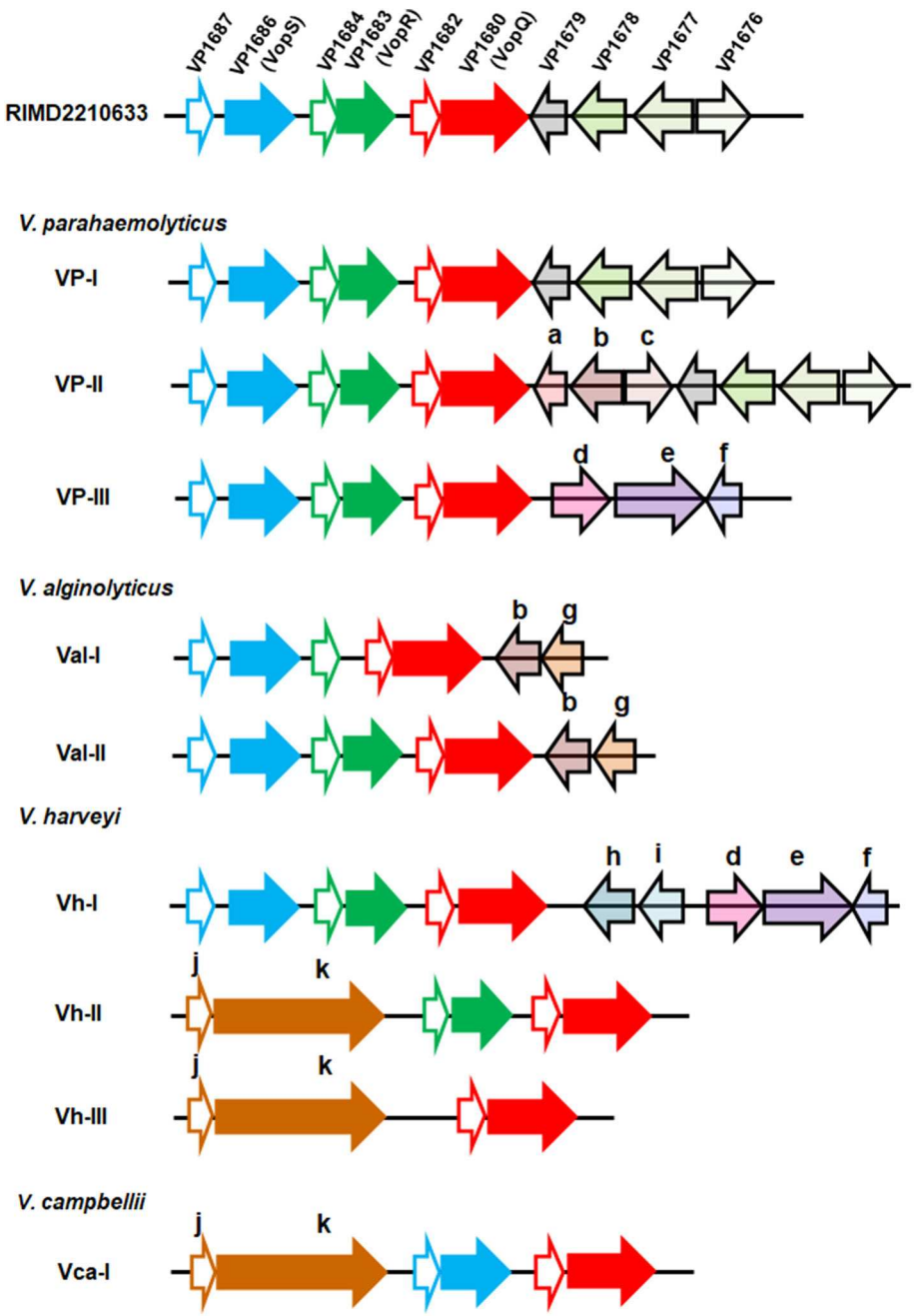

FIGURE 1 | Genetic organization of the T3SS1 effector coding regions in four *Vibrio* species. Each gene was represented by an arrow indicating the approximate size and the direction of transcription based on the position of methionine initiation and the termination codons. The effector coding region of T3SS1 in the *V. parahaemolyticus* strain RIMD2210633 was set as a reference, and different genes within this region were highlighted with different colors. The one-to-one relationship between each indicated effector protein and its adjacent chaperone were shown by identical color code, and the latter was filled with white color. Nine types of genomic organization were classified based on gene content and the order of the T3SS1 effector coding regions from 62 *Vibrio* strains across the four species (*V. parahaemolyticus*, *V. alginolyticus*, *V. harveyi,* and *V. campbellii*). The gene (arrow) in the nine types was marked with the same color if it had an ortholog in the reference strain RIMD2210633 or with another color and indicated with a lower case letter as follows: a: GNAT family N-acetyltransferase; b: EamA family transporter, c: LysR family transcriptional regulator; d: HlyD family secretion protein; e: MFS transporter; f: TetR/AcrR family transcriptional regulator; g: AraC family transcriptional regulator; h: SDR family oxidoreductase; i: MarR family transcriptional regulator; j: class I chaperone; k: Afp17.

the medium of cells infected with all of the *V. alginolyticus* strains were not significantly different from that of cells infected with the reference strain RIMD2210633 (**Figure 2B**). For *V. harveyi* strains, the difference in cytotoxicity effects was quite obvious among these strains (**Figure 2C**). The five strains (HN385, HN435, HN453, E385, and HS14) of *V. harveyi* with the *Afp17*

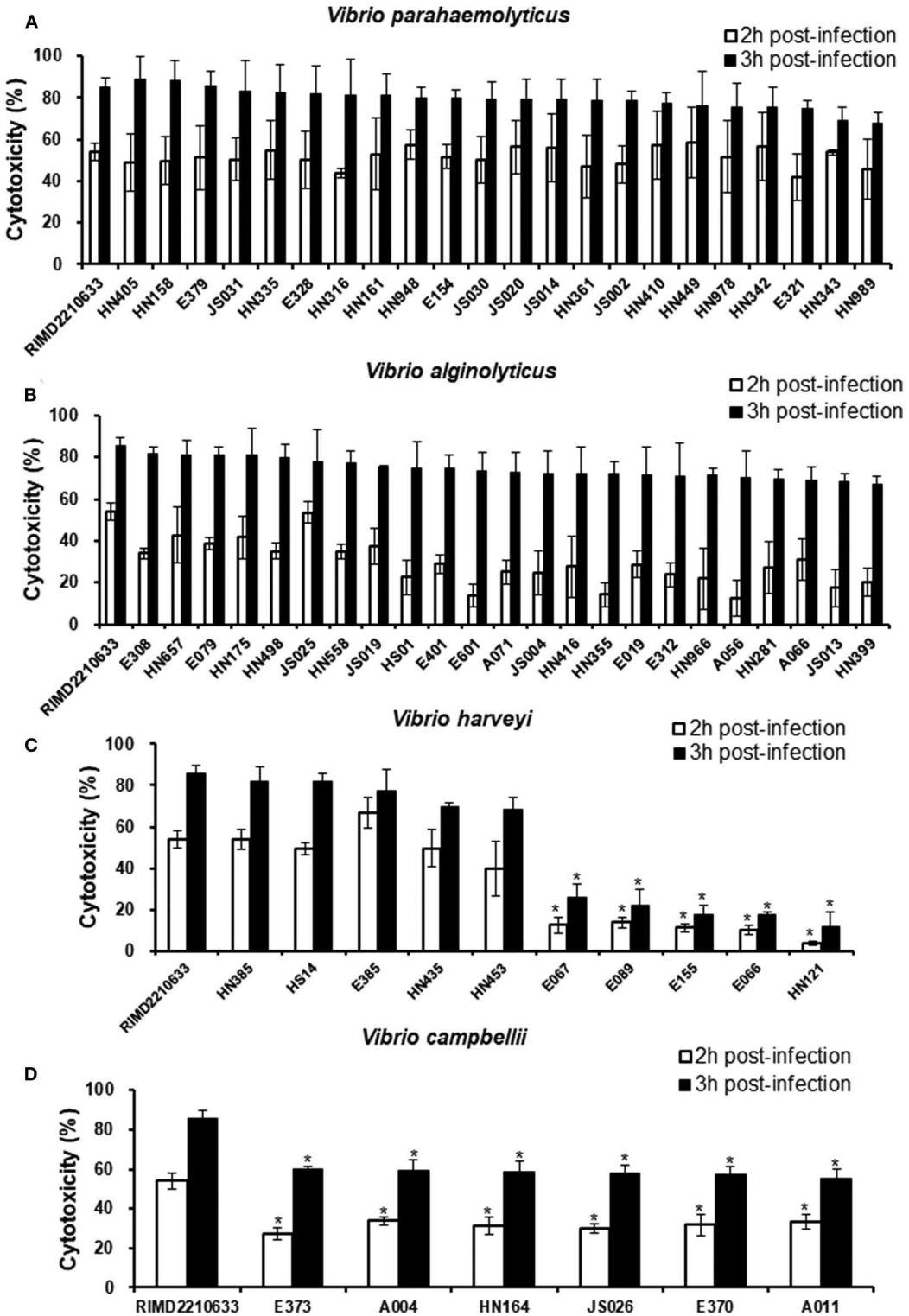

FIGURE 2 | Cytotoxicity toward fish cells induced by different *Vibrio* strains. EPC cells were infected with different strains from *V. parahaemolyticus* **(A)**, *V. alginolyticus* **(B)**, *V. harveyi* **(C)**, and *V. campbellii* **(D)** as described in the Materials and Methods. At the indicated time points, the culture supernatants were measured for the release of LDH, followed by the calculation of cytotoxicity as a percentage of total cellular lysis. The data are expressed as the means ± SE from three independent experiments ($n = 3$). *$P < 0.05$ by one-way ANOVA and Tukey's multiple comparison test.

produced equivalent LDH release levels on fish cells when compared to the reference strain RIMD2210633, whereas another five strains (E066, E067, E089, E155, and HN121) caused the lowest cytotoxicity effect, with ∼20% total LDH release at 3 h post-infection. Additionally, six *V. campbellii* strains showed a moderate cytotoxicity effect when compared to the reference strain and the *V. harveyi* strains.

Adhesion Ability Affects T3SS-Mediated Cytotoxicity

Adherence is a critical first step in the establishment of infection, which then affects the subsequent events, including bacterial pathogenesis (Kline et al., 2009). Since some strains of *V. harveyi* were shown to cause a lower cytotoxicity than the reference strain RIMD2210633, even though they possessed the same effector repertoires (VopS, VopR, and VopQ), it was assumed that differences may exist in the adhesion ability between these strains. For this reason, seventeen strains, as indicated in **Figure 3**, were selected to measure their adhesion ability. The data showed that the *V. harveyi* strains with a low cytotoxicity effect appeared to have a weaker adhesion ability than the *V. harveyi* strains with high cytotoxicity and the reference strain RIMD2210633 at 1 h post-infection (**Figures 2**, **3**). Furthermore, all *V. campbellii* strains also exhibited low adhesion and consequently did not produce cytotoxicity levels as high as expected, even if they carried the three key effector genes (Afp17, VopS, and VopQ) in their T3SS1 gene cluster. We therefore surmised that the initial adhesion to host cells is a prerequisite factor that affects T3SS-mediated cytotoxicity in *Vibrio* species.

DISCUSSION

Vibrio is a genetically and metabolically diverse group of bacteria that often predominate in the aquatic environment and accounts for more than 10% of the culturable bacterial community (Yooseph et al., 2010; Gilbert et al., 2012; Takemura et al., 2014). In this study, we obtained 19 different *Vibrio* species from the coastal areas of South China and the Jiangsu province, and the most abundant species were found to be *V. parahaemolyticus*, *V. alginolyticus,* and *V. harveyi.* This was in agreement with the previous reports indicating that the members of the harveyi clade are usually the dominant groups in Chinese coastal environments (Xie et al., 2005; Austin and Zhang, 2006; Chen et al., 2011; Han et al., 2015; Zuo et al., 2019).

The T3SS genes are commonly used as virulence markers for pathogenic bacteria. The T3SS in the *Vibrio* species was discovered from a *V. parahaemolyticus* clinical strain that carried the T3SS1 and T3SS2 gene clusters (Makino et al., 2003). In addition to *V. parahaemolyticus*, the T3SS1 and T3SS2 gene clusters were also found to be present in many other *Vibrio* species. Of these, the T3SS1 gene cluster was mainly present in several species of the harveyi clade, such as *V. alginolyticus*, *V. harveyi,* and *V. campbellii* (Henke and Bassler, 2004; Park et al., 2004; Zhao et al., 2010; Liu et al., 2017). This conclusion was well-supported by our data showing that all tested strains of *V. parahaemolyticus, V. alginolyticus*, *V. harveyi,* and *V. campbellii* in our collections possessed the T3SS1 gene cluster. T3SS2-related gene cluster is located within an 80 kb pathogenicity island (Vp-PAI) and the T3SS2 has two distinct subtypes, T3SS2α and T3SS2β (Noriea et al., 2010), and has been reported in some specific strains of non-O1/O139 *V. cholerae*, non-toxigenic O1 *V. cholerae* and *V. mimicus* (Dziejman et al., 2005; Okada et al., 2010; Mahmud et al., 2014). However, six genes within the T3SS2α and T3SS2β were not detected in our isolates, including all the *V. parahaemolyticus* strains. This may have been possible because our *Vibrio* isolates belonged to environmental strains (isolated from sea water or common marine animals), while the T3SS2 genes tend to be closely linked with clinical strains (Okada et al., 2010).

Effector diversity was commonly observed in many T3SS from several different bacterial taxa (Troisfontaines and Cornelis, 2005). The three secreted effectors (VopS, VopR and VopQ) were identified within the T3SS1 effector coding region between *vscL* and *vscU* genes from *V. parahaemolyticus* (Ono et al., 2006). These effectors play a central role in T3SS1-mediated cell death, with a temporal regulation of events, including autophagy, cell rounding and ultimately cell lysis, in HeLa cells (Burdette et al., 2009; Yarbrough et al., 2009; Salomon et al., 2013). Therefore, the specific regions from all the T3SS1-positive strains were highlighted to characterize the variations in the effectors. The orthologs of VopQ were highly conserved in all strains across four different *Vibrio* species and was referred to here as a core effector. This effector was not only responsible for *V. parahaemolyticus* T3SS1-induced autophagy in HeLa cells (Burdette et al., 2009) but also contributed to T3SS1-induced LDH release in HeLa cells and fish cells (Burdette et al., 2009; Zhao et al., 2018). Another core effector, VopS, was of equal importance for T3SS1-induced cell death and was required for the T3SS1-induced cell rounding phenotype in *V. parahaemolyticus* (Yarbrough et al., 2009). The *V. alginolyticus* ortholog (Val1686) of effector VopS was necessary and sufficient to cause cell rounding and apoptosis (Zhao et al., 2018). It was therefore not surprising that the VopS orthologs were found to be present in all strains of *V. parahaemolyticus*, *V. alginolyticus* and *V. campbellii.* The exception was in certain *V. harveyi* strains that lacked the VopS homolog in their effector coding regions. Surprisingly, a novel T3SS effector protein (Afp17) containing an ADP-ribosyltransferase domain, was discovered in the strains lacking the VopS homolog. The bacterial proteins carrying this domain are usually toxins, known as ADP-ribosylating toxins, that covalently transfer the ADP-ribose portion of NAD to host proteins and result in a variety of cytotoxic effects (Deng and Barbieri, 2008); for example, many T3SS effectors, including AexT of *Aeromonas salmonicida*, ExoS, and ExoT of *Pseudomonas aeruginosa* and SpvB of *Salmonella* spp., have been verified for their toxin activities (Kaufman et al., 2000; Krall et al., 2000; Burr et al., 2003; Cheng and Wiedmann, 2019). In addition, a strong type III secretion signal was found in the N-terminal of almost all under-investigated Afp17 from several different *Vibrio* species (**Supplemental Table 4**). Notably, the only exception was found in *V. harveyi* strain HENC-02, of which the T3SS signal for Afp17 was determined to be very low (0.00044). Further studies concerning the prediction of type

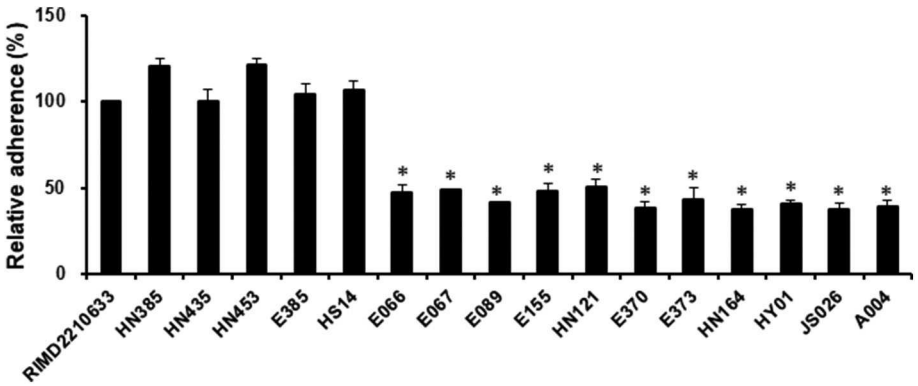

FIGURE 3 | Assay to test adhesion of the *V. harveyi* and *V. campbellii* strains to fish cells. EPC monolayers were infected with all *V. harveyi* and *V. campbellii* strains as described in the Materials and Methods. The *V. parahaemolyticus* strain RIMD2210633 was included as a control. After 1 h of infection, the adherent bacteria were enumerated. The y-axis represented the adhesion efficiency of each strain indicated in the x-axis, relative to strain RIMD2210633. The data are expressed as the means ± SE from three independent experiments ($n = 3$). *$P < 0.05$ by one-way ANOVA and Tukey's multiple comparison test.

III secretion signal in Vibrios as well as functional comparisons among these Afp17 orthologs will contribute to an in-depth understanding of the evolution and functional implication of T3SS effector signal. Moreover, current knowledge about the T3SS effectors has suggested that certain signal motif in its N-terminal, which served as binding sites for chaperone proteins to facilitate effectors secretion, can be identified by using machine learning approach (Samudrala et al., 2009; McDermott et al., 2011). However, such CCBD was not found in any of the under-investigated Afp17 orthologs, which possibly could be explained by the lacking of *Vibrio*-originated sequences in the training dataset that had been used in CCBD prediction (Costa et al., 2012; Eichinger et al., 2015). Whilst, considering the existence of structural linkage between afp17 and its upstream chaperone gene in several Vibrios other than *V. harveyi* and *V. campbellii*, it's highly likely that the Afp17 could be a *bona fide* effector within the T3SS1 gene cluster that may exert functions similar to VopS during infection. The effector VopR also existed in the majority of the strains but was not found to be in some strains from the *V. alginolyticus*, *V. harveyi,* and *V. campbellii* species. It is tempting to speculate that VopR may not be indispensable for T3SS1-induced cell death since the *V. alginolyticus* strain ZJ51 lacking the VopR homolog still exerts a comparative cytotoxic effect with *V. parahaemolyticus* T3SS1 on HeLa cells (Zhou et al., 2009; Zhao et al., 2010, 2011), although VopR was suggested to contribute to cell rounding (Salomon et al., 2013).

Many additional genes were frequently found in the vicinity of effector VopQ in many *Vibrio* strains. Although these genes were located within the effector coding regions of the T3SS1 gene cluster, their products, such as transcriptional regulators, transporters and enzymes, did not appear to be related to the T3SS effectors, according to gene functional annotation and the T3SEdb (Tay et al., 2010). We also predicted the type III secretion signals for their products using EffectiveDB, but no T3SS secretion signal was found in their amino terminus. Furthermore, we also had deleted a gene encoding AraC family transcriptional regulator in T3SS1 of *V. alginolyticus* strain ZJ51, however, the deletion has no any effect on T3SS1-mediated cytotoxicity toward fish cells (data not shown). Sequence analysis showed that those "non-related" genes have the similar GC contents to the effector genes in the effector coding region. Therefore, their presence increased gene diversity within the region encoding the T3SS1 effectors, and a functional correlation with T3SS1 remains elusive.

T3SS function is essentially dependent on its effectors. We therefore compared the cytotoxicity toward cultured fish cell lines of all *Vibrio* strains harboring T3SS1. As expected, all strains of *V. parahaemolyticus* and *V. alginolyticus* exhibited cytotoxicity effects similar to the reference strain RIMD2210633 since they all had homologs of two core effectors, VopQ and VopS. Additionally, five *V. harveyi* strains carrying VopQ and Afp17 also produced equal cytotoxicity, although these *V. harveyi* strains lacked VopS. The data further supported the hypothesis that Afp17 is a novel T3SS1 effector and can substitute for VopS, and experimental evidence for this is currently being generated. Surprisingly, another five *V. harveyi* strains harboring the VopQ and VopS orthologs demonstrated quite low cytotoxicities. This phenomenon was explained by bacterial adhesion ability since *V. harveyi* strains harboring the VopQ and VopS orthologs exhibited a significant reduction in adhesion compared to the reference strain RIMD2210633 and other *V. harveyi* strains. It is reasonable that the translocation of effectors into the host cell cytoplasm by T3SS requires direct contact between pathogen and host (Krachler and Orth, 2011; Erwin et al., 2012). We concluded that the initial adhesion to host cells was a prerequisite factor that affected the cytotoxicity effect of *Vibrio* T3SS1. This point was further supported by cytotoxicity and adhesion assays of *V. campbellii* strains. Our *V. campbellii* strains not only had the two core effectors but also carried the Apf17, and it was therefore expected that they possessed a

higher cytotoxicity than other *Vibrio* strains. However, due to their weak adhesion, their cytotoxicity effect was lower than that of the reference strain RIMD2210633. Bacterial adhesion is a complicated process of interaction between a pathogen and its host, and requires adhesive molecules on their surfaces. For Vibrio species, many proteins, such as MAM7, VpadF, and flagellar assembly-associated proteins (flrA, flrB, and flrC), have been reported to be linked to bacterial adhesion (Krachler and Orth, 2011; Liu and Chen, 2015; Luo et al., 2016); however, whether the T3SS1 pathway is involved into the regulation of bacterial adhesion remained to be elucidated.

In summary, we here examined the distribution of the T3SS gene cluster from 110 *Vibrio* strains of 26 different species, including 98 strains isolated from Chinese coastal areas, and found that the T3SS1 gene cluster, but not the T3SS2 (T3SS2α and T3SS2β) gene cluster, was extensively present in our isolated *V. parahaemolyticus*, *V. alginolyticus*, *V. harveyi,* and *V. campbellii* strains. We further examined their T3SS1 effector coding regions, revealing that the T3SS1 effectors varied among not only the four different *Vibrio* species, but also the different strains of *V. harveyi*. Importantly, we discovered a potential novel effector, Afp17, in the T3SS1 effector coding region of some *V. harveyi* and *V. campbellii* strains, which may substitute for the core effector VopS and perform a similar function in inducing cytotoxicity. Moreover, we also shown that the cytotoxicity effect of T3SS1 was dependent not only on their effectors but also on the initial bacterial adhesion to host cells.

DATA AVAILABILITY STATEMENT

The datasets generated for this study can be found in the GenBank.

AUTHOR CONTRIBUTIONS

CW, YL, XZ, and ML carried out the experiments. CW, YS, and ZZ designed the experiments and analyzed the data. PL contributed the *Vibrio* strains. CW and ZZ wrote the manuscript. All authors have read and agreed to the published version of the manuscript.

FUNDING

This study was supported by the National Natural Science Foundation of China (31872597), the Natural Science Foundation of Jiangsu Province (BK20171431), the Jiangsu Agriculture Science and Technology Innovation Fund (CX [19]2033), and the Earmarked Fund for Jiangsu Agricultural Industry Technology System (JATS [2019]477).

SUPPLEMENTARY MATERIAL

The Supplementary Material for this article can be found online at: https://www.frontiersin.org/articles/10.3389/fcimb.2020.00301/full#supplementary-material

Supplemental Figure 1 | Phylogenetic tree of different *Vibrio* strains. The phylogenetic analysis was based on multiple sequences alignment of 164 concatenated sequences of 16S rRNA gene-*gapA-recA-rpoA* and conducted by MEGA7 using the Kimura 2-parameter model with the maximum-likelihood method, and then the tree was further edited using the Evolview online. Values of bootstrap after 1,000 replications were shown in each node branch represented by the sized circles. 14 *Vibrio* clades defined in the previous study (Sawabe et al., 2013; Gabriel et al., 2014) were shown and strains belonging to the same clade were labeled with the same color. Among 164 concatenated sequences, 110 of them were obtained by amplification from 98 unknown *Vibrio* strains isolated in this study and 12 standard *Vibrio* strains (See Materials and Methods); while the remaining 54 sequences of reference that have been previously used in MLSA analysis for identification of Species in the Genus *Vibrio* (Gabriel et al., 2014) were retrieved from Genbank.

Supplemental Figure 2 | Phylogenetic tree based on the nucleotide sequence of T3SS1 effector coding regions from 62 T3SS1-positive strains. Phylogenetic analysis was conducted as described in **Supplemental Figure 1**, and the tree was also edited using the Evolview online. Values of bootstrap after 1,000 replications were shown in each node branch represented by the sized circles. Strains belonging to the same species were labeled with the same color.

Supplemental Figure 3 | Comparisons of the T3SS1 effector coding region of *V. harveyi* with other *Vibrio* species. The *Vibrio* genomes that contain the genomic loci spanning the T3SS1 effectors were inspected and compared by MultiGeneBLAST. The colors of the size-scaled gene arrows represented BLAST identities across both intra- and inter-specific comparisons. The white gene arrows denote flanking genes without BLAST hits to the query. Syntenic gene tracks showed the co-occurrence of afp17 and its adjacently upstream gene were widely found in several different *Vibrio* species.

Supplemental Table 1 | Strains used in this study.

Supplemental Table 2 | The primer sequences used in this study.

Supplemental Table 3 | GeneBank accession number of nucleotide sequences.

Supplemental Table 4 | Sequences used to analyze Afp17 and the results of prediction.

REFERENCES

Akeda, Y., and Galan, J. E. (2005). Chaperone release and unfolding of substrates in type III secretion. *Nature* 437, 911–915. doi: 10.1038/nature03992

Austin, B., and Zhang, X. H. (2006). *Vibrio harveyi*: a significant pathogen of marine vertebrates and in vertebrates. *Lett. Appl. Microbiol.* 43, 119–124. doi: 10.1111/j.1472-765X.2006.01989.x

Broberg, C. A., Calder, T. J., and Orth, K. (2011). *Vibrio parahaemolyticus* cell biology and pathogenicity determinants. *Microbes. Infect.* 13, 992–1001. doi: 10.1016/j.micinf.2011.06.013

Brugirard-Ricaud, K., Givaudan, A., Parkhill, J., Boemare, N., Kunst, F., et al. (2004). Variation in the effectors of the type III secretion system among photorhabdus species as revealed by genomic analysis. *J. Bacteriol.* 186, 4376–4381. doi: 10.1128/JB.186.13.4376-4381.2004

Burdette, D. L., Seemann, J., and Orth, K. (2009). *Vibrio* VopQ induces PI3-kinase-independent autophagy and antagonizes phagocytosis. *Mol. Microbiol.* 73, 639–649. doi: 10.1111/j.1365-2958.2009.06798.x

Burr, S. E., Stuber, E., and Frey, J. (2003). The ADP-ribosylating toxin, AexT, from *Aeromonas salmonicida* subsp. salmonicida is translocated via a type III secretion pathway. *J. Bacteriol.* 185, 6583–6591. doi: 10.1128/JB.185.22.6583-6591.2003

Chen, M. X., Li, H. Y., Li, G., and Zheng, T. L. (2011). Distribution of *vibrio alginolyticus*-like species in shenzhen coastal waters, China. *Braz. J. Microbiol.* 42, 884–896. doi: 10.1590/S1517-83822011000300007

Cheng, R. A., and Wiedmann, M. (2019). The ADP-ribosylating toxins of *salmonella*. *Toxins*. 11:416. doi: 10.3390/toxins11070416

Coburn, B., Sekirov, I., and Finlay, B. B. (2007). Type III secretion systems and disease. *Clin. Microbiol. Rev*. 20:535. doi: 10.1128/CMR.00013-07

Costa, S. C., Schmitz, A. M., Jahufar, F. F., Boyd, J. D., Cho, M. Y., et al. (2012). A new means to identify type 3 secreted effectors: functionally interchangeable class IB chaperones recognize a conserved sequence. *mBio* 3:e00243-11. doi: 10.1128/mBio.00243-11

Deng, Q., and Barbieri, J. T. (2008). Molecular mechanisms of the cytotoxicity of ADP-ribosylating toxins. *Annu. Rev. Microbiol.* 62, 271–288. doi: 10.1146/annurev.micro.62.081307.162848

Diepold, A., and Armitage, J. P. (2015). Type III secretion systems: the bacterial flagellum and the injectisome. *Philos. Trans. R. Soc. Lond. B Biol. Sci.* 370:20150020. doi: 10.1098/rstb.2015.0020

Dziejman, M., Serruto, D., Tam, V. C., Sturtevant, D., Diraphat, P., Faruque, S. M., et al. (2005). Genomic characterization of non-O1, non-O139 *Vibrio cholerae* reveals genes for a type III secretion system. *Proc. Natl. Acad. Sci. U.S.A*. 102, 3465–3470. doi: 10.1073/pnas.0409918102

Eichinger, V., Nussbaumer, T., Platzer, A., Jehl, M. A., Arnold, R., and Rattei, T. (2015). EffectiveDB-updates and novel features for a better annotation of bacterial secreted proteins and Type III, IV, VI secretion systems. *Nucleic Acids Res*. 4:gkv1269. doi: 10.1093/nar/gkv1269

Erwin, D. P., Nydam, S. D., and Call, D. R. (2012). *Vibrio parahaemolyticus* ExsE is requisite for initial adhesion and subsequent type III secretion system 1-dependent autophagy in HeLa cells. *Microbiology* 158, 2303–2314. doi: 10.1099/mic.0.059931-0

Finn, R. D., Coggill, P., Eberhardt, R. Y., Eddy, S. R., Mistry, J., et al. (2016). The pfam protein families database: towards a more sustainable future. *Nucleic Acids Res*. 4:gkv1344. doi: 10.1093/nar/gkv1344

Gabriel, M. W., Matsui, G. Y., Friedman, R., and Lovell, C. R. (2014). Optimization of multilocus sequence analysis for identification of species in the genus *vibrio*. *Appl. Environ. Microbiol*. 80, 5359–5365. doi: 10.1128/AEM.01206-14

Gilbert, J. A., Steele, J. A., Caporaso, J. G., Steinbrück, L., Reeder, J., Temperton, B., et al. (2012). Defining seasonal marine microbial community dynamics. *ISME J*. 6, 298–308. doi: 10.1038/ismej.2011.107

Han, H., Li, F., Yan, W., Guo, Y., Li, N., Liu, X., et al. (2015). Temporal and spatial variation in the abundance of total and pathogenic *vibrio parahaemolyticus* in shellfish in China. *PLoS ONE* 10:e0130302. doi: 10.1371/journal.pone.0130302

Henke, J. M., and Bassler, B. L. (2004). Quorum sensing regulates type III secretion in *Vibrio harveyi* and *vibrio parahaemolyticus*. *J. Bacteriol*. 186, 3794–3805. doi: 10.1128/JB.186.12.3794-3805.2004

Hiyoshi, H., Kodama, T., Iida, T., and Honda, T. (2010). Contribution of *Vibrio parahaemolyticus* virulence factors to cytotoxicity, enterotoxicity, and lethality in mice. *Infect. Immun*. 78, 1772–1780. doi: 10.1128/IAI.01051-09

Hu, B., Morado, D. R., Margolin, W., Rohde, J. R., Arizmendi, O., Picking, W. L., et al. (2014). Visualization of the type III secretion sorting platform of *Shigella flexneri*. *Proc. Natl. Acad. Sci. U.S.A*. 112, 1047–1052. doi: 10.1073/pnas.1411610112

Hueck, C. J. (1998). Type III protein secretion systems in bacterial pathogens of animals and plants. *Microbiol. Mol. Biol. Rev*. 62, 379–433. doi: 10.1128/MMBR.62.2.379-433.1998

Jones, M. K., and Oliver, J. D. (2009). *Vibrio vulnificus*: disease and pathogenesis. *Infect Immun*. 77, 1723–1733. doi: 10.1128/IAI.01046-08

Kaufman, M. R., Jia, J., Zeng, L., Ha, U., Chow, M., and Jin, S. (2000). *Pseudomonas aeruginosa* mediated apoptosis requires the ADP-ribosylating activity of exoS. *Microbiology* 146, 2531–2541. doi: 10.1099/00221287-146-10-2531

Kline, K. A., Fälker, S., Dahlberg, S., Normark, S., and Henriques-Normark, B. (2009). Bacterial adhesins in host-microbe interactions. *Cell Host Microbe*. 5, 580–592. doi: 10.1016/j.chom.2009.05.011

Klose, K. E. (2001). Regulation of virulence in *Vibrio cholerae*. *Int. J. Med. Microbiol*. 291, 81–88. doi: 10.1078/1438-4221-00104

Krachler, A. M., and Orth, K. (2011). Functional characterization of the interaction between bacterial adhesin multivalent adhesion molecule 7 (MAM7) protein and its host cell ligands. *J. Biol. Chem*. 286, 38939–38947. doi: 10.1074/jbc.M111.291377

Krall, R., Schmidt, G., Aktories, K., and Barbieri, J. T. (2000). *Pseudomonas aeruginosa* exoT is a Rho GTPase activating protein. *Infect. Immun*. 68, 6066–6068. doi: 10.1128/IAI.68.10.6066-6068.2000

Lin, H., Yu, M., Wang, X., and Zhang, X. H. (2018). Comparative genomic analysis reveals the evolution and environmental adaptation strategies of vibrios. *BMC Genomics*. 19:135. doi: 10.1186/s12864-018-4531-2

Liu, J. X., Zhao, Z., Deng, Y. Q., Shi, Y., Liu, Y. P., Wu, C., et al. (2017). Complete genome sequence of *vibrio campbellii* LMB 29 isolated from red drum with four native megaplasmids. *Front. Microbiol*. 8:2035. doi: 10.3389/fmicb.2017.02035

Liu, M., and Chen, S. (2015). A novel adhesive factor contributing to the virulence of *Vibrio parahaemolyticus Sci Rep*. 24:14449. doi: 10.1038/srep14449

Luo, G., Huang, L., Su, Y., Qin, Y., Xu, X., Zhao, L., et al. (2016). flrA, flrB and flrC regulate adhesion by controlling the expression of critical virulence genes in *Vibrio alginolyticus*. *Emerg. Microbes. Infect.* 5:e85. doi: 10.1038/emi.2016.82

Mahmud, J., Rashed, S. M., Islam, T., Islam, S., Watanabe, H., Cravioto, A., et al. (2014). Type three secretion system in non-toxigenic *Vibrio cholerae* O1, Mexico. *J. Med. Microbiol*. 63, 1760–1762. doi: 10.1099/jmm.0.078295-0

Makino, K., Oshima, K., Kurokawa, K., Yokoyama, K., Uda, T., Tagomori, K., et al. (2003). Genome sequence of *Vibrio parahaemolyticus*: a pathogenic mechanism distinct from that of *V. cholera*. *Lancet* 361, 743–749. doi: 10.1016/S0140-67360312659-1

McDermott, J. E., Corrigan, A., Peterson, E., Oehmen, C., Niemann, G., et al. (2011). Computational prediction of type III and IV secreted effectors in gram-negative bacteria. *Infect Immun*. 79, 23–32. doi: 10.1128/IAI.00537-10

Medema, M. H., Takano, E., and Breitling, R. (2013). Detecting sequence homology at the gene cluster level with MultiGeneBlast. *Mol. Biol. Evol*. 30,1218–1223. doi: 10.1093/molbev/mst025

Miller, K. A., Tomberlin, K. F., and Dziejman, M. (2019). *Vibrio* variations on a type three theme. *Curr. Opin. Microbiol*. 7, 66–73. doi: 10.1016/j.mib.2018.12.001

Noriea, N. F., Johnson, C. N., Griffitt, K. J., and Grimes, D. J. (2010). Distribution of type III secretion systems in *Vibrio parahaemolyticus* from the northern gulf of mexico. *J. Appl. Microbiol*. 109, 953–962. doi: 10.1111/j.1365-2672.2010.04722.x

Okada, N., Iida, T., Park, K. S., Goto, N., Yasunaga, T., Hiyoshim, H., et al. (2009). Identification and characterization of a novel type III secretion system in trh-positive *Vibrio parahaemolyticus* strain TH3996 reveal genetic lineage and diversity of pathogenic machinery beyond the species level. *Infect. Immun.* 77, 904–913. doi: 10.1128/IAI.01184-08

Okada, N., Matsuda, S., Matsuyama, J., Park, K. S., de los Reyes, C., Kogure, K., et al. (2010). Presence of genes for type III secretion system 2 in *Vibrio mimicus* strains. *BMC Microbiol*. 10:302. doi: 10.1186/1471-2180-10-302

Ono, T., Park, K. S., Ueta, M., Iida, T., and Honda, T. (2006). Identification of proteins secreted via *Vibrio parahaemolyticus* type III secretion system 1. *Infect. Immun*. 74, 1032–1042. doi: 10.1128/IAI.74.2.1032-1042.2006

Park, K. S., Ono, T., Rokuda, M., Jang, M. H., Okada, K., Iida, T., et al. (2004). Functional characterization of two type III secretion systems of *Vibrio parahaemolyticus*. *Infect. Immun.* 72, 6659–6665. doi: 10.1128/IAI.72.11.6659-6665.2004

Salomon, D., Guo, Y., Kinch, L. N., Grishin, N. V., Gardner, K. H., and Orth, K. (2013). Effectors of animal and plant pathogens use a common domain to bind host phosphoinositides. *Nat Commun*. 4:2973. doi: 10.1038/ncomms3973

Samudrala, R., Heffron, F., and McDermott, J. E. (2009). Accurate prediction of secreted substrates and identification of a conserved putative secretion signal for type III secretion systems. *PLoS Pathog*. 5:e1000375. doi: 10.1371/journal.ppat.1000375

Sawabe, T., Ogura, Y., Matsumura, Y., Feng, G., Amin, A. K., Mino, S., et al. (2013). Updating the *Vibrio* clades defined by multilocus sequence phylogeny: proposal of eight new clades, and the description of *Vibrio tritonius sp.* nov. *Front. Microbiol*. 4:414. doi: 10.3389/fmicb.2013.00414

Takemura, A. F., Chien, D. M., and Polz, M. F. (2014). Associations and dynamics of Vibrionaceae in the environment, from the genus to the population level. *Front. Microbiol*. 5:38. doi: 10.3389/fmicb.2014.00038

Tay, D. M., Govindarajan, K. R., Khan, A. M., Ong, T. Y., Samad, H. M., Soh, W. W., et al. (2010). T3SEdb: data warehousing of virulence effectors secreted by the bacterial Type III Secretion System. *BMC Bioinform*. 11:S4. doi: 10.1186/1471-2105-11-S7-S4

Thompson, F. L., Iida, T., and Swings, J. (2004). Biodiversity of vibrios. *Microbiol. Mol. Biol. Rev*. 68, 403–431, doi: 10.1128/MMBR.68.3.403-431.2004

Troisfontaines, P., and Cornelis, G. R. (2005). Type III secretion: more systems than you think. *Physiology*. 20, 326–339. doi: 10.1152/physiol.00011.2005

Wagner, S., Grin, I., Malmsheimer, S., Singh, N., Torres-Vargas, C. E., and Westerhausen, S. (2018). Bacterial type III secretion systems: a complex device for the delivery of bacterial effector proteins into eukaryotic host cells. *FEMS Microbiol. Lett*. 365:fny201. doi: 10.1093/femsle/fny201

Xie, Z. Y., Hu, C., Chen, C., Zhang, L. P., and Ren, C. H. (2005). Investigation of seven *Vibrio* virulence genes among *Vibrio alginolyticus* and *Vibrio parahaemolyticus* strains from the coastal mariculture systems in Guangdong, China. *Lett. Appl. Microbiol*. 41, 202–207. doi: 10.1111/j.1472-765X.2005.01688.x

Yarbrough, M. L., Li, Y., Kinch, L. N., Grishin, N. V., Ball, H. L., and Orth, K. (2009). AMPylation of Rho GTPases by *Vibrio* VopS disrupts effector binding and downstream signaling. *Science* 323, 269–272. doi: 10.1126/science.1166382

Yooseph, S., Nealson, K. H., Rusch, D. B., McCrow, J. P., Dupont, C. L., Kim, M., et al. (2010). Genomic and functional adaptation in surface ocean planktonic prokaryotes. *Nature* 468, 60–66. doi: 10.1038/nature09530

Zhao, Z., Chen, C., Hu, C. Q., Ren, C. H., Zhao, J. J., Zhang, L. P., et al. (2010). The type III secretion system of *Vibrio alginolyticus* induces rapid apoptosis, cell rounding and osmotic lysis of fish cells. *Microbiology* 156, 2864–2872. doi: 10.1099/mic.0.040626-0

Zhao, Z., Liu, J. X., Deng, Y. Q., Huang, W., Ren, C., Call, D. R., et al. (2018). The *Vibrio alginolyticus* T3SS effectors, val1686 and Val1680, induce cell rounding, apoptosis and lysis of fish epithelial cells. *Virulence* 9, 318–330. doi: 10.1080/21505594.2017.1414134

Zhao, Z., Zhang, L., Ren, C., Zhao, J., Chen, C., Jiang, X., et al. (2011). Autophagy is induced by the type III secretion system of *Vibrio alginolyticus* in several mammalian cell lines. *Arch. Microbiol*. 193, 53–61. doi: 10.1007/s00203-010-0646-9

Zhou, X., Konkel, M. E., and Call, D. R. (2009). Type III secretion system 1 of *Vibrio parahaemolyticus* induces oncosis in both epithelial and monocytic cell lines. *Microbiology* 155, 837–851. doi: 10.1099/mic.0.024919-0

Zuo, Y. F., Zhao, L. M., Xu, X. J., Zhang, J. N., Zhang, J. L., Yan, Q. P., et al. (2019). Mechanisms underlying the virulence regulation of new *Vibrio alginolyticus* ncRNA Vvrr1 with a comparative proteomic analysis. *Emerg. Microbes. Infect.* 8, 1604–1618. doi: 10.1080/22221751.2019.1687261

Conflict of Interest: The authors declare that the research was conducted in the absence of any commercial or financial relationships that could be construed as a potential conflict of interest.

frontiers in Cellular and Infection Microbiology

ORIGINAL RESEARCH
published: 24 September 2020
doi: 10.3389/fcimb.2020.00482

Analysis of the *Zonula occludens* Toxin Found in the Genome of the Chilean Non-toxigenic *Vibrio parahaemolyticus* Strain PMC53.7

Diliana Pérez-Reytor[1], Alequis Pavón[1], Carmen Lopez-Joven[2], Sebastián Ramírez-Araya[1], Carlos Peña-Varas[1], Nicolás Plaza[1], Melissa Alegría-Arcos[3], Gino Corsini[1], Víctor Jaña[4], Leonardo Pavez[5,6], Talia del Pozo[7], Roberto Bastías[8], Carlos J. Blondel[1,9†], David Ramírez[1] and Katherine García[1*]*

[1] Facultad de Ciencias de la Salud, Instituto de Ciencias Biomédicas, Universidad Autónoma de Chile, Santiago, Chile, [2] Facultad de Ciencias Veterinarias, Instituto de Medicina Preventiva Veterinaria, Universidad Austral de Chile, Valdivia, Chile, [3] Facultad de Ciencias, Centro Interdisciplinario de Neurociencias de Valparaíso, Universidad de Valparaíso, Valparaíso, Chile, [4] Facultad de Medicina Veterinaria y Agronomía, Universidad de las Américas, Santiago, Chile, [5] Departamento de Ciencias Químicas y Biológicas, Universidad Bernardo O'Higgins, Santiago, Chile, [6] Instituto de Ciencias Naturales, Universidad de Las Américas, Santiago, Chile, [7] Centro Tecnológico de Recursos Vegetales, Escuela de Agronomía, Universidad Mayor, Huechuraba, Chile, [8] Laboratorio de Microbiología, Instituto de Biología, Pontificia Universidad Católica de Valparaíso, Valparaíso, Chile, [9] Facultad de Medicina y Facultad de Ciencias de la Vida, Instituto de Ciencias Biomédicas, Universidad Andrés Bello, Santiago, Chile

Vibrio parahaemolyticus non-toxigenic strains are responsible for about 10% of acute gastroenteritis associated with this species, suggesting they harbor unique virulence factors. *Zonula occludens* toxin (Zot), firstly described in *Vibrio cholerae*, is a secreted toxin that increases intestinal permeability. Recently, we identified Zot-encoding genes in the genomes of highly cytotoxic Chilean *V. parahaemolyticus* strains, including the non-toxigenic clinical strain PMC53.7. To gain insights into a possible role of Zot in *V. parahaemolyticus*, we analyzed whether it could be responsible for cytotoxicity. However, we observed a barely positive correlation between Caco-2 cell membrane damage and Zot mRNA expression during PMC53.7 infection and non-cytotoxicity induction in response to purified PMC53.7-Zot. Unusually, we observed a particular actin disturbance on cells infected with PMC53.7. Based on this observation, we decided to compare the sequence of PMC53.7-Zot with Zot of human pathogenic species such as *V. cholerae*, *Campylobacter concisus*, *Neisseria meningitidis*, and other *V. parahaemolyticus* strains, using computational tools. The PMC53.7-Zot was compared with other toxins and identified as an endotoxin with conserved motifs in the N-terminus and a variable C-terminal region and without FCIGRL peptide. Notably, the C-terminal diversity among Zots meant that not all of them could be identified as toxins. Structurally, PMC53.7-Zot was modeled as a transmembrane protein. Our results suggested that it has partial 3D structure similarity with *V. cholerae*-Zot. Probably, the PMC53.7-Zot would affect the actin cytoskeletal, but, in the absence of FCIGRL, the mechanisms of actions must be elucidated.

Keywords: *Vibrio parahaemolyticus*, non-toxigenic strains, *Zonula occludens* toxin, Zot, *Vibrio cholerae*, *Campylobacter concisus*, intestinal permeability, Protein structure prediction

OPEN ACCESS

Edited by:
Lixing Huang,
Jimei University, China

Reviewed by:
Li Zhang,
University of New South Wales, Australia
Wei Xu,
State Oceanic Administration, China

***Correspondence:**
David Ramírez
david.ramirez@uautonoma.cl
Katherine García
katherine.garcia@uautonoma.cl

†Present address:
Carlos J. Blondel, Facultad de Medicina y Facultad de Ciencias de la Vida, Instituto de Ciencias Biomédicas, Universidad Andrés Bello, Santiago, Chile

Specialty section:
This article was submitted to Molecular Bacterial Pathogenesis, a section of the journal Frontiers in Cellular and Infection Microbiology

Received: *13 June 2020*
Accepted: *04 August 2020*
Published: *24 September 2020*

Citation:
Pérez-Reytor D, Pavón A, Lopez-Joven C, Ramírez-Araya S, Peña-Varas C, Plaza N, Alegría-Arcos M, Corsini G, Jaña V, Pavez L, del Pozo T, Bastías R, Blondel CJ, Ramírez D and García K (2020) Analysis of the Zonula occludens Toxin Found in the Genome of the Chilean Non-toxigenic Vibrio parahaemolyticus Strain PMC53.7. Front. Cell. Infect. Microbiol. 10:482. doi: 10.3389/fcimb.2020.00482

INTRODUCTION

Inshore marine waters around the world are densely populated with *Vibrio parahaemolyticus*, which is the leading cause of seafood-associated bacterial gastroenteritis (Raghunath, 2014; Letchumanan et al., 2017), even though few strains can cause infections in humans and most environmental strains are non-pathogenic (Shinoda, 2011). The most characteristic virulence-associated factors are thermostable direct hemolysin (TDH) and TDH-related hemolysin (TRH), encoded by the *tdh* and *trh* genes, respectively (Nishibuchi et al., 1992; Shinoda, 2011; Zhang and Orth, 2013; Raghunath, 2014), although other virulence factors such as the type III secretion systems of both chromosomes (T3SS1 and T3SS2) and several genomic islands (VPaIs) have been identified (Broberg et al., 2011; Yu et al., 2012; Ceccarelli et al., 2013). Various studies have reported that isolates of non-toxigenic *V. parahaemolyticus*, named like that because of the lack of *tdh*, *trh*, and T3SS2, can be highly cytotoxic to human gastrointestinal cells (Mahoney et al., 2010; Castillo et al., 2018a), suggesting that other virulence factors must exist (Pérez-Reytor and García, 2018; Wagley et al., 2018). In Chile, the disappearance of the pandemic strain from coasts was associated with a severe diminishing of clinical cases; however, *V. parahaemolyticus* is still considered a significant pathogen associated with food-borne diseases (MINSAL, 2017).

In our recent work, we identified prophages encoding putative *zonula occludens* toxins (Zots) in the genome of highly cytotoxic southern Chilean *V. parahaemolyticus* strains, including the clinical non-toxigenic strain PMC53.7, which does not possess any other known virulence factor in its genome (Castillo et al., 2018a). In *Vibrio cholerae*, Zot is the most important toxin in the absence of the classical cholera toxin (CT), and it is encoded by the CTX prophage (Fasano, 2002; Schmidt et al., 2007; Castillo et al., 2018b). The N-terminal domain of the *V. cholerae*-Zot protein is involved in bacteriophage morphogenesis, while the C-terminal domain is cleaved and secreted into the intestinal lumen (Uzzau et al., 2001; Schmidt et al., 2007; Mahendran et al., 2016). Structure-function analyses indicate that the biologically active fragment of Zot (FCIGRL) can be mapped to amino acids 288–293. The FCIGRL fragment is structurally similar to another motif (SLIGRL) that activates an intracellular signaling pathway by binding to proteinase-activated receptor-2 (PAR-2). This receptor has been implicated in the regulation of paracellular permeability, inducing a transient reduction in the transepithelial resistance and an increase in transepithelial flux along concentration gradients by affecting the tight junction (TJ) (Fasano et al., 1995; Gopalakrishnan et al., 2009; Goldblum et al., 2011; Vanuytsel et al., 2013). Notably, it has been shown that IEC6 cell monolayers treated with *V. cholerae*-Zot in its supernatant displayed a redistribution of actin cytoskeleton, decreasing G-actin while increasing F-actin and the disturbance of paracellular permeability (Fasano et al., 1995). Also, it was reported that toxigenic *Campylobacter concisus* strains producing Zot have the potential to initiate inflammatory bowel disease or could be aggravators of Crohn's disease (Kaakoush et al., 2014; Zhang et al., 2014). This Zot protein causes sustained intestinal barrier damage, induces the release of proinflammatory cytokines, and increases the response of macrophages to other microorganisms (Mahendran et al., 2016). Although there are no reports assigning a role of Zot in the *V. parahaemolyticus* virulence, 77.9% of the clinical isolates of *V. parahaemolyticus* possess *Zot*-encoding prophages, including the f237 of the pandemic RIMD2210633 reference strain (VpKX) (Castillo et al., 2018b). These prophages belong to the Inoviridae family and play an important role in the evolution and pathogenesis of multiple bacterial species (Castillo et al., 2018b).

In this work, we proposed that PMC53.7-Zot is an endotoxin with conserved motifs in the N-terminal end, probably anchored to the membrane and with a structure similar to Zot of other human pathogenic strains. It would be associated with the actin cytoskeletal disturbances observed in PMC53.7-infected Caco-2 cells and with the purified PMC53.7-Zot. However, the mechanisms of action of this toxin and its effects on the intestinal barrier will be the subject of future research.

MATERIALS AND METHODS

Bacterial Strains and Cell Culture

V. parahaemolyticus clinical strain PMC53.7 (Harth et al., 2009) and VpKX (Fuenzalida et al., 2006) strains were cultured overnight at 37°C with shaking in Luria-Bertani (LB) broth containing 3% NaCl. The PMC53.7 strain was used to infect Caco-2 cells, as a mammalian intestinal epithelium cell model. The Caco-2 cells are human colonic adenocarcinoma cells that physiologically mimic the mature small intestine villous epithelium (Hidalgo et al., 1989). The cells were grown in Eagle's minimal essential medium (MEM; Sigma-Aldrich, St. Louis, MO, USA) supplemented with 10% fetal bovine serum (FBS; Gibco®, Grand Island, NY, USA) plus 1% antibiotic (Pen-strep; Gibco®, Grand Island, NY, USA). They were maintained in 75 cm^2 flasks at 37°C under a 5% CO_2 atmosphere in a humidified incubator until semiconfluence.

Fluorescent Staining of Cells Infected With Bacteria

The Caco-2 cells were grown on glass slides until ∼70% of confluence for staining analysis. Cells were incubated with *V. parahaemolyticus* PMC53.7 and VpKX bacterial culture at a multiplicity of infection (MOI) = 10 or H_2O_2 1 mM. After 3 h (post infection), the slides were washed three times with phosphate-buffered saline (PBS), fixed in paraformaldehyde (PFA) 4% with PBS for 20 min at room temperature, permeabilized with Triton X-100 0.1%, and blocked with 1.0% (w/v) BSA. The F-actin was counterstained using rhodamine phalloidin (Cytoskeleton Inc., Denver, CO, USA) at a dilution of 1:200 in PBS, and nuclei were counterstained with Hoechst stain (H6024; Sigma-Aldrich, St. Louis, MO, USA) solution at 1:5,000 dilution in PBS. The slides were carefully mounted on coverslips and analyzed with an epifluorescence microscope (Leica LX6000, Germany).

Cytotoxicity Assay

The cellular membrane damage was measured by the release of lactate dehydrogenase (LDH) into the supernatants, using the

CytoTox 96 Non-Radioactive Cytotoxicity Assay kit (Promega, Madison, WI, USA) according to the manufacturer's guidelines. The percentage of cytotoxicity was calculated with the equation described by Tanabe et al. (2015). All the experiments were done in triplicate and repeated three times.

Infection Assay and Zot mRNA Expression

The Caco-2 cells were seeded in a six-well plate (5×10^6 cells per well) and incubated in MEM (Sigma-Aldrich, St. Louis, MO, USA) supplemented with 10% FBS until ∼80–90% of confluence. The growth media was removed from monolayers, and cells were washed three times with PBS. A culture in exponential phase ($OD_{600} = 0.6$) of *V. parahaemolyticus* PMC53.7 strain was centrifuged, and subsequently, a bacterial suspension was prepared in MEM (Sigma-Aldrich, St. Louis, MO, USA), without phenol red and antibiotics, at an MOI = 10, previously standardized. At the onset of infection, cells were centrifuged at 250 g for 4 min to synchronize cell–cell and incubated for 4 h at 37°C and 5% CO_2. The supernatants and the cells were collected post infection, at 1, 2, 3, and 4 h. The cellular membrane damage was measured by the release of LDH, as described above. All the experiments were done in triplicate and repeated three times. Total RNA from supernatants and cells were isolated with the E.Z.N.A. total RNA kit (Omega Bio-tek, GA, USA) according to the manufacturer's instructions and quantified using an Infinite M200 PRO spectrophotometer (Tecan Austria GmbH). The complementary DNA (cDNA) was synthesized through random hexamer-primed reactions using ImProm-II Reverse Transcriptase (Promega, Madison, WI, USA), according to the manufacturer's instructions, except that we treated the RNA with DNase for twice the time recommended by the kit. Then, the PMC53.7-*Zot* product was analyzed in a Roche LC480 Real-Time PCR system (Roche Diagnostics, Nederland, BV) using Brilliant SYBR Green II single-step quantitative RT-PCR (qRT-PCR) Master Mix (Stratagene–Agilent Technologies, La Jolla, CA, USA) and specific primers for each gene. Briefly, each reaction contained 10 μl, and the optimized cycling profile was performed at 95°C for 30 s, followed by 40 cycles at 95°C for 5 s, at 55°C for 34 s, and at 72°C for 45 s and the melting curve analysis at 95°C for 15 s and then at 60°C for 1 min. Each PCR was conducted in three technical triplicates. The *rpoS* gene (Ma et al., 2015) was used as reference, and positive and negative controls were included in all reaction mixtures.

Cloning, Expression, and Purification of *V. parahaemolyticus* PMC53.7-*Zot* Gene in the *Escherichia coli* BL21 System

The full-length *V. parahaemolyticus* PMC53.7-*Zot* gene was amplified from the genomic DNA by PCR. The strains and plasmids used in this study are listed in **Table 1**. The amplified *Zot* gene was cloned into plasmid vector pBAD33.1 with 6-histidines tagged at the C-terminus and expressed following the manufacturer's instructions. The *E. coli* strain used for recombinant protein expression was BL21(DE3). The sequences of the primers used for *Zot* gene cloning are listed in **Table 2**. Vector control (pBAD33.1 without insert) was also subjected to identical treatment to that of *Zot* insert.

The expression of Zot from BL21(DE3) pBAD33.1_ZotPMC53.7 was induced by the addition of 0.2% of L-arabinose at $OD_{600} = 0.2$ growth and harvested 3 h later to reach an $OD_{600} = 0.5$–0.6. The cells were harvested by centrifugation at 4,000 *g* for 20 min; resuspended in lysis buffer containing 50 mM Tris-HCl (pH = 7.4), 150 mM NaCl, Triton X-100 1%, 1 mM PSMF, 2% glycerol, lysozyme 1 mg/ml, and DNase I 10 μg/ml; and incubated on ice for 45 min before sonication. The mixture was sonicated with

TABLE 1 | Bacterial strains and plasmid used in this study.

Bacterial strains	Relevant characteristics	Reference or source
V. parahaemolyticus PMC 53.7	Clinical strain isolated from Puerto Montt, Chile	Laboratory collection
E. coli DH5α	F$^-$ *endA1 glnV44 thi-1 recA1 relA1 gyrA96 deoR nupG purB20* ϕ80d*lacZ*ΔM15 Δ(*lacZYA-argF*)U169, hsdR17($r_K^- m_K^+$), λ$^-$	Laboratory collection
E. coli BL21(DE3)	*E. coli* str. B F$^-$ *ompT gal dcm lon hsdS$_B$*($r_B^- m_B^-$) λ(DE3 [*lacI lacUV5-T7p07 ind1 sam7 nin5*]) [*malB*$^+$]$_{K-12}$(λ^S)	Laboratory collection
Plasmids	**Relevant characteristics**	**Reference or source**
pBAD33.1	pBAD33 including ribosomal binding site, chloramphenicol resistant	pBAD33.1 was a gift from Christian Raetz (Addgene plasmid #36267)

The amplified Zot gene was cloned into plasmid vector pBAD33.1 with 6-histidines tagged at the C-terminus and expressed following the manufacturer's instructions.

TABLE 2 | Sequences of primers used for *Zot* gene cloning.

Primers	Sequence (5′ – 3′)*	Reference
F1_pBAD33.1_ZotPMC53.7	*CTT*CATATG**GCTGTTATCTTTCGTCAC**	This study
R1_pBAD33.1_ZotPMC53.7	*AAC*AAGCTTtta*GTGGTGATGATGGTGATG***GCCCTCATTTAAGTTGAAAATATC**	

**Extra base pairs on the 5′ end of each sequence denote primer leader (italicized); sequences with restriction sites of NdeI (forward) and HindIII (reverse) are underlined; Zot sequence residues are in boldface; tta represents the stop codon.*

24–25% amplitude for 5–7 min of total on time and 10–12 min of off time. The lysate was clarified by centrifugation, and the soluble fraction was used for purification of recombinant Zot protein. *V. parahaemolyticus* PMC53.7-Zot was purified by affinity-based purification using the nickel-IMAC resin HisPur Ni-NTA (Thermo Fisher Scientific, MA, USA) according to the manufacturer's instructions. As proteins eluted from the Ni-NTA columns contained both the PMC53.7-Zot and *E. coli* proteins, *E. coli* BL21(DE3) cells were transformed with pBAD33.1 vector without insert. The induction and purification of these proteins were performed using protocols identical to those for the purification of Zot. These *E. coli* proteins (EPs) were included as controls in all the experiments. The proteins eluted from Ni-NTA columns were filtered through 0.22 μm filters and concentrated through a buffer exchanged to DPBS using an Amicon Ultra 10K column (Merck Millipore Ltd, Carrigtwohill, Ireland). The total protein concentrations were determined using a Coomassie Plus (Bradford) assay kit (Thermo Fisher Scientific, MA, USA). The presence of *V. parahaemolyticus* PMC53.7-Zot was confirmed by SDS/PAGE followed by Coomassie staining and western blot analysis using anti-6xHis monoclonal mouse antibodies (Thermo Fisher Scientific, MA, USA).

Actin Cytoskeletal Staining of Cells Incubated With Recombinant Zot Protein

The post-confluent Caco-2 cells were treated overnight with 25, 50, and 100 μg of PMC53.7-Zot or EP as control for actin cytoskeletal staining. Cells were washed three times with PBS without Ca^{+2} and Mg^{+2}, fixed with PFA 4%, washed three times with PBS, and permeabilized with Triton X-100 0.1%. F-actin was stained using Alexa-Fluor 488 phalloidin (Thermo Fisher Scientific, MA, USA) at a dilution of 1:200 with PBS. Cells were subsequently rinsed, mounted, and viewed using an epifluorescence microscope (Leica LX6000, Germany). The mean pixel intensity value for actin was quantified using the NIH ImageJ software.

Bacterial Toxin Prediction

The amino acid sequences of the Zot proteins from *V. parahaemolyticus* clinical strains PMC53.7 and VpKX (Q9KGQ7), *V. parahaemolyticus* environmental strains PMA2.15 and PMA3.15, *V. cholerae* N16961 (P38442), *C. concisus* 13826 (A7ZF54), and *Neisseria meningitidis* MC58 (Q9JY47) were obtained from UniProtKB. The toxin prediction from the primary amino acid sequence of Zot found in the *V. parahaemolyticus* clinical non-toxigenic strain PMC53.7, *V. cholerae* N16961, and other strains was performed using the BTXpred server (Saha and Raghava, 2007). This server uses SVM, HMM, and PSI-Blast to predict and classify exotoxins and endotoxins with an accuracy above 95%, besides identifying the function of enterotoxins with 100% overall accuracy.

Multiple Sequence Alignment for Zot Proteins

The multiple sequence alignment (MSA) of the Zot amino acid sequences from *V. parahaemolyticus* PMC53.7, VpKX, PMA2.15 and PMA3.15, *V. cholerae* N16961 (VcN16961), *C. concisus* 13826 (Cc13826), and *N. meningitidis* MC58 (NmMC58) was performed with T-Coffee server and the PSI/TM-Coffee option (Notredame et al., 2000). The motifs and domains analyses were performed with the Conserved Domains Search tool (CD-Search) from NCBI (Marchler-Bauer et al., 2017). The figures were generated with Jalview (Waterhouse et al., 2009) and the WebLogo server (Crooks et al., 2004).

Structure Prediction of *V. parahaemolyticus* PMC53.7-Zot Protein

The Protter (Omasits et al., 2014) and Phobius (Käll et al., 2004) servers were used for prediction of transmembrane topology of PMC53.7-Zot, as well as N-terminal and C-terminal domains. The potential phosphorylation sites were predicted with the NetPhos 3.1 server (Blom et al., 1999). Due to the lack of templates available in databases such as the Protein Data Bank (PDB), to perform conventional homology modeling, we modeled the 3D structure of PMC53.7-Zot with the I-TASSER server (Yang and Zhang, 2015). Residues 272–290 were preselected as the residues of the transmembrane segment, with α-helix as the predetermined secondary structure, according to the predictions made with the other servers to guide the modeling. The other I-TASSER parameters were set by default. Two threading templates were found and used by the server (PDB codes 2R2A and 3JC8) to finally generate five models. The top 1 model according to I-TASSER selection parameters (Zhang, 2008; Roy et al., 2010; Yang and Zhang, 2015) was validated with PROCHECK (Laskowski et al., 1993) and the ProSA-web server (Wiederstein and Sippl, 2007) and was selected for further modeling and analysis.

Model 1 was manually modified using the Maestro suite (Schrödinger Release 2019-3) to generate clear N-terminal (intracellular) and C-terminal (extracellular) domains as well as the transmembrane segment. Later, the protein was optimized and minimized using the Protein Preparation Wizard included in the Maestro Suite and subjected to two molecular dynamics simulations (MDs) using the Desmond MD package (Jorgensen et al., 1996) and the OPLS3 force field (Harder et al., 2016). The PMC53.7-Zot model was embedded into a 1-palmitoyl-2-oleoyl-phosphatidylcholine (POPC) preequilibrated membrane model (111 phospholipids per layer) and solvated with single-point charge (SPC) waters (57,315 molecules). The Cl^- ions were used as counterions in order to neutralize the systems, and 150 mM of NaCl was added to the system. For the first 25 ns, the default relax protocol of Desmond was applied. Then a restraint spring constant of 1 kcal * mol^{-1} * $^{-2}$ was applied to the backbone atoms of the protein. The last frame was taken, and a second non-restricted 250 ns MDs was performed. The temperature was maintained at 300 K, while pressure was kept at 1 atm, employing the Nosé–Hoover thermostat method with a relaxation time of 1 ps using the MTK algorithm (Martyna et al., 1994), with a 2 fs integration time step. Data were collected every 5 ps during the MDs for further analysis.

Statistical Analysis

The values of LDH obtained in the cytotoxicity assay were analyzed with one-way ANOVA and a *post-hoc* Bonferroni test

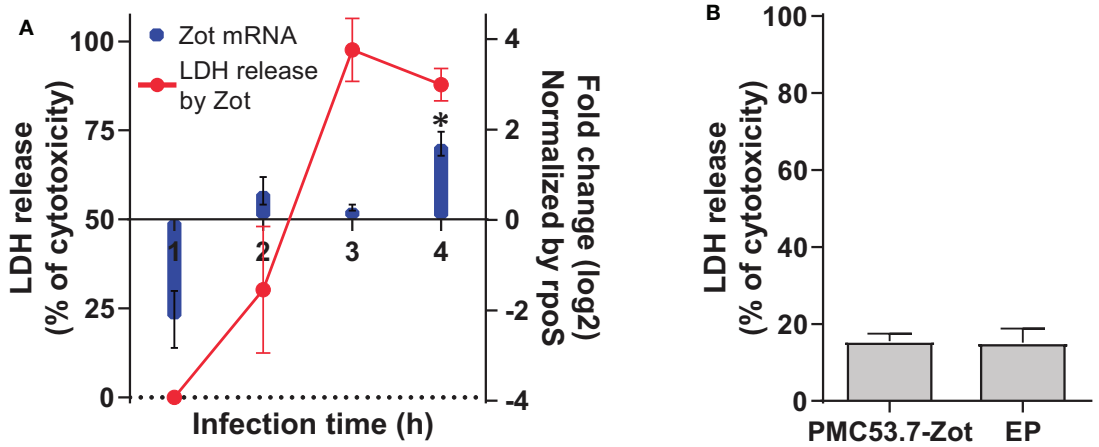

FIGURE 1 | Transcriptional level of *Zot* mRNA during course of infection and cytotoxicity. **(A)** Zot expression levels of PMC53.7 strain and cytotoxicity (%) during the course of infection of Caco-2 cells. * Up-regulated vs rpoS (reference gene) **(B)** Cytotoxicity (%) of Caco-2 cells induced by treatment with 100 μg of purified PMC53.7-Zot and *E. coli* proteins (EP) control. All the experiments were done in triplicate and repeated three times.

with 95% significance, using GraphPad Prism 6.0 software. The Zot data expression was analyzed using REST 2009 software (Pfaffl et al., 2002). The differences were considered statistically significant when $^{*}p < 0.05$, $^{**}p < 0.01$, and $^{***}p < 0.001$. The correlation analysis between the variables "Zot mRNA expression" and "cytotoxicity" was determined using Pearson correlation analysis, and it was interpreted that a value ≥0.7 indicates a significant and positive relationship between both variables (Nettleton, 2014).

RESULTS

Contribution of Zot-PMC53.7 to Cytotoxicity in Caco-2 Cells

In our previous work, we identified Zot-encoding genes in the genomes of highly cytotoxic Chilean *V. parahaemolyticus* strains (Castillo et al., 2018a). Then, we hypothesized that PMC53.7-Zot could contribute to cytotoxicity. To assess whether Zot expression occurred during *V. parahaemolyticus* PMC53.7 infection of Caco-2 cells, a kinetic infection was performed for 4 h. The analysis of gene *Zot* by qPCR showed detectable levels of expression after 2 h post infection and a gene overexpression at 4 h post infection, relative to the reference gene *rpoS* (**Figure 1A**). In parallel, we evaluated if Zot mRNA levels could be correlated with the cytotoxicity induced by *V. parahaemolyticus* PMC53.7. The LDH release was measured at each time point during PMC53.7 infection kinetics of Caco-2 cells (**Figure 1A**). Pearson analysis showed that there was a barely positive correlation between Zot mRNA expression and LDH release, with a global correlation coefficient of 0.7 (Nettleton, 2014). Pearson correlation coefficients for each independent experiment were 0.87, 0.61, and 0.76. PMC53.7-Zot, previously expressed in a heterologous system of *E. coli* BL21, was purified and was visualized by western blot as a band of ∼57 kDa, according to the fully transcribed *Zot* gene (56 kDa), while a second band of ∼27 kDa was observed (**Supplementary Figure 1**). Unexpectedly, Caco-2 cells treated with purified PMC53.7-Zot (100 μg) did not exhibit cytotoxicity (**Figure 1B**); instead, we observed that they were impaired to be attached to the plate surface at 4 h post treatment, which was not detected in the control treatment with *E. coli* proteins (EP) (**Supplementary Figure 2**).

Cellular Damage Provoked by Infection With PMC53.7

It is well-known that the main contributor of cytotoxicity in *V. parahaemolyticus* is the T3SS-1, which is completely present in PMC53.7 as also in VpKX strains. If Zot was not contributing to cytotoxicity over T3SS1, we hypothesized that detrimental effects exclusively displayed by PMC53.7 infection could be associated with its unique putative virulence factor Zot, in the absence of TDH, TRH, and T3SS-2. In parallel to cytotoxicity assays, we decided to compare effects of both strains over the cell culture. We infected Caco-2 cells with *V. parahaemolyticus* PMC53.7 and VpKX at an MOI = 10 and performed fluorescence microscopy at 3 h post infection. We observed that uninfected monolayers of Caco-2 cells had an organized actin cytoskeleton in a network of filaments normally distributed beneath the plasma membrane and throughout the cytoplasm (**Figure 2A**). On the other hand, infected cells showed cytoskeletal rearrangement and detachment of adjacent cells from each other with PMC53.7 and VpKX (**Figure 2A**). Interestingly, we observed the absence of actin in several cells infected with PMC53.7 (yellow arrows, **Figure 2A**), which was not observed in the VpKX infection. As an additional control of cellular damage, we treated Caco-2 cells with 1 mM H_2O_2, but its effects over cellular nuclei were not observed in the infected cells (**Figure 2A**). In addition, we visualized the actin cytoskeleton of Caco-2 incubated with PMC53.7-Zot, through immunofluorescence with fluorescent phalloidin. These cells showed a higher percentage of F-actin redistribution, compared

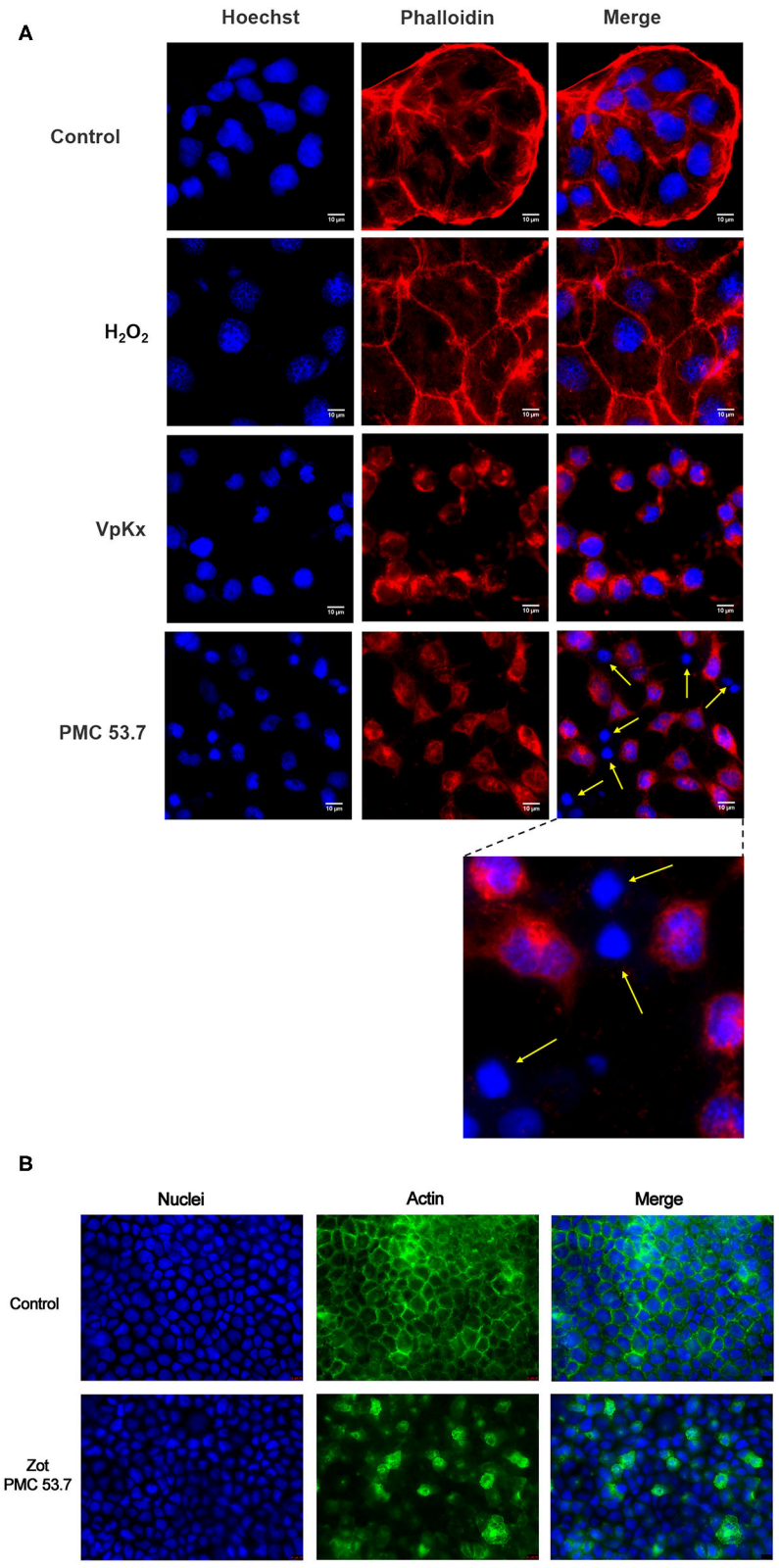

FIGURE 2 | Effect of PMC53.7 infection over the morphology of Caco-2 cells. **(A)** PMC53.7 infection (MOI 10) produces disruption of the actin cytoskeleton in infected cells at 3 h post infection. The yellow arrows indicate the absence of actin in several cells infected with PMC53.7. **(B)** Caco-2 exposed to 100 μg of purified PMC53.7-Zot showed an increased percentage (at 24 h incubation) of cells displaying redistribution of F-actin compared to the control-exposed cells.

TABLE 3 | Bacterial toxin prediction using BTXpred.

Species	Strain	Toxin classification	Exotoxin function
V. parahaemolyticus	PMC53.7	Endotoxin	–
V. parahaemolyticus	VpKX	Exotoxin	Guanylate cyclase activating enterotoxin
V. parahaemolyticus	PMA2.15	Exotoxin	Guanylate cyclase activating enterotoxin
V. parahaemolyticus	PMA3.15	Not match	–
V. cholerae	N16961	Endotoxin	–
C. concisus	13826	Exotoxin	Not found
N. meningitidis	MC58	Not match	–

We used the Zot amino acid sequences of V. parahaemolyticus VpKX, PMC53.7, PMA2.15, and PMA3.15; V. cholerae VcN16961; C. concisus Cc13826; and N. meningitidis MC58, comparing each sequence against known toxin databases using the BTXpred program (Saha and Raghava, 2007).

to control cells, with a peak at 24 h of incubation. Both Caco-2 control and EP incubated cells had stabilized F-actin with normal, continuous, and smooth distribution of actin at the membrane boundaries (**Figure 2B**). Instead, the treatment with 100 μg of PMC53.7-Zot produced rearrangement of actin in the cells (**Figure 2B**). These results suggest that Zot could play a key role in *V. parahaemolyticus* PMC53.7 infection, inducing the loss of actin cytoskeleton integrity in Caco-2 cells (**Figure 2B**).

Bioinformatics Analysis

Since we observed that PMC53.7 infection produces disruption of the actin cytoskeleton in infected cells, which is an effect associated to the Zot action of *V. cholerae* over IEC6 cellular culture (Fasano et al., 1995), we decided to perform a bioinformatics analysis, comparing the sequence of *V. parahaemolyticus* PMC53.7-Zot with Zot sequences of other important human pathogens: *V. cholerae* N16961 (VcN16961) and *C. concisus* 13826 (Cc13826), which have been reported as biologically active toxins (Fasano et al., 1995; Mahendran et al., 2016); and we also included *N. meningitidis* MC58 (NmMC58) and other strains of *V. parahaemolyticus* (PMA2.15, PMA3.15, and the reference strain VpKX).

Prediction of *V. parahaemolyticus* PMC53.7-Zot as Toxin

To investigate if the Zot amino acid sequence found in PMC53.7 was a toxin, we performed a comparison of this sequence against known toxin databases using BTXpred (Saha and Raghava, 2007). As control, we used the Zot sequences of VcN16961 and Cc13826. The results showed that PMC53.7-Zot and VcN16961-Zot were recognized as endotoxin, while Cc13826-Zot matched with an exotoxin (**Table 3**). Additionally, we performed the same analysis with Zot sequences of other *V. parahaemolyticus* strains. We observed that VpKX-Zot and PMA2.15-Zot were classified as exotoxin with a guanylate cyclase-activating enterotoxin function, while PMA3.15-Zot and NmMC58-Zot did not match with any toxin (**Table 3**).

MSA in Different Zot Proteins and Their Walker A and Walker B Motifs

To detect conserved domains and motifs present in the Zot protein sequences of *V. parahaemolyticus*, an MSA was performed comparing Zot of different species of human pathogens, including strains previously mentioned (**Supplementary Figure 3**). A detailed analysis of the protein sequences showed that these proteins belong to the P-loop containing nucleoside triphosphate hydrolases. Members of the P-loop NTPase domain superfamily are characterized by a conserved nucleotide phosphate-binding motif, also referred as the Walker A motif (GxxxxGK[S/T], where x is any residue), and the Walker B motif (hhhh[D/E], where *h* is a hydrophobic residue) (Hanson and Whiteheart, 2005). Respect to PMC53.7, the protein sequence identity of NmMC58, VcN16961, Cc13826, and VpKX/PMA2.15 is 30.9, 23.8, 38.5, and 40.7%, respectively. We noticed that Zot sequences of *V. parahaemolyticus* strains, including both clinical PMC53.7 and VpKX and environmental strains PMA 2.15 and PMA 3.15, besides VcN16961, have a tyrosine (Y) instead of a glycine (G) in the Walker A motif: GxxxxYK[S/T] (**Figure 3A**). Both Walker motifs were located at the N-terminal side prior to the transmembrane domains, approximately 1–270, as defined for *V. cholerae*-Zot (Uzzau et al., 1999). As these Walker motifs belong to the proteins of the P-loop NTPase superfamily, we aligned the sequence of *V. parahaemolyticus* PMC53.7 against the protein sequence of PHA00350 (**Supplementary Figure 4**), member of the P-loop NTPase superfamily (conserved protein domain family accession number: cl21455).

No sequences of the Zot proteins in *V. parahaemolyticus* isolates had the FCIGRL active fragment previously identified in *V. cholerae* and located in the C-terminal domain (Goldblum et al., 2011), neither the Zot sequences of *C. concisus* nor *N. meningitidis* (**Figure 3B**). Additionally, we noticed that PMC53.7, *C. concisus*, *N. meningitidis*, and VpKX do not have a glycine aligned with the *V. cholerae* position 298, which has been proposed as a key amino acid involved in the opening of the intercellular tight junctions (TJ) (**Figure 3B**). Instead, PMC53.7 and *N. meningitidis* have a threonine residue, while VpKX, PMA2.15, and PMA3.15 have a serine in this position. This G-298 position is the last amino acid of an octapeptide motif (GxxxVQxG) proposed as the putative receptor-binding site shared by Zot and human zonulin (Di Pierro et al., 2001). The octapeptide motif was not found in any other pathogenic bacterial strains besides *V. cholerae* (**Figure 3B**).

Structure Prediction of *V. parahaemolyticus* Zot Proteins

Besides the prediction of *V. parahaemolyticus* PMC53.7-Zot as an endotoxin, similar to *V. cholerae*-Zot, we focused on predicting its structure, because the *Zot*-coding gene was the unique putative virulence factor found in the genome of this clinical strain (Castillo et al., 2018a). In addition, it has been suggested that the structure and not the sequence is responsible for the biological effects of Zot on the epithelial barrier (Kaakoush et al., 2010), and also cytoskeletal disturbances occurred in response to

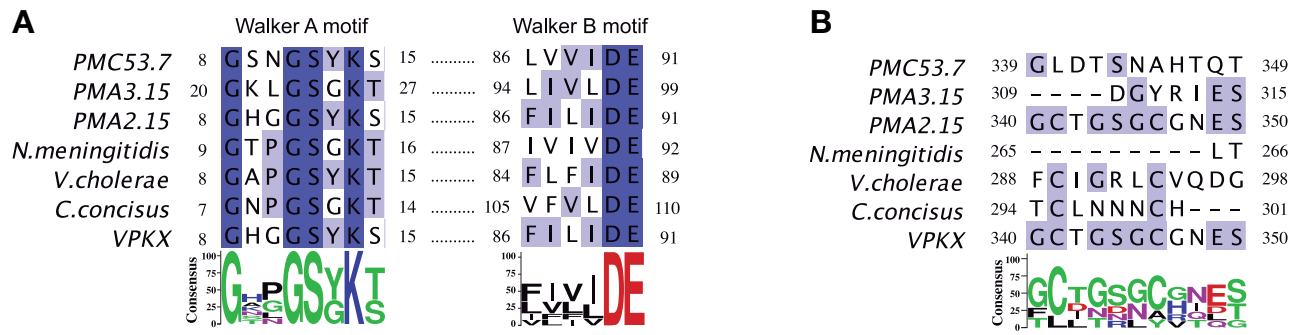

FIGURE 3 | Multiple sequence alignment of Zot protein. **(A)** Conserved Walker A (GxxxxGK[S/T]) and B (hhhh[D/E]) motifs. **(B)** Zot-active domain and putative Zot-receptor-binding site proposed to V. cholerae N16961.

V. cholerae-Zot (Fasano et al., 1995). So, despite some differences reported among *V. parahaemolyticus*-Zot and *V. cholerae*-Zot sequences, we decided to perform 3D structure prediction of PMC53.7-Zot. First, we predicted a transmembrane domain of PMC53.7-Zot (**Supplementary Figures 5A–D**), as *V. cholerae*-Zot has been reported as a transmembrane protein. Three well-defined domains were identified for PMC53.7-Zot as follows: an N-terminus from residues 1 to 272; one transmembrane segment from 273 to 294; and a C-terminus from 295 to 466. We also predicted the phosphorylation sites in the PMC53.7-Zot (above the threshold value in **Supplementary Figure 5B** using NetPhos 3.1 server; Blom et al., 1999). Specifically, the PMC53.7-Zot was predicted to possess 23 serine-, 21 threonine-, and 6 tyrosine-phosphorylation sites, all of them equally distributed at the N-terminal and C-terminal domains. Finally, properties such as solvent accessible surface area (SASA), hydropathy, and the inherent thermal mobility of the residues/atoms in PMC53.7 protein were also predicted (**Supplementary Figures 5E–G**).

The I-TASSER server was found, by threading two suitable templates, to generate multiple PMC53.7-Zot models (PDB codes: 2R2A and 3JC8). The software used the templates 2R2A and 3JC8 to model the PMC53.7-Zot N-terminal and C-terminal domains, respectively. PMC53.7-Zot shared 25.71% of sequence identity with 35% of coverage to 2R2A (chain A) and 60% of sequence identity with 10% of coverage to 3JC8 (chain Q). The coverage is the number of aligned residues of each template divided by the length of PMC53.7-Zot; in both cases, the coverage is very low. The I-TASSER server generated an MSA with both template sequences (**Supplementary Figure 6**) and then a large ensemble of structural conformations. The top five models (according to I-TASSER scoring function) generated were further analyzed (**Supplementary Figure 7**). It is clear that the only valid template to generate a valid model is 2R2A; therefore, in this work, we assume that the structure of the N-terminal domain of PMC53.7-Zot modeled using 2R2A as a template is reliable. This can be corroborated according to the I-TASSER estimated accuracy (the lower, the better) of models 1 to 5, where residues of the C-terminal domain present higher estimated accuracy than the transmembrane segment as well as the N-terminal domain (**Supplementary Figure 7**).

Then, model 1 was selected and manually modified to generate clear N-terminal (cytoplasmic) and C-terminal (extracellular) domains (**Figure 4**), as well as the transmembrane segment, previously predicted (**Supplementary Figure 5**). After the generation of clear domains, the model was embedded into a POPC membrane (111 phospholipids per layer) and solvated with water (57.315 molecules). Later, the system was subjected to two molecular dynamics simulations (MDs). The first 25 ns of simulation was performed with application of a restraint spring constant of 1 kcal * mol^{-1} * $^{-2}$ to the backbone atoms of the protein; then, the last frame was taken, and a second non-restricted 250 ns MDs was performed (**Figure 4**).

The root mean square deviation (RMSD) of the backbone atoms, as a function of simulation time, was analyzed to know how stable the model was after the 250 ns MDs, using their initial configuration (0 ns) as reference (**Supplementary Figure 8**). It is possible to observe that the protein is not stable because the global RMSD is around 10–20 Å after 20 ns, due to the mobility of the C-terminal and N-terminal domains. When the three different domains were analyzed separately, we observed that the transmembrane segment was very stable (RMSD $<$ 5 Å), followed by the N-terminal (RMSD $<$ 10 Å) and C-terminal (RMSD $<$ 20 Å) domains. This allows us to evidence that the N-terminal domain was indeed well-modeled and that it is stable over time, as well as the transmembrane segment. The quality of the C-terminal domain cannot be verified due to the fact that it was modeled without a suitable template. To characterize changes in the PMC53.7-Zot residue position along the 250 ns unrestrained MDs of our final model, the root mean square fluctuation (RMSF) was calculated, showing the mobility of the protein residues along the MDs (**Supplementary Figure 8C**). The major fluctuations were identified in the C-terminal domain. This is in agreement with the stable time dependence of RMSD for the N-terminal domain as well as the transmembrane segment in our model, and it indicates that the major rearrangement of its conformation during the MDs occurs at the C-terminal domain, as expected. The model was validated using PROCHECK (Laskowski et al., 1993) and ProSA (Wiederstein and Sippl, 2007). The validations were done with the initial model 1 obtained from I-TASSER, the model before (0 ns) and after

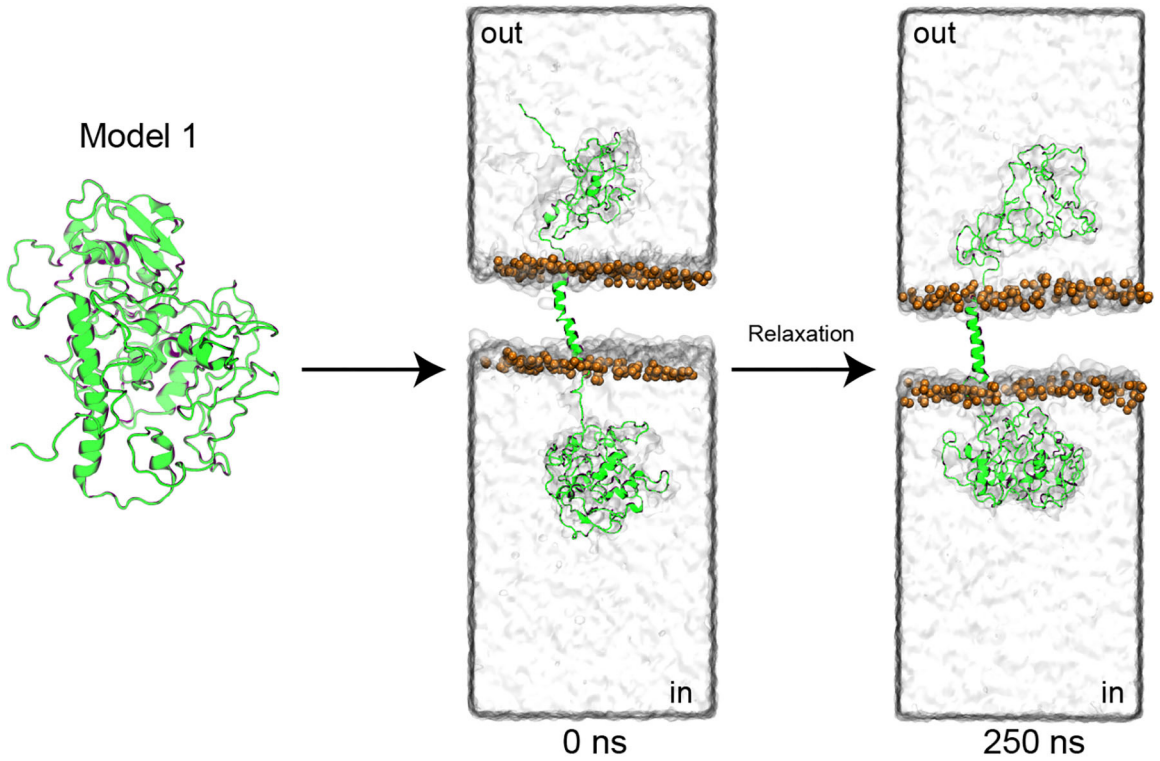

FIGURE 4 | PMC53.7-Zot model refinement. The top-1 PMC53.7 model generated by I-TASSER was manually modified to produce the N-terminal and C-terminal domains at the intracellular and extracellular compartments, respectively. The protein is shown as a cartoon representation; the solvent is displayed as a water-surface box; only the phosphates atoms from the POPC membrane are displayed as orange spheres for better visualization.

(250 ns) MDs, and finally with the model without the C-terminal domain (**Supplementary Figure 9**), because (as stated above) this region was modeled with an unsuitable template (low residue identity %). This result indicated that the model was reasonable for the transmembrane segment and N-terminal domain. Furthermore, the validations showed that as the model is refined, the quality of the 3D structure modeled improves. While the model does not show residues in the more favorable regions above 75% of the Ramachandran plots (Bertini et al., 2003) (**Supplementary Figure 9**), it is clear that residues in disallowed regions begin to shift to allowed regions as the model is refined through MDs. The final quality of the model indicates that the C-terminal and N-terminal parts are quite mobile and that as the model is refined, the number of residues in permitted regions increases. To obtain a better-quality 3D structure, it is necessary to find templates with higher percentages of sequence identity and coverage, but unfortunately, in our case, we do not have templates with these characteristics. The *z*-score of the stabilized model after 250 ns is in the same range as the experimentally determined structure proteins of the PDB (Wiederstein and Sippl, 2007) (**Supplementary Figure 10**).

Finally, we monitored the protein secondary structure elements (SSE) like α-helices and β-strands during the simulation. **Supplementary Figure 11A** shows the percentage of SSE distribution by residue index throughout the protein structure. We found that out of 100% of the PMC53.7-Zot model, 8.82% corresponds to α-helix and 2.25% to β-strands (total of SSE assigned = 11.41%). **Supplementary Figure 11B** summarizes each residue, and its SSE assignment over the 250 ns MDs. And the 3D structure of the equilibrated model (at 250 ns) is displayed with α-helices, β-strands, and loops highlighted in **Supplementary Figure 11C**. The most stable secondary structure is the transmembrane segment, followed by the α-helices and β-strands at the N-terminal domain. These results are in concordance with the initial prediction of the secondary structure of the protein (**Supplementary Figure 5**).

DISCUSSION

The present study identifies and characterizes novel virulence factors that could explain the pathogenicity of non-toxigenic strains of *V. parahaemolyticus*. In our previous work, we identified that some of these strains possess *Zot* genes in their accessory genome associated with prophages (Castillo et al., 2018a). The studies across diverse marine *Vibrio* species have shown that filamentous prophages play a key role in the emergence of novel pathogenic strains from the environment (Hay and Lithgow, 2019). In addition, we showed that the identification of Zot occurred exclusively in highly cytotoxic strains (Castillo et al., 2018a), suggesting a possible role for

V. parahaemolyticus-Zot. In this work, we observed that there was a barely positive correlation between *Zot* mRNA expression occurring during *V. parahaemolyticus* PMC53.7 infection of Caco-2 cells and cellular membrane damage represented by LDH release (% of cytotoxicity). Additionally, the treatment of Caco-2 cells with purified PMC53.7-Zot heterologous produced in *E. coli* BL21 did not induce cytotoxicity. Although the main band observed by Western blot corresponded to the expected size for the complete transcribed *Zot* gene (56 kDa), a second band of ∼27 kDa was observed (**Supplementary Figure 1**). The significance of the second one is unknown, but the *V. cholerae*-Zot undergoes a proteolytic cleavage after the transmembrane domain, which releases the biologically active C-terminal fragment (12 kDa) into the intestinal micro milieu (Goldblum et al., 2011). We cannot affirm whether the two bands obtained for PMC53.7-Zot occurred due to the action of bacterial proteases in the *E. coli* host or by autoproteolysis. However, the ∼27 kDa of the second band is close to the predicted size of the C-terminal fragment (22 kDa, **Supplementary Figure 1**), plus the histidine tail (4.5 kDa). This suggests that there probably exists a sequence site that favors the PMC53.7-Zot cleavage after the transmembrane domain. Nonetheless, the absence of correlation among Zot and cytotoxicity observed to PMC53.7-Zot had been previously reported to *V. cholerae*-Zot (Fasano et al., 1995). Interestingly, despite not finding a strong cytotoxicity correlation, we observed that PMC53.7-Zot impaired the attachment of Caco-2 cells to the plate surface (**Supplementary Figure 2**), suggesting disturbance of focal adhesions. In addition, we also observed alterations of actin cytoskeleton associated with the infection with PMC53.7, which were not observed with VpKX (**Figure 2A**) and actin rearrangements in response to the protein treatment (**Figure 2B**). Based on both observations, we suggest that probably *V. parahaemolyticus* PMC53.7-Zot contributes to cause redistribution of actin cytoskeleton also described for the *V. cholerae*-Zot. The effect observed in Caco-2 cells could be explained by differences in the actin distribution, since it is the F-actin cytoskeleton, as well as its connection to the plasma membrane, that is responsible for providing the structure and shape of epithelial cells (Brückner et al., 2019). Regrettably, despite all efforts to obtain a PMC53.7-ΔZot strain, it was not possible, even using diverse methodologies. However, the similar effects observed in Caco-2 cells infected with PMC53.7 (**Figure 2A**) and treated with PMC53.7-Zot (**Figure 2B**) suggest that the actin cytoskeleton alterations observed exclusively during the infection with PMC53.7 (yellow arrows in **Figure 2A**) occurred due to the Zot action. On the other hand, although the H_2O_2 effects over cellular nuclei were not detected in any of the infected cells, the nucleus fragmentation observed with Hoechst staining and the cytoskeletal alteration detected with phalloidin in Caco-2 cells infected with PMC53.7 suggest preliminarily that it could be a type of death related to apoptosis; however, the result did not support by itself that conclusion, and additional experiments should be done to elucidate the type of cell death induced by the *V. parahaemolyticus* PMC53.7 strain. Future research will address the unanswered aspects of this study.

It would be expected that similar functions are being attributed to similar domains of Zot protein. In fact, the bioinformatics analysis showed several similarities between Zots of *Vibrio* pathogens. The N-terminal region of PMC53.7-Zot was highly conserved among *Vibrio* strains, *Vibrio* species, and other human pathogenic bacterial species which possess Zot associated with prophages in its accessory genomes. The unique highly conserved protein among the filamentous phages is the pI, which has a conserved Zot domain (Pfam PF05707) at the N-terminus. This domain is essential for the assembly and export of phage virion, and it was named for the homolog in the *Vibrio* CTX phage (Hay and Lithgow, 2019). We also identified two Walker motifs located toward the N-terminal region, prior to the transmembrane domain of *V. parahaemolyticus*-Zot. Walker A and B motifs belong to the proteins of the P-loop NTPase superfamily (Hanson and Whiteheart, 2005). In fact, the sequence of *V. parahaemolyticus* PMC53.7-Zot aligned against the protein sequence of PHA00350, a putative assembly protein, which is a member of the P-loop_NTPase superfamily (accession number: cl21455). The P-loop_NTPase binds to NTP, typically ATP or GTP, through the Walker A and B motifs. Specifically, the N-terminus of Zot is predicted to act as an ATPase, powering the assembly and transport of phages through the envelope, as has been observed for *E. coli* Ff-type phages (Feng et al., 1997). It has been identified that P-loop in NTPases is able to affect focal adhesion and actin fibers of cells (Steele-Mortimer et al., 2000); thus, there exists the possibility that the conserved motifs located toward the N-terminal end of the toxin could be responsible for the attachment impairment seen after PMC53.7-Zot treatment in the cells (**Supplementary Figure 2**). Besides, a change of glycine (non-polar aliphatic amino acid) to tyrosine (aromatic amino acid) into the Walker A motif (GxxxxGK[S/T]) observed in most *V. parahaemolyticus* strains was also observed in *V. cholerae* (GxxxxYK[S/T]) but did not occur in *N. meningitidis* and other *Campylobacter* species (Liu et al., 2016). Despite this change, the *V. cholerae*-Zot maintains the functionality (Schmidt et al., 2007).

The mechanism of action of *V. cholerae*-Zot has been deeply studied, and it is known that it depends on the active fragment FCIGRL and its binding to the zonulin receptor PAR-2 (Goldblum et al., 2011). However, FCIGRL is absent in PMC53.7-Zot, any *V. parahaemolyticus* strain contained the active fragment described for *V. cholerae* in its Zot sequences, and there was a high variability on the C-terminal end of Zot between different pathogens and among *Vibrio* species and strains. Interestingly, we observed that differences of these regions were responsible for the diversity between Zot sequences of *V. parahaemolyticus* strains. In fact, three Zot sequences of PMC53.7, PMA2.15, and PMA3.15 strains were classified into three categories using BTXpred: endotoxin, exotoxin with guanylate cyclase activating enterotoxin activity, and non-toxin, respectively. Likewise, PMA3.15 was less cytotoxic on Caco-2 cells than other non-toxigenic strains (see Figure 7 in Castillo et al., 2018a). On the other hand, VcN16961-Zot was classified as endotoxin while Cc13826-Zot was identified as an exotoxin with an unknown activity. The diversity among Zot sequences, found in diverse *Vibrio* species, was suggested in our previous work. The phylogenetic analysis of different toxin

sequences showed that *V. parahaemolyticus* PMA2.15-Zot was identical to that found in the phage f237 of VpKX, while *V. parahaemolyticus* PMC53.7-Zot was grouped, in other nearby clades, with *V. parahaemolyticus*_A0A1J0JZE6, *Vibrio campbellii*, and *V. parahaemolyticus*_A0A0N1IWZ0 strains. Interestingly, PMA3.15-Zot, not recognized as a toxin in this work, was the most divergent sequence, and it was grouped with *Vibrio celticus* in a distant clade, suggesting major variability. This Zot divergence between different clades was observed for *V. campbellii* and *Vibrio splendidus*; however, Zot of *V. cholerae* had a major similarity among them, and all sequences were grouped in only one clade (see Figure 5 in Castillo et al., 2018a). If the diversity of Zot sequences can have an impact on its definition as toxin, we would expect that Zot of *V. cholerae* strains would act as endotoxins, but not all Zots of *V. parahaemolyticus* would have the same mechanism of action. Even more, not all Zots found in *V. parahaemolyticus* should be considered as active toxins; thus, Zot sequences with the ability to produce detrimental effects over human cells must be clearly recognized and subsequently detected.

The absence of the FCIGRL fragment is also observed in the Zot sequence of *C. concisus*, which is able to affect the paracellular pathway in spite of its absence (Mahendran et al., 2016), suggesting that the presence of this peptide sequence would not be strictly necessary to perform the action of all Zots. Similarly, a glycine in position 298 of *V. cholerae*-Zot, with a proposed crucial role in the opening of intracellular TJ, was also absent in all *V. parahaemolyticus* and *C. concisus* strains. The above observations are related to those previously reported by Kaakoush et al. (2010), so it would be the structure and not the sequence that is responsible for the biological effects of Zot on the epithelial barrier. For this reason, we modeled the PMC53.7-Zot sequence. The structure prediction suggested the presence of a transmembrane helix, which would allow PMC53.7-Zot to be specifically anchored to the membrane, as also has been reported to *V. cholerae* (Di Pierro et al., 2001). Considering that Zot could be responsible for cellular actin disturbances in Caco-2 cells, we suggest that the high number of phosphorylation sites could constitute a mechanism for regulation of protein secretion. In this regard, we reported a model for PMC57.3-Zot with the aim of contributing a structural approach to understand the function of this protein. The prediction and refinement of the structural model of the Zot protein, carried out in this work, show that a relatively stable model can be established for the N-terminal and transmembrane domains of the protein. However, it was not possible to obtain a reliable prediction for the C-terminal domain because there is no suitable model. Despite a molecular dynamic of 250 ns for the whole structure, the C-terminal domain showed high fluctuations between 10 and 20 Å. We hope that this partially stable structural model of Zot will contribute to future research to elucidate its function as a possible virulence determinant.

In conclusion, our results show that PMC53.7-Zot cannot induce cytotoxicity in Caco-2 cells, as we previously suspected. Instead, we suggest that it would be responsible for the actin cytoskeletal disturbance in the infected cells, as also described for *V. cholerae*-Zot (Goldblum et al., 2011). However, whether this effect is due to the conserved NTPase activity of the N-terminus, the 3D structural similarity with the *V. cholerae*-Zot, or a combination of both is a matter of future studies. Furthermore, the present study offers the entire model of PMC57.3-Zot as we consider it important to highlight that there are no suitable templates to model all the domains. However, a good approach to understanding the function of this protein through its structure can be made by following a rigorous modeling process.

DATA AVAILABILITY STATEMENT

All datasets generated for this study are included in the article/**Supplementary Material**.

AUTHOR CONTRIBUTIONS

KG and DP-R conceived the idea. KG, DR, CB, DP-R, and AP designed the experiments and wrote the manuscript. DR, CP-V, NP, MA-A, and CB performed the bioinformatics analysis and structure prediction. SR-A, VJ, LP, and AP performed infection and staining analysis. DP-R and RB performed Zot cloning, expression, and purification experiments. CL-J, GC, AP, and TP performed time course infection for cytotoxicity measures and made the statistical analysis. Fluorescence microscopy was performed by DP-R and SR-A. All the authors read, discussed, and approved the final version of this manuscript.

FUNDING

This work was supported by Fondecyt (Fondo Nacional de Desarrollo Cientï£¡fico y Tecnológico) Iniciación no. 11140257 to KG, no. 11160901 to CB, no. 11180604 to DR, and no. 11160642 to CL-J; Fondecyt Regular no. 1190957 to KG; REDI170296 to CB, Competitive Funds of Universidad de Las Américas PI2018026 to VJ; CONICYT-Programa de Cooperación Internacional grant no. REDES190074 to DR; CONICYT PCHA/Doctorado Nacional 2017-21172039 fellowship and ICM-Economía P09-022-F Centro Interdisciplinario de Neurociencias de Valparaíso to MA-A, and PDCBM doctoral fellowship of Universidad Autónoma de Chile to NP.

ACKNOWLEDGMENTS

We thank Beatriz Calzadilla for English editing.

SUPPLEMENTARY MATERIAL

The Supplementary Material for this article can be found online at: https://www.frontiersin.org/articles/10.3389/fcimb.2020.00482/full#supplementary-material

REFERENCES

Bertini, I., Cavallaro, G., Luchinat, C., and Poli, I. (2003). A use of Ramachandran potentials in protein solution structure determinations. *J. Biomol. NMR*. 26, 355–366. doi: 10.1023/A:1024092421649

Blom, N., Gammeltoft, S., and Brunak, S. (1999). Sequence and structure-based prediction of eukaryotic protein phosphorylation sites. *J. Mol. Biol*. 294, 1351–1362. doi: 10.1006/jmbi.1999.3310

Broberg, C. A., Calder, T. J., and Orth, K. (2011). Vibrio parahaemolyticus cell biology and pathogenicity determinants. *Microbes Infect*. 13, 992–1001. doi: 10.1016/j.micinf.2011.06.013

Brückner, B. R., Nöding, H., Skamrahl, M., and Janshoff, A. (2019). Mechanical and morphological response of confluent epithelial cell layers to reinforcement and dissolution of the F-actin cytoskeleton. *Prog. Biophys. Mol. Biol*. 144, 77–90. doi: 10.1016/j.pbiomolbio.2018.08.010

Castillo, D., Kauffman, K., Hussain, F., Kalatzis, P., Rørbo, N., Polz, M. F., et al. (2018b). Widespread distribution of prophage-encoded virulence factors in marine Vibrio communities. *Sci. Rep*. 8:9973. doi: 10.1038/s41598-018-28326-9

Castillo, D., Pérez-Reytor, D., Plaza, N., Ramírez-Araya, S., Blondel, C. J., Corsini, G., et al. (2018a). Exploring the genomic traits of non-toxigenic Vibrio parahaemolyticus strains isolated in southern Chile. *Front. Microbiol*. 9:161. doi: 10.3389/fmicb.2018.00161

Ceccarelli, D., Hasan, N. A., Huq, A., and Colwell, R. R. (2013). Distribution and dynamics of epidemic and pandemic Vibrio parahaemolyticus virulence factors. *Front. Cell Infect. Microbiol*. 3:97. doi: 10.3389/fcimb.2013.00097

Crooks, G. E., Hon, G., Chandonia, J. M., and Brenner, S. E. (2004). WebLogo: a sequence logo generator. *Genome Res*. 14, 1188–1190. doi: 10.1101/gr.849004

Di Pierro, M., Lu, R., Uzzau, S., Wang, W., Margaretten, K., Pazzani, C., et al. (2001). Zonula occludens toxin structure-function analysis. *J. Biol. Chem*. 276, 19160–19165. doi: 10.1074/jbc.M009674200

Fasano, A. (2002). Toxins and the gut: role in human disease. *Gut* 50(Suppl. III), iii9–iii14. doi: 10.1136/gut.50.suppl_3.iii9

Fasano, A., Fiorentini, C., Donelli, G., Uzzau, S., Kaper, J. B., Margaretten, K., et al. (1995). Zonula occludens toxin modulates tight junctions through protein kinase C-dependent actin reorganization, *in vitro*. *J. Clin. Invest*. 96, 710–720. doi: 10.1172/JCI118114

Feng, J. N., Russel, M., and Model, P. (1997). A permeabilized cell system that assembles filamentous bacteriophage. *Proc. Natl. Acad. Sci. U.S.A*. 94, 4068–4073. doi: 10.1073/pnas.94.8.4068

Fuenzalida, L., Hernández, C., Toro, J., Rioseco, M. L., Romero, J., and Espejo, R. T. (2006). Vibrio parahaemolyticus in shellfish and clinical samples during two large epidemics of diarrhoea in southern Chile. *Environ. Microbiol*. 8, 675–683. doi: 10.1111/j.1462-2920.2005.00946.x

Goldblum, S. E., Rai, U., Tripathi, A., Thakar, M., De Leo, L., Di Toro, N., et al. (2011). The active Zot domain (aa 288-293) increases ZO-1 and myosin 1C serine/threonine phosphorylation, alters interaction between ZO-1 and its binding partners, and induces tight junction disassembly through proteinase activated receptor 2 activation. *FASEB J*. 25, 144–158. doi: 10.1096/fj.10-158972

Gopalakrishnan, S., Pandey, N., Tamiz, A. P., Vere, J., Carrasco, R., Somerville, R., et al. (2009). Mechanism of action of ZOT-derived peptide AT-1002, a tight junction regulator and absorption enhancer. *Int. J. Pharm*. 365, 121–130. doi: 10.1016/j.ijpharm.2008.08.047

Hanson, P. I., and Whiteheart, S. W. (2005). AAA+ proteins: have engine, will work. *Nat. Rev. Mol. Cell Biol*. 6, 519–529. doi: 10.1038/nrm1684

Harder, E., Damm, W., Maple, J., Wu, C., Reboul, M., Xiang, J. Y., et al. (2016). OPLS3: a force field providing broad coverage of drug-like small molecules and proteins. *J. Chem. Theory Comput*. 12, 281–296. doi: 10.1021/acs.jctc.5b00864

Harth, E., Matsuda, L., Hernández, C., Rioseco, M. L., Romero, J., González-Escalona, N., et al. (2009). Epidemiology of Vibrio parahaemolyticus outbreaks, Southern Chile. *Emerg. Infect. Dis*. 15, 163–168. doi: 10.3201/eid1502.071269

Hay, I. D., and Lithgow, T. (2019). Filamentous phages: masters of a microbial sharing economy. *EMBO Rep*. 20:e47427. doi: 10.15252/embr.201847427

Hidalgo, I. J., Raub, T. J., and Borchardt, R. T. (1989). Characterization of the human colon carcinoma cell line (Caco-2) as a model system for intestinal epithelial permeability. *Gastroenterology* 96, 736–749. doi: 10.1016/S0016-5085(89)80072-1

Jorgensen, W. L., Maxwell, D. S., and Tirado-Rives, J. (1996). Development and testing of the OPLS all-atom force field on conformational energetics and properties of organic liquids. *J. Am. Chem. Soc*. 118, 11225–11236. doi: 10.1021/ja9621760

Kaakoush, N. O., Man, S. M., Lamb, S., Raftery, M. J., Wilkins, M. R., Kovach, Z., et al. (2010). The secretome of *Campylobacter concisus*. *FEBS J*. 277, 1606–1617. doi: 10.1111/j.1742-4658.2010.07587.x

Kaakoush, N. O., Mitchell, H. M., and Man, S. M. (2014). Role of emerging Campylobacter species in inflammatory bowel diseases. *Inflamm. Bowel Dis*. 20, 2189–2197. doi: 10.1097/MIB.0000000000000074

Käll, L., Krogh, A., and Sonnhammer, E. L. L. (2004). A combined transmembrane topology and signal peptide prediction method. *J. Mol. Biol*. 338, 1027–1036. doi: 10.1016/j.jmb.2004.03.016

Laskowski, R. A., MacArthur, M. W., Moss, D. S., and Thornton, J. M. (1993). PROCHECK: a program to check the stereochemical quality of protein structures. *J. Appl. Cryst*. 26:283–291. doi: 10.1107/S0021889892009944

Letchumanan, V., Chan, K. G., Khan, T. M., Bukhari, S. I., Mutalib, N. S. A., Goh, B. H., et al. (2017). Bile sensing: the activation of Vibrio parahaemolyticus virulence. *Front. Microbiol*. 8:728. doi: 10.3389/fmicb.2017.00728

Liu, F., Lee, H., Lan, R., and Zhang, L. (2016). Zonula occludens toxins and their prophages in Campylobacter species. *Gut Pathog*. 8:43. doi: 10.1186/s13099-016-0125-1

Ma, Y. J., Sun, X. H., Xu, X. Y., Zhao, Y., Pan, Y. J., Hwang, C. A., et al. (2015). Investigation of reference genes in Vibrio parahaemolyticus for gene expression analysis using quantitative RT-PCR. *PLoS ONE* 10:e0144362. doi: 10.1371/journal.pone.0144362

Mahendran, V., Liu, F., Riordan, S. M., Grimm, M. C., Tanaka, M. M., and Zhang, L. (2016). Examination of the effects of *Campylobacter concisus* zonula occludens toxin on intestinal epithelial cells and macrophages. *Gut Pathog*. 8:18. doi: 10.1186/s13099-016-0101-9

Mahoney, J. C., Gerding, M. J., Jones, S. H., and Whistler, C. A. (2010). Comparison of the pathogenic potentials of environmental and clinical Vibrio parahaemolyticus strains indicates a role for temperature regulation in virulence. *Appl. Environ. Microbiol*. 76, 7459–7465. doi: 10.1128/AEM.01450-10

Marchler-Bauer, A., Bo, Y., Han, L., He, J., Lanczycki, C. J., Lu, S., et al. (2017). CDD/SPARCLE: functional classification of proteins via subfamily domain architectures. *Nucl. Acids Res*. 45, D200–D203. doi: 10.1093/nar/gkw1129

Martyna, G. J., Tobias, D. J., and Klein, M. L. (1994). Constant pressure molecular dynamics algorithms. *J. Chem. Phys*. 101, 4177–4189. doi: 10.1063/1.467468

MINSAL (2017). *Base de datos RANKIN-ETA DEIS, Ministerio de Salud*. Avaliable online at: https://public.tableau.com/profile/deis4231#!/vizhome/BrotesdeEnfermedadesTransmitidasporAlimentoETA_Aos2011-2017/BrotesETAChile2011-2017 (accessed March 15, 2020).

Nettleton, D. (2014). "Chapter 6 - Selection of Variables and Factor Derivation in "Commercial data mining" Processing," in *Analysis and Modeling for Predictive Analytics Projects. The Savvy Manager's Guides*. (MA: Morgan Kaufmann Publishers Elsevier Inc.), 79–104. doi: 10.1016/B978-0-12-416602-8.00006-6

Nishibuchi, M., Fasano, A., Russell, R. G., and Kaper, J. B. (1992). Enterotoxigenicity of Vibrio parahaemolyticus with and without genes encoding thermostable direct hemolysin. *Infect. Immun*. 60, 3539–3545. doi: 10.1128/IAI.60.9.3539-3545.1992

Notredame, C., Higgins, D. G., and Heringa, J. (2000). T-coffee: a novel method for fast and accurate multiple sequence alignment. *J. Mol. Biol*. 302, 205–217. doi: 10.1006/jmbi.2000.4042

Omasits, U., Ahrens, C. H., Müller, S., and Wollscheid, B. (2014). Protter: interactive protein feature visualization and integration with experimental proteomic data. *Bioinformatics* 30, 884–886. doi: 10.1093/bioinformatics/btt607

Pérez-Reytor, D., and García, K. (2018). Galleria mellonella: a model of infection to discern novel mechanisms of pathogenesis of non-toxigenic Vibrio parahaemolyticus strains. *Virulence* 9, 22–24. doi: 10.1080/21505594.2017.1388487

Pfaffl, M. W., Horgan, G. W., and Dempfle, L. (2002). Relative expression software tool (REST(C)) for group-wise comparison and statistical analysis of relative expression results in real-time PCR. *Nucl. Acids Res*. 30:e36. doi: 10.1093/nar/30.9.e36

Raghunath, P. (2014). Roles of thermostable direct hemolysin (TDH) and TDH-related hemolysin (TRH) in Vibrio parahaemolyticus. *Front. Microbiol*. 5:805. doi: 10.3389/fmicb.2014.00805

Roy, A., Kucukural, A., and Zhang, Y. (2010). I-TASSER: a unified platform for automated protein structure and function prediction. *Nat. Protoc.* 5, 725–738. doi: 10.1038/nprot.2010.5

Saha, S., and Raghava, G. P. S. (2007). BTXpred: prediction of bacterial toxins. *In Silico Biol.* 7, 405–412. Available online at: https://pubmed.ncbi.nlm.nih.gov/18391233/

Schmidt, E., Kelly, S. M., and van der Walle, C. F. (2007). Tight junction modulation and biochemical characterisation of the zonula occludens toxin C-and N-termini. *FEBS Lett.* 581, 2974–2980. doi: 10.1016/j.febslet.2007.05.051

Shinoda, S. (2011). Sixty years from the discovery of Vibrio parahaemolyticus and some recollections. *Biocontrol Sci.* 16, 129–137. doi: 10.4265/bio.16.129

Steele-Mortimer, O., Knodler, L. A., and Brett Finlay, B. (2000). Poisons, ruffles and rockets: bacterial pathogens and the host cell cytoskeleton. *Traffic* 1, 107–118. doi: 10.1034/j.1600-0854.2000.010203.x

Tanabe, T., Miyamoto, K., Tsujibo, H., Yamamoto, S., and Funahashi, T. (2015). The small RNA Spot 42 regulates the expression of the type III secretion system 1 (T3SS1) chaperone protein VP1682 in Vibrio parahaemolyticus. *FEMS Microbiol. Lett.* 362:fnv173. doi: 10.1093/femsle/fnv173

Uzzau, S., Cappuccinelli, P., and Fasano, A. (1999). Expression of Vibrio cholerae zonula occludens toxin and analysis of its subcellular localization. *Microb. Pathog.* 27, 377–385. doi: 10.1006/mpat.1999.0312

Uzzau, S., Lu, R., Wang, W., Fiore, C., and Fasano, A. (2001). Purification and preliminary characterization of the zonula occludens toxin receptor from human (CaCo2) and murine (IEC6) intestinal cell lines. *FEMS Microbiol. Lett.* 194, 1–5. doi: 10.1111/j.1574-6968.2001.tb09437.x

Vanuytsel, T., Vermeire, S., and Cleynen, I. (2013). The role of Haptoglobin and its related protein, Zonulin, in inflammatory bowel disease. *Tissue Barriers* 1:e27321. doi: 10.4161/tisb.27321

Wagley, S., Borne, R., Harrison, J., Baker-Austin, C., Ottaviani, D., Leoni, F., et al. (2018). Galleria mellonella as an infection model to investigate virulence of Vibrio parahaemolyticus. *Virulence* 9, 197–207. doi: 10.1080/21505594.2017.1384895

Waterhouse, A. M., Procter, J. B., Martin, D. M. A., Clamp, M., and Barton, G. J. (2009). Jalview version 2–a multiple sequence alignment editor and analysis workbench. *Bioinformatics* 25, 1189–1191. doi: 10.1093/bioinformatics/btp033

Wiederstein, M., and Sippl, M. J. (2007). ProSA-web: interactive web service for the recognition of errors in three-dimensional structures of proteins. *Nucl. Acids Res.* 35, W407–W410. doi: 10.1093/nar/gkm290

Yang, J., and Zhang, Y. (2015). I-TASSER server: new development for protein structure and function predictions. *Nucl. Acids Res.* 43, W174–W181. doi: 10.1093/nar/gkv342

Yu, Y., Yang, H., Li, J., Zhang, P., Wu, B., Zhu, B., et al. (2012). Putative type VI secretion systems of Vibrio parahaemolyticus contribute to adhesion to cultured cell monolayers. *Arch. Microbiol.* 194, 827–835. doi: 10.1007/s00203-012-0816-z

Zhang, L., and Orth, K. (2013). Virulence determinants for Vibrio parahaemolyticus infection. *Curr. Opin. Microbiol.* 16, 70–77. doi: 10.1016/j.mib.2013.02.002

Zhang, L., Lee, H., Grimm, M. C., Riordan, S. M., Day, A. S., and Lemberg, D. A. (2014). *Campylobacter concisus* and inflammatory bowel disease. *World J. Gastroenterol.* 20, 1259–1267. doi: 10.3748/wjg.v20.i5.1259

Zhang, Y. (2008). I-TASSER server for protein 3D structure prediction. *BMC Bioinformatics* 9:40. doi: 10.1186/1471-2105-9-40

Conflict of Interest: The authors declare that the research was conducted in the absence of any commercial or financial relationships that could be construed as a potential conflict of interest.

frontiers in Cellular and Infection Microbiology

REVIEW
published: 30 September 2020
doi: 10.3389/fcimb.2020.572096

Virulence Regulation and Innate Host Response in the Pathogenicity of *Vibrio cholerae*

Thandavarayan Ramamurthy[1]*, *Ranjan K. Nandy*[1], *Asish K. Mukhopadhyay*[1], *Shanta Dutta*[1], *Ankur Mutreja*[2], *Keinosuke Okamoto*[3,4], *Shin-Ichi Miyoshi*[3], *G. Balakrish Nair*[5] and *Amit Ghosh*[1]

[1] Division of Bacteriology, National Institute of Cholera and Enteric Diseases, Kolkata, India, [2] Global Health-Infectious Diseases, Department of Medicine, University of Cambridge, Cambridge, United Kingdom, [3] Graduate School of Medicine, Dentistry and Pharmaceutical Sciences, Okayama University, Okayama, Japan, [4] Collaborative Research Center of Okayama University for Infectious Diseases in India, National Institute of Cholera and Enteric Diseases, Kolkata, India, [5] Microbiome Laboratory, Rajiv Gandhi Centre for Biotechnology, Thiruvananthapuram, India

OPEN ACCESS

Edited by:
Jo Brzostek,
National University of Singapore, Singapore

Reviewed by:
Pramod Kumar,
National Centre for Disease Control (NCDC), India
Yingxue Qin,
Jimei University, China
Youyu Zhang,
Xiamen University, China

***Correspondence:**
Thandavarayan Ramamurthy
ramamurthy.t@icmr.gov.in

Specialty section:
This article was submitted to Molecular Bacterial Pathogenesis, a section of the journal Frontiers in Cellular and Infection Microbiology

Received: 12 June 2020
Accepted: 19 August 2020
Published: 30 September 2020

Citation:
Ramamurthy T, Nandy RK, Mukhopadhyay AK, Dutta S, Mutreja A, Okamoto K, Miyoshi S-I, Nair GB and Ghosh A (2020) Virulence Regulation and Innate Host Response in the Pathogenicity of Vibrio cholerae. Front. Cell. Infect. Microbiol. 10:572096. doi: 10.3389/fcimb.2020.572096

The human pathogen *Vibrio cholerae* is the causative agent of severe diarrheal disease known as cholera. Of the more than 200 "O" serogroups of this pathogen, O1 and O139 cause cholera outbreaks and epidemics. The rest of the serogroups, collectively known as non-O1/non-O139 cause sporadic moderate or mild diarrhea and also systemic infections. Pathogenic *V. cholerae* circulates between nutrient-rich human gut and nutrient-deprived aquatic environment. As an autochthonous bacterium in the environment and as a human pathogen, *V. cholerae* maintains its survival and proliferation in these two niches. Growth in the gastrointestinal tract involves expression of several genes that provide bacterial resistance against host factors. An intricate regulatory program involving extracellular signaling inputs is also controlling this function. On the other hand, the ability to store carbon as glycogen facilitates bacterial fitness in the aquatic environment. To initiate the infection, *V. cholerae* must colonize the small intestine after successfully passing through the acid barrier in the stomach and survive in the presence of bile and antimicrobial peptides in the intestinal lumen and mucus, respectively. In *V. cholerae*, virulence is a multilocus phenomenon with a large functionally associated network. More than 200 proteins have been identified that are functionally linked to the virulence-associated genes of the pathogen. Several of these genes have a role to play in virulence and/or in functions that have importance in the human host or the environment. A total of 524 genes are differentially expressed in classical and El Tor strains, the two biotypes of *V. cholerae* serogroup O1. Within the host, many immune and biological factors are able to induce genes that are responsible for survival, colonization, and virulence. The innate host immune response to *V. cholerae* infection includes activation of several immune protein complexes, receptor-mediated signaling pathways, and other bactericidal proteins. This article presents an overview of regulation of important virulence factors in *V. cholerae* and host response in the context of pathogenesis.

Keywords: *V. cholerae*, virulence, toxins, quorum sensing, host response, microbiome

INTRODUCTION

In many developing and underdeveloped countries, cholera remains a major public health problem. Historically, this disease is well-known for being associated with several large epidemics and pandemics. The causative agent of cholera, a Gram-negative bacterium *Vibrio cholerae*, has both environmental and human stages in its life cycle. This bacterium has a high capacity to adapt to varying conditions of salt concentration, pH, osmolarity and bile salts prevailing in the environment, and in human host. *V. cholerae* is classified into more than 200 somatic O antigen serogroups (Yamai et al., 1997). The O1 serogroup has two biotypes, classical and El Tor, both could individually be serotyped as either Ogawa or Inaba. The other toxigenic *V. cholerae* serogroup O139, emerged in the Indian subcontinent during 1992 and spread to other Asian countries (Ramamurthy et al., 2003). The rest of the serogroups are commonly known as *V. cholerae* non-O1, non-O139, or non-agglutinable vibrios (NAG). Apart from sporadic mild diarrhea, the non-O1/non-O139 serogroups of *V. cholerae* have also been found to be involved in invasive and extra-intestinal infections (Maraki et al., 2016; Zhang et al., 2020).

V. cholerae has several arsenal of virulence factors. Serotype switching, expression of toxins, biofilm formation, multiple transcriptional circuits, genome plasticity, adherence and invasions, cytolytic proteins, secretion systems, and the ability to respond to multiple stresses are some of the major determinants of *V. cholerae* pathogenecity. In addition to the interaction and association among all of these factors, the existence of multiple genetic and functional networks plays an important role in its pathogenesis. Bacterial pathogens have evolved mechanisms to sense the host environment and to adapt constantly to the specific niche they colonize, exquisitely regulating the production of specialized virulence factors (Ribet and Cossart, 2015). Expression of virulence factors to specific stimuli is controlled at the transcriptional and translational levels through intricate regulatory links. During chronic infection state, the bacterial regulatory genes are geared to sustain their fitness to adapt host conditions (Hindré et al., 2012; Damkiær et al., 2013). The innate host immune response to *V. cholerae* infection includes activation of the nuclear factor (NF)-κB, mitogen-activated protein kinase Toll-like receptor-mediated signaling pathways and other bactericidal proteins. This article provides a comprehensive review of the mechanisms involved in virulence of *V. cholerae* and the host immune responses it induces.

MAJOR TOXINS PRODUCED BY *V. CHOLERAE* AND THEIR REGULATION

Cholera Toxin (CT)

Cholera toxin is the main virulence factor of *V. cholerae*, which is composed of one A subunit (toxic domain) and five B subunits (receptor-binding domain). The basic mechanism of action of CT is shown in **Figure 1**. Secreted CT-B binds to monosialoganglioside (GM1) on the surface of host cells to facilitate internalization of CT-A that prompts fluid loss *via* cAMP-mediated activation of anion secretion and inhibition of electroneutral NaCl absorption. The action of the barrier-disrupting effects of CtxA with massive Cl^- secretion leads to the severe diarrhea, which is characteristic of cholera.

While there is no variation in the CT-A subunit, CT-B has several amino acid substitutions and some are specific to biotypes (Ramamurthy et al., 2019). These AA residues do not take part in binding to GM1 and hence unlikely to influence affinity for the receptor. On the other hand the AA changes might influence toxin immunity and hence play an important role in the severity of the infection. The gene encoding the CT (*ctx*) is located in the CT cassette, which has been shown to be a prophage (CTXΦ) that could integrates in the *V. cholerae* chromosome using Tcp (toxin-coregulated pili) as a receptor (Davis and Waldor, 2003). However, *V. cholerae* O139 uses mannose-sensitive hemagglutinin (MSHA) pilus as a receptor VGJFΦ or its satellite phage RS1 (Campos et al., 2003). Hence, strains that are not expressing the Tcp may use other mechanisms to acquire CTXΦ. The typical genome of CTXΦ consists of the core and RS2 regions. The core region is constituted with seven genes, *psh*, *cep*, *gIIICTX*, *ace*, *zot*, *ctxA*, and *ctxB*. Except for *ctxA* and *ctxB*, rest of the genes in the core region are involved in phage morphogenesis. RS2 region contains three genes, *rstA*, *rstB*, and *rstR*, which are associated with CTXΦ replication, integration and regulation, respectively (Waldor et al., 1997). In addition, an antirepressor RstC located within the RS1 promotes the expression and transmission of CTXΦ genes. The regulatory aspects of CT have been discussed in the ToxRST system. Apart from ToxR, a three-component signal transduction system VieSAB was shown to enhance the CT expression indirectly through controlled ToxT expression (Tischler et al., 2002). However, the role of environmental factors controlling this signal system has not been established.

Accessory Cholera Enterotoxin (Ace) and Zonula Occludens Toxin (Zot)

Apart from CT, accessory cholera enterotoxin (Ace) and zonula occludens toxin (Zot) are present in the core region and contribute to *V. cholerae* pathogenesis by inducing changes in the intestinal barrier. The genes encoding them are present in the N-terminal side of the core region, which is involved in CTXΦ morphogenesis (Pérez-Reytor et al., 2018). Ace is an integral membrane protein that stimulates Ca^{2+} -dependent Cl^-/HCO^{3-} cotransporters, induces fluid secretion in the rabbit ileal loop and alters short-circuit current (I_{sc}) in the Ussing chambers (Somarny et al., 2002). The process of secretion by Ace involves Ca^{2+} as a second messenger, as there is no secretory response to cAMP or cGMP agonists (Trucksis et al., 2000). It appears that Ace may cause initial intestinal secretion *in vivo* during *V. cholerae* infection before the slow action of CT. Anoctamins (ANOs) are the transmembrane protein on the cell surface, which are essential for the calcium-dependent exposure of phosphatidylserine. The role of ANOs in diarrhea is well-investigated in NSP-4 of rotavirus. It was found that phosphatidylinositol 4,5-bisphosphate (PIP_2) influences the ANO6 function by Ace stimulation in intestinal epithelium for

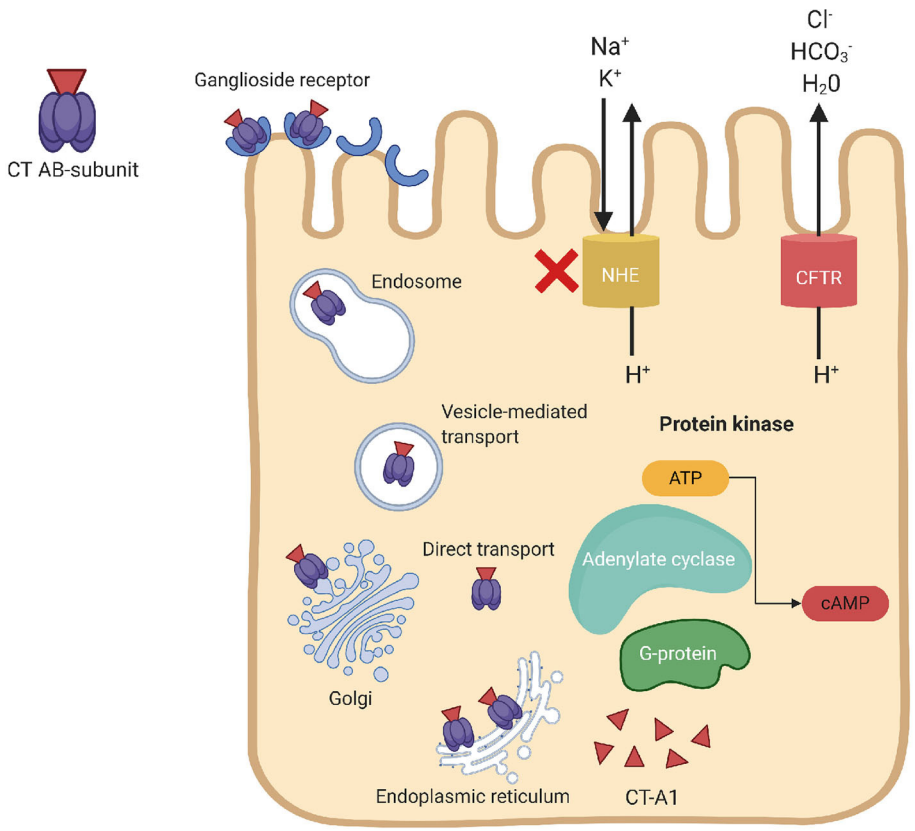

FIGURE 1 | Mechanism of action of the cholera toxin. CT binds to the ganglioside receptor on the host epithelial cells, triggers endocytosis of the holotoxin. The internalized CT moves from the endosomes to the Golgi complex and endoplasmic reticulum (ER). The catalytic CT-A1 polypeptide transfers from the ER to the cytosol by retro-translocation through the action of the ER-linked degradation pathway to activate the Gsα subunit of guanine nucleotide-binding regulatory ($G\alpha_s$) protein. Activation of $G\alpha_s$-protein leads to increased adenylate cyclase (AC) activity, which cleaves ATP to cyclic adenosine monophosphate (cAMP) and subsequently activates protein kinase-A (PKA). Activation of PKA inhibits NaCl absorption through Na^+/H^+ exchanger (NHE transporters) and phosphorylate the cystic fibrosis transmembrane conductance regulator (CFTR) chloride channel proteins, which leads to ATP-mediated efflux of chloride ions and induce secretion of HCO_3^-, Na^+, K^+, and H_2O. Loss of chloride ions induces massive fluid secretion in the small intestine, deposing the resorptive ability of the large intestine, which results in severe watery diarrhea.

Cl^- secretion to induce diarrhea (Aoun et al., 2016). ANO6 and PIP_2 act as additional mechanisms of secretory diarrhea. Overall, a comprehensive study on the role of Ace from the pathophysiological point of view is still lacking.

Zot is involved in the CTXΦ morphogenesis and its promoter activity has been identified within the *ace* sequence. Zot affects the structure of epithelial tight junction (TJs) of the small intestine. This modification leads to increase of mucosal permeability, resulting passage of macromolecules through the paracellular route. Binding of Zot to the human α-1-chimaerin receptor, which is a neuron-specific GTPase-activating protein that induces a reduction in epithelial electrical resistance and increases the trans-epithelial flux and permeability of TJs (Uzzau et al., 2001). This binding modifies the cytoskeleton and the TJ complex inside of the cell *via* an intracellular signaling that reduces the actin filaments by changing the F- and G-actin pools. This action increases intestinal epithelial permeability by affecting the TJs (Goldblum et al., 2011). Though the TJ molecular structure and its assembly during morphogenesis are well-studied, its physiological regulation and response to toxins still remains incomplete.

Heat-Stable Enterotoxin (ST)

Some strains of *V. cholerae* elaborate heat-stable enterotoxin (ST) that signal cyclic guanosine monophosphate (cGMP) pathways to activate the cystic fibrosis transmembrane conductance regulator (CFTR) chloride channel, and elevates intracellular cGMP to induce anion secretion and diarrhea (**Figure 2**). ST expression by *V. cholerae* O1 strains is rare, but is mostly reported in enterotoxigenic *Escherichia coli* and NAGs. The basis of NAG-ST expression by environmental strains of *V. cholerae* is not known. NAG/O1-ST binds to guanylyl cyclase C (GC-C) on the apical surface of enterocytes, signals intracellular cGMP, and a cGMP-dependent kinase (PGKII) to phosphorylate CFTR on the apical membrane. The activation of cGMP and CFTR signaling stimulates chloride and fluid secretion (Al-Majali et al., 2000). PGKII plays an important role in regulating cGMP-dependent translocation of CFTR and ST-dependent anion secretion, which

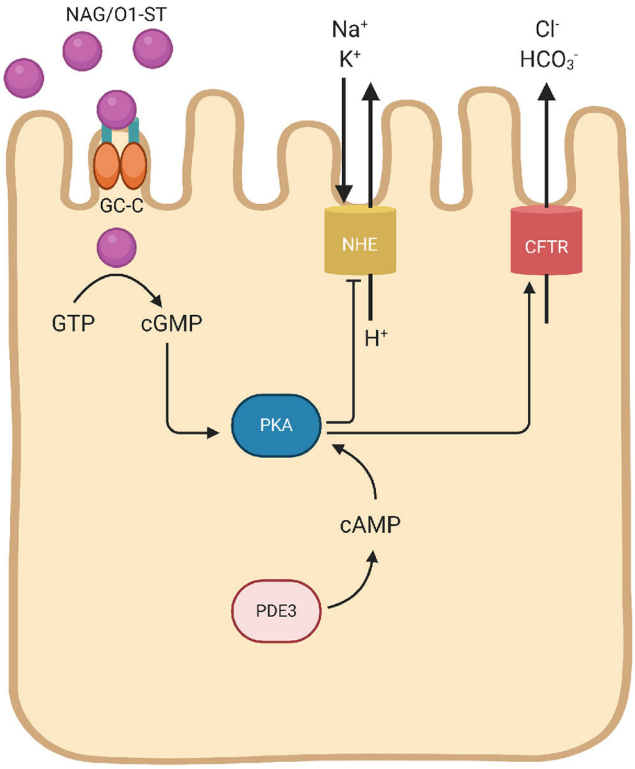

FIGURE 2 | Schematic mechanisms of *V. cholerae* heat-stable eterotoxin (NAG/O1-ST). NAG/O1-ST bind to the intestinal guanylate cyclase (GC-C). Activation of intracellular catalytic domain of GC-C result in the formation of cyclic guanosine monophosphate (cGMP) from guanosine triphosphate (GTP). This intracellular transformation activates cGMP-cAMP-dependent PKA leads to CFTR phosphorylation. cGMP reduces Na^+ and Cl^- absorption through the NHE, and also inhibits phosphodiesterase-3 (PDE3) leading to cellular accumulation of cAMP, and subsequent activation of PKA. Phosphorylation of the CFTR leads to secretion of Cl^- with HCO_3^- and decreased NaCl absorption, which results in diarrhea.

is independent of CT regulation (Golin-Bisello et al., 2005). It has been seen in *E. coli* STa, that GC-C is also implicated in the regulation of the intestinal pH, as CFTR transport Cl^- as well as HCO_3^- to prevent the tissue damage. This HCO_3^- secretion is unaided either by PKGII or CFTR (Weiglmeier et al., 2010). *E. coli* STp is encoded within a transposon (Tn1681) flanked by inverted repeats of insertion sequence 1 (IS*1*) and hence able to spread widely by gene transfer. The flanking regions of gene encoding the NAG-ST lack any transposon, but has direct repeats (DRs). DRs are known for chromosomal rearrangements such as transpositions, duplications, and deletions.

Cholix Toxin (Chx)

Cholix toxin is a member of the diphthamide-specific class of ADP-ribose transferases that has a specific ADP-ribose transferase activity against ribosomal eukaryotic elongation factor-2 (eEF2) (Jørgensen et al., 2008). Chx has been mostly identified in environmental *V. cholerae* non-O1, non-O139 strains. Though lipoprotein receptor-related protein has been shown to bind with Chx, the specific receptor for cholix bining is not known, as the sensitivity of human cell lines to cholix is variable. Recently, prohibitin (PHB) was identified acts as a Chx-binding protein (Yahiro et al., 2019), which is expressed by some cell membranes, and also by mitochondria and nucleus. *V. cholerae* ChxA has some homology with exotoxin A (ToxA) of *Pseudomonas aeruginosa*, but there is no evidence for lateral transfer (Purdy et al., 2010). In addition, *chxA* gene present on chromosome 1 (between VC1644 and VC1645) is not flanked by phage-like sequences or IS elements.

The mechanism of action of Chx is shown in **Figure 3**. Chx transports across intestinal epithelium through a vesicular trafficking pathway that rapidly reaches vesicular apical to basal transcytosis by avoiding the lysosomes (Ogura et al., 2017). This toxin has the necessary attributes required for the infection of host cells by receptor-mediated endocytosis, translocation to the cytoplasm, and inhibition of protein synthesis by specific modification of eEF-2. Transfer of an ADP-ribose group from NAD^+ to a diphthamide in eEF2 inhibits protein synthesis leading to cell death (Jørgensen et al., 2008). The pathways responsible for Chx-induced hepatocyte (HepG2) death involves reactive oxygen species (ROS) and MAPK-dependent effects (Ogura et al., 2017). Chx interacts with PHB and induces mitochondrial dysfunction and cytoskeletal rearrangement by rho-associated coiled-coil-containing protein kinase-1 activation during apoptosis. This alters the respiratory supercomplexes formation, followed by elevation of ROS-production. However, the role for cholix in causing diseases has not been clearly proven. Of the three types of Chx (ChxA-I, ChxA-II, and ChxA-III) detected in *V. cholerae*, chxA-I and ChxA-II have been shown to cause severe damage to internal organs in mice, which suggests the involvement of cholix in extraintestinal infections (Awasthi et al., 2013).

Multifunctional Autoprocessing Repeats-in-toxin (MARTX Also Known as RTX)

RTX is one of the pore-forming accessory toxins that translocates specific effector molecules into a target eukaryotic cell to carry out distinct functions. The RTX toxins comprise proteins encoded by four genes (*rtxACBD*) in two operons, located adjacent to the *ctxAB* on the large chromosome: *rtxA* encoding the toxin; *rtxB/rtxE*, an ATP-binding cassette transporter of RtxA; *rtxC*, an acylase of RtxA; and *rtxD*, with unknown function (Linhartová et al., 2010). These distinct virulence activity proteins are responsible for the RTX effect. RTX is produced both by clinical and environmental strains of *V. cholerae*. Early studies showed that the non-toxigenic *V. cholerae* O1, exerts cell rounding effect by using the RTX that causes depolymerization of actin stress fibers and covalent cross-linking of cellular actin into multimers targeting the G-actin (Fullner and Mekalanos, 2000). This direct catalyzation of RTX leads to covalent cross-linking of monomeric G-actin into oligomeric chains that cause permanent disassembly of the cytoskeleton (Cordero et al., 2006). *rtxA* gene is one of the largest ORFs of the *V. cholerae* genome. The *rtx* locus is linked to the CTXΦ integration site and the

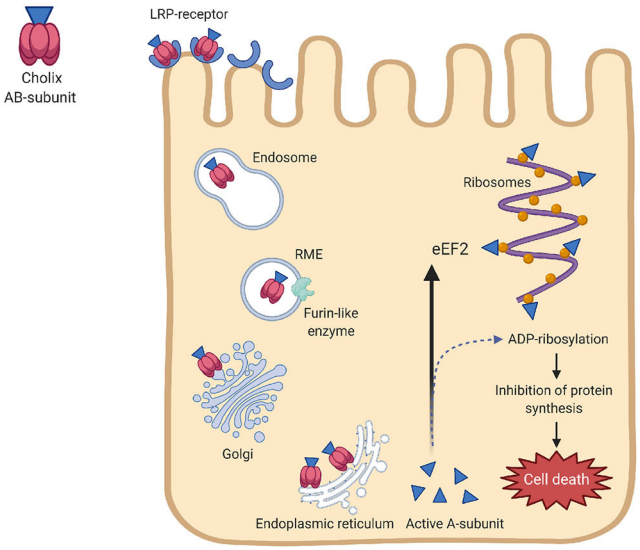

FIGURE 3 | Mechanisms of action of cholix toxin. Chx binds to the lipoprotein receptor-related protein (LRP-receptor) of the eukaryotic cells, followed by internalization by receptor-mediate endocytosis (RME). A furin-like enzyme is believed to be responsible for nicking cholix in its arginine-rich loop. After passing the Golgi complex, cholix follows the retrograde pathway in the endoplasmic reticulum to form the A and B-subunits. The A-subunit translocate into the cytoplasm and prevents protein synthesis by altering the diphthamide residue of elongation factor 2 (eEF2) through its ADP-ribosylation activity. Inhibition of protein synthesis by specific modification of eEF2 leads to cell death.

putative repressor that regulates *rtxBDE* lies outside of the *rtx* locus. In classical biotype strains, there is a deletion at the 5′ end of the *rtxA* gene along with the *rtx* promoter region. This deletion affects RTX toxin maturation and secretion deactivates the RTX.

RTX is exported to the extracellular milieu by an atypical type 1 secretion system (T1SS) that disrupts the actin cytoskeleton followed by inactivation of small Rho GTPases, Rho, Rac, and Cdc42 (Kudryashov et al., 2008; Prochazkova and Satchell, 2008). This T1SS regulation of RTX at the transcriptional level is independent of quorum sensing (QS). In certain strains of *V. cholerae*, QS indirectly regulates the RTX activity. RTX is autoprocessed by an internal cysteine protease domain (CPD), which is activated by the eukaryote-specific small molecule inositol hexakisphosphate (Lupardus et al., 2008). Under *in vitro* conditions, the exported bacterial proteases can damage the RTX activity and thus play a role in its own growth phase regulation. Presence of CPD proteolytically activates the RTX in *V. cholerae* for colonization in intestinal epithelial cells. In addition, the host response to bacterial factors also reduces the RTX toxicity, resulting in a non-inflammatory diarrheal disease response (Woida and Satchell, 2020).

Hemagglutinin Protease (HAP)

Hemagglutinin protease expression is a stationary phase growth-specific system and induces a hemorrhagic response with symptoms like necrosis, acute myofibre degeneration and degeneration of laminin, and collagen of vascular endothelial cells. HAP is secreted through the type II secretion (T2SS) pathway of *V. cholerae*. Expression of *hapA* is complex that involves a combination of several environmental signals through many global regulators, including cyclic AMP (cAMP) receptor protein (CRP), and RNA polymerase sigma (RpoS) subunit (Silva and Benitez, 2004). The RNA polymerase-binding transcription factor (DksA)-HapR-RpoS axis regulates hemagglutinin protease production in *V. cholerae* (Basu et al., 2017). HapR is expressed at high cell density. Repression of *hapR* takes place at low cell density, a condition conducive for expression of *aphA*. By binding to their respective promoter regions, HapR directly repress *tcpP*, *tcpA*, and *toxT* transcription in an indirect mode *via* AphA and a ferric uptake regulator (Fur) and directly activates the transcription of *tcpP*, *toxT*, and *tcpA*. However, the mechanisms of the Fur-dependent activation of Tcp expression needs further investigation. HapR and Fur seemed to have no regulatory actions on *toxR* transcription.

Endogenous nitric oxide (NO) production modulates HAP-mediated cytotoxicity. HAP causes degradation of the mucus barrier, modification of some of the toxins and also acts on TJ-associated proteins (Wu et al., 2000). Cleavage of occludin by HAP causes a reorganization of one of the zonulae occludents, the F-actin cytoskeleton and disruption of paracellular barrier function (Benitez and Silva, 2016). CRP is important for the expression of multiple HapR-regulated genes (Liang et al., 2007). Inactivation of *crp* represses *ompU, ompT*, and *ompW* encoding outer-membrane proteins, the alternative sigma factor (σE) required for intestinal colonization and genes involved in anaerobic energy metabolism. Most strains of *V. cholerae* O1 and NAGs carry a gene *hlyA*, which codes for hemolysin (HlyA). Production of HlyA is controlled by QS that is regulated by transcription factor HapR, at two levels-at the transcription level, independent of the metalloprotease HapA and also at the post-translational level mediated by HapA (Tsou and Zhu, 2010).

HAP can potentially contribute to the nicking and activation CT-A subunit and process pro-HlyA to active and mature form of HlyA during infection at low cell density. In addition, HAP supports long persistence of *V. cholerae* in the small intestine, delivery of CT in the vicinity of its receptor, proteolysis of biofilm protein RbmA that increase cell-to-cell adhesion by supporting interaction between biofilm cells and planktonic cells, controlling the VarS/VarA-CsrA/B/C/D sensory system. Thus, HAP has multiple targets during infection to increase the severity of the infection.

Mannose-Sensitive Hemagglutinin (MSHA)

The mannose-sensitive hemagglutinin (MSHA) is a member of the family of type 4 pili, which is important as host colonization factors, bacteriophage receptors, and mediators of DNA transfer in Gram-negative bacteria. Presence of MSHA pilus is another phenotypic marker for the El Tor vibrios and is associated with biofilm formation and environmental survival of *V. cholerae*. MSHA locus is organized as two operons and many of the genes

located upstream of the *mshA* and involved in the secretion and assembly of MSHA pilin subunits. Presence of a 7-bp direct repeat flanking *msh* suggests that the MSHA gene locus may have been acquired as a transposable or a mobilizable genetic element.

V. cholerae with MSHA phenotype become inactive in the intestine due to the binding of host's secretory immunoglobulins. In order to establish successful gut colonization, Tcp represses *msh* genes while activating *tcp* genes during infection (Hsiao et al., 2008). The ability of *V. cholerae* to regulate this switch over process determines its survival in the host. The two pili systems are intertwined post-transcriptionally through the ToxT-regulated pre-pilin peptidase that degrades MshA in a TcpJ-dependent manner. Expression of the MSHA biosynthesis is directly regulated by ToxT by binding to three different promoters within the *msh* locus. *V. cholerae* binds S-IgA in an MSHA-dependent and mannose-sensitive manner that prevents bacteria from crossing mucus barriers and attaching to the surface of epithelial cells (Hsiao et al., 2008).

V. cholerae Cytolysin (VCC)

V. cholerae cytolysin (VCC) is a member of the β-barrel pore-forming toxin (β-PFT) family and has mostly been reported in non-toxigenic strains. VCC has membrane-damaging cell-killing activity and acts on the target cells by making transmembrane oligomeric β-barrel pores leading to permeabilization of the target cell membranes (Rai and Chattopadhyay, 2015). Encoded in the *hlyA* gene of *V. cholerae,* VCC initiates mitochondria-dependent apoptosis due to its anion channel activity through several signal transduction pathways (Kanoktippornchai et al., 2014). These anion channels in the apical membrane of enterocytes trigger an outer transcellular flux of Cl^-. This ion movement, associated with the external movement of Na^+ and water is responsible for the diarrhea caused by the non-toxigenic strains of *V. cholerae*. The QS regulator HapR, along with Fur and HlyU has been shown to regulate the transcription of *hlyA* in El Tor vibrios (Gao et al., 2018). This complex regulation helps *V. cholerae* in invasion and pathogenesis during the different infective stages. VCC pro-inflammatory responses significantly rest on the activation of the transcription factor nuclear factor-κB and mitogen-activated protein kinase (MAPK) family (Khilwani et al., 2015).

This pore formation by VCC needs the presence of cholesterol in the liposome membranes. Specific binding of VCC with the membrane lipid components using the distinct loop sequences within the membrane-proximal region of VCC is considered to play a key role in determining the efficacy of the pore-forming process. Membrane binding of VCC, oligomerization, and pore-formation activity are facilitated by several regulatory mechanisms and physicochemical factors, which are not fully established. It was observed that in comparison with freely secreted VCC, VCC-associated with outer membrane vesicles (OMVs), which might play a role in its stability enhanced its biological activities (Bitar et al., 2019). OMV-associated VCC triggers an autophagy response in the target cell, which acts as a cellular defense mechanism against an OMV-associated bacterial virulence factor. VCC causes extensive vacuolation and death of cultured cells and forms an anion-selective channel in planar lipid bilayers and in cells. The formation of the anion channel is important for the progression of the vacuoles and for the cell death induced by VCC (Moschioni et al., 2002).

CONTROL OF VIRULENCE BY THE TOXR REGULON

ToxR is a DNA-binding protein and a member of the outer membrane protein regulator-R (OmpR) subclass of two-component activator (TA) systems. ToxR tightly regulates expression several virulence encoding genes in response to environmental stimuli and also plays an important role in de-repressing genes that are silenced by H-NS. It coordinately regulates the expression of a number of genes aided by the products of two other genes, *toxS* and *toxT*. **Figure 4** shows involvement of multiple signaling facilitated by ToxR, ToxS, and ToxT in controlling expression virulence genes. OmpT, a dominant outer membrane porin regulated by *V. cholerae* in response to different environmental factors. ToxR directly repress the *ompT* promoter and activate the *ompU* promoter, but involves a second activator, TcpP, to initiate the *toxT* promoter that encodes the transcription factor. Modulation of OmpU and OmpT is critical for *V. cholerae* bile resistance, virulence factor expression, and intestinal colonization (Provenzano and Klose, 2000; Morgan et al., 2019). Strains expressing only the OmpT show considerably reduced *in vitro* expression of virulence factors and intestinal colonization (Provenzano and Klose, 2000). It was also found that two transcriptional regulators, cAMP receptor protein (CRP) and ToxR, compete in the *ompT* promoter region. ToxR functions as an antiactivator and repressor, depending on its interplay with CRP, which activates *ompT* transcription by a loop-forming mechanism (Song et al., 2010). In classical vibrios, ToxR directly induce CT expression independent of ToxT and the presence of bile salts enhances this activation. The antimicrobial bactericidal/permeability-increasing (BPI) protein and a BPI-derived peptide P2 kills invading pathogens by increasing outer membrane permeability and inhibiting the O_2 consumption. ToxR regulates the outer membrane protein OmpU so as to confer resistance to P2. It was demonstrated that *V. cholerae* lacking *toxR* is sensitive to P2 than is wild type strain (Mathur and Waldor, 2004).

ToxR and ToxS function as direct mediators of signal transduction by detecting signals with their periplasmic domains and control transcription of regulated genes with their cytoplasmic domains. For full activity, ToxR requires ToxS, a periplasmic integral membrane protein, which stabilizes the ToxR by protecting it from premature proteolysis. ToxRS interact through their corresponding periplasmic domains, ToxRp and ToxSp (Midgett et al., 2017). For gut colonization and pathogenesis, *V. cholerae* has to recognize and respond to the environmental signals and cell density to ensure proper expression of genes. The molecular mechanism of cell-density dependent expression of *toxR*, needs further investigation. Bile sensory system facilitates the ToxRS complex to achieve this

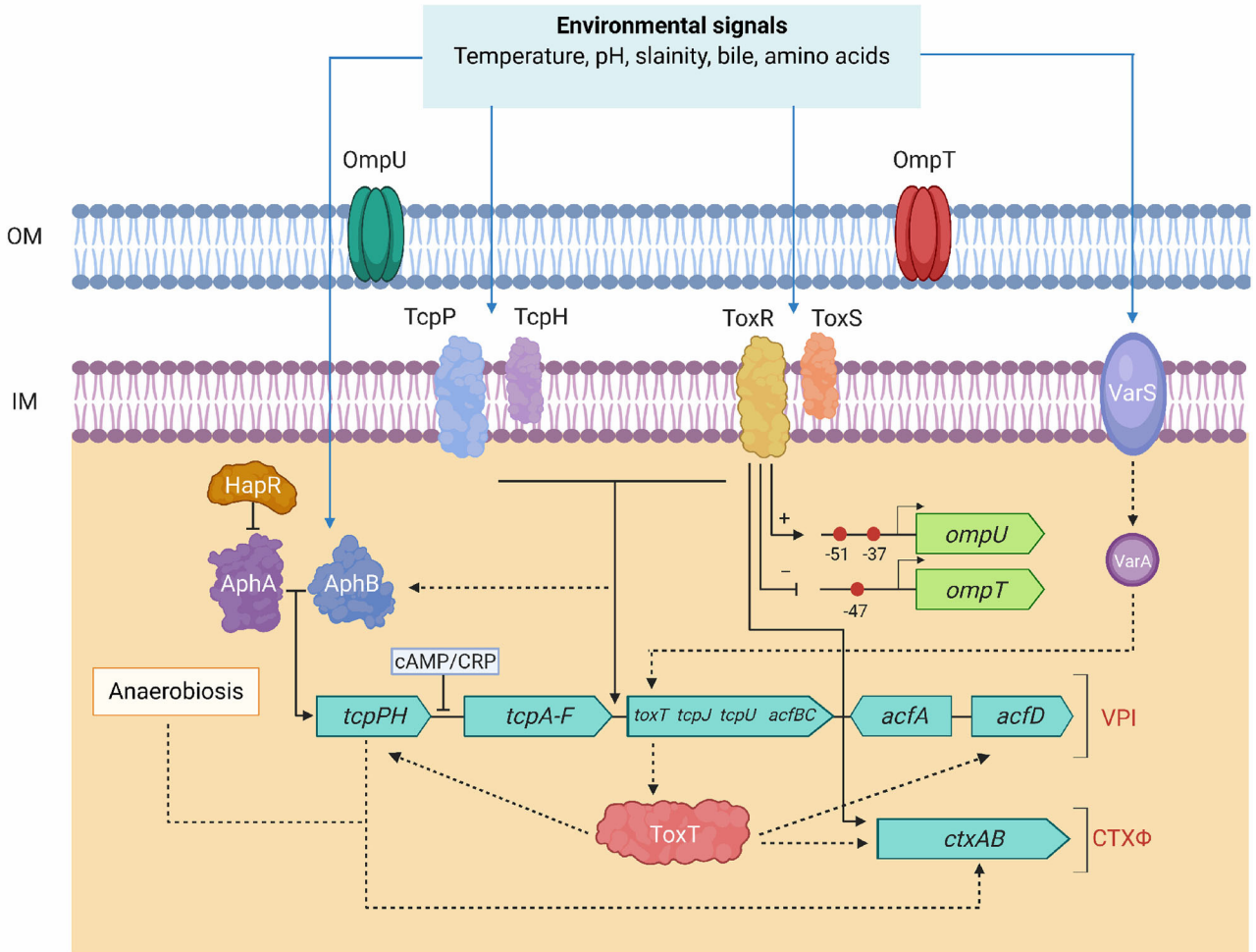

FIGURE 4 | Regulation model of Tox-mediated virulence genes in *V. chlerae*. TcpP/TcpH and ToxR/ToxS function together in activating transcription of *toxT*. ToxR and TcpP need accessory proteins (ToxS and TcpH, respectively) for maximal activity. ToxT initiates transcription of the full *tcp* operon, *ctxAB*, and *acf*. AphA and AphB activate transcription of the *tcpPH* operon in response to environmental conditions. *tcpPH* promoter is negatively influenced by the global regulator, CRP. ToxR/ToxS, and AphA/AphB also regulate genes other than *ctx* and *acf*. ToxRS, AphAB, TcpPH, and ToxT coordinately regulate the transcription of *ctx* and *tcp*. AphA and AphB activates expression of the *tcpPH*. TcpPH and ToxRS regulate *ctx* and *tcp* genes through ToxT. AphB has been linked to the expression of *tcpPH* for anaerobiosis that enhances the production of CT. The direct activator and the second activator are differentiated by black solid and dotted arrows, respectively. Blue arrows indicate different environmental conditions sensed by the ToxRS and TcpPH, AphAB, and VarS regulatory systems. The two-component VarS-VarA system responds to environmental factors and signals *toxT*. ToxR, independently activates and represses transcription of *ompU* and *ompT*. ToxR modulation was shown by an arrow (*ompU*) and line with base (*ompT*) through + for the transcription of *ompU* and—for repressing the transcription of *ompT*. Red circles in *ompU* and *ompT* indicate the ToxR binding sites and the transcriptional start sites are marked with arrows for each promoter.

(Mey et al., 2015; Lembke et al., 2018). ToxR activation by bile salts depends on the function of ToxS. Bile inhibits ToxR degradation under starvation and alkaline pH condition or when the serine protease DegPS acts on the reduced disulfide bonds. In the subsequent stage, bile is coupled with ToxRS complex and it triggers transcription (Thomson and Withey, 2014). Even though the basic functional hierarchy of the ToxR regulon is known, there are still certain gaps that need to be addressed clearly. For instance, CT and Tcp are both induced by the same pathway, but can be expressed differently. Similarly, it is not clear how a different expression of ToxR regulon components affects the virulence factors during colonization of *V. cholerae* in the host.

The second transcriptional activator, ToxT, is positively regulated by ToxR. Coordinated expression of virulence genes is regulated by the ToxR, TcpP, and ToxT proteins (**Figure 4**). The amino-terminal region of TcpP has a sequence homology to the DNA-binding domains of many regulatory proteins, including ToxR. Pairs of ToxT-binding sites in the promoters are important for dimerization of ToxT, which facilitate the binding of DNA and activate the expression of virulence genes. Depending on the structure of the promoter, ToxT can function

as a monomer or a dimer. ToxR and TcpP are the two inner membrane proteins that activate transcription of *toxT* and ToxT directly initiates virulence gene expression, especially the CT and Tcp. In response to human host signals, TcpP also stimulates virulence factors. ToxT is also responsible for the activation of putative accessory virulence genes, such as *aldA* (aldehyde dehydrogenase), *tagA* (ToxR-activated gene-A), *acfA,D* (accessory colonization factor), and *tarAB* (ToxT-activated RNA) (Thomson and Withey, 2014). ToxT activity is negatively modulated by bile and unsaturated fatty acids existing in the upper small intestine and the presence of bicarbonate in the same milieu increases the ToxT binding affinity raising the level of virulence gene transcription. Anaerobiosis has been shown to affect the production of virulence factors. Aerobic respiration control protein (ArcA) detects the signal of low oxygen to enhance biofilm formation. ArcA may upregulate virulence gene expression under the anaerobic condition by activating *toxT* expression (Sengupta et al., 2003). However, influences of environmental factors responsible for the activation of virulence system through ToxT have not been elucidated.

ToxR is not a direct activator in the *toxT* expression system but, it enhances the activity of TcpP, perhaps by recruiting it to the *toxT* promoter (Krukonis et al., 2000). TcpP/TcpH comprise a pair of regulatory proteins that have functional similarity with ToxR/ToxS and these regulatory proteins are required for *toxT* transcription. ToxR directly activates the porin encoded *ompU* promoter along with TcpP as a second activator to initiate the transcription factor, which activates virulence factors including CT and Tcp (Morgan et al., 2011). In association with TcpH, TcpP form TcpP/TcpH transcription activation complex and activate downstream virulence gene expression grouping with ToxR/ToxS complex. Of the four cysteine residues present in the cytoplasmic domain of TcpP, C58 is essential for its function and also for activation of virulence gene expression and gut colonization in infant mice model (Shi et al., 2020). Currently, there is no evidence that Tcp directly binds to intestinal cells. In addition, the interaction between Tcp and a specific receptor on host cells has not been established.

Expression of genes encoding the Tcp differs between classical and El Tor biotypes. Intergenic regions between *tcpI* (methyl-accepting chemotaxis protein) and *tcpP* (trans-cytoplasmic membrane protein), and between *tcpH* (periplasmic or exported protein) and *tcpA* (cytoplasmic membrane protein) have substantial sequence differences in these two biotypes. These sequence differences in *tcp* influence their response to pH and temperature signals. AphB, which is the activator of *tcpP* and *tcpH*, belongs to the family of LysR transcriptional regulators and along with AphA plays a role in the differential regulation of virulence genes in classical and El Tor vibrios by activating ToxR virulence cascade that leads to the transcription of the *tcpPH* operon in response to any environmental stimuli. The global regulator, CRP represses tcpPH transcription *via* its ability to influence AphA and AphB-dependent transcriptional activation. This is likely because the CRP binding site is completely within the binding sites of AphA and AphB. A single base-pair change at positions−65 and−66 of *tcpPH* promoters was shown to be responsible for the differential regulation of virulence gene expression in classical and El Tor vibrios, respectively (Kovacikova and Skorupski, 2000). Reciprocal interchange of the *tcpPH* promoter between the two biotypes showed that their ability to activate the transcription is essentially dependent on the *tcpPH* promoter with the presence of either an A or a G at position−65 or−66 in classical and El Tor, respectively. Interaction of ToxRS, ToxT, TcpPH, and other virulence related proteins/genes in are shown in **Table 1**. Several *in vitro* studies have shown the role of complex ToxR regulatory network in modulating the expression of virulence genes, but their coordinated regulatory responses during infection process still remain largely unknown.

TABLE 1 | Interaction of ToxRS, ToxT, TcpPH, and other virulence related proteins/genes in *V. cholerae*.

Protein	Action/significance
ToxR/S	Interaction of ToxR with ToxS is required for full transcriptional activation by enhancing dimerization of ToxR.
	ToxR is protected from degradation and alkaline pH by ToxS. break ToxRS detect and transduce signals into transcriptional regulation programs.
	Activation of CT, Tcp, Acf through ToxT. ToxR act as a coactivator by increasing transcriptional activation of *toxT* by promoting TcpP recruitment and/or binding to the *toxT* promoter.
	Directly repress *ompT* expression and activate *ompU* transcription that changes the outer-membrane porin composition. break Upregulation of OmpU is important for resistance to bile acids and antimicrobial peptides present in the host.
	Enhances TcpP binding and activation of transcription.
	ToxR-regulated *tcpI* and *acfB* function with a two-component system to regulate chemotaxis.
ToxT	Activate about eight different virulence gene promoters, including the *ctxAB*, *tcpA* and *acf* promoters, as part of a virulence gene regulatory cascade.
	Transcription is influenced by bile, unsaturated fatty acids and bicarbonate. break Influenced by environmental signals through VarS and VarA.
	Represses expression of MSHA.
	Transcription is regulated by ToxRS and TcpPH.
	H-NS directly represses the expression of the *toxT*.
TcpP	Transcription is stimulated by AphAB.
	Temperature and pH influence the levels of TcpP through intramembrane proteolysis.
	Activation is signaled by HapR.
TcpH	Required for stability of TcpP and co-expressed with *tcpP* as an operon. break TcpH protect TcpP against this proteolytic degradation.
AphA/B	AphA activate transcription in the presence of AphB.
	Synergistic function of AphAB activates *tcpPH* transcription.
	Alteration of dyad symmetry due to base pair changes in the *tcpPH* promoter and binding of AphB is responsible for the differential expression of virulence genes in *V. cholerae* classical and El Tor biotypes.
	The promoters directly activated by AphB respond to intracellular pH and anaerobiosis during the early stages of the infection.
	A main transcriptional activator of biofilm formation, virulence genes, and pH homeostasis.
	HapR represses transcription.

REGULATION OF SECRETION SYSTEMS (T2SS/T3SS/T6SS)

Secretion systems are used to transport macromolecules across the membranes. Some of the factors such as motility (required for successful colonization), intestinal colonization and expression virulence are dependent on the secretion of effector molecules in the cellular environment and host cytoplasm. Of the eight types of secretion systems that described, T2SS, T3SS, and T6SS are well-studied in *V. cholerae*.

The T2SS, also known as extracellular protein secretion (Eps) system, is involved in transport of hydrolytic enzymes and may play a role in ameliorating the cellular environments and generating nutrients to support bacterial fitness. T2SS secreted proteins and protein complexes are folded and accumulated in the periplasm of the bacterial cells. The T2SS selectively translocates toxins and several enzymes in their folded state across the outer membrane. CT is translocated as a folded protein complex from the periplasm across the outer membrane through the T2S channel and is captured within the large periplasmic vestibule of *V. cholerae* general secretory protein-D (VcGspD) before its secretion (Reichow et al., 2011). The other T2SS secreted proteins, such as *V. cholerae* extracellular serine proteases (VesA), Hap, and sialidase are functionally associated with CT (Sikora et al., 2011). The pilin-like proteins of T2SS assemble into a pseudopilus and are exported by the extracellular polysaccharide synthesis protein (EpsD), which is an itegral outer membrane pore and also helps in exclusion of intact CTXphi from *V. cholerae* (Yanez et al., 2008; Faruque and Mekalanos, 2012). Proteases present in the OMVs of *V. cholerae* also play a role in its pathogenesis. It is believed that QS plays an important role in directing the activation of the T2SS and the initiation of exoprotein release under favorable environmental conditions (Sandkvist, 2001). Using the T2SS, *V. cholerae* produces calcium-dependent trypsin-like serine protease (VesC) and Zn-dependent HAP, which is important in the initial phase of intestinal colonization, hemorrhagic fluid response, necrosis, increased interleukin-8 (IL-8) response, and apoptosis (Mondal et al., 2016).

The second messenger nucleotide cyclic dimeric guanosine monophosphate (c-di-GMP) regulates T2S, however, the range of phenotypes regulated by c-di-GMP is not fully known. At least for biofilm life style of *V. cholerae,* it is established that high intracellular c-di-GMP concentration has a strong association. T2SS contains 13 proteins, of which 12 are encoded by the extracellular protein secretion (*eps*) gene cluster. VpsR seems to have a molecular-link involving the intracellular c-di-GMP concentration to both *Vibrio* polysaccharide (Vps) biosynthesis and T2S. The c-di-GMP-dependent transcription factor VpsR activated by c-di-GMP, induces transcription of the extracellular protein secretion encoding *eps* operon and putative transcription factor encoding *tfoY* for the expression of T2SS and T6SS, respectively (Fernandez et al., 2018). In addition, T2SS also secretes the three proteins RbmA, RbmC, and Bap1, which are necessary for biofilm formation.

T3SSs are commonly detected in Gram-negative bacterial pathogens, but their mode of action and functions vary, as each species make different effector proteins. Some segments of the *V. cholerae* T3SS genomic island are analogous in gene organization and protein coding content of T3SS2 in *V. parahaemolyticus*. However, the flanking sequences are less conserved between these two species. After translocation, effector proteins of T3SS can enact a wide variety of functions to promote pathogenesis. T3SS-positive *V. cholerae* strains encode three regulators; $VttR_A$, $VttR_B$, and ToxR. $VttR_A$ and $VttR_B$ are the transmembrane transcriptional regulatory proteins encoded within the horizontally acquired T3SS genomic island, whereas ToxR is encoded on the chromosome. $VttR_A$ and $VttR_B$ are integral membrane proteins with N-terminal, cytoplasmic DNA binding domains and overall sequence similarity to ToxR (Miller et al., 2016a).

Most of the non-toxicgenic *V. cholerae* use T3SS as their prime virulence mechanism. The T3SS pathogenicity islands have a tripartite structure. A conserved "core" region encodes functions necessary for colonization and disease, including modulation of innate immune signaling pathways and actin dynamics, whereas regions bordering core sequences mostly encode effector proteins that perform a diverse array of activities. T3SS-mediated machinery helps the pathogen to colonize host cells and interrupt homeostasis. It was observed that T3SS induced toxicity does not progress to apoptotic or necrotic mechanisms, but displays osmotic lysis (Miller et al., 2016b). The collective effect of translocated proteins (VopS) and other effectors contributes to the colonization of T3SS-positive strains in the host epithelial cells (Chaand et al., 2015). All the three T3SS regulators are important for eukaryotic cell death as ToxR and $VttR_A$ act upstream of $VttR_B$ and modify the level of either *vttRA* or *vttRB* and strongly influence T3SS gene expression. Suppression of T3SS-encoded VttR regulatory proteins showed attenuated colonization *in vivo* (Alam et al., 2010).

T6SS is a contact-dependent factor, which resembles a contractile phage tail, but with an orientation that is opposite of the phage tail. It eliminates the competitors in the gut through the translocation of proteinaceous toxins. *V. cholerae* can use T6SS to damage both host cells and other members of the gut microbiota (Ho et al., 2014). T6SS genes are encoded in a major and at three auxiliary clusters. Activation of the major cluster induces transcription of more than one auxiliary clusters and the production of an assembled T6SS. The genes coding for the secreted core components (Hcp, VgrG, PAAR) are found in auxiliary clusters together with the genes that encode the effectors-immunity pairs. T6SS machinery is ATP-dependent actions involving expression of more than 10 genes. Some of these genes are regulated by the TfoY (encodes a putative transcription factor in *Vibrio* spp.) that responds to c-di-GMP levels. But, the mechanisms or external signals that induce the secretion activity is not fully known. LonA belongs to the superfamily of ATPases that repress the T6SS and influence T6SS-dependent killing phenotypes differently in *V. cholerae* strains with high and low levels of c-d-GMP (Joshi et al., 2020).

Four T6SS effectors mediate bacterial killing that includes cell membrane targeting TseL (putative lipase), VasX (pore forming colicin), peptidoglycan targeting VgrG-3 (lysozyme), and TseH (amidase) (Joshi et al., 2017). Effectors like VgrG proteins could

damage substrates present in the periplasm or cytosol of target bacteria. Presence of immunity proteins prevent self intoxication by neutralizing effectors. For this, *V. cholerae* expresses an anti-toxin encoded immediately downstream of *vgrG-3* that inhibits lysis through direct interaction (Brooks et al., 2013). In addition, three protein-encoding genes *tsiV1-tsiV3* provides *V. cholerae* strains with T6SS immunity (Miyata et al., 2013).

The T6SS is controlled through the QS, catabolite repression, and nucleoside scavenging pathways that are influenced by temperature, osmolarity, c-di-GMP, mucin, and bile acid. When exposed to different environments, *V. cholerae* have distinct regulatory pathways that maintain the function of T6SS. In hosts, mucins from intestinal cells increase the ability of *V. cholerae* to kill target bacterial cells while bile acids regulate expression of T6SS genes. High osmolarity conditions induce T6SS gene expression through the osmolarity controlled regulator (OscR), while cold shock protein CspV increases expression of T6SS genes. QS and the protein TsrA (VC0070) repress T6SS. Disruption of TsrA and the LuxO induces expression and secretion of a hemolysin-coregulated protein (Hcp), which is dependent on the downstream regulator HapR. HapR binds directly to the promoter regions of the T6SS genes *hcp1* and *hcp2* to induce their expression (Zheng et al., 2010). Thus, TsrA functions as a global regulator to activate expression of hemagglutinin protease and repress CT and Tcp. In *Drosophila* model, Fast et al. (2020) have shown that *V. cholerae* lacking VasK (T6SS inner-membrane protein), or VipA (a component of T6SS outer sheath), did not prevent intestinal proliferation. T6SS genes are repressed by QS response regulator LuxO at low cell density and activated by the HapR at high cell density. Quorum regulatory small RNAs (Qrr sRNAs) in the QS cascade are required for these regulatory effects to control T6SS by repressing the expression of the large cluster through base pairing and they in turn repress HapR, the activator of the two small clusters (Shao and Bassler, 2014).

FLAGELLAR REGULATORY SYSTEM

A fully functional flagellum is required for attachment and colonization of *V. cholerae*. During the process of colonization, *V. cholerae* detaches its flagellum and penetrates the mucosal layer of the intestinal epithelium. Flagellar regulatory system controls the expression of non-flagellar genes. The loss flagellum results in the secretion of the anti-σ factor FlgM, followed by activation of another σ-factor FliA, which represses HapR, facilitating increased expression of CT and Tcp (Tsou et al., 2008). It was also shown that the major virulence genes encoding CT, Tcp, HlyA, and T6SS genes are upregulated in *V. cholerae* strains with mutated flagellar regulatory genes (*rpoN, flrA, flrC,* and *fliA*) (Syed et al., 2009). These regulatory genes are important in increased hemolysis of human erythrocytes. Derepression of virulence factor occurs concomitantly with the entry of the pathogen into the intestinal mucosal layer. Stringent response stimulated by the accumulation of guanosine pentaphosphate/tetraphosphate (p)ppGpp under stress conditions play an important role in the growth and virulence of *V. cholerae*. Administration of glucose, which is present in the oral rehydartion solution might reduce (p)ppGpp-mediated CT-production and growth of the pathogen under the influence of anaerobic glucose metabolism (Oh et al., 2016). Genome-wide screening has revealed that flagellin FlaC is involved in flagellum function and toxin production at higher (p)ppGpp levels (Kim et al., 2018). The other flagellar protein FlgT is essential for motility, attachment and colonization of *V. cholerae* (Martinez et al., 2010). In addition, the flagellar regulatory system positively regulates transcription of a diguanylate cyclase (CdgD), which regulates transcription of a hemagglutinin (*frhA*) that helps in adherence of the pathogen to chitin and epithelial cells and increases biofilm formation and intestinal colonization.

In *V. cholerae* flagellar synthesis, more than 40 gene products are known to take part. These genes belong to four classes and among these, the role of *flrD* encoding the flagellar regulatory protein D has been investigated in detail (Moisi et al., 2009). *flrD* has been transcribed independently and FlrD positively regulates class III and IV flagellar gene transcription that contributes to intestinal colonization in mice. In addition to *flr* genes, the class II operon commencing with *flhA* also encodes five chemotaxis genes (*cheY3, cheZ, cheA, cheB*, and *cheW1*). Hypervirulent *V. cholerae* strains display high levels of *flhA* expression, but decreased expression of *cheW1* needed for chemotaxis. Thus, in the life cycle of *V. cholerae*, the flagellar and chemotaxis gene cluster have different regulations. In the disease process, flagellar genes briefly repress chemotaxis genes and maintain motility to accelerate infectivity.

ROLE OF HISTONE-LIKE NUCLEOID-STRUCTURING (H-NS) IN REPRESSION OF VIRULENCE-REALTED GENES

Inherent gene silencing controls expression several virulence factors and gut colonization of *V. cholerae*. Generally, gene silencing can occur during transcription or translation depending on the environmental factors. H^+Cl^- transporter chloride channel (ClcA), which is repressed *in vivo* has a spatiotemporal expression pattern. It is induced in the stomach for acid tolerance response during stomach passage, but is silenced in the lower gastrointestinal tract by proton-motive force under alkaline pH to avoid detrimental effects and ensure better colonization (Cakar et al., 2019).

Histone-like nucleoid-structuring (H-NS) protein belongs to a family of small nucleoid-associated proteins that are involved in the maintenance of chromosomal architecture in bacteria and play a role in silencing the expression of a variety of virulence and environmentally regulated genes (Silva et al., 2008). H-NS targets genes with a high A + T base content and inhibits their transcription by RNA polymerase. This transcription silencing activity is said to be one of the evolutionary processes that assist the pathogens to acquire new genes and integrate them into their genome. H-NS is required for adaptation of the pathogen to specific environments, including its ability to shift

between different lifestyles (Ayala et al., 2017). Genes within these specific clusters are activated in response to environmental fluctuations by the action of transcription factors that negate H-NS repression. The major repression targets by H-NS are shown in **Figure 5**. H-NS directly represses the transcription of *hlyA* and *rtx* (Wang et al., 2015). It was also shown that H-NS silences the virulence gene expression by repressing transcription of the ToxR cascade at various levels, including *toxT*, *tcpA*, and *ctxA* promoters (Nye et al., 2000). Binding of the positive regulator ToxT to *ctxA* and *tcpA* promoters displaces H-NS and allows the RNA polymerase to initiate transcription (Yu and DiRita, 2002). Interestingly, the hns mutants of *V. cholerae* exhibited reduced bile- and anaerobiosis-mediated repression of *ctxA* expression and the ability to colonize in the intestine (Krishnan et al., 2004; Ghosh et al., 2006).

ROLE OF BILE ACIDS IN VIRULENCE REGULATION

V. cholerae encounters bile acids in the early stages of infection. Seen in this light, many investigations proved the role of bile as an environmental cue to influence virulence genes (Krukonis and DiRita, 2003). *V. cholerae* uses small intestinal bile to modify the intracellular concentration of c-di-GMP which consequently impacts virulence gene expression. The ability of bile acids for stimulation and activation of *ctxAB* by ToxRS is governed by the transmembrane domain of ToxR in the inner membrane (Hung and Mekalanos, 2005). *In vitro* expression of CT by the classical vibrios in the presence of bile acids is due to the direct ToxRS activity at the *ctx* promoter and not through ToxT. Inability of bile acids to stimulate ToxRS-dependent expression of CT in El Tor biotype is related to the difference in *ctx* promoter responsiveness, which differ in the number of heptad TTTTGAT repeats in the upstream region (Hung and Mekalanos, 2005). El Tor strains carry only two to four copies of heptad repeats, whereas classical strains typically have eight repeats. The number of repeats forms binding regions for the activator, there by increasing higher CT-expression.

Depending on oxygen limitation and bile salts, cysteine residues are known to form homodimers or intramolecular disulfide bonds, which are important for the regulation or protein stability of ToxR, AphB, TcpP, and TcpH. Homodimer configuration of TcpP is important in the activation of *toxT* transcription. Bile increase TcpP homodimerization by limiting periplasmic disulfide interchange protein DsbA reoxidation that form intermolecular TcpP-TcpP disulfide bonds (Xue et al., 2016). Unsaturated fatty acids (UFAs) in bile inhibit the activity of ToxT. It was hypothesized that ToxT will be in an inactive state when it binds with UFAs in the small intestine and due to its inability to dimerize the virulence genes are repressed. Inside the mucus or epithelial cells, ToxT can dimerize and activate the expression of virulence genes due to the low concentration of bile inside the cellular milieu (Cruite et al., 2019). This complex interaction and complex virulence regulatory network require detailed investigation.

Bile acids also control the gut colonization of *V. cholerae*. Although two effective bile-regulated resistance-nodulation-division (RND)-family efflux systems, *vexAB* and *vexCD* provide high-level bile resistance, deletion of these genes was found not related to the colonization of *V. cholerae* in infant mice (Bina et al., 2006). In the gut, bile acids along with the Ca^{2+} function as host signals to activate *V. cholerae* virulence cascade through the dimerization of TcpP by inducing the formation of intermolecular disulphide bonds in its periplasmic domain (Yang et al., 2013). Ca^{2+} alone does not affect virulence, but it enhances bile salt-dependent induction of Tcp and also promotes bile salt-induced TcpP-TcpP interaction (Hay et al., 2016). Thus, Ca^{2+} and bile salts together may affect TcpP membrane movement and regulate TcpP activity.

Bile salts interact and destabilize ToxRp. Remarkably, the destabilized ToxRp augments interaction with ToxSp to promote the ToxR activity. In contrast, alkaline pH, which is one of the factors that leads to ToxR proteolysis, decreases the interaction between ToxRp and ToxSp (Midgett et al., 2017). As a consequence, *V. cholerae* alkalinizes its environment, which decreases the interaction between these two proteins and allows the ToxR proteolysis to progress. OmpT and OmpU are pore-forming outer membrane proteins of *V. cholerae*. Interaction between ToxR and ToxS has been controlled by the binding of bile acids, which increases active transcriptional complex and OmpU and OmpT expression. Bile stimulates ToxR-mediated transcription of *ompU* making *V. cholerae* more resistant to bile than the *ompT*-expressing ones (Wibbenmeyer et al., 2002). As the OmpU-OmpT system provides a channel that allows hydrophilic solutes to pass through the outer membrane, this effect indicates that bile might interfere with this traffic in OmpT-producing cells by functionally inhibiting the OmpT pore.

ROLE OF QUORUM SENSING (QS) AND BIOFILM FORMATION

Quorum sensing is a cell-to-cell communication leading to the synchronization of various bacterial functions, such as biofilm formation, expression of virulence, production of secondary metabolites, and competition adaptation mechanisms through secretion systems. *V. cholerae* uses QS to regulate the expression of virulence genes in response to changes in cell density. The QS circuit of *V. cholerae* consists of two autoinducer/sensor systems, cholera autoinducer-1/cholera quorum-sensing receptor (CAI-1/CqsS) and autoinducer-2 (AI-2)/LuxPQ, and the virulence associated regulator/carbon storage regulator/CsrB,C,D (VarS/VarA-CsrA/BCD) growth-phase regulatory system (Lenz and Bassler, 2007). The function of these systems depends on the *V. cholerae* cell density (**Figure 6**). Generally, QS is controlled by global quorum regulator, LuxO. VarS/VarA is a two-component system that acts on the phosphorelay pathway, upstream of HapR to regulate its expression.

Using QS, *V. cholerae* coordinates gene expression through the production, secretion, and detection of signaling molecules using AIs. Accumulation of AIs triggers repression of genes

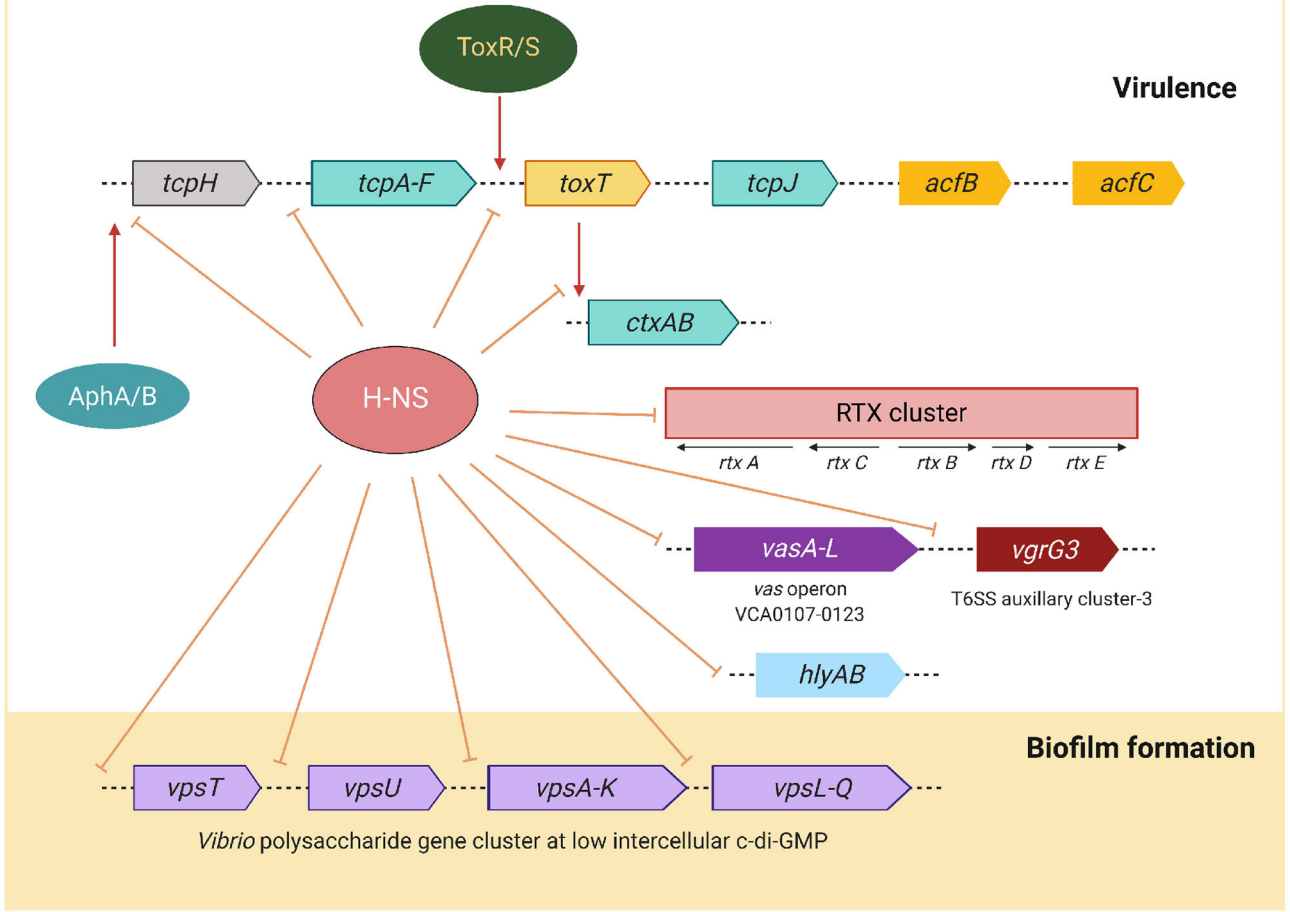

FIGURE 5 | Schematic representation of *V. cholerae* H-NS mediated negative modulation virulence and biofilm expression. Apart from the *ctxAB* operon, most of the genes are silenced by H-NS is located in the *tcp*, *rtx* gene clusters, *vas* T6SS operon, *hlyA* hemolysin/cytolysin, and the *vps* biofilm utilization genes at low c-di-GMP. Lines with base near the intergenic regions represent H-NS repression. Red arrow indicates activation of corresponding genes.

responsible for virulence factors and biofilm formation. These AIs function in parallel while, CAI-1 detects cell abundance, and the AI-2 allows *V. cholerae* to assess the adjacent bacterial community (Bridges and Bassler, 2019). QS is connected to virulence gene expression through AI molecules that share single signal transduction pathway to control the production of AphA, a key transcriptional activator of biofilm formation and virulence genes (Herzog et al., 2019). Expression of AphA is regulated by the HapR, which is regulated by the *V. cholerae* QS system. At a high cell density, the QS reduces intracellular AphA levels and this in turn lowers CT synthesis. At low cell densities, AphA levels increase, which activates expression of CT. The CAI-1 QS pathway is activated when less number of *V. cholerae* cells are present, whereas the AI-2 pathway is activated at a much higher cell density (HCD, **Figure 6**). For the latter, the response regulator LuxO does not reduce the expression of HapR but represses the expression of the virulence cascade with the activation of *tcpPH* expression by AphA and AphB (Kovacikova and Skorupski, 2002).

Histidine kinases (LuxPQ, CqsS, CqsR, and VpsS) have been identified as QS receptors that initiate virulence gene expression when the cell numbers are less (LCD, **Figure 6**). Any one of the receptors is sufficient for colonization of *V. cholerae* in the host small intestine (Watve et al., 2020). Detection of AIs by these receptors leads to virulence gene repression when the cell numbers are high. Recently, it was shown that the AI, QS autoinducer 3,5-dimethyl-pyrazin-2-ol (DPO) binds the receptor and transcription factor *V. cholerae* QS protein (VqmA) and this DPO-VqmA complex activates expression of a gene encoding the VqmR small RNA. Inside the host, several metabolites seem to act as an environmental cue for the expression of QS. Ethanolamine is a common metabolite in mammalian intestine, which has been used as an external signal for niche sensing and modulation of QS by *V. cholerae* using the cholera QS receptor (CqsR) (Watve et al., 2020). VqmR small RNA in turn post-transcriptionally controls many target genes by repressing translation of *ctx*, *rtxA*, *vpsT*, and *aphA*. *vpsT* encodes component required for biofilm formation and

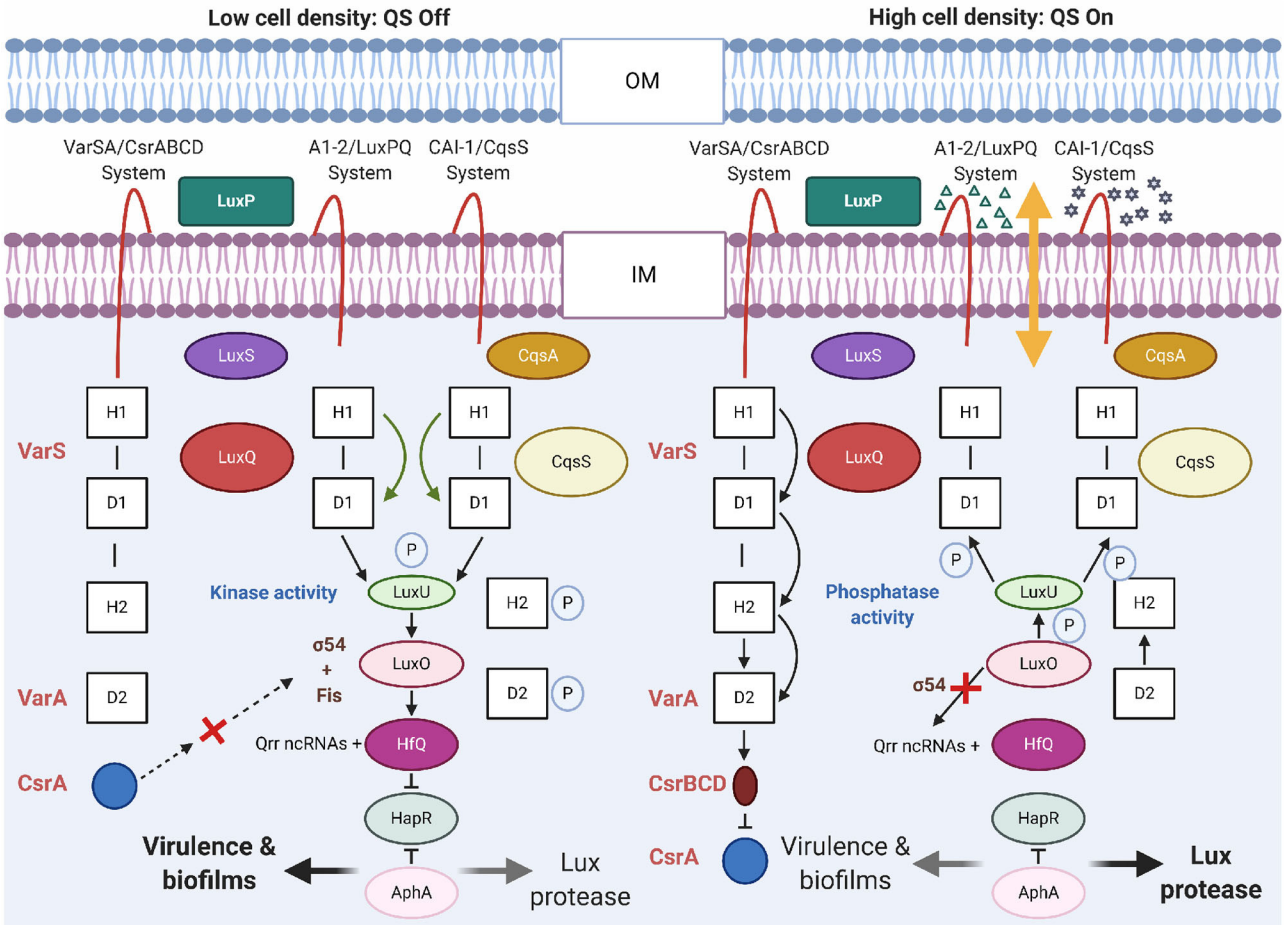

FIGURE 6 | Quorum sensing circuits in *V. cholerae*. In *V. cholerae*, QS outcome depends on the cell density. At a low cell density (LCD), QS will be in a switch-off mode. With low autoinducer concentration, the membrane proteins LuxPQ and CqsS act as kinases and direct phosphate (P) through LuxO to LuxU. With σ54 of RNA polymerase, LuxO initiates transcription of genes encoding regulatory Qrr ncRNAs. The Qrr ncRNAs activate translation of AphA and with Hfq, it represses translation of HapR. The above mentioned conditions promotes expression of genes encoding virulence factors and biofilm formation. At a high cell density (HCD), the QS will be in a switch-on mode. At this phase, the autoinducers are accrued, AI-2 (Δ) and CAI-1 (★) bind to their respective receptors LuxPQ and CqsS. Binding of AI act as phosphatases to reverse the flow of phosphate (P) across the regulatory circuit and deactivate LuxO. As a result, the Qrr ncRNAs are not formed and hence, HapR translation is not repressed and AphA translation is not activated. HapR represses the virulence-related functions. Other receptors, VarSA/CsrABCD with unknown ligands, also transduce QS information through LuxU. DNA-binding protein Fis functions together with AI-2/LuxPQ, CAI-1/CqsS, and VarS/VarA-CsrABCD systems to increase the activity of LuxO-phosphate at LCD. At the HCD, Fis and VarS/A-CsrABCD are inactive. OM and IM, indicate outer- and inner-membrane, respectively. H and D in the boxes denote histidine and aspartate sites of phosphorylation, respectively. Dotted arrows denote hypothetical interaction.

aphA, encodes the low cell density QS master regulator AphA (Huang et al., 2020).

Non-coding RNAs (ncRNAs) have complex regulatory roles in *V. cholerae* and constitute a dynamic system that allows communication among bacterial cells to synchronize several activities. At early stages of infection with LCD, phosphorylation of the regulator LuxO stimulates transcription of five quorum regulatory RNAs (Qrr 1–5, ncRNAs). These ncRNAs activate translation of *aphA*, the LCD master regulator, and repress translation of *hapR*, the HCD master regulator (**Figure 6**). At this stage, AphA activates the ToxT virulence regulon with expression of the Tcp and the CT. At the late stages of infection with HCD, the phosphorylation of LuxO is repressed and HapR is expressed (Rutherford et al., 2011; Shao and Bassler, 2012). HapR represses *aphA* transcription, production of Tcp and CT virulence factors, but activates expression of hemagglutinin/protease genes (Zhu et al., 2002).

Biofilm formation enhances the survival and persistence of *V. cholerae* in natural ecosystems and protects the pathogen during its passage through the stomach. Vibrio polysaccharide (Vps) is the major component of the biofilm matrix encoded in the *vps-I* and *vps-II* clusters (Fong et al., 2010). An intergenic region with the *rbm* gene cluster that encodes biofilm matrix proteins separates these clusters. In-frame deletions of the *vps* and *rbm* gene clusters drastically reduce the biofilm formation and intestinal colonization, indicating the functional association of these clusters.

In *V. cholerae*, c-di-GMP regulates several cellular activities. c-di-GMP and QS are important signaling systems that support *V. cholerae* in the aquatic environment and an intestinal milieu by positively regulating biofilm formation and negatively regulating virulence (Conner et al., 2017). Due to the low intracellular concentration during infection, c-di-GMP represses the expression of virulence factors. During its transmission within the host, several proteins degrade and produce c-di-GMP. This process recognizes distinct microenvironments within the gut using bile salts and bicarbonate as chemical cues and responds by modulating the intracellular concentration of c-di-GMP (Hammer and Bassler, 2009). At high c-di-GMP concentrations, c-di-GMP-dependent transcription factors VpsR and VpsT induce the expression of genes required for biofilm formation, in particular, the VPS operons and the gene cluster *rbmBCDEF* encoding biofilm matrix proteins. In addition, the c-di-GMP upregulates expression of the extracellular protein secretion (*eps*) genes encoding the T2SS via the c-di-GMP-dependent transcription factor VpsR (Sloup et al., 2017). Modulation of c-di-GMP levels, which controls biofilm formation in response to distinct sensory pathways is dependent on the *V. cholerae* biotypes. Overexpression of QS-activated HD-GYP protein (histidine [H] and/or aspartate [D] superfamily of metal dependent phosphohydrolases contain an additional GYP motif) in El Tor vibrios, decreases the intracellular concentration of c-di-GMP, which in turn reduces the exopolysaccharide production and biofilm formation. In classical vibrios, the global regulator VieA signaling pathway controls the c-di-GMP levels and biofilm formation (Hammer and Bassler, 2009).

OTHER SECRETED AND INDIGENOUS REGULATORY FACTORS

Several other factors either secreted by *V. cholerae* or available in the gut milieu, aid in its survival, colonization and expression of virulence. *V. cholerae* neuraminidase releases intestinal epithelial sialic acids as a nutrition source and also modifies intestinal polysialylated gangliosides into GM1 (Alisson-Silva et al., 2018). Utilization of sialic acid as a carbon and energy source possibly helps *V. cholerae* in colonizing the mucus-rich environment of the gut. Neuraminidase may act synergistically with CT and increase the secretory response by binding and penetration of the toxin to enterocytes. Loci VC1758 to VC1809 (*nan-nag* gene cluster) present in the VPI-2 was identified to be involved in the transport and catabolism of sialic acid (Almagro-Moreno and Boyd, 2009). During the infection process, the host cells produce nitric oxide (NO), which is a toxic radical and disrupts the function of bacterial proteins. Conversely, *V. cholerae* genome encodes a NO sensor (NorR) and a NO detoxifying enzyme (HmpA). These sensor and detoxification systems play a significant role in the survival of *V. cholerae* during gut colonization (Stern et al., 2012). The host-inducible NO synthase (iNOS) is suppressed by the *V. cholerae* regulatory protein NorR, which is expressed by NO detoxification genes *hmpA* and *nnrS* under microaerobic conditions. In adult mouse colonization model, it was shown that during prolonged colonization of *V. cholerae*, both the *hmpA* and *norR* are important for the iNOS- and non-iNOS resistance (Stern et al., 2012). *V. cholerae* secretes GlcNAc binding protein A (GbpA) that acts as adherence factor and supports attachment of the pathogen to *N*-acetylglucosamine (GlcNAc)-containing carbohydrates (chitin) as well as to intestinal mucin. GbpA has been shown to enhance gut colonization and fluid accumulation in mouse models (Wong et al., 2012).

Bacteria employ specific transduction pathways in sensing and responding to a wide variety of signals. Two component systems (TCS) are signaling pathway involved in stress response. The Cpx (conjugative plasmid expression) pathway is a TCS, which exerts extracytoplasmic stress response and helps the bacteria to maintain the integrity of the cell envelope by detecting and responding to damage by changing the protein composition of the outer and inner membranes. Cpx is also associated with the regulation of envelope-localized virulence determinants (Acosta et al., 2015a). The Cpx envelope stress response is mediated by membrane-localized sensor histidine kinase CpxA and the cytoplasmic response regulator CpxR. In *V. cholerae*, activation of the Cpx pathway decreases the expression of CT and Tcp through repression of ToxT regulator and TcpP (Acosta et al., 2015b). Cpx dysfunctions Crp, which results in reduction in TcpP production.

Bicarbonate present in the upper small intestine is an important chemical stimulus that induces virulence in *V. cholerae* O1 by enhancing ToxT activity during the course of infection. The ethoxyzolamide inhibition assay has shown the conversion of CO_2 into bicarbonate by carbonic anhydrase plays a role in virulence induction (Abuaita and Withey, 2009). Efflux systems present in *V. cholerae* remove substances detrimental to it from its cytosol. For example, RND family efflux systems help in developing antimicrobial resistance and virulence expression in *V. cholerae* (Bina et al., 2008; Taylor et al., 2012). RND-null strain expresses less CT, Tcp, and colonization in infant mouse and was also linked to the reduced transcription of *tcpP* and *toxT*. It was shown that the loss of RND efflux affected the activation state of periplasmic sensing systems, including the virulence regulator ToxR (Bina et al., 2018).

For *V. cholerae,* the human intestine is the best milieu for the maximal expression of virulence genes. TcpI is a methyl-accepting chemotaxis protein that recognize pH and influence *tcpA* transcription. The role of TcpI is important for *V. cholerae* for the penetration from the neutral pH lumen into the acidic brush border of the small intestine and pilus synthesis (Selvaraj et al., 2015). AphB activates the expression of ToxR and TcpP, which jointly control the expression of ToxT (Xu et al., 2010). Anaerobiosis enhances dimerization and the activity of transcriptional activator AphB that is required for the expression of Tcp. Under aerobic conditions, AphB is modified at the C(235) residue, which is reversible between oxygen-rich aquatic environments and oxygen-limited human hosts (Liu et al., 2011). This thiol-based switch mechanism senses intestinal signals and activates virulence. Other chromosomally encoded putative virulence related genes/proteins are provided in **Supplementary Table 1**.

REGULATION OF INVASIVE MECHANISMS

V. cholerae O1/O139 colonizes in the small intestine, but does not invade the intestinal tissue (i.e., noninvasive). *V. cholerae* non-O1, non-O139 serogroups occasionally can cause extraintestinal disease, mostly through their invasive mechanisms. In *V. cholerae*, the invasive mechanisms are complex and multifactorial. During the different stages of infection, regulation of an extracellular pore-forming hemolysin encoding gene (*hlyA*) by HapR, Fur, and HlyU was considered advantageous to the invasion of *V. cholerae*. However, the pathogenesis of invasive infections caused by these vibrios have not been fully investigated. Patients with predisposing factors such as cirrhotic condition and thrombocytopenia are susceptible to *V. cholerae* non-O1, non-O139 bloodstream invasion, bacteremic skin, and soft tissue infections including necrotizing fasciitis (Lee et al., 2007; Maraki et al., 2016). Remarkably, majority of these vibrios have *tcpA* and that could suggest its role in the pathogenesis. In some of the clinical cases, it was shown that the *V. cholerae* non-O1 and non-O139 causes invasive infection using the Zot by increasing the permeability of epithelial barrier and destabilizing the TJs junctions (Kharlanova et al., 2004). *Vibrio parahaemolyticus* has a second T3SS2 in its chromosome-II that mediates invasion into non-phagocytic cells using an effector, VopC that has a deamidase/transglutaminase activity (Park et al., 2004). Some of the pathogenic *V. cholerae* non-O1, non-O139 strains shown to contain a T3SS2-like gene cluster with the VopC and was found to be responsible for the invasion in HeLa cells (Zhang et al., 2012).

HOST RESPONSE

V. cholerae evokes long lasting immunity, responding to several antigens, in the host. During the infection process, there is a strong interaction between the host and the pathogen. At first, a number of non-specific defense mechanisms present in the host come into play, which is followed by a strong immune response mounted by the host. To initiate infection, *V. cholerae* must elude the host intestinal innate immune system; breach the mucus layer of the small intestine, adhere, and proliferate on the surface of microvilli and produce toxin(s) through the action of virulence encoded genes. In the *in vivo* model, CT-induced intestinal barrier disruption and TLR-4-NF-κB-mediated COX-2 expression has been illustrated in the pathogenesis of *V. cholerae* O1. It has been found small intestinal epithelial cells expresses the immunomodulatory microRNAs at the acute stage of infection. *V. cholerae*, like other Gram-negative bacteria discharges spherical membrane-enclosed virulence molecules called OMVs that help it to translocate its cytolysin by inducing immunomodulatory micro-RNAs (miR-146a) for colonization, reducing the epithelial innate immune defense system and preventing inflammation in the mucosa (Bitar et al., 2019).

Response to Toxins and Somatic Antigens

CT is the prime virulence factor of *V. cholerae*, but the antitoxin responses to CT do not induce long-term protective immunity against cholera. Household cholera contact studies indicated that CtxB-IgG antibodies and CtxB-specific memory B cells do not play a role in providing protective immunity, whereas elevated levels of CtxB-IgA have shown to be associated with protection (Harris et al., 2008). However, serum IgA wanes rapidly after natural infection (Harris et al., 2009). It was also shown that Ctx-B activates immune cells by inducing interleukin-1β production from the peritoneal macrophages via the pyrin inflammasome as well as the nucleotide-binding domain (NOD)-like receptor protein 3 (NLRP3) inflammasome (Orimo et al., 2019). In several cholera vaccine trials, immunomodulatory role of Ctx-B was shown to give higher protective efficacy.

Somatic antigen (O)-specific polysaccharide antigen (OSP) immunity has been maintained for long in the memory B-cell compartment at the mucosal surface. Hence, host OSP antibody responses are more important in protection against cholera than the CT antibodies. The main responses of OSP antibodies include, inhibition of motility of OSP-targeted IgA antibodies by interfering with flagellar function and pathogen trapping and elimination preceding the colonization of the small intestine (Levinson et al., 2016; Harris, 2018). Serum vibriocidal responses have long been considered as a best surrogate marker for immuno-protection upon vaccination (Chen et al., 2016; Ritter et al., 2019). Though strong vibriocidal responses are evident in children below 5 years of age, vaccine efficacy was found to be low with shorter duration of protection (Ritter et al., 2019).

Generally, *V. cholerae* infection may not trigger clinically overt inflammation, but disruption of intestinal homeostasis for extended duration may be associated with long-lasting cholera immunity (Bourque et al., 2018). Some of the innate signaling pathways upregulated in response to *V. cholerae* infection are not similar to the innate immune response to other bacterial infections. For example, in cholera, the nucleotide-binding domain leucine-rich repeat pyrin domain-3 (NLRP3) inflammasome, and type I interferon signaling pathways are activated to a level similar to viral infections (Bourque et al., 2018). Innate immunity functions as a primary defense, but in severe cholera this protection may be ineffective. The innate immune system recognizes *V. cholerae* and generates signals to direct T- and B-lymphocytes. This immune modulation is accomplished through the increased production of cytokines, including interleukin-1β (IL-1β), IL-6, and IL-17. An innate signaling pathway activated during infection process is to induce the expression of proteins that produce ROS. Dual oxidase-2 and inducible nitric oxide synthase are some of the upregulated proteins identified in duodenal tissue during *V. cholerae* infection (Bourque et al., 2018). Nontoxigenic El Tor vibrios infection is distinguished by the upregulation of IL-6, IL-10, and macrophage inflammatory protein-2α in the intestine, indicating an acute innate immune response. From several reports, it could be seen that the innate immune system directs the progression of subsequent adaptive immunity (Weil et al., 2019).

Phosphate, a component of nucleotides plays an important role in biological systems serves as an energy repository within cells (ATP) or in linking nucleotides together to form nucleic acids. It is also an important component of membrane phospholipids that is incorporated into proteins

during post-translational modifications, mainly as a regulatory tool, which plays a role in signal transduction of TCS. At the high phosphate conditions of the gut, the AphA/AphB regulatory cascade promotes Tcp and CT-production. At low phosphate conditions, the transcriptional-response regulator (PhoB) controls the *V. cholerae* virulence regulation cascade by binding and repressing the *tcpPH* promoter (Chekabab et al., 2014).

Inflammatory Response

Unlike O1/O139 serogroups, the nontoxigenic *V. cholerae* generally induces gastritis. *V. cholerae* colonizes in the small intestine and along with other factors causes acute inflammation. The mRNA expression of pro-inflammatory and anti-inflammatory cytokines revealed coordinated activity of up-regulation of IL-1α, IL-6, granulocyte-macrophage colony-stimulating factor (GM-CSF), monocyte chemoattractant protein-1 (MCP-1) and down-regulation of TGF-β in *V. cholerae* infected Int407 cells. It is evident that the whole action is modulated by NF-κ-B and in part by the adherence or motility of *V. cholerae* (Bandyopadhaya et al., 2007). *V. cholerae* mediates induction of host cell nuclear responses through signal transduction pathway and activation of proinflammatory cytokines in cultured intestinal epithelial cells. This cellular infection result in the activation of extracellular signal-regulated kinases and p38 of the mitogen activated protein kinase (MAPK) family. The intracellular infection activates protein kinase A (PKA) and protein tyrosine kinase (PTK) in the upstream of MAPK and NF-κB pathway (Bandyopadhaya et al., 2009a).

The outer membrane protein OmpU, which is one of the major porins in *V. cholerae*, has been shown to play an important role in intestinal inflammation by inducing IL-8 expression at the mRNA and protein levels in human intestinal epithelial cell line (Yang et al., 2018). Only the apical exposure to OmpU induce IL-8 secretion in polarized HT-29 cells. Mitochondria play a crucial role in the OmpU-mediated cell death. OmpU translocate to the mitochondria and directly initiates membrane permeability modifications and apoptosis-inducing factor release, which probably opens the mitochondrial permeability transition pore (Gupta et al., 2015).

V. cholerae is affected by host-derived hormones and neurotransmitters, the adrenaline and non-adrenaline signaling molecules. These molecules modulate the growth and virulence of the pathogen. Adrenaline transformed by *V. cholerae* to adrenochrome during the process of its respiration not only stimulates the growth of the pathogen, but also elicits specific responses in immune cells (Toulouse et al., 2019). In the host, adrenochrome inhibited lipopolysaccharide activates formation of TNF-α by THP-1 monocytes. The adrenochrome formed from adrenaline thus functions as an effector molecule during pathogen-host interaction. In addition, stress-associated hormones epinephrine and norepinephrine of the human host also act as signal molecules to support *V. cholerae* growth by the sequestration of the host's iron and production of virulence factors (Halang et al., 2015).

As mentioned before, GbpA is a secretory protein of *V. cholerae* that accelerates its adherence to human intestine. Binding of *V. cholerae* to intestinal mucin by GbpA results in increased mucus production, which draws more bacteria for better colonization (Rothenbacher and Zhu, 2014). GbpA interaction causes accumulation of reactive oxygen species that leads to mitochondrial dysfunction, relocation of NF-κB into nucleus, and necrotic response of the host cells (Mandal and Chatterjee, 2016). Protein kinase-B, also known as Akt, is a serine/threonine-specific protein kinase that plays a key role in the regulation of cellular survival. In *V. cholerae* infected Int cells, inhibition of Akt significantly decreases IL-1α, IL-6, and TNF-α by the NF-κ-B activation (Bandyopadhaya et al., 2009b).

The disease processes and the host responses to infection caused by toxigenic and non-toxigenic *V. cholerae* are inherently different. Infection caused by the non-toxigenic *V. cholerae* is characterized by involvement of extraintestinal organs, and a systemic inflammatory response mostly associated with immunosuppression, which induces more inflammatory gastrointestinal symptoms (Queen and Satchell, 2013). The role of neutrophils is to protect the host against pathogens and limit the infection to the intestine and control its spread to extraintestinal organs. They also control the levels of IL-1β and tumor necrosis factor-α. Invasive infections caused by non-toxigenic *V. cholerae* is characterized by upregulation of interleukin-6 (IL-6), IL-10, and macrophage inflammatory protein-2α in the intestine (Queen and Satchell, 2012). Strong evidence for this comes from the observation that reducing neutrophils from mice with anti-Ly6G-IA8 (a member of the Ly-6 superfamily of glycosylphosphatidylinositol-anchored cell surface proteins with roles in cell signaling and cell adhesion) monoclonal antibody led to decreased survival of mice infected by non-toxigenic *V. cholerae*. However, it seems that neutrophils are not protective during infection with a CT-expressing strains (Queen and Satchell, 2013).

Stimulation of the inflammasome in human THP-1 monocytes and in primary human peripheral blood mononuclear cells (PBMCs) is mediated by both nucleotide-binding oligomerization domain-like receptor family pyrin domain-containing 3 (NLRP3)-dependent and -independent pathways. However, the degree of stimulation depends on *V. cholerae* biotypes. El Tor biotype induces release of interleukin-1β (IL-1β) dependent on NLRP3 and apoptosis-associated speck-like protein-containing a caspase recruitment domain (ASC), due to the secreted pore-forming toxin hemolysin. Classical biotype strains do not produce either hemolysin or the MARTX toxin. Induction of low-level IL-1β release is due to CT and dependent on ASC but independent of NLRP3 and pyroptosis (Queen et al., 2015).

INFLUENCE OF MICROBIOME ON *V. CHOLERAE* PATHOGENESIS

Symptoms of cholera is essentially due to CT, which *V. cholerae* elaborates after it colonizes the human gut, a place where millions of other microbes reside and interact. Recently, the importance of

gut microbiome has been recognized for their role in controlling the enteric infections as they provide colonization resistance, nutrient competition, secretion of antimicrobial compounds, gut barrier integrity, mucosal adjuvant activity, etc. The disease cholera eliminates the normal gut microbes in two ways. First, the efflux of secreted water and salts into the intestinal lumen removes the protective mucus along with the gut microbiota. Second, the reduction of the microbiota may be exacerbated large amounts of oral rehydration solution used in the treatment of cholera and T6SS by the pathogen.

In gnotobiotic mice model, improved CT-IgA response was observed after colonizing with diet-specific microbiome (Di Luccia et al., 2020). In several studies, it was shown that the commensal microbes act as a barrier against enteric pathogens. In grem-free adult mice, colonization of *Bacteroides vulgatus* was shown to reduce *V. cholerae* colonization after conditional challenge (You et al., 2019). On the other hand, some microbes make gut as a conducive milieu for the proliferation of enteric pathogens through their metabolic process. In the adult mice model, it was shown that a decrease of ROS in the gut by the non-lactose fermenting *E. coli* support the growth of *V. cholerae* (Yoon et al., 2016). The host derived metabolites also play a role in supporting the such pathogens in the gut, but the studies focused on this line are very less.

Gut microbial composition determines susceptibility to *V. cholerae* infection and can be used as a epidemiologic tool to predict risk factors (Midani et al., 2018). With the development of large scale microbial sequencing, microbiome studies are increasingly available. It has been shown that in case of cholera, rapid loss of normal flora occurs due to massive loss of body fluids through the intestine and/or due to the influence of antibiotic treatment. Restoration of normal gut microbiota requires bacterial species succession after cholera infection, which has been demonstrated with different stages. In all these stages, relative abundance of oxygen tension and nutrient availability play a crucial role (David et al., 2015). Knowledge of the role of gut microbes that impact host-pathogen interactions in *V. cholerae* infection increasing. Investigations of the specific bacterial groups associated with susceptibility may provide understanding of relationships between *V. cholerae* infection and the gut microbiome. Considering several benefits provided by gut microbes and the dynamic nature of the gut environment, use of microbiome in the development of therapeutic strategies.

CONCLUSION

As this review has attempted to highlight virulence regulation and host responses during the infection process of *V. cholerae*. The risk of infections associated with not just *V. cholerae,* but also other *Vibrio* species is increasing, as a consequence of unhealthy environment, food contamination and global warming. *V. cholerae* has several virulence factors, and for some of them, the mechanisms associated with the infections are not completely understood. Horizontal gene transfer plays a significant role in the transmission of genes encoding the toxins. This mechanism constantly changes the phenotypic and genetic characteristics of *V. cholerae*. As far as the virulence is concerned, the role of RNA-mediated regulation factors and specific ncRNA population that regulates different target molecules are not known at the single-bacterial cell level. Mechanisms by which the gut microbes interact with *V. cholerae* remain unknown. Based on the voluminous data that we have in hand, trans-disciplinary approaches using pan-omic technologies have to be developed to recognize patho-adaptation, environmental signals and host responses that participate in the genetic regulatory networks. The information on these factors is crucial for developing novel therapeutics and prevention strategies against *V. cholerae* mediated infections.

AUTHOR CONTRIBUTIONS

TR, RN, AM, and AG conceived and structured the review. TR and RN wrote the manuscript. AKM, SD, KO, S-IM, and GN critically analyzed the presentation. All authors discussed the results, reviewed, and commented on the manuscript.

FUNDING

This work was supported in part by the Japan Initiative for Global Research Network on Infectious Diseases (J-GRID), the Ministry of Education, Culture, Sports, Science and Technology in Japan, the Japan Agency for Medical Research and Development (AMED; Grant No. JP19fm0108002), Indian Council of Medical Research, Indian National Science Academy (INSA), and the National Academy of Sciences (NASI), India. TR is INSA-Senior Scientist, AG is J. C. Bose Chair Professor of the NASI, India.

ACKNOWLEDGMENTS

We thank Dharanidharan R, Medical Biotechnology and Immunothreapy Research Unit, Faculty of Health Sciences, University of Cape Town, South Africa in preparation of figures using BioRender.com.

SUPPLEMENTARY MATERIAL

The Supplementary Material for this article can be found online at: https://www.frontiersin.org/articles/10.3389/fcimb.2020.572096/full#supplementary-material

REFERENCES

Abuaita, B. H., and Withey, J. H. (2009). Bicarbonate induces *Vibrio cholerae* virulence gene expression by enhancing ToxT activity. *Infect. Immun.* 77, 4111–4420. doi: 10.1128/IAI.00409-09

Acosta, N., Pukatzki, S., and Raivio, T. L. (2015a). The *Vibrio cholerae* Cpx envelope stress response senses and mediates adaptation to low iron. *J. Bacteriol.* 197, 262–276. doi: 10.1128/JB.01957-14

Acosta, N., Pukatzki, S., and Raivio, T. L. (2015b). The Cpx system regulates virulence gene expression in *Vibrio*

cholerae. *Infect. Immun.* 83, 2396–2408. doi: 10.1128/IAI.03056-14

Alam, A., Tam, V., Hamilton, E., and Dziejman, M. (2010). *vttRA* and *vttRB* encode ToxR family proteins that mediate bile-induced expression of type three secretion system genes in a non-O1/non-O139 *Vibrio cholerae* strain. *Infect. Immun.* 78, 2554–2570. doi: 10.1128/IAI.01073-09

Alisson-Silva, F., Liu, J. Z., Diaz, S. L., Deng, L., Gareau, M. G., Marchelletta, R., et al. (2018). Human evolutionary loss of epithelial Neu5Gc expression and species-specific susceptibility to cholera. *PLoS Pathog.* 14:e1007133. doi: 10.1371/journal.ppat.1007133

Almagro-Moreno, S., and Boyd, E. F. (2009). Sialic acid catabolism confers a competitive advantage to pathogenic *Vibrio cholerae* in the mouse intestine. *Infect. Immun.* 77, 3807–3816. doi: 10.1128/IAI.00279-09

Al-Majali, A. M., Asem, E. K., Lamar, C. H., Robinson, J. P., Freeman, M. J., and Saeed, A. M. (2000). Studies on the mechanism of diarrhoea induced by *Escherichia coli* heat-stable enterotoxin (STa) in newborn calves. *Vet. Res. Commun.* 24, 327–338. doi: 10.1023/A:1006444105846

Aoun, J., Hayashi, M., Sheikh, I. A., Sarkar, P., Saha, T., Ghosh, P., et al. (2016). Anoctamin 6 contributes to Cl^- secretion in accessory cholera enterotoxin (Ace)-stimulated diarrhea: an essential role for phosphatidylinositol 4,5-bisphosphate (pip2) signaling in cholera. *J. Biol. Chem.* 291, 26816–26836. doi: 10.1074/jbc.M116.719823

Awasthi, S. P., Asakura, M., Chowdhury, N., Neogi, S. B., Hinenoya, A., Golbar, H. M., et al. (2013). Novel cholix toxin variants, ADP-ribosylating toxins in *Vibrio cholerae* non-O1/non-O139 strains, and their pathogenicity. *Infect. Immun.* 81, 531–541. doi: 10.1128/IAI.00982-12

Ayala, J. C., Silva, A. J., and Benitez, J. A. (2017). H-NS: an overarching regulator of the *Vibrio cholerae* life cycle. *Res. Microbiol.* 168, 16–25. doi: 10.1016/j.resmic.2016.07.007

Bandyopadhaya, A., Bhowmick, S., and Chaudhuri, K. (2009b). Activation of proinflammatory response in human intestinal epithelial cells following *Vibrio cholerae* infection through PI3K/Akt pathway. *Can. J. Microbiol.* 55, 1310–1318. doi: 10.1139/W09-093

Bandyopadhaya, A., Das, D., and Chaudhuri, K. (2009a). Involvement of intracellular signaling cascades in inflammatory responses in human intestinal epithelial cells following *Vibrio cholerae* infection. *Mol. Immunol.* 46, 1129–1139. doi: 10.1016/j.molimm.2008.11.003

Bandyopadhaya, A., Sarkar, M., and Chaudhuri, K. (2007). Human intestinal epithelial cell cytokine mRNA responses mediated by NF-kappaB are modulated by the motility and adhesion process of *Vibrio cholerae*. *Int. J. Biochem. Cell Biol.* 39, 1863–1876. doi: 10.1016/j.biocel.2007.05.005

Basu, P., Pal, R. R., Dasgupta, S., and Bhadra, R. K. (2017). DksA-HapR-RpoS axis regulates haemagglutinin protease production in *Vibrio cholerae*. *Microbiology* 163, 900–910. doi: 10.1099/mic.0.000469

Benitez, J. A., and Silva, A. J. (2016). *Vibrio cholerae* hemagglutinin(HA)/protease: an extracellular metalloprotease with multiple pathogenic activities. *Toxicon* 115, 55–62. doi: 10.1016/j.toxicon.2016.03.003

Bina, J. E., Provenzano, D., Wang, C., Bina, X. R., and Mekalanos, J. J. (2006). Characterization of the *Vibrio cholerae vexAB* and *vexCD* efflux systems. *Arch. Microbiol.* 186, 171–181. doi: 10.1007/s00203-006-0133-5

Bina, X. R., Howard, M. F., Taylor-Mulneix, D. L., Ante, V. M., Kunkle, D. E., and Bina, J. E. (2018). The *Vibrio cholerae* RND efflux systems impact virulence factor production and adaptive responses via periplasmic sensor proteins. *PLoS Pathog.* 14:e1006804. doi: 10.1371/journal.ppat.1006804

Bina, X. R., Provenzano, D., Nguyen, N., and Bina, J. E. (2008). *Vibrio cholerae* RND family efflux systems are required for antimicrobial resistance, optimal virulence factor production, and colonization of the infant mouse small intestine. *Infect. Immun.* 76, 3595–3605. doi: 10.1128/IAI.01620-07

Bitar, A., Aung, K. M., Wai, S. N., and Hammarström, M. (2019). *Vibrio cholerae* derived outer membrane vesicles modulate the inflammatory response of human intestinal epithelial cells by inducing microRNA-146a. *Sci. Rep.* 9:7212. doi: 10.1038/s41598-019-43691-9

Bourque, D. L., Bhuiyan, T. R., Genereux, D. P., Rashu, R., Ellis, C. N., Chowdhury, F., et al. (2018). Analysis of the human mucosal response to cholera reveals sustained activation of innate immune signaling pathways. *Infect. Immun.* 86, e00594–e00517. doi: 10.1128/IAI.00594-17

Bridges, A. A., and Bassler, B. L. (2019). The intragenus and interspecies quorum-sensing autoinducers exert distinct control over *Vibrio cholerae* biofilm formation and dispersal. *PLoS Biol.* 17:e3000429. doi: 10.1371/journal.pbio.3000429

Brooks, T. M., Unterweger, D., Bachmann, V., Kostiuk, B., and Pukatzki, S. (2013). Lytic activity of the *Vibrio cholerae* type VI secretion toxin VgrG-3 is inhibited by the antitoxin TsaB. *J. Biol. Chem.* 288, 7618–7625. doi: 10.1074/jbc.M112.436725

Cakar, F., Zingl, F. G., and Schild, S. (2019). Silence is golden: gene silencing of *V. cholerae* during intestinal colonization delivers new aspects to the acid tolerance response. *Gut Microbes.* 10, 228–234. doi: 10.1080/19490976.2018.1502538

Campos, J., Martínez, E., Marrero, K., Silva, Y., Rodríguez, B. L., Suzarte, E., et al. (2003). Novel type of specialized transduction for CTX phi or its satellite phage RS1 mediated by filamentous phage VGJ phi in *Vibrio cholerae*. *J. Bacteriol.* 185, 7231–7240. doi: 10.1128/JB.185.24.7231-7240.2003

Chaand, M., Miller, K. A., Sofia, M. K., Schlesener, C., Weaver, J. W., Sood, V., et al. (2015). Type 3 secretion system island encoded proteins required for colonization by non-O1/non-O139 serogroup *Vibrio cholerae*. *Infect. Immun.* 83, 2862–2869. doi: 10.1128/IAI.03020-14

Chekabab, S. M., Harel, J., and Dozois, C. M. (2014). Interplay between genetic regulation of phosphate homeostasis and bacterial virulence. *Virulence* 5, 786–793. doi: 10.4161/viru.29307

Chen, W. H., Cohen, M. B., Kirkpatrick, B. D., Brady, R. C., Galloway, D., Gurwith, M., et al. (2016). Single-dose live oral cholera vaccine CVD 103-HgR protects against human experimental infection with *Vibrio cholerae* O1 El Tor. *Clin. Infect. Dis.* 62, 1329–1335. doi: 10.1093/cid/ciw145

Conner, J. G., Zamorano-Sánchez, D., Park, J. H., Sondermann, H., and Yildiz, F. H. (2017). The ins and outs of cyclic di-GMP signaling in *Vibrio cholerae*. *Curr. Opin. Microbiol.* 36, 20–29. doi: 10.1016/j.mib.2017.01.002

Cordero, C. L., Kudryashov, D. S., Reisler, E., and Satchell, K. J. (2006). The Actin cross-linking domain of the *Vibrio cholerae* RTX toxin directly catalyzes the covalent cross-linking of actin. *J. Biol. Chem.* 281, 32366–32374. doi: 10.1074/jbc.M605275200

Cruite, J. T., Kovacikova, G., Clark, K. A., Woodbrey, A. K., Skorupski, K., and Kull, F. J. (2019). Structural basis for virulence regulation in *Vibrio cholerae* by unsaturated fatty acid components of bile. *Commun. Biol.* 2:440. doi: 10.1038/s42003-019-0686-x

Damkiær, S., Yang, L., Molin, S., and Jelsbak, L. (2013). Evolutionary remodeling of global regulatory networks during long-term bacterial adaptation to human hosts. *Proc. Natl. Acad. Sci. U. S. A.* 110, 7766–7771. doi: 10.1073/pnas.1221466110

David, L. A., Weil, A., Ryan, E. T., Calderwood, S. B., Harris, J. B., Chowdhury, F., et al. (2015). Gut microbial succession follows acute secretory diarrhea in humans. *mBio* 6, e00381–e00315. doi: 10.1128/mBio.00381-15

Davis, B. M., and Waldor, M. K. (2003). Filamentous phages linked to virulence of *Vibrio cholerae*. *Curr. Opin. Microbiol.* 6, 35–42. doi: 10.1016/S1369-5274(02)00005-X

Di Luccia, B., Ahern, P. P., Griffin, N. W., Cheng, J., Guruge, J. L., Byrne, A. E., et al. (2020). Combined prebiotic and microbial intervention improves oral cholera vaccination responses in a mouse model of childhood undernutrition. *Cell Host Microbe*. 27, 899–908.e5. doi: 10.1016/j.chom.2020.04.008

Faruque, S. M., and Mekalanos, J. J. (2012). Phage-bacterial interactions in the evolution of toxigenic *Vibrio cholerae*. *Virulence* 3, 556–565. doi: 10.4161/viru.22351

Fast, D., Petkau, K., Ferguson, M., Shin, M., Galenza, A., Kostiuk, B., et al. (2020). *Vibrio cholerae*-symbiont interactions inhibit intestinal repair in *Drosophila*. *Cell Rep.* 30, 1088–1100. doi: 10.1016/j.celrep.2019.12.094

Fernandez, N. L., Srivastava, D., Ngouajio, A. L., and Waters, C. M. (2018). Cyclic di-GMP positively regulates DNA repair in *Vibrio cholerae*. *J. Bacteriol.* 200, e00005–18. doi: 10.1128/JB.00005-18

Fong, J. C. N., Syed, K. A., Klose, K. E., and Yildiz, F. H. (2010). Role of Vibrio polysaccharide (*vps*) genes in VPS production, biofilm formation and *Vibrio cholerae* pathogenesis. *Microbiology* 156, 757–2769. doi: 10.1099/mic.0.040196-0

Fullner, K. J., and Mekalanos, J. J. (2000). *In vivo* covalent cross-linking of cellular actin by the *Vibrio cholerae* RTX toxin. *EMBO J.* 19, 5315–5323. doi: 10.1093/emboj/19.20.5315

Gao, H., Xu, J., Lu, X., Li, J., Lou, J., Zhao, H., et al. (2018). Expression of hemolysin is regulated under the collective actions of HapR, Fur, and

HlyU in *Vibrio cholerae* El Tor serogroup O1. *Front. Microbiol.* 9:1310. doi: 10.3389/fmicb.2018.01310

Ghosh, A., Paul, K., and Chowdhury, R. (2006). Role of the histone-like nucleoid structuring protein in colonization, motility, and bile-dependent repression of virulence gene expression in *Vibrio cholerae*. *Infect. Immun.* 74, 3060–3064. doi: 10.1128/IAI.74.5.3060-3064.2006

Goldblum, S. E., Rai, U., Tripathi, A., Thakar, M., De Leo, L., Di Toro, N., et al. (2011). The active Zot domain (aa 288-293) increases ZO-1 and myosin 1C serine/threonine phosphorylation, alters interaction between ZO-1 and its binding partners, and induces tight junction disassembly through proteinase activated receptor 2 activation. *FASEB J.* 25,144–158. doi: 10.1096/fj.10-158972

Golin-Bisello, F., Bradbury, N., and Ameen, N. (2005). STa and cGMP stimulate CFTR translocation to the surface of villus enterocytes in rat jejunum and is regulated by protein kinase G. *Am. J. Physiol. Cell Physiol.* 289, C708–C716. doi: 10.1152/ajpcell.00544.2004

Gupta, S., Prasad, G. V., and Mukhopadhaya, A. (2015). *Vibrio cholerae* porin OmpU induces caspase-independent programmed cell death upon translocation to the host cell mitochondria. *J. Biol. Chem.* 290, 31051–31068. doi: 10.1074/jbc.M115.670182

Halang, P., Toulouse, C., Geißel, B., Michel, B., Flauger, B., Müller, M., et al. (2015). Response of *Vibrio cholerae* to the catecholamine hormones epinephrine and norepinephrine. *J. Bacteriol.* 197, 3769–3778. doi: 10.1128/JB.00345-15

Hammer, B. K., and Bassler, B. L. (2009). Distinct sensory pathways in *Vibrio cholerae* El Tor and classical biotypes modulate cyclic dimeric GMP levels to control biofilm formation. *J. Bacteriol.* 191, 169–177. doi: 10.1128/JB.01307-08

Harris, A. M., Bhuiyan, M. S., Chowdhury, F., Khan, A. I., Hossain, A., Kendall, E. A., et al. (2009). Antigen-specific memory B-cell responses to *Vibrio cholerae* O1 infection in Bangladesh. *Infect. Immun.* 77, 3850–3856. doi: 10.1128/IAI.00369-09

Harris, J. B. (2018). Cholera: immunity and prospects in vaccine development. *J. Infect. Dis.* 218, S141–S146. doi: 10.1093/infdis/jiy414

Harris, J. B., LaRocque, R. C., Chowdhury, F., Khan, A. I., Logvinenko, T., Faruque, A. S., et al. (2008). Susceptibility to *Vibrio cholerae* infection in a cohort of household contacts of patients with cholera in Bangladesh. *PLoS Negl. Trop. Dis.* 2:e221. doi: 10.1371/journal.pntd.0000221

Hay, A. J., Yang, M., Xia, X., Liu, Z., Hammons, J., Fenical, W., et al. (2016). Calcium enhances bile salt-dependent virulence activation in *Vibrio cholerae*. *Infect. Immun.* 85, e00707–e00716. doi: 10.1128/IAI.00707-16

Herzog, R., Peschek, N., Fröhlich, K. S., Schumacher, K., and Papenfort, K. (2019). Three autoinducer molecules act in concert to control virulence gene expression in *Vibrio cholerae*. *Nucleic Acids Res.* 47, 3171–3183. doi: 10.1093/nar/gky1320

Hindré, T., Knibbe, C., Beslon, G., and Schneider, D. (2012). New insights into bacterial adaptation through *in vivo* and *in silico* experimental evolution. *Nat. Rev. Microbiol.* 10, 352–365. doi: 10.1038/nrmicro2750

Ho, B. T., Dong, T. G., and Mekalanos, J. J. (2014). A view to a kill: the bacterial type VI secretion system. *Cell Host Microbe.* 15, 9–21. doi: 10.1016/j.chom.2013.11.008

Hsiao, A., Toscano, K., and Zhu, J. (2008). Post-transcriptional cross-talk between pro-and anti-colonization pili biosynthesis systems in *Vibrio cholerae*. *Mol. Microbiol.* 67, 849–860. doi: 10.1111/j.1365-2958.2007.06091.x

Huang, X., Duddy, O. P., Silpe, J. E., Paczkowski, J. E., Cong, J., Henke, B. R., et al. (2020). Mechanism underlying autoinducer recognition in the *Vibrio cholerae* DPO-VqmA quorum-sensing pathway. *J. Biol. Chem.* 295, 2916–2931. doi: 10.1074/jbc.RA119.012104

Hung, D. T., and Mekalanos, J. J. (2005). Bile acids induce cholera toxin expression in *Vibrio cholerae* in a ToxT-independent manner. *Proc. Natl. Acad. Sci. U. S. A.* 102, 3028–3033. doi: 10.1073/pnas.0409559102

Jørgensen, R., Purdy, A. E., Fieldhouse, R. J., Kimber, M. S., Bartlett, D. H., and Merrill, A. R. (2008). Cholix toxin, a novel ADP-ribosylating factor from *Vibrio cholerae*. *J. Biol. Chem.* 283, 10671–10678. doi: 10.1074/jbc.M710008200

Joshi, A., Kostiuk, B., Rogers, A., Teschler, J., Pukatzki, S., and Yildiz, F. H. (2017). Rules of engagement: the type VI secretion system in *Vibrio cholerae*. *Trends Microbiol.* 25, 267–279. doi: 10.1016/j.tim.2016.12.003

Joshi, A., Mahmoud, S. A., Kim, S. K., Ogdahl, J. L., Lee, V. T., Chien, P., et al. (2020). c-di-GMP inhibits LonA-dependent proteolysis of TfoY in *Vibrio cholerae*. *PLoS Gen.* 16:e1008897. doi: 10.1371/journal.pgen.1008897

Kanoktippornchai, B., Chomvarin, C., Hahnvajanawong, C., and Nutrawong, T. (2014). Role of *hlyA*-positive *Vibrio cholerae* non-O1/non-O139 on apoptosis and cytotoxicity in a Chinese hamster ovary cell line. *Southeast Asian J. Trop. Med. Public Health.* 45, 1365–1375.

Kharlanova, N. G., Lomov, Y. M., Bardykh, I. D., Monakhova, E. V., and Bardakhch'yan, E. A. (2004). Ultrastructural evidence of invasive activity of *Vibrio cholerae*. *Bull. Exp. Biol. Med.* 137, 403–406. doi: 10.1023/B:BEBM.0000035143.55617.04

Khilwani, B., Mukhopadhaya, A., and Chattopadhyay, K. (2015). Transmembrane oligomeric form of *Vibrio cholerae* cytolysin triggers TLR2/TLR6-dependent proinflammatory responses in monocytes and macrophages. *Biochem. J.* 466, 147–161. doi: 10.1042/BJ20140718

Kim, H. Y., Yu, S. M., Jeong, S. C., Yoon, S. S., and Oh, Y. T. (2018). Effects of *flaC* mutation on stringent response-mediated bacterial growth, toxin production, and motility in *Vibrio cholerae*. *J. Microbiol. Biotechnol.* 28, 816–820. doi: 10.4014/jmb.1712.12040

Kovacikova, G., and Skorupski, K. (2000). Differential activation of the *tcpPH* promoter by AphB determines biotype specificity of virulence gene expression in *Vibrio cholerae*. *J. Bacteriol.* 182, 3228–3238. doi: 10.1128/JB.182.11.3228-3238.2000

Kovacikova, G., and Skorupski, K. (2002). Regulation of virulence gene expression in *Vibrio cholerae* by quorum sensing: HapR functions at the *aphA* promoter. *Mol. Microbiol.* 46, 1135–1147. doi: 10.1046/j.1365-2958.2002.03229.x

Krishnan, H. H., Ghosh, A., Paul, K., and Chowdhury, R. (2004). Effect of anaerobiosis on expression of virulence factors in *Vibrio cholerae*. *Infect. Immun.* 72, 3961–3967. doi: 10.1128/IAI.72.7.3961-3967.2004

Krukonis, E. S., and DiRita, V. J. (2003). From motility to virulence: sensing and responding to environmental signals in *Vibrio cholerae*. *Curr. Opin. Microbiol.* 6, 186–190. doi: 10.1016/S1369-5274(03)00032-8

Krukonis, E. S., Yu, R. R., and Dirita, V. J. (2000). The *Vibrio cholerae* ToxR/TcpP/ToxT virulence cascade: distinct roles for two membrane-localized transcriptional activators on a single promoter. *Mol. Microbiol.* 38, 67–84. doi: 10.1046/j.1365-2958.2000.02111.x

Kudryashov, D. S., Durer, Z. A., Ytterberg, A. J., Sawaya, M. R., Pashkov, I., Prochazkova, K., et al. (2008). Connecting actin monomers by iso-peptide bond is a toxicity mechanism of the *Vibrio cholerae* MARTX toxin. *Proc. Natl. Acad. Sci. U. S. A.* 105, 18537–18542. doi: 10.1073/pnas.0808082105

Lee, Y. L., Hung, P. P., Tsai, C. A., Lin, Y. H., Liu, C. E., and Shi, Z. Y. (2007). Clinical characteristics of non-O1/non-O139 *Vibrio cholerae* isolates and polymerase chain reaction analysis of their virulence factors. *J. Microbiol. Immunol. Infect.* 40, 474–480.

Lembke, M., Pennetzdorfer, N., Tutz, S., Koller, M., Vorkapic, D., Zhu, J., et al. (2018). Proteolysis of ToxR is controlled by cysteine-thiol redox state and bile salts in *Vibrio cholerae*. *Mol. Microbiol.* 110, 796–810. doi: 10.1111/mmi.14125

Lenz, D. H., and Bassler, B. L. (2007). The small nucleoid protein Fis is involved in *Vibrio cholerae* quorum sensing. *Mol. Microbiol.* 63, 859–871. doi: 10.1111/j.1365-2958.2006.05545.x

Levinson, K. J., Baranova, D. E., and Mantis, N. J. (2016). A monoclonal antibody that targets the conserved core/lipid A region of lipopolysaccharide affects motility and reduces intestinal colonization of both classical and El Tor *Vibrio cholerae* biotypes. *Vaccine* 34, 5833–5836. doi: 10.1016/j.vaccine.2016.10.023

Liang, W., Pascual-Montano, A., Silva, A. J., and Benitez, J. A. (2007). The cyclic AMP receptor protein modulates quorum sensing, motility and multiple genes that affect intestinal colonization in *Vibrio cholerae*. *Microbiology* 153, 2964–2975. doi: 10.1099/mic.0.2007/006668-0

Linhartová, I., Bumba, L., Mašín, J., Basler, M., Osička, R., Kamanová, J., et al. (2010). RTX proteins: a highly diverse family secreted by a common mechanism. *FEMS Microbiol Rev.* 34, 1076–1112. doi: 10.1111/j.1574-6976.2010.00231.x

Liu, Z., Yang, M., Peterfreund, G. L., Tsou, A. M., Selamoglu, N., Daldal, F., et al. (2011). *Vibrio cholerae* anaerobic induction of virulence gene expression is controlled by thiol based switches of virulence regulator AphB. *Proc. Natl. Acad. Sci. U. S. A.* 108, 810–815. doi: 10.1073/pnas.1014640108

Lupardus, P. J., Shen, A., Bogyo, M., and Garcia, K. C. (2008). Small molecule-induced allosteric activation of the *Vibrio cholerae* RTX cysteine protease domain. *Science* 322, 265–268. doi: 10.1126/science.1162403

Mandal, S., and Chatterjee, N. S. (2016). *Vibrio cholerae* GbpA elicits necrotic cell death in intestinal cells. *J. Med. Microbiol.* 65, 837–847. doi: 10.1099/jmm.0.000298

Maraki, S., Christidou, A., Anastasaki, M., and Scoulica, E. (2016). Non-O1, non-O139 *Vibrio cholerae* bacteremic skin and soft tissue infections. *Infect. Dis.* 48, 171–176. doi: 10.3109/23744235.2015.1104720

Martinez, R. M., Jude, B. A., Kirn, T. J., Skorupski, K., and Taylor, R. K. (2010). Role of FlgT in anchoring the flagellum of *Vibrio cholerae*. *J. Bacteriol.* 192, 2085–2092. doi: 10.1128/JB.01562-09

Mathur, J., and Waldor, M. K. (2004). The *Vibrio cholerae* ToxR-regulated porin OmpU confers resistance to antimicrobial peptides. *Infect. Immun.* 72, 3577–3583. doi: 10.1128/IAI.72.6.3577-3583.2004

Mey, A. R., Butz, H. A., and Payne, S. M. (2015). *Vibrio cholerae* CsrA regulates ToxR levels in response to amino acids and is essential for virulence. *mBio* 6:e01064. doi: 10.1128/mBio.01064-15

Midani, F. S., Weil, A. A., Chowdhury, F., Begum, Y. A., Khan, A. I., Debela, M. D., et al. (2018). Human gut microbiota predicts susceptibility to *Vibrio cholerae* infection. *J. Infect. Dis.* 218, 645–653. doi: 10.1093/infdis/jiy192

Midgett, C. R., Almagro-Moreno, S., Pellegrini, M., Taylor, R. K., Skorupski, K., and Kull, F. J. (2017). Bile salts and alkaline pH reciprocally modulate the interaction between the periplasmic domains of *Vibrio cholerae* ToxR and ToxS. *Mol. Microbiol.* 105, 258–272. doi: 10.1111/mmi.13699

Miller, K. A., Chaand, M., Gregoire, S., Yoshida, T., Beck, L. A., Ivanov, A. I., et al. (2016b). Characterization of *V. cholerae* T3SS-dependent cytotoxicity in cultured intestinal epithelial cells. *Cell Microbiol.*18, 1857–1870. doi: 10.1111/cmi.12629

Miller, K. A., Sofia, M. K., Weaver, J., Seward, C. H., and Dziejman, M. (2016a). Regulation by ToxR-like proteins converges on $vttR_B$ expression to control Type 3 secretion system-dependent Caco2-BBE cytotoxicity in *Vibrio cholerae*. *J. Bacteriol.* 198, 1675–1682. doi: 10.1128/JB.00130-16

Miyata, S. T., Unterweger, D., Rudko, S. P., and Pukatzki, S. (2013). Dual expression profile of type VI secretion system immunity genes protects pandemic *Vibrio cholerae*. *PLoS Pathog.* 9:e1003752. doi: 10.1371/journal.ppat.1003752

Moisi, M., Jenul, C., Butler, S. M., New, A., Tutz, S., Reidl, J., et al. (2009). A novel regulatory protein involved in motility of *Vibrio cholerae*. *J. Bacteriol.* 191, 7027–7038. doi: 10.1128/JB.00948-09

Mondal, A., Tapader, R., Chatterjee, N. S., Ghosh, A., Sinha, R., Koley, H., et al. (2016). Cytotoxic and inflammatory responses induced by outer membrane vesicle-associated biologically active proteases from *Vibrio cholerae*. *Infect. Immun.* 84, 1478–1490. doi: 10.1128/IAI.01365-15

Morgan, S. J., Felek, S., Gadwal, S., Koropatkin, N. M., Perry, J. W., Bryson, A. B., et al. (2011). The two faces of ToxR: activator of *ompU*, co-regulator of *toxT* in *Vibrio cholerae*. *Mol. Microbiol.* 81, 113–128. doi: 10.1111/j.1365-2958.2011.07681.x

Morgan, S. J., French, E. L., Plecha, S. C., and Krukonis, E. S. (2019). The wing of the ToxR winged helix-turn-helix domain is required for DNA binding and activation of *toxT* and *ompU*. *PLoS ONE*. 14:e0221936. doi: 10.1371/journal.pone.0221936

Moschioni, M., Tombola, F., de Bernard, M., Coelho, A., Zitzer, A., Zoratti, M., et al. (2002). The *Vibrio cholerae* haemolysin anion channel is required for cell vacuolation and death. *Cell Microbiol.* 4, 397–409. doi: 10.1046/j.1462-5822.2002.00199.x

Nye, M. B., Pfau, J. D., Skorupski, K., and Taylor, R. K. (2000). *Vibrio cholerae* H-NS silences virulence gene expression at multiple steps in the ToxR regulatory cascade. *J. Bacteriol.* 182, 4295–4303. doi: 10.1128/JB.182.15.4295-4303.2000

Ogura, K., Terasaki, Y., Miyoshi-Akiyama, T., Terasaki, M., Moss, J., Noda, M., et al. (2017). *Vibrio cholerae* cholix toxin-induced HepG2 cell death is enhanced by tumor necrosis factor-alpha through ROS and intracellular signal-regulated kinases. *Toxicol Sci.* 156, 455–468. doi: 10.1093/toxsci/kfx009

Oh, Y. T., Lee, K. M., Bari, W., Kim, H. Y., Kim, H. J., and Yoon, S. S. (2016). Cholera toxin production induced upon anaerobic respiration is suppressed by glucose fermentation in *Vibrio cholerae*. *J. Microbiol. Biotechnol.* 26, 627–636. doi: 10.4014/jmb.1512.12039

Orimo, T., Sasaki, I., Hemmi, H., Ozasa, T., Fukuda-Ohta, Y., Ohta, T., et al. (2019). Cholera toxin B induces interleukin-1β production from resident peritoneal macrophages through the pyrin inflammasome as well as the NLRP3 inflammasome. *Int. Immunol.* 31, 657–668. doi: 10.1093/intimm/dxz004

Park, K. S., Ono, T., Rokuda, M., Jang, M. H., Okada, K., Iida, T., et al. (2004). Functional characterization of two type III secretion systems of *Vibrio parahaemolyticus*. *Infect. Immun.* 72, 6659–6665. doi: 10.1128/IAI.72.11.6659-6665.2004

Pérez-Reytor, D., Jaña, V., Pavez, L., Navarrete, P., and García, K. (2018). Accessory toxins of Vibrio pathogens and their role in epithelial disruptiond during infection. *Front Microbiol.* 9:2248. doi: 10.3389/fmicb.2018.02248

Prochazkova, K., and Satchell, K. J. (2008). Structure-function analysis of inositol hexakisphosphate-induced autoprocessing of the *Vibrio cholerae* multifunctional autoprocessing RTX toxin. *J. Biol. Chem.* 283, 23656–23664. doi: 10.1074/jbc.M803334200

Provenzano, D., and Klose, K. E. (2000). Altered expression of the ToxR-regulated porins OmpU and OmpT diminishes *Vibrio cholerae* bile resistance, virulence factor expression, and intestinal colonization. *Proc. Natl. Acad. Sci. U. S. A.* 97, 10220–10224. doi: 10.1073/pnas.170219997

Purdy, A. E., Balch, D., Lizárraga-Partida, M. L., Islam, M. S., Martinez-Urtaza, J., Huq, A., et al. (2010). Diversity and distribution of cholix toxin, a novel ADP-ribosylating factor from *Vibrio cholerae*. *Environ. Microbiol. Rep.* 2, 198–207. doi: 10.1111/j.1758-2229.2010.00139.x

Queen, J., Agarwal, S., Dolores, J. S., Stehlik, C., and Satchell, K. J. (2015). Mechanisms of inflammasome activation by *Vibrio cholerae* secreted toxins vary with strain biotype. *Infect. Immun.* 83, 2496–2506. doi: 10.1128/IAI.02461-14

Queen, J., and Satchell, K. J. (2012). Neutrophils are essential for containment of *Vibrio cholerae* to the intestine during the proinflammatory phase of infection. *Infect. Immun.* 80, 2905–2913. doi: 10.1128/IAI.00356-12

Queen, J., and Satchell, K. J. (2013). Promotion of colonization and virulence by cholera toxin is dependent on neutrophils. *Infect. Immun.* 81, 3338–3345. doi: 10.1128/IAI.00422-13

Rai, A. K., and Chattopadhyay, K. (2015). Revisiting the membrane interaction mechanism of a membrane-damaging β-barrel ore-forming toxin *Vibrio cholerae* cytolysin. *Mol. Microbiol.* 97, 1051–1062. doi: 10.1111/mmi.13084

Ramamurthy, T., Mutreja, A., Weill, F. X., Das, B., Ghosh, A., and Nair, G. B. (2019). Revisiting the global epidemiology of cholera in conjunction with the genomics of *Vibrio cholerae*. *Front. Public Health.* 7:203. doi: 10.3389/fpubh.2019.00203

Ramamurthy, T., Yamasaki, S., Takeda, Y., and Nair, G. B. (2003). *Vibrio cholerae* O139 Bengal: odyssey of a fortuitous variant. *Microbes Infect.* 5, 329–344. doi: 10.1016/S1286-4579(03)00035-2

Reichow, S. L., Korotkov, K. V., Gonen, M., Sun, J., Delarosa, J. R., Hol, W. G., et al. (2011). The binding of cholera toxin to the periplasmic vestibule of the type II secretion channel. *Channels* 5, 215–218. doi: 10.4161/chan.5.3.15268

Ribet, D., and Cossart, P. (2015). How bacterial pathogens colonize their hosts and invade deeper tissues. *Microbes Infect.* 17, 173–183. doi: 10.1016/j.micinf.2015.01.004

Ritter, A. S., Chowdhury, F., Franke, M. F., Becker, R. L., Bhuiyan, T. R., and Khan, A. I. (2019). Vibriocidal titer and protection from cholera in children. *Open Forum Infect. Dis.* 6:ofz057. doi: 10.1093/ofid/ofz057

Rothenbacher, F. P., and Zhu, J. (2014). Efficient responses to host and bacterial signals during *Vibrio cholerae* colonization. *Gut Microbes.* 5, 120–128. doi: 10.4161/gmic.26944

Rutherford, S. T., van Kessel, J. C., Shao, Y., and Bassler, B. L. (2011). AphA and LuxR/HapR reciprocally control quorum sensing in vibrios. *Genes Dev.* 25, 397–408. doi: 10.1101/gad.2015011

Sandkvist, M. (2001). Type II secretion and pathogenesis. *Infect. Immun.* 69, 3523–3535. doi: 10.1128/IAI.69.6.3523-3535.2001

Selvaraj, P., Gupta, R., and Peterson, K. M. (2015). The *Vibrio cholerae* ToxR regulon encodes host-specific chemotaxis proteins that function in intestinal colonization. *SOJ Microbiol. Infect. Dis.* 3:10. doi: 10.15226/sojmid/3/3/00141

Sengupta, N., Paul, K., and Chowdhury, R. (2003). The global regulator ArcA modulates expression of virulence factors in *Vibrio cholerae*. *Infect. Immun.* 71, 5583–5589. doi: 10.1128/IAI.71.10.5583-5589.2003

Shao, Y., and Bassler, B. L. (2012). Quorum-sensing non-coding small RNAs use unique pairing regions to differentially control mRNA targets. *Mol. Microbiol.* 83, 599–611. doi: 10.1111/j.1365-2958.2011.07959.x

Shao, Y., and Bassler, B. L. (2014). Quorum regulatory small RNAs repress type VI secretion in *Vibrio cholerae*. *Mol. Microbiol.* 92, 921–930. doi: 10.1111/mmi.12599

Shi, M., Li, N., Xue, Y., Zhong, Z., and Yang, M. (2020). The 58th Cysteine of TcpP is essential for *Vibrio cholerae* virulence factor production and pathogenesis. *Front. Microbiol.* 11:118. doi: 10.3389/fmicb.2020.00118

Sikora, A. E., Zielke, R. A., Lawrence, D. A., Andrews, P. C., and Sandkvist, M. (2011). Proteomic analysis of the *Vibrio cholerae* type II secretome reveals new proteins, including three related serine proteases. *J. Biol. Chem.* 286, 16555–16566. doi: 10.1074/jbc.M110.211078

Silva, A. J., and Benitez, J. A. (2004). Transcriptional regulation of *Vibrio cholerae* hemagglutinin/protease by the cyclic AMP receptor protein and RpoS. *J. Bact.* 186, 6374–6382. doi: 10.1128/JB.186.19.6374-6382.2004

Silva, A. J., Sultan, S. Z., Liang, W., and Benitez, J. A. (2008). Role of the histone-like nucleoid structuring protein in the regulation of *rpoS* and RpoS-dependent genes in *Vibrio cholerae*. *J. Bacteriol.* 190, 7335–7345. doi: 10.1128/JB.00360-08

Sloup, R. E., Konal, A. E., Severin, G. B., Korir, M. L., Bagdasarian, M. M., Bagdasarian, M., et al. (2017). Cyclic Di-GMP and VpsR induce the expression of type II secretion in *Vibrio cholerae*. *J. Bacteriol.* 199, e00106–e00107. doi: 10.1128/JB.00106-17

Somarny, W. M., Mariana, N. S., Neela, V., Rozita, R., and Raha, A. R. (2002). Optimization of parameters for accessory cholera enterotoxin (Ace) protein expression. *Med. Sci.* 2, 74–76. doi: 10.3923/jms.2002.74.76

Song, T., Sabharwal, D., and Wai, S. N. (2010). VrrA mediates Hfq-dependent regulation of OmpT synthesis in *Vibrio cholerae*. *J. Mol. Biol.* 400, 682–688. doi: 10.1016/j.jmb.2010.05.061

Stern, A. M., Hay, A. J., Liu, Z., Desland, F. A., Zhang, J., Zhong, Z., et al. (2012). The NorR regulon is critical for *Vibrio cholerae* resistance to nitric oxide and sustained colonization of the intestines. *mBio* 3, e00013–e00012. doi: 10.1128/mBio.00013-12

Syed, K. A., Beyhan, S., Correa, N., Queen, J., Liu, J., Peng, F., et al. (2009). The *Vibrio cholerae* flagellar regulatory hierarchy controls expression of virulence factors. *J. Bacteriol.* 191, 6555–6570. doi: 10.1128/JB.00949-09

Taylor, D. L., Bina, X. R., and Bina, J. E. (2012). *Vibrio cholerae* VexH encodes a multiple drug efflux pump that contributes to the production of cholera toxin and the toxin co-regulated pilus. *PLoS ONE.* 7:e38208. doi: 10.1371/journal.pone.0038208

Thomson, J. J., and Withey, J. H. (2014). Bicarbonate increases binding affinity of *Vibrio cholerae* ToxT to virulence gene promoters. *J. Bacteriol.* 196, 3872–3880. doi: 10.1128/JB.01824-14

Tischler, A. D., Lee, S. H., and Camilli, A. (2002). The *Vibrio cholerae vieSAB* locus encodes a pathway contributing to cholera toxin production. *J Bacteriol.* 184, 4104–4113. doi: 10.1128/JB.184.15.4104-4113.2002

Toulouse, C., Schmucker, S., Metesch, K., Pfannstiel, J., Michel, B., Starke, I., et al. (2019). Mechanism and impact of catecholamine conversion by *Vibrio cholerae*. *Biochim. Biophys Acta Bioenerg.* 1860, 478–487. doi: 10.1016/j.bbabio.2019.04.003

Trucksis, M., Conn, T. L., Wasserman, S. S., and Sears, C. L. (2000). *Vibrio cholerae* ACE stimulated Ca (2+)- dependent Cl(-)/HCO(3) (-) secretion in T84 cells *in vitro*. *Am. J. Physiol. Cell Physiol.* 279, C567–577. doi: 10.1152/ajpcell.2000.279.3.C567

Tsou, A. M., Frey, E. M., Hsiao, A., Liu, Z., and Zhu, J. (2008). Coordinated regulation of virulence by quorum sensing and motility pathways during the initial stages of *Vibrio cholerae* infection. *Commun. Integr. Biol.* 1, 42–44. doi: 10.4161/cib.1.1.6662

Tsou, A. M., and Zhu, J. (2010). Quorum sensing negatively regulates hemolysin transcriptionally and posttranslationally in *Vibrio cholerae*. *Infect. Immun.* 78, 461–467. doi: 10.1128/IAI.00590-09

Uzzau, S., Lu, R., Wang, W., Fiore, C., and Fasano, A. (2001). Purification and preliminary characterization of the zonula occludens toxin receptor from human (CaCo2) and murine (IEC6) intestinal cell lines. *FEMS Microbiol. Lett.* 194, 1–5. doi: 10.1111/j.1574-6968.2001.tb09437.x

Waldor, M. K., Rubin, E. J., Pearson, G. D., Kimsey, H., and Mekalanos, J. J. (1997). Regulation, replication, and integration functions of the *Vibrio cholerae* CTXphi are encoded by region RS2. *Mol. Microbiol.* 24, 917–926. doi: 10.1046/j.1365-2958.1997.3911758.x

Wang, H., Ayala, J. C., Benitez, J. A., and Silva, A. J. (2015). RNA-seq analysis identifies new genes regulated by the histone-like nucleoid structuring protein (H-NS) affecting *Vibrio cholerae* virulence, stress response and chemotaxis. *PLoS ONE.* 10:e0118295. doi: 10.1371/journal.pone.0118295

Watve, S., Barrasso, K., Jung, S. A., Davis, K. J., Hawver, L. A., Khataokar, A., et al. (2020). Parallel quorum-sensing system in *Vibrio cholerae* prevents signal interference inside the host. *PLoS Pathog.* 16:e1008313. doi: 10.1371/journal.ppat.1008313

Weiglmeier, P. R., Rösch, P., and Berkner, H. (2010). Cure and curse: *E. coli* heat-stable enterotoxin and its receptor guanylyl cyclase C. *Toxins.* 2, 2213–2229. doi: 10.3390/toxins2092213

Weil, A. A., Becker, R. L., and Harris, J. B. (2019). *Vibrio cholerae* at the intersection of immunity and the microbiome. *mSphere* 4, e00597–e00619. doi: 10.1128/mSphere.00597-19

Wibbenmeyer, J. A., Provenzano, D., Landry, C. F., Klose, K. E., and Delcour, A. H. (2002). *Vibrio cholerae* OmpU and OmpT porins are differentially affected by bile. *Infect. Immun.* 7, 121–126. doi: 10.1128/IAI.70.1.121-126.2002

Woida, P. J., and Satchell, K. J. F. (2020). The *Vibrio cholerae* MARTX toxin silences the inflammatory response to cytoskeletal damage before inducing actin cytoskeleton collapse. *Sci. Signal.* 13:eaaw9447. doi: 10.1126/scisignal.aaw9447

Wong, E., Vaaje-Kolstad, G., Ghosh, A., Hurtado-Guerrero, R., Konarev, P. V., Ibrahim, A. F., et al. (2012). The *Vibrio cholerae* colonization factor GbpA possesses a modular structure that governs binding to different host surfaces. *PLoS Pathog.* 8:e1002373. doi: 10.1371/journal.ppat.1002373

Wu, Z., Nybom, P., and Magnusson, K. E. (2000). Distinct effects of *Vibrio cholerae* haemagglutinin/protease on the structure and localization of the tight junction associated proteins occludin and ZO-1. *Cell Microbiol.* 2, 11–17. doi: 10.1046/j.1462-5822.2000.00025.x

Xu, X., Stern, A. M., Liu, Z., Kan, B., and Zhu, J. (2010). Virulence regulator AphB enhances toxR transcription in *Vibrio cholerae*. *BMC Microbiol.* 10:3. doi: 10.1186/1471-2180-10-3

Xue, Y., Tu, F., Shi, M., Wu, C. Q., Ren, G., Wang, X., et al. (2016). Redox pathway sensing bile salts activates virulence gene expression in *Vibrio cholerae*. *Mol. Microbiol.* 102, 909–924. doi: 10.1111/mmi.13497

Yahiro, K., Ogura, K., Terasaki, Y., Satoh, M., Miyagi, S., Terasaki, M., et al. (2019). Cholix toxin, an eukaryotic elongation factor 2 ADP-ribosyltransferase, interacts with prohibitins and induces apoptosis with mitochondrial dysfunction in human hepatocytes. *Cell. Microbiol.* 21:e13033. doi: 10.1111/cmi.13033

Yamai, S., Okitsu, T., Shimada, T., and Kaatsube, Y. (1997). Serogroup of *Vibrio cholerae* non-O1/non-O139 with specific reference to their ability to produce cholera toxin and addition of novel serogroups. *J. Jpn. Infect. Dis.* 71, 1037–1045. doi: 10.11150/kansenshogakuzasshi1970.71.1037

Yanez, M. E., Korotkov, K. V., Abendroth, J., and Hol, W. G. (2008). Structure of the minor pseudopilin EpsH from the Type 2 secretion system of *Vibrio cholerae*. *J. Mol. Biol.* 377, 91–103. doi: 10.1016/j.jmb.2007.08.041

Yang, J. S., Jeon, J. H., Jang, M. S., Kang, S. S., Ahn, K. B., Song, M., et al. (2018). *Vibrio cholerae* OmpU induces IL-8 expression in human intestinal epithelial cells. *Mol. Immunol.* 93, 47–54. doi: 10.1016/j.molimm.2017.11.005

Yang, M., Liu, Z., Hughes, C., Stern, A. M., Wang, H., Zhong, Z., et al. (2013). Bile salt-induced intermolecular disulfide bond formation activates *Vibrio cholerae* virulence. *Proc. Natl. Acad. Sci. U. S. A.* 110, 2348–2353. doi: 10.1073/pnas.1218039110

Yoon, M. Y., Min, K. B., Lee, K. M., Yoon, Y., Kim, Y., Oh, Y. T., et al. (2016). A single gene of a commensal microbe affects host susceptibility to enteric infection. *Nat. Commun.* 7:11606. doi: 10.1038/ncomms11606

You, J. S., Yong, J. H., Kim, G. H., Moon, S., Nam, K. T., Ryu, J. H., et al. (2019). Commensal-derived metabolites govern *Vibrio cholerae* pathogenesis in host intestine. *Microbiome* 7:132. doi: 10.1186/s40168-019-0746-y

Yu, R. R., and DiRita, V. J. (2002). Regulation of gene expression in *Vibrio cholerae* by ToxT involves both antirepression and RNA polymerase stimulation. *Mol. Microbiol.* 4, 119–134. doi: 10.1046/j.1365-2958.2002.02721.x

Zhang, L., Krachler, A. M., Broberg, C. A., et al. (2012). Type III effector VopC mediates invasion for *Vibrio* species. *Cell Rep.* 1, 453–460. doi: 10.1016/j.celrep.2012.04.004

Zhang, X., Lu, Y., Qian, H., Liu, G., Mei, Y., Jin, F., et al. (2020). Non-O1, Non-O139 *Vibrio cholerae* (NOVC) bacteremia: case report and literature review, 2015–2019. *Infect. Drug Resist.* 13, 1009–1016. doi: 10.2147/IDR.S245806

Zheng, J., Shin, O. S., Cameron, D. E., and Mekalanos, J. J. (2010). Quorum sensing and a global regulator TsrA control expression of type VI secretion and virulence in *Vibrio cholerae*. *Proc. Natl. Acad. Sci.U. S. A.* 107, 21128–22133. doi: 10.1073/pnas.1014998107

Zhu, J., Miller, M. B., Vance, R. E., Dziejman, M., Bassler, B. L., and Mekalanos, J. J. (2002). Quorum-sensing regulators control virulence gene expression in *Vibrio cholerae*. *Proc. Natl. Acad. Sci. U. S. A.* 99, 3129–3134. doi: 10.1073/pnas.052694299

Conflict of Interest: The authors declare that the research was conducted in the absence of any commercial or financial relationships that could be construed as a potential conflict of interest.

frontiers in Cellular and Infection Microbiology

REVIEW
published: 06 October 2020
doi: 10.3389/fcimb.2020.561296

Vibrio Pathogenicity Island-1: The Master Determinant of Cholera Pathogenesis

Ashok Kumar[1,2], *Bhabatosh Das*[1,2*] *and Niraj Kumar*[1,2*]

[1] *Translational Health Science and Technology Institute, Faridabad, India,* [2] *Centre for Doctoral Studies, Advanced Research Centre, Manipal Academy of Higher Education, Manipal, India*

Cholera is an acute secretory diarrhoeal disease caused by the bacterium *Vibrio cholerae*. The key determinants of cholera pathogenicity, cholera toxin (CT), and toxin co-regulated pilus (TCP) are part of the genome of two horizontally acquired Mobile Genetic Elements (MGEs), CTXΦ, and Vibrio pathogenicity island 1 (VPI-1), respectively. Besides, *V. cholerae* genome harbors several others MGEs that provide antimicrobial resistance, metabolic functions, and other fitness traits. VPI-1, one of the most well characterized genomic island (GI), deserved a special attention, because (i) it encodes many of the virulence factors that facilitate development of cholera (ii) it is essential for the acquisition of CTXΦ and production of CT, and (iii) it is crucial for colonization of *V. cholerae* in the host intestine. Nevertheless, VPI-1 is ubiquitously present in all the epidemic *V. cholerae* strains. Therefore, to understand the role of MGEs in the evolution of cholera pathogen from a natural aquatic habitat, it is important to understand the VPI-1 encoded functions, their acquisition and possible mode of dissemination. In this review, we have therefore discussed our present understanding of the different functions of VPI-1 those are associated with virulence, important for toxin production and essential for the disease development.

Keywords: cholera pathogenesis, mobile genetic elements (MGEs), VPI-1, quorum sensing, toxin co-regulated pilus

OPEN ACCESS

Edited by:
Yang Fu,
Southern University of Science and Technology, China

Reviewed by:
Jiandong Chen,
University of Pennsylvania, United States
Zhi Liu,
Huazhong University of Science and Technology, China

****Correspondence:***
Niraj Kumar
nkumar@thsti.res.in
Bhabatosh Das
bhabatosh@thsti.res.in

Specialty section:
This article was submitted to Molecular Bacterial Pathogenesis, a section of the journal Frontiers in Cellular and Infection Microbiology

Received: *12 May 2020*
Accepted: *11 September 2020*
Published: *06 October 2020*

Citation:
Kumar A, Das B and Kumar N (2020) Vibrio Pathogenicity Island-1: The Master Determinant of Cholera Pathogenesis. Front. Cell. Infect. Microbiol. 10:561296. doi: 10.3389/fcimb.2020.561296

INTRODUCTION

Cholera is an acute gastrointestinal diarrheal disease that is caused by a bacterium, *Vibrio cholerae* (Kaper et al., 1995). The complete genome sequences of clinical and environmental strains of *V. cholerae* revealed that their genome consists of two circular non-homologous chromosomes that carry nearly 3,900 open reading frames (ORFs). Both the chromosomes of *V. cholerae* consist of core and acquired genomes. The acquired genome of *V. cholerae* harbor several mobile genetic elements (MGEs) and linked with DNA mobility genes and other metabolic functions (Mutreja et al., 2011). Almost all the 7th pandemic *V. cholerae* strains harbor four pathogenicity islands namely (i) Vibrio pathogenicity island-1 (VPI-1), ∼41.3 kb in size (ii) Vibrio pathogenicity island-2 (VPI-2), ∼57 kb in size, (iii) Vibrio seventh pandemic island-I (VSP-1), ∼16 kb in size, and (iv) Vibrio seventh pandemic island-2 (VSP-2), ∼26.9 kb in size (Heidelberg et al., 2000). Virulence functions of cholera pathogens are not endogenous, but they are part of the acquired MGEs.

V. cholerae strains devoid of CTXΦ or VPI-1, two important MGEs ubiquitously present in the toxigenic strains, are non-toxigenic and can't develop cholera in animal model and human volunteer (Pang et al., 2007). Like other bacterial species MGEs present in the genome of *V. cholerae* have several typical characteristics of horizontally acquired elements such as (i) sporadic distribution (ii) encode DNA recombinases (iii) located in *tRNA/ssrA* or *dif* loci (iv) direct repeat sequences at the borders (v) distinct GC content and (vi) unstable.

In this review, we discuss dynamics of VPI-1; different functions encoded by the VPI-1 linked with its mobility and modulate the virulence cascades. Special focus is given to understand how VPI-1 contributed in the emergence of toxigenic pandemic strains.

THE PATHOGEN (*V. cholerae*) AND INTEGRATIVE MOBILE GENETIC ELEMENTS (MGEs)

Over the period, *V. cholera* has evolved as one of the most successful pathogen in the history of mankind. To attain the fitness for survival, the pathogen has acquired a number of MGEs belongs to different classes such as prophages (CTXΦ, VGJΦ, RS1, TLCΦ), pathogenicity islands (VPI-1, VPI-2, VSP-1 & VSP-2) and integrative conjugative elements (ICEs) (**Table 1**). The key virulence factor of cholera, cholera toxin (CT) is encoded by the *ctxA* and *ctxB* genes that induces the secretion of fluid and electrolytes from the intestinal epithelial cells and causes the diarrhea. CT is acquired through irreversible integration of a single stranded DNA (+ssDNA) phage CTXΦ into the *dif* sites of either or both the chromosome of *V. cholerae* (Val et al., 2005). The second most crucial virulence factor of cholera pathogen, toxin-coregulated pilus (TCP), encoded by the genes present in the TCP locus of VPI-1, helps the pathogen in colonization in the gastrointestinal tract of the host and also act as a cell surface receptor for CTXΦ (Manning, 1997). This altogether suggests that the acquisition of the MGEs is the key for the fitness and evolution of the cholera pathogen for different pandemics. Therefore, understanding the role of MGEs acquired by pathogen over time is critical to develop strategies for managing the patient and the disease.

CHOLERA AND ITS INDISPENSIBLE ASSOCIATION WITH VPI-1

The first cholera pandemic was recorded in 1817 and seven pandemics have been recorded till to date (**Figure 1**) (Hu et al., 2016). The ongoing 7th pandemic was first evolved on the island of Sulawesi in Indonesia in 1961 (Karaolis et al., 1995). All of the seven cholera pandemics are caused by the O1 serotype of *V. cholerae*, except the spatial emergences of O139 Bengal in eastern part of India and Bangladesh in 1992 (Johnson et al., 1994). Interestingly, all of these pathogenic strains harbored VPI-1 as well as CTXΦ in their chromosomes (Li et al., 2003). Since VPI-1 encoded TcpA acts as a receptor for CTXΦ, sequential acquisition of VPI-1 and CTXΦ probably convert the environmental *V. cholerae* strains into toxigenic strains. Although no such experimental evidences or validation or natural phenomenon has been reported yet (Singh et al., 2001). But this is most accepted hypothesis across the scientific community that environmental *V. cholerae* strain may become pathogenic if it acquires VPI-1 and CTXΦ. Besides, loss of VPI-1 could revert a pathogenic strain into a non-pathogenic strain. Other than VPI-1 and CTXΦ, *V. cholerae* O1 El Tor biotype strains have acquired RS1 element (Choi et al., 2010) and two other pathogenicity-associated islands (VSP-1 & VSP-2). However, it is believed that RS1, VSP-1 & VSP-2 are not the pre-requisite for *V. cholerae* pathogenesis but involved in the fitness and robustness of 7th pandemic *V. cholerae* strains over the classical strain of O1 serotype.

VIBRIO PATHOGENICITY ISLAND-1 (VPI-1)

The Vibrio pathogenicity island-1 (VPI-1) is a ∼41.3 kb long DNA fragment present in all the epidemic strains including sixth-pandemic classical biotype and seventh-pandemic El Tor biotype strains. Previously, VPI-1 was experimentally demonstrated to be a filamentous bacteriophage (Karaolis et al., 1999). The authors reported that the cell-free preparations can transmit VPI-1 between *V. cholerae* strains by transduction. However, the protection of VPI-1 genomic DNA in a phage preparation from DNase and RNase treatment insisted the authors to conclude that the VPI-1 genes in the phage preparations are possibly wrapped with the protein coat TcpA. The authors further reported that replicative dsDNA genome of VPI-1 were detectable in toxigenic *V. cholerae* by DNA hybridization. However, no other laboratories were able to reproduce these findings (Faruque and Mekalanos, 2003). Nevertheless, the same group later on reported that VPI-1 is a pathogenicity island (Rajanna et al., 2003).

In the whole genome sequenced reference *V. cholerae* strain N16961, VPI-1 harbors 31 genes (*VC0817* to *VC0847*) with known and unknown functions (Rajanna et al., 2003) (**Table 2**, **Figure 2A**). Like other genomic islands, VPI-1 has following typical characteristics:

(i) Sporadic distribution among environmental isolates
(ii) Distinct GC content (35% of the total in VPI-1 alone)
(iii) Flanked by direct repeat sequences (30–31 bp); one at left (*attL*) and another at right (*attR*) borders
(iv) Located downstream of a tmRNA locus
(v) Encodes two DNA mobility enzymes; one transposase [VpiT encoded by *vpiT* (Gene Map ID: VC0817)] and one integrase [Int_{vpi} encoded by *intV* (Gene Map ID: VC0847)]
(vi) Harbors a number of virulence associated and accessory colonization factors.

The role of VPI-1 in the pathogenicity of cholera was identified while investigating the differences between pathogenic and non-pathogenic *V. cholerae* strains (Karaolis et al., 1998). Several proteins (ToxT, TcpA, TcpP, TcpH, ACFs gene cluster) encoded by the VPI-1 are crucial for *V. cholerae* pathogenesis and justified the name of the genomic island as Vibrio pathogenicity islands.

TABLE 1 | Significance of integrative mobile genetic elements (IMGEs) in the *V. cholerae* pathogenesis and fitness.

S. no.	IMGEs	Size (kb)	Cholera pathogenesis				Brief description and function
			Required for conversion of environmental non-pathogenic strains to pathogenic clones	Colonization	Role in toxin production	Overall enhanced pathogenicity	
1.	CTXΦ	6.7	+	−	+	+	Integrates in the chromosome of *V. cholerae*, form stable lysogens and encodes cholera toxin Kimsey and Waldor, 1998
2.	RS1Φ	3	−	−	−	+	Carries gene for an anti-repressor RstC that effect CTXΦ replication Faruque et al., 2003a
3.	VGJΦ	7.5	−	−	−	+	Integrates into same *dif* site as CTXΦ Das et al., 2010
4.	TLCΦ	5.3	−	−	−	+	Generates a functional *dif* site in *dif* defective strains and facilitates stable integration of CTXΦ Hassan et al., 2010
5.	VPI-I	41.3	+	+	+	+	Encodes receptor for CTXΦ that also helps acquisition of the CTXΦ into the *V. cholerae*, bacterial colonization in the human-gut, regulates toxin production and helps the bacteria to achieve fitness in harsh environmental conditions Boyd et al., 2000
6.	VPI-II	57.3	−	−	−	+	Encodes neuraminidase which converts higher order sialogangliosides to GM-1 gangliosides, receptor for cholera toxin Jermyn and Boyd, 2002
7.	VSP-I	16	−	−	−	+	Encodes a putative XerCD like integrase Faruque and Mekalanos, 2003
8.	VSP-II	27	−	−	−	+	Encodes RNase H1 protein, a type IV pilus O'Shea et al., 2004

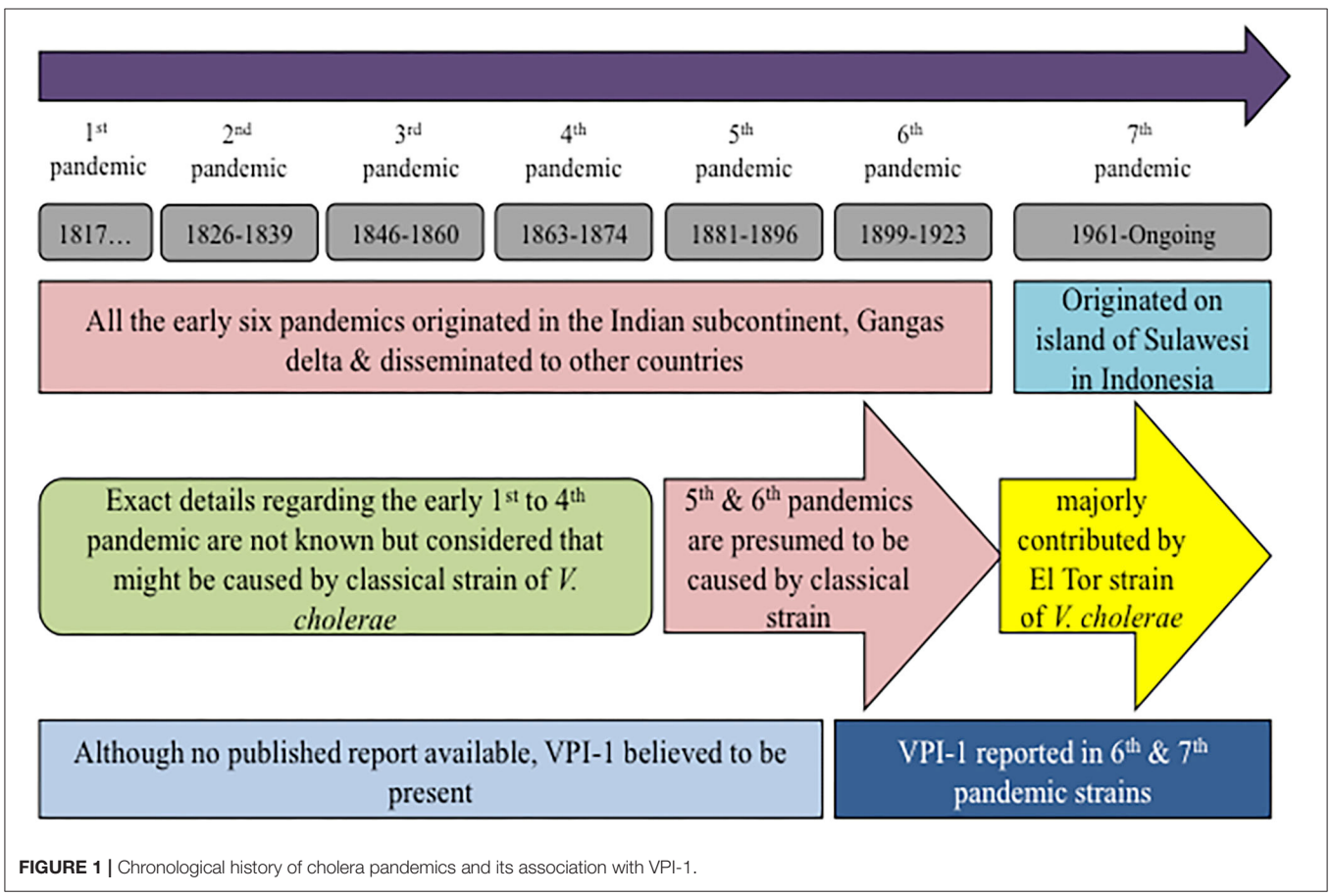

FIGURE 1 | Chronological history of cholera pandemics and its association with VPI-1.

TABLE 2 | Properties and function of VPI-1 encoded genes.

Gene map ID	Gene symbol	Size[#] (bp)	Mw (kDa)	Functions(s)
VC0817	*vpiT*	984	38.2	Transposase, mediates integration, and excision Faruque et al., 2003b
VC0818	N/A	680	N/A	Pseudo gene, function N/A
VC0819	*aldA*	1,440	52.7	Expressed under the control of ToxR and may be associated with virulence Mishra et al., 2003
VC0820	*tagA*	3,042	115.9	A mucinase, involved in modification of intestinal cells surface during *V. cholerae* infection Hammer and Bassler, 2003
VC0821	N/A	4,501	N/A	Pseudo gene, function N/A
VC0822	N/A	3,331	N/A	Hypothetical protein, function N/A
VC0823	N/A	939	N/A	Hypothetical protein, function N/A
VC0824	*tpx*	495	17.9	A thiol-specific peroxidase that protect *V. cholerae* cells against oxidative stress Cha et al., 2004
VC0825	*tcpI*	1,863	69.0	Negatively regulates the *tcpA* expression in non-permissive conditions and promotes colonization in response to environmental single and also maximize *tcpA* expression in permissive growth conditions Harkey et al., 1994
VC0826	*tcpP*	666	25.7	Transcriptional activator of *toxT* Hase and Mekalanos, 1998
VC0827	*tcpH*	411	15.2	Required for stability of TcpP Carroll et al., 1997
VC0828	*tcpA*	675	23.2	Receptor for CTXΦ, helps in forming micro-colonies and play role in intestinal colonization of *V. cholerae* Rhine and Taylor, 1994
VC0829	*tcpB*	1,293	47.1	Mediates uptake of CTXΦ in to *V. cholerae* cells and also initiate the assembly of TCP Gao et al., 2016
VC0830	*tcpQ*	453	17.2	Required for the stability of TcpC and also help in outer membrane localization Bose and Taylor, 2005
VC0831	*tcpC*	1,470	53.8	Encode outer membrane lipoprotein required for pilus biogenesis and provide resistance from host complement system.
VC0832	*tcpR*	456	17.7	Helps in high osmolality tolerance in intestinal lumen and promotes colonization Tripathi and Taylor, 2007
VC0833	*tcpD*	837	31.7	TCP pilus biogenesis Parsot et al., 1991
VC0834	*tcpS*	459	17.3	Essential for colonization Davies et al., 2012
VC0835	*tcpT*	1,512	57.2	A cognate putative ATPase located on inner membrane, required for TCP biogenesis and also for all other TCP-mediated functions Chang et al., 2017
VC0836	*tcpE*	1,023	38.0	Probably involved in cholera toxin receptor (GM1) interaction Kolappan and Craig, 2013
VC0837	*tcpF*	1,017	38.1	A soluble protein, role in colonization Megli et al., 2011
VC0838	*toxT*	831	32.0	Master regulator of virulence associated genes, directly activates expression of cholera toxin and TCP, and also auto-regulates its own expression Schuhmacher and Klose, 1999
VC0839	*tcpJ*	762	29.3	Encode type IV prepilin peptidase, required for the processing of TcpA Kaufman et al., 1991
VC0840	*acfB*	1,880	69.1	Required for intestinal colonization, disruption of any of the four genes exhibits 10-fold decreases in colonization Hughes et al., 1995; Klose, 2000
VC0841	*acfC*	771	28.5	
VC0844	*acfA*	648	24.6	
VC0845	*acfD*	4,562	167.8	
VC0843	*tagE*	909	34.4	Probably encodes an endo-peptidase Almagro-Moreno et al., 2010
VC0846	N/A	1,701	N/A	Pseudo gene, function N/A
VC0847	*intV*	1,269	48.3	Integrase, mediates integration and excision Kumar et al., 2018

[#]*Size and molecular weight are obtained from NCBI server and ExPASy portal of Swiss institute of Bioinformatics.*
N/A = Not available.

DISTRIBUTION OF VPI-1 IN *V. cholerae* ISOLATES

Genomic analyses of thousands of clinical *V. cholerae* isolates revealed that VPI-1 is widely conserved in the genome of all the epidemic and pandemic cholera pathogen (Mutreja et al., 2011; Domman et al., 2017; Weill et al., 2019). However, VPI-1 distribution is sporadic among nonO1-nonO139 environmental *V. cholerae* strain (Chun et al., 2009). Whole genome sequence analysis of environmental strains revealed that VPI-1 is absent in several isolates belonging to serogroup O37 (MZO-3), O39 (AM-19226), O12 (1587), O14 (MZO-2), O141 (V51), and O135 (RC 385). Interestingly, VPI-1 was detected in the nonO1-nonO139 environmental *V. cholerae* strains belonging to serogroup O141 (V51). The same group has also reported absence of VPI-1 in the genome of environmental O1 El Tor strains 12129 and TM11079-80 (Chun et al., 2009). As expected, the genome of all the VPI-1 negative *V. cholerae* strains are also negative for CTX-prophage. This finding indicates that VPI-1 is absolutely important for the conversion of a non-toxigenic strain to a toxigenic variant. In addition, VPI-1 encoded functions are also essential for colonization of cholera pathogen in the host intestine. Since, colonization and toxin are the sole components for development of cholera, VPI-1 is an indispensible component for the emergence and evolution of epidemic and pandemic *V. cholerae*.

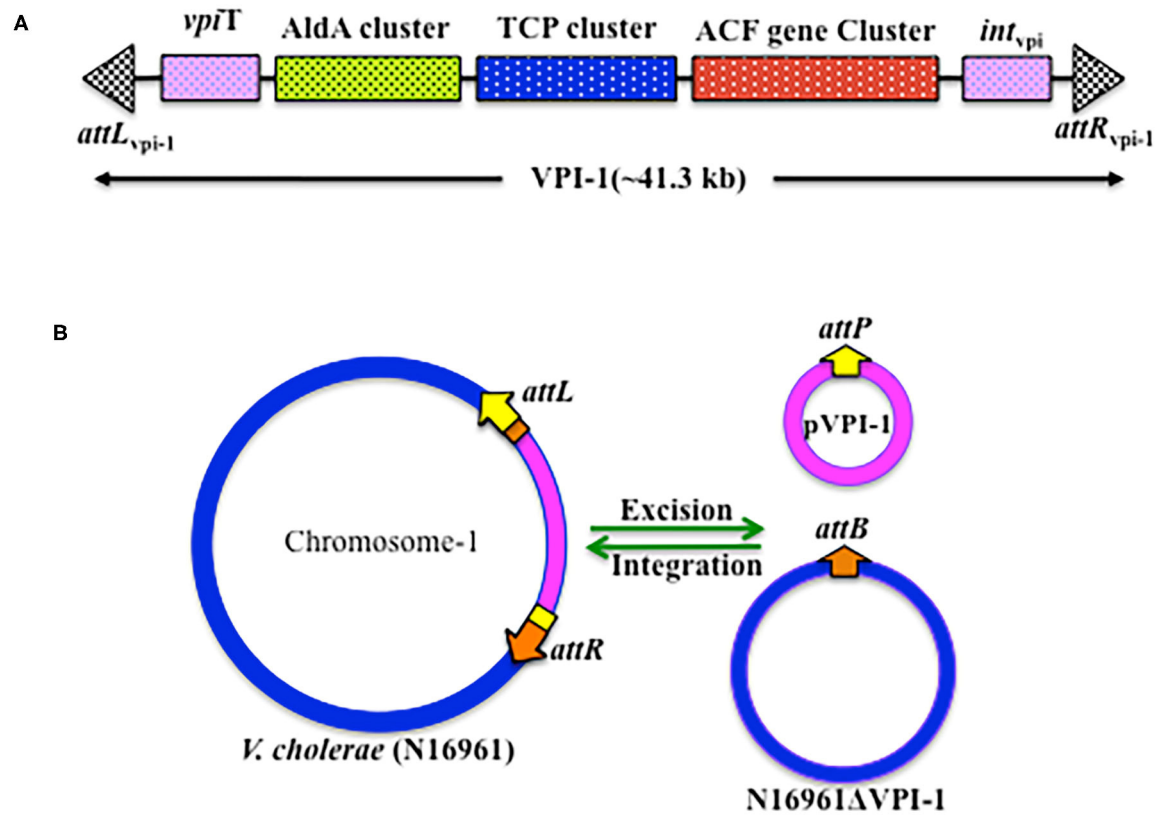

FIGURE 2 | Genetic organization of VPI-1. **(A)** Schematic representation of the VPI-1 genetic element, **(B)** Schematic representation of the integration and excision mechanisms of VPI-1 genetic element.

MOBILITY OF VPI-1: ACQUISITION AND DISSEMINATION

VPI-1 has been reported to precisely excise from the *V. cholerae* chromosome and form an extra-chromosomal circular product (Rajanna et al., 2003) (**Figure 2B**). However, this study could not provide information about the loss frequency of VPI-1 from the genome of *V. cholerae*. To address this issue, Kumar et al. (2018) have engineered the genome of *V. cholerae* and developed a reporter strain to monitor the loss frequency of VPI-1 and isolated VPI-1 devoid clone from a mixed population of *V. cholerae*. Authors used an antibiotic resistance gene (*cat*) as selectable marker and a sucrose sensitive confirming counter selectable gene (*sacB*) to tagged the VPI-1 element. The engineered strain was used to measure loss frequency of VPI-1 in *in vitro* (test tube) and *in vivo* (rabbit ileal loop model) growth conditions. *V. cholerae* cell containing functional *sacB* in the genome is unable to grown in room temperature (∼24°C) in the presence of excess sucrose (10–15%) sucrose in growth medium. Using the said vector, excision frequency of VPI-1 was investigated in the *in vitro*. VPI-1 was found highly stable in the animal model (excision frequency, $\sim10^{-9}$) compared to the *in vitro* laboratory growth condition (excision frequency, $\sim10^{-4}$) (Kumar et al., 2018).

The VPI-1 doesn't encode any known conjugative function. The pathogenicity island also has no *oriT* sequence. Thus, horizontal transmission of VPI-1 between different *V. cholerae* strains couldn't be through conjugation. Since *V. cholerae* is naturally competent (Meibom et al., 2005), the bacterium could uptake naked genomic DNA including VPI-1 through transformation. We believe that different *V. cholerae* serogroups living in the biofilms during aquatic and inflectional phases of its life cycle acquired MGEs through natural transformation. However, currently substantial experimental evidences are lacking to support this hypothesis. In another study, VPI-1 has also been shown to get transferred from *V. cholerae* O1 strain C6709 to VPI-negative *V. cholerae* isolates (468-83, GP6, V69, and 1528-79) by a generalized transducing phage CP-T1.This study proposed an alternative mode of dissemination of VPI-1 between *V. cholerae* strains (O'Shea and Boyd, 2002). Once inside the cell, both the tyrosine recombinases encoded by the VPI-1 helps the GI to integrate at the *prfC* locus by site-specific recombination. The reaction is reversible; hence the *attL* and *attR* sites generated due to integration of VPI-1 come together, possibly with the help of recombination directionality factors (RDFs), and excised from the chromosome.

Although VPI-1 has already been shown indispensable for *V. cholerae* pathogenicity, the molecular mechanisms and

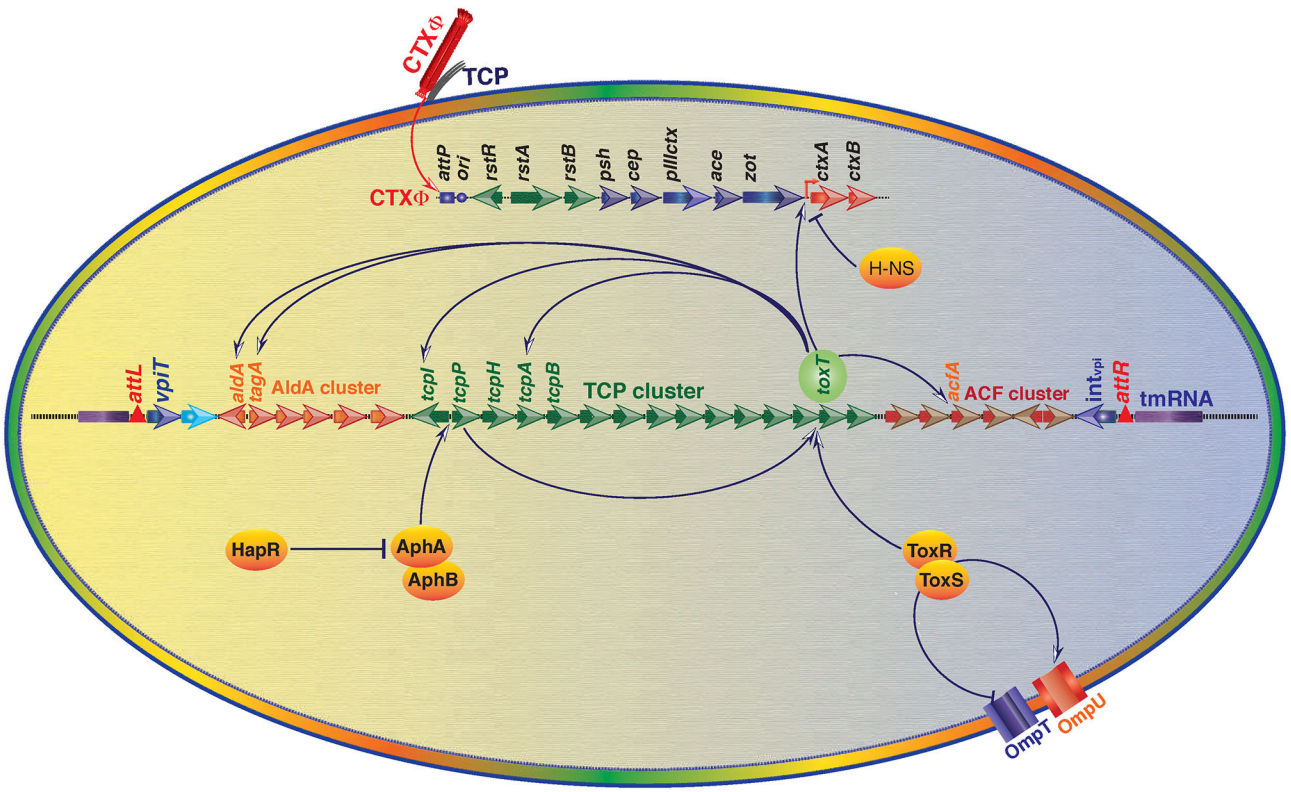

FIGURE 3 | An overview of regulation of *V. cholerae* virulence gene expression through Vibrio Pathogenicity Island 1 (VPI-1) and core genome encoded functions. Transcriptional factor ToxT is the key positive regulator of cholera toxin (CT) encoding genes *ctxA* and *ctxB*. ToxT also positively modulates expression of toxin co-regulated pilus (TCP) genes and several other genes located in the VPI-1. ToxR-ToxS and AphA-AphB proteins positively regulate expression of *toxT*. ToxR-ToxS proteins also modulate expression of outer membrane proteins OmpU and OmpT. Histone-like nucleoid-structuring (H-NS) protein negatively regulates expression of CT. Transcriptional regulator HapR negatively regulates expression of AphA and AphB encoding gene expression. Positive regulation is depicted by arrowhead and T head depicts negative regulation.

factors that modulate integration and excision of VPI-1 into chromosomes are still largely unknown.

VPI-1 AND CHOLERA PATHOGENESIS

Although CT is the crucial factor for developing cholera, but it is not the only virulence factor for developing the disease. There are several other virulence-associated factors (ToxT, TCP, AphAB, ToxRS) that also contribute substantially in cholera pathogenesis. Production of CT, and intestinal colonization of *V. cholerae* in the host intestine are pivotal for disease development (Krukonis et al., 2000). VPI-1 plays critical role in both the processes by encoding CT expression transcriptional factor ToxT and intestinal colonization factor TCP. Nevertheless, VPI-1 also plays crucial role in the acquisition of CT encoding gene through horizontal gene transfer. The detailed role of VPI-1 in cholera pathogenesis is as given below and depicted in **Figure 3**.

Acquisition of CTXΦ in *V. cholerae*

Acquisition of CTXΦ is the first and critical step for the conversion of a non-toxigenic *V. cholerae* strain into toxigenic clone. The VPI-1 encoded TCP is a homopolymer of multiple subunits of major pillin protein, TcpA. After its production, TcpA trans-located to the cell surface and serve as the receptor for the CTXΦ (Lim et al., 2010). Once CTXΦ recognizes TcpA pili on the surface, it injects it's (+)ssDNA genome in to the host cytoplasm of the host cell(s) (Karaolis et al., 1999). The (+)ssDNA genome of CTXΦ either converted into replicative double stranded pCTXΦ or exploits the two tyrosine recombinases, XerC and XerD, for irreversible integration into chromosomal DNA (Boyd, 2010). XerC and XerD recombinases are conserved among the bacteria chromosomes and their native function is to resolve the chromosome dimers. XerC and XerD recognize 28 bp *dif* sequences as a substrate to resolve the chromosomal dimers before cell division (Das et al., 2013). The CTXΦ has two *dif* like attachment sequences, *attP1* and *attP2*, on its pCTXΦ genome. In (+) ssDNA genome of CTXΦ both the attachment sites are separated by 90 bp DNA sequences. The single stranded genome of CTXΦ forms intra-strand base pairing and developed a double-forked hairpin like structure. The stem of the hairpin harbors a functional attachment site (+)*attP* resembles with the *dif1* and *dif2* site of *V. cholerae* chromosomes

(McLeod and Waldor, 2004). Due to similar DNA sequences between *dif* and (+)*attP*, the XerC and XerD recognizes the (+)*attP* as their binding substrate and mediate CTXΦ integration into the *dif* site by site specific recombination. Once the CTXΦ gets integrated into the chromosome, the host DNA replication machinery converts (+) ssDNA CTXΦ genome into double stranded. Once integrated, the dsDNA of prophage genome is unable to excise due to lack of two functional dif like sequences. This irreversible integration of CTXΦ into the chromosomal DNA of *V. cholerae* is one of the important events in the *V. cholerae* evolution as a pathogen. Tandemly integrated CTX-prophage can initiate rolling replication for production of new virion and disseminate to other *V. cholerae* cells. In addition to TcpA, several other VPI-1 functions including TcpB and TcpE helps acquisition and dissemination of CTXΦ (Gutierrez-Rodarte et al., 2019).

Intestinal Colonization of *V. cholerae*

V. cholerae is the natural inhabitant of estuaries where it can survive as free-living cells or as biofilms. The stomach is not a suitable environment for *V. cholerae* to survive and multiply since, the bacterium is highly sensitive to low pH (Almagro-Moreno et al., 2015). However, on ingestion with contaminated food/water, *V. cholerae* strains have the ability to pass through such adverse environments and colonized in the small intestine of human gut and produce sufficient amount of cholera toxin to develop the clinical symptoms.

Historically chemotactic movement was proposed to be responsible for colonization of *V. cholerae* (Castro-Rosas and Escartin, 2002), however various reports later suggested that intestinal colonization of *V. cholerae* is the complex outcome of interplay of VPI-1, chromosomally encoded proteins and host factors that are involved in motility, chemo-taxsis, and penetration. During the initial stages of colonization that is at the proximal ends of small intestine, bacterium flagellum, and a few general (neuraminidase etc.) and *V. cholerae*-specific proteolytic enzymes (haemagglutinin/protease, Hap) helps in the movement and penetration of thick mucosal layer (Zhu and Mekalanos, 2003). TagA, a VPI-1 encoded metalloprotease, is known to modify the mucin glycoproteins that are attached to the host cell surface (Szabady et al., 2011). TagA is specifically expressed and secreted by the pathogen under virulence-inducing conditions. TagA has been reported to be positively coregulated along with TCP and other virulence genes and hence may potentially play critical role in colonization of the pathogen by facilitating the movement through the intestinal mucosa (Szabady et al., 2011). Along with a few pathogen-derived adhesin molecules (i.e., flagellin, Mam7, GbpA, OmpU, and FrhA etc.), TCP is also reported to help the pathogen to adhere to the epithelium and facilitate bacteria-bacteria interaction to form micro-colonies (Tam et al., 2007). The aberrant production or function of the TCP has been shown to result in reduced colonization in both humans and mice. In addition, other four VPI-1 encoded proteins called as accessory colonization factors encoded by *acfA*, *acfB*, *acfC*, *acfD* also play critical role in colonization (Everiss et al., 1994; Withey and DiRita, 2005; Valiente et al., 2018). Disruption of any of the four genes has been reported to cause ∼10-fold decreases in colonization as compared to wild type.

Clinical Appearance of the Disease

Once the *V. cholerae* colonized inside the gut it starts producing CT and other virulence factors. CT is A_1B_5 multimeric protein complex, where B-subunit binds to GM1 ganglioside receptor. The receptor-toxin complex is endocytosed to endoplasmic reticulum and A1-subunit of toxin activates adenylate cyclase that ultimately opens chloride ions channels (CFTR Cystic fibrosis trans-membrane conductance regulator) and causes the secretion of fluids and ions into the lumen of gut (Vanden Broeck et al., 2007). Clinical onset of cholera may be sudden or delayed, depending upon the inoculation size. But in general after the incubation period in range of 18 h to 5 days, clinical symptoms of diseases appeared that included secretion of voluminous stools, resembling like rice-water (Due to presence of mucus in the stool), abdominal discomfort, anorexia with or without vomiting (Sack et al., 2004). Although ∼2–11% of the infected person with the El Tor and Classical strain of *V. cholerae*, respectively showed the severe clinical manifestation (Kaper et al., 1995). In the case of severe cholera, the rate of diarrhea reaches up to 500–1,000 ml/h, which leads to decrease in the turner pressure, low blood pressure, sunken eyes and wrinkled hand, and feet skin. Although cholera patients can be easily treated with simple electrolytes replacement therapy but severe patients of cholera may die within few hours if left untreated (Bhattacharya, 2003).

VPI-1 encoded transcriptional activator ToxT activates the transcription of CT; ToxT is a 32-kDa AraC family transcriptional activator of *ctxA*/*ctxB* as well as *tcpA*, *acfs*, *aldA*. It has two helix-turn-helix-motifs, an N-terminal dimerization and environmental-sensing domain, along with C-terminal DNA binding domain (Lowden et al., 2010). Once induced, the ToxT directly bind via direct repeats of the sequence TTTTGAT called as Tox boxes to the promoter of *ctxA, ctxB, tcpA, acfs, aldA*. However, configuration of tox boxes differs at different promoters. For example, binding to the promoter of *ctxA*/*B*, ToxT required minimum three direct repeats of Tox boxes (Prouty et al., 2005). For t*cpA* promoter, ToxT binds to two tox boxes arranged as a direct repeat between position −44 and −67. Whereas, for *acfA* and *acfD* promoters, ToxT binds to two tox boxes organized as an inverted repeat (Krukonis et al., 2000). In contrast to *tcpA*, *acfA,* and *acfD*, ToxT binds to a single tox box for *aldA* promoter. ToxT is located downstream of *tcpF* and auto-regulates its own transcription. A histone-like nucleoid structural protein (H-NS) that binds to DNA in sequence-independent manner at AT-rich sequences competes with ToxT binding promoters and causes the repression of virulence protein (Ayala et al., 2017). Probably this mechanism might help in the shutdown of virulence protein expression under non-permissive conditions. Same finding was supported with mutational studies; *h-ns* mutants are reported to have de-repressed expression of *toxT*, *ctxA*/*B,* and *tcpA* (Nye and Taylor, 2003). As compared to *tcpA* promoter, H-NS strongly binds to *ctxAB* promoter and subsequently strongly represses the transcription of *ctxAB* (Nye et al., 2000).

Interaction Between VPI-1 and Chromosomally Encoded Function and Its Influence on *V. cholerae* Pathogenesis

The functioning of *V. cholerae* as a pathogen is strongly regulated by the function encoded by its core genome, genomic islands and intestinal environmental conditions in the host associated phage. In this review, we also included role of human intestinal environment in the *V. cholerae* pathogenesis. The human gut environment consists of a number of poorly characterized chemical components harboring thousands of host derived signaling molecules. In addition, microbiota residing in the intestine contribute in further complexity by producing and secreting several small molecules in the milieu. Auto-inducers that triggers the expression of number of virulence factors in *V. cholerae* are one of the important bacterial component that modulate disease severity and dissemination of bacteria from host to the environment (Higgins et al., 2007). A number of host and microbial origin molecule have been discovered to-date and majority of which have integrated molecular circuit with VPI-1 encoded transcriptional regulators that play role at various stages of cholera pathogenesis.

Core Genome Encoded HapR Repressed VPI-1 Encoded ToxT

The *aphA*/*hapR* mediated quorum sensing is the central mechanism that regulates the virulence-associated cascade in toxigenic *V. cholerae*. The low cell density of the pathogen in the gut is typically sensed by a membrane bound sensor kinase (the CqsS), based on the concentration of a cholera auto-inducer 1 (CAI-1). CAI-1 triggers the expression of *aphA*, which induces the expression of *tcpP* and *tcpH* (Haycocks et al., 2019; Herzog et al., 2019). This quorum sensing of *V. cholerae* modulates the virulence gene expression cascades for development of the disease and its severity. Besides at low cell density, CqsS activates LuxO (a sigma-54 dependent protein) that represses the expression of *hapR* which favors the bacterial growth and pathogenesis (Zhu et al., 2002). Whereas, at high cell density, LuxO is unable to activate the repressor protein of HapR, and hence it remains available to *aphA* promoter between −85 and −58 and repress its expression, which leads to deficiency of TcpP and TcpH. Ultimately because of this, ToxR/ToxS regulon becomes unable to activate the *toxT*; the master regulator of VPI-1 encoded factors and cholera toxin production (Kovacikova and Skorupski, 2002). Interestingly in *V. cholerae* strain N16961, *hapR* is not active due to a frame-shift mutation (Joelsson et al., 2006). Since, N16961 is a clinical isolate and it can develop typical disease phenotype in animal model indicating HapR is dispensable for disease development. For a clear understanding of the HapR mediated regulation, the interactions of HapR with the transcriptional factors AphAB has been depicted in the **Figure 3**. Some additional modulators like ToxT, H-NS, ToxR/S involved in the regulation of toxin production, colonization and disease development can compensate the absence of HapR in N16961.

ToxR and TcpP Mediated Activation of ToxT

ToxR is a 32.5-kDa inner trans-membrane transcriptional activator consisting of 294 amino acids. It has three functional domains: a 180 amino acids long cytoplasmic domain, 16 amino acids long trans-membrane domain, and 100 amino acids long peri-plasmic domain (Miller et al., 1987). ToxR helps *V. cholerae* in sensing external intestinal environmental conditions (like pH, bile, temperature) and facilitates bacterial adaptation (Childers and Klose, 2007). ToxR modulates the expression of CT, OmpU, OmpT, and ToxT by binding to their promoters and modulating their transcription (Provenzano and Klose, 2000). However, experimental data indicates that ToxR alone is unable to activate the ToxT expression and need another membrane bound protein TcpP. Possibly, ToxR act as an enhancer for TcpP at the *toxT* promoter. ToxR also interact with another co-transcribed protein, ToxS (Bina et al., 2003), which is required for the maximal transcriptional activation of ToxT regulated genes. Like ToxR, TcpP interacts with another protein, TcpH that is required for TcpP stability. Experimental data showed that when *V. cholerae* cells shifted from permissive to non-permissive growth conditions, TcpP gets degraded even in presence of TcpH suggesting the role of TcpP at the initial stage of virulence cascade as a switch of ToxT dependent virulence associated genes in permissive and non-permissive growth conditions (Raskin et al., 2020). Once the bacteria sense the gut environment through its quorum sensing, ToxR and TcpP binds to *toxT* promoter at −100 to −69 and at −51 to −32 region with respect to transcription start site, respectively and subsequently activates the expression *toxT*, the master regulator of *V. cholerae* pathogenesis and hence the disease.

VarS/VarA Mediated Activation of Virulence-Associated Genes

It is reported that VarS/VarA, two-component system acting downstream of ToxR/S signaling cascade, also independently controls the expression of ToxT and other virulence proteins in response to environmental signals. *V. cholerae* O395 *varA* mutant are reported to have reduced expression of *tcpA* and *ctxA* and *ctxB* (Tsou et al., 2011). VarS mutant of classical O395 and El Tor C6706 strains exhibit the decreased production of TcpA (134-fold), CT (2.5-fold), *ctxA* (1.75-fold) and *ctxB* (1.72-fold) as compared to wild types (Jang et al., 2011). Recently, downstream target of VarS/VarA system, PckA which is a key player in central carbon metabolism and affects the levels of many metabolic intermediates, has been shown to modulate HapR activity (Jang et al., 2010). Although more evidences are required, this supported to hypothesize that VarS/VarA system to be a way for *V. cholerae* to combine information about surrounding cell density and nutrient availability to fine-tune its gene expression profile precisely to the surrounding microenvironmental conditions.

GENETIC VARIATION IN VPI-1, AMONG VARIOUS CLINICAL ISOLATES OF *V. cholerae*

Classical strains of *V. cholerae* represent the remnant of the sixth-pandemics toxigenic clones, while El Tor and O139 Bengal represent the current seventh-pandemic toxigenic clones (Karaolis et al., 1995). Comparative studies of VPI-1 of sixth and seventh pandemics strains found that the GI integrate in

TABLE 3 | Genetic variation among the important genes of classical and El Tor strains.

Gene	Percentage variation
tagD	1.21%
tcpP	1.50%
tcpH	2.67%
tcpB	1.46%
tcpQ	1.98%
tcpC	2.17%
tcpA	22.5%

the same locus of chromosome 1 of both the biotypes of O1 isolates. VPI-1 is very similar in both the biotypes and has similar numbers of ORFs. However, ∼483 polymorphic nucleotides were reported between both the biotypes. The central region of VPI-1 that harbors gene for TcpI, TcpP, TcpH, and TcpA was found to have interestingly highest level of polymorphic nucleotides (Karaolis et al., 2001). Highest variation was observed for *tcpA*, gene encoding the type IV pilus that works as a receptor for CTXΦ, around 22.5% variation at nucleotide level and 16.9% at the protein level. The accessory colonization factor, AcfD that help in the intestinal colonization contained longer open reading frame in El Tor strain (**Table 3**). Despite the huge importance of VPI-1 encoded genes in the pathogenesis of *V. cholerae*, yet a detail comparative study of their contents including the characterization of genetic, proteomic, and phenotypic variations among the various pathogenic clones of *V. cholerae* is not available. Therefore, in order to understand the reason behind the disappearance of O1 classical strains and emergences of O1 El Tor strain and the temporal emergences of O139 Bengal in 1992, further investigations are of much demand.

CONCLUSION

Cholera, an acute gastrointestinal diarrheal disease caused by the *V. cholerae*, is still a major public health concern to many developing countries including India. Improved understanding of the cholera pathogenesis at molecular level is a pre-requisite for the development of appropriate strategies for disease management.

Acquisition of MGEs through HGT is among the most common approaches of the pathogens to achieve fitness and survival traits in hostile and/or changing environments. Two important virulence factors for cholera pathogenesis, CT and TCP, are part of two MGEs, CTXΦ and VPI-1, respectively. This indicates that understanding the MGEs biology, their integration mechanisms, stable inheritance and dissemination between bacterial species, may help in reducing the disease burden and development of novel therapeutics for treating the disease. To date, *V. cholerae* have acquired a number of MGEs (CTXΦ, VPI-1, VPI-2, RS1, VSP-1, & VSP-2) that help the pathogen survival under the changing environmental conditions and contribute in causing the pathogenesis. The VPI-1 is unique, as it has been involved in regulation of almost all the stages of cholera pathogenesis. First, the VPI-1 encoded TCP helps the CTXΦ to recognize the host bacterium and introduce their (+) ssDNA inside the host cell. The *V. cholerae* strains that lack CTXΦ are typically non-pathogenic. Then, VPI-1 encoded factors, including TCP, TagA, AcfA, AcfB, AcfC, and AcfD, facilitate the pathogenic bacterium to colonize in the human gut. The VPI-1 encoded ToxT induces the expression of CT, the most critical virulence factor of cholera pathogenesis and helps the pathogen to cause the disease. TCP, Tpx, and ToxT are also integral part of quorum sensing mechanisms that protects the pathogen from harsh micro-environmental conditions in the gut. Deregulation of VPI-1 or its encoded factor(s) have already been reported to negatively impact the ability of the pathogen to cause the disease. This altogether supports the role of VPI-1 as the master regulator of cholera pathogenesis and hence suggesting it as potential therapeutic target for disease control and/or management.

AUTHOR CONTRIBUTIONS

AK provided the general concept. AK and NK drafted the initial concept of manuscript. AK, NK, and BD wrote the manuscript. All the authors have seen and approved the final manuscript.

FUNDING

The work has been supported by funding from Department of Biotechnology, India and Indian Council of Medical Research.

ACKNOWLEDGMENTS

We are grateful to Professor Gagandeep Kang (Translational Health Science and Technology Institute Faridabad), for her support and Indian council of Medical Research for providing the Junior/Senior Research Fellowship to pursue AK for perusal of Doctoral degree.

REFERENCES

Almagro-Moreno, S., Napolitano, M. G., and Boyd, E. F. (2010). Excision dynamics of Vibrio pathogenicity island-2 from *Vibrio cholerae*: role of a recombination directionality factor VefA. *BMC Microbiol.* 10:306. doi: 10.1186/1471-2180-10-306

Almagro-Moreno, S., Pruss, K., and Taylor, R. K. (2015). Intestinal colonization dynamics of *Vibrio cholerae*. *PLoS Pathog.* 11:e1004787. doi: 10.1371/journal.ppat.1004787

Ayala, J. C., Silva, A. J., and Benitez, J. A. (2017). H-NS: an overarching regulator of the *Vibrio cholerae* life cycle. *Res. Microbiol.* 168, 16–25. doi: 10.1016/j.resmic.2016.07.007

Bhattacharya, S. K. (2003). An evaluation of current cholera treatment. *Expert Opin. Pharmacother.* 4, 141–146. doi: 10.1517/14656566.4.2.141

Bina, J., Zhu, J., Dziejman, M., Faruque, S., Calderwood, S., and Mekalanos, J. (2003). ToxR regulon of *Vibrio cholerae* and its expression in vibrios shed by cholera patients. *Proc. Natl. Acad. Sci. U.S.A.* 100, 2801–2806. doi: 10.1073/pnas.2628026100

Bose, N., and Taylor, R. K. (2005). Identification of a TcpC-TcpQ outer membrane complex involved in the biogenesis of the toxin-coregulated pilus of *Vibrio cholerae*. *J. Bacteriol.* 187, 2225–2232. doi: 10.1128/JB.187.7.2225-2232.2005

Boyd, E. F. (2010). Efficiency and specificity of CTXphi chromosomal integration: dif makes all the difference. *Proc. Natl. Acad. Sci. U.S.A.* 107, 3951–3952. doi: 10.1073/pnas.1000310107

Boyd, E. F., Moyer, K. E., Shi, L., and Waldor, M. K. (2000). Infectious CTXPhi and the vibrio pathogenicity island prophage in *Vibrio mimicus*: evidence for recent horizontal transfer between *V. mimicus* and *V. cholerae*. *Infect. Immun.* 68, 1507–1513. doi: 10.1128/IAI.68.3.1507-1513.2000

Carroll, P. A., Tashima, K. T., Rogers, M. B., DiRita, V. J., and Calderwood, S. B. (1997). Phase variation in tcpH modulates expression of the ToxR regulon in *Vibrio cholerae*. *Mol. Microbiol.* 25, 1099–1111. doi: 10.1046/j.1365-2958.1997.5371901.x

Castro-Rosas, J., and Escartin, E. F. (2002). Adhesion and colonization of *Vibrio cholerae* O1 on shrimp and crab carapaces. *J. Food Prot.* 65, 492–498. doi: 10.4315/0362-028X-65.3.492

Cha, M. K., Hong, S. K., Lee, D. S., and Kim, I. H. (2004). *Vibrio cholerae* thiol peroxidase-glutaredoxin fusion is a 2-Cys TSA/AhpC subfamily acting as a lipid hydroperoxide reductase. *J. Biol. Chem.* 279, 11035–11041. doi: 10.1074/jbc.M312657200

Chang, Y. W., Kjaer, A., Ortega, D. R., Kovacikova, G., Sutherland, J. A., Rettberg, L. A., et al. (2017). Architecture of the *Vibrio cholerae* toxin-coregulated pilus machine revealed by electron cryotomography. *Nat. Microbiol.* 2:16269. doi: 10.1038/nmicrobiol.2016.269

Childers, B. M., and Klose, K. E. (2007). Regulation of virulence in *Vibrio cholerae*: the ToxR regulon. *Future Microbiol.* 2, 335–344. doi: 10.2217/17460913.2.3.335

Choi, S. Y., Lee, J. H., Kim, E. J., Lee, H. R., Jeon, Y. S., von Seidlein, L., et al. (2010). Classical RS1 and environmental RS1 elements in *Vibrio cholerae* O1 El Tor strains harbouring a tandem repeat of CTX prophage: revisiting Mozambique in 2005. *J. Med. Microbiol.* 59(Pt 3), 302–308. doi: 10.1099/jmm.0.017053-0

Chun, J., Grim, C. J., Hasan, N. A., Lee, J. H., Choi, S. Y., Haley, B. J., et al. (2009). Comparative genomics reveals mechanism for short-term and long-term clonal transitions in pandemic *Vibrio cholerae*. *Proc. Natl. Acad. Sci. U.S.A.* 106, 15442–15447. doi: 10.1073/pnas.0907787106

Das, B., Bischerour, J., Val, M. E., and Barre, F. X. (2010). Molecular keys of the tropism of integration of the cholera toxin phage. *Proc. Natl. Acad. Sci. U.S.A.* 107, 4377–4382. doi: 10.1073/pnas.0910212107

Das, B., Martinez, E., Midonet, C., and Barre, F. X. (2013). Integrative mobile elements exploiting Xer recombination. *Trends Microbiol.* 21, 23–30. doi: 10.1016/j.tim.2012.10.003

Davies, B. W., Bogard, R. W., Young, T. S., and Mekalanos, J. J. (2012). Coordinated regulation of accessory genetic elements produces cyclic di-nucleotides for *V. cholerae* virulence. *Cell* 149, 358–370. doi: 10.1016/j.cell.2012.01.053

Domman, D., Quilici, M. L., Dorman, M. J., Njamkepo, E., Mutreja, A., Mather, A. E., et al. (2017). Integrated view of *Vibrio cholerae* in the Americas. *Science* 358, 789–793. doi: 10.1126/science.aao2136

Everiss, K. D., Hughes, K. J., Kovach, M. E., and Peterson, K. M. (1994). The *Vibrio cholerae* acfB colonization determinant encodes an inner membrane protein that is related to a family of signal-transducing proteins. *Infect. Immun.* 62, 3289–3298. doi: 10.1128/IAI.62.8.3289-3298.1994

Faruque, S. M., Kamruzzaman, M., Asadulghani, Sack, D. A., Mekalanos, J. J., and Nair, G. B. (2003a). CTXphi-independent production of the RS1 satellite phage by *Vibrio cholerae*. *Proc. Natl. Acad. Sci. U.S.A.* 100, 1280–1285. doi: 10.1073/pnas.0237385100

Faruque, S. M., and Mekalanos, J. J. (2003). Pathogenicity islands and phages in *Vibrio cholerae* evolution. *Trends Microbiol.* 11, 505–510. doi: 10.1016/j.tim.2003.09.003

Faruque, S. M., Zhu, J., Asadulghani, Kamruzzaman, M., and Mekalanos, J. J. (2003b). Examination of diverse toxin-coregulated pilus-positive *Vibrio cholerae* strains fails to demonstrate evidence for Vibrio pathogenicity island phage. *Infect Immun.* 71, 2993–2999. doi: 10.1128/IAI.71.6.2993-2999.2003

Gao, Y., Hauke, C. A., Marles, J. M., and Taylor, R. K. (2016). Effects of *tcpB* mutations on biogenesis and function of the toxin-coregulated pilus, the type IVb pilus of *Vibrio cholerae*. *J. Bacteriol.* 198, 2818–2828. doi: 10.1128/JB.00309-16

Gutierrez-Rodarte, M., Kolappan, S., Burrell, B. A., and Craig, L. (2019). The *Vibrio cholerae* minor pilin TcpB mediates uptake of the cholera toxin phage CTXphi. *J. Biol. Chem.* 294, 15698–15710. doi: 10.1074/jbc.RA119.009980

Hammer, B. K., and Bassler, B. L. (2003). Quorum sensing controls biofilm formation in *Vibrio cholerae*. *Mol. Microbiol.* 50, 101–104. doi: 10.1046/j.1365-2958.2003.03688.x

Harkey, C. W., Everiss, K. D., and Peterson, K. M. (1994). The *Vibrio cholerae* toxin-coregulated-pilus gene tcpI encodes a homolog of methyl-accepting chemotaxis proteins. *Infect. Immun.* 62, 2669–2678. doi: 10.1128/IAI.62.7.2669-2678.1994

Hase, C. C., and Mekalanos, J. J. (1998). TcpP protein is a positive regulator of virulence gene expression in *Vibrio cholerae*. *Proc. Natl. Acad. Sci. U.S.A.* 95, 730–734. doi: 10.1073/pnas.95.2.730

Hassan, F., Kamruzzaman, M., Mekalanos, J. J., and Faruque, S. M. (2010). Satellite phage TLCphi enables toxigenic conversion by CTX phage through dif site alteration. *Nature* 467, 982–985. doi: 10.1038/nature09469

Haycocks, J. R. J., Warren, G. Z. L., Walker, L. M., Chlebek, J. L., Dalia, T. N., Dalia, A. B., et al. (2019). The quorum sensing transcription factor AphA directly regulates natural competence in *Vibrio cholerae*. *PLoS Genet.* 15:e1008362. doi: 10.1371/journal.pgen.1008362

Heidelberg, J. F., Eisen, J. A., Nelson, W. C., Clayton, R. A., Gwinn, M. L., Dodson, R. J., et al. (2000). DNA sequence of both chromosomes of the cholera pathogen *Vibrio cholerae*. *Nature* 406, 477–483. doi: 10.1038/35020000

Herzog, R., Peschek, N., Frohlich, K. S., Schumacher, K., and Papenfort, K. (2019). Three autoinducer molecules act in concert to control virulence gene expression in *Vibrio cholerae*. *Nucleic Acids Res.* 47, 3171–3183. doi: 10.1093/nar/gky1320

Higgins, D. A., Pomianek, M. E., Kraml, C. M., Taylor, R. K., Semmelhack, M. F., and Bassler, B. L. (2007). The major *Vibrio cholerae* autoinducer and its role in virulence factor production. *Nature* 450, 883–886. doi: 10.1038/nature06284

Hu, D., Liu, B., Feng, L., Ding, P., Guo, X., Wang, M., et al. (2016). Origins of the current seventh cholera pandemic. *Proc. Natl. Acad. Sci. U.S.A.* 113, E7730–E7739. doi: 10.1073/pnas.1608732113

Hughes, K. J., Everiss, K. D., Kovach, M. E., and Peterson, K. M. (1995). Isolation and characterization of the *Vibrio cholerae acfA* gene, required for efficient intestinal colonization. *Gene* 156, 59–61. doi: 10.1016/0378-1119(95)00054-A

Jang, J., Jung, K.-T., Yoo, C.-K., and Rhie, G.-E. (2010). Regulation of hemagglutinin/protease expression by the VarS/VarA–CsrA/B/C/D system in *Vibrio cholerae*. *Microb. Pathog.* 48, 245–250. doi: 10.1016/j.micpath.2010.03.003

Jang, J., Jung, K. T., Park, J., Yoo, C. K., and Rhie, G. E. (2011). The *Vibrio cholerae* VarS/VarA two-component system controls the expression of virulence proteins through ToxT regulation. *Microbiology* 157(Pt 5), 1466–1473. doi: 10.1099/mic.0.043737-0

Jermyn, W. S., and Boyd, E. F. (2002). Characterization of a novel Vibrio pathogenicity island (VPI-2) encoding neuraminidase (*nanH*) among toxigenic *Vibrio cholerae* isolates. *Microbiology* 148(Pt 11), 3681–3693. doi: 10.1099/00221287-148-11-3681

Joelsson, A., Liu, Z., and Zhu, J. (2006). Genetic and phenotypic diversity of quorum-sensing systems in clinical and environmental isolates of *Vibrio cholerae*. *Infect. Immun.* 74, 1141–1147. doi: 10.1128/IAI.74.2.1141-1147.2006

Johnson, J. A., Salles, C. A., Panigrahi, P., Albert, M. J., Wright, A. C., Johnson, R. J., et al. (1994). *Vibrio cholerae* O139 synonym bengal is closely related to *Vibrio cholerae* El Tor but has important differences. *Infect. Immun.* 62, 2108–2110. doi: 10.1128/IAI.62.5.2108-2110.1994

Kaper, J. B., Morris, J. G. Jr., and Levine, M. M. (1995). Cholera. *Clin. Microbiol. Rev.* 8, 48–86. doi: 10.1128/CMR.8.1.48

Karaolis, D. K., Johnson, J. A., Bailey, C. C., Boedeker, E. C., Kaper, J. B., and Reeves, P. R. (1998). A *Vibrio cholerae* pathogenicity island associated with epidemic and pandemic strains. *Proc. Natl. Acad. Sci. U.S.A.* 95, 3134–3139. doi: 10.1073/pnas.95.6.3134

Karaolis, D. K., Lan, R., Kaper, J. B., and Reeves, P. R. (2001). Comparison of *Vibrio cholerae* pathogenicity islands in sixth and seventh pandemic strains. *Infect. Immun.* 69, 1947–1952. doi: 10.1128/IAI.69.3.1947-1952.2001

Karaolis, D. K., Lan, R., and Reeves, P. R. (1995). The sixth and seventh cholera pandemics are due to independent clones separately derived from environmental, nontoxigenic, non-O1 *Vibrio cholerae*. *J. Bacteriol.* 177, 3191–3198. doi: 10.1128/JB.177.11.3191-3198.1995

Karaolis, D. K., Somara, S., Maneval, D. R. Jr., Johnson, J. A., and Kaper, J. B. (1999). A bacteriophage encoding a pathogenicity island, a type-IV pilus and a phage receptor in cholera bacteria. *Nature* 399, 375–379. doi: 10.1038/20715

Kaufman, M. R., Seyer, J. M., and Taylor, R. K. (1991). Processing of TCP pilin by TcpJ typifies a common step intrinsic to a newly recognized pathway of extracellular protein secretion by gram-negative bacteria. *Genes Dev.* 5, 1834–1846. doi: 10.1101/gad.5.10.1834

Kimsey, H. H., and Waldor, M. K. (1998). CTXphi immunity: application in the development of cholera vaccines. *Proc. Natl. Acad. Sci. U.S.A.* 95, 7035–7039. doi: 10.1073/pnas.95.12.7035

Klose, K. E. (2000). The suckling mouse model of cholera. *Trends Microbiol.* 8, 189–191. doi: 10.1016/S0966-842X(00)01721-2

Kolappan, S., and Craig, L. (2013). Structure of the cytoplasmic domain of TcpE, the inner membrane core protein required for assembly of the *Vibrio cholerae* toxin-coregulated pilus. *Acta Crystallogr. D Biol. Crystallogr.* 69(Pt 4), 513–519. doi: 10.1107/S0907444912050330

Kovacikova, G., and Skorupski, K. (2002). Regulation of virulence gene expression in *Vibrio cholerae* by quorum sensing: HapR functions at the *aphA* promoter. *Mol. Microbiol.* 46, 1135–1147. doi: 10.1046/j.1365-2958.2002.03229.x

Krukonis, E. S., Yu, R. R., and Dirita, V. J. (2000). The *Vibrio cholerae* ToxR/TcpP/ToxT virulence cascade: distinct roles for two membrane-localized transcriptional activators on a single promoter. *Mol. Microbiol.* 38, 67–84. doi: 10.1046/j.1365-2958.2000.02111.x

Kumar, A., Bag, S., and Das, B. (2018). Novel genetic tool to study the stability of genomic islands. *Recent Pat. Biotechnol.* 12, 200–207. doi: 10.2174/1872208312666180223113618

Li, M., Kotetishvili, M., Chen, Y., and Sozhamannan, S. (2003). Comparative genomic analyses of the vibrio pathogenicity island and cholera toxin prophage regions in nonepidemic serogroup strains of *Vibrio cholerae*. *Appl. Environ. Microbiol.* 69, 1728–1738. doi: 10.1128/AEM.69.3.1728-1738.2003

Lim, M. S., Ng, D., Zong, Z., Arvai, A. S., Taylor, R. K., Tainer, J. A., et al. (2010). *Vibrio cholerae* El Tor TcpA crystal structure and mechanism for pilus-mediated microcolony formation. *Mol. Microbiol.* 77, 755–770. doi: 10.1111/j.1365-2958.2010.07244.x

Lowden, M. J., Skorupski, K., Pellegrini, M., Chiorazzo, M. G., Taylor, R. K., and Kull, F. J. (2010). Structure of *Vibrio cholerae* ToxT reveals a mechanism for fatty acid regulation of virulence genes. *Proc. Natl. Acad. Sci. U.S.A.* 107, 2860–2865. doi: 10.1073/pnas.0915021107

Manning, P. A. (1997). The *tcp* gene cluster of *Vibrio cholerae*. *Gene* 192, 63–70. doi: 10.1016/S0378-1119(97)00036-X

McLeod, S. M., and Waldor, M. K. (2004). Characterization of XerC- and XerD-dependent CTX phage integration in *Vibrio cholerae*. *Mol. Microbiol.* 54, 935–947. doi: 10.1111/j.1365-2958.2004.04309.x

Megli, C. J., Yuen, A. S., Kolappan, S., Richardson, M. R., Dharmasena, M. N., Krebs, S. J., et al. (2011). Crystal structure of the *Vibrio cholerae* colonization factor TcpF and identification of a functional immunogenic site. *J. Mol. Biol.* 409, 146–158. doi: 10.1016/j.jmb.2011.03.027

Meibom, K. L., Blokesch, M., Dolganov, N. A., Wu, C. Y., and Schoolnik, G. K. (2005). Chitin induces natural competence in *Vibrio cholerae*. *Science* 310, 1824–1827. doi: 10.1126/science.1120096

Miller, V. L., Taylor, R. K., and Mekalanos, J. J. (1987). Cholera toxin transcriptional activator *toxR* is a transmembrane DNA binding protein. *Cell* 48, 271–279. doi: 10.1016/0092-8674(87)90430-2

Mishra, A., Srivastava, R., Pruzzo, C., and Srivastava, B. S. (2003). Mutation in *tcpR* gene (VC0832) of *Vibrio cholerae* O1 causes loss of tolerance to high osmolarity and affects colonization and virulence in infant mice. *J. Med. Microbiol.* 52(Pt 11), 933–939. doi: 10.1099/jmm.0.05171-0

Mutreja, A., Kim, D. W., Thomson, N. R., Connor, T. R., Lee, J. H., Kariuki, S., et al. (2011). Evidence for several waves of global transmission in the seventh cholera pandemic. *Nature* 477, 462–465. doi: 10.1038/nature10392

Nye, M. B., Pfau, J. D., Skorupski, K., and Taylor, R. K. (2000). *Vibrio cholerae* H-NS silences virulence gene expression at multiple steps in the ToxR regulatory cascade. *J. Bacteriol.* 182, 4295–4303. doi: 10.1128/JB.182.15.4295-4303.2000

Nye, M. B., and Taylor, R. K. (2003). *Vibrio cholerae* H-NS domain structure and function with respect to transcriptional repression of ToxR regulon genes reveals differences among H-NS family members. *Mol. Microbiol.* 50, 427–444. doi: 10.1046/j.1365-2958.2003.03701.x

O'Shea, Y. A., and Boyd, E. F. (2002). Mobilization of the *Vibrio* pathogenicity island between *Vibrio cholerae* isolates mediated by CP-T1 generalized transduction. *FEMS Microbiol. Lett.* 214, 153–157. doi: 10.1111/j.1574-6968.2002.tb11339.x

O'Shea, Y. A., Finnan, S., Reen, F. J., Morrissey, J. P., O'Gara, F., and Boyd, E. F. (2004). The *Vibrio* seventh pandemic island-II is a 26.9 kb genomic island present in *Vibrio cholerae* El Tor and O139 serogroup isolates that shows homology to a 43.4 kb genomic island in *V. vulnificus*. *Microbiology* 150(Pt 12), 4053–4063. doi: 10.1099/mic.0.27172-0

Pang, B., Yan, M., Cui, Z., Ye, X., Diao, B., Ren, Y., et al. (2007). Genetic diversity of toxigenic and nontoxigenic *Vibrio cholerae* serogroups O1 and O139 revealed by array-based comparative genomic hybridization. *J. Bacteriol.* 189, 4837–4849. doi: 10.1128/JB.01959-06

Parsot, C., Taxman, E., and Mekalanos, J. J. (1991). ToxR regulates the production of lipoproteins and the expression of serum resistance in *Vibrio cholerae*. *Proc. Natl. Acad. Sci. U.S.A.* 88, 1641–1645. doi: 10.1073/pnas.88.5.1641

Prouty, M. G., Osorio, C. R., and Klose, K. E. (2005). Characterization of functional domains of the *Vibrio cholerae* virulence regulator ToxT. *Mol. Microbiol.* 58, 1143–1156. doi: 10.1111/j.1365-2958.2005.04897.x

Provenzano, D., and Klose, K. E. (2000). Altered expression of the ToxR-regulated porins OmpU and OmpT diminishes *Vibrio cholerae* bile resistance, virulence factor expression, and intestinal colonization. *Proc. Natl. Acad. Sci. U.S.A.* 97:10220. doi: 10.1073/pnas.170219997

Rajanna, C., Wang, J., Zhang, D., Xu, Z., Ali, A., Hou, Y. M., et al. (2003). The vibrio pathogenicity island of epidemic *Vibrio cholerae* forms precise extrachromosomal circular excision products. *J. Bacteriol.* 185, 6893–6901. doi: 10.1128/JB.185.23.6893-6901.2003

Raskin, D. M., Mishra, A., He, H., and Lundy, Z. (2020). Stringent response interacts with the ToxR regulon to regulate *Vibrio cholerae* virulence factor expression. *Arch. Microbiol.* 202, 1359–1368. doi: 10.1007/s00203-020-01847-6

Rhine, J. A., and Taylor, R. K. (1994). TcpA pilin sequences and colonization requirements for O1 and O139 *Vibrio cholerae*. *Mol. Microbiol.* 13, 1013–1020. doi: 10.1111/j.1365-2958.1994.tb00492.x

Sack, D. A., Sack, R. B., Nair, G. B., and Siddique, A. K. (2004). Cholera. *Lancet* 363, 223–233. doi: 10.1016/S0140-6736(03)15328-7

Schuhmacher, D. A., and Klose, K. E. (1999). Environmental signals modulate ToxT-dependent virulence factor expression in *Vibrio cholerae*. *J. Bacteriol.* 181, 1508–1514. doi: 10.1128/JB.181.5.1508-1514.1999

Singh, D. V., Matte, M. H., Matte, G. R., Jiang, S., Sabeena, F., Shukla, B. N., et al. (2001). Molecular analysis of *Vibrio cholerae* O1, O139, non-O1, and non-O139 strains: clonal relationships between clinical and environmental isolates. *Appl. Environ. Microbiol.* 67, 910–921. doi: 10.1128/AEM.67.2.910-921.2001

Szabady, R. L., Yanta, J. H., Halladin, D. K., Schofield, M. J., and Welch, R. A. (2011). TagA is a secreted protease of *Vibrio cholerae* that specifically cleaves mucin glycoproteins. *Microbiology* 157(Pt 2), 516–525. doi: 10.1099/mic.0.044529-0

Tam, V. C., Serruto, D., Dziejman, M., Brieher, W., and Mekalanos, J. J. (2007). A type III secretion system in *Vibrio cholerae* translocates a formin/spire hybrid-like actin nucleator to promote intestinal colonization. *Cell Host Microbe* 1, 95–107. doi: 10.1016/j.chom.2007.03.005

Tripathi, S. A., and Taylor, R. K. (2007). Membrane association and multimerization of TcpT, the cognate ATPase ortholog of the *Vibrio cholerae* toxin-coregulated-pilus biogenesis apparatus. *J. Bacteriol.* 189, 4401–4409. doi: 10.1128/JB.00008-07

Tsou, A. M., Liu, Z., Cai, T., and Zhu, J. (2011). The VarS/VarA two-component system modulates the activity of the *Vibrio cholerae* quorum-sensing transcriptional regulator HapR. *Microbiology* 157(Pt 6), 1620–1628. doi: 10.1099/mic.0.046235-0

Val, M. E., Bouvier, M., Campos, J., Sherratt, D., Cornet, F., Mazel, D., et al. (2005). The single-stranded genome of phage CTX is the form used for integration into the genome of *Vibrio cholerae*. Mol. Cell 19, 559–566. doi: 10.1016/j.molcel.2005.07.002

Valiente, E., Davies, C., Mills, D. C., Getino, M., Ritchie, J. M., and Wren, B. W. (2018). *Vibrio cholerae* accessory colonisation factor AcfC: a chemotactic protein with a role in hyperinfectivity. *Sci. Rep.* 8:8390. doi: 10.1038/s41598-018-26570-7

Vanden Broeck, D., Horvath, C., and De Wolf, M. J. (2007). *Vibrio cholerae*: cholera toxin. *Int. J. Biochem. Cell Biol.* 39, 1771–1775. doi: 10.1016/j.biocel.2007.07.005

Weill, F. X., Domman, D., Njamkepo, E., Almesbahi, A. A., Naji, M., Nasher, S. S., et al. (2019). Genomic insights into the 2016-2017 cholera epidemic in Yemen. *Nature* 565, 230–233. doi: 10.1038/s41586-018-0818-3

Withey, J. H., and DiRita, V. J. (2005). Activation of both *acfA* and *acfD* transcription by *Vibrio cholerae* ToxT requires binding to two centrally located DNA sites in an inverted repeat conformation. *Mol. Microbiol.* 56, 1062–1077. doi: 10.1111/j.1365-2958.2005.04589.x

Zhu, J., and Mekalanos, J. J. (2003). Quorum sensing-dependent biofilms enhance colonization in *Vibrio cholerae*. *Dev. Cell* 5, 647–656. doi: 10.1016/S1534-5807(03)00295-8

Zhu, J., Miller, M. B., Vance, R. E., Dziejman, M., Bassler, B. L., and Mekalanos, J. J. (2002). Quorum-sensing regulators control virulence gene expression in *Vibrio cholerae*. *Proc. Natl. Acad. Sci. U.S.A.* 99, 3129–3134. doi: 10.1073/pnas.052694299

Conflict of Interest: The authors declare that the research was conducted in the absence of any commercial or financial relationships that could be construed as a potential conflict of interest.

frontiers in Cellular and Infection Microbiology

MINI REVIEW
published: 22 October 2020
doi: 10.3389/fcimb.2020.582947

Diguanylate Cyclases in *Vibrio cholerae*: Essential Regulators of Lifestyle Switching

Sumit Biswas, Om Prakash Chouhan and Divya Bandekar*

ViStA Lab, Department of Biological Sciences, Birla Institute of Technology and Sciences (BITS), Pilani–KK Birla Goa Campus, Goa, India

Biofilm formation in *Vibrio cholerae* empowers the bacteria to lead a dual lifestyle and enhances its infectivity. While the formation and dispersal of the biofilm involves multiple components—both proteinaceous and non-proteinaceous, the key to the regulatory control lies with the ubiquitous secondary signaling molecule, cyclic-di-GMP (c-di-GMP). A number of different cellular components may interact with c-di-GMP, but the onus of synthesis of this molecule lies with a class of enzymes known as diguanylate cyclases (DGCs). DGC activity is generally associated with proteins possessing a GGDEF domain, ubiquitously present across all bacterial systems. *V. cholerae* is also endowed with multiple DGCs and information about some of them have been pouring in over the past decade. This review summarizes the DGCs confirmed till date in *V. cholerae*, and emphasizes the importance of DGCs and their product, c-di-GMP in the virulence and lifecycle of the bacteria.

Keywords: biofilm, GGDEF, cyclic-di-GMP, virulence, diguanylate cyclase

OPEN ACCESS

Edited by:
Yang Fu,
Southern University of Science and Technology, China

Reviewed by:
Umesh Ahuja,
UCLA Health System, United States
Badreddine Douzi,
INRA Centre Nancy-Lorraine, France

****Correspondence:***
Sumit Biswas
sumit@goa.bits-pilani.ac.in

Specialty section:
This article was submitted to Molecular Bacterial Pathogenesis, a section of the journal Frontiers in Cellular and Infection Microbiology

Received: *13 July 2020*
Accepted: *14 September 2020*
Published: *22 October 2020*

Citation:
Biswas S, Chouhan OP and Bandekar D (2020) Diguanylate Cyclases in Vibrio cholerae: Essential Regulators of Lifestyle Switching. Front. Cell. Infect. Microbiol. 10:582947. doi: 10.3389/fcimb.2020.582947

INTRODUCTION

Vibrio cholerae: Dual Lifestyle and Biofilm

Formation of biofilm enables the bacteria to survive and propagate despite the presence of antibiotics or other external stress. *Vibrio cholerae* is no exception. This bacterium adopts two different lifestyles—the motile pathogenic form in the human host, and the sessile form in waterbodies existing in associated biofilms. The biofilm allows the bacteria to survive nutrient limitations, fluctuations in oxygen levels, and massive changes in osmolarity (Rodney, 2002; Tischler and Camilli, 2004; Waters et al., 2008). Additionally, it also allows changes in the bacterial proteome by inducing favorable genes or suppressing unfavorable genes in order to adapt better.

Biofilm formation in *V. cholerae* is a three-step cyclic process, involving (a) surface attachment, (b) colony formation, and (c) dispersal. In the initial step (surface attachment), motile *V. cholerae* scan solid surfaces—with a preference for the chitinous exoskeleton of zooplanktons or phytoplanktons (Tamplin et al., 1990; Rawlings et al., 2007). The bacterium, powered by the single polar flagellum (with a Na^+-driven motor and regulated by the Flh proteins) seeks a suitable surface (Echazarreta and Klose, 2019), and has been suggested to be quite selective in assaying the surface before selecting it for attachment (Utada et al., 2014). The Mannose-Sensitive Haemagglutinin type 4 surface pili (MSHA-pili) contribute to strong surface attachment during the initial attachment steps (Watnick et al., 1999; Wong, 2016).

After multiplication and the progression of colony formation, the size of the average member cell keeps on decreasing to increase the compaction in the biofilm. The size decreased from 2.4 μm (Drescher et al., 2016) at the beginning of biofilm to 1.8 μm for cellular communities

having ∼1,000 cells (Wong, 2016). Consequently, interbacterial distances in the biofilm matrix also show a significant decrease. The directionality of colony growth also changes incrementally with increase in colony size—while the initial growth is only one dimensional, growth happens in all three directions when cell number crosses 200. It is during this three-dimensional growth phase, the extracellular matrix composed of polysaccharides, proteins, and a small amount of nucleic acids (Joachim and Karl, 2002; Wong, 2016) is secreted. Vibrio polysaccharides (VPS) are essential for keeping the cells together and maintenance of the 3D structure. Proteins of the extracellular matrix, *viz.,* RbmA, RbmC and Bap1 play critical roles in the biofilm as well. The RbmA protein has been implicated in cellular adhesion, architecture and biofilm stability process, while the RbmC secreted on the outer surface of the cells creates flexible scaffolds where the cells can grow and multiply. The Bap1 protein maintains pellicle strength and hydrophobicity allowing the biofilm to propagate at the water-air interface (Römling et al., 2013; Hay and Zhu, 2015).

The last phase of biofilm formation is the dispersal of the bacterial cells from the biofilm to search and colonize a new substratum when conditions are favorable. Environmental conditions such as high/low oxygen level, the concentration of phosphate, Ca^{2+}, etc, have negative effects (inhibition of *vps* gene transcription) on biofilm formation and induce the dispersal of the *V. cholerae* biofilm (Colwell and Huq, 1994; Hay and Zhu, 2015). Atleast two deoxyribonucleases and the Xds protein have also been reported to play crucial roles in biofilm dispersal (Römling et al., 2013; Sisti et al., 2013). The degradation of biofilm and extracellular matrix is induced by various environmental signals and other proteins, many of which are yet to be elucidated.

REGULATION OF BIOFILM FORMATION IN *V. CHOLERAE* AND PATHOGENESIS

Formation of the biofilm comes at a premium—the amount of resources diverted and spent toward the formation is substantial, but the benefits are huge. Being able to thrive in adverse conditions accords the bacterium a different strategy for survival. Therefore, the process needs to be highly regulated and that is how it happens, with the interplay of various factors. In *V. cholerae*, transcriptional activators, repressor proteins and sigma factors RpoS and RpoE have been demonstrably involved in the process (He et al., 2012).

The structural genes for VPS synthesis have been reported to be essential for exopolysaccharide biosynthesis and biofilm formation (Yildiz and Schoolnik, 1999). These genes, located on *vps-1* (*vpsA* to *vpsK*) and *vps-2* (*vpsL* to *vpsQ*) operons, are positively regulated by VpsR and VpsT, while HapR negatively regulates the expression of the *vps* genes, and the positive regulators VpsR and VpsT themselves (Casper-Lindley and Yildiz, 2004; Beyhan et al., 2007). Both VpsR and VpsT bind directly to the *vps* promoter regions and have recognition sites in *vps-1, vps-2* and *vps-L* operons which act as regulatory sequences in the expression of extracellular polysaccharide and matrix protein synthesis (Fong et al., 2010). A recent report relates the activation of the *vps* operons to the concentration of VpsR as well as c-di-GMP (Hsieh et al., 2020) directly affecting the σ70 RNAP. Additionally, VpsT can act as a regulatory protein with recognition sequences for RbmA, whereas RbmC and Bap1 promoters also contain recognition sites for VpsR (Boyd and O'Toole, 2012; Zhao-Xun, 2015).

Activation of HapR is an important precursor to the process of biofilm dispersion. The N-terminal HTH domain of HapR directly binds to the *vps-2* operon at *vpsL* and *vpsT* (Jonas et al., 2008; Sudarsan et al., 2008). The activation of HapR is controlled by small molecules involved in the quorum sensing pathway. During the biofilm phase, lower concentrations of the quorum sensing molecules AI-2 and CAI-1 activate the transcription of quorum sensing regulatory RNAs (sRNA, via phosphorylation of RpoN and LuxO), which prevent the synthesis of HapR. With the increase in concentrations of AI-2 and CAI-1, LuxO is dephosphorylated, and the sRNAs are repressed, leading to the expression of HapR, eventually resulting in the dispersal of the biofilm (Tchigvintsev et al., 2010). Other negative regulators include the cAMP and the cAMP-receptor protein complex (Liang et al., 2007).

Intricately involved with all these regulatory elements, including those involved in pathogenesis is the secondary signaling messenger molecule cyclic-di-GMP (**Figure 1**; Watnick and Kolter, 2000; Tischler and Camilli, 2005). Both the biofilm activators, VpsT and VpsR can bind to c-di-GMP and has been shown to be responsive to fluctuations in the intracellular concentrations of c-di-GMP in *V. cholerae* (Krasteva et al., 2012; Hay and Zhu, 2015). An increase in the cellular c-di-GMP pool leads to the dimerization and activation of VpsT to induce biofilm formation (Shikuma et al., 2012). Similarly, allosteric activation of VpsR happens when the intracellular concentration of c-di-GMP rises. The activation of both VpsR and VpsT enhances the expression of genes essential for the formation of the biofilm. The third major component which responds to changes in c-di-GMP concentration is the σ^{54}-dependent activator FlrA, which is linked to the expression of flagellar motility. Increased c-di-GMP levels lead to binding of c-di-GMP to FlrA, and inhibition of its activity which in turn diminishes flagellar gene expression (Srivastava et al., 2013). The dynamic extension and retraction of the MSHA pilus (Jones et al., 2015; Wang et al., 2016) is regulated by c-di-GMP via interaction with the ATPase MshE (Floyd et al., 2020). The role of c-di-GMP in the regulation of large adhesins which control reversible cell attachment during biofilm formation also highlights the essentiality of the molecule (Kitts et al., 2019). It is safe to state that c-di-GMP is a crucial and essential regulatory element for surface attachment and biofilm formation in *V. cholerae*.

Biofilm formation would therefore, be ideally associated with the loss of motility and switch toward the sessile, non-pathogenic lifestyle. However, the formation of biofilm is not just an essential ability which enhances the infectivity of *V. cholerae* (Zamorano-Sánchez et al., 2019), but also has been found to be crucial to the process of intestinal colonization. Interestingly, Xu et al. (2003) found that the expression of biofilm genes (*vpsA and rbmA)* was higher in rabbit ileal loop models. However, other biofilm-promoting genes like the *rbmC* and *bap1* did not seem to have any role to play in intestinal infection models (Fong

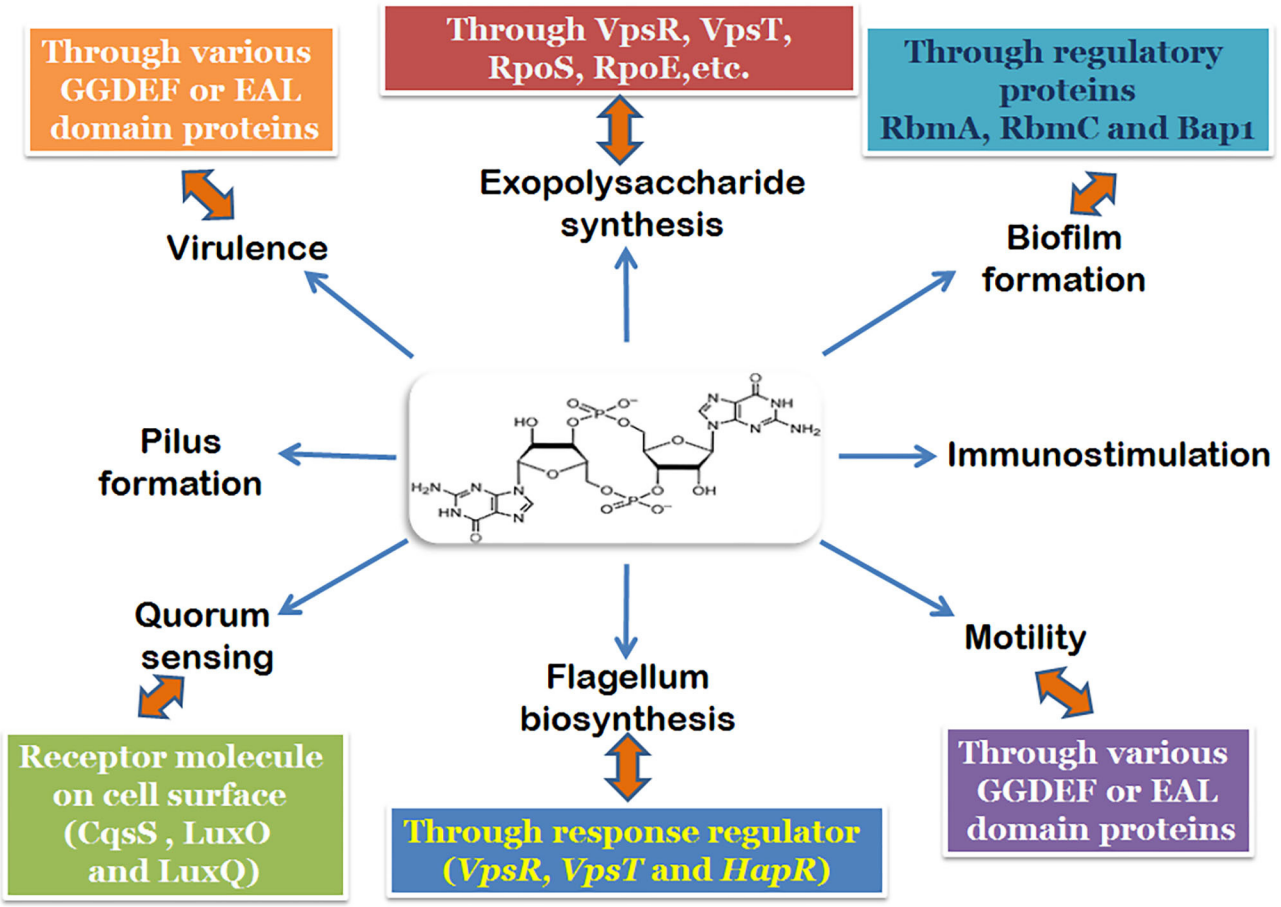

FIGURE 1 | Regulatory pathways and components of the biofilm formation mechanism involving c-di-GMP in *V.* cholerae.

et al., 2006), suggesting that the biofilms formed during intestinal colonization do not proceed beyond the RbmA-dependent primary cell aggregates (Silva and Benitez, 2016). Once in the intestine, the bacterium is exposed to multiple reverses like the effect of taurocholate salts in bile (Hay and Zhu, 2015) which is believed to degrade the VPS of the biofilm. Further repression of *vps* expression happens when the mucus layer is encountered, and the subsequent dispersal of the biofilm (Liu et al., 2007) results in the faster movement of the released bacterium in mucus. It has been postulated that the components of mucin might repress *vps* expression by actually regulating intracellular c-di-GMP concentrations (Liu et al., 2015) during *V. cholerae* infection. However, there has been no further elucidation of the interactions between mucin and c-di-GMP to explain the possible switch in the intestine.

c-di-GMP AND DIGUANYLATE CYCLASES IN *V. CHOLERAE*

Cellular c-di-GMP levels are regulated by the synthesis of activities of c-di-GMP by diguanylate cyclases (DGCs), and degraded by phosphodiesterases (Römling et al., 2013; Bandekar et al., 2017). Apart from *Mycobacterium smegmatis* (only two DGCs) (Kumar and Chatterjee, 2008), there is an abundance of DGCs in different bacterial systems (Römling et al., 2013; Chouhan et al., 2016). The multitude of functionalities regulated by DGCs and phosphodiesterases is very wide and even after years of investigation, the roles that they execute in these processes are not fully understood. The consensus is that the competitive action of the DGCs (and even the phosphodiesterases) results in the complex interactions between various pathways, but how or why these happen is yet to be elucidated. Even the response of DGCs to various extracellular signals and quorum sensing involves an intricate, network-modulated pathway, which might need years to unravel.

In *V. cholerae*, sensing environmental cues in the surrounding water or in the small intestine have been closely associated with fluctuations in the intracellular c-di-GMP pool. Generally, an increase in the levels of cellular c-di-GMP is associated with the suppression of the virulence genes in *V. cholerae* (Tischler and Camilli, 2005; Tamayo et al., 2007). Currently, it is accepted that the bacterium invades the gastrointestinal (GI) cavity with augmented levels of c-di-GMP, which are acted

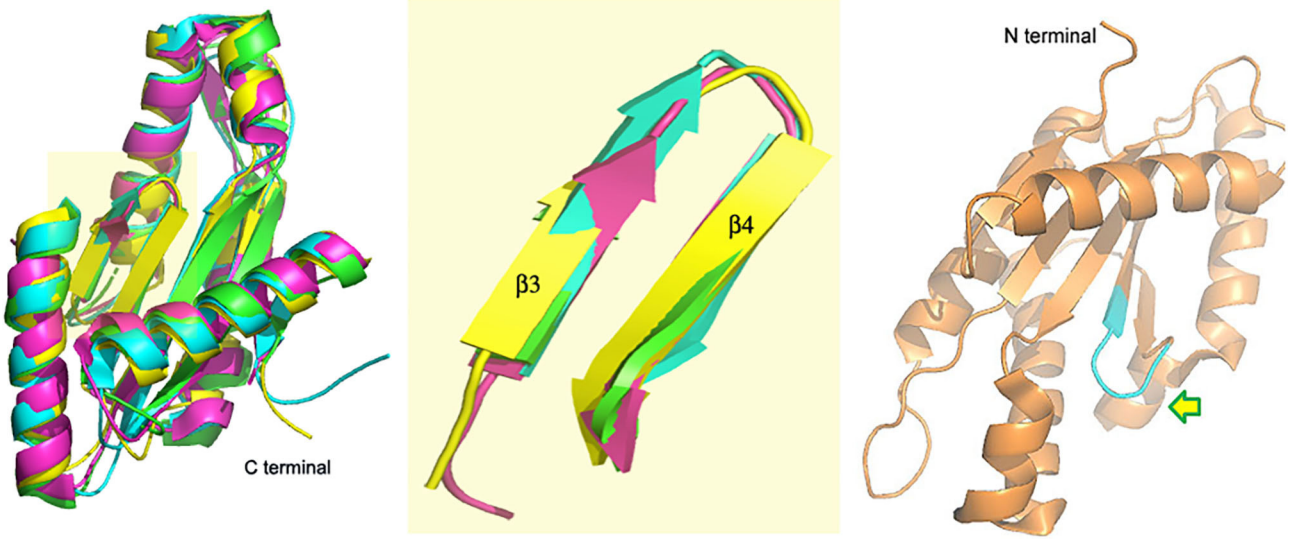

FIGURE 2 | VC0395_0300$_{(161-321)}$ (yellow, 6EIB) aligned with SadC (blue, 4WXW, *Pseudomonas aeruginosa*) and DGCs from *Thermotoga maritima* (green, 4URG) and *Bdellovibrio bacteriovorus* (pink, 6HBZ) Highlight: Alignment of GGDEF domains. Right: Active site of VC0395_0300 in cyan. Arrow shows direction of entry of GTP.

upon by the mucin components and eventually, the action of the phosphodiesterases bring down the c-di-GMP concentration (Koestler and Waters, 2014). During the late infection phase, though, there have been reports of a spurt in c-di-GMP concentration with expression of DGCs (Tamayo et al., 2007). The fluorescent visualization of the distribution of vibrios in the small intestine (Millet et al., 2014) has also brought to light the differential localizations in distinct niches along the small intestine, limited by the abundance of mucin. Together, these cues point to the following scenario—*V. cholerae* invades the GI tract with high levels of cellular c-di-GMP, which is brought down subsequently during the infective stage of the lifecycle. Once the bacteria is in the distal parts of the small intestine, where mucus is less abundant, c-di-GMP levels are raised again, as if in preparation for the life upon exit from the human host.

Diguanylate Cyclases of *V. cholerae*

Diguanylate cyclases, responsible for c-di-GMP synthesis in bacteria, have been associated with a conserved GGD(/E)EF motif across different families (Ryjenkov et al., 2005). In line with the multiplicity of these proteins in bacteria, *V. cholerae* has been known to have 31 different proteins with a conserved GGD(/E)EF domain and 10 with a GGD(/E)EF and EAL (phosphodiesterase) domain in tandem distributed across its two chromosomes (https://www.ncbi.nlm.nih.gov/Complete_Genomes/c-di-GMP.html) (Conner et al., 2017). However, not all of these are associated with motility and/or biofilm formation, and some have not been demonstrated to have DGC activity. Generally DGCs have an active site (A site) where the synthesis of c-di-GMP takes place and a site for allosteric control (RXXD) which regulates the synthesis. We would elaborate on the few DGCs from *V. cholerae* which have been elucidated over the years.

CdgD

When the GGDEF domain was still named as a domain of unknown function (DUF), Yildiz et al. (2004) had identified five genes encoding proteins with GGDEF and GGDEF plus EAL domains which were differentially expressed between the smooth and rugose variants of *V. cholerae*. The proteins encoded by these genes were named Cdg A-E and assayed for their expression. Of these, the CdgD and CdgC deletion mutants showed significant alteration in the biofilm formation of the strains harboring them. While CdgD had a GGDEF domain along with a sensory PAS domain, CdE showed the presence of both GGDEF and EAL domains (Lim et al., 2006). While deletion of *cdgD* caused an increase in motility, *cdgC* mutants were associated with a 2.3-fold decrease in motility. CdgD was later characterized as a diguanylate cyclase and CdgC was responsible for negative regulation of VPS biosynthesis (Lim et al., 2007).

CdgH

Subsequently, (Beyhan et al., 2007) reported the activity of another protein with a predicted GGDEF domain, which they named CdgH. Overexpression of *cdgH* resulted in a high amount of c-di-GMP accumulation in the cell, which established CdgH as a diguanylate cyclase. Additionally, CdgH positively regulated the rugosity of the cell. The structure of CdgH is one of the two solved *V. cholerae* DGC structures, and displayed the presence of two N-terminal tandem periplasmic substrate-binding (PBPb) domains for signal recognition (Xu et al., 2017). Additionally, the same group had characterized several other predicted GGDEF domain proteins, which were not however DGCs.

VCA0965

A further DGC in *V. cholerae* was reported by the Waters lab in 2014 (Hunter et al., 2014). Interestingly, this protein did

not have the conserved GGDEF motif, but had a degenerate AGDEF site. Significantly, expression of VCA0965 in *V. cholerae* was shown to cause a three-fold reduction in flagellar-based motility. This was noteworthy as many of the other predicted GGDEF proteins with conserved sequence did not show DGC activity, whereas VCA0965, despite its degenerate active site, could synthesize c-di-GMP.

VC0395_0300

A DGC with a GGEEF domain was reported by our group in 2017 (Bandekar et al., 2017; Chouhan and Biswas, 2018). While VC0395_0300 was shown to synthesize c-di-GMP actively and had an essential role to play in the biofilm formation of *V. cholerae*, mutations at the central positions of the GGEEF sequence were detrimental to the functional activity of the protein (Chouhan et al., 2016). The structure of the protein though showed similar architecture (**Figure 2**) associated with diguanylate cyclases from other bacterial systems (Chouhan et al., 2020). Another deviation in this DGC was that it lacked the site for allosteric inhibition found in the other DGCs of *V. cholerae*, suggesting a different mode of inhibitory control in this DGC.

CONCLUDING REMARKS

The secondary messenger c-di-GMP plays the most crucial role in the regulation of biofilm formation and motility of *V. cholerae*. The levels of intracellular c-di-GMP are modulated by a host of factors including the diguanylate cyclases from which these are synthesized, the phosphodiesterases which lead to their degradation, and other receptor molecules including several virulence genes. The abundance of GGDEF domains in bacterial species, coupled with the uncertainty around their function as diguanylate cyclases renders further complexity to the mechanism of action of this class of enzymes. To add to the conundrum, the ability of degenerate GGDEF domains to synthesize c-di-GMP and the variance of allosteric inhibitory mechanisms in the DGCs are also systems of interest. It has been hypothesized that the multiple DGCs don't fire in unison—one or a few of them might be expressed at a time, possibly in response to an environmental cue. The association of the DGCs with an extra sensory domain in most cases points to the interaction of the DGC with the extracellular environment. Elucidation of the modes of action of the other DGCs and their regulation vis-à-vis the sensory domain will lead to solving the enigma of multiplicity of the DGCs.

The hitherto unexplored role of c-di-GMP against the host immune system is also an area of intrigue which has been poorly explored. In mammals, c-di-GMP was found to activate the innate immune system by binding to STING (stimulator of interferon genes) (Burdette et al., 2011). However, how the host immune response affects the levels of intercellular c-di-GMP also needs to be explored and should open up newer areas of understanding of this signaling messenger. The observation of hyperinfectivity (a short-lived but elevated infectious state where the virulence gene expression is high) in biofilm-grown cells of *V. cholerae* in comparison to planktonic cells (Gallego-Hernandez et al., 2020), makes it extremely important to understand the mechanism of biofilm-formation in the bacteria.

AUTHOR CONTRIBUTIONS

SB, OC, and DB contributed to the drafting and writing of the manuscript. All authors contributed to the article and approved the submitted version.

REFERENCES

Bandekar, D., Chouhan, O. P., Mohapatra, S., Hazra, M., Hazra, S., and Biswas, S. (2017). Putative protein VC0395_0300 from *Vibrio cholerae* is a diguanylate cyclase with a role in biofilm formation. *Microbiol. Res.* 202, 61–70. doi: 10.1016/j.micres.2017.05.003

Beyhan, S., Bilecen, K., Salama, S. R., Casper-Lindley, C., and Yildiz, F. H. (2007). Regulation of rugosity and biofilm formation in *Vibrio cholerae*: comparison of VpsT and VpsR regulons and epistasis analysis of vpsT, vpsR, and hapR. *J. Bacteriol.* 189, 388–402. doi: 10.1128/JB.00981-06

Boyd, C. D., and O'Toole, G. A. (2012). Second messenger regulation of biofilm formation: breakthroughs in understanding c-di-GMP effector systems. *Annu. Rev. Cell Dev. Biol.* 28, 439–462. doi: 10.1146/annurev-cellbio-101011-155705

Burdette, D. L., Monroe, K. M., Sotelo-Troha, K., Iwig, J. S., Eckert, B., Hyodo, M., et al. (2011). STING is a direct innate immune sensor of cyclic di-GMP. *Nature* 478, 515–518. doi: 10.1038/nature10429

Casper-Lindley, C., and Yildiz, F. H. (2004). VpsT is a transcriptional regulator required for expression of vps biosynthesis genes and the development of rugose colonial morphology in *Vibrio cholerae* O1 El Tor. *J. Bacteriol.* 186, 1574–1578. doi: 10.1128/JB.186.5.1574-1578.2004

Chouhan, O. P., Bandekar, D., Hazra, M., Baghudana, A., Hazra, S., and Biswas, S. (2016). Effect of site-directed mutagenesis at the GGEEF do- main of the biofilm forming GGEEF protein from *Vibrio cholerae*. *AMB Express* 6:2. doi: 10.1186/s13568-015-0168-6

Chouhan, O. P., and Biswas, S. (2018). Subtle changes due to mutations in the GGDEF domain result in loss of biofilm forming activity in the VC0395_0300 protein from *Vibrio cholerae*, but no major change in the overall structure. *Protein Pept. Lett.* 25, 740–747. doi: 10.2174/0929866525666180628162405

Chouhan, O. P., Roske, Y., Heinemann, U., and Biswas, S. (2020). Structure of the active GGEEF domain of a diguanylate cyclase from *Vibrio cholerae*. *Biochem. Biophys. Res.Commun.* 523, 87–292. doi: 10.1016/j.bbrc.2019.11.179

Colwell, R. R., and Huq, A. (1994). Environmental reservoir of *Vibrio cholerae*. the causative agent of cholera. *Ann. N. Y. Acad. Sci.* 740, 44–54. doi: 10.1111/j.1749-6632.1994.tb19852.x

Conner, J. G., Zamorano-Sánchez, D., Park, J. H., Sondermann, H., and Yildiz, F. H. (2017). The ins and outs of cyclic di-GMP signaling in *Vibrio cholerae*. *Curr. Opin. Microbiol.* 36, 20–29. doi: 10.1016/j.mib.2017.01.002

Drescher, K., Jörn, D., Carey, D. N., Sven van, T., Ivan, G., Ned, S. W., et al. (2016). Architectural transitions in *Vibrio cholerae* biofilms at single-cell resolution. *Proc. Natl. Acad. Sci. U.S.A.* 113, E2066–E2072. doi: 10.1073/pnas.1601702113

Echazarreta, M. A., and Klose, K. E. (2019). Vibrio flagellar synthesis. *Front. Cell. Infect. Microbiol.* 9:131. doi: 10.3389/fcimb.2019.00131

Floyd, K. A., Lee, C. K., Xian, W., Nametalla, M., Valentine, A., Crair, B., et al. (2020). c-di-GMP modulates type IV MSHA pilus retraction and surface attachment in *Vibrio cholerae*. *Nat. Commun.* 11:1549. doi: 10.1038/s41467-020-15331-8

Fong, J. C., Karplus, K., Schoolnik, G. K., and Yildiz, F. H. (2006). Identification and characterization of RbmA, a novel protein required for the development of rugose colony morphology and biofilm structure in *Vibrio cholerae*. *J. Bacteriol.* 188, 1049–1059. doi: 10.1128/JB.188.3.1049-1059.2006

Fong, J. C., Syed, K. A., Klose, K. E., and Yildiz, F. H. (2010). Role of Vibrio polysaccharide (vps) genes in VPS production, biofilm

formation and *Vibrio cholerae* pathogenesis. *Microbiology* 156, 2757–2765. doi: 10.1099/mic.0.040196-0

Gallego-Hernandez, A. L., DePas, W. H., Park, J. H., Teschler, J. K., Hartmann, R., Jeckel, H., et al. (2020). Upregulation of virulence genes promotes *Vibrio cholerae* biofilm hyperinfectivity. *Proc. Natl. Acad. Sci. U.S.A.* 117, 11010–11017. doi: 10.1073/pnas.1916571117

Hay, A. J., and Zhu, J. (2015). Host intestinal signal-promoted biofilm dispersal induces *Vibrio cholerae* colonization. *Infect. Immun.* 83, 317–323. doi: 10.1128/IAI.02617-14

He, H., Cooper, J. N., Mishra, A., and Raskin, D. M. (2012). Stringent response regulation of biofilm formation in *Vibrio cholerae*. *J. Bacteriol.* 194, 2962–2972. doi: 10.1128/JB.00014-12

Hsieh, M. L., Waters, C. M., and Hinton, D. M. (2020). VpsR directly activates transcription of multiple biofilm genes in *Vibrio cholerae*. *J. Bacteriol.* 202, e00234–e00220. doi: 10.1128/JB.00234-20

Hunter, J. L., Severin, G. B., Koestler, B. J., and Waters, C. M. (2014). The *Vibrio cholerae* diguanylate cyclase VCA0965 has an AGDEF active site and synthesizes cyclic di-GMP. *BMC Microbiol.* 14:22. doi: 10.1186/1471-2180-14-22

Joachim, R., and Karl, E. K. (2002). *Vibrio cholerae* and cholera: out of the water and into the host. *FEMS Microb. Rev.* 26, 125–139. doi: 10.1111/j.1574-6976.2002.tb00605.x

Jonas, K., Edwards, A. N., Simm, R., Romeo, T., Römling, U., and Melefors, O. (2008). The RNA binding protein CsrA controls cyclic di-GMP metabolism by directly regulating the expression of GGDEF proteins. *Mol. Microbiol.* 70, 236–257. doi: 10.1111/j.1365-2958.2008.06411.x

Jones, C. J., Utada, A., Davis, K. R., Thongsomboon, W., Zamorano-Sánchez, D., Banakar, V., et al. (2015). c-di-GMP regulates motile to sessile transition by modulating MshA pili biogenesis and near-surface motility behavior in *Vibrio cholerae*. *PLoS Pathog* 11:e1005068. doi: 10.1371/journal.ppat.1005068

Kitts, G., Giglio, K. M., Zamorano-Sánchez, D., Park, J. H., Townsley, L., Cooley, R. B., et al. (2019). A conserved regulatory circuit controls large adhesins in *Vibrio cholerae*. *mBio* 10, e02822-19. doi: 10.1128/mBio.02822-19

Koestler, B. J., and Waters, C. M. (2014). Bile acids and bicarbonate inversely regulate intracellular cyclic di-GMP in *Vibrio cholerae*. *Infect. Immun.* 82, 3002–3014. doi: 10.1128/IAI.01664-14

Krasteva, P. V., Giglio, K. M., and Sondermann, H. (2012). Sensing the messenger: the diverse ways that bacteria signal through c-di-GMP. *Protein Sci.* 21, 929–948. doi: 10.1002/pro.2093

Kumar, M., and Chatterjee, D. (2008). Cyclic di-GMP: a second messenger required for long-term survival, but not for biofilm formation in *Mycobacterium smegmatis*. *Microbiology* 154, 2942–2955. doi: 10.1099/mic.0.2008/017806-0

Liang, W., Silva, A. J., and Benitez, J. A. (2007). The cyclic AMP receptor protein modulates colonial morphology in *Vibrio cholerae*. *Appl. Environ. Microbiol.* 73, 737482–737487. doi: 10.1128/AEM.01564-07

Lim, B., Beyhan, S., Meir, J., and Yildiz, F. H. (2006). Cyclic-diGMP signal transduction systems in *Vibrio cholerae*: modulation of rugosity and biofilm formation. *Mol. Microbiol.* 60, 331–348. doi: 10.1111/j.1365-2958.2006.05106.x

Lim, B., Beyhan, S., and Yildiz, F. H. (2007). Regulation of Vibrio polysaccharide synthesis and virulence factor production by CdgC a GGDEF-EAL domain protein in *Vibrio cholerae*. *J. Bacteriol.* 189, 717–729. doi: 10.1128/JB.00834-06

Liu, Z., Stirling, F. R., and Zhu, J. (2007). Temporal quorum-sensing induction regulates *Vibrio cholerae* biofilm architecture. *Infect. Immun.* 75, 122–126. doi: 10.1128/IAI.01190-06

Liu, Z., Wang, Y., Liu, S., Sheng, Y., Rueggeberg, K. G., Wang, H., et al. (2015). *Vibrio cholerae* represses polysaccharide synthesis to promote motility in mucosa. *Infect. Immun.* 83, 1114–1121. doi: 10.1128/IAI.02841-14

Millet, Y. A., Alvarez, D., Ringgaard, S., von Andrian, U. H., Davis, B. M., and Waldor, M. K. (2014). Insights into *Vibrio cholerae* intestinal colonization from monitoring fluorescently labeled bacteria. *PLoS Pathog.* 10:e1004405. doi: 10.1371/journal.ppat.1004405

Rawlings, T. K., Ruiz, G. M., and Colwell, R. R. (2007). Association of *Vibrio cholerae* O1 El Tor and O139 Bengal with the copepods acartia tonsa and Eurytemora affinis. *Appl. Environ. Microbiol.* 73, 7926–7933. doi: 10.1128/AEM.01238-07

Rodney, M. D. (2002). Biofilms: microbial life on surfaces. *Emerg. Infect. Dis.* 8, 881–890. doi: 10.3201/eid0809.020063

Römling, U., Galperin, M. Y., and Gomelsky, M. (2013). Cyclic di GMP: the first 25 years of a universal bacterial second messenger. *Microbiol. Mol. Biol. Rev.* 77, 1–52. doi: 10.1128/MMBR.00043-12

Ryjenkov, D. A., Tarutina, M., Moskvin, O. V., and Gomelsky, M. (2005). Cyclic diguanylate is a ubiquitous signaling molecule in bacteria: insights into biochemistry of the GGDEF protein domain. *J. Bacteriol.* 187, 1792–1798. doi: 10.1128/JB.187.5.1792-1798.2005

Shikuma, N. J., Fong, J. C. N., and Yildiz, F. H. (2012). Cellular levels and binding of c-di-GMP control subcellular localization and activity of the *Vibrio cholerae* transcriptional regulator VpsT. *PLoS Pathog.* 8: e1002719. doi: 10.1371/journal.ppat.1002719

Silva, A. J., and Benitez, J. A. (2016). *Vibrio cholerae* biofilms and cholera pathogenesis. *PLoS Negl. Trop. Dis.* 10:e0004330. doi: 10.1371/journal.pntd.0004330

Sisti, F., Ha, D. G., O'Toole, G. A., Hozbor, D., and Fernández, J. (2013). Cyclic-di-GMP signalling regulates motility and biofilm formation in *Bordetella bronchiseptica*. *Microbiology* 159, 869–879. doi: 10.1099/mic.0.064345-0

Srivastava, D., Hsieh, M. L., Khataokar, A., Neiditch, M. B., and Waters, C. M. (2013). Cyclic di-GMP inhibits *Vibrio cholerae* motility by repressing induction of transcription and inducing extracellular polysaccharide production. *Mol. Microbiol.* 90, 1262–1276. doi: 10.1111/mmi.12432

Sudarsan, N., Lee, E. R., Weinberg, Z., Moy, R. H., Kim, J. N., Link, K. H., et al. (2008). Riboswitches in eubacteria sense the second messenger cyclic di-GMP. *Science* 321, 411–413. doi: 10.1126/science.1159519

Tamayo, R., Pratt, J. T., and Camilli, A. (2007). Roles of cyclic diguanylate in the regulation of bacterial pathogenesis. *Annu. Rev. Microbiol.* 61, 131–148. doi: 10.1146/annurev.micro.61.080706.093426

Tamplin, M. L., Gauzens, A. L., Huq, A., Sack, D. A., and Colwell, R. R. (1990). Attachment of *Vibrio cholerae* serogroup O1 to zooplankton and phytoplankton of Bangladesh waters. *Appl. Env. Microbiol.* 56, 1977–1980. doi: 10.1128/AEM.56.6.1977-1980.1990

Tchigvintsev, A., Xu, X., Singer, A., Chang, C., Brown, G., Proudfoot, M., et al. (2010). Structural insight into the mechanism of c-di-GMP hydrolysis by EAL domain phosphodiesterases. *J. Mol. Biol.* 402, 524–538. doi: 10.1016/j.jmb.2010.07.050

Tischler, A. D., and Camilli, A. (2004). Cyclic diguanylate (c-di-GMP) regulates *Vibrio cholerae* biofilm formation. *Mol. Microbiol.* 53, 857–869. doi: 10.1111/j.1365-2958.2004.04155.x

Tischler, A. D., and Camilli, A. (2005). Cyclic diguanylate regulates *Vibrio cholerae* virulence gene expression. *Infect. Immun.* 73, 5873–5882. doi: 10.1128/IAI.73.9.5873-5882.2005

Utada, A. S., Bennett, R. R., Fong, J. C. N., Gibiansky, M. L., Yildiz, F. H., Golestanian, R., et al. (2014). *Vibrio cholerae* use pili and flagella synergistically to effect motility switching and conditional surface attachment. *Nat. Commun.* 5:4913. doi: 10.1038/ncomms5913

Wang, Y.-C., Chin, K.-H., Tu, Z.-L., He, J., Jones, C. J., Zamorano-Sánchez, D., et al. (2016). Nucleotide binding by the widespread high-affinity cyclic di-GMP receptor MshEN domain. *Nat. Commun.* 7:12481. doi: 10.1038/ncomms12481

Waters, C. M., Lu, W., Rabinowitz, J. D., and Bassler, B. L. (2008). Quorum sensing controls biofilm formation in *Vibrio cholerae* through modulation of cyclic di-GMP levels and repression of vpsT. *J. Bacteriol.* 190, 2527–2536. doi: 10.1128/JB.01756-07

Watnick, P. I., Fullner, K. J., and Kolter, R. (1999). A role for the mannose-sensitive hemagglutinin in biofilm formation by *Vibrio cholerae* El Tor. *J. Bacteriol.* 181, 3606–3609. doi: 10.1128/JB.181.11.3606-3609.1999

Watnick, P. I., and Kolter, R. (2000). Biofilm, city of microbes. *J. Bacteriol.* 182, 2675–2679. doi: 10.1128/JB.182.10.2675-2679.2000

Wong, G. C. L. (2016). Three-dimensional architecture of *Vibrio cholerae* biofilms. *Proc. Natl. Acad. Sci. U.S.A.* 113, 3711–3713. doi: 10.1073/pnas.1603016113

Xu, M., Wang, Y. Z., Yang, X. A., Jiang, T., and Xie, W. (2017). Structural studies of the periplasmic portion of the diguanylate cyclase CdgH from *Vibrio cholerae*. *Sci. Rep.* 7:1861. doi: 10.1038/s41598-017-01989-6

Xu, Q., Dziejman, M., and Mekalanos, J. J. (2003). Determination of the transcriptome of *Vibrio cholerae* during intraintestinal growth and

midexponential phase *in vitro*. *Proc. Natl. Acad. Sci. U.S.A*. 100, 1286–1291. doi: 10.1073/pnas.0337479100

Yildiz, F. H., Liu, X. S., Heydorn, A., and Schoolnik, G. K. (2004). Molecular analysis of rugosity in a *Vibrio cholerae* O1 El Tor phase variant. *Mol. Microbiol.* 53, 497–515. doi: 10.1111/j.1365-2958.2004.04154.x

Yildiz, F. H., and Schoolnik, G. K. (1999). *Vibrio cholerae* O1 El Tor: identification of a gene cluster required for the rugose colony type, exopolysaccharide production, chlorine resistance, and biofilm formation. *Proc. Natl. Acad. Sci. U.S.A*. 96, 4028–4033. doi: 10.1073/pnas.96.7.4028

Zamorano-Sánchez, D., Xian, W., Lee, C. K., Salinas, M., Thongsomboon, W., Cegelski, L., et al. (2019). Functional specialization in *Vibrio cholerae* diguanylate cyclases: distinct modes of motility suppression and c-di-GMP production. *mBio* 10, e00670–e00619. doi: 10.1128/mBio.00670-19

Zhao-Xun, L. (2015). The expanding roles of c-di-GMP in the biosynthesis of exopolysaccharides and secondary metabolites. *Nat. Prod. Rep*. 32, 663–683. doi: 10.1039/C4NP00086B

Conflict of Interest: The authors declare that the research was conducted in the absence of any commercial or financial relationships that could be construed as a potential conflict of interest.

frontiers in Cellular and Infection Microbiology

REVIEW
published: 23 October 2020
doi: 10.3389/fcimb.2020.582554

Crosstalks Between Gut Microbiota and *Vibrio Cholerae*

Zixin Qin†, *Xiaoman Yang*†, *Guozhong Chen*†, *Chaiwoo Park and Zhi Liu**

Department of Biotechnology, College of Life Science and Technology, Huazhong University of Science and Technology, Wuhan, China

Vibrio cholerae, the causative agent of cholera, could proliferate in aquatic environment and infect humans through contaminated food and water. Enormous microorganisms residing in human gastrointestinal tract establish a special microecological system, which immediately responds to the invasion of *V. cholerae*, through "colonization resistance" mechanisms, such as antimicrobial peptide production, nutrients competition, and intestinal barrier maintenances. Meanwhile, *V. cholerae* could quickly sense those signals and modulate the expression of relevant genes to circumvent those stresses during infection, leading to successful colonization on the surface of small intestinal epithelial cells. In this review, we summarized the crosstalks profiles between gut microbiota and *V. cholerae* in the terms of Type VI Secretion System (T6SS), Quorum Sensing (QS), Reactive Oxygen Species (ROS)/pH stress, and Bioactive metabolites. These mechanisms can also be applied to molecular bacterial pathogenesis of other pathogens in host.

Keywords: gut microbiota, *Vibrio cholerae*, T6SS, QS, ROS, pH, Bioactive metabolites

OPEN ACCESS

Edited by:
Yang Fu,
Southern University of Science and Technology, China

Reviewed by:
Xiaohui Zhou,
University of Connecticut, United States
Govind Vediyappan,
Kansas State University, United States

***Correspondence:**
Zhi Liu
zhiliu@hust.edu.cn

†*These authors have contributed equally to this work*

Specialty section:
This article was submitted to Molecular Bacterial Pathogenesis, a section of the journal Frontiers in Cellular and Infection Microbiology

Received: *12 July 2020*
Accepted: *17 September 2020*
Published: *23 October 2020*

Citation:
Qin Z, Yang X, Chen G, Park C and Liu Z (2020) Crosstalks Between Gut Microbiota and Vibrio Cholerae. Front. Cell. Infect. Microbiol. 10:582554. doi: 10.3389/fcimb.2020.582554

INTRODUCTION

To date, the devastating diarrheal disease cholera pandemics have been occurred seven times, and it is still endemics in the world, responsible for up to 3 million cases and 100,000 deaths annually (Theriot and Petri, 2020). *Vibrio cholerae* is the causal organism of the disease cholera, usually infects humans through ingestion of contaminated water and food, colonizes on the surface of small intestine villi with the aid of toxin coregulated pilus (TCP), and then secretes cholera toxin (CT), causing watery diarrhea and vomiting that lead to severe dehydration and even death (Yoon and Waters, 2019). *V. cholerae* is gram-negative, curved and facultative bacterium, with a long unipolar flagellum. According to the serological characteristics of its surface O-antigens, *V. cholerae* has over 200 serotypes, in which only O1 serotype cause the cholera pandemics. Based on the genotypes, O1 *V. cholerae* are further classified into classical biotype and El Tor type (Kaper et al., 1995). Classical biotype was the causative agent of the first six cholera epidemics, while El Tor *V. cholerae* caused the seventh epidemic (Albert, 1994).

In 1894, Metchnikoff, the Russian Nobel laureate, claimed that cholera was a disease to humans due to the fact that the phenotype of human infections could not be precisely replicated in the infections of laboratory model animals (Ritchie and Waldor, 2009). He further speculated that experimental animals could not be infected with *V. cholerae* because of the presence of microorganisms in the gut and suggested that animal cubs could be used as an experimental model because of their significantly lower abundance of gut microbes. Indeed, the 3–5-day-old infant mouse is used as the most common model for *V. cholerae* pathogenesis research. However, there are enormous bacteria resided in host gastrointestinal environment, with the 10 times more

population than those of host cell, those gut microbes provide "colonization resistance" against pathogen invasion. Gut microbiota can produce short-chain fatty acids, antibacterial substances, signal molecules, and bioactive metabolites to benefit host health and to defend pathogenic bacterial infection, such as *V. cholerae* (Ducarmon et al., 2019). Correspondingly, *V. cholerae* can also sense the change of environments and adjust gene expression to increase adaptability (Parker and Sperandio, 2009).

In recent years, an increasing number of researchers turned to study *V. cholerae* pathogenesis under the microbiota background. This review will elaborate the crosstalk profiles between gut microbiota and *V. cholerae* and reveal their synergistic and antagonistic effects from the following aspects: (1) Type VI Secretion System (T6SS), (2) Quorum Sensing (QS), (3) Reactive Oxygen Species (ROS) and pH, (4) Bioactive metabolites. In this review, we aspire to shine the light on the gut microbiota modulation as a promising therapy for *V. cholerae* and related enteric pathogens infection.

T6SS-DEPENDED CROSSTALK BETWEEN GUT MICROBIOTA AND *V. CHOLERAE*

T6SS is a syringe-like protein apparatus, affects the physiological function of susceptible cells by injecting toxic effectors into the cells, including prokaryotes as well as eukaryotes, and even lysing susceptible cells (Pukatzki et al., 2006; Schwarz et al., 2010). Up to 25% of Gram-negative bacteria, including *V. cholerae*, have been reported to contain T6SS (Pukatzki et al., 2006; Bingle et al., 2008; Basler et al., 2012), The *V. cholerae* T6SS consists of the following components: substrate proteins (HisF, VasA, VasB, VasE, and VasJ) attached to the cell outer membrane via protein-to-protein linkages, secretion-promoting tubular sheath exoskeleton protein VipA/VipB (Basler et al., 2012; Broms et al., 2013), sheath protein-coated a tubule of hemolysin co-regulated proteins (Hcps), VgrG protein responsible for punching holes in receptor cells and effector toxin (Shneider et al., 2013; Cianfanelli et al., 2016). Until now, six T6SS effectors with corresponding functions were reported in *V. cholerae*, among them, TleV1 (lipase), TseH (amidase), the C-terminal domain of VgrG-3 (lysozyme) targeted to prokaryotic cells, the C-terminal domain of VgrG-1 (actin-crosslinking) attacked eukaryotes, and VasX (pore formation), TseL (lipase) acted on both prokaryotic and eukaryotic cells (Pukatzki et al., 2007; Miyata et al., 2011; Russell et al., 2011, 2013). Function of *V. cholerae* T6SS only performed when its VipA/VipB protein was contracted rather than extended (**Figure 1**). Susceptible strains can be attacked by T6SS with its toxic effectors, so they have evolved a number of protective mechanisms, such as the production of cognate immune proteins or extracellular polysaccharides (Dong et al., 2013; Fu et al., 2013; Toska et al., 2018). The protective mechanisms, while remaining to be further excavated, may explain why some gut microbes are less vulnerable to T6SS attacks (Fast et al., 2018). Overall, T6SS plays an important role in the interaction between gut microbiota and *V. cholerae*.

Gut microbiota can suppress the expression of *V. cholerae* T6SS by converting bile acids to de-conjugated bile acids through the production of bile salt hydrolase (BSH) (Bachmann et al., 2015; Alavi et al., 2020). While the antagonistic interaction of intestinal microbes with *V. cholerae* T6SS enhances the virulence of *V. cholerae* either in mouse (Zhao et al., 2018), rabbit (Fu et al., 2018) or *Drosophila* model (Fast et al., 2018, 2020), concomitantly, the regenerative function and cell differentiation of intestinal cell are inhibited, resulting in massive intestinal cells shedding and then the exacerbation of the cholera symptoms (Fast et al., 2018, 2020). However, the precise mechanism of interaction between gut microbiota and *V. cholerae* by T6SS is largely unknown and needs to be further explored.

Conversely, *V. cholerae* can use T6SS to enhance its own adaptation in the gut. *V. cholerae* T6SS has direct lethal effect on the Prokaryotic organisms such as *Escherichia coli* MG1655, *Pseudomonas aeruginosa* (Basler et al., 2012, 2013; Dong et al., 2013; Fu et al., 2013; Fast et al., 2018). It can also stimulate the peristalsis of intestinal epithelial cells for excluding gut microbiota, like *Aeromonas veronii*, to improve the efficiency of the colonization (Logan et al., 2018; Booth and Smith, 2020). This suggests that T6SS is a critical method of communication between gut microbiota and *V. cholerae* (**Figure 1**).

QS-DEPENDED CROSSTALK BETWEEN GUT MICROBIOTA AND *V. CHOLERAE*

QS is widely present in different bacteria and adjusts the behavioral changes of the entire population according to the cell density. Different gut microbiota produces different quorum sensing molecules. For example, Acyl-homoserine lactone (AHL) as autoinducer molecule is produced by gram-negative bacteria. Small-molecule polypeptides are produced by gram-positive bacteria. Both types of bacteria can produce the furanyl dibasic compound (2S, 4S)-2-methyl-2,3,3,4-tetrahydroxytetrahydrofuran borate (AI-2). Intestinal microbiota also communicates with each other via quorum sensing signals, transforming intestinal pathogenic commensal bacteria into pathogenic bacteria, and thus impacts on host health (Kim et al., 2020). While *V. cholerae* itself can produce three QS signal molecules, including inter-species communication autoinducer AI-2 (Schauder et al., 2001; Chen et al., 2002), intra-genus-specific autoinducer (S)-3-hydroxytridecan-4-one (CAI-1) (Kelly et al., 2009) and 3,5-dimethylpyrazin-2-ol (DPO) (Herzog et al., 2019). *V. cholerae* adapts to the gut environment through QS signals either by influencing the expression of the primary regulator *hapR*, or through the *vqmA* pathway, which regulates a number of physiological pathways, such as the expression of virulence factors, biofilms, T6SS, the formation of natural transformation states, cell aggregation, and other behaviors (Miller et al., 2002; Zhu et al., 2002; Hammer and Bassler, 2003; Beyhan et al., 2007; Shikuma et al., 2009; Suckow et al., 2011; Lo Scrudato and Blokesch, 2012; Shao and Bassler, 2014; Hawver et al., 2016; Jemielita et al., 2018). It is not surprised that QS is important for communication between gut microbiota and *V. cholerae*.

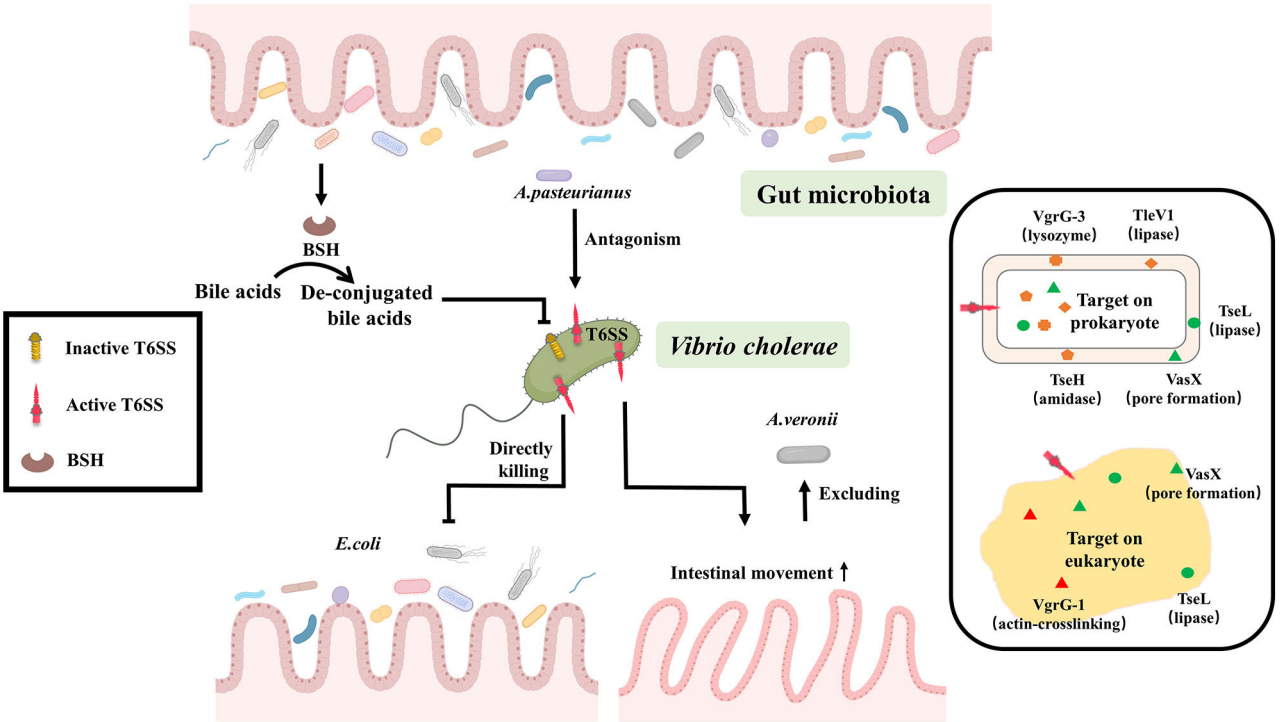

FIGURE 1 | T6SS-depended crosstalk between gut microbiota and *V. cholerae*. Gut microbiota can suppress the expression of *V. cholerae* T6SS by converting bile acids to de-conjugated bile acids through the production of BSH, or some gut bacteria like *A. pasteurianus* can enhance the virulence of *V. cholerae* through antagonizing with *V. cholerae* T6SS. Conversely, *V. cholerae* T6SS has direct lethal effects on the prokaryote, such as *Escherichia coli*. Or it can stimulate the peristalsis of intestinal epithelial cells for excluding gut microbiota, like *Aeromonas veronii*, to improve the efficiency of the colonization. The effector of T6SS plays an important role in those reactions. Six T6SS effectors with corresponding functions were reported in *V. cholerae*, among them, TleV1 (lipase), TseH (amidase), the C-terminal domain of VgrG-3 (lysozyme) targeted to prokaryotic cells, the C-terminal domain of VgrG-1 (actin-crosslinking) attacked eukaryotes, and VasX (pore formation), TseL (lipase) acted on both prokaryotic and eukaryotic cells.

Gut microbiota can influence the physiological status of *V. cholerae* through QS. Ansel Hsiao found that the abundance of *Ruminococcus obeum* was significantly increased in the gut microbiota involved in recovery from *V. cholerae* infection. Further analysis of the function of *R. obeum* on *V. cholerae* revealed that the AI-2 signal produced by *R. obeum* significantly enhanced the colonization of *V. cholerae*. Interestingly, the AI-2 synthesized by *R. obeum luxS* does not act through the *V. cholerae* AI-2 sensor, LuxP, but rather affects the expression of *V. cholerae* virulence through another pathway that involves high expression of *vqmA* (Hsiao et al., 2014). Some researchers speculated that this phenotype may be related to the accumulation of signal molecule DPO, which can activate the QS system via *vqmA* pathway, but the actual mechanism is controversial (Papenfort et al., 2017). Also, recently reported intestinal metabolite ethanolamine, is recognized by CqsR and then up-regulate the expression of *hapR* (Watve et al., 2020), can activate the QS system of *V. cholerae*. It shows that the QS signals produced by gut microbiota are complex and diverse, and it remains to be discovered if there is any communication of other group-sensing signals between gut microbiota and *V. cholerae*.

On the contrary, QS signals produced by *V. cholerae* may also have an effect on the physiological function of other microorganisms. For example, the CAI-1 produced by *V. cholerae* enhances the expression of T3SS virulence of enteropathogenic *Escherichia coli* (EPEC) E2348/69 and subsequent diarrhea in the host (Gorelik et al., 2019). Also, the *V. cholerae* QS system is still poorly understood, so there may be other factors by which *V. cholerae* communicates with gut microbiota via QS signals.

Because QS plays a critical role in interbacterial communication, the combination of QS signaling and synthetic biology methods to modify intestinal probiotics for detection, prevention, and treatment of *V. cholerae* infections has become a new therapeutic approach. For example, modified *Escherichia coli* Nissle1917 can produce *V. cholerae*-derived CAI-1 to reduce colonization of *V. cholerae* (Duan and March, 2008, 2010), or engineered *Lactococcus* lactis subsp. cremoris MG1363 can detect *V. cholerae* in the fecal through CAI-1 signals which is applied for the readily detection of *V. cholerae* (Higgins et al., 2007; Holowko et al., 2016; Mao et al., 2018). In summary, the *V. cholerae* QS will perform different functions depending on various environmental conditions. For *V. cholerae*, either external addition of CAI-1 chemicals (Higgins et al., 2007) or overexpression of CAI-1 using probiotics as carriers (Duan and March, 2008, 2010) inhibits the colonization of *V.*

cholerae, whereas for other intestinal microorganisms, such as EPEC, CAI-1 activates their T3SS expression to enhance virulence. This also reflects the complexity and diversity of the gut environment. Therefore, better understanding of the *V. cholerae* QS system can provide a solid theoretical basis for the clinical treatment for cholera. It is becoming an increasingly promising therapy to mitigate and prevent the *V. cholerae* infection via interfering with the QS signal (**Figure 2**).

ROS/PH-DEPENDED CROSSTALK BETWEEN GUT MICROBIOTA AND *V. CHOLERAE*

Pathogens invading the intestinal environment primarily challenge intestinal innate immunity, which includes ROS and low pH. It is reported that the diversity of the gut microbiota is related to the level of ROS (Yardeni et al., 2019). Gut microbiota can produce ROS by itself (Chen et al., 2019). Meanwhile, L-lactate produced by *Lactobacillus* plantarum can either mediate the consumption of NADH by NOX enzymes or be metabolized in mitochondria through the generation of pyruvate, enhancing ROS levels in the intestine (Iatsenko et al., 2018). Whereas, gut microbiota can also reduce ROS production by metabolizing Short-chain fatty acids (SCFAs) such as N-butyrate (Mottawea et al., 2016) or scavenge ROS by peroxidase (Yoon et al., 2016) to diminish ROS levels in the gut.

To better adapt to the intestinal environment, *V. cholerae* has also evolved a series of mechanisms to defend against or scavenge ROS, including the production of antioxidant molecule like glutathione (Meister and Anderson, 1983), catalase like KatB/KatG (Xia et al., 2017), superoxide dismutase like OhrA/AphC (Cha et al., 2004; Liu et al., 2011, 2016; Wang et al., 2017), even it can protect itself from damaging by high levels of ROS in the intestinal environment through transforming its morphology, such as reversible phase variation between the rugose and smooth colony variants to response to ROS or biofilm formation (Faruque et al., 2006; Sengupta et al., 2016; Wang et al., 2018). Conversely, under inflammatory conditions *V. cholerae* impacts the structure and composition of intestinal microorganisms in multiple pathways. *V. cholerae* can produce a cholera toxin (CT), which causes electrolyte imbalance in the intestine, leading to diarrhea and thus disrupts the structure of intestinal commensal bacteria. Besides, under inflammatory conditions, the concentrations of NO_3^- increases and the available iron concentration decreases, while *V. cholerae* can make better use of NO_3^- as a receptor for the electron respiratory chain and thus multiply faster and occupy an ecological niche (Bueno et al., 2018). *V. cholerae* also could promote their own proliferation by competing with gut microbiota and the host with iron (Rivera-Chavez and Mekalanos, 2019).

Apart from ROS, the host gut environment also has low pH pressure. pH is an important factor for bacterial growth in the gut. Gut microbiota can also alter pH to resist the invasion of *V. cholerae*. Culture supernatants of *Lactobacillus lactis* isolated from feces of healthy children inhibited the biofilm formation of *V. cholerae*. The phenotype that inhibited biofilm formation largely vanished after neutralization of the culture supernatant (Kaur et al., 2018). In addition, *Escherichia coli* 40 and Nissle 1917 isolated from the gut of healthy human volunteers were co-cultured with *V. cholerae* N16961 in LB medium containing glucose, respectively. It was found that both of them reduced the pH value in the medium and affected on the survival rate of *V. cholerae* (Sengupta et al., 2017). In the zebrafish model, the glucose combination with *Escherichia coli* 40 or Nissle 1917 reduced the colonization of *V. cholerae* N16961 by changing the pH in the gut (Nag et al., 2018). This is consistent with the use of glucose-based oral rehydration (ORS) combination with probiotic *Escherichia coli* during cholera treatment. These suggest that gut microbiota and their compositions can inhibit the colonization of *V. cholerae* by changing pH.

Low pH in the intestinal microenvironment affects colonization of *V. cholerae*, and the reason may be that *V. cholerae* can respond to low pH by multiple mechanisms. For example, under hypoxic growth condition, *V. cholerae* can use nitrate as an oxidative phosphorylation electron acceptor, and adjust the process of nitrate/nitrite according to the environmental pH, affecting its own adaptability by inhibiting glycolysis and proton motive force (PMF) (Bueno et al., 2018). In addition, NhaP1, as an antiporter of $K^+(Na^+)/H^+$, enables *V. cholerae* to grow under low pH condition and maintain internal pH homeostasis by removing K^+/Na^+ from the cytoplasm and ingesting H^+. The H^+ enters the respiratory chain and is consumed. This mechanism is more suitable for *V. cholerae* to adapt intestinal microenvironment (Quinn et al., 2012). *V. cholerae* can also regulate lysine decarboxylase by AphB to consume H^+ so that it can alleviate low pH states (Kovacikova et al., 2010). Under alkaline conditions, *V. cholerae* can suppress related acid tolerance genes via OmpR and increase fitness (Kunkle et al., 2020). Indeed, *V. cholerae* itself has different pH patterns of fermentation depended on glucose. El Tor N16961 can produce 2, 3-butanediol as the neutral product of fermentation, avoiding the acidification of the medium. In contrast, classic biotype O395 is unable to synthesize 2, 3-butanediol, therefore its viability is diminished during mixed fermentation with glucose due to the acidification of the medium by synthetic organic acids (Lee et al., 2020).

The mechanism by which *V. cholerae* affects gut microbiota by changing pH is unknown. However, *V. cholerae* can produce cholera toxin to cause intestinal inflammation of the host, resulting in intestinal electrolyte imbalance. This may affect pH changes to compete for niches.

Thus, it is known that gut microbiota can influence the ROS or pH of the gut environment to interfere with the colonization and infection of *V. cholerae*. In turn, *V. cholerae* can develop mechanisms to defend against it. This indicates that the interaction between gut microbiota and *V. cholerae* is complex and versatile (**Figure 3**).

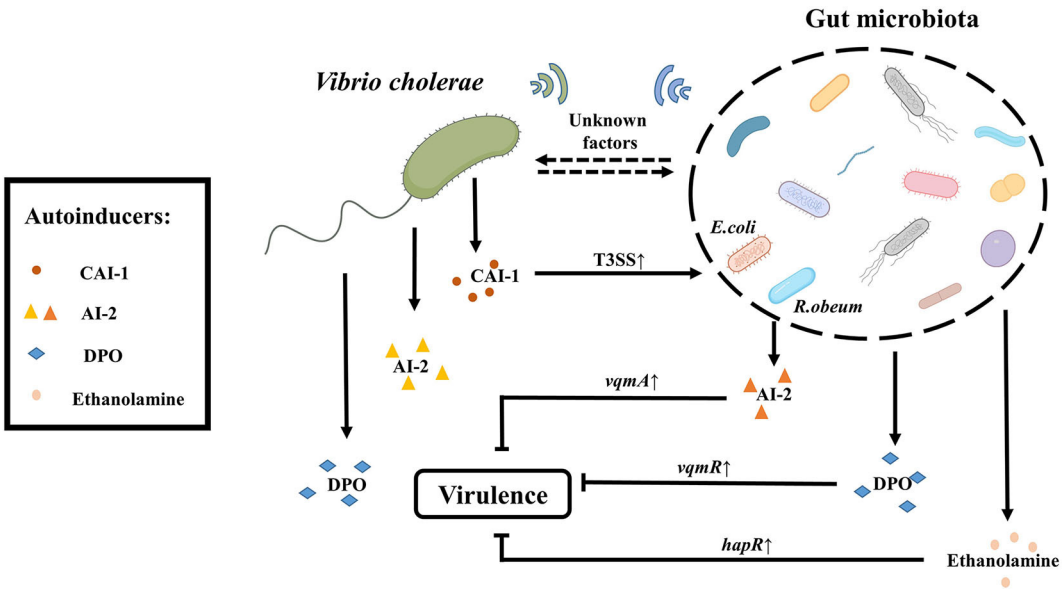

FIGURE 2 | QS- depended crosstalk between gut microbiota and *V. cholerae*. The gut microbiota like *R. obeum* can reduce the colonization of *V. cholerae* in the intestine by generating the quorum sensing signal AI-2 (different from the *V. cholerae* AI-2). The gut microbiota can also suppress the virulence of *V. cholerae* through metabolites such as ethanolamine or DPO mediated by *hapR* and *vqmR,* respectively. In addition, there are a series of unknown signaling molecules to be exploited. Conversely, *V. cholerae* itself can produce three kinds of autoinducers including CAI-1, AI-2, and DPO. CAI-1 produced by *V. cholerae* can enhance the pathogenicity of *E. coli* by up-regulating the expression of T3SS-associated genes. And there may be other factors by which *V. cholerae* communicates with gut microbiota via QS signals.

BIOACTIVE METABOLITES-DEPENDED CROSSTALK BETWEEN GUT MICROBIOTA AND *V. CHOLERAE*

Bioactive metabolites are also an important way for the gut microbiota to communicate with each other. The main bioactive metabolites include SCFAs, bacteriocins, and bile acids.

SCFAs are fatty acid fermentation products of microorganisms with indigestible polysaccharides as substrates. The concentration of SCFAs is relatively abundant in the proximal colon of the host. SCFAs are metabolites of gut microbiota and participate in the regulation of various host physiological process (Dalile et al., 2019). Surveillance of clinical samples of *V. cholerae* infection found that the content of SCFAs in the host decreased and the probiotic *Bifidobacterium* abundance decreased after *V. cholerae* infection. As the treatment progresses, the abundance of *Bifidobacterium* and SCFAs were return to normal levels (Monira et al., 2010). Besides, mice treated with clindamycin reduced the abundance of *Bacteroides* and the content of SCFAs to enhance the colonization ability of *V. cholerae* (You et al., 2019). All these indicate that probiotics in the host can antagonize the colonization of *V. cholerae* by secreting SCFAs. In the process of infecting the host, *V. cholerae* can also activate the transcription of acetyl-CoA synthase-1 (ACS-1) through the two-component system CrbRS, thereby regulating the conversion of *V. cholerae* acetate to deplete the acetate in the intestinal environment for protecting itself. The absence of this acetate will cause the host's insulin signal transduction pathway to be blocked and the accumulation of lipids, which will affect the host's health (Hang et al., 2014).

Antimicrobial peptide is a kind of peptide with antibacterial activity, which can be divided into two categories in the intestinal environment: host-derived antimicrobial peptides and microbial-derived antimicrobial peptides (also known as bacteriocins). The host-derived antimicrobial peptides are mainly produced by intestinal epithelial cells and Pan's cells, including defensins, cathelicidins, lysozymes, chemokines, etc. (Chung and Raffatellu, 2019). During *V. cholerae* infection, the expression of host-derived antimicrobial peptides is upregulated, including α-defensin (HD-5 and−6), β-defensin (hBD-1-4), cathelicidin (LL-37), etc. (Qadri et al., 2004; Shirin et al., 2011). Human α-defensin generally damages bacteria by disrupting cell membranes, while HD-6 defends against pathogenic bacteria by trapping microbes in the intestinal lumen (Chairatana and Nolan, 2017). Human β-defensin can also mediate membrane lysis to exert antimicrobial activity, as well as capture or kill bacteria by inducing self-nets and neutrophil extracellular traps (NETs) (Alvarez et al., 2018). In addition, cathelicidin can mediate membrane perturbation and induce ROS production to inhibit bacterial growth (Rowe-Magnus et al., 2019). *V. cholerae* has also evolved a response mechanism that uses the major virulence protein cholera toxin CT to activate several intracellular signaling pathways involving protein kinase A (PKA), ERK-MAPKinase, and Cox-2 to downregulate the transcription of AMPs with cAMP accumulation (Chakraborty et al., 2008). The antimicrobial peptides or bacteriocin derived from bacteria can be divided

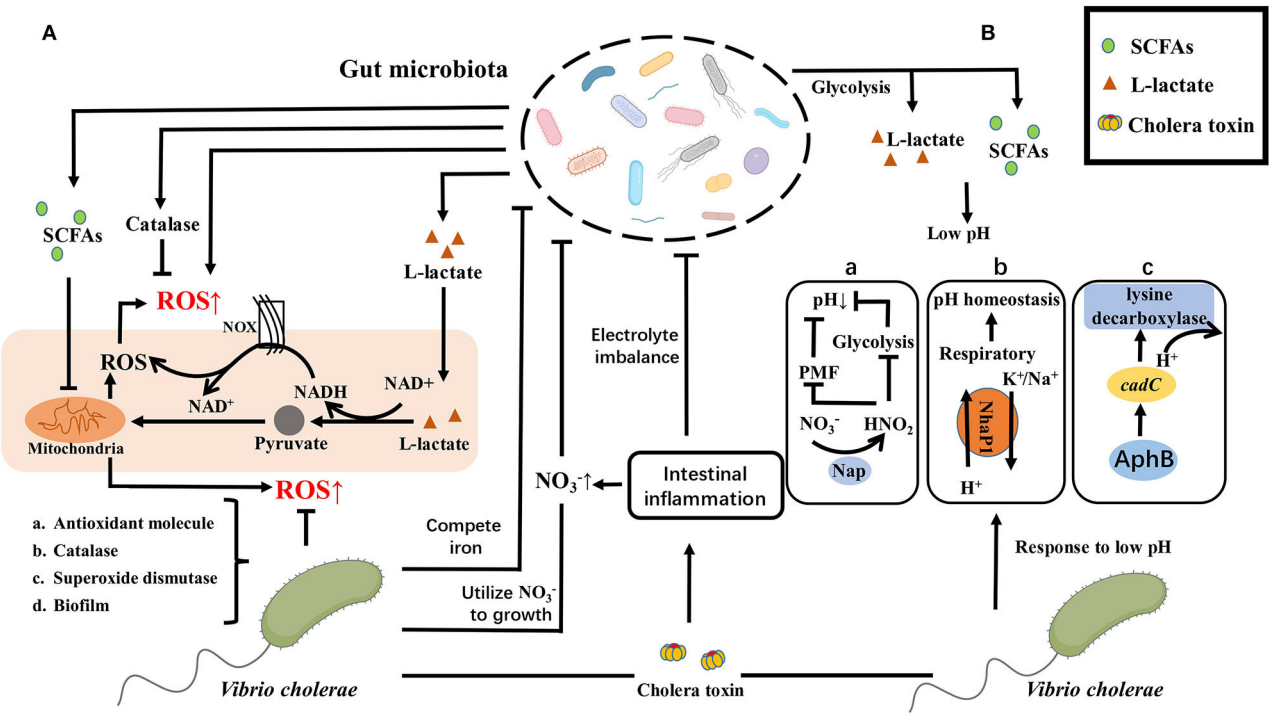

FIGURE 3 | ROS/pH-depended crosstalk between gut microbiota and *V. cholerae*. **(A)** Gut microbiota can produce ROS directly or activate the host to produce ROS, such as L-lactate produced by *Lactobacillus Plantarum* can either mediate the consumption of NADH by NOX enzymes or metabolized in mitochondria through the generation of pyruvate, increasing ROS levels in the gut. While gut microbiota can also reduce ROS production by metabolizing SCFAs such as N-butyrate or scavenge ROS by peroxidase to diminish ROS levels in the gut. To better adapt to the intestinal microenvironment, *V. cholerae* has also evolved a series of mechanisms to defend against or scavenge ROS, including the production of (a) antioxidant molecule, (b) catalase, (c) superoxide dismutase, or (d) transform its morphology, like biofilm formation. Conversely, *V. cholerae* impacts the structure and composition of intestinal microorganisms in multiple pathways, including causing electrolyte imbalance in the intestine through the production of CT to disrupt the structure of intestinal commensal bacteria, or making better use of NO_3^- as a receptor for the electron respiratory chain and competing with gut microbiota and the host with iron to promote their own proliferation and occupy an ecological niche. **(B)** *E. coli* glucose fermentation and *lactobacillus* metabolites create a low pH environment to prevent the *V. cholerae* from colonizing in the small intestine by producing SCFAs and L-Lactate. While *V. cholerae* has a variety of response strategies, containing (a) anaerobic nitrate respiration of *V. cholerae* on bacterial expansion dependent on pH by inhibiting glycolysis and PMF to reduce the acid formation; (b) the cytoplasmic K^+/Na^+ exchanged at low pH to maintain pH homeostasis; (c) the expression of *cadC* activated by AphB to consume H^+. Same as ROS response, *V. cholerae* can also cause electrolyte imbalance in the intestine by producing CT to disrupt the structure of intestinal commensal bacteria.

into gram-positive bacteriocin and gram-negative bacteriocin according to the type of bacteria. In the study of bacteriocin, Nisin produced by the genus streptococcus is relatively extensive (Hammami et al., 2013). The culture supernatant of *Pediococcus acidilacticii* QC38 isolated from food producing bacteriocin, showed inhibitory activity on the growth of *V. cholerae in vitro*, indicating that bacteriocins produced by probiotic QC38 had antagonistic effect on *V. cholerae* (Morales-Estrada et al., 2016). Previously, *Lactobacillus casei* OGM12 isolated from the food also showed inhibitory activity against *V. cholerae*, which produces bacteriocin casein A (Olasupo et al., 1995). Also, the bacteriocin produced by *Streptococcus lactis* 11451 showed inhibitory activity against *V. cholerae in vitro* (Spelhaug and Harlander, 1989). These indicate that the bacteriocin produced by probiotics has antibacterial activity against *V. cholerae*.

V. cholerae possesses its own antagonistic mechanism against this antimicrobial active peptide. Resistance-nodulation-division (RND) mutants are sensitive to antimicrobial peptides *in vitro* and showed colonization defects on infant mice experiments. These phenotypes indicate RND efflux pump is important for *V. cholerae* to resist the toxicity of antimicrobial peptides (Bina et al., 2008). Besides, the outer membrane vesicles (OMV) of *V. cholerae* also play a crucial role in this stress condition. In the presence of antimicrobial peptides, the OMV content secreted by *V. cholerae* does not change, while the structure is altered, including the two outer membrane proteins OmpV and OmpW, as well as the Bap1 protein. Research showed that Bap1 protein can be combined with OmpT protein on the surface of OMV and can also be used as a ligand to capture antibacterial peptides to achieve the protection of bacteria (Duperthuy et al., 2013). *V. cholerae* also has a periplasmic space protein SipA, which can interact with the outer membrane protein OmpA. After the antibacterial peptide enters the periplasmic space, it may be captured by SipA, and

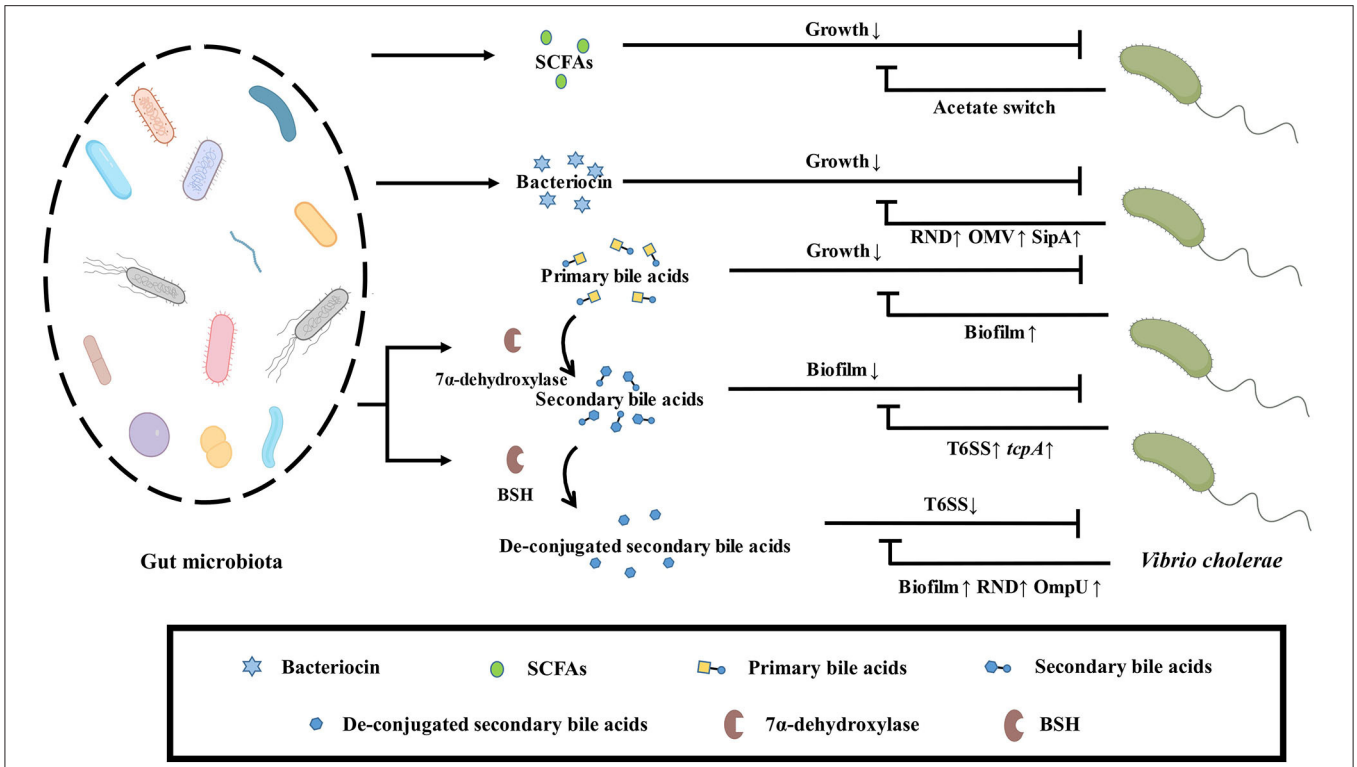

FIGURE 4 | Effect of bioactive metabolites produced by gut microbiota on *V. cholerae*. SCFAs secreted by the gut microbiota inhibit the growth of *V. cholerae*, which depletes the intestinal microenvironment of acetate via acetate switch to resist this stress. Bacteriocins secreted by the gut microbiota also inhibit the growth of *V. cholerae*, which excretes bacteriocins through upregulation of the RND efflux pump family related-genes, outer membrane vesicles, and the periplasmic space protein SipA to avoid accumulating toxicity. Primary bile salts inhibit the growth of *V. cholerae*, which resists stress by forming biofilms. Secondary bile acids formed by the metabolism of primary bile salts by gut microbiota dissociate the biofilm of *V. cholerae*, but *V. cholerae* kills gut microbiota by upregulating virulence and T6SS to gain ecological niche. Gut microbiota can reduce the toxicity of T6SS by de-conjugation of secondary bile salts by BSH, but *V. cholerae* can enhance colonization by forming biofilms, upregulating the RND efflux pump family related-genes and the porin OmpU to resist stress.

then interact with OmpA to transport out antimicrobial peptides (Saul-McBeth and Matson, 2019).

Bile acids are an important substance involved in the regulation of the hepatic-intestinal axis. Primary bile acids are produced from the body's liver using cholesterol as a substrate, followed by bile and discharged into the intestinal cavity, and then metabolized by the gut microbiota secondarily, in the terminal jejunum or ileum through the portal vein reabsorption back to the liver. In the human body, the primary bile acids produced by the liver mainly include cholic acid (CA) and chenodeoxycholic acid (CDCA), and then form conjugated bile acid (CBA) with taurine or glycine to enter the gallbladder and transport to small intestine (Ridlon et al., 2016). Most bile salts would be absorbed by the body from the terminal ileum, but some bile salts will be metabolized by gut microbiota to produce secondary bile salts (Wahlström et al., 2016). *V. cholerae* in the mature biofilm state is disrupted by taurocholate by altering the biofilm matrix and promoting biofilm disintegration (Hay and Zhu, 2015). Besides, taurocholate stimulates the formation of C207-C207 disulfide bonds between TcpP molecules, thereby activating the expression of the virulence gene *toxT* (Yang et al., 2013). In the case of mucin-activated *V. cholerae* T6SS expression, the taurine and glycine groups in the conjugated deoxycholic acid will enhance the killing effect of *V. cholerae* T6SS on intestinal commensal bacteria. Thus, while conjugated secondary bile acids inhibit *V. cholerae* biofilm formation, *V. cholerae* can also kill gut microbiota to gain ecological niche by increasing T6SS and virulence. The free deoxycholic acid metabolized by the gut microbiota in turn inhibits the toxicity of *V. cholerae* T6SS. Therefore, gut microbiota can resist the killing effect of pathogenic bacteria by adjusting bile acid metabolism (Bachmann et al., 2015). Pathogen-susceptible mice can acquire colonization resistance to *V. cholerae* by fecal microbiota transplantation (FMT). Further research has found that *Blautia obeum*'s BSH enzyme deconjugate *tcpA* expression dependent secondary conjugated bile salts to down-regulate the expression of virulence gene in *V. cholerae* (Alavi et al., 2020). *V. cholerae* has reduced cell membrane permeability and upregulate *acrAB* gene expression to encode RND family outflow pump for avoiding accumulation toxicity of intracellular bile acids after sensing bile acid stimulation *in vitro*. This phenomenon is also found in rabbit isolated intestine models (Chatterjee et al., 2004). In addition, *V. cholerae* upregulates the porin OmpU and downregulates OmpT to resist deoxycholic acid stress via toxR (Provenzano

and Klose, 2000; Ante et al., 2015). Biofilm-free *V. cholerae* activates *vps* gene and *vpsR* transcriptional activator expression to form biofilms against bile acids toxicity after deoxycholic acid and cholic acid salt stimulation (Hung et al., 2006). Thus, while the gut microbiota can de-conjugate secondary conjugated bile salts to reduce *V. cholerae* T6SS and virulence, *V. cholerae* enhances colonization by forming biofilms, upregulating the RND efflux pump family proteins, and regulating porins against bile acids toxicity.

Probiotic flora abundance correlates with the concentration of SCFAs in the intestinal environment, and correspondingly, SCFAs resist *V. cholerae* infection. SCFAs, the metabolites involved in the regulation of many physiological functions, and their mechanism of protecting against *V. cholerae* infection are unclear. At present, the research on the antagonism of bacteriocin produced by gut microbiota to *V. cholerae* mainly focuses on the genus *Streptococcus*, and little research has been done on the production of bacteriocins by other commensal gut bacteria. Also, the research on the molecular mechanism of *V. cholerae* in response to antimicrobial peptides mainly uses host-derived antimicrobial peptides, and the interaction mechanism between *V. cholerae* and bacteriocins is also unclear. Studies on bile acids and *V. cholerae* have focused on the effects of bile acid salts conjugation and de-conjugation on the virulence of *V. cholerae*. In addition, bile acids are metabolized by BSH enzymes from the gut microbiota and then undergo metabolic pathways such as 7α-HSDH and 3α-HSDH to produce other types of bile acids. The interaction of these kinds of bile acids with *V. cholerae* need more research (**Figure 4**).

CONCLUSIONS AND PERSPECTIVES

The virulence regulation network of *V. cholerae* has been well-studied. However, the classical animal model and the germ-free animal model of *V. cholerae* have ignored the role of gut microbiota. Interestingly, gut microbiota can not only use intestinal barrier to directly resist the invasion of *V. cholerae*, but also inhibit the colonization of *V. cholerae* through their metabolites, including autoinducer signaling molecules, antimicrobial peptides, short-chain fatty acids, bile salts and so on (Ducarmon et al., 2019). Correspondingly, *V. cholerae*, an intestinal pathogen, adjusts the expressions of its genes to respond to stress in the terms of T6SS, QS, ROS/pH, biofilm.

So far, the ways in which many QS signaling molecules produced by host or gut microbiota communicate with pathogens remain unknown, making it difficult to find novel quorum quenching molecules to reduce the pathogenicity of *V. cholerae*. Furthermore, traditional antibiotic therapy is facing a big challenge, which involves the drug resistance and the accelerating evolution of pathogens. Thus, the treatment of cholera by regulating the microecology of gut microbiota will be a potential therapy.

The intestine is a complex micro-ecological system, in which gut microbes have complex composition, with dynamic adjustment according to the external environment disturbance. So, the investigation of gut microbes and pathogen interactions require multidisciplinary technology platforms, including big data analysis, Next-generation sequencing, *in situ* fluorescence microscopic imagination, and lab-in-chip automatic systems (Baumler and Sperandio, 2016). Gut microbiota is the important and active component in the gastrointestinal tract, which activity should be considered in studies of the pathogenesis of enteric pathogens, representatively, *V. cholerae*. The detailed information of molecular crosstalk between commensal gut bacteria and enteric pathogens would shed a light on the prevention and control of all infectious disease.

AUTHOR CONTRIBUTIONS

ZL provided the general concept. ZQ, XY, GC, and ZL drafted the initial concept of manuscript, and wrote the manuscript. CP provided the critical review of the manuscript. All the authors have seen and approved the final manuscript.

FUNDING

This work was supported by the National Key R&D Program of China (2019YFA0905600), the National Natural Science Foundation of China (31770132 and 81873969).

ACKNOWLEDGMENTS

We thank all the members of Liu lab for helpful discussion, Quanxian She for critically reading the manuscript.

REFERENCES

Alavi, S., Mitchell, J. D., Cho, J. Y., Liu, R., Macbeth, J. C., and Hsiao, A. (2020). Interpersonal gut microbiome variation drives susceptibility and resistance to cholera infection. *Cell* 181, 1533–1546.e13. doi: 10.1016/j.cell.2020.05.036

Albert, M. J. (1994). *Vibrio cholerae* O139 Bengal. *J. Clin. Microbiol.* 32, 2345–2349. doi: 10.1128/JCM.32.10.2345-2349.1994

Alvarez, A. H., Martinez Velazquez, M., and Prado Montes de Oca, E. (2018). Human beta-defensin 1 update: potential clinical applications of the restless warrior. *Int. J. Biochem. Cell. Biol.* 104, 133–137. doi: 10.1016/j.biocel.2018.09.007

Ante, V. M., Bina, X. R., Howard, M. F., Sayeed, S., Taylor, D. L., and Bina, J. E. (2015). *Vibrio cholerae leuO* transcription is positively regulated by ToxR and contributes to bile resistance. *J. Bacteriol.* 197, 3499–3510. doi: 10.1128/JB.00419-15

Bachmann, V., Kostiuk, B., Unterweger, D., Diaz-Satizabal, L., Ogg, S., and Pukatzki, S. (2015). Bile salts modulate the mucin-activated type VI secretion system of pandemic *Vibrio cholerae*. *PLoS Negl. Trop. Dis.* 9:e0004031. doi: 10.1371/journal.pntd.0004031

Basler, M., Ho, B. T., and Mekalanos, J. J. (2013). Tit-for-tat: type VI secretion system counterattack during bacterial cell-cell interactions. *Cell* 152, 884–894. doi: 10.1016/j.cell.2013.01.042

Basler, M., Pilhofer, M., Henderson, G. P., Jensen, G. J., and Mekalanos, J. J. (2012). Type VI secretion requires a dynamic contractile phage tail-like structure. *Nature* 483, 182–186. doi: 10.1038/nature10846

Baumler, A. J., and Sperandio, V. (2016). Interactions between the microbiota and pathogenic bacteria in the gut. *Nature* 535, 85–93. doi: 10.1038/nature18849

Beyhan, S., Bilecen, K., Salama, S. R., Casper-Lindley, C., and Yildiz, F. H. (2007). Regulation of rugosity and biofilm formation in *Vibrio cholerae*: comparison of VpsT and VpsR regulons and epistasis analysis of *vpsT*, *vpsR*, and *hapR*. *J. Bacteriol.* 189, 388–402. doi: 10.1128/JB.00981-06

Bina, X. R., Provenzano, D., Nguyen, N., and Bina, J. E. (2008). *Vibrio cholerae* RND family efflux systems are required for antimicrobial resistance, optimal virulence factor production, and colonization of the infant mouse small intestine. *Infect. Immun.* 76, 3595–3605. doi: 10.1128/IAI.01620-07

Bingle, L. E., Bailey, C. M., and Pallen, M. J. (2008). Type VI secretion: a beginner's guide. *Curr. Opin. Microbiol.* 11, 3–8. doi: 10.1016/j.mib.2008.01.006

Booth, S. C., and Smith, W. P. J. (2020). Light sheets unveil host-microorganism interactions. *Nat. Rev. Microbiol.* 18:65. doi: 10.1038/s41579-019-0318-y

Broms, J. E., Ishikawa, T., Wai, S. N., and Sjostedt, A. (2013). A functional VipA-VipB interaction is required for the type VI secretion system activity of *Vibrio cholerae* O1 strain A1552. *BMC Microbiol.* 13:96. doi: 10.1186/1471-2180-13-96

Bueno, E., Sit, B., Waldor, M. K., and Cava, F. (2018). Anaerobic nitrate reduction divergently governs population expansion of the enteropathogen *Vibrio cholerae*. *Nat. Microbiol.* 3, 1346–1353. doi: 10.1038/s41564-018-0253-0

Cha, M. K., Hong, S. K., Lee, D. S., and Kim, I. H. (2004). *Vibrio cholerae* thiol peroxidase-glutaredoxin fusion is a 2-Cys TSA/AhpC subfamily acting as a lipid hydroperoxide reductase. *J. Biol. Chem.* 279, 11035–11041. doi: 10.1074/jbc.M312657200

Chairatana, P., and Nolan, E. M. (2017). Human alpha-defensin 6: a small peptide that self-assembles and protects the host by entangling microbes. *Acc. Chem. Res.* 50, 960–967. doi: 10.1021/acs.accounts.6b00653

Chakraborty, K., Ghosh, S., Koley, H., Mukhopadhyay, A. K., Ramamurthy, T., Saha, D. R., et al. (2008). Bacterial exotoxins downregulate cathelicidin (hCAP-18/LL-37) and human beta-defensin 1 (HBD-1) expression in the intestinal epithelial cells. *Cell. Microbiol.* 10, 2520–2537. doi: 10.1111/j.1462-5822.2008.01227.x

Chatterjee, A., Chaudhuri, S., Saha, G., Gupta, S., and Chowdhury, R. (2004). Effect of bile on the cell surface permeability barrier and efflux system of *Vibrio cholerae*. *J. Bacteriol.* 186, 6809–6814. doi: 10.1128/JB.186.20.6809-6814.2004

Chen, D., Wu, J., Jin, D., Wang, B., and Cao, H. (2019). Fecal microbiota transplantation in cancer management: current status and perspectives. *Int. J. Cancer* 145, 2021–2031. doi: 10.1002/ijc.32003

Chen, X., Schauder, S., Potier, N., Van Dorsselaer, A., Pelczer, I., Bassler, B. L., et al. (2002). Structural identification of a bacterial quorum-sensing signal containing boron. *Nature* 415, 545–549. doi: 10.1038/415545a

Chung, L. K., and Raffatellu, M. (2019). G.I. Pros: Antimicrobial defense in the gastrointestinal tract. *Semin. Cell. Dev. Biol.* 88, 129–137. doi: 10.1016/j.semcdb.2018.02.001

Cianfanelli, F. R., Alcoforado Diniz, J., Guo, M., De Cesare, V., Trost, M., and Coulthurst, S. J. (2016). VgrG and PAAR proteins define distinct versions of a functional type VI secretion system. *PLoS Pathog.* 12:e1005735. doi: 10.1371/journal.ppat.1005735

Dalile, B., Van Oudenhove, L., Vervliet, B., and Verbeke, K. (2019). The role of short-chain fatty acids in microbiota-gut-brain communication. *Nat. Rev. Gastroenterol. Hepatol.* 16, 461–478. doi: 10.1038/s41575-019-0157-3

Dong, T. G., Ho, B. T., Yoder-Himes, D. R., and Mekalanos, J. J. (2013). Identification of T6SS-dependent effector and immunity proteins by Tn-seq in *Vibrio cholerae*. *Proc. Natl. Acad. Sci. U.S.A.* 110, 2623–2628. doi: 10.1073/pnas.1222783110

Duan, F., and March, J. C. (2008). Interrupting *Vibrio cholerae* infection of human epithelial cells with engineered commensal bacterial signaling. *Biotechnol. Bioeng.* 101, 128–134. doi: 10.1002/bit.21897

Duan, F., and March, J. C. (2010). Engineered bacterial communication prevents *Vibrio cholerae* virulence in an infant mouse model. *Proc. Natl. Acad. Sci. U.S.A.* 107, 11260–11264. doi: 10.1073/pnas.1001294107

Ducarmon, Q. R., Zwittink, R. D., Hornung, B. V. H., van Schaik, W., Young, V. B., and Kuijper, E. J. (2019). Gut microbiota and colonization resistance against bacterial enteric infection. *Microbiol. Mol. Biol. Rev.* 83:e00007-19. doi: 10.1128/MMBR.00007-19

Duperthuy, M., Sjostrom, A. E., Sabharwal, D., Damghani, F., Uhlin, B. E., and Wai, S. N. (2013). Role of the *Vibrio cholerae* matrix protein Bap1 in cross-resistance to antimicrobial peptides. *PLoS Pathog.* 9:e1003620. doi: 10.1371/journal.ppat.1003620

Faruque, S. M., Biswas, K., Udden, S. M., Ahmad, Q. S., Sack, D. A., Nair, G. B., et al. (2006). Transmissibility of cholera: *in vivo*-formed biofilms and their relationship to infectivity and persistence in the environment. *Proc. Natl. Acad. Sci. U.S.A.* 103, 6350–6355. doi: 10.1073/pnas.0601277103

Fast, D., Kostiuk, B., Foley, E., and Pukatzki, S. (2018). Commensal pathogen competition impacts host viability. *Proc. Natl. Acad. Sci. U.S.A.* 115, 7099–7104. doi: 10.1073/pnas.1802165115

Fast, D., Petkau, K., Ferguson, M., Shin, M., Galenza, A., Kostiuk, B., et al. (2020). *Vibrio cholerae*-symbiont interactions inhibit intestinal repair in *drosophila*. *Cell Rep. 30*, 1088–1100.e1085. doi: 10.1016/j.celrep.2019.12.094

Fu, Y., Ho, B. T., and Mekalanos, J. J. (2018). Tracking *Vibrio cholerae* cell-cell interactions during infection reveals bacterial population dynamics within intestinal microenvironments. *Cell Host Microbe 23*, 274–281.e272. doi: 10.1016/j.chom.2017.12.006

Fu, Y., Waldor, M. K., and Mekalanos, J. J. (2013). Tn-Seq analysis of *Vibrio cholerae* intestinal colonization reveals a role for T6SS-mediated antibacterial activity in the host. *Cell Host Microbe* 14, 652–663. doi: 10.1016/j.chom.2013.11.001

Gorelik, O., Levy, N., Shaulov, L., Yegodayev, K., Meijler, M. M., and Sal-Man, N. (2019). *Vibrio cholerae* autoinducer-1 enhances the virulence of enteropathogenic *Escherichia coli*. *Sci. Rep.* 9:4122. doi: 10.1038/s41598-019-40859-1

Hammami, R., Fernandez, B., Lacroix, C., and Fliss, I. (2013). Anti-infective properties of bacteriocins: an update. *Cell. Mol. Life Sci.* 70, 2947–2967. doi: 10.1007/s00018-012-1202-3

Hammer, B. K., and Bassler, B. L. (2003). Quorum sensing controls biofilm formation in *Vibrio cholerae*. *Mol. Microbiol* 50, 101–104. doi: 10.1046/j.1365-2958.2003.03688.x

Hang, S., Purdy, A. E., Robins, W. P., Wang, Z., Mandal, M., Chang, S., et al. (2014). The acetate switch of an intestinal pathogen disrupts host insulin signaling and lipid metabolism. *Cell Host Microbe.* 16, 592–604. doi: 10.1016/j.chom.2014.10.006

Hawver, L. A., Giulietti, J. M., Baleja, J. D., and Ng, W. L. (2016). Quorum sensing coordinates cooperative expression of pyruvate metabolism genes to maintain a sustainable environment for population stability. *MBio* 7:16. doi: 10.1128/mBio.01863-16

Hay, A. J., and Zhu, J. (2015). Host intestinal signal-promoted biofilm dispersal induces *Vibrio cholerae* colonization. *Infect. Immun.* 83, 317–323. doi: 10.1128/IAI.02617-14

Herzog, R., Peschek, N., Fröhlich, K. S., Schumacher, K., and Papenfort, K. (2019). Three autoinducer molecules act in concert to control virulence gene expression in *Vibrio cholerae*. *Nucleic Acids Res.* 47, 3171–3183. doi: 10.1093/nar/gky1320

Higgins, D. A., Pomianek, M. E., Kraml, C. M., Taylor, R. K., Semmelhack, M. F., and Bassler, B. L. (2007). The major *Vibrio cholerae* autoinducer and its role in virulence factor production. *Nature* 450, 883–886. doi: 10.1038/nature06284

Holowko, M. B., Wang, H., Jayaraman, P., and Poh, C. L. (2016). Biosensing *Vibrio cholerae* with genetically engineered *Escherichia coli*. *ACS Synth. Biol* 5, 1275–1283. doi: 10.1021/acssynbio.6b00079

Hsiao, A., Ahmed, A. M., Subramanian, S., Griffin, N. W., Drewry, L. L., Petri, W. A., et al. (2014). Members of the human gut microbiota involved in recovery from *Vibrio cholerae* infection. *Nature* 515, 423–426. doi: 10.1038/nature13738

Hung, D. T., Zhu, J., Sturtevant, D., and Mekalanos, J. J. (2006). Bile acids stimulate biofilm formation in *Vibrio cholerae*. *Mol. Microbiol.* 59, 193–201. doi: 10.1111/j.1365-2958.2005.04846.x

Iatsenko, I., Boquete, J. P., and Lemaitre, B. (2018). Microbiota-derived lactate activates production of reactive oxygen species by the intestinal NADPH oxidase nox and shortens *drosophila* lifespan. *Immunity* 49, 929–942.e925. doi: 10.1016/j.immuni.2018.09.017

Jemielita, M., Wingreen, N. S., and Bassler, B. L. (2018). Quorum sensing controls *Vibrio cholerae* multicellular aggregate formation. *Elife* 7:e42057. doi: 10.7554/eLife.42057

Kaper, J. B., Morris, J. G. Jr., and Levine, M. M. (1995). Cholera. *Clin. Microbiol. Rev.* 8, 48–86. doi: 10.1128/CMR.8.1.48

Kaur, S., Sharma, P., Kalia, N., Singh, J., and Kaur, S. (2018). Anti-biofilm properties of the fecal probiotic lactobacilli against *vibrio* spp. *Front. Cell. Infect. Microbiol* 8:120. doi: 10.3389/fcimb.2018.00120

Kelly, R. C., Bolitho, M. E., Higgins, D. A., Lu, W., Ng, W. L., Jeffrey, P. D., et al. (2009). The *Vibrio cholerae* quorum-sensing autoinducer CAI-1: analysis of the biosynthetic enzyme CqsA. *Nat. Chem. Biol* 5, 891–895. doi: 10.1038/nchembio.237

Kim, E. K., Lee, K. A., Hyeon, D. Y., Kyung, M., Jun, K. Y., Seo, S. H., et al. (2020). Bacterial nucleoside catabolism controls quorum sensing and commensal-to-pathogen transition in the *drosophila* gut. *Cell Host Microbe.* 27, 345–357.e346. doi: 10.1016/j.chom.2020.01.025

Kovacikova, G., Lin, W., and Skorupski, K. (2010). The LysR-type virulence activator AphB regulates the expression of genes in *Vibrio cholerae* in response to low pH and anaerobiosis. *J. Bacteriol.* 192, 4181–4191. doi: 10.1128/JB.00193-10

Kunkle, D. E., Bina, X. R., and Bina, J. E. (2020). *Vibrio cholerae* OmpR contributes to virulence repression and fitness at alkaline pH. *Infect. Immun* 88:e00141–20. doi: 10.1128/IAI.00141-20

Lee, D., Kim, E. J., Baek, Y., Lee, J., Yoon, Y., Nair, G. B., et al. (2020). Alterations in glucose metabolism in *Vibrio cholerae* serogroup O1 El Tor biotype strains. *Sci. Rep.* 10:308. doi: 10.1038/s41598-019-57093-4

Liu, Z., Wang, H., Zhou, Z., Sheng, Y., Naseer, N., Kan, B., et al. (2016). Thiol-based switch mechanism of virulence regulator AphB modulates oxidative stress response in *Vibrio cholerae*. *Mol. Microbiol.* 102, 939–949. doi: 10.1111/mmi.13524

Liu, Z., Yang, M., Peterfreund, G. L., Tsou, A. M., Selamoglu, N., Daldal, F., et al. (2011). *Vibrio cholerae* anaerobic induction of virulence gene expression is controlled by thiol-based switches of virulence regulator AphB. *Proc. Natl. Acad. Sci. U.S.A.* 108, 810–815. doi: 10.1073/pnas.1014640108

Lo Scrudato, M., and Blokesch, M. (2012). The regulatory network of natural competence and transformation of *Vibrio cholerae*. *PLoS Genet.* 8:e1002778. doi: 10.1371/journal.pgen.1002778

Logan, S. L., Thomas, J., Yan, J., Baker, R. P., Shields, D. S., Xavier, J. B., et al. (2018). The *Vibrio cholerae* type VI secretion system can modulate host intestinal mechanics to displace gut bacterial symbionts. *Proc. Natl. Acad. Sci. U.S.A.* 115, E3779–E3787. doi: 10.1073/pnas.1720133115

Mao, N., Cubillos-Ruiz, A., Cameron, D. E., and Collins, J. J. (2018). Probiotic strains detect and suppress cholera in mice. *Sci. Transl. Med.*10:eaao2586. doi: 10.1126/scitranslmed.aao2586

Meister, A., and Anderson, M. E. (1983). Glutathione. *Annu. Rev. Biochem.* 52, 711–760. doi: 10.1146/annurev.bi.52.070183.003431

Miller, M. B., Skorupski, K., Lenz, D. H., Taylor, R. K., and Bassler, B. L. (2002). Parallel quorum sensing systems converge to regulate virulence in *Vibrio cholerae*. *Cell* 110, 303–314. doi: 10.1016/S0092-8674(02)00829-2

Miyata, S. T., Kitaoka, M., Brooks, T. M., McAuley, S. B., and Pukatzki, S. (2011). *Vibrio cholerae* requires the type VI secretion system virulence factor VasX to kill Dictyostelium discoideum. *Infect. Immun.* 79, 2941–2949. doi: 10.1128/IAI.01266-10

Monira, S., Hoq, M. M., Chowdhury, A. K., Suau, A., Magne, F., Endtz, H. P., et al. (2010). Short-chain fatty acids and commensal microbiota in the faeces of severely malnourished children with cholera rehydrated with three different carbohydrates. *Eur. J. Clin. Nutr.* 64, 1116–1124. doi: 10.1038/ejcn.2010.123

Morales-Estrada, A. I., Lopez-Merino, A., Gutierrez-Mendez, N., Ruiz, E. A., and Contreras-Rodriguez, A. (2016). Partial characterization of bacteriocin produced by halotolerant *pediococcus acidilactici* strain QC38 isolated from traditional cotija Cheese. *Pol. J. Microbiol.* 65, 279–285. doi: 10.5604/17331331.1215607

Mottawea, W., Chiang, C. K., Mühlbauer, M., Starr, A. E., Butcher, J., Abujamel, T., et al. (2016). Altered intestinal microbiota-host mitochondria crosstalk in new onset Crohn's disease. *Nat. Commun.* 7:13419. doi: 10.1038/ncomms13419

Nag, D., Breen, P., Raychaudhuri, S., and Withey, J. H. (2018). glucose metabolism by *Escherichia coli* inhibits *vibrio cholerae* intestinal colonization of zebrafish. *Infect. Immun.* 86:18. doi: 10.1128/IAI.00486-18

Olasupo, N. A., Olukoya, D. K., and Odunfa, S. A. (1995). Studies on bacteriocinogenic *Lactobacillus* isolates from selected Nigerian fermented foods. *J. Basic Microbiol.* 35, 319–324. doi: 10.1002/jobm.3620350507

Papenfort, K., Silpe, J. E., Schramma, K. R., Cong, J. P., Seyedsayamdost, M. R., and Bassler, B. L. (2017). A *Vibrio cholerae* autoinducer-receptor pair that controls biofilm formation. *Nat. Chem. Biol.* 13, 551–557. doi: 10.1038/nchembio.2336

Parker, C. T., and Sperandio, V. (2009). Cell-to-cell signalling during pathogenesis. *Cell. Microbiol.* 11, 363–369. doi: 10.1111/j.1462-5822.2008.01272.x

Provenzano, D., and Klose, K. E. (2000). Altered expression of the ToxR-regulated porins OmpU and OmpT diminishes *Vibrio cholerae* bile resistance, virulence factor expression, and intestinal colonization. *Proc. Natl. Acad. Sci. U.S.A.* 97, 10220–10224. doi: 10.1073/pnas.170219997

Pukatzki, S., Ma, A. T., Revel, A. T., Sturtevant, D., and Mekalanos, J. J. (2007). Type VI secretion system translocates a phage tail spike-like protein into target cells where it cross-links actin. *Proc. Natl. Acad. Sci. U.S.A.* 104, 15508–15513. doi: 10.1073/pnas.0706532104

Pukatzki, S., Ma, A. T., Sturtevant, D., Krastins, B., Sarracino, D., Nelson, W. C., et al. (2006). Identification of a conserved bacterial protein secretion system in *Vibrio cholerae* using the *Dictyostelium* host model system. *Proc. Natl. Acad. Sci. U.S.A.* 103, 1528–1533. doi: 10.1073/pnas.0510322103

Qadri, F., Bhuiyan, T. R., Dutta, K. K., Raqib, R., Alam, M. S., Alam, N. H., et al. (2004). Acute dehydrating disease caused by *Vibrio cholerae* serogroups O1 and O139 induce increases in innate cells and inflammatory mediators at the mucosal surface of the gut. *Gut* 53, 62–69. doi: 10.1136/gut.53.1.62

Quinn, M. J., Resch, C. T., Sun, J., Lind, E. J., Dibrov, P., and Hase, C. C. (2012). NhaP1 is a K+(Na+)/H+ antiporter required for growth and internal pH homeostasis of *Vibrio cholerae* at low extracellular pH. *Microbiology 158*, 1094–1105. doi: 10.1099/mic.0.056119-0

Ridlon, J. M., Harris, S. C., Bhowmik, S., Kang, D. J., and Hylemon, P. B. (2016). Consequences of bile salt biotransformations by intestinal bacteria. *Gut Microbes* 7, 22–39. doi: 10.1080/19490976.2015.1127483

Ritchie, J. M., and Waldor, M. K. (2009). *Vibrio cholerae* interactions with the gastrointestinal tract: lessons from animal studies. *Curr. Top. Microbiol. Immunol.* 337, 37–59. doi: 10.1007/978-3-642-01846-6_2

Rivera-Chavez, F., and Mekalanos, J. J. (2019). Cholera toxin promotes pathogen acquisition of host-derived nutrients. *Nature* 572, 244–248. doi: 10.1038/s41586-019-1453-3

Rowe-Magnus, D. A., Kao, A. Y., Prieto, A. C., Pu, M., and Kao, C. (2019). Cathelicidin peptides restrict bacterial growth via membrane perturbation and induction of reactive oxygen species. *MBio* 10:19. doi: 10.1128/mBio.02021-19

Russell, A. B., Hood, R. D., Bui, N. K., LeRoux, M., Vollmer, W., and Mougous, J. D. (2011). Type VI secretion delivers bacteriolytic effectors to target cells. *Nature* 475, 343–347. doi: 10.1038/nature10244

Russell, A. B., LeRoux, M., Hathazi, K., Agnello, D. M., Ishikawa, T., Wiggins, P. A., et al. (2013). Diverse type VI secretion phospholipases are functionally plastic antibacterial effectors. *Nature* 496, 508–512. doi: 10.1038/nature12074

Saul-McBeth, J., and Matson, J. S. (2019). A periplasmic antimicrobial peptide-binding protein is required for stress survival in *vibrio cholerae*. *Front. Microbiol.* 10:161. doi: 10.3389/fmicb.2019.00161

Schauder, S., Shokat, K., Surette, M. G., and Bassler, B. L. (2001). The LuxS family of bacterial autoinducers: biosynthesis of a novel quorum-sensing signal molecule. *Mol. Microbiol.* 41, 463–476. doi: 10.1046/j.1365-2958.2001.02532.x

Schwarz, S., West, T. E., Boyer, F., Chiang, W. C., Carl, M. A., Hood, R. D., et al. (2010). *Burkholderia* type VI secretion systems have distinct roles in eukaryotic and bacterial cell interactions. *PLoS Pathog.* 6:e1001068. doi: 10.1371/journal.ppat.1001068

Sengupta, C., Ekka, M., Arora, S., Dhaware, P. D., Chowdhury, R., and Raychaudhuri, S. (2017). Cross feeding of glucose metabolism byproducts of *Escherichia coli* human gut isolates and probiotic strains affect survival of *Vibrio cholerae*. *Gut Pathog.* 9:3. doi: 10.1186/s13099-016-0153-x

Sengupta, C., Mukherjee, O., and Chowdhury, R. (2016). Adherence to Intestinal Cells Promotes Biofilm Formation in *Vibrio cholerae*. *J. Infect. Dis.* 214, 1571–1578. doi: 10.1093/infdis/jiw435

Shao, Y., and Bassler, B. L. (2014). Quorum regulatory small RNAs repress type VI secretion in *Vibrio cholerae*. *Mol. Microbiol.* 92, 921–930. doi: 10.1111/mmi.12599

Shikuma, N. J., Fong, J. C., Odell, L. S., Perchuk, B. S., Laub, M. T., and Yildiz, F. H. (2009). Overexpression of VpsS, a hybrid sensor kinase, enhances biofilm formation in *Vibrio cholerae*. *J. Bacteriol.* 191, 5147–5158. doi: 10.1128/JB.00401-09

Shirin, T., Rahman, A., Danielsson, A., Uddin, T., Bhuyian, T. R., Sheikh, A., et al. (2011). Antimicrobial peptides in the duodenum at the acute and convalescent stages in patients with diarrhea due to *Vibrio cholerae* O1 or enterotoxigenic *Escherichia coli* infection. *Microbes. Infect.* 13, 1111–1120. doi: 10.1016/j.micinf.2011.06.014

Shneider, M. M., Buth, S. A., Ho, B. T., Basler, M., Mekalanos, J. J., and Leiman, P. G. (2013). PAAR-repeat proteins sharpen and diversify the type VI secretion system spike. *Nature* 500, 350–353. doi: 10.1038/nature12453

Spelhaug, S. R., and Harlander, S. K. (1989). Inhibition of foodborne bacterial pathogens by bacteriocins from *Lactococcus lactis* and *Pediococcus pentosaceous* (1). *J. Food Prot.* 52, 856–862. doi: 10.4315/0362-028X-52.12.856

Suckow, G., Seitz, P., and Blokesch, M. (2011). Quorum sensing contributes to natural transformation of *Vibrio cholerae* in a species-specific manner. *J. Bacteriol.* 193, 4914–4924. doi: 10.1128/JB.05396-11

Theriot, C. M., and Petri, W. A. Jr. (2020). Role of microbiota-derived bile acids in enteric infections. *Cell* 181, 1452–1454. doi: 10.1016/j.cell.2020.05.033

Toska, J., Ho, B. T., and Mekalanos, J. J. (2018). Exopolysaccharide protects *Vibrio cholerae* from exogenous attacks by the type 6 secretion system. *Proc. Natl. Acad. Sci. U.S.A.* 115, 7997–8002. doi: 10.1073/pnas.1808469115

Wahlström, A., Sayin, S. I., Marschall, H. U., and Bäckhed, F. (2016). Intestinal crosstalk between bile acids and microbiota and its impact on host metabolism. *Cell Metab.* 24, 41–50. doi: 10.1016/j.cmet.2016.05.005

Wang, H., Naseer, N., Chen, Y., Zhu, A. Y., Kuai, X., Galagedera, N., et al. (2017). OxyR2 Modulates OxyR1 activity and *Vibrio cholerae* oxidative stress response. *Infect. Immun.* 85:e00929–16. doi: 10.1128/IAI.00929-16

Wang, H., Xing, X., Wang, J., Pang, B., Liu, M., Larios-Valencia, J., et al. (2018). Hypermutation-induced *in vivo* oxidative stress resistance enhances *Vibrio cholerae* host adaptation. *PLoS Pathog* 14:e1007413. doi: 10.1371/journal.ppat.1007413

Watve, S., Barrasso, K., Jung, S. A., Davis, K. J., Hawver, L. A., Khataokar, A., et al. (2020). Parallel quorum-sensing system in *Vibrio cholerae* prevents signal interference inside the host. *PLoS Pathog* 16:e1008313. doi: 10.1371/journal.ppat.1008313

Xia, X., Larios-Valencia, J., Liu, Z., Xiang, F., Kan, B., Wang, H., et al. (2017). OxyR-activated expression of Dps is important for *Vibrio cholerae* oxidative stress resistance and pathogenesis. *PLoS ONE* 12:e0171201. doi: 10.1371/journal.pone.0171201

Yang, M., Liu, Z., Hughes, C., Stern, A. M., Wang, H., Zhong, Z., et al. (2013). Bile salt-induced intermolecular disulfide bond formation activates *Vibrio cholerae* virulence. *Proc. Natl. Acad. Sci. U.S.A.* 110, 2348–2353. doi: 10.1073/pnas.1218039110

Yardeni, T., Tanes, C. E., Bittinger, K., Mattei, L. M., Schaefer, P. M., Singh, L. N., et al. (2019). Host mitochondria influence gut microbiome diversity: A role for ROS. *Sci. Signal* 12:aaw3159. doi: 10.1126/scisignal.aaw3159

Yoon, M. Y., Min, K. B., Lee, K. M., Yoon, Y., Kim, Y., Oh, Y. T., et al. (2016). A single gene of a commensal microbe affects host susceptibility to enteric infection. *Nat. Commun.* 7:11606. doi: 10.1038/ncomms11606

Yoon, S. H., and Waters, C. M. (2019). *Vibrio cholerae*. *Trends Microbiol.* 27, 806–807. doi: 10.1016/j.tim.2019.03.005

You, J. S., Yong, J. H., Kim, G. H., Moon, S., Nam, K. T., Ryu, J. H., et al. (2019). Commensal-derived metabolites govern *Vibrio cholerae* pathogenesis in host intestine. *Microbiome* 7:132. doi: 10.1186/s40168-019-0746-y

Zhao, W., Caro, F., Robins, W., and Mekalanos, J. J. (2018). Antagonism toward the intestinal microbiota and its effect on *Vibrio cholerae* virulence. *Science* 359, 210–213. doi: 10.1126/science.aap8775

Zhu, J., Miller, M. B., Vance, R. E., Dziejman, M., Bassler, B. L., and Mekalanos, J. J. (2002). Quorum-sensing regulators control virulence gene expression in *Vibrio cholerae*. *Proc. Natl. Acad. Sci. U.S.A.* 99, 3129–3134. doi: 10.1073/pnas.052694299

Conflict of Interest: The authors declare that the research was conducted in the absence of any commercial or financial relationships that could be construed as a potential conflict of interest.

frontiers in Cellular and Infection Microbiology

ORIGINAL RESEARCH
published: 09 December 2020
doi: 10.3389/fcimb.2020.595709

Prophage-Related Gene *VpaChn25_0724* Contributes to Cell Membrane Integrity and Growth of *Vibrio parahaemolyticus* CHN25

Lianzhi Yang[1,2†], *Yaping Wang*[1,2,3†], *Pan Yu*[1,2†], *Shunlin Ren*[3], *Zhuoying Zhu*[1,2], *Yinzhe Jin*[1,2], *Jizhou Yan*[4], *Xu Peng*[5] and *Lanming Chen*[1,2*]

[1] Key Laboratory of Quality and Safety Risk Assessment for Aquatic Products on Storage and Preservation (Shanghai), China Ministry of Agriculture, Shanghai, China, [2] College of Food Science and Technology, Shanghai Ocean University, Shanghai, China, [3] Department of Internal Medicine, Virginia Commonwealth University/McGuire VA Medical Centre, Richmond, VA, United States, [4] College of Fishers and Life Science, Shanghai Ocean University, Shanghai, China, [5] Archaea Centre, Department of Biology, University of Copenhagen, Copenhagen, Denmark

Vibrio parahaemolyticus is a leading seafood-borne pathogen that can cause acute gastroenteritis and even death in humans. In aquatic ecosystems, phages constantly transform bacterial communities by horizontal gene transfer. Nevertheless, biological functions of prophage-related genes in *V. parahaemolyticus* remain to be fully unveiled. Herein, for the first time, we studied one such gene *VpaChn25_0724* encoding an unknown hypothetical protein in *V. parahaemolyticus* CHN25. This gene deletion mutant Δ*VpaChn25_0724* was constructed by homologous recombination, and its complementary mutant Δ*VpaChn25_0724*-com was also obtained. The Δ*VpaChn25_0724* mutant exhibited a sever defect in growth and swimming motility particularly at lower temperatures. Biofilm formation and cytotoxicity capacity of *V. parahaemolyticus* CHN25 was significantly lowered in the absence of *VpaChn25_0724*. Comparative secretomic analysis revealed an increase in extracellular proteins of Δ*VpaChn25_0724*, which likely resulted from its damaged cell membrane. Comparison of transcriptome data showed twelve significantly altered metabolic pathways in Δ*VpaChn25_0724*, suggesting inactive transport and utilization of carbon sources, repressed energy production and membrane biogenesis in *ΔVpaChn25_0724*. Comparative transcriptomic analysis also revealed several remarkably down-regulated key regulators in bacterial gene regulatory networks linked to the observed phenotypic variations. Overall, the results here facilitate better understanding of biological significance of prophage-related genes remaining in *V. parahaemolyticus*.

Keywords: ***Vibrio parahaemolyticus*, prophage, virulence, gene knockout, secretome, transcriptome**

OPEN ACCESS

Edited by:
Lixing Huang,
Jimei University, China

Reviewed by:
Yanni Zhao,
Shaanxi University of Science and Technology, China
Xiaojun Zhang,
Yangzhou University, China

***Correspondence:**
Lanming Chen
lmchen@shou.edu.cn

†These authors have contributed equally to this work

Specialty section:
This article was submitted to Molecular Bacterial Pathogenesis, a section of the journal Frontiers in Cellular and Infection Microbiology

Received: *17 August 2020*
Accepted: *06 November 2020*
Published: *09 December 2020*

Citation:
Yang L, Wang Y, Yu P, Ren S, Zhu Z, Jin Y, Yan J, Peng X and Chen L (2020) Prophage-Related Gene VpaChn25_0724 Contributes to Cell Membrane Integrity and Growth of Vibrio parahaemolyticus CHN25. Front. Cell. Infect. Microbiol. 10:595709. doi: 10.3389/fcimb.2020.595709

INTRODUCTION

Vibrio parahaemolyticus is a gram-negative bacterium and thrives in marine, riverine, and aquaculture environments worldwide (Ghenem et al., 2017). Consumption of raw, undercooked or mishandled seafood contaminated by pathogenic *V. parahaemolyticus* can cause acute gastroenteritis in humans and even death (Kim et al., 2017). The bacterium was originally identified in 1950 in Osaka, Japan, where an outbreak of acute gastroenteritis, caused by contaminated semidried juvenile sardines, sickened 272 and killed 20 people (Fujino et al., 1953). Since then, the infectious disease caused by *V. parahaemolyticus* has been reported in many Asian countries, and subsequently in Africa, America, and Europe, arguing a pandemic of *V. parahaemolyticus* worldwide (Ghenem et al., 2017). In China, *V. parahaemolyticus* is a leading cause of foodborne bacterial disease, especially among adults in coastal regions in recent years (Jiang et al., 2019). Most pathogenic *V. parahaemolyticus* strains of clinical origin have two major virulence factors, a thermostable direct hemolysin (TDH) and a TDH-related hemolysin (TRH). Both toxins have hemolytic activity, enterotoxin activity, cardiotoxicity and cytotoxicity to the host (Li et al., 2019). Nevertheless, some *V. parahaemolyticus* isolates of environmental origins lacking the *tdh* and/or *trh* genes also show cytotoxicity to human intestinal cells, suggesting additional virulence-associated factors exist in the bacterium (Raghunath, 2014). Thus, identification of risk factors in *V. parahaemolyticus* is imperative for assuming food safety.

In aquatic ecosystems, phages are the most abundant biological entity involved in numerous biological cycles and constantly transform bacterial communities by horizontal gene transfer (HGT) (Penades et al., 2015; Castillo et al., 2018). Phage genomic DNA can integrate into and replicate as part of bacterial chromosomes, which is a typical feature of mild phages for a lysogen cycle (Feiner et al., 2015; Howard-Varona et al., 2017). HGT can result in pandemic or pathogenic clones with expanded ecological persistence and dispersibility, e.g., the filamentous phage VfO3:K6 in *V. parahaemolyticus* O3:K6 (Loyola et al., 2015). It constitutes important driving forces in host evolution, and bestows a wide range of phenotypes upon hosts with transmitted gene cassettes, such as phage-coded virulence, cell adhesion, antibiotic resistance, and metabolizing enzyme determinants (Harrison and Brockhurst, 2017; Castillo et al., 2018). Previous studies have revealed phages or prophage gene clusters present in *V. parahaemolyticus* (e.g., Jensen et al., 2013; Gomez-Gil et al., 2014; Kalburge et al., 2014). For instance, the phage Vp58.5 enhances ultraviolet sensitivity of *V. parahaemolyticus* O3:K6 (Zabala et al., 2009), and phage Vp882 transmits DNA adenine methylase and quorum sensing (QS) transcription factors to *V. parahaemolyticus* O3:K6 (Lan et al., 2009). A recently reported lytic *Vibrio* phage VP06 can infect a broad range of hosts, including *Vibrio alginolyticus, Vibrio azureus, Vibrio harveyi*, and *V. parahaemolyticus*. This *Vibrio* phage is resistant to environmental stresses, displaying potential as a candidate biocontrol agent (Wong et al., 2019).

In our prior studies, *V. parahaemolyticus* CHN25 strain (serotype: O5:KUT) was isolated, identified, and characterized (Song et al., 2013; Sun et al., 2014; He et al., 2015; Zhu et al., 2017). The complete genome sequence of *V. parahaemolyticus* CHN25 contains 5,443,401 bp with 45.2% G+C content (Zhu et al., 2017). Comparative genomic analysis revealed five prophage gene clusters in *V. parahaemolyticus* CHN25. The largest one has sequence similarity with a 33,277-bp *Vibrio* phage Martha 12B12 (GenBank accession no. HQ316581). Nevertheless, this prophage sequence exists in a truncated version in the bacterial genome, where approximately 37.5% of the remaining genes encode predicted proteins of unknown function. Identification of these hypothetical proteins is yet to be determined. We, therefore, asked whether *V. parahaemolyticus* CHN25 would be affected by the absence of these prophage-related genes. In this study, we aimed to address possible function of one such gene *VpaChn25_0724* in *V. parahaemolyticus* CHN25.

MATERIALS AND METHODS

Bacterial Strains, Plasmids, and Culture Conditions

The *V. parahaemolyticu* CHN25 strain was used in this study. *Escherichia coli* DH5α λpir [BEINUO Biotech (Shanghai) Co. Ltd., China] was used as a host strain for DNA cloning. The pDS132 plasmid and *E. coli* β2155 λpir were used as a suicide vector and a donor strain in conjugation experiments, respectively (Zhu et al., 2017). The pMMB207 plasmid (Biovector Science Lab, Inc., China) was used as an expression vector to construct the reverse mutant. The *E. coli* strains were routinely incubated in Luria-Bertani (LB) medium (1% NaCl, pH 7.2) at 37°C, and the *V. parahaemolyticus* strains were grown in LB (3% NaCl, pH 8.5) or Tryptic Soy Broth (TSB) (3% NaCl, pH8.5) media. The growth medium was supplemented as needed with chloramphenicol to a final concentration of 30 μg/ml for *E. coli* and 5 μg/ml for *V. parahaemolyticus* (Zhu et al., 2017).

Construction of Deletion Mutant and Reverse Mutant of the VpaChn25_0724 Gene

Genomic DNA was prepared using TaKaRa MiniBEST Bacterial Genomic DNA Extraction Kit (Japan TaKaRa BIO, Dalian Company, China). Plasmid DNA was isolated using TIANpure Midi Plasmid Kit (Tiangen Biotech Beijing Co. Ltd., China). Oligonucleotide primers (**Table 1**) were designed using Primier 5.0 software (https://www.premierbiosoft.com), and synthesized by the Sangon Biotech (Shanghai) Co. Ltd., China. A markerless in-frame gene deletion mutant of the *VpaChn25_0724* gene was constructed using the homologous recombination method (Zhu et al., 2017). Briefly, based on the *VpaChn25_0724* gene sequence (294 bp) in *V. parahaemolyticus* CHN25 genome, the primer pairs (*VpaChn25_0724*-up-F/R and *VpaChn25_0724*-down-F/R) (**Table 1**) were designed to target the upstream (464 bp) and downstream (444 bp) sequences of the *VpaChn25_0724* gene, respectively. The amplified products by polymerase chain reaction (PCR) were individually digested with corresponding

TABLE 1 | Oligonucleotide primers designed and used in this study.

Primer	Sequence (5′->3′)	Product size (bp)
VpaChn25_0724-up-F	GCTCTAGAATCGACCTATTCAGGC	464
VpaChn25_0724-up-R	TGGCGGCTCCATGAACCTCTATTTATC	
VpaChn25_0724-down-F	AGAGGTTCATGGAGCCGCCATGAAG	444
VpaChn25_0724-down-R	CGAGCTC TGGCGGCTTGCTCGATACGC	
VpaChn25_0724- up-ex-F	GAACTCGACCTGATATTG	1663
VpaChn25_0724-down-ex- R	CACATCCTCCTCAACCGC	
Vpachn25_0724-com-F	CGAGCTCATGTCCTTTAAAGATGTATTA	294
Vpachn25_0724- com-R	GCTCTAGATTACTTAGCGCGAGGGCGCTT	
tlh-F	AAAGCGGATTATGCAGAAGCACTG	596
tlh-R	ACTTTCTAGCATTTTCTCTGC	
Vpachn25_0724 -F	ACCAGCGGTTAGTCATCTTG	154
Vpachn25_0724 -R	ATTAGGCTTTGCTCTTCCAG	
16s RNA-F	GACACGGTCCAGACTCCTAC	179
16s RNA-R	GGTGCTTCTTCTGTCGCTAAC	
VpaChn25_RS01720-F	CTTAGCCACATCCCAACACC	196
VpaChn25_RS01720-R	TAGGACAAACAACCGCAATC	
VpaChn25_RS03850-F	ACCAGCGGTTAGTCATCTTG	154
VpaChn25_RS03850-R	ATTAGGCTTTGCTCTTCCAG	
VpaChn25_RS04440-F	ATGGGTCATCTTTATCTTTCG	183
VpaChn25_RS04440-R	CAGTCCGTTTAGCAGGTTCT	
VpaChn25_RS06735-F	GTAATAACCGACGCCTGCTC	165
VpaChn25_RS06735-R	ACGGGTGAATACGAAACGAA	
VpaChn25_RS07910-F	CTGCCGTGTTACCGATAAAG	184
VpaChn25_RS07910-R	CATCTCACCGCAATGAAAGC	
VpaChn25_RS08070-F	AGAACCAACTCTTAGGCTGGAC	114
VpaChn25_RS08070-R	TTAATGAACGCATTCGCTGT	
VpaChn25_RS08820-F	CAATCTTTAATTGCGTTGAG	144
VpaChn25_RS08820-R	AACCGATGTTCGTCACTATG	
VpaChn25_RS11070-F	GGTCTCGTTCATTGCACCTT	122
VpaChn25_RS11070-R	CTGCGGGTCTACAAATCTCG	
VpaChn25_RS04175-F	GACTAAACCGTATCGCTGAA	123
VpaChn25_RS04175-R	TGCCCATAGAAAGCATTACA	
VpaChn25_RS13780-F	GGTTTCGTTTAGGTCACG	277
VpaChn25_RS13780-R	ACGTCGAAATGTCGGCGG	
VpaChn25_RS14070-F	TGGTCGCGTAAGCAATGC	209
VpaChn25_RS14070-R	TTCGTCAGCTAGAGGAAG	

The underlined sequences represent the recognition sites of restriction endonucleases that were introduced via the forward and reverse primers, respectively.

restriction endonucleases (TaKaRa, Japan), purified, and ligated into *XbaI* and *SacI* cloning sites on the pDS132. The ligated DNA was transformed into *E. coli* DH5α λpir competent cells and positive transformants were screened (Zhu et al., 2017). The recombinant plasmid pDS132+*VpaChn25_0724* was subsequently prepared and transformed into diaminopimelic acid (DAP) auxotroph *E. coli* β2155 competent cells grown in LB medium supplemented with 0.3 mM DAP (Sigma-Aldrich, USA). Plate mating assay was performed (Zhu et al., 2017). Exconjugants with successful double crossover deletions of the *VpaChn25_0724* gene were screened by colony PCR assay using the *VpaChn25_0724*-up-ex-F and *VpaChn25_0724*-down-ex-R primer pair (**Table 1**). The obtained Δ*VpaChn25_0724* mutant was confirmed by DNA sequencing, quantitative reverse transcription-PCR (RT-qPCR), and transcriptome analysis (see below). DNA sequences were determined by the Sangon (China).

The 294-bp *VpaChn25_0724* gene was amplified from the genomic DNA of *V. parahaemolyticus* CHN25 by PCR with the *VpaChn25_0724*-com-F/-R primers (**Table 1**). The PCR product was ligated into the expression vector pMMB207. The ligated DNA was transformed into *E. coli* DH5α and positive transformants were screened as described above. The recombinant plasmid pMMB207+*VpaChn25_0724* was then prepared and transformed into the Δ*VpaChn25_0724* mutant by electrotransformation as described previously (Zhu et al., 2017). The positive electrotransformants (Δ*VpaChn25_0724*-com mutant) were screened by colony PCR with primers *VpaChn25_0724*-com-F/R and *tlh*-F/R (**Table 1**), and confirmed using the aforementioned methods.

Swimming Mobility and Biofilm Formation Assays

Swimming motility was examined according to the method described previously (Huang et al., 2017; Yang et al., 2017). Briefly, *V. parahaemolyticus* strains were individually incubated at 37°C in the TSB medium (pH 8.5, 3% NaCl) to the middle-logarithmic growth phase (mid-LGP) with OD_{600nm} values of about 0.8 to 1.0. Growth curves were measured using Bioscreen Automatic Growth Curve Analyzer (BioTek, USA). The differential growth phases were calculated on the basis of OD_{600nm} values between the wild type and mutant strains (Zhu et al., 2017). A 0.5 μl of each cell culture were inoculated into semi-solid TSB agar plates containing 0.25% agar, and incubated at 15°C, 25°C, and 37°C for 48, 24, and 12 h,

respectively. The bacterial clones formed on the plates were measured and recorded.

Biofilm formation was quantified using the crystal violet staining method (Tan et al., 2018). Briefly, *V. parahaemolyticus* strains from overnight culture were individually diluted in the TSB medium to an absorption value at OD_{600nm} of about 0.4, and then 1 ml of the dilutions was individually inoculated into 24-well polystyrene microtiter plates (Sangon, China). After incubation at 37°C for 12 h, 24 h, 36 h, 48 h, and 60 h, the planktonic bacteria were removed, and biofilms were gently washed with 1 ml of 0.1M phosphate-buffered saline (PBS, pH 7.2 to 7.4, Sangon, China) for three times. The biofilms were then fixed using 0.1% (w/v) crystal violet (Sangon, China), washed, dissolved, and measured for absorbance values at OD_{600nm} using BioTek Synergy 2 (BioTek, USA) (Tan et al., 2018).

Bacterial Cell Membrane Damage, Hydrophobicity, and Fluidity Assays

Cell membrane damage was analyzed using the method described by Collado et al. (Collado et al., 2017). The bacterial cell suspension was double dyed using propidium iodide (PI) (final concentration 10 mM) (Sangon, China) and 5(6)-carboxydiacetate fluorescein succinimidyl ester (CFDA) (final concentration 10 μM) (Beijing Solarbio Science & Technology Co. Ltd., China). Bacterial cell forward scatter, lateral astigmatism, and fluorescent channels FL1 (green) and FL2 (red) were determined using a flow cytometer BD FACSVerse™ (Becton, Dickinson and Company, USA). 1,000 cells were detected in each sample.

The cell membrane hydrophobicity and fluidity assays were performed as described by Pelletier et al. (Pelletier et al., 1997), and Voss and Montville (Voss and Montville, 2014), respectively.

Secretome Analysis

Extracellular proteins of *V. parahaemolyticus* strains were extracted according to the method described previously (He et al., 2015). The 2-dimensional gel electrophoresis (2-DE) was performed according to the method by Zhu et al. (Zhu et al., 2020). Briefly, approximately 20 μg of extracellular proteins was diluted with the rehydration buffer [8 M urea, 4% (w/v) CHAPS, 65 mM dithiothreitol, 0.2% (vol/vol) Bio-Lyte 3/10 ampholyte and 0.0001% (wt/vol) bromophenol blue (Sangon, China)] to a final volume of 200 μl per sample. The mixture of each sample was applied to the pH gradient gel (IPG) strips (pH 4–7, 7 cm, Bio-Rad, USA) and passive rehydrated for 16 h at 17°C. After rehydration, IEF (isoelectric focusing) was run with a six-step program (Zhu et al., 2020). Following the electrophoresis in the first dimension, the strips were first equilibrated for 15 min in equilibration buffer I, and then washed for a further 15 min with equilibration buffer II (Zhu et al., 2020). The second-dimension separation was performed using SDS-polyacrylamide gel electrophoresis (SDS-PAGE). The strips were individually transferred onto 12.5% separation gel using a Mini-PROTEANW electrophoresis cell (Bio-Rad, USA) with a 2-step program (Zhu et al., 2020). The gels were stained, imaged, and analyzed as described previously (He et al., 2015). Additionally, amino acid sequences of protein spots were determined using liquid chromatography tandem mass spectrometry (LC-MS/MS) technique at Shanghai Houji Biology Co Ltd., China as described previously (Zhu et al., 2020).

Human Intestinal Epithelial Cell Viability and Apoptosis Assay

Human intestinal epithelial cell viability infected by *V. parahaemolyticus* strains was determined as described previously (Tsai et al., 2018) with minor modifications. Human rectal cancer epithelial cell line Caco-2 (ATCC number : HTB-37™) was purchased from Stem Cell Bank, Chinese Academy of Sciences (Shanghai, China). Briefly, Caco-2 cells were seeded into 96-well cell culture plates at a concentration of 5×10^4 cells/ml per well, and cultured in Dulbecco's modified eagle medium (DMEM, Gibco, USA) at 37°C, 5% CO_2 for 24 h using a CO_2 Cell Incubator (Thermo, USA). The cell culture fluid was aspirated off, and cells were washed twice with 0.1 M PBS (pH 7.2–7.4, Sangon, China). Meanwhile, *V. parahaemolyticus* strains grown to the mid-LGP at 37°C were individually harvested, and cell pellet was washed twice with 0.1 M PBS, and resuspended with the phenol red-free DMEM medium to adjust OD_{490nm} values of about 0.2 ± 0.02. A 100 μl of the bacterial suspension was added into each well containing the Caco-2 cells, and 10 μl of [2-(2-methoxy-4-nitrophenyl)-3-(4-nitrophenyl)-5-(2,4-disulfonate)-2h-tetrazole monosodium salt (CCK-8, Sigma-Aldrich, USA)] was also added and incubated for 4 h at 5% CO_2, 37°C. Caco-2 cell viability was calculated according to the following formula: cell viability (%) = [A (bacteria) − A (blank)]/[A (0 bacteria) − A (blank)] × 100, in which A (bacteria) represents an absorbance at OD_{450nm} of the cell culture wells with Caco-2 cells, CCK-8 solution and bacterial suspension; A (blank) represents a OD_{450nm} value without Caco-2 cells, DME medium and CCK-8 solution; A (0 bacteria) represents a OD_{450nm} value with Caco-2 cells and CCK-8 solution but without bacterial suspension.

A 2 ml of Caco-2 cells (1×10^5 cells/ml) was inoculated into 6-well cell culture plates, and individually infected by *V. parahaemolyticus* strains for 4 h at 5% CO_2, 37°C. Then a 200-μl trypsin (Gibco, USA) was added into each cell culture well to digest for 3 min. Then the supernatant was discarded, and cells were collected by centrifugation at 800 rpm for 4 min. Apoptosis of the Caco-2 cells was assayed using Annexin-V-FITC/PI Apoptosis Detection Kit (Solarbio, China), according to the manufacturer's protocol. The treated samples were detected by BD FACSVerse™ flow cytometry (Becton, Dickinson and Company, USA), and data analysis was performed using FlowJo software (https://www.flowjo.com).

Illumina RNA Sequencing

Total RNA was prepared using RNeasy Protect Bacteria Mini Kit (QIAGEN Biotech Co. Ltd., Germany) and QIAGEN RNeasy Mini Kit (QIAGEN) according to the manufacturer's protocols. The DNA was removed from the samples using RNase-Free DNase Set (QIAGEN). Three independently prepared RNA samples were used in each Illumina RNA-sequencing experiment. The sequencing library construction and Illumina

sequencing were conducted at Shanghai Majorbio Bio-pharm Technology Co. Ltd., China using Illumina HiSeq 2500 platform as described previously (Zhu et al., 2017). High quality reads that passed the Illumina quality filters were used for sequence analyses.

Real-Time Reverse Transcription-PCR Assay

The RT-qPCR was performed as described previously (Wang et al., 2013). *V. parahaemolyticus* cultures grown to the mid-LGP were harvested for RNA extraction. The RNeasy Mini Kit (Qiagen, Germany) was used to extract total RNA. Reverse transcription reactions were performed using PrimeScript™ RT reagent Kit with gDNA Eraser (Perfect Real Time) (TaKaRa, Japan) kit. Relative quantitative PCR reactions were performed with TB Green® Premix Ex Taq™ II (Tli RNaseH Plus) (TaKaRa, Japan) kit using 7500 Fast Real-Time PCR Instrument (Applied Biosystems, USA). The 16S rRNA gene was used as the internal reference gene, and $2^{-\Delta\Delta Ct}$ method was used to calculate the relative expression between the target and the internal reference genes. The representative eighteen differentially expressed genes (DEGs) in the transcriptome of Δ*VpaChn25_0724* mutant were confirmed by the RT-qPCR assay, and listed in **Table S1**.

Detection of VpaChn25_0724 Gene by PCR

Total 138 V. *parahaemolyticus* strains isolated from commonly consumed aquatic products collected in Shanghai, China (Su et al. unpublished) were used in this study. The *VpaChn25_0724* gene was amplified with the primers *VpaChn 25_0724* –F/R (**Table 1**) by PCR (Song et al., 2013). A 6 μl of each PCR product was analyzed by agarose gel (1%) electrophoresis, imaged and recorded, and validated by DNA sequencing as described above.

Transmission Electron Microscope Assay

The TEM observation of *V. parahaemolyticus* strains was conducted using ultrathin edge-cutting method (Morgelin, 2017; Xu et al., 2017) *via* a transmission electron (JEM2100, JEOL, Japan, ×80,000) at the Instrumental Analysis Center at Shanghai Jiao Tong University, Shanghai, China.

Enzyme Activity Assays

The wild type and mutant strains grown to the mid-LGP were individually harvested by centrifugation at 8,000 g for 10 min at 4°C. The supernant was removed, and the bacterial cell pellets were used for the malate dehydrogenase and citrate synthase activity assays using the corresponding kits (Product Nos. BC1040, and BC1060, Beijing Solarbio Science & Technology Co. Ltd., China), according to the manufecturer's instructions. Approximately 0.05 ± 0.002 g and 0.1 ± 0.02 g of each sample was used in the malate dehydrogenase and citrate synthase reactions, and their OD_{340nm} and OD_{412nm} values were recorded using BioTek Synergy 2 (BioTek, USA), respectively.

Data Analysis

Quality filtration of raw RNA-seq data were performed using theSeqPrep (https://github.com/jstjohn/SeqPrep) and Sickle version 1.33 software (https://github.com/najoshi/sickle) as described previously (Zhu et al., 2017). The resulting clean reads were aligned to the *V. parahaemolyticus* CHN25 genome using the Bowtie2 version 2.0.5 software (http://bowtie-bio.sourceforge.net/bowtie2/index.shtml). Expression of each gene was calculated using RNA-Seq by Expectation-Maximization (RSEM, http://deweylab.github.io/RSEM/). Genes with the criteria, fold-changes ≥ 2.0 or ≤ 0.5, and p-values by BH (fdr correction with Benjamini/Hochberg) < 0.05 relative to the control, were defined as DEGs. These DEGs were used for gene set enrichment analysis (GSEA) against the Kyoto Encyclopedia of Genes and Genomes (KEGG) database (http://www.genome.jp/kegg/) and gene set annotation analysis (GSAA) against the Gene Ontology (GO) database (http://www.geneontology.org) as described previously (Zhu et al., 2017). Significantly changed GSEA were identified when the enrichment test p-value fell below 0.05.

Prophage gene clusters were searched and analyzed using Prophage Finder (http://phast.wishartlab.com/) and Basic Local Alignment Search Tool (BLAST) (http://www.ncbi.nlm.nih.gov/BLAST) software. All tests in this study were conducted in at least triplicate. The data were analyzed using SPSS statistical analysis software version 17.0 (SPSS Inc., USA).

RESULTS

Gene Organization of the Largest Prophage Gene Cluster in Vibrio parahaemolyticus CHN25 Genome

Comparative genomic analysis revealed that the largest prophage gene cluster in *V. parahaemolyticus* CHN25 genome has sequence similarity to the *Vibrio* phage Martha 12B12 that contains 50 predicted genes. Approximately 24 genes thereof were present in chromosome 1 (3,416,467 bp) of *V. parahaemolyticus* CHN25 genome, where they located in the locus from 816,554 bp to 846,961 bp (**Figure 1**). Among the 24 genes, 7 coded for potential phage proteins (i.e., phage head, tail, and baseplate), 8 for predicted regulators, and 9 for hypothetical structural proteins of unknown function. Within the gene cluster, genes encoding DNA endonuclease, DNA transport protein, conjugal transfer protein TraR, and additional proteins were also identified, suggesting that the bacterium underwent extensive genetic recombination *via* HGT during its evolution (Zhu et al., 2017). Among the genes encoding unknown hypothetical proteins, the 294-bp *VpaChn25_0724* gene was further investigated and reported in this study.

Deletion and Reverse Complementation of the VpaChn25_0724 Gene

To study biological function of the *VpaChn25_0724* gene, we constructed an unmarked in-frame gene deletion mutant Δ*VpaChn25_0724* using the homologous recombination method (**Figure S1**). The upstream and downstream sequences (approximately 0.5 kb) that flank the *VpaChn25_0724* gene were obtained by PCR (**Table 1**), and then cloned into a suicide vector

pDS132 to yield a recombinant vector pDS132+*VpaChn25_0724*. The 908-bp inserted sequence was validated by DNA sequencing (data not shown). The recombinant vector was transformed into *E. coli* β2155, and the chloramphenicol-resistant transformant was obtained and conjugated with *V. parahaemolyticus* CHN25. Positive exconjugants were obtained using the two-step allelic exchange method. Deletion of the 294-bp *VpaChn25_0724* gene from *V. parahaemolyticus* CHN25 genome was validated by PCR and DNA sequencing assays (data not shown), as well as by RT-qPCR and transcriptomic analysis (see below).

To facilitate a complementation assay, a reverse mutant Δ*VpaChn25_0724*-com was also successfully constructed. The 294-bp *VpaChn25_0724* gene was amplified from genomic DNA of *V. parahaemolyticus* CHN25 by PCR, and then cloned into an expression vector pMMB207, which yielded a recombinant vector pMMB207-*VpaChn25_0724*. The inserted 294-bp sequence was confirmed by DNA sequencing (data not shown). This recombinant vector was then electrotransformed into the Δ*VpaChn25_0724* mutant, and generated the reverse mutant Δ*VpaChn25_0724*-com that was further confirmed using the aforementioned methods.

Growth of the ΔVpaChn25_0724 Mutant at Different Temperatures

To gain insights into possible impact of the *VpaChn25_0724* gene deletion on bacterial growth, we determined growth curves of *V. parahaemolyticus* CHN25, Δ*VpaChn25_0724*, and Δ*VpaChn25_0724*-com strains at 37°C, 25°C, and 15°C, which are within the temperature range experienced by *V. parahaemolyticus* during its life cycle (Desai and Kenney, 2019). As illustrated in **Figure 2**, the Δ*VpaChn25_0724* mutant exhibited a significantly extended lag phase, which was 4-fold, 6-fold, and 2.5-fold of that of the wild type strain at 37°C, 25°C, and 15°C, respectively. Complementation with a plasmid-borne *VpaChn25_0724* (Δ*VpaChn25_0724*-com) restored the growth almost completely at 37°C and partially at 25°C, but not at all at 15°C. These results highlighted the importance of *VpaChn25_0724* gene for the growth of *V. parahaemolyticus* CHN25, particularly at the lower temperatures.

Swimming Motility and Biofilm Formation of the ΔVpaChn25_0724 Mutant

As shown in **Figure 3**, on the semi-solid swimming plates, the lower temperatures notably shrunk swimming cycles of wild type, Δ*VpaChn25_0724*, and Δ*VpaChn25_0724*-com strains. However, swimming capacity of the wild type was about 2-fold and 3-fold higher than that of the Δ*VpaChn25_0724* mutant at 25°C and 15°C, respectively ($p<0.05$). No significant difference in swimming cycles was observed among the three strains at 37°C ($p > 0.05$). Additionally, the lower temperatures appeared to inhibit restoring the different phenotypes by the Δ*VpaChn25_0724*-com strain. Therefore, we focused on the

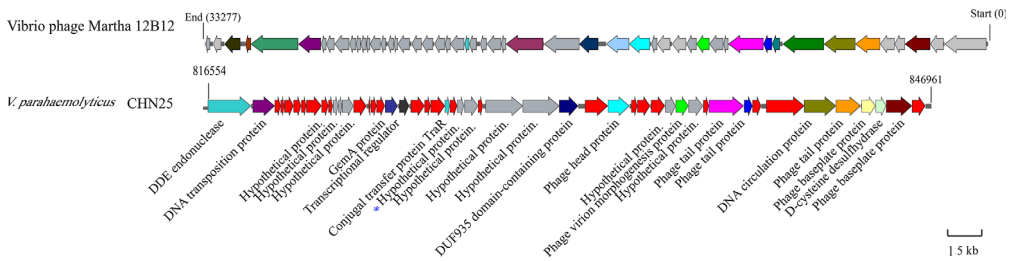

FIGURE 1 | Gene organization of the *Vibrio* phage Martha 12B12-like sequence in chromosome 1 of *V. parahaemolyticus* CHN25 genome. Genes in gray color represent predicted hypothetical proteins, and those in red represent additional proteins absent from the *Vibrio* phage Martha 12B12. The *VpaChn25_0724* gene was marked with a star in blue.

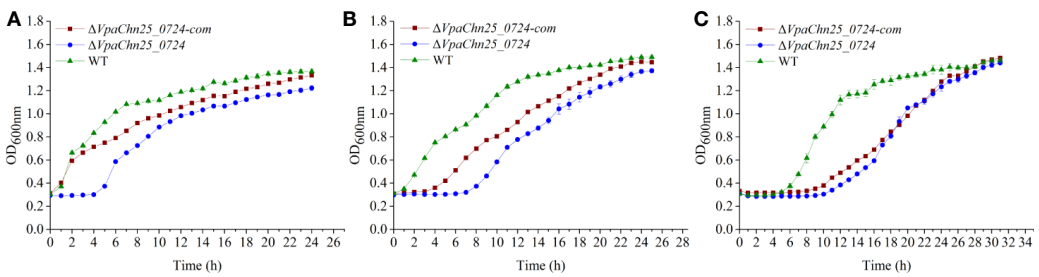

FIGURE 2 | Survival of *V. parahaemolyticus* CHN25 (WT), Δ*VpaChn25_0724*, and Δ*VpaChn25_0724*-com strains at different temperatures. The strains were incubated in the TSB medium at 37°C **(A)**, 25°C **(B)**, 15°C **(C)**, respectively. WT, wild type.

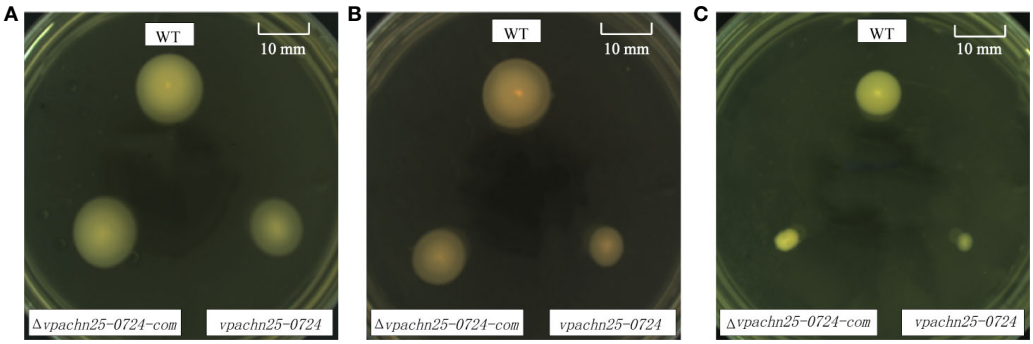

FIGURE 3 | Swimming motility of *V. parahaemolyticus* CHN25 (WT), Δ*VpaChn25_0724*, and Δ*VpaChn25_0724*-com strains at different temperature. A: 37°C; B: 25°C; C: 15°C; WT: wild type. The strains were incubated on the semi-solid TSB agar plates containing 0.25% agar at 37°C **(A)**, 25°C **(B)**, 15°C **(C)**, respectively. WT, wild type.

optimal growth temperature 37°C in the following analysis in this study. These results indicated that the severe defect in growth elicited by the *VpaChn25_0724* gene deletion likely led to the variant swimming motility of *V. parahaemolyticus* CHN25 at the lower temperatures.

In addition, we analyzed and quantified the bacterial biofilms formed under static incubation conditions using the crystal violet staining assay. The dynamic process of biofilm formation was followed for the wild type, Δ*VpaChn25_0724*, and Δ*VpaChn25_0724*-com strains grown at 37°C for 60 h (**Figure 4**). We observed that biofilms were built at three different stages (development, maturation and diffusion) by all the three strains, consistent with previous studies. At the early formation stage (24 h), the Δ*VpaChn25_0724* mutant exhibited a 1.5-fold decrease in biomass compared with the wild type ($p<0.01$). No significant difference was observed at the other stages among the three strains ($p>0.05$), except a notably decrease in biomass of Δ*VpaChn25_0724*-com at the latter stage. These results showed a defect in early biofilm formation of *V. parahaemolyticus* CHN25 in the absence of the *VpaChn25_0724* gene.

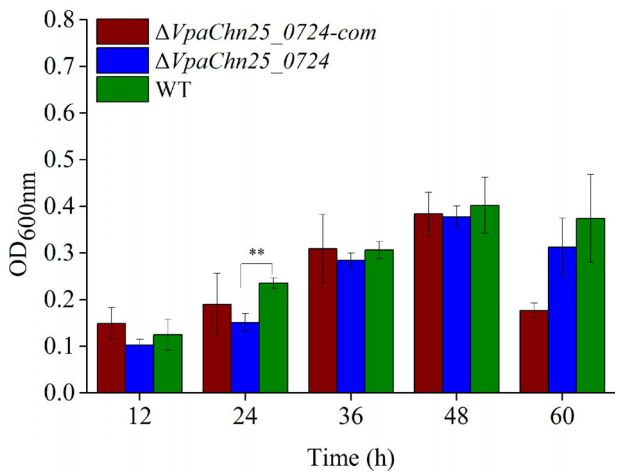

FIGURE 4 | Biofilm formation of *V. parahaemolyticus* CHN25 (WT), Δ*VpaChn25_0724*, and Δ*VpaChn25_0724*-com strains. The strains were incubated in the TSB medium at 37°C under static conditions. WT: wild type. **$p<0.01$ compared with the WT.

Cell Membrane Damage, Hydrophobicity, and Fluidity of the ΔVpaChn25_0724 Mutant

On the basis of the above results, we, therefore, asked whether bacterial cell membrane structure would be affected by the *VpaChn25_0724* gene deletion. We evaluated cell membrane damage, hydrophobicity and fluidity of the three strains grown in the TSB medium to mid-LGP at 37°C. As shown in **Figure 5**, no significant difference in cell membrane fluidity was observed among the three strains ($p>0.05$). However, the proportion of Δ*VpaChn25_0724* cells with damaged membrane was about twofold of that of the wild type ($p < 0.01$). The Δ*VpaChn25_0724* mutant also showed a twofold cell surface hydrophobicity ($p<0.01$) in comparison to the wild type. In correlation to the almost full restoration of cellular growth by the plasmid-borne *VpaChn25_0724* at 37°C (**Figure 1**), the complementation also restored the membrane integrity and hydrophobicity phenotypes. These results indicated that the *VpaChn25_0724* gene is important for cell membrane integrity of *V. parahaemolyticus* CHN25.

Differential Secretomes Mediated by the VpaChn25_0724 Gene Deletion

Given the altered cell membrane trait mediated by the *VpaChn25_0724* gene deletion, we next conducted comparative secretomic analysis of the three strains. When incubated in the TSB medium at 37°C without shaking, the Δ*VpaChn25_0724* mutant also grew more slowly than wild type (data not shown). The supernatant of bacterial cultures at the mid-LGP were collected, and extracellular proteins were isolated, and analyzed by 2-DE assay. This analysis revealed different secretome profiles among the wild type, Δ*VpaChn25_0724* and Δ*VpaChn25_0724*-com strains, showing various numbers of visible protein spots (**Figure 6**). The patterns yielded from three independent 2-DE

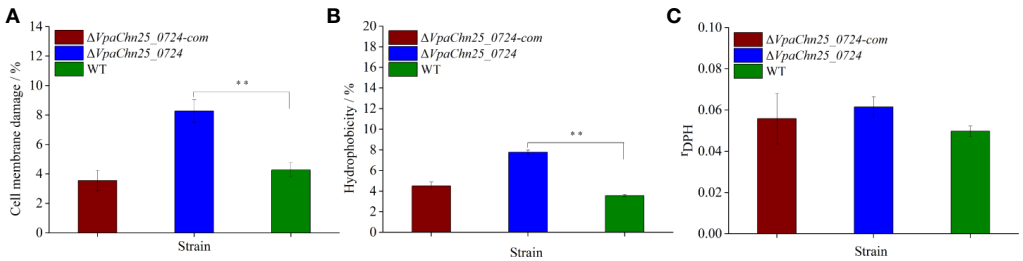

FIGURE 5 | Cell membrane damage **(A)**, hydrophobicity **(B)** and fluidity **(C)** of *V. parahaemolyticus* CHN25 (WT), Δ*VpaChn25_0724*, and Δ*VpaChn25_0724*-com. The strains were incubated in the TSB medium at 37°C to the mid-LGP. WT: wild type. **p<0.01 compared with the WT.

gels per biological sample were consistent (data not shown). These varied protein spots were excised from the 2-DE gels and digested with the trypsin. The resulting peptides were further identified by LC-MS/MS analysis.

The results yielded from the LC-MS/MS analysis were summarized in **Table 2**. Sequences of seven differentially expressed extracellular proteins among the three strains were obtained. Six proteins thereof were secreted by the Δ*VpaChn25_0724* mutant. For instance, the protein Spot 24-b-1 was identified as an 8-stranded β-barrel protein (OmpW). The protein Spots 24-b-2 and 24-b-3 were identified as FlaB/D and FlaA flagellins, respectiely, while the 24-b-6 and 24-C-1 were identified as an aldehyde-alcohol dehydrogenase (AdhE), and a 2-hydroxyacid dehydrogenase, respectively. These results indicated that the *VpaChn25_0724* gene deletion resulted in increased numbers of extracellular proteins, which was likely associated with damaged cell membrane structure of *V. parahaemolyticus* CHN25.

Effects of the VpaChn25_0724 Gene Deletion on V. parahaemolyticus CHN25-Host Intestinal Epithelial Cell Interaction

Consequently, we reasoned that the changed secretome may affect *V. parahaemolyticus* CHN25-host intestinal epithelial cell interaction, whereby the bacterium elicits gastroenteritis disease (O'Boyle and Boyd, 2013). The human rectal cancer epithelial cell line Caco-2 was used as an *in vitro* model for the cell interaction analysis in this study. As shown in **Figure 7**, after infected with the *ΔVpaChn25_0724* mutant at 37°C for 4 h, the viability of Caco-2 cells was significantly higher (97.05% ± 0.84) than those infected with the wild type (66.97% ± 1.04) and Δ*VpaChn25_0724*-com (62.38% ± 1.34) strains (p<0.01). Moreover, apoptosis of Caco-2 cells was examined using Annexin V-FITC and propidium iodide (PI) double stainings by flow cytometry assay. Unexpectedly, the results showed that at 4 h post infection, *ΔVpaChn25_0724* induced an early apoptosis in Caco-2 cells at a much higher rate (32.67% ± 2.12%) than the

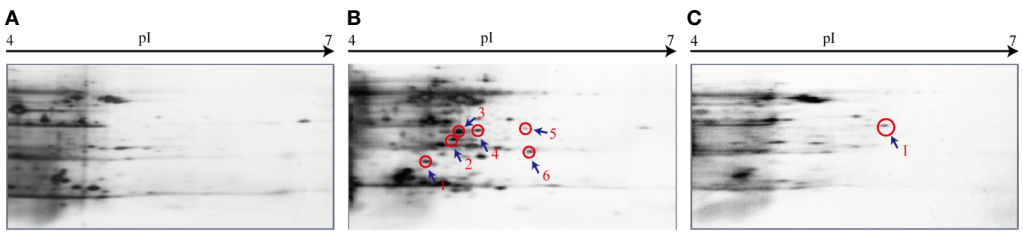

FIGURE 6 | The 2-DE analysis of extracellular proteins of *V. parahaemolyticus* CHN25, Δ*VpaChn25_0724*, and Δ*VpaChn25_0724*-com strains. **(A)** Wild type; **(B)** Δ*VpaChn25_0724*; **(C)** Δ*VpaChn25_0724*-com.

TABLE 2 | Identification of the protein spots on the secretome profiles by LC-MS/MS analysis.

Protein spot	Uniprot No.	Protein	Gene	MW (Da)	pI	Score	Sequence coverage
24-b-1	Z2ENQ0	Outer membrane protein	*ompW*	23467.38	4.98	34.42	6.54%
24-b-2	A6BAT3	Polar flagellin B/D	*A79_3829*	39327.82	5.01	64.04	3%
24-b-3	C8CP39	Flagellin flaA	*flaA*	39776.44	4.9	63.57	5.32%
24-b-4	A0A2R9VMM8	Phage head morphogenesis protein	*C1S91_15620*	48343.9	4.79	23.63	1.62%
24-b-5	S5IY46	D-lactate dehydrogenase	*M634_18815*	36750.66	5.6	30.14	2.72%
24-b-6	A0A0M9C4Z3	Aldehyde-alcohol dehydrogenase	*ACX03_17620*	97061.86	5.68	34.29	1.11%
24-c-1	A0A0L8BEZ4	2-hydroxyacid dehydrogenase	*C9I78_22190*	36706.56	5.49	23.88	2.72%

wild type (11.27% ± 0.94) and the Δ*VpaChn25_0724*-com (10.94% ± 2.12%) strains ($p<0.01$). Interestingly, an opposite pattern was observed where late apoptosis elicited by *ΔVpaChn25_0724* was significantly less (48.50% ± 0.30%) than by wild type (77.53% ± 5.59%) and Δ*VpaChn25_0724*-com (74.57% ± 4.56%) strains ($p<0.01$).

Differential Transcriptomes Mediated by the VpaChn25_0724 Gene Deletion

To get insights into global-level gene expression change mediated by the *VpaChn25_0724* gene deletion, we next determined transcriptomes of *V. parahaemolyticus* CHN25, *ΔVpaChn25_0724* and Δ*VpaChn25_0724*-com strains using Illumina RNA sequencing technique. This analysis revealed that approximately 13.7% of the bacterial genes were differentially expressed in the *ΔVpaChn25_0724* mutant, when compared with the wild type and *ΔVpaChn25_0724*-com strains grown at 37°C to the mid-LGP. Of these genes, 190 showed higher transcriptional levels (fold change ≥ 2.0), while 569 genes were down-regulated (fold change ≤ 0.5). These DEGs in *ΔVpaChn25_0724* were grouped into one hundred and twenty-six gene functional catalogues in the KEGG database (data not shown). A complete list of the DEGs in the three strains is available in the NCBI SRA database (http://www.ncbi.nlm.nih.gov/sra/) under the accession number SRP258529. To validate the transcriptome data, we examined 18 representative genes (**Table S1**) in the *ΔVpaChn25_0724* mutant by RT-qPCR analysis. The resulting data were correlated with those yielded from the transcriptome analysis (**Table S1**).

The Major Altered Metabolic Pathways in the ΔVpaChn25_0724 Mutant

Based on the GSEA of the transcriptome data against the KEGG database, approximately twelve significantly altered metabolic pathways were identified in the *VpaChn25_0724* mutant, including the galactose, glyoxylate and dicarboxylate, fructose and mannose, butanoate and thiamine metabolisms; citrate cycle (TCA); pentose and glucuronate interconversions; valine, leucine, and isoleucine degradation and glycerolipid metabolism; QS; ATP-binding cassette (ABC) transporters; and phosphotransferase system (PTS) (**Table 3**).

Remarkably, approximately sixty DEGs involved in the galactose metabolism, fructose and mannose metabolism, TCA, glycerolipid metabolism, PTS, and thiamine metabolism were all significantly down-regulated in the *ΔVpaChn25_0724* mutant (0.034- to 0.487-fold) ($p<0.05$), when compared with the wild type and *ΔVpaChn25_0724-com* strains (**Table 3**). Also, all the DEGs in the pentose and glucuronate interconversions were greatly down-regulated (0.097- to 0.393-fold), except one encoding aldehyde dehydrogenase. These changes were directly related to the observed phenotypic variations of *ΔVpaChn25_0724*. For example, in the galactose metabolism, eleven DEGs encoding key metabolizing enzymes were significantly repressed at the transcriptional level (0.171–0.441 fold) ($p<0.05$), including the galactokinase (*VpaChn25_RS11750* and *VpaChn25_RS21100*), galactose-1-epimerase (*VpaChn25_RS11745*), alpha and beta-galactosidase (*VpaChn25_RS21125*, *VpaChn25_RS06235*, *VpaChn25_RS11770* and *VpaChn25_RS11775*), UDP-glucose 4-epimerase GalE (*VpaChn25_RS21110* and *VpaChn25_RS11760*), and UDP-glucose-hexose-1-phosphate uridylyltransferase (*VpaChn25_RS11755* and *VpaChn25_RS21105*), which may have resulted in reduced important metabolites (e.g., galactose-1-phosphate, and UDP-glucose/galactose/fructose 1,6-diphosphate) in the metabolic pathway. Similarly, in the fructose and mannose metabolism, the DEGs encoding key metabolizing enzymes, e.g., 1-phosphofructokinase (*VpaChn25_RS19525*) and mannose-6-phosphate isomerase (*VpaChn25_RS22285*, *VpaChn25_RS20215*), were also significantly down-regulated (0.156- to 0.326-fold) ($p<0.05$). Moreover, approximately all the DEGs linked to PTS showed a significant decrease in transcription in *ΔVpaChn25_0724* (0.191- to 0.473-fold) ($p<0.05$). Interestingly, expression of the gene encoding glucose transporter subunit IIBC (*VpaChn25_RS10110*) was notably down-regulated (0.199-fold). Meanwhile, expression of about nine DEGs involved in TCA was slightly down-regulated (0.365- to 0.486-fold) ($p<0.05$). In addition, in the thiamine metabolism, expression of thiamine phosphorylase (*VpaChn25_RS16405*) was also down-regulated (0.310-fold) ($p<0.05$). These data suggested inactive transport and utilization of the carbon sources as well as repressed energy production in the *ΔVpaChn25_0724* mutant.

Additionally, five DEGs involved in the glycerolipid metabolism were strikingly down-regulated (0.034- to 0.041-fold) ($p<0.05$), including the glycerol kinase (*VpaChn25_RS16340* and *VpaChn25_RS11685*), glycerol dehydrogenase (*VpaChn25_RS01900*), dihydroxyacetone kinase ADP-binding

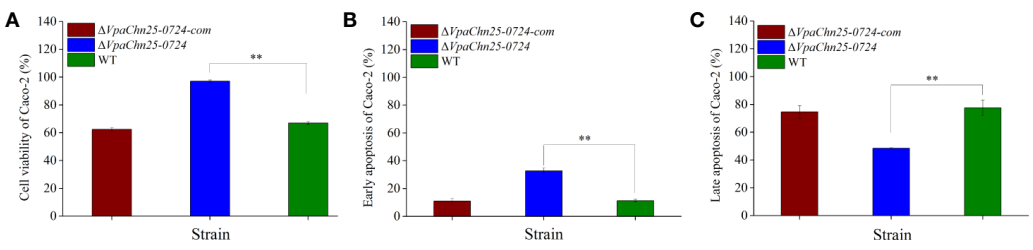

FIGURE 7 | The viability and apoptosis of Caco-2 cells infected by *V. parahaemolyticus* CHN25 (WT), Δ*VpaChn25_0724*, and Δ*VpaChn25_0724-com* strains. The infection was performed at 37°C for 4 h. **(A)** Cell viability; **(B)** Early stage of apoptosis; **(C)** Late stage of apoptosis. **p<0.01 compared with the WT.

TABLE 3 | Major altered metabolic pathways in the *ΔVpaChn25_0724* mutant.

Metabolic pathway	Gene ID	Fold change	Description
Galactose metabolism	*VpaChn25_RS11745*	0.441	Galactose-1-epimerase
	VpaChn25_RS11750	0.318	Galactokinase
	VpaChn25_RS11755	0.215	UDP-glucose-hexose-1-phosphate uridylyltransferase
	VpaChn25_RS11760	0.376	UDP-glucose 4-epimerase GalE
	VpaChn25_RS11770	0.403	beta-galactosidase subunit alpha
	VpaChn25_RS21125	0.185	beta-galactosidase
	VpaChn25_RS06235	0.452	alpha-galactosidase
	VpaChn25_RS21110	0.167	UDP-glucose 4-epimerase GalE
	VpaChn25_RS11775	0.406	beta-galactosidase subunit beta
	VpaChn25_RS21100	0.233	Galactokinase
	VpaChn25_RS21105	0.171	UDP-glucose–hexose-1-phosphate uridylyltransferase
Fructose and mannose metabolism	*VpaChn25_RS19530*	0.326	Fused PTS fructose transporter subunit IIA/HPr protein
	VpaChn25_RS21730	0.273	PTS mannitol transporter subunit IICB
	VpaChn25_RS21735	0.156	PTS mannitol transporter subunit IIA
	VpaChn25_RS21725	0.276	L-sorbose 1-phosphate reductase
	VpaChn25_RS22280	0.244	PTS fructose transporter subunit IIC
	VpaChn25_RS22285	0.129	Mannose-6-phosphate isomerase%2C class I
	VpaChn25_RS01915	0.191	Phosphoenolpyruvate–protein phosphotransferase
	VpaChn25_RS20215	0.385	Mannose-6-phosphate isomerase%2C class I
	VpaChn25_RS19525	0.307	1-phosphofructokinase
	VpaChn25_RS17315	0.254	PTS sugar transporter subunit IIA
	VpaChn25_RS19520	0.310	PTS fructose transporter subunit IIBC
Glyoxylate and dicarboxylate metabolism	*VpaChn25_RS02855*	3.967	Malate synthase A
	VpaChn25_RS12740	0.409	Dihydrolipoyl dehydrogenase
	VpaChn25_RS07820	0.393	Twin-arginine translocation signal domain-containing protein
	VpaChn25_RS07825	0.305	4Fe-4S dicluster domain-containing protein
	VpaChn25_RS07830	0.413	Formate dehydrogenase subunit gamma
	VpaChn25_RS16830	2.986	Malate synthase
	VpaChn25_RS22250	0.484	Catalase
	VpaChn25_RS02860	2.131	Isocitrate lyase
	VpaChn25_RS18565	2.087	Thiolase family protein
	VpaChn25_RS01720	0.420	Malate dehydrogenase
	VpaChn25_RS16175	0.465	Bifunctional 4-hydroxy-2-oxoglutarate Aldolase/2-dehydro-3-deoxy-phosphogluconate aldolase
	VpaChn25_RS13855	2.071	Alanine–glyoxylate aminotransferase family protein
Citrate cycle	*VpaChn25_RS12750*	0.421	Pyruvate dehydrogenase (acetyl-transferring)%2C homodimeric type
	VpaChn25_RS09275	0.486	Fumarate hydratase
	VpaChn25_RS04480	0.475	Succinate–CoA ligase subunit alpha
	VpaChn25_RS00605	0.365	Phosphoenolpyruvate carboxykinase (ATP)
	VpaChn25_RS12745	0.398	Pyruvate dehydrogenase complex dihydrolipoyllysine-residue acetyltransferase
	VpaChn25_RS04475	0.439	ADP-forming succinate–CoA ligase subunit beta
	VpaChn25_RS04465	0.485	2-oxoglutarate dehydrogenase E1 component
	VpaChn25_RS04455	0.440	Succinate dehydrogenase flavoprotein subunit
	VpaChn25_RS04440	0.472	Citrate synthase
Pentose and glucuronate interconversions	*VpaChn25_RS23490*	0.393	L-arabinose isomerase
	VpaChn25_RS07015	5.792	Aldehyde dehydrogenase (NADP(+))
	VpaChn25_RS23600	0.321	Mannonate dehydratase
	VpaChn25_RS23625	0.331	Fructuronate reductase
	VpaChn25_RS23630	0.370	Glucuronate isomerase
	VpaChn25_RS23480	0.097	Ribulokinase
Butanoate metabolism	*VpaChn25_RS07255*	0.460	4-aminobutyrate-2-oxoglutarate transaminase
	VpaChn25_RS18405	2.693	Acetoacetate-CoA ligase
	VpaChn25_RS16990	0.104	Aspartate aminotransferase family protein
	VpaChn25_RS18185	2.591	Class I poly(R)-hydroxyalkanoic acid synthase
	VpaChn25_RS01855	0.394	Acetolactate synthase small subunit
	VpaChn25_RS01850	0.436	Acetolactate synthase 3 large subunit
	VpaChn25_RS10475	0.470	Bifunctional acetaldehyde-CoA/alcohol dehydrogenase
	VpaChn25_RS22970	0.479	Formate C-acetyltransferase/glycerol dehydratase family glycyl radical enzyme
ABC transporters	*VpaChn25_RS20680*	2.168	ABC transporter ATP-binding protein
	VpaChn25_RS18435	2.674	Branched-chain amino acid ABC transporter permease

(Continued)

TABLE 3 | Continued

Metabolic pathway	Gene ID	Fold change	Description
	VpaChn25_RS15795	0.489	Amino acid ABC transporter substrate-binding protein
	VpaChn25_RS07075	3.318	ATP-binding cassette domain-containing protein
	VpaChn25_RS07770	0.320	Tungsten ABC transporter substrate-binding protein
	VpaChn25_RS23465	0.252	L-arabinose ABC transporter permease AraH
	VpaChn25_RS18440	2.085	Branched-chain amino acid ABC transporter permease
	VpaChn25_RS18445	2.037	Branched-chain amino acid ABC transporter substrate-binding protein
	VpaChn25_RS23380	0.422	Fe(3+) dicitrate ABC transporter ATP-binding protein FecE
	VpaChn25_RS22050	2.141	iron ABC transporter permease
	VpaChn25_RS23470	0.108	L-arabinose ABC transporter ATP-binding protein AraG
	VpaChn25_RS23475	0.141	Arabinose ABC transporter substrate-binding protein
	VpaChn25_RS16420	0.217	ABC transporter ATP-binding protein
	VpaChn25_RS18450	2.058	ABC transporter ATP-binding protein
	VpaChn25_RS16425	0.257	ABC transporter permease
	VpaChn25_RS21150	2.079	sn-glycerol-3-phosphate ABC transporter ATP-binding protein UgpC
	VpaChn25_RS07085	5.165	ABC transporter permease subunit
	VpaChn25_RS07080	4.177	ATP-binding cassette domain-containing protein
	VpaChn25_RS20855	2.741	Transporter substrate-binding domain-containing protein
	VpaChn25_RS20850	3.288	Arginine ABC transporter permease ArtQ
	VpaChn25_RS18745	0.192	Ribose ABC transporter substrate-binding protein RbsB
	VpaChn25_RS21135	0.294	Sugar ABC transporter permease
	VpaChn25_RS16430	0.315	ABC transporter ATP-binding protein
	VpaChn25_RS21145	0.209	Extracellular solute-binding protein
	VpaChn25_RS21140	0.325	Sugar ABC transporter permease
	VpaChn25_RS07095	4.736	Peptide ABC transporter substrate-binding protein
	VpaChn25_RS07090	5.473	Oligopeptide ABC transporter permease OppB
	VpaChn25_RS20845	4.173	Arginine ABC transporter permease ArtM
	VpaChn25_RS03505	0.442	MetQ/NlpA family lipoprotein
	VpaChn25_RS20860	2.059	Arginine ABC transporter ATP-binding protein ArtP
	VpaChn25_RS18620	0.063	Choline ABC transporter substrate-binding protein
	VpaChn25_RS18625	0.076	Choline ABC transporter permease subunit
	VpaChn25_RS18740	0.362	Ribose ABC transporter permease
	VpaChn25_RS22165	0.221	Maltose/maltodextrin ABC transporter substrate-binding protein MalE
	VpaChn25_RS18630	0.132	Choline ABC transporter ATP-binding protein
	VpaChn25_RS17000	0.498	Putative 2-aminoethylphosphonate ABC transporter substrate-binding protein
	VpaChn25_RS18730	0.127	D-ribose pyranase
	VpaChn25_RS18735	0.327	Ribose ABC transporter ATP-binding protein RbsA
	VpaChn25_RS18425	2.079	ABC transporter ATP-binding protein
Quorum sensing	*VpaChn25_RS14495*	0.459	Protein-export chaperone SecB
	VpaChn25_RS12590	2.502	ABC transporter ATP-binding protein
	VpaChn25_RS15815	0.388	ABC transporter ATP-binding protein
	VpaChn25_RS18430	3.205	Long-chain fatty acid–CoA ligase
	VpaChn25_RS12580	2.162	ABC transporter permease
	VpaChn25_RS12585	2.557	ABC transporter ATP-binding protein
	VpaChn25_RS19030	0.412	Quorum-sensing autoinducer synthase
	VpaChn25_RS07050	9.639	ABC transporter permease
	VpaChn25_RS25650	0.474	GTP cyc Meng ydrolase II
	VpaChn25_RS09025	0.424	Response regulator
	VpaChn25_RS09695	0.442	Anthranilate synthase component 1
	VpaChn25_RS00230	0.497	ABC transporter permease
	VpaChn25_RS09030	0.188	Two-component sensor histidine kinase
	VpaChn25_RS07030	6.574	Extracellular solute-binding protein
	VpaChn25_RS07045	6.497	ABC transporter ATP-binding protein
	VpaChn25_RS17545	0.461	Extracellular solute-binding protein
	VpaChn25_RS07055	8.372	ABC transporter permease
	VpaChn25_RS09700	0.386	Aminodeoxychorismate/anthranilate synthase component II
Glycerolipid metabolism	*VpaChn25_RS16340*	0.162	Glycerate kinase
	VpaChn25_RS01910	0.167	Dihydroxyacetone kinase ADP-binding subunit DhaL
	VpaChn25_RS11685	0.034	Glycerol kinase
	VpaChn25_RS01905	0.153	Dihydroxyacetone kinase subunit DhaK
	VpaChn25_RS01900	0.041	Glycerol dehydrogenase
Phosphotransferase system	*VpaChn25_RS16970*	0.353	PTS sugar transporter subunit IIB
	VpaChn25_RS10110	0.199	PTS glucose transporter subunit IIBC

(Continued)

TABLE 3 | Continued

Metabolic pathway	Gene ID	Fold change	Description
	VpaChn25_RS03530	0.416	PTS trehalose transporter subunit IIBC
	VpaChn25_RS04190	0.487	Phosphoenolpyruvate-protein phosphotransferase PtsI
	VpaChn25_RS13660	0.473	HPr family phosphocarrier protein
Valine, leucine and isoleucine degradation	*VpaChn25_RS18590*	2.510	3-hydroxyisobutyrate dehydrogenase
	VpaChn25_RS18535	2.274	Hydroxymethylglutaryl-CoA lyase
	VpaChn25_RS18570	2.783	CoA-acylating methylmalonate-semialdehyde dehydrogenase
	VpaChn25_RS18550	2.559	Methylcrotonoyl-CoA carboxylase
	VpaChn25_RS18540	2.521	Acetyl/propionyl/methylcrotonyl-CoA carboxylase subunit alpha
Thiamine metabolism	*VpaChn25_RS15465*	0.279	Phosphomethylpyrimidine synthase ThiC
	VpaChn25_RS15460	0.171	Thiamine phosphate synthase
	VpaChn25_RS16435	0.420	Bifunctional hydroxymethylpyrimidine kinase/phosphomethylpyrimidine kinase
	VpaChn25_RS16405	0.310	Thiamine phosphate synthase
	VpaChn25_RS15455	0.158	Thiazole biosynthesis adenylyltransferase ThiF
	VpaChn25_RS16410	0.289	Hydroxyethylthiazole kinase
	VpaChn25_RS16415	0.244	Thiaminase II
	VpaChn25_RS15445	0.134	Thiazole synthase
	VpaChn25_RS15440	0.163	2-iminoacetate synthase ThiH

subunit DhaL (*VpaChn25_RS01910*), and dihydroxyacetone kinase subunit DhaK genes (*VpaChn25_RS01905*). The reaction product (glycerol 3-phosphate, G3P) catalyzed by glycerol kinase is also an important metabolite in phospholipid biosynthesis under all growth conditions (Holtman et al., 2001), which plays a vital role in the regulation of membrane biogenesis.

On the other aspect, the deletion of *VpaChn25_0724* also triggered significant changes in the other five metabolic pathways in the *ΔVpaChn25_0724* mutant. Many DEGs thereof showed higher transcriptional levels. For instance, most DEGs linked to the valine, leucine and isoleucine degradation were slightly up-regulated in *ΔVpaChn25_0724* (2.179- to 2.783-fold) ($p<0.05$), which may have resulted in an increases in acetyl-CoA and subsequent entry into TCA. Remarkably, approximately 39 DEGs associated with ABC transporters were significantly altered at the transcriptional level. Consistent with the down-regulated carbon metabolism as well as repressed energy production in *ΔVpaChn25_0724*, some ABC transporters for sugar uptake were also greatly down-regulated (0.192- to 0.362-fold) ($p<0.05$), e.g., sugar ABC transporter permease (*VpaChn25_RS21140* and *VpaChn25_RS21135*), maltose/maltodextrin ABC transporter substrate-binding protein MalE (*VpaChn25*_RS22165), ribose ABC transporter permease (*VpaChn25_RS18740*), ribose ABC transporter ATP-binding protein RbsAB (*VpaChn25_RS18735* and *VpaChn25_RS187450*), and extracellular solute-binding protein (*VpaChn25_RS21145*). In marked contrast, the DEGs encoding arginine ABC transporter permease ArtM (*VpaChn25_RS20845*), peptide ABC transporter substrate-binding protein (*VpaChn25_RS07095*), and oligopeptide ABC transporter permease (*VpaChn25_RS07090*) were notably up-regulated (4.173- to 5.473-fold). Likewise, some DEGs encoding ABC transporter ATP-binding protein (*VpaChn25_RS07045*), ABC transporter permease (*VpaChn25_RS07085*, *VpaChn25_RS07050* and *VpaChn25_RS07055*), and extracellular solute-binding protein (*VpaChn25_RS07030*) were also greatly up-regulated in the QS (5.165- to 9.639-fold) ($p<0.05$), suggesting that the *VpaChn25_0724* gene may act as a suppressor of these ABC transporters in *V. parahaemolyticus* CHN25.

Major Altered DGEs Related with Phenotypic Variations of the ΔVpaChn25_0724 Mutant

On the basis of the transcriptome data, the GSAA against the GO database also revealed major altered DGEs related with phenotypic variations of the Δ*VpaChn25_0724* mutant compared with the wild type and Δ*VpaChn25_0724-com* strain.

Expression of the DEGs encoding flagellar basal body protein FliL (*VpaChn25_RS22910*) (0395-fold), rod protein FlgD (*VpaChn25_RS17140*) (0.389-fold), and export and assembly protein FliR (*VpaChn25_RS22850*) (0.094-fold) were all significantly down-regulated in the Δ*VpaChn25_0724* mutant ($p<0.05$). The remarkably repressed FliR (0.094-fold) belongs to a membrane-embedded part of flagellar export apparatus. These data suggested a defective flagellar basal body in the Δ*VpaChn25_0724* mutant that may have contributed to its affected swimming and biofilm formation.

Some biofilm formation-associated genes were also repressed at the transcriptional level in the Δ*VpaChn25_0724* mutant, e.g., QS autoinducer synthase (*VpaChn25_RS19030*), anthranilate synthase component 1 (*VpaChn25_RS09695*), aminodeoxychorismate/anthranilate synthase component II (*VpaChn25_RS09700*), and PTS glucose transporter subunit IIBC (*VpaChn25_RS10110*) (0.199- to 0.442-fold) ($p<0.05$). QS impacts bacterial motility, biofilm formation, and construction (Whiteley et al., 2017). The conserved phage shock protein (Psp) system functions in cell envelope stress response, and links to antibiotic resistance, biofilm formation and virulence in a diverse group of bacteria (Flores-Kim and Darwin, 2016). In this study, the genes encoding core components of the Psp system PspB (*VpaChn25_RS06290*) (0.385-fold) and PspC (*VpaChn25_RS06295*) (0.342-fold) were

significantly down-regulated in the Δ*VpaChn25_0724* mutant ($p<0.05$).

The genes encoding T3SS chaperones SycN (*VpaChn25_RS08695*) (0.197-fold) and YopN-like gatekeeper (*VpaChn25_RS08705*) (0.399-fold), YopR-like regulator (*VpaChn25_RS08820*) (0.461-fold), and export apparatus protein (*VpaChn25_RS08740*) (0.244-fold) were all greatly down-regulated in Δ*VpaChn25_0724* ($p<0.05$). Additionally, expression of the genes encoding OmpA (*VpaChn25_RS22825*) (0.164-fold) and OmpW (*VpaChn25_RS16240)* (0.331-fold) were significantly decreased ($p<0.05$). In contrast, the gene encoding T3SS chaperone CesT (*VpaChn25_RS08785*) was notably up-regulated in the Δ*VpaChn25_0724* mutant (6.221-fold) ($p<0.05$).

Remarkably, several differentially expressed response and transcriptional regulators were greatly repressed in the Δ*VpaChn25_0724* mutant, which are key components in bacterial gene regulatory networks, and can sense fluctuations under internal and external conditions (Brinkrolf et al., 2007). For example, two genes (*VpaChn25_RS08860* and *VpaChn25_RS22275*) encoded DNA-binding transcriptional regulator AraC, one of the most common positive regulators in bacteria, were notably down-regulated (0.270-fold and 0.204-fold) ($p<0.05$). Regulators belonging to this family have three major regulatory functions in common: carbon metabolism, stress response, and pathogenesis (Gallegos et al., 1997). Moreover, the gene (*VpaChn25_RS04915*) encoding a TetR/AcrR family transcriptional regulator was strikingly down-regulated (0.021-fold) ($p<0.05$). Another interesting observation was that expression of a regulator BetI (*VpaChn25_RS18605*) was also strikingly down-regulated in the Δ*VpaChn25_0724* mutant (0.022-fold) ($p<0.05$). Additionally, TEM images provided additional evidence for the global-level gene expression change in *ΔVpaChn25_0724*, as cell morphological characteristics of this mutant appeared different from those of the wild type and Δ*VpaChn25_0724*-com strains, such as the changed intracellular structure with more cytocysts in *ΔVpaChn25_0724* (**Figure 8**).

On the other hand, to further verify the differential transcriptomic data, two representative DEGs *Vpachn25_RS01720* and *Vpachn25_RS04440* (**Table S1**) encoding key enzymes were chosen for enzyme activity analyses, given their detection methods are available in literature to date. The results showed significantly reduced malate dehydrogenase and citrate synthase activities in *ΔVpaChn25_0724* compared with the wild type strain ($p<0.05$) (**Figure S2**), which were encoded by the *Vpachn25_RS01720* and *Vpachn25_RS04440*, respectively. These results were correlated with those yielded from the transcriptome analysis and confirmed by the RT-qPCR analyses (**Table S1**).

On the basis of the findings, we tried to locate the protein encoded by *VpaChn25_0724* in *V. parahaemolyticus* CHN25 using routine immunochemistry method, but failed to find its exact cellular position. It will be interesting to investigate its protein property and regulation in the bacterium in the future research.

Transmission of the VpaChn25_0724 Gene in Bacteria

The *VpaChn25_0724* gene was examined in 138 V. *parahaemolyticus* strains isolated from aquatic products

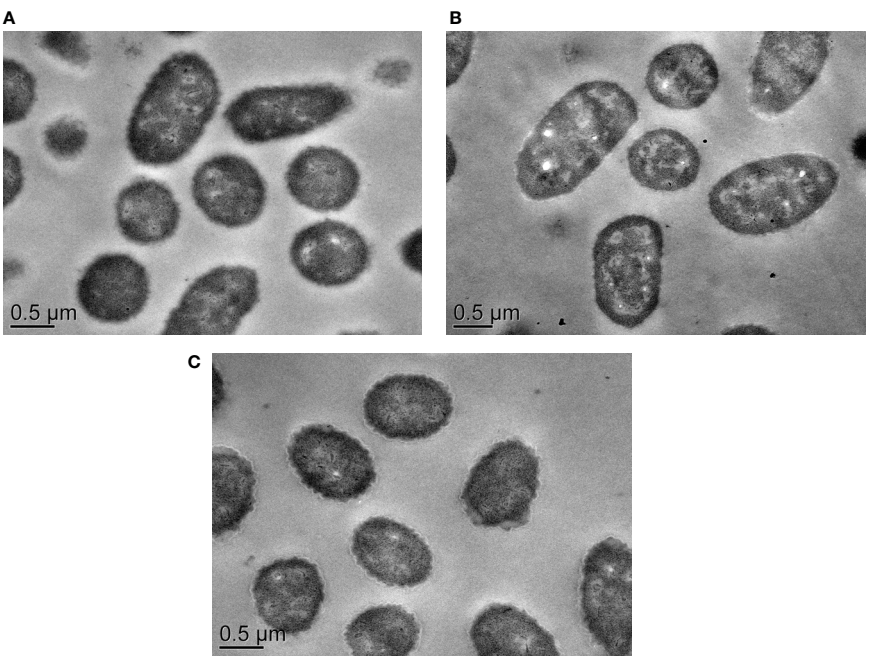

FIGURE 8 | The TEM observation of cell structure of *V. parahaemolyticus* CHN25, Δ*VpaChn25_0724*, and Δ*VpaChn25_0724-com* strains. **(A)** Wild type; **(B)** Δ*VpaChn25_0724*; **(C)** Δ*VpaChn25_0724*-com.

collected in Shanghai, China (Su et al. under review) by PCR assay. The resulting data showed that approximately 5.8% (n=8) of the *V. parahaemolyticus* isolates carried the *VpaChn25_0724* gene. Moreover, BLAST analysis against the GenBank database revealed that the *VpaChn25_0724* gene is present in three *Vibrio* phages, four *Vibrio* species including *Vibrio cholera*e, *Vibrio campbellii, Vibrio mimicus*, and *V. parahaemolyticus*, as well as the other two bacterial genera such as *Marinomonas primoryensis*, and *Shewanella oneidensis*. These data indicated that transmission of the *VpaChn25_0724* gene occurred among *V. parahaemolyticus* population in aquatic products, within *Vibrio* genus, and even across bacterial genera during the evolution history.

DISCUSSION

Vibrio parahaemolyticus is a leading seafood-borne pathogen worldwide. In aquatic ecosystems, phages constantly transform bacterial communities by HGT (Penades et al., 2015; Castillo et al., 2018). Nevertheless, biological functions of prophage-related genes remaining in *V. parahaemolyticus* are not yet fully understood. In this study, for the first time, we studied one such gene *VpaChn25_0724* encoding an unknown hypothetical protein in the largest prophage gene cluster identified in *V. parahaemolyticus* CHN25 genome (Zhu et al., 2017). An unmarked in-frame gene deletion mutant Δ*VpaChn25_0724* was successfully constructed, and its complementary mutant Δ*VpaChn25_0724*-com was also obtained in this study. Our data unveiled that the *VpaChn25_0724* gene deletion resulted in a sever defect in growth of *V. parahaemolyticus* CHN25, particularly at the lower temperatures.

Motility is closely associated with bacterial virulence and affects their attachment, colonization and invasion toward host cells (Guo et al., 2019). *V. parahaemolyticus* is motile by means of a single, sheathed polar flagellum that propels the swimmer cell in liquid environments (Kim and McCarter, 2000). The bacterial flagellum is essential in forming biofilm (i.e., matrix enclosed and surface-associated communities), which is critical for *V. parahaemolyticus* persistence in aquatic environments and pathogenicity in the host (Yildiz and Visick, 2009). In this study, we observed significantly lowered swimming capacity of the Δ*VpaChn25_0724* mutant at 25°C and 15°C, when compared with the wild type ($p < 0.05$). Moreover, our data showed a decrease in the development of biofilm by *V. parahaemolyticus* CHN25 in the absence of the *VpaChn25_0724* gene. The severe defect in growth elicited by the *VpaChn25_0724* gene deletion likely led to the variant swimming motility and biofilm formation of *V. parahaemolyticus* CHN25.

Bacterial secretion systems play a vital role in virulence, symbiosis, interbacterial interactions, and environmental stress (De Nisco et al., 2017). In this study, we found differential secretomes mediated by the *VpaChn25_0724* gene deletion. Among the differentially expressed extracellular proteins, the protein Spot 24-b-1 is an important outer membrane protein and protects bacteria against host phagocytosis (Li et al., 2016). The protein Spots 24-b-2 and 24-b-3, identified as FlaB/D and FlaA flagellins, respectiely, are involved in polar flagellar biosynthesis in *V. parahaemolyticus* (Kim and McCarter, 2000). The latter is involved in P-ring assembly of flagellar structure and swimming motility (Kim and McCarter, 2000). Recently, Echazarreta et al. reported that FlaA also facilitated filament formation of *V. cholerae* flagellum (Echazarreta et al., 2018). The protein Spot 24-b-6 was identified as an AdhE that forms a high-order spirosome architecture for its activity (Kim et al., 2019). This multi-functional enzyme is essential for the fermentation of glucose to sustain the glycolytic pathway, and the deletion of *adhE* gene in pathogenic *E. coli* O157:H7 strongly suppressed type III secretion systems (T3SS) and induced over-expression of non-functional flagella (Kim et al., 2019). The Spot 24-C-1, identified as a 2-hydroxyacid dehydrogenase, plays an important role in cell stability at high saline concentrations (Bonete et al., 2000). These results indicated that the *VpaChn25_0724* gene deletion resulted in increased numbers of extracellular proteins, which was likely associated with damaged cell membrane of the Δ*VpaChn25_0724* mutant.

The damaged cell membrane elicited by the *VpaChn25_0724* gene deletion also significantly affected *V. parahaemolyticus* CHN25-host intestinal epithelial cell interaction. Based on the *in vitro* Caco-2 cell model, our data showed that the *ΔVpaChn25_0724* mutant induced much higher viability and early apoptosis rate of Caco-2 cells than the wild type and the Δ*VpaChn25_0724*-com strains ($p < 0.01$). Nevertheless, an opposite pattern was observed in the late apoptosis elicited by *ΔVpaChn25_0724*. The cell membrane of Caco-2 cells at the early apoptosis phase was still intact, whereas at the later stage was damaged. The most possible explanation for the above observation was that the increased number of extracellular proteins secreted by the *ΔVpaChn25_0724* mutant may have contributed to the higher apoptosis occurrence at the early stage, however, the significantly changed membrane surface structure and cellular process (see below) of the mutant likely lowered its cytotoxicity to the host cells at the later stage.

Transcriptomes of *V. parahaemolyticus* CHN25, *ΔVpaChn25_0724* and Δ*VpaChn25_0724*-com strains were determined to get insights into global-level gene expression change mediated by the *VpaChn25_0724* gene deletion. Based on the GSEA of the transcriptome data against the KEGG database, approximately twelve significantly altered metabolic pathways were identified in the *VpaChn25_0724* mutant (**Table 3**). For instance, PTS is known as a major sugar transport multicomponent system in bacteria, by which many sugars are transported into bacteria, concomitantly phosphorylated, and then fed into glycolysis (Postma et al., 1993). In this study, approximately all the DEGs linked to PTS showed a significant decrease in transcription in *ΔVpaChn25_0724* (0.191- to 0.473-fold) ($p<0.05$), which encode fructose, glucose. mannitol, trehalose, and sugar transporter subunits. Moreover,

expression of the gene encoding glucose transporter subunit IIBC (*VpaChn25_RS10110*) was notably down-regulated (0.199-fold), which may be related with the repressed galactose, fructose, mannose and glycerol metabolisms, because glucose controls utilization of several other carbon sources including lactose, melibiose, maltose, and glycerol in *E. coli* (Holtman et al., 2001). Meanwhile, expression of about nine DEGs involved in TCA was slightly down-regulated ($p<0.05$). In addition, in the thiamine metabolism, expression of thiamine phosphorylase (*VpaChn25_RS16405*) was also down-regulated ($p<0.05$), which may result in decreased thiamine pyrophosphate, a cofactor for many essential enzymes in glucose and energy metabolisms (Rodionov et al., 2017). These data suggested inactive transport and utilization of the carbon sources as well as repressed energy production in the *ΔVpaChn25_0724* mutant.

On the basis of the transcriptome data, major altered DGEs related with the phenotypic variations of the Δ*VpaChn25_0724* mutant were also identified. For instance, bacterial polar flagellum is powered by a rotary motor and acts as semirigid helical propeller, which is attached *via* a flexible coupling, known as the hook, to the basal body. The latter consists of rings and rods that penetrate the membrane and peptidoglycan layers (Kim and McCarter, 2000). In this study, expression of the DEGs encoding flagellar basal body structure protein FliL (*VpaChn25_RS22910*), rod structure protein FlgD (*VpaChn25_RS17140*), and export and assembly structure protein FliR (*VpaChn25_RS22850*) were all significantly down-regulated in the Δ*VpaChn25_0724* mutant ($p<0.05$). Recently, Takekawa et al. reported that FliL is a new stomatin-like protein that assists the *Vibrio* flagellar motor function (Takekawa et al., 2019). In this study, the FliR that belongs to a membrane-embedded part of flagellar export apparatus was greatly down-regulated in expression (0.094-fold). These data suggested a defective flagellar basal body in the Δ*VpaChn25_0724* mutant that may have contributed to its affected swimming and biofilm formation.

T3SS was identified in *V. parahaemolyticus* CHN25 genome, which is necessary for bacterial survival in the environment (De Nisco et al., 2017; Matsuda et al., 2019). In this study, the genes encoding T3SS chaperones SycN (*VpaChn25_RS08695*) and YopN-like gatekeeper (*VpaChn25_RS08705*), YopR-like regulator (*VpaChn25_RS08820*), and export apparatus protein (*VpaChn25_RS08740*) were all greatly down-regulated in Δ*VpaChn25_0724* ($p<0.05$). In *Yersinia pestis*, the secretion of toxic *Yersinia* outer proteins (Yops) is regulated by a YopN/SycN/YscB/TyeA complex (Joseph and Plano, 2013). It has been reported that YopN functions to prevent the secretion of Yops until T3SS apparatuses are in direct contact with a targeted eukaryotic cell and activated, which avoids the spurious loss of effector proteins to the extracellular environment (Plano and Schesser, 2013). Additionally, expression of the genes encoding OmpA (*VpaChn25_RS22825*) and OmpW (*VpaChn25_RS16240)* were significantly decreased ($p<0.05$). OmpA family proteins are heat-modifiable, surface-exposed, and porin proteins that are in high-copy number in the outer membrane of many gram-negative pathogenic bacteria. They are involved in bacterial adhesion, invasion or intracellular survival, as well as evasion of host defenses or stimulation of pro-inflammatory cytokine production (Confer and Ayalew, 2013). In this study, in contrast, the gene encoding T3SS chaperone CesT (*VpaChn25_RS08785*) was notably up-regulated in the Δ*VpaChn25_0724* mutant (6.221-fold) ($p<0.05$). It has been reported that the enteropathogenic *E. coli* (EPEC) multicargo chaperone CesT interacts with at least ten effector proteins and contributes pathogenesis (Ramu et al., 2013).

The distinct transcriptome data also revealed strikingly down-regulated five key genes involved in the glycerolipid metabolism in the *ΔVpaChn25_0724* mutant (0.034- to 0.041-fold), suggesting reduced important metabolites in the bacterial phospholipid biosynthesis, such as the G3P (Holtman et al., 2001) that plays a vital role in the regulation of membrane biogenesis. Meanwhile, a defective flagellar basal body in Δ*VpaChn25_0724* was also revealed by the comparative transcriptomic analyses (see above). These results, coupled with the inactive transport and utilization of the carbon sources as well as repressed energy production in *ΔVpaChn25_0724* may have significantly affected the cell membrane integrity of the mutant.

In addition, several key components in bacterial gene regulatory networks were greatly repressed in the Δ*VpaChn25_0724* mutant, which can sense fluctuations under internal and external conditions (Brinkrolf et al., 2007). For instance, the gene (*VpaChn25_RS04915*) encoding a TetR/AcrR family transcriptional regulator was strikingly down-regulated (0.021-fold) ($p<0.05$). Regulators of this family are involved in a series of regulatory cascades, e.g., cell response to environmental insults, control of catabolic pathways, differentiation processes, and pathogenicity (Ramos et al., 2005). Another interesting observation was that expression of a regulator BetI (*VpaChn25_RS18605*) was also strikingly down-regulated in the Δ*VpaChn25_0724* mutant (0.022-fold) ($p<0.05$), which negatively regulates *betT* and *betIBA* genes that govern glycine betaine (GB) biosynthesis from choline in *E. coli* (Rkenes et al., 1996). The down-regulated BetI possibly in turn activated the target genes in Δ*VpaChn25_0724*, which perhaps led to increased amount of GB to maintain the integrity of cell membranes against the damaging effects, as in other stress responses to excessive salt, cold, heat and freezing in bacteria (Sun et al., 2014).

Taken together, the results in this study facilitate better understanding of biological function of prophage-related genes remaining in *V. parahaemolyticus*, and meet the increasing need for novel diagnosis candidates of the leading seafood-borne pathogen worldwide.

DATA AVAILABILITY STATEMENT

A complete list of the DEGs is available in the NCBI SRA database (http://www.ncbi.nlm.nih.gov/sra/) under the accession number SRP258529.

AUTHOR CONTRIBUTIONS

LY, YW, PY, SR, ZZ, YJ, JY, XP, and LC participated in the design and or discussion of the study. LY, YW, and ZZ carried out the major experiments. PY analyzed the data. SR supervised this study. JY helped the bacteria-host intestinal epithelial cell interaction experiments. LY, YW, ZZ, and LC wrote the manuscript. XP, and LC revised the manuscript. All authors contributed to the article and approved the submitted version.

FUNDING

This study was supported by grants from the Science and Technology Commission of Shanghai Municipality (No. 17050502200) and the National Natural Science Foundation of China (No. 31671946).

ACKNOWLEDGMENTS

We acknowledge Professor Dominique Schneider, for kindly providing us the plasmid pDS132 for construction of the gene deletion mutant, and Professor Weicheng Bei for the *E. coli* β2155 λpir for conjugation experiments in this study.

SUPPLEMENTARY MATERIAL

The Supplementary Material for this article can be found online at: https://www.frontiersin.org/articles/10.3389/fcimb.2020.595709/full#supplementary-material

SUPPLEMENTARY FIGURE 1 | Construction of the Δ*VpaChn25_0724*, and Δ*VpaChn25_0724-com* mutants by agarose gel electrophoresis analysis. **(A)** amplicons of upstream (Lane 1) and downstream (Lane 2) sequences of the *VpaChn25_0724* gene. **(B)** amplicons franking the upstream and downstream sequence of *VpaChn25_0724*. **(C)** amplicons of the upstream and downstream sequence of *VpaChn25_0724* in the recombinant pDS132+*VpaChn25_0724* plasmids. Lines 1–6, positive recombinant plasmids; Line 7, blank control; Line 8, positive control. **(D)** amplicons of transformants with the *VpaChn25_0724*-up-F and *VpaChn25_0724*-down-R primers. Lines 1–5, positive strain of the first change; Lines 6–7, positive control; Lines 8 to 9, blank control. **(E)** amplicons of the *tlh* gene. Lines 1–5, positive exconjugants; Line 6, positive control; Line 7, blank control. **(F)** amplicons of exconjugants with the *VpaChn25_0724*-up-ex-F and *VpaChn25_0724*-down-ex-R primers. Lines 1–22, selected exconjugants strains; Line 23, blank control; Line 24, genomic DAN control. **(G)** Amplicons of the *tlh* gene from Δ*VpaChn25_0724* mutants. Lines 1–5, positive Δ*VpaChn25_0724* mutants; Line 6, positive control; Line 7, blank control. **(H)** Amplicons of the *VpaChn25_0724* gene. Lines 1–2, positive bands; Line 3, blank control. **(I)** double digestion of the recombinant pMMB207+*VpaChn25_0724* plasmid. **(J)** amplicons of *VpaChn25_0724* from positive transformants. **(K)** amplicons of *tlh from* Δ*VpaChn25_0724-com* mutants. M, 100 bp DNA Ladder.

SUPPLEMENTARY FIGURE 2 | Activities of the malate dehydrogenase and citrate synthase encoded by the DEGs *Vpachn25_RS01720* and *Vpachn25_RS04440* in *V. parahaemolyticus* CHN25 (WT), Δ*VpaChn25_0724*, and Δ*VpaChn25_0724*-com strains. A. Malate dehydrogenase. B. Citrate synthase.

SUPPLEMENTARY TABLE S1 | Expression of representative DEGs in ΔVpaChn25_0724 mutant by RT-qPCR analysis.

REFERENCES

Bonete, M. J., Ferrer, J., Pire, C., Penades, M., and Ruiz, J. L. (2000). 2-Hydroxyacid dehydrogenase from *Haloferax mediterranei*, a D-isomer-specific member of the 2-hydroxyacid dehydrogenase family. *Biochimie* 82 (12), 1143–1150. doi: 10.1016/s0300-9084(00)01193-7

Brinkrolf, K., Brune, I., and Tauch, A. (2007). The transcriptional regulatory network of the amino acid producer *Corynebacterium glutamicum*. *J. Biotechnol.* 129 (2), 191–211. doi: 10.1016/j.jbiotec.2006.12.013

Castillo, D., Kauffman, K., Hussain, F., Kalatzis, P., Rorbo, N., Polz, M. F., et al. (2018). Widespread distribution of prophage-encoded virulence factors in marine *Vibrio* communities. *Sci. Rep.* 8 (1), 9973. doi: 10.1038/s41598-018-28326-9

Collado, S., Oulego, P., Alonso, S., and Diaz, M. (2017). Flow cytometric characterization of bacterial abundance and physiological status in a nitrifying-denitrifying activated sludge system treating landfill leachate. *Environ. Sci. Pollut. Res. Int.* 24 (26), 21262–21271. doi: 10.1007/s11356-017-9596-y

Confer, A. W., and Ayalew, S. (2013). The OmpA family of proteins: roles in bacterial pathogenesis and immunity. *Vet. Microbiol.* 163 (3-4), 207–222. doi: 10.1016/j.vetmic.2012.08.019

De Nisco, N. J., Kanchwala, M., Li, P., Fernandez, J., Xing, C., and Orth, K. (2017). The cytotoxic type 3 secretion system 1 of *Vibrio* rewires host gene expression to subvert cell death and activate cell survival pathways. *Sci. Signal.* 10 (479), eaal4501. doi: 10.1126/scisignal.aal4501

Desai, S. K., and Kenney, L. J. (2019). Switching lifestyles is an in vivo adaptive strategy of bacterial pathogens. *Front. Cell. Infect. Microbiol.* 9:421. doi: 10.3389/fcimb.2019.00421

Echazarreta, M. A., Kepple, J. L., Yen, L. H., Chen, Y., and Klose, K. E. A. (2018). Critical Region in the FlaA Flagellin Facilitates Filament Formation of the *Vibrio cholerae* Flagellum. *J. Bacteriol.* 200 (15), e00029–e00018. doi: 10.1128/jb.00029-18

Feiner, R., Argov, T., Rabinovich, L., Sigal, N., Borovok, I., and Herskovits, A. A. (2015). A new perspective on lysogeny: prophages as active regulatory switches of bacteria. *Nat. Rev. Microbiol.* 13 (10), 641–650. doi: 10.1038/nrmicro3527

Flores-Kim, J., and Darwin, A. J. (2016). Interactions between the cytoplasmic domains of PspB and PspC silence the *Yersinia* enterocolitica phage shock protein response. *J. Bacteriol.* 198 (24), 3367–3378. doi: 10.1128/jb.00655-16

Fujino, T., Okuno, Y., Nakada, D., Aoyama, A., Fukai, K., Mukai, T., et al. (1953). On the bacteriological examination of Shirasu food poisoning. *Med. J. Osaka Univ.* 4, 299–304.

Gallegos, M. T., Schleif, R., Bairoch, A., Hofmann, K., and Ramos, J. L. (1997). Arac/XylS family of transcriptional regulators. *Microbiol. Mol. Biol. Rev.* 61 (4), 393–410. doi: 10.1128/.61.4.393-410.1997

Ghenem, L., Elhadi, N., Alzahrani, F., and Nishibuchi, M. (2017). *Vibrio parahaemolyticus*: a review on distribution, pathogenesis, virulence determinants and epidemiology. *Saudi J. Med. Med. Sci.* 5 (2), 93–103. doi: 10.4103/sjmms.sjmms_30_17

Gomez-Gil, B., Soto-Rodriguez, S., Lozano, R., and Betancourt-Lozano, M. (2014). Draft genome sequence of *Vibrio parahaemolyticus* strain M0605, which causes severe mortalities of shrimps in Mexico. *Genome Announc.* 2 (2), e00055–e00014. doi: 10.1128/genomeA.00055-14

Guo, D., Yang, Z., Zheng, X., Kang, S., Yang, Z., Xu, Y., et al. (2019). Thymoquinone inhibits biofilm formation and attachment-invasion in host cells of *Vibrio parahaemolyticus*. *Foodborne Pathog. Dis.* 16 (10), 671–678. doi: 10.1089/fpd.2018.2591

Harrison, E., and Brockhurst, M. A. (2017). Ecological and evolutionary benefits of temperate phage: what does or doesn't kill you makes you stronger. *Bioessays* 39, 1700112. doi: 10.1002/bies.201700112

He, Y., Wang, H., and Chen, L. (2015). Comparative secretomics reveals novel virulence-associated factors of *Vibrio parahaemolyticus*. *Front. Microbiol.* 6:707. doi: 10.3389/fmicb.2015.00707

Holtman, C. K., Pawlyk, A. C., Meadow, N. D., and Pettigrew, D. W. (2001). Reverse genetics of *Escherichia coli* glycerol kinase allosteric regulation and glucose control of glycerol utilization in vivo. *J. Bacteriol.* 183 (11), 3336–3344. doi: 10.1128/JB.183.11.3336–3344

Howard-Varona, C., Hargreaves, K. R., Abedon, S. T., and Sullivan, M. B. (2017). Lysogeny in nature: mechanisms, impact and ecology of temperate phages. *ISME J.* 11 (7), 1511–1520. doi: 10.1038/ismej.2017.16

Huang, H. H., Chen, W. C., Lin, C. W., Lin, Y. T., Ning, H. C., Chang, Y. C., et al. (2017). Relationship of the CreBC two-component regulatory system and inner membrane protein CreD with swimming motility in *Stenotrophomonas maltophilia*. *PLoS One* 12 (4), e0174704. doi: 10.1371/journal.pone.0174704

Jensen, R. V., Depasquale, S. M., Harbolick, E. A., Hong, T., Kernell, A. L., Kruchko, D. H., et al. (2013). Complete genome sequence of prepandemic *Vibrio parahaemolyticus* BB22OP. *Genome Announc.* 1 (1), e00002–e00012. doi: 10.1128/genomeA.00002-12

Jiang, Y., Chu, Y., Xie, G., Li, F., Wang, L., Huang, J., et al. (2019). Antimicrobial resistance, virulence and genetic relationship of *Vibrio parahaemolyticus* in seafood from coasts of Bohai Sea and Yellow Sea, China. *Int. J. Food. Microbiol.* 290, 116–124. doi: 10.1016/j.ijfoodmicro.2018.10.005

Joseph, S. S., and Plano, G. V. (2013). The SycN/YscB chaperone-binding domain of YopN is required for the calcium-dependent regulation of Yop secretion by *Yersinia* pestis. *Front. Cell. Infect. Microbiol.* 3, 1. doi: 10.3389/fcimb.2013.00001

Kalburge, S. S., Polson, S. W., Boyd Crotty, K., Katz, L., Turnsek, M., Tarr, C. L., et al. (2014). Complete genome sequence of *Vibrio parahaemolyticus* environmental strain UCM-V493. *Genome Announc.* 2 (2), e00159–e00114. doi: 10.1128/genomeA.00159-14

Kim, Y. K., and McCarter, L. L. (2000). Analysis of the polar flagellar gene system of *Vibrio parahaemolyticus*. *J. Bacteriol.* 182 (13), 3693–3704. doi: 10.1128/jb.182.13.3693-3704.2000

Kim, H. W., Hong, Y. J., Jo, J.II, Ha, S. D., Kim, S. H., Lee, H. J., et al. (2017). Raw ready-to-eat seafood safety: microbiological quality of the various seafood species available in fishery, hyper and online markets. *Lett. Appl. Microbiol.* 64 (1), 27–34. doi: 10.1111/lam.12688

Kim, G., Azmi, L., Jang, S., Jung, T., Hebert, H., Roe, A. J., et al. (2019). Aldehyde-alcohol dehydrogenase forms a high-order spirosome architecture critical for its activity. *Nat. Commun.* 10 (1), 4527. doi: 10.1038/s41467-019-12427-8

Lan, S. F., Huang, C. H., Chang, C. H., Liao, W. C., Lin, I. H., Jian, W. N., et al. (2009). Characterization of a new plasmid-like prophage in a pandemic *Vibrio parahaemolyticus* O3:K6 strain. *Appl. Environ. Microbiol.* 75 (9), 2659–2667. doi: 10.1128/aem.02483-08

Li, W., Wen, L., Li, C., Chen, R., Ye, Z., Zhao, J., et al. (2016). Contribution of the outer membrane protein OmpW in *Escherichia coli* to complement resistance from binding to factor H. *Microb. Pathog.* 98, 57–62. doi: 10.1016/j.micpath.2016.06.024

Li, L., Meng, H., Gu, D., Li, Y., and Jia, M. (2019). Molecular mechanisms of *Vibrio parahaemolyticus* pathogenesis. *Microbiol. Res.* 222, 43–51. doi: 10.1016/j.micres.2019.03.003

Loyola, D. E., Navarro, C., Uribe, P., Garcia, K., Mella, C., Diaz, D., et al. (2015). Genome diversification within a clonal population of pandemic *Vibrio parahaemolyticus* seems to depend on the life circumstances of each individual bacteria. *BMC Genomics* 16, 176. doi: 10.1186/s12864-015-1385-8

Matsuda, S., Okada, R., Tandhavanant, S., Hiyoshi, H., Gotoh, K., Iida, T., et al. (2019). Export of a *Vibrio parahaemolyticus* toxin by the Sec and type III secretion machineries in tandem. *Nat. Microbiol.* 4 (5), 781–788. doi: 10.1038/s41564-019-0368-y

Morgelin, M. (2017). Negative Staining and transmission electron microscopy of bacterial surface structures. *Methods Mol. Biol.* 1535, 211–217. doi: 10.1007/978-1-4939-6673-8_13

O'Boyle, N., and Boyd, A. (2013). Manipulation of intestinal epithelial cell function by the cell contact-dependent type III secretion systems of *Vibrio parahaemolyticus*. *Front. Cell. Infect. Microbiol.* 3:114. doi: 10.3389/fcimb.2013.00114

Pelletier, C., Bouley, C., Cayuela, C., Bouttier, S., Bourlioux, P., and Bellon-Fontaine, M. N. (1997). Cell surface characteristics of *Lactobacillus casei* subsp. casei, *Lactobacillus paracasei* subsp. paracasei, and *Lactobacillus rhamnosus* strains. *Appl. Environ. Microbiol.* 63 (5), 1725–1731. doi: 10.1128/AEM.63.5.1725-1731.1997

Penades, J. R., Chen, J., Quiles-Puchalt, N., Carpena, N., and Novick, R. P. (2015). Bacteriophage-mediated spread of bacterial virulence genes. *Curr. Opin. Microbiol.* 23, 171–178. doi: 10.1016/j.mib.2014.11.019

Plano, G. V., and Schesser, K. (2013). The *Yersinia* pestis type III secretion system: expression, assembly and role in the evasion of host defenses. *Immunol. Res.* 57 (1-3), 237–245. doi: 10.1007/s12026-013-8454-3

Postma, P., Lengeler, J., and Jacobson, G. (1993). Phosphoenolpyruvate: carbohydrate phosphotransferase systems of bacteria. *Microbiol. Rev.* 57 (3), 543–594. doi: 10.1128/MMBR.57.3.543-594.1993

Raghunath, P. (2014). Roles of thermostable direct hemolysin (TDH) and TDH-related hemolysin (TRH) in *Vibrioparahaemolyticus*. *Front. Microbiol.* 5:805. doi: 10.3389/fmicb.2014.00805

Ramos, J. L., Martínez-Bueno, M., Molina-Henares, A. J., Terán, W., Watanabe, K., Zhang, X., et al. (2005). The TetR family of transcriptional repressors. *Microbiol. Mol. Biol. Rev.* 69 (2), 326–356. doi: 10.1128/MMBR.69.2.326-356.2005

Ramu, T., Prasad, M. E., Connors, E., Mishra, A., Thomassin, J. L., Leblanc, J., et al. (2013). A novel C-terminal region within the multicargo type III secretion chaperone CesT contributes to effector secretion. *J. Bacteriol.* 195 (4), 740–756. doi: 10.1128/jb.01967-12

Rkenes, T., Lamark, T., and Strøm, A. R. (1996). DNA-binding properties of the BetI repressor protein of *Escherichia coli*: The inducer choline stimulates BetI-DNA complex formation. *J. Bacteriol.* 178 (6), 1663–1670. doi: 10.1128/jb.178.6.1663-1670.1996

Rodionov, D. A., Leyn, S. A., Li, X., and Rodionova, I. A. (2017). A novel transcriptional regulator related to thiamine phosphate synthase controls thiamine metabolism genes in archaea. *J. Bacteriol.* 199 (4), e00743–e00716. doi: 10.1128/jb.00743-16

Song, Y., Yu, P., Li, B., Pan, Y., Zhang, X., Cong, J., et al. (2013). The mosaic accessory gene structures of the SXT/R391-like integrative and conjugative elements derived from *Vibrio* spp. isolated from aquatic products and environment in the Yangtze River estuary, China. *BMC Microbiol.* 13:214. doi: 10.1186/1471-2180-13-214

Sun, X., Liu, T., Peng, X., and Chen, L. (2014). Insights into *Vibrio parahaemolyticus* CHN25 response to artificial gastric fluid stress by transcriptomic analysis. *Int. J. Mol. Sci.* 15 (12), 22539–22562. doi: 10.3390/ijms151222539

Takekawa, N., Isumi, M., Terashima, H., Zhu, S., Nishino, Y., Sakuma, M., et al. (2019). Structure of *Vibrio* FliL, a new stomatin-like protein that assists the bacterial flagellar motor function. *MBio* 10 (2), e00292–e00219. doi: 10.1128/mBio.00292-19

Tan, L., Zhao, F., Han, Q., Zhao, A., Malakar, P. K., Liu, H., et al. (2018). High correlation between structure development and chemical variation during biofilm formation by *Vibrio parahaemolyticus*. *Front. Microbiol.* 9:1881. doi: 10.3389/fmicb.2018.01881

Tsai, C. C., Hung, Y. H., and Chou, L. C. (2018). Evaluation of lactic acid bacteria on the inhibition of *Vibrio parahaemolyticus* infection and its application to food systems. *Molecules* 23 (5):1238. doi: 10.3390/molecules23051238

Voss, D., and Montville, T. J. (2014). 1,6-Diphenyl-1,3,5-hexatrine as a reporter of inner spore membrane fluidity in *Bacillus subtilis* and *Alicyclobacillus acidoterrestris*. *J. Microbiol. Methods* 96, 101–103. doi: 10.1016/j.mimet.2013.11.009

Wang, L., Ling, Y., Jiang, H., Qiu, Y., Qiu, J., Chen, H., et al. (2013). AphA is required for biofilm formation, motility, and virulence in pandemic *Vibrio parahaemolyticus*. *Int. J. Food. Microbiol.* 160 (3), 245–251. doi: 10.1016/j.ijfoodmicro.2012.11.004

Whiteley, M., Diggle, S. P., and Greenberg, E. P. (2017). Progress in and promise of bacterial quorum sensing research. *Nature* 551 (7680), 313–320. doi: 10.1038/nature24624

Wong, H. C., Wang, T. Y., Yang, C. W., Tang, C. T., Ying, C., Wang, C. H., et al. (2019). Characterization of a lytic vibriophage VP06 of *Vibrio parahaemolyticus*. *Res. Microbiol.* 170 (1), 13–23. doi: 10.1016/j.resmic.2018.07.003

Xu, F., Feng, X., Sui, X., Lin, H., and Han, Y. (2017). Inactivation mechanism of *Vibrio parahaemolyticus* via supercritical carbon dioxide treatment. *Food. Res. Int.* 100 (Pt 2), 282–288. doi: 10.1016/j.foodres.2017.08.038

Yang, A., Tang, W. S., Si, T., and Tang, J. X. (2017). Influence of physical effects on the swarming motility of *Pseudomonas aeruginosa*. *Biophys. J.* 112 (7), 1462–1471. doi: 10.1016/j.bpj.2017.02.019

Yildiz, F. H., and Visick, K. L. (2009). *Vibrio* biofilms: so much the same yet so different. *Trends Microbiol.* 17 (3), 109–118. doi: 10.1016/j.tim.2008.12.004

Zabala, B., Hammerl, J. A., Espejo, R. T., and Hertwig, S. (2009). The linear plasmid prophage Vp58.5 of *Vibrio parahaemolyticus is* closely related to the

integrating phage VHML and constitutes a new incompatibility group of telomere phages. *J. Virol.* 83 (18), 9313–9320. doi: 10.1128/jvi.00672-09

Zhu, C., Sun, B., Liu, T., Zheng, H., Gu, W., He, W., et al. (2017). Genomic and transcriptomic analyses reveal distinct biological functions for cold shock proteins (VpaCspA and VpaCspD) in *Vibrio parahaemolyticus* CHN25 during low-temperature survival. *BMC Genomics* 18 (1), 436. doi: 10.1186/s12864-017-3784-5

Zhu, Z., Yang, L., Yu, P., Wang, Y., Peng, X., and Chen, L. (2020). Comparative proteomics and secretomics revealed virulence and antibiotic resistance-associated factors in *Vibrio parahaemolyticus* recovered from commonly consumed aquatic products. *Front. Microbiol.* 11, 1453. doi: 10.3389/fmicb.2020.01453

Conflict of Interest: The authors declare that the research was conducted in the absence of any commercial or financial relationships that could be construed as a potential conflict of interest.

frontiers in Cellular and Infection Microbiology

ORIGINAL RESEARCH
published: 03 February 2021
doi: 10.3389/fcimb.2020.591751

cheA, *cheB*, *cheR*, *cheV*, and *cheY* Are Involved in Regulating the Adhesion of *Vibrio harveyi*

Xiaojin Xu[1,2,3,4,5*†], *Huiyao Li*[1,2,3†], *Xin Qi*[1,2,3], *Yunong Chen*[1,2,3], *Yingxue Qin*[1,2,3], *Jiang Zheng*[1,2,3,4] *and Xinglong Jiang*[1,2,3*]

[1] Fisheries College, Jimei University, Xiamen, China, [2] Engineering Research Centre of Eel Modern Industrial Technology, Ministry of Education, Xiamen, China, [3] Jimei University, Xiamen, China, [4] State Key Laboratory of Large Yellow Croaker Breeding, Ningde Fufa Fisheries Company Limited, Ningde, China, [5] Fujian Province Key Laboratory of Special Aquatic Formula Feed, Fujian Tianma Science and Technology Group Co., Ltd., Fuzhou, China

OPEN ACCESS

Edited by:
Wenxiang Sun,
The University of Utah, United States

Reviewed by:
Julia Van Kessel,
Indiana University Bloomington, United States
Evgeniya V. Nazarova,
Immunology Discovery, Genentech, United States

***Correspondence:**
Xiaojin Xu
xiaojinxu@jmu.edu.cn
Xinglong Jiang
xnlongjiang@jmu.edu.cn

†These authors have contributed equally to this work and share first authorship

Specialty section:
This article was submitted to Molecular Bacterial Pathogenesis, a section of the journal Frontiers in Cellular and Infection Microbiology

Received: 05 August 2020
Accepted: 01 December 2020
Published: 03 February 2021

Citation:
Xu X, Li H, Qi X, Chen Y, Qin Y, Zheng J and Jiang X (2021) cheA, cheB, cheR, cheV, and cheY Are Involved in Regulating the Adhesion of Vibrio harveyi. Front. Cell. Infect. Microbiol. 10:591751. doi: 10.3389/fcimb.2020.591751

Diseases caused by *Vibrio harveyi* lead to severe economic losses in the aquaculture industry. Adhesion is an important disease-causing factor observed in bacteria with chemotactic activity. In our study, we measured the adhesion of *V. harveyi* by subjecting the bacteria to stress using Cu^{2+}, Pb^{2+}, Hg^{2+}, and Zn^{2+}. The genes responsible for chemotaxis (*cheA*, *cheB*, *cheR*, *cheV*, and *cheY*), which are also crucial for adhesion, were identified and silenced *via* RNAi. We observed that a decrease in chemotactic gene expression reduced the ability of the organism to demonstrate adhesion, motility, chemotaxis, and biofilm formation. Upon comparing the *cheA*-RNAi bacteria to the wild-type strain, we observed that the transcriptome of *V. harveyi* was significantly altered. Additionally, the expression of key genes and the adhesion ability were affected by the pH (pH of 5, 6, 7, 8, and 9), salinity (NaCl at concentrations of 0.8, 1.5, 2.5, 3.5, or 4.5%), and temperature (4, 15, 28, 37, and 44°C) of the medium. Based on these results, the following conclusions were made: (1) The chemotactic genes *cheA*, *cheB*, *cheR*, *cheV*, and *cheY* may regulate the adhesion ability of *V. harveyi* by affecting bacterial motility, and participate in the regulation of adhesion at different temperatures, salinities, and pH values; (2) stable silencing of *cheA* could alter the transcriptional landscape of *V. harveyi* and regulate the expression of genes associated with its adhesion mechanisms.

Keywords: adhesion, chemotactic gene, environmental factors, RNAi, *Vibrio harveyi*

INTRODUCTION

Vibrio harveyi is a pathogen that affects marine organisms (Austin and Zhang, 2006); it has been reported to cause the death of cage-cultured Asian catfish (Tendencia, 2002). The frequency of bacterial diseases affecting marine organisms has been increasing, and *V. harveyi* infections could cause severe economic losses in the aquaculture industry. Adhesion is the first step in bacterial infection, in which pathogenic bacteria adhere to the intestines or injured skin of the host, causing infection (Chen et al., 2008). Thus, inhibition of this step has gained interest among researchers (Kirk et al., 2010; Liu et al., 2013).

Bacteria can perceive gradients of environmental stimuli, including pH, temperature, osmolality, and the concentration of various chemicals. Active bacteria will move toward a favorable living environment (Colin and Sourjik, 2017). Chemotactic behavior allows bacteria to determine their course of action quickly and strategically in complex environments, which is essential for the induction of biofilm-related infections and pathogenic invasion into the host (Xue, 2015; Guo M. et al., 2017). Bacterial chemotaxis is a tightly regulated process, in which chemotactic signals are detected by methyl-accepting chemotaxis proteins (MCPs). MCPs can link to histidine protein kinases encoded by the *cheA* gene with the help of an adaptor protein encoded by *cheW*. CheV is a chemotactic connexin that can replace or enhance the function of *cheW* (Wadhams and Armitage, 2004). *CheA* and *cheY* are important constituents of a two-component system (Stock et al., 2000), the presence of repellents in the environment can stimulate the *cheA*, phosphorylated histidine kinase (CheA-P) phosphorylates CheB and CheY. The phosphorylated response regulator (CheY-P) increases its attraction to the motor protein *fliM* due to conformational changes, and the combination of the two makes the bacterial flagella movement clockwise (also called tumbling) to change direction stay away from repellents. On the contrary, the inducer in the environment can inhibit the autophosphorylation of *cheA*, and the response regulator (*cheY*) cannot be phosphorylated. The bacterial flagella move counterclockwise (also called swim), thereby tending to inducer. On the other hand, CheB-P and CheR change the methylation state of the receptor (MCPs) at a slower rate: CheR methylates it and CheB-P demethylates it. This methylation-demethylation cycle restores the activity of the associated CheA (Hess et al., 1988; Borkovich et al., 1989; Roman et al., 1992; Sockett et al., 1992). In *Salmonella enterica* (Haiko and Westerlund-Wikström, 2013) and *V. alginolyticus* (Huang et al., 2017), studies have confirmed that bacterial adhesion is controlled by chemotaxis-related genes.

Bacterial adhesion is a very complex process, and the ability of bacteria to adhere can be significantly affected by environmental factors (Yan et al., 2007). Studies have shown that bacterial adhesion is affected by physical and chemical factors such as temperature, salinity, ion concentration, and pH (Pianetti et al., 2012). The pH value affects the thickness of the electric double layer on the surface of pathogenic bacteria, thereby affecting the adhesion of bacteria to the surface of the substrate (Gorden et al., 1981). Different concentrations of monovalent ions have an effect on the adhesion of *Vibrio alginolyticus*, and the concentration of Na^+ has the greatest effect on adhesion (Kogure et al., 1998). Na^+ is the power source of *V. alginolyticus* polar flagella, thereby affecting its adhesion (Atsumi et al., 1992).

The process of adhesion of bacteria is connected to the movement of bacteria in response to a chemical stimulus. Chemical gradients are sensed through multiple transmembrane receptors, called methylaccepting chemotaxis proteins (MCPs), which vary in the molecules that they detect. These receptors may bind attractants or repellents directly or indirectly through interaction with proteins of the periplasmic space. The signals from these receptors are transmitted across the plasma membrane into the cytosol, where the two-component system is activated. The two-component system then induces tumbling by interacting with the flagellar switch protein FliM, inducing a change from counterclockwise to clockwise rotation of the flagellum. In the study of *V. alginolyticus*, the expression levels of "Bacterial chemotaxis" genes was consistent with the extent their adhesion decreased after the metal ion stress treatment (Kong et al., 2015). Subsequent studies also showed that chemotactic genes could affect the adhesion of *V. alginolyticus* (Wang et al., 2015).

Chemotactic genes are present in some bacteria, including *V. harveyi*. However, their roles in the adhesion of pathogenic bacteria still need to be identified. The aims of this research were as follows: (1) to identify chemotactic genes, which could potentially be associated with adhesion, (2) to determine the relationship between *V. harveyi* adhesion and *cheA*, *cheB*, *cheR*, *cheV*, and *cheY* activity, (3) to determine whether these genes participate in regulating adhesion under natural conditions, and (4) to detect the changes in the transcriptome of *V. harveyi* after silencing *cheA via* RNA interference (RNAi).

MATERIALS AND METHODS

Bacterial Strain and Culture Conditions

V. harveyi (VH6110) was isolated from diseased *Larimichthys crocea*. The strain was identified to be pathogenic based on the regression of infection and was confirmed as *V. harveyi* by biochemical identification and 16S rRNA sequencing (Xu et al., 2010). The reference genome sequences were obtained through *de novo* assembly reference to near-source species. *V. harveyi* was cultivated in lysogeny broth at 28°C (LB; pH = 7, 2% NaCl, shaking at 200 rpm). *Escherichia coli* SM10 was purchased from TransGen Biotech (Beijing, China) and cultivated in LB broth or agar at 37°C. The pathogens and plasmids used in the study are presented in **Supplementary Table 1**.

To identify the chemotactic genes potentially associated with *V. harveyi* adhesion, the bacteria were subjected to stress with different concentrations of metal ions (Cu^{2+}, Pb^{2+}, Hg^{2+}, or Zn^{2+}) (Kong et al., 2015). *V. harveyi* grown in LB broth (pH = 7) was used as the control. Quantitative real-time polymerase chain reaction (qRT-PCR) was used to confirm gene expression in the adhesion-defective strain. All treatments were carried out using three independent replicates.

Stable Gene Silencing

The methods used for stably silencing *V. harveyi* genes and treating *E. coli* SM10 have been reported previously (Darsigny et al., 2010; Huang et al., 2017), in which, pACYC184 vectors were *digested* using *Bam*HI and *Sph*I. Short hairpin (sh) RNA was obtained from Generay Biotech Co., Ltd. (Shanghai, China). The pACYC184 vectors were ligated using T4 DNA ligase (TaKaRa, Shiga, Japan). Recombinant plasmids were transformed into *E. coli* SM10 by heat-shock. Conjugation experiments were carried out by transferring the plasmids from *E. coli* SM10 to *V. harveyi*. An empty pACYC184 plasmid was transformed into *V. harveyi* as the control. LB medium containing chloramphenicol (34 μg/ml) and shRNA

was used to select stably silenced *V. harveyi* cells (**Supplementary Table 2**).

RNA Isolation

Total RNA was extracted using the TRIzol reagent (TransGen Biotech, Beijing, China). cDNA was synthesized using the TransScript® ALL-in-One First-Strand cDNA Synthesis SuperMix and qPCR Assay Kit (TransGen Biotech, Beijing, China). The experiment was performed according to the manufacturer's instructions.

qRT-PCR

Gene silencing was confirmed by qRT-PCR (QuantStudio 6 Flex, Grand Island, NY, USA) using the SYBR Green qPCR Mix (Dongsheng Biotech, Guangdong, China). 16rRNA was used as the reference gene. All reactions were carried out in triplicate, and quantification was performed using the $2^{-\Delta\Delta CT}$ method (Cikos et al., 2007). Primer sequences are listed in **Supplementary Table 3**.

Mucus Preparation

Experiments on *L. crocea* were conducted in accordance with the specifications stated in the "Guide for the Care and Use of Laboratory Animals" published by the National Institutes of Health. Healthy *L. crocea* specimens were obtained from Fujian Fuding Seagull Fishing Food Co., Ltd. (Fujian, China). Mucus from the skin was collected according to a previously reported method (Huang et al., 2015). Briefly, *L. crocea* was washed with sterile PBS and the mucus from the skin was collected using a soft rubber spatula. Articulate material was removed by centrifuging twice (20,000 × *g*, 4°C, 30 min). The supernatant was passed through filters with pore sizes of 0.45 and 0.22 μm. The protein concentration was adjusted to 1 mg protein/ml using sterile PBS (Bradford, 1976).

Adhesion Assay

The experiment on bacterial adhesion was performed as described previously (Huang et al., 2015). Briefly, 20 μl of mucus from *L. crocea* was applied to a glass slide (22 mm × 22 mm) and fixed with methanol at 28°C for 20 min. Then, 200 μl of the suspension of *V. harveyi* adjusted to an OD_{600} of 0.3 (concentration of 3.0×10^8 CFU/ml) was applied evenly on the mucus-coated glass slides. The slides were incubated at 28°C for 2 h and washed thrice with PBS. The *V. harveyi* cells were fixed with 4% methanol for 30 min and stained with 1% crystal violet for 3 min. The slides were examined under a light microscope at *1,000*× magnification. The number of *V. harveyi* cells was counted in 20 sections. The experiment was carried out using *positive controls with V. harveyi only* and *negative controls* with sterile PBS.

In Vitro Biofilm Assay

A 12 h-old culture of V. harveyi was resuspended in sterile PBS, and its OD_{600} was adjusted to 0.2 (2.0×10^8 CFU/ml) using sterile LB. Then, 200 μl of this suspension was added to the wells of a 96-well plate. Sterile LB was used in the blank control group. The plates were incubated at 28°C for 24 h. The plate contents were shaken and washed thrice using 200 μl of sterile PBS to remove the non-adherent bacteria. The microtiter plates were dried at 60°C for 10 min, and 125 μl of a 0.1% crystal violet solution (Merck KGaA, Darmstadt, Germany) was added to each well; the plates were then incubated for 10 min. The microtiter plates were washed thrice using sterile PBS. Then, the biofilms were solubilized using 33% acetic acid, and OD_{590} was measured using a microtiter plate reader (Bio-Rad, Hercules, CA, USA). Each experiment was performed in *triplicate*.

Soft Agar Plate Motility Assay

Bacterial motility was determined using a *soft agar* plate *according to* a method described previously (Luo et al., 2016). The OD_{600} of bacterial cultures grown overnight in LB was adjusted to 0.3, and plates of LB agar (0.3% agar) were seeded using 1 μl of the culture suspension. After incubating the *plates* at 28°C for 24 h, the diameters of the bacterial colonies were measured. Each experiment was performed in triplicate.

Capillary Assay

Bacterial chemotaxis was tested using a method reported previously (Huang et al., 2017). A capillary tube with an *inside diameter* of *0.1* mm *was filled with* mucus, leaving one end open. Then, the tube was filled with 2.5 ml of bacterial suspension (1.0×10^9 CFU/ml), the open end of the capillary is placed in the bacterial solution. After incubation for 1 h at 28°C, the LB agar plates were inoculated with the contents of the tube to accurately determine the number of bacteria present in the capillary tube. Bacterial chemotaxis was determined by comparing the number of bacteria in the tube with that of the negative control, which consisted of a capillary filled with mucus-free buffer. Samples were tested in triplicate in each group.

Transcriptomic Analysis

Library Preparation and Sequencing

Total RNA was isolated and purified from the bacterial solution (sample collected in triplicate), and the concentration was measured using the Nanodrop 2000. The RNA integrity number (RIN) was measured using an Agilent 2100 Bioanalyzer System. The TruSeq™ RNA sample preparation Kit (Illumina, San Diego, CA, USA) was used to construct the rRNA-depleted and RNA-fragmented libraries. Here, dUTP was used for construction of the second strand of cDNA, which resulted in the presence of A/U/C/G in the new strand. End repair and *adapter ligation led to the* adenylation of the 3' ends. Then, the UNG enzyme was used to digest the second strand of cDNA; thus, the first strand only was included in the libraries. Transcriptome sequencing (2 × 150 bp, paired-ended) was performed using an Illumina Hiseq from Majorbio Biotech Co., Ltd. (Shanghai, China).

Data Analysis

The original sequencing data was filtered to obtain clean data using Sickle and SeqPrep. Based on the method of Burrows-Wheeler, high-quality sequence data were compared to those of the reference genome obtained from NCBI (NZ_CP009467.1). EdgeR (http://www.bioconductor.org/packages/2.12/bioc/html/

edgeR.html) was used to detect differentially expressed genes (DEGs) between the two samples with significant false discovery rate (FDR) P value < 0.05 and $|\log2FC| \geq 1$, where FC = fold change.

The H-cluster method was used for cluster analysis to determine the expression patterns of DEGs. All DEGs and gene ontology (GO) terms were mapped to a reference database (http://www.geneontology.org/) to indicate gene function in the samples. Enrichment analysis of DEGs in the Kyoto Encyclopedia of Genes and Genomes (KEGG) pathway was conducted using the KOBAS software, and Fisher's exact test was used for calculations. The Benjamini-Hochberg Procedure (FDR) was used to analyze for KEGG pathway *enrichment*. $P < 0.05$ was considered statistically significant. The data of significantly expressed genes was validated using qRT-PCR. Genes and primer sequences are listed in **Supplementary Table 4**.

Environmental Impact on Adhesion Ability

To investigate the effects of different temperatures, *V. harveyi* was cultured in LB broth (supplemented with 2% NaCl, pH = 7) at 4, 15, 28, 37, and 44°C. To investigate the effects of different pH levels, *V. harveyi* was cultured in LB broth (supplemented with 2% NaCl) adjusted to a pH of 5, 6, 7, 8, or 9 at 28°C. To investigate the effects of different salinities, *V. harveyi* was cultured in LB broth (pH = 7) with 0.8, 1.5, 2.5, 3.5, or 4.5% NaCl at 28°C. Each treatment consisted of six independent replicates. After harvesting and re-suspending, the adhesion ability of *V. harveyi* was measured, RNA was extracted from the bacteria, and reverse transcription were performed, expression levels of *cheA*, *cheB*, *cheR*, *cheV*, and *cheY* were determined using qRT-PCR according to the method described in *qRT-PCR*.

Data Processing

The data are summarized as the mean ± standard deviation. The data was analyzed by *one-way ANOVA* using 17.0 Statistics (Chicago, IL, USA). $P < 0.05$ was considered statistically significant.

RESULTS

Adhesion and Gene Expression of *Vibrio harveyi* Under Stress

We observed that the ability of *V. harveyi* to adhere to crocea mucus changed significantly after the bacteria were subjected to stress, and most of the cases were decreased (**Figure 1**, $P < 0.01$). In addition, the results of qRT- PCR showed that chemotactic genes were very sensitive to metal ions, most of the times, treatment with Cu^{2+}, Hg^{2+}, Zn^{2+}, and Pb^{2+} significantly reduced the expression of *cheA*, *cheB*, *cheR*, *cheV*, and *cheY*. Hg^{2+} had the greatest effect on adhesion and gene expression. In particular, the expression of *chaA* gene was significantly upregulated most frequently after ion stress (**Figure 2**, $P < 0.01$). The adhesion ability of *V. harveyi* may be regulated by chemotactic genes, but the regulation mechanism is complex.

Effects of Stable Gene Silencing

The correlation between genes and adhesion was confirmed through RNAi and adhesion experiments. Expression of the stably silenced *cheA*, *cheB*, *cheR*, *cheV*, and *cheY* genes decreased by 2.1-, 10.4-, 13.4-, 2.2, and 2.3-fold, respectively, compared to the control gene (**Figure 3**, $P < 0.01$). The ability of the clones with silenced genes to adhere to mucus was significantly reduced. The number of adherent *V. harveyi* colonies in the control group was 1,081 ± 112 cells/field. The

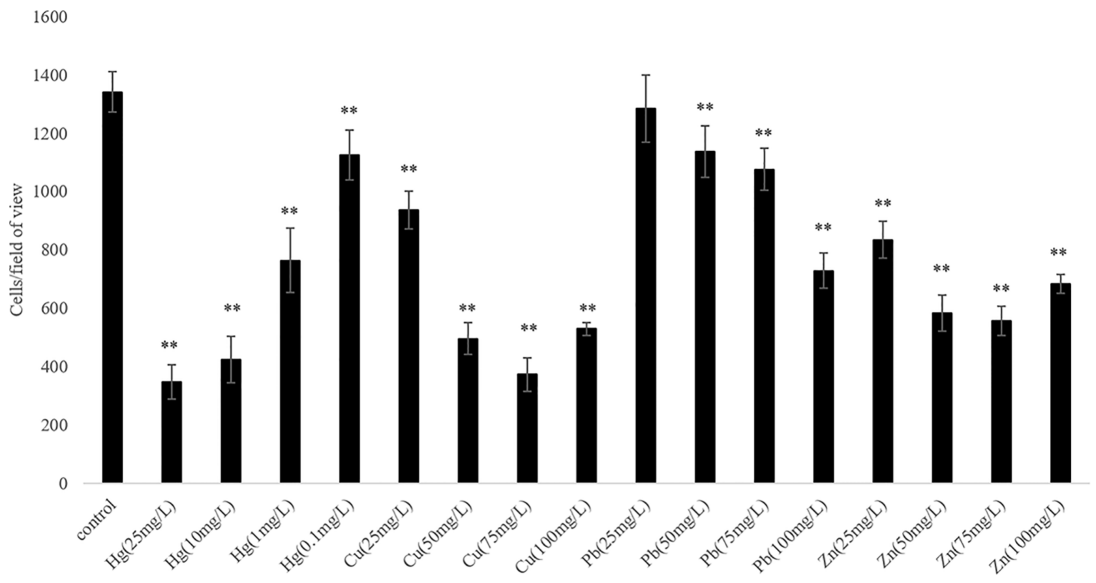

FIGURE 1 | The adhesion abilities of the wild-type and stressed *Vibrio harveyi* cells. Data are presented as the mean ± SD; experiments were performed on three independent replicates per group. $^{**}P < 0.01$ compared to the control.

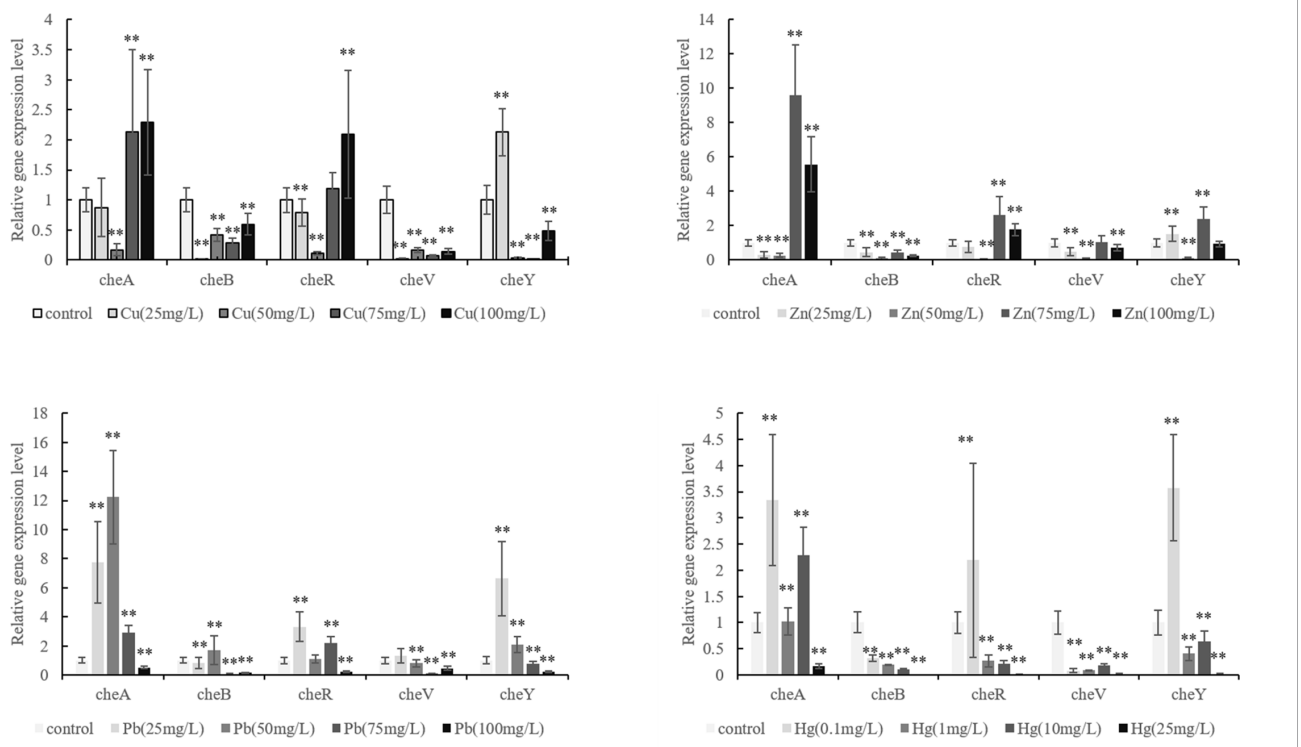

FIGURE 2 | Expression of *cheA*, *cheB*, *cheR*, *cheV*, and *cheY* in the control and stressed *Vibrio harveyi* cells confirmed *via* qRT-PCR. Data are presented as the mean ± SD; experiments were performed on three independent replicates per group. $^{**}P < 0.01$ compared the control.

number of adherent *V. harveyi* colonies in the *cheA*-, *cheB*-, *cheR*-, *cheV*-, and *cheY*-RNAi groups was 309 ± 38, 512 ± 50, 354 ± 26, 460 ± 32, and 344 ± 35 cells/field, respectively (**Figure 4**, $P < 0.05$). These results suggest that bacterial adhesion could be reduced by stably silencing *cheA*, *cheB*, *cheR*, *cheV*, and *cheY*.

A comparison between the abilities of the control *V. harveyi* and the stably silenced strains to form bacterial biofilms is presented in **Figure 5**. Compared to the control strain, the strains silenced with *cheA*-, *cheB*-, *cheR*-, and *cheV*-RNAi demonstrated an increased ability to form biofilms after 24-h incubation. This phenomenon was not observed in *cheY*-RNAi strains. The *cheY* gene silenced

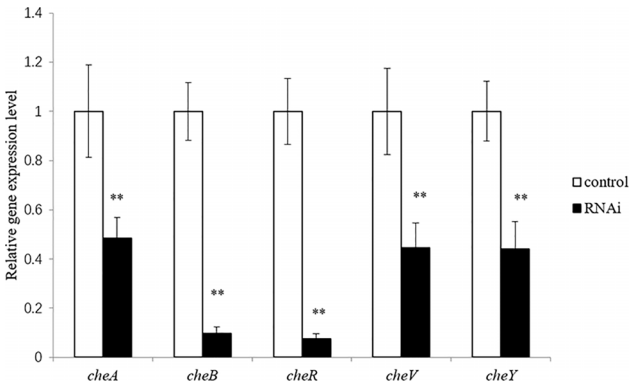

FIGURE 3 | Expression of *cheA*, *cheB*, *cheR*, *cheV*, and *cheY* in the control and RNAi-silenced *Vibrio harveyi* cells confirmed *via* qRT-PCR. Data are presented as the mean ± SD; experiments were performed on three independent replicates per group. $^{**}P < 0.01$ compared to the control.

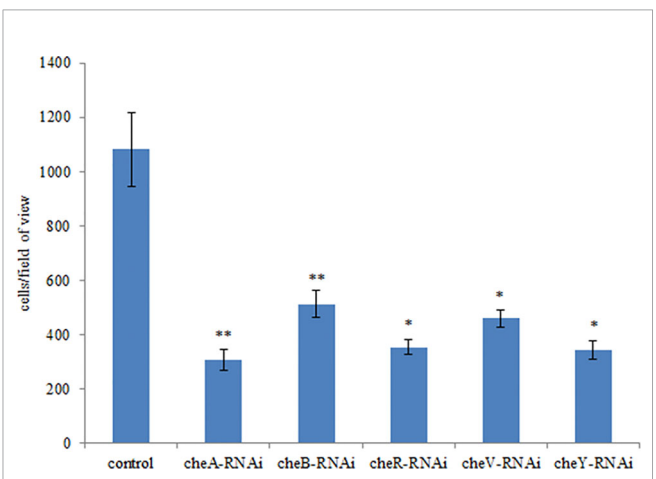

FIGURE 4 | Adhesion abilities of the control and stably silenced *Vibrio harveyi* cells. Data are presented as the mean ± SD; experiments were performed on three independent replicates per group. $^{**}P < 0.01$, $^{*}P < 0.05$ compared to the control.

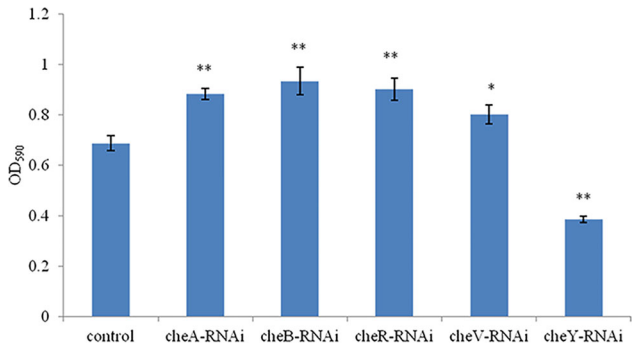

FIGURE 5 | The ability of the control and stably silenced *Vibrio harveyi* cells to form biofilms in lysogeny broth (LB) medium at 28°C. Data are presented as the mean ± SD; experiments were performed on three independent replicates per group. $^{**}P < 0.01$, $^{*}P < 0.05$ compared to the control.

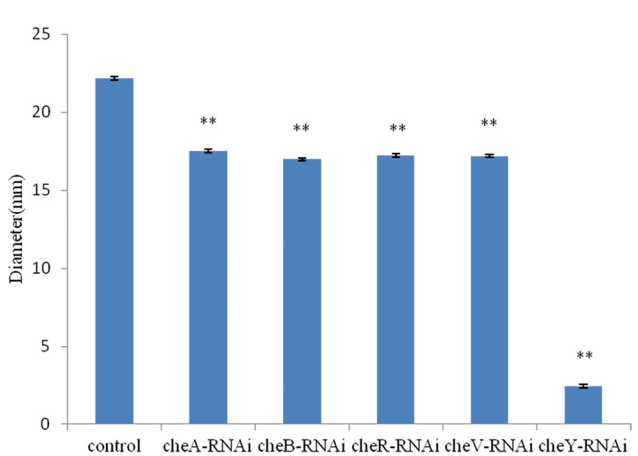

FIGURE 6 | Motility of *Vibrio harveyi* on soft agar plates. Data are presented as the mean ± SD; experiments were performed on three independent replicates per group. $^{**}P < 0.01$ compared to the control.

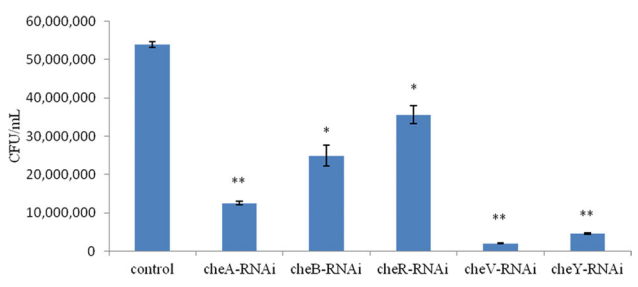

FIGURE 7 | Chemotactic ability of stably silenced *Vibrio harveyi* strains and the control to move toward the mucus. Data are presented as the mean ± SD (n = 3). $^{**}P < 0.01$, $^{*}P < 0.05$ compared to the control.

V. harveyi showed a reduced ability to form biofilms, this phenomenon needs further explanation.

The bacterial motility of stably silenced strains was significantly reduced, and the *cheY*-RNAi bacteria was the least motile (**Figure 6**). Typical images of the spreading of stably silenced *V. harveyi* strains and control were showed in **Supplementary Figure 1**. Interestingly, we found that *cheY* gene-silencing strains always show more special phenomena than other silent strains.

We observed that the extent of chemotaxis toward the skin mucus of *L. crocea* was higher in the control *V. harveyi*. Stable silencing of the genes significantly reduced the chemotactic ability of the bacteria. The chemotactic ability decreased by 4.2-fold (*cheA*-RNAi), 2.1-fold (*cheB*-RNAi), 1.5-fold (*cheR*-RNAi), 26.7-fold (*cheV*-RNAi), and 11.7-fold (*cheY*-RNAi), compared to the control *V. harveyi* strain (**Figure 7**, $P < 0.05$). The *cheY* gene silenced strain did not show the lowest chemotaxis ability, but the *cheV* silenced strain. The biofilm formation ability, motility, and chemotaxis of wild *V. harveyi* strains under stress by Cu^{2+} (50mg/L) and Zn^{2+} (50mg/L) were showed a certain degree of reduction, proved that these assays were working properly and with expected dynamic ranges (**Supplementary Figure 2**).

The *cheA* gene is located at the core of the bacterial chemotactic system, and *cheA* gene silenced strains show the lowest adhesion ability, thus, RNA sequencing libraries were constructed using the control *V. harveyi* and *cheA*-RNAi strains. Quality control on raw Illumina reads provided high-quality reads, which were mapped to the *V. harveyi* reference genome. The mapping rate was 89.63 and 89.73% for the control *V. harveyi* and *cheA*-RNAi strains, respectively. EdgeR was used to calculate the DEGs between the two samples, and 5,348 genes were identified from the *cheA*-RNAi strains. Compared to the control, 134 genes were significantly differentially expressed in the *cheA*-RNAi cells. There were 45 downregulated and 89 upregulated genes (**Figure 8**).

The detected differentially expressed genes of *cheA*-RNAi strains were annotated with GO function to clarify gene function, among which 89 significantly upregulated genes were mapped to 27 GO terms and 45 significantly downregulated genes were mapped to 20 GO terms (**Supplementary Figure 3**). These significantly upregulated genes are mainly involved in functions such as biological regulation, cellular processes, metabolic processes, regulation of biological processes, formation of macromolecular complexes, binding, catalytic activities, localization, and establishment of localization.

According to the KEGG database, DEGs in *V. harveyi* were mapped to 62 KEGG pathways. The largest number of pathways mapped included those for the "biosynthesis of amino acids," "metabolic pathways," "biosynthesis of secondary metabolites," "two-component system," "bacterial secretion system," and "ABC transporters," among others. Among all the KEGG pathways, "biofilm formation-*Vibrio cholerae*," "ABC transporters," "bacterial secretion system," "oxidative phosphorylation," and "quorum sensing" were associated with bacterial adhesion (Kolenbrander et al., 1998; Watnick and Kolter, 1999;

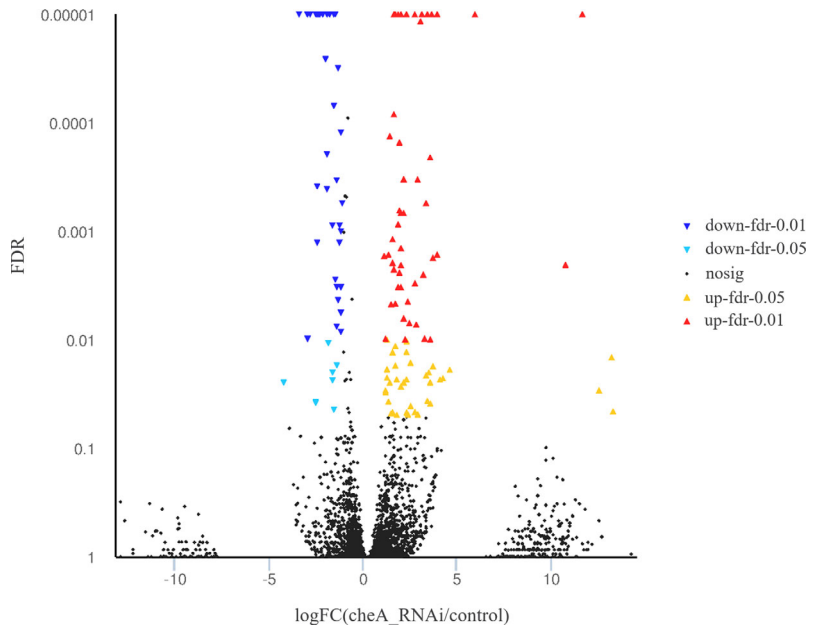

FIGURE 8 | Volcano plot of all genes. X and y axes represent the fold change values of the *cheA*-RNAi strain/control strain and statistical test value [false discovery rate (FDR)], respectively. Higher values represent more significant differences. Each dot represents one gene. Red and blue dots indicate significantly upregulated and downregulated genes, respectively. Black dots represent genes with expression changes that are not significant.

Paola et al., 2003; Koutsoudis et al., 2006; Guo L. et al., 2017). Upon analyzing the expression of the DEGs involved in these pathways, we determined that the expression of many of the genes in these pathways was significantly upregulated in *cheA*-RNAi cells (**Figure 9**). The relationships between genes and KEGG pathways are presented in **Figure 10**. We used qRT-PCR to experimentally confirm DEG expression changes and validate the RNA-seq results (**Supplementary Figure 4**). qRT-PCR yielded similar expression patterns, which supports the reliability and accuracy of the RNA-seq data.

Effects of Different Environmental Conditions

Many pathogenic bacteria can induce an adaptable response to environmental stimuli, so studying the influence of environmental factors on the gene expression will help to understand the molecular mechanism of the adhesion of *V. harveyi* in the environment. The adhesion ability of *V. harveyi* under different environmental conditions is presented in **Figure 11**. The adhesion of *V. harveyi* to mucus was found to be stronger under acidic and neutral environments than under alkaline conditions (**Figure 11A**). Moreover, the adhesion of *V. harveyi* was reduced at both high and low temperatures (**Figure 11B**). The adhesion ability of *V. harveyi* also was reduced under conditions of high salinity; however, no significant difference was observed with 0.8, 1.5, and 2.5% salinity (**Figure 11C**). The environmental conditions significantly affected the expression of all five genes. The expression of *cheA* and *cheR* increased significantly under acidic and alkaline conditions, whereas the expression of the other three genes was the highest at pH = 7 (**Supplementary Figure 5**). Gene expression decreased at low temperatures, whereas *cheV* expression increased at 37 and 44°C and *cheA* expression increased at 44°C. *cheR* expression was the most stable over the different temperature conditions (**Supplementary Figure 6**). The lowest expression of *cheA*, *cheB*, *cheR*, *cheV*, and *cheY* was observed under 3.5% salinity (**Supplementary Figure 7**). These data indicate that *cheA*, *cheB*, *cheR*, *cheV*, and *cheY* may participate in regulation of adhesion in the natural environment.

DISCUSSION

V. harveyi is an important pathogen (Yang and Defoirdt, 2015), and studies on *V. harveyi* have mainly focused on quorum sensing (Yang and Defoirdt, 2015; Van Kessel et al., 2018; McRose et al., 2018). Bacterial adhesion is a virulence factor and leads to infection through the attachment of bacteria to the surfaces of host membranes (Hamed et al., 2018). Understanding the mucus adhesion mechanisms of pathogens will aid in the prevention of bacterial diseases. Bacterial adhesion is regulated by known genes, such as *CdiA* gene, flagellum genes (*flrA*, *flrB*, and *flrC*) and global regulator RpoN and GacS, which have been reported in *E. coli* (Ruhe et al., 2015), *V. alginolyticus* (Luo et al., 2016), and *Pseudomonas aeruginosa* (Duque et al., 2013). However, it has not been reported in *V. harveyi*. The detailed adhesion mechanisms have not yet been fully elucidated.

Using RNA-seq, Huang et al. (2017) and Kong et al. (2015) confirmed that a relationship exists between adhesion and the

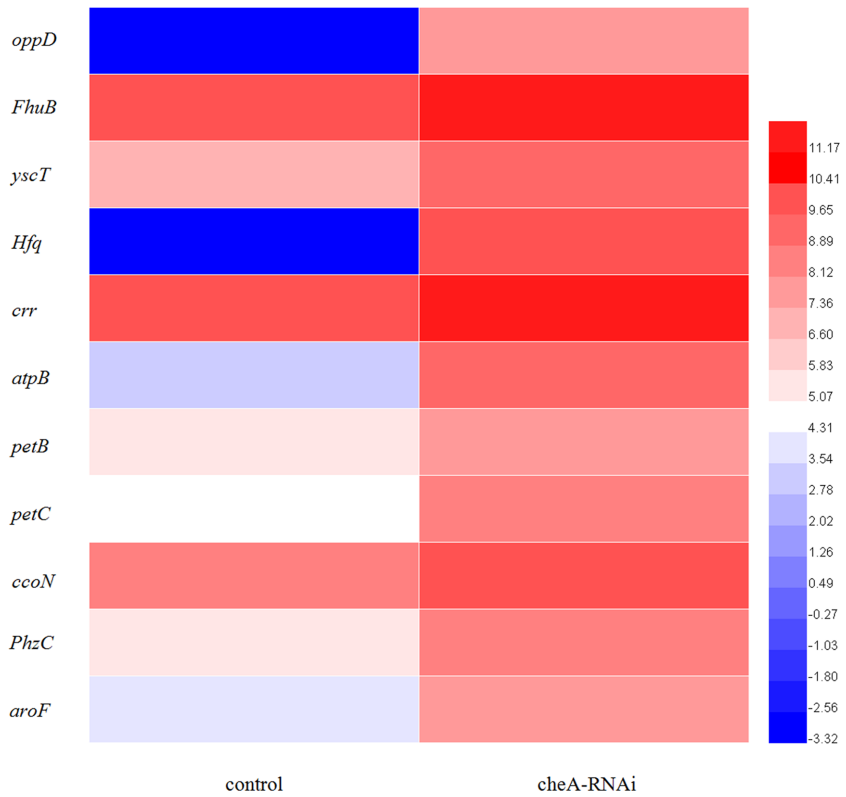

FIGURE 9 | Heat map of the DEGs involved in adhesion-related pathways (adjusted FDR < 0.05; |log2FC| ≥ 1; three replicates). Values represent log2-fold change. Colors of the log-transformed transcripts represent the mean FPKM values. Blue and red indicate decreased and increased expression, respectively.

bacterial chemotaxis pathway. In our study, the adhesion ability of *V. harveyi* was significantly decreased upon treatment with Cu^{2+}, Pb^{2+}, Hg^{2+}, and Zn^{2+}. Additionally, results of qRT-PCR demonstrated that the five genes responsible for chemotactic activity (*cheA*, *cheB*, *cheR*, *cheV*, and *cheY*) had been significantly changed in adhesion-deficient strains. Bacterial adhesion of *V. harveyi* was reduced upon RNAi-mediated gene silencing (**Figure 4**), thus indicating that *cheA*, *cheB*, *cheR*, *cheV*, and *cheY* may play important roles in this process.

We observed that the chemotaxis and motility of *cheA*-, *cheB*-, *cheR*-, *cheV*-, and *cheY*-RNAi cells had significantly decreased. Chemotaxis is the activity of bacteria that involves movement away from the surface of the zooplankton toward the mucus; however, it is not directly related to adhesion (Bordas et al., 1998). The chemotactic system plays a vital role in inducing motility (Burkart et al., 1998). The chemotaxis system integrates the signals from external and internal sensors through a signal transduction cascade consisting of MCPs, CheW/CheV, CheA and CheY, while other factors such as CheB, CheR, CheC, CheZ, or CheX may modulate and fine-tune the signal transduction cascade, with diverse combinations observed throughout the bacterial kingdom. It is known that *cheA* and *cheB* are putatively involved in pilus-mediated twitching motility (Sonnenschein et al., 2012). *cheV* encodes a chemotactic connexin that can affect the ATPase activity of CheA. The CheY protein is the final effector protein in the signal transduction cascade, directly interacting with the flagellar switch. The observation that lowest mobility of *cheY*-RNAi supports this theory. Interestingly, we observed that the ability of *cheA*-, *cheB*-, *cheR*-, and *cheV*-RNAi cells to form biofilms had increased, whereas that of *cheY*-RNAi had decreased. This result is similar to that described previously, suggesting that, although bacterial adhesion and biofilm formation are complex multi-step processes causing diseases, they are not directly related, biofilm formation is not dependent on the extent of initial adherence of bacteria to the substrate. Biofilm formation is more likely to be dependent on cell-to-cell adhesion rather than on the amount of cells initially attached to the surface. Adherence is a complex phenomenon involving a variety of surface factors on the bacterium (Cerca et al., 2005). Previous studies have implicated chemotaxis sensors were involved in biofilm formation. Tlp3 (Cj1564) mutants showed increased biofilm formation (Rahman et al., 2014), while CetZ (Tlp8) mutants showed decreased biofilm formation (Chandrashekhar et al., 2015). Defect in motility reduces the opportunities for bacteria to come into contact with surfaces, and the deletion of *plzB* in wild-type *V. cholerae* results in a decrease in biofilm formation and motility (Pratt et al., 2007). Thus, a serious decline in the motility of *cheY*-RNAi may decrease the extent of biofilm formation. Bacterial adhesion is severely affected by motility

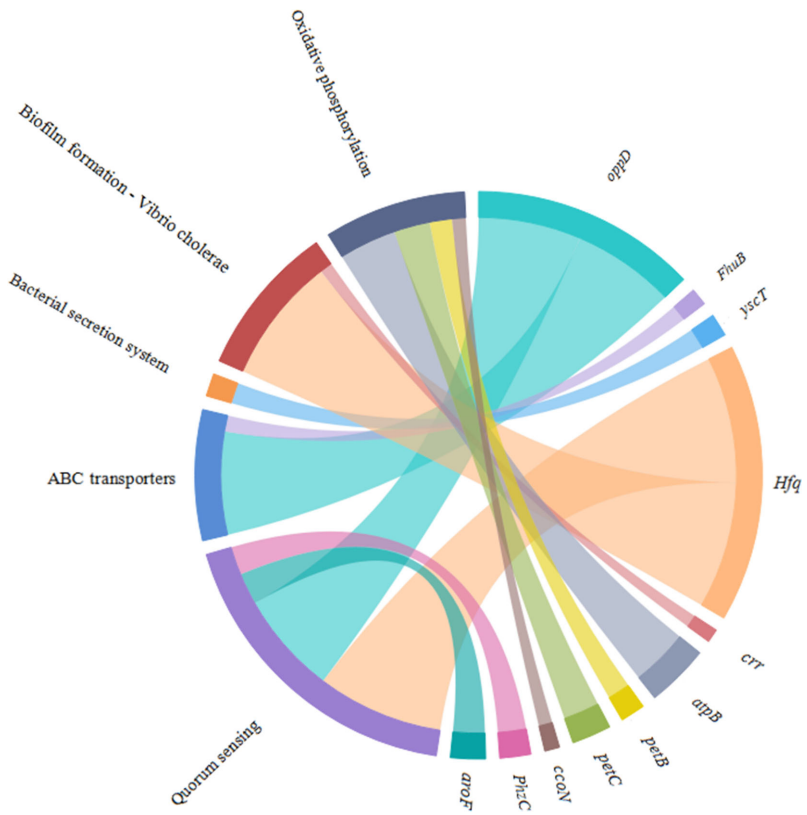

FIGURE 10 | Chordal graph of the DEGs to KEGG pathways. The width of the chordal represents the log2FC value.

(Beier and Gross, 2006), the result shows that motility is one of the approaches through which chemotactic genes influence adhesion, however, further research is required to fully understand these processes.

The loss of a single gene can significantly alter the transcriptional landscape of a bacterium (Richmond et al., 2016). In our study, silencing *cheA* significantly altered the transcriptome of *V. harveyi*. GO analysis revealed that many DEGs were involved in localization and the response to stimuli, which were relevant to bacterial adhesion (Kong et al., 2015). Changes in genes in the KEGG pathway related to adhesion ("biofilm formation-*Vibrio cholerae*," "ABC transporters," "oxidative phosphorylation," "quorum sensing," and "bacterial secretion system") prompt us *V. harveyi* may regulate the expression of these genes to cope with the decreased adhesion ability caused by *cheA* silencing.

The process of bacterial adhesion is linked to the movement of bacteria in response to chemical stimuli, which depends on bacterial chemotaxis. In this process, the bacteria sense signals transmitted to the cytosol, and the two-component system is activated. The two-component system interacts with the bacterial flagella and affects its adhesion (Benhamed et al., 2014). Additionally, the process of bacterial adhesion is affected by adhesins (Haiko and Westerlund-Wikström, 2013). Thus, a "bacterial secretion system" could mediate adhesion by controlling the secretion of intercellular polysaccharide adhesins. The results indicated that the DEGs identified in this study could affect bacterial adhesion. It is likely that *V. harveyi* could adapt to the reduced stimulus for adhesion caused by *cheA* silencing by regulating adhesion-related pathways. In the process of bacterial adhesion, cheA gene may affect adhesion by regulating bacterial response to environmental stimuli, which needs to be further confirmed.

The adhesion capacity of bacteria was dependent on environmental factors, particularly salinity and temperature (Benhamed et al., 2014), and the RNA-seq results suggest that the regulation of chemotactic genes on adhesion may be related to environmental stimuli. Therefore, we studied the adhesion ability and gene expression of *V. harveyi* in different environments. At different temperatures, an inverted U-shaped trend was observed in the adhesion ability of *V. harveyi*, with the highest adhesion occurring at 28°C, which is the same as that observed for *V. alginolyticus* (Huang et al., 2016). The expression of both *cheA* and *cheV* increased at high temperatures, whereas that of *cheR* was minimal under different temperature conditions. The expression of *cheB* and *cheY* was highly downregulated under both high and low temperature conditions. In summary, *cheB* and *cheY* could be the key

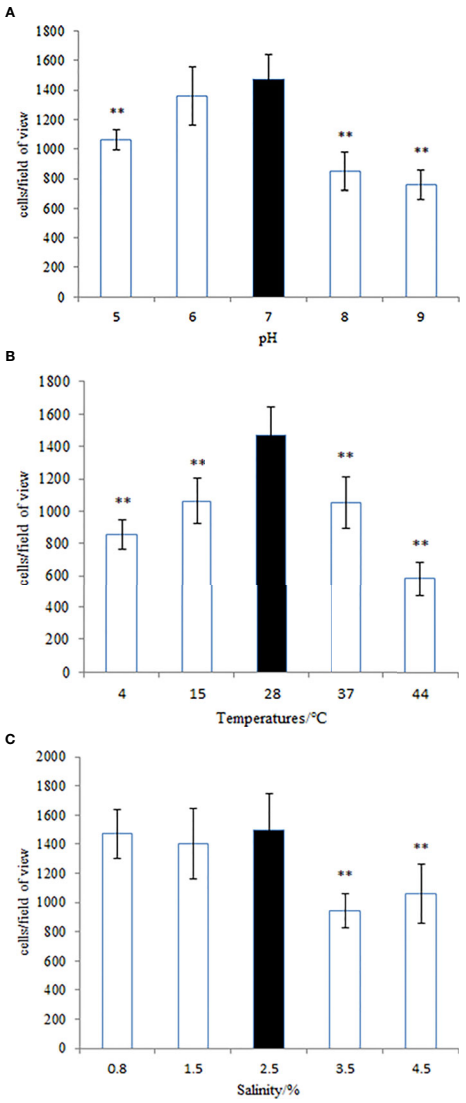

FIGURE 11 | The adhesion ability of the wild-type *Vibrio harveyi* strain under different conditions of **(A)** pH, **(B)** temperature, and **(C)** salinity. Data are presented as the mean ± SD, and each treatment was performed on six independent replicates. **P < 0.01 compared to the control.

regulatory genes responsible for the adhesion of the bacterium at different temperatures. Additionally, expression of these genes was highly impacted by low temperatures, potentially owing to a decrease in the metabolic levels of *V. harveyi* under these conditions. No similar trends in the expression of the five genes and the adhesion ability of *V. harveyi* under varying salinities were observed. *cheR* is essential for stable adhesion of *V. harveyi* at salinities of 1.5 and 2.5%, and further research is needed to explain the regularity of the effect of salinity on the adhesion of *V. harveyi*. A higher adhesion ability of *Vibrio anguillarum* (Balebona et al., 1995) and *V. alginolyticus* (Yan et al., 2007) was observed in acidic environments, and this result was similar to that observed with *V. harveyi*. In this study, under acidic conditions, the expression of *cheA* was the highest. However, the lowest expression of *cheA* was observed under neutral conditions, indicating that it has no obvious correlation with the adhesion ability of the bacteria. The results showed that the expression of *cheB*, *cheV*, and *cheY* showed trends similar to the bacterial adhesion ability, suggesting that their expression may be linked to the regulation of bacterial adhesion in a variable pH environment. Although the expression of *cheR* was upregulated to suit different pH conditions, no significant effect on adhesion was observed. This indicates that environmental conditions can affect bacterial adhesion and the expression of chemotactic genes, but how the genes regulate the adhesion of bacteria in a complex environment requires further research.

CONCLUSION

In conclusion, our study revealed the following results: (1) The chemotactic genes *cheA*, *cheB*, *cheR*, *cheV*, and *cheY* may regulate the adhesion ability of *V. harveyi* by affecting bacterial motility, and participate in the regulation of adhesion at different temperatures, salinities, and pH values; (2) RNAi-mediated *cheA* silencing altered the transcriptional landscape of *V. harveyi* and regulated the expression of genes involved in adhesion-related pathways. Understanding the relationship between the expression of *cheA*, *cheB*, *cheR*, *cheV*, and *cheY* and bacterial adhesion will provide insights on the mechanisms by which pathogens adhere to the mucus and assist in uncovering new avenues to prevent bacterial diseases.

DATA AVAILABILITY STATEMENT

The datasets presented in this study can be found in online repositories. The names of the repository/repositories and accession number(s) can be found below: https://www.ncbi.nlm.nih.gov/, PRJNA541796.

ETHICS STATEMENT

The animal study was reviewed and approved by the Animal Ethics Committee of Xiamen University.

AUTHOR CONTRIBUTIONS

XX conceived the experiments. HL, XQ, YC, YQ, JZ, and XJ conducted the experiments. All authors assisted in the collection and interpretation of data. XX and HL have the same contribution to this paper. All authors contributed to the article and approved the submitted version.

FUNDING

This research was supported by Open Research Fund Project of State Key Laboratory of Large Yellow Croaker Breeding

(No.LYC2018RS04), the Natural Science Foundation of Fujian Province (# 2020J01673), the National Key Research and Development Program of China (NO. 2018YFC1406305), the Foreign Cooperation Project of Fujian Province(No.2019I1008), the Scientific Research Fund of Engineering Research Center of the Modern Industry Technology for Eel Ministry of Education (No.RE202014, RE-R202007), the Science and Technology Platform Construction of Fujian Province (No.2018N2005, 2017L3019), the NSFC (General Program No.31702384), the Scientific Research Fund of Fujian Provincial Department of Education (No.JA15292), and the open fund of the Fujian Province Key Laboratory of Special Aquatic Formula Feed (Fujian Tianma Science and Technology Group Co., Ltd.) (No.TMKJZ1907), Science and technology commissioner of fujian province (No.MinKeNong [2019] No.11, ZP2021001), the national key Research and development plan(No.2020YFD0900102).

SUPPLEMENTARY MATERIAL

The Supplementary Material for this article can be found online at: https://www.frontiersin.org/articles/10.3389/fcimb.2020.591751/full#supplementary-material

REFERENCES

Atsumi, T., Mccarter, L., and Imae, Y. (1992). Polar and lateral flagellar motors of marine Vibrio are driven by different ion-motive forces. *Nature* 355, 182–184. doi: 10.1038/355182a0

Austin, B., and Zhang, X. (2006). Vibrio harveyi: A significant pathogen of marine vertebrates and invertebrates. *Lett. Appl. Microbiol.* 43 (2), 119–124. doi: 10.1111/j.1472-765X.2006.01989.x

Balebona, M. C., Moriñigo, M. A., Faris, A., Krovacek, K., Månsson, I., Bordas, M. A., et al. (1995). Influence of salinity and pH on the adhesion of pathogenic Vibrio strains to Sparusaurata skinmucus. *Aquaculture* 132, 113–120. doi: 10.1016/0044-8486(94)00376-Y

Beier, D., and Gross, R. (2006). Regulation of bacterial virulence by two-component systems. *Curr. Opin. Microbiol.* 9, 143–152. doi: 10.1016/j.mib.2006.01.005

Benhamed, S., Guardiola, F. A., Mars, M., and Esteban, M. Á. (2014). Pathogen bacteria adhesion to skin mucus of fishes. *Veterinary Microbiol.* 171 (1-2), 1. doi: 10.1016/j.vetmic.2014.03.008

Bordas, M. A., Balebona, M. C., Rodriguezmaroto, J. M., Borrego, J. J., and Morinigo, M. A. (1998). Chemotaxis of Pathogenic Vibrio Strains towards Mucus Surfaces of Gilt-Head Sea Bream (Sparus aurata L). *Appl. Environ. Microbiol.* 64 (4), 1573–1575. doi: 10.1128/AEM.64.4.1573-1575.1998

Borkovich, K. A., Kaplan, N., Hess, J. F., and Simon, M. I. (1989). Transmembrane signal transduction in bacterial chemotaxis involves ligand- dependent activation of phosphate group transfer. *Proc. Natl. Acad. Sci.* 86, 1208–1212. doi: 10.1073/pnas.86.4.1208

Bradford, N. M. (1976). A rapid and sensitive method for the quantification of microgram quantities of protein utilizing the principle of protein-dye binding. *Anal. Biochem.* 72, 248–254. doi: 10.1016/0003-2697(76)90527-3

Burkart, M., Toguchi, A., and Harshey, R. M. (1998). The chemotaxis system, but not chemotaxis, is essential for swarming motility in Escherichia coli. *Proc. Natl. Acad. Sci. U. States America* 95 (5), 2568. doi: 10.1073/pnas.95.5.2568

Cerca, N., Gerald, B., Pier, G. B., Rosário, M., Oliveira, R., and Azeredo, J. (2005). Quantitative analysis of adhesion and biofilm formation on hydrophilic and hydrophobic surfaces of clinical isolates of Staphylococcus epidermidis. *Res. Microbiol.* 156 (4), 506. doi: 10.1016/j.resmic.2005.01.007

Chandrashekhar, K., Gangaiah, D., Pina-Mimbela, R., Kassem, I., Jeon, B. H., and Rajashekara, G. (2015). Transducer like proteins of Campylobacter jejuni 81-176: role in chemotaxis and colonization of the chicken gastrointestinal tract. *Front. Cell Infect. Microbiol.* 5, 46. doi: 10.3389/fcimb.2015.00046

Chen, Q., Yan, Q., Wang, K., Zhuang, Z., and Wang, X. (2008). Portal of entry for pathogenic Vibrio alginolyticus into Pseudosciaene crocea and characteristic of bacterial adhesion to the mucus. *Dis. Aquat. Organisms* 80 (3), 181–188. doi: 10.3354/dao01933

Cikos, S., Bukovská, A., and Koppel, J. (2007). Relative quantification of mRNA: comparison of methods currently used for real-time PCR data analysis. *BMC Mol. Biol.* 8, 113. doi: 10.1186/1471-2199-8-113

Colin, R., and Sourjik, V. (2017). Emergent properties of bacterial chemotaxis pathway. *Curr. Opin. Microbiol.* 39, 24–33. doi: 10.1016/j.mib.2017.07.004

Darsigny, M., Babeu, J. P., Seidman, E. G., Gendron, F. P., Levy, E., Carrier, J., et al. (2010). Hepatocyte nuclear factor-4alpha promotes gut neoplasia in mice and protects against the production of reactive oxygen species. *Cancer Res.* 70, 9423. doi: 10.1158/0008-5472.CAN-10-1697

Duque, E., Torre, J., Bernal, P., Molina-Henares, M. A., Alaminos, M., Espinosa-Urgel, M., et al. (2013). Identification of reciprocal adhesion genes in pathogenic and non-pathogenic Pseudomonas. *Environ. Microbiol.* 15, 36–48. doi: 10.1111/j.1462-2920.2012.02732.x

Gorden, A. S., Gerchakov, S. M., and Udey, L. R. (1981). The effect of polarization on the attachement of marine to copper and platinum surfaces. *Can. J. Microbiol.* 27 (7), 698–703. doi: 10.1139/m81-108

Guo, L., Huang, L., Su, Y., Qin, Y. X., Zhao, L. M., and Yan, Q. P. (2017). secA, secD, secF, yajC, and yidC contribute to the adhesion regulation of Vibrio alginolyticus. *Microbiologyopen* 7 (2), e00551. doi: 10.1002/mbo3.551

Guo, M., Huang, Z., and Yang, J. (2017). Is there any crosstalk between the chemotaxis and virulence induction signaling in Agrobacterium tumefaciens? *Biotechnol. Adv.* 35 (4), 505–511. doi: 10.1016/j.biotechadv.2017.03.008

Haiko, J., and Westerlund-Wikström, B. (2013). The role of the bacterial flagellum in adhesion and virulence. *Biology* 2, 1242–1267. doi: 10.3390/biology2041242

Hamed, S. B., Ranzani-Paiva, M. J. T., Tachibana, L., Dias, D., Ishikawa, C. M., et al. (2018). Fish pathogen bacteria: Adhesion, parameters influencing virulence and interaction with host cells. *Fish Shellfish Immunol.* 80, 550–562. doi: 10.1016/j.fsi.2018.06.053

Hess, J. F., Oosawa, K., Kaplan, N., and Simon, M. I. (1988). Phosphorylation of three proteins in the signaling pathway of bacterial chemotaxis. *Cell* 53), 79–87. doi: 10.1016/0092-8674(88)90489-8

Huang, L., Qin, Y. X., Yan, Q. P., Lin, G. F., Huang, L. X., Huang, B., et al. (2015). MinD plays an important role in Aeromonas hydrophila adherence to Anguilla japonica mucus. *Gene* 565, 275–281. doi: 10.1016/j.gene.2015.04.031

Huang, L., Huang, L., Yan, Q., Qin, Y., Ma, Y., Lin, M., et al. (2016). The TCA pathway is an important player in the regulatory network governing Vibrio alginolyticus adhesion under adversity. *Front. Microbiol.* 7, 40. doi: 10.3389/fmicb.2016.00040

Huang, L., Wang, L., Lin, X., et al. (2017). mcp, aer, cheB, and cheV contribute to the regulation of Vibrio alginolyticus (ND-01) adhesion under gradients of environmental factors. *MicrobiologyOpen* 6 (6), e00517. doi: 10.1002/mbo3.517

Kirk, S., Vanessa, K., Deanna, L. G., Caixia, M., Marinieve, M., Ho, P. S., et al. (2010). Muc2 protects against lethal infectious colitis by disassociating pathogenic and commensal bacteria from the colonic mucosa. *PloS Pathog.* 6, e1000902. doi: 10.1371/journal.ppat.1000902

Kogure, K., Ikemoto, E., and Morisaki, H. (1998). Attachment of Vibrio alginolyticus to glass surfaces is dependent on swimming speed. *J. Bacteriol.* 180, 932–937. doi: 10.1128/JB.180.4.932-937.1998

Kolenbrander, P. E., Andersen, R. N., Baker, R. A., and Jenkinson, H. F. (1998). The Adhesion-Associated sca Operon inStreptococcus gordonii Encodes an Inducible High-Affinity ABC Transporter for Mn2+ Uptake. *J. Bacteriol.* 180 (2), 290–295. doi: 10.1128/JB.180.2.290-295.1998

Kong, W., Huang, L., Su, Y., Qin, Y. X., Ma, Y., Xu, X. J., et al. (2015). Investigation of possible molecular mechanisms underlying the regulation of adhesion in Vibrio alginolyticus with comparative transcriptome analysis. *Antonie van Leeuwenhoek* 107 (5), 1197–1206. doi: 10.1007/s10482-015-0411-9

Koutsoudis, M. D., Tsaltas, D., Minogue, T. D., and Bodman, S. B. (2006). Quorum-sensing regulation governs bacterial adhesion, biofilm development, and host colonization in Pantoea stewartii subspecies stewartii. *Proc. Natl. Acad. Sci.* 103 (15), 5983–5988. doi: 10.1073/pnas.0509860103

Liu, W., Ren, P., He, S., Xu, L., Yang, Y. L., Gu, Z. M., et al. (2013). Comparison of adhesive gut bacteria composition, immunity, and disease resistance in juvenile

hybrid tilapia fed two different Lactobacillus strains. *Fish Shellfish Immunol.* 35, 54–62. doi: 10.1016/j.fsi.2013.04.010

Luo, G., Huang, L., Su, Y., Qin, Y. X, Xu, X. J., Zhao, L. M., et al. (2016). flrA, flrB and flrC regulate adhesion by controlling the expression of critical virulence genes in Vibrio alginolyticus. *Emerg. Microbes Infect.* 5 (8), e85. doi: 10.1038/emi.2016.82

McRose, D. L., Baars, O., Seyedsayamdost, M. R., and Morel, F. M. (2018). Quorum sensing and iron regulate a two-for-one siderophore gene cluster in Vibrio harveyi. *Proc. Natl. Acad. Sci.* 115 (29), 7581–7586. doi: 10.1073/pnas.1805791115

Paola, C., Giovambattista, P., Elisa, G., Letizia, T., Renata, C., Giovanni, R., et al. (2003). Reactive oxygen species as essential mediators of cell adhesion: the oxidative inhibition of a FAK tyrosine phosphatase is required for cell adhesion. *J. Cell Biol.* 161 (5), 933–944. doi: 10.1083/jcb.200211118

Pianetti, A., Battistelli, M., Barbieri, F., Bruscolini, F., Falcieri, E., Manti, A., et al. (2012). Changes in adhesion ability of Aeromonas hydrophila during long exposure to salt stress conditions. *J. Appl. Microbiol.* 113 (4), 974–982. doi: 10.1111/j.1365-2672.2012.05399.x

Pratt, J. T., Tamayo, R., Tischler, A. D., and Camilli, A. (2007). PilZ domain proteins bind cyclic diguanylate and regulate diverse processes in Vibrio cholerae. *J. Biol. Chem.* 282 (17), 12860–12870. doi: 10.1074/jbc.M611593200

Rahman, H., King, R. M., Shewell, L. K., Semchenko, E. A., Hartley-Tassell, L. E., Wilson, J. C., et al. (2014). Characterisation of a multi-ligand binding chemoreceptor CcmL (Tlp3) of Campylobacter jejuni. *PloS Pathog.* 10, e1003822. doi: 10.1371/journal.ppat.1003822

Richmond, G. E., Evans, L. P., Anderson, M. J., Wand, M. E., Bonney, L. C., Ivens, A., et al. (2016). The Acinetobacter baumannii two-component system AdeRS regulates genes required for multidrug efflux, biofilm formation, and virulence in a strain-specific manner. *MBio* 7 (2), e00430–e00416. doi: 10.1128/mBio.00852-16

Roman, S. J., Meyers, M., Volz, K., and Matsumura, P. (1992). A chemotactic signaling surface on CheY defined by suppressors of flagellar switch mutations. *J. Bacteriol.* 174), 6247–6255. doi: 10.1128/JB.174.19.6247-6255.1992

Ruhe, Z. C., Townsley, L., Wallace, A. B., King, A., Woude, M., David, A. L., et al. (2015). CdiA promotes receptor-independent intercellular adhesion. *Mol. Microbiol.* 98, 175–192. doi: 10.1111/mmi.13114

Sockett, H., Yamaguchi, S., Kihara, M., Irikura, V. M., and Macnab, R. M. (1992). Molecular analysis of the flagellar switch protein FliM of Salmonella typhimurium. *J. Bacteriol.* 174, 793–806. doi: 10.1128/JB.174.3.793-806.1992

Sonnenschein, E. C., Syit, D. A., Grossart, H. P., and Ullrich, M. S. (2012). Chemotaxis of Marinobacter adhaerens and Its Impact on Attachment to the Diatom Thalassiosira weissflogii. *Appl. Environ. Microbiol.* 78 (19), 6900. doi: 10.1128/AEM.01790-12

Stock, A. M., Robinson, V. L., and Goudreau, P. N. (2000). Two-component signal transduction. *Annu. Rev. Biochem.* 69, 183–215. doi: 10.1146/annurev.biochem.69.1.183

Tendencia, E. A. (2002). V. harveyi isolated from cage-cultured seabass Lates calcarifer Bloch in the Philippines. *Aquaculture Res.* 33, 455–458. doi: 10.1046/j.1365-2109.2002.00688.x

van Kessel, J. C., Rutherford, S. T., Cong, J. P., Quinodoz, S., Healy, J., and Bassler, B. L. (2015). Quorum sensing regulates the osmotic stress response in Vibrio harveyi. *J. Bacteriol.* 197 (1), 73–80. doi: 10.1128/JB.02246-14

Wadhams, G. H., and Armitage, J. P. (2004). Making sense of it all: bacterial chemotaxis. *Nat. Rev. Mol. Cell Biol.* 5 (12), 1024. doi: 10.1038/nrm1524

Wang, L., Huang, L., Su, Y. Q., Qin, Y. X., Kong, W. D., Ma, Y., et al. (2015). Involvement of the flagellar assembly pathway in Vibrio alginolyticus adhesion under environmental stresses. *Front. Cell Infect. Microbiol.* 5, 59. doi: 10.3389/fcimb.2015.00059

Watnick, P.II, and Kolter, R. (1999). Steps in the development of a Vibrio cholerae El Tor biofilm. *Mol. Microbiol.* 34 (3), 586–595. doi: 10.1046/j.1365-2958.1999.01624.x

Xu, X. J., Xu, B., Wang, J., Su, Y. Q., Zhang, Z. W., and Chen, X. (2010). Plate Effect of V. harveyi on the head kidney and liver of P. crocea (histopathological and electronic microscope section). *J. Fish. China* (4), 618–625.

Xue, C. (2015). Macroscopic equations for bacterial chemotaxis: integration of detailed biochemistry of cell signaling. *J. Math. Biol.* 70 (1-2), 1–44. doi: 10.1007/s00285-013-0748-5

Yan, Q. P., Chen, Q., Ma, S., Zhuang, Z. X., and Wang, X. R. (2007). Characteristics of adherence of pathogenic Vibrio alginolyticus to the intestinal mucus of large yellow croakers (Pseudosciaena crocea). *Aquaculture* 269, 21–30. doi: 10.1016/j.aquaculture.2007.02.042

Yang, Q., and Defoirdt, T. (2015). Quorum sensing positively regulates flagellar motility in pathogenic Vibrio harveyi. *Environ. Microbiol.* 17 (4), 960–968. doi: 10.1111/1462-2920.12420

Conflict of Interest: XX was employed by Ningde Fufa Fisheries Company Limited and Fujian Tianma Science and Technology Group Co., Ltd. JZ was employed by Ningde Fufa Fisheries Company Limited.

The authors declare that this study received funding from Fujian Tianma Science and Technology Group Co., Ltd.. The funder had the following involvement in the study: the funder bodies were involved in the study design, interpretation of data.

The remaining authors declare that the research was conducted in the absence of any commercial or financial relationships that could be construed as a potential conflict of interest.

frontiers in Cellular and Infection Microbiology

ORIGINAL RESEARCH
published: 05 February 2021
doi: 10.3389/fcimb.2020.626574

First Succinylome Profiling of *Vibrio alginolyticus* Reveals Key Role of Lysine Succinylation in Cellular Metabolism and Virulence

Fuyuan Zeng[1,2,3†], Huanying Pang[1,2,3,4†], Ying Chen[2,3], Hongwei Zheng[2,3], Wanxin Li[5*], Srinivasan Ramanathan[5], Rowena Hoare[6], Sean J. Monaghan[6], Xiangmin Lin[5] and Jichang Jian[1,2,3,4]*

[1] Shenzhen Institute, Guangdong Ocean University, Shenzhen, China, [2] Fisheries College, Guangdong Ocean University, Zhanjiang, China, [3] Guangdong Provincial Key Laboratory of Pathogenic Biology and Epidemiology for Aquatic Economic Animals, Guangdong Key Laboratory of Control for Diseases of Aquatic Economic Animals, Southern Marine Science and Engineering Guangdong Laboratory (Zhan jiang), Zhanjiang, China, [4] Key Laboratory of Experimental Marine Biology, Institute of Oceanology, Chinese Academy of Sciences, Qingdao, China, Laboratory for Marine Biology and Biotechnology, Qingdao National Laboratory for Marine Science and Technology, Qingdao, China, [5] Fujian Provincial Key Laboratory of Agroecological Processing and Safety Monitoring, School of Life Sciences, Fujian Agriculture and Forestry University, Fuzhou, China, [6] Institute of Aquaculture, University of Stirling, Stirling, United Kingdom

Recent studies have shown that a key strategy of many pathogens is to use post-translational modification (PTMs) to modulate host factors critical for infection. Lysine succinylation (Ksuc) is a major PTM widespread in prokaryotic and eukaryotic cells, and is associated with the regulation of numerous important cellular processes. *Vibrio alginolyticus* is a common pathogen that causes serious disease problems in aquaculture. Here we used the affinity enrichment method with LC-MS/MS to report the first identification of 2082 lysine succinylation sites on 671 proteins in *V. alginolyticus*, and compared this with the lysine acetylation of *V. alginolyticus* in our previous work. The Ksuc modification of SodB and PEPCK proteins were further validated by Co-immunoprecipitation combined with Western blotting. Bioinformatics analysis showed that the identified lysine succinylated proteins are involved in various biological processes and central metabolism pathways. Moreover, a total of 1,005 (25.4%) succinyl sites on 502 (37.3%) proteins were also found to be acetylated, which indicated that an extensive crosstalk between acetylation and succinylation in *V. alginolyticus* occurs, especially in three central metabolic pathways: glycolysis/gluconeogenesis, TCA cycle, and pyruvate metabolism. Furthermore, we found at least 50 (7.45%) succinylated virulence factors, including LuxS, Tdh, SodB, PEPCK, ClpP, and the Sec system to play an important role in bacterial virulence. Taken together, this systematic analysis provides a basis for further study on the pathophysiological role of lysine succinylation in *V. alginolyticus* and provides targets for the development of attenuated vaccines.

Keywords: ***Vibrio alginolyticus*, lysine succinylation, acetylation, crosstalk, virulence factors**

OPEN ACCESS

Edited by:
Lixing Huang,
Jimei University, China

Reviewed by:
Huan Liu,
Shaanxi University of Science and Technology, China
Yang Zhou,
Huazhong Agricultural University, China
Hui Li,
Sun Yat-Sen University, China

****Correspondence:***
Huanying Pang
phying1218@163.com
Wanxin Li
953454965@qq.com

†These authors have contributed equally to this work and share first authorship

Specialty section:
This article was submitted to Molecular Bacterial Pathogenesis, a section of the journal Frontiers in Cellular and Infection Microbiology

Received: *06 November 2020*
Accepted: *22 December 2020*
Published: *05 February 2021*

Citation:
Zeng F, Pang H, Chen Y, Zheng H, Li W, Ramanathan S, Hoare R, Monaghan SJ, Lin X and Jian J (2021) First Succinylome Profiling of Vibrio alginolyticus Reveals Key Role of Lysine Succinylation in Cellular Metabolism and Virulence. Front. Cell. Infect. Microbiol. 10:626574. doi: 10.3389/fcimb.2020.626574

INTRODUCTION

Protein post-translational modifications (PTMs) are vital regulatory mechanisms, which are involved in a plethora of cellular events such as gene expression, virulence, and cellular metabolism in both prokaryotic and eukaryotic cells (Avison et al., 2002; Xie et al., 2014). During these processes simple chemical groups such as a methyl, hydroxyl, phosphate, and acetyl groups or more complex groups such as sugars, lipids, AMP, and ADP-ribose may be added to the protein molecules (Ribet and Cossart, 2010). Several types of PTMs have been discovered that are involved in bacterial virulence and physiology. Hence, determining bacterial proteomes alone may be limiting and characterization of PTMs is vital to better understand adaption, virulence, and resistance of bacterial pathogens (Wu et al., 2019). Among the 20 amino acids residues, lysine is frequently targeted for a variety of PTMs, for example the protein Nε-acylation targets lysine residues and is an extensively dispersed PTM (Komine-Abe et al., 2017). Recent research has consistently revealed that lysine can be post-translationally modified by numerous types of acylation (Weinert et al., 2013). Among the hundreds of diverse PTMs, acylation on lysine residues, such as lysine crotonylation (K_{cr}), lysine propionylation (K_{pr}), lysine glutarylation (K_{glu}), lysine butyrylation (K_{bu}), lysine malonylation (K_{mal}), lysine β-hydroxybutyrylation (K_{bhb}), and lysine 2-hydroxyisobutyrylation (K_{hib}) are vital for efficient regulation of many prokaryotic and eukaryotic proteins (Yang et al., 2015).

Protein lysine succinylation (K_{suc}), also referred to as Nε-succinylation, is a newly identified and evolutionarily conserved reversible PTM from prokaryotes to eukaryotes. It transfers the succinyl group (-CO-CH_2-CH_2-CO-) from the succinyl-CoA to the lysine residue of the protein moiety, resulting in the formation of succinyl-lysine (Zhang et al., 2011). Recently, numerous lysine-succinylated proteins have been identified in various bacterial pathogens, such as *Mycobacterium tuberculosis*, *Porphyromonas gingivalis*, *Candida albicans* (Yang et al., 2015; Zheng et al., 2016; Wu et al., 2019), and so on. Many are enzymes involved in various metabolic pathways and regulation of several central metabolic processes in the bacteria such as glycolysis, gluconeogenesis, the tricarboxylic acid cycle (TCA cycle), and fatty acid metabolism (Xie et al., 2014). Furthermore, Nε-succinylation has been reported in many protein substrates and involved in the regulation of cellular physiology and metabolism in both prokaryotic and eukaryotic cells (Nadine et al., 2017). This PTM can make prominent modifications in structure regulation and protein function. The identification of protein succinylation sites has important implications with regards to understanding of cellular physiology and pathology, potentially leading to valuable information for drug development and biomedical research. In recent times, high-throughput approaches in conjunction with mass spectrometry have been widely applied to identify the K_{suc} in several organisms ranging from bacteria to humans (Colak et al., 2013; Li et al., 2014; Jin and Wu, 2016; Xu et al., 2016; Feng et al., 2017; Song et al., 2017; Xie et al., 2017; Zhang et al., 2017).

Vibrio alginolyticus is a Gram-negative halophilic bacterium and an etiological agent of vibriosis, mainly found in marine and estuarine environments. Outbreaks cause high mortality in marine animals with serious economic losses worldwide. Being a zoonotic pathogen, it not only causes vibriosis in marine animals, but also causes foodborne related infections in humans by consumption of contaminated raw and half-cooked seafood (Dan et al., 2019; Zheng et al., 2019). Moreover, several researchers frequently reported antibiotic resistant strains of the bacterium from aquaculture and clinical settings (Horii et al., 2005; Ferrini et al., 2008; Xiong et al., 2010). *V. alginolyticus* is able to form biofilms and is capable of flagellar mediated motility (Echazarreta and Klose, 2019). It also secretes several virulence factors such as, serine protease, hemolysin, exopolysaccharide, siderophores, and cell surface hydrophobicity products through various metabolic pathways (Yang et al., 2015; Hernández-Robles et al., 2016; Santhakumari et al., 2017; Huang et al., 2018), which all contribute to mechanisms of pathogenicity that require further understanding.

Comprehensive lysine succinylome studies conducted in different bacterial pathogens have revealed the importance of this PTM. However, to the best of our knowledge, no succinylated proteins have been discovered so far in *V. alginolyticus*, which presents a foremost obstacle for understanding the regulatory mechanism of K_{suc} in this pathogen. We have therefore conducted the first systematic analysis to identify the targets of this K_{suc} in *V. alginolyticus*. Following enrichment of succinylated peptides from digested cell lysates we used mass spectrometry to explore Nε-succinylation PTMs and identified 2082 K_{suc} sites on 671 proteins in *V. alginolyticus*. Further, the bioinformatic analysis showed that a large quantity of the succinylation sites were present on proteins associated with metabolism pathway, followed by biosynthesis of antibiotics, but also associated with diverse biological processes and functions, such as ribosomes, biosynthesis of secondary metabolites. The results obtained provide the first global lysine succinylation profiling of *V. alginolyticus* and sets a foundation for further investigations on the biological role of lysine succinylation in this bacterial pathogen.

MATERIALS AND METHODS

Bacterial Strains and Sample Preparation

V. alginolyticus strain HY9901 was isolated from diseased fish *Lutjanus erythopterus* in Zhanjiang harbor area of Guangdong Province (Cai et al., 2007), China, and cultured in Dulbecco's Modified Eagle Medium (DMEM) media. The strain was grown overnight in DMEM media, and culture was diluted 1:100 ratio in the fresh DMEM media. Cell were harvested when OD600nm reached 1.0, centrifuged at 8,000×g, and then washed twice with phosphate buffered saline (PBS, NaCl 136.89 mM, KCl 2.67 mM, Na_2HPO_4 8.1 mM, KH_2PO_4 1.76 mM, pH 7.4). The pellets were resolved in 8 M urea and 0.2% SDS in 50 mM Tris-HCl buffer (pH 8.0) and cells were broken by super-sonication on ice for a total of 10 min with 9 s intervals, and the lysate centrifuged at

12,000×g for 15 min at 4°C. The supernatant dithiothreitol (DTT) was added until a final concentration of 2 mM DTT was obtained. The sample was then incubated at 56°C for 1 h, and then the equivalent of 4× the sample volume of pre-cooled acetone was added to precipitate proteins at −20°C for >2 h. The sample pellet was washed twice by centrifugation with pre-cooled acetone. Finally the pellet was dissolved in dissolution buffer containing 0.1 M triethylammonium bicarbonate (TEAB, pH 8.5) and 8 M urea. Protein concentration was determined with a Bradford assay (He et al., 2016).

Enrichment of Lysine-Succinylated Peptides

Approximately 10 mg of protein sample was used for reduction and alkylation with 10 mM DTT and 20 mM iodoacetamide (IAA), respectively, as described previously (Yao et al., 2019). The treated sample was digested to peptides using trypsin at 1:20 ratio (m/v) at 37°C for 16 h. The lysine-succinylated peptides were enriched by immunoaffinity using agarose-conjugated anti-succinyllysine antibody (PTM Biolabs Inc., Hangzhou, China), as previously described (Yang et al., 2015). Briefly, the digested peptides were incubated with anti-succinyllysine agarose beads overnight at 4°C in NETN buffer (100 mM NaCl, 50 mM Tris-HCl, 1 mM EDTA, and 0.5% (v/v) Nonidet P-40, pH 8.0). The enriched peptides were eluted with 1% trifluoroacetic acid (TFA) and desalted with C18 ZipTips (Millipore, Burlington, MA, USA) before being subjected to MS identification.

LC-MS/MS Analysis

Proteomic analyses were performed using an EASY-nLC^{TM} 1200 UHPLC system (ThermoFisher Scientific, Germany) coupled to an Orbitrap Q Exactive HF-X mass spectrometer (ThermoFisher) operating in the data-dependent acquisition (DDA) mode which was carried out as previously described (Pang et al., 2020).

Data Processing

The resulting MS raw data were processed using Proteome Discoverer2.2 software for database retrieval and protein quantification. Tandem mass spectra were compared against the Uniprot_*Vibrio alginolyticus* protein database (4,338 sequences). Trypsin was specified as a cleavage enzyme allowing up to two missing cleavages. The precursor and fragment ion mass tolerance were set to 10 ppm and 0.02 Da. Carbamidomethylation on Cys was specified as a fixed modification and succinylation on protein N-terminals were specified as variable modifications. False discovery rate (FDR) thresholds for peptide and protein were specified at 0.05. Minimum peptide length was set at 7. Lysine succinylation sites were identified with a localization probability set as >0.75. The mass spectrometry proteomics data have been deposited to the ProteomeXchange Consortium (http://proteomecentral.proteomexchange.org) *via* the iProX partner repository with the dataset identifier PXD023153.

Co-Immunoprecipitation and Western Blotting

Specific polyclonal antibodies to SodB and PEPCK (Phosphoenolpyruvate carboxykinase, one of the key enzymes in gluconeogenesis pathway) were used to precipitate target proteins. *V. alginolyticus* strain cell lysates (500 μg) were interacted with SodB and PEPCK antibody at 4°C overnight. Protein A/G beads washed three times with PBS buffer were added to the lysates at 4°C for 1–3 h (Cheng et al., 2019). The beads were pelleted at 4°C, followed by five washes with PBS buffer. Then 50 μl of loading sample buffer (250 mM Tric-HCl pH = 6.8, 10% SDS, 0.5% bromophenol blue, 50% glycerol, and 5% β-mercaptoethanol) was added to the pellet, boiled for 5 min, and subsequently analyzed by SDS-PAGE and Western blotting.

For Western blotting, proteins were run on 12% 1-DE gels and transferred to a polyvinylidene fluoride (PVDF, Millipore, Billerica, MA, USA) membrane. The membranes were blocked in Tris buffered saline (TBS, 500 mM Tris-HCl; 2.8 M NaCl; 60 mM KCl; pH7.4) containing 0.05% (v/v) Tween 20 with 5% (w/v) skimmed milk and incubated for 1 h at room temperature. The primary antibodies used in the western blot were anti-SodB (1:4,000), anti-PEPCK (1:4,000), and anti-succinyllysine mouse mAb (PTM Biolabs Inc., Hangzhou, China) (1:5m000 in TBST with 5% skimmed milk) and incubated overnight at 4°C. Horseradish peroxidase (HRP) conjugated goat anti-mouse IgG (H+L) (Beyotime Biotechnology, Shanghai, China) was used as the secondary antibody at a 1:10,000 dilution in TBST with 3% skimmed milk. Finally, the membrane was visualized using the ECL system (Bio-Rad, Hercules, CA, USA), and recorded by the ChemiDoc^{TM} MP (Bio-Rad, Hercules, CA, USA) imaging system (Wang et al., 2019).

Bioinformatics

Gene Ontology (GO, including cellular components, molecular functions, and biological processes) and the Kyoto Encyclopedia of Genes and Genomes (KEGG) pathway annotation of identified succinylated proteins were performed using online software OmicsBean (http://www.omicsbean.cn/). The Cluster of Orthologous Groups of proteins (COG) was analyzed using the COG database of NCBI (https://www.ncbi.nlm.nih.gov/COG/). STRING software (version 11.0) was used to annotate protein domains. Amino acid sequence motifs were analyzed using online software MoMo (Modification Motifs, version 5.1.1, http://meme-suite.org/tools/momo?tdsourcetag=s_pcqq_aiomsg) (Cheng et al., 2017). All analyses with a corrected p-value <0.05 were considered significant, and using GraphPad Prism 8.0 software to generate images. Protein-Protein interactions (PPIs) were predicted using STRING (https://string-db.org/) combined with Cyctoscape 3.7.1 software.

RESULTS AND DISCUSSION

Identification of Lysine-Succinylated Peptides and Proteins in *V. alginolyticus*

We combined immunoaffinity enrichment of lysine-succinylated peptides with a highly specific succinylation antibody and LC-MS/MS to profile the succinylated proteins and peptides of *V. alginolyticus*. With FDR thresholds below 5% for peptides, 2,082 unique succinylated peptides with 2,082 succinylation sites from

671 proteins were identified in *V. alginolyticus* (**Supplemental Tables S1**, **S2**). The mass error of succinylated peptides ranged from −5 to 5 ppm, illustrating that the MS dataset was controlled within an expected error rate (**Figure 1A**). The peptides exhibit distinct abundance depending on their lengths, and most were in range of 7–24 segments (97.65%), with a small number of peptides with lengths of 24–38, which accounted for about 2.35% (**Figure 1B**). Moreover, of the 671 succinylated proteins, 43.4% were succinylated at a sole site, 16.7, 12.5, and 7.7% were modified at two, three, and four sites, respectively, whereas 19.7% were modified at five or more sites (**Figure 1C**). In *V. alginolyticus* the most heavily succinylated protein was DNA-directed RNA polymerase subunit beta RpoS (28 sites). In addition, nine proteins exhibited high abundances (>15) of succinylated sites including translation process related proteins D0WXZ6 (RpsA, 19 sites), D0WW35 (RpoC, 18), D0WYY9 (FusA, 17), and D0WX73 (Frr, 16); the major chaperone proteins D0WYT6 (GroL, 18) and D0WUB9 (DnaK, 16); pyruvate dehydrogenase E1 component D0WZ79 (18); dihydrolipoyl dehydrogenase D0WZ77 (LpdA, 16); AAA_PrkA domain-containing protein A0A2I3BY81 (16). The abundance of lysine succinylation sites in chaperone proteins found in this study, which are consistent with the results of pathogenic bacteria such as *Aeromonas hydrophila* and *M. tuberculosis*, is worthy of further investigation (Xie et al., 2014; Yao et al., 2019).

Functional Annotation of the Lysine Succinylome in *V. alginolyticus*

To understand the roles of lysine succinylation, we performed GO, KEGG, COG, and domain analysis of all identified succinylated proteins. The classification results relating to molecular function, biological process, and cellular component categories showed that the largest protein group of succinyl proteins are associated with catalytic activity, organonitrogen compound biosynthetic processes, and cytoplasm, which accounts for 24, 33, and 34% of the total succinyl proteins, respectively (**Figure 2**). Moreover, other molecular functions include small molecule binding, ion binding, and structural constituents of ribosomes, representing 22, 12, and 8% of all identified proteins, respectively (**Figure 2A**). The other large groups in terms of biological processes are proteins associated with organonitrogen compound metabolic processes (14%), organic substance metabolic processes (13%), and metabolic processes (8%) (**Figure 2B**). Cell (11%), other cell components (7%), intracellular (3%), and macromolecular complexes (1%) are classified in cellular components (**Figure 2C**). The GO analysis of the succinylome suggests that the succinylated proteins are related to different molecular functions, biological processes, and cellular components, and closely related to bacterial life activities.

The KEGG analysis of the succinylated proteins showed that most identified proteins were enriched in metabolic pathways (17%), biosynthesis of antibiotics (15%), ribosomes (8%), and 29% succinylated protein were not enriched in the metabolic pathway category (**Figure 2D**). In this study, we found that 54 ribosomal proteins were succinylated, including 21 30S ribosomal proteins and 33 50S ribosomal proteins were related to translation processes. Interestingly, succinylation of ribosomal proteins was also found in *M. tuberculosis*, *A. hydrophila*, and *E. coli* (Colak et al., 2013; Xie et al., 2014; Yao et al., 2019).

The COG is a tool for genome-scale analysis of protein functions and evolution. In this study, COG analysis revealed that translation, ribosomal structure and biogenesis (134 succinylated proteins), amino acid transport and metabolism (97), posttranslational modification, protein turnover, chaperones (62), and general function prediction mechanisms (51), were significant (**Figure 3A**). Our results were consistent with previous succinyl-proteome studies conducted in *E. coli*, *M. tuberculosis*, *B. subtilis*, and *V. parahaemolyticus* (Colak et al., 2013; Kosono et al., 2015; Pan et al., 2015; Yang et al., 2015), which revealed that the majority of succinyl-proteins consisted of translation and metabolic proteins.

The domain is the structural basis of protein physiological function, thus in order to further identify the function associated with succinylation, the domain of the identified succinylated proteins were annotated. The results shown in **Figure 3B**, indicate enriched succinylated substrates with functional domains including NAD(P)-binding domain superfamily,

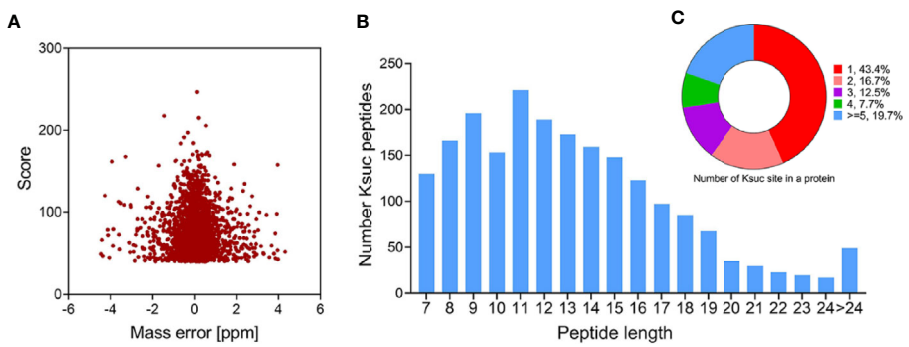

FIGURE 1 | Profile of *V. alginolyticus* lysine succinylation proteome. **(A)** Distributions of mass errors for lysine succinylated peptides. **(B)** Distribution of lysine succinylated peptides based on their length. **(C)** The pie chart shows the distribution of succinylation sites in each protein.

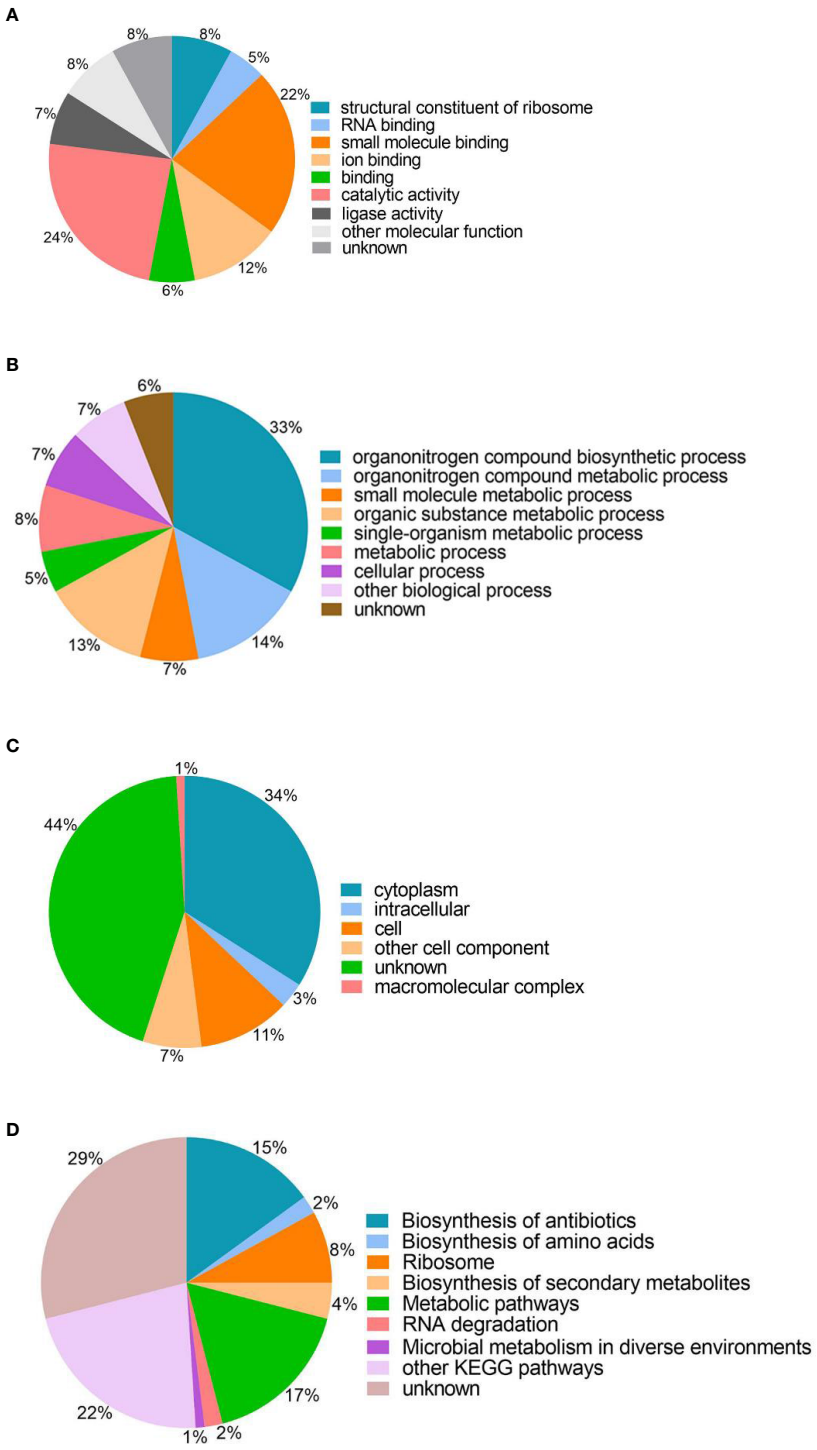

FIGURE 2 | Gene ontology functional classification and KEGG pathway analysis of the identified succinylated proteins. **(A)** Molecular function. **(B)** Biological processes. **(C)** Cell components. **(D)** KEGG pathway analysis.

nucleic acid-binding, OB-fold, NAD(P)-binding domain, and Rossmann-like alpha/beta/alpha sandwich fold, were the largest. In addition, 16 aminoacyl-tRNA synthetases and 9 ATP dependent proteases underwent succinylation, suggesting that succinylation modification may be involved in the protein synthesis and regulation of ATPase activity, which is consistent

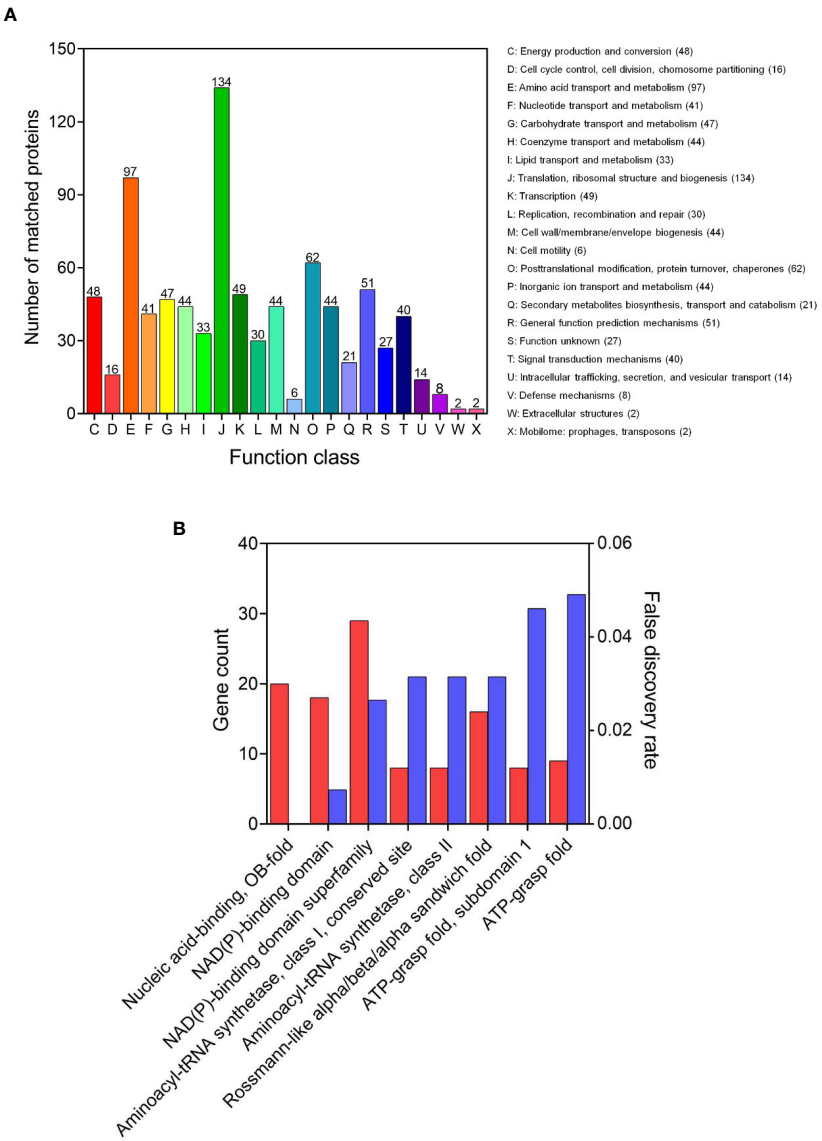

FIGURE 3 | Functional annotation of the lysine succinylome in *V. alginolyticus*. **(A)** The COG analysis and **(B)** domains enrichment analysis of the succinylated proteins.

with the succinylation observed in the fish pathogen *A. hydrophila* (Yao et al., 2019).

Motif of Succinylated Peptides in *V. alginolyticus*

We further evaluated the position-specific amino acid of succinylated peptides, using MoMo software to analyze the surrounding sequences (10 amino acids to both termini) of succinylated lysine sites in the *V. alginolyticus* succinylproteome (p-value <0.000001). The results showed that four conserved motifs were significantly over-represented around the lysine succinylation sites, which tended to have arginine (R) at position -7, lysine (K) at position -5, methionine (M) at position -2, and alanine (A) at position +1 (**Figure 4A**). The frequency of $K_{suc}A$ motif was the highest, $K_{(-5)}K_{suc}$ and $R_{(-7)}K_{suc}$ motif the second highest, and $M_{(-2)}K_{suc}$ motif the lowest (**Figure 4B**). Similar results were observed for the succinylome of *Deinococcus radiodurans* ($K_{(-5)}K_{suc}$ motif), *V. parahaemolyticus* and rice leaves ($R_{(-7)}K_{suc}$ motif), which suggests bacteria and plants may share common conserved motifs surrounding lysine succinylated sites (Pan et al., 2015; Zhou et al., 2018; Zhou et al., 2019). Then, when we compared our motifs to the reported succinylome of fish pathogens *A. hydrophila* and *V. parahaemolyticus*, the result found conserved motifs in arginine (R) and lysine (K), although the precise positions varied (Pan et al., 2015; Yao et al., 2019). Furthermore, we also found that the preference for alanine (A) at position +1 (KsucA motif) is a unique feature of a succinylated modified protein in *V. alginolyticus*.

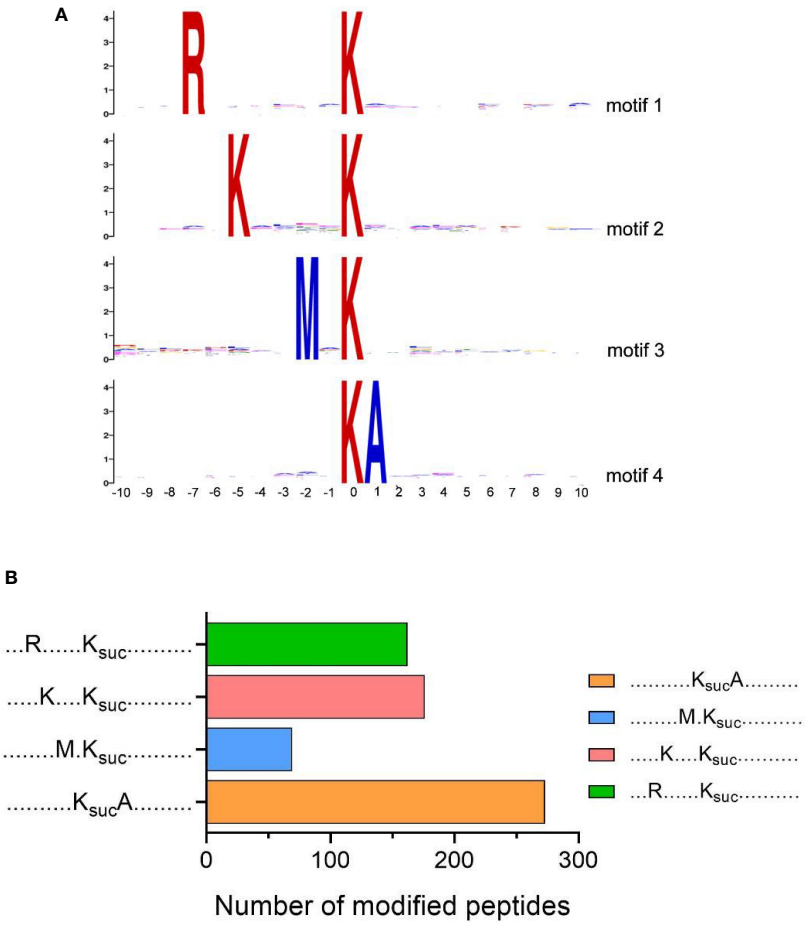

FIGURE 4 | Motif analysis of lysine succinylation sites. **(A)** Sequence logos of motifs (*P*-value <0.000001) identified by MoMo software. **(B)** Numbers of each identified motifs.

Validation of SodB and PEPCK Lysine-Succinylated Proteins Using Co-Immunoprecipitation and Western Blotting

To further validate the identified lysine-succinylated results, two Ksuc proteins (SodB and PEPCK) were selected and analyzed by Co-IP and Western blotting. The SodB and PEPCK proteins were captured by their respective antibodies and then Western blotting was performed with anti-succinylation and anti-target protein antibody, respectively (**Figure 5**). The results showed that SodB and PEPCK proteins exhibited succinylation modifications consistent with lysine-succinylated proteomic data, further validating our proteomics results.

Overlap Between Lysine Succinylation and Acetylation in *V. alginolyticus*

Previous studies have shown that there are various modifications in lysine residues, such as acetylation, succinylation, propionylation, formylation, ubiquitination (Yang and Seto, 2008). In our previous report on the acetylome of *V. alginolyticus* we identified 2,883 acetylated sites within 1,178 proteins. In order to determine whether succinylation and acetylation "crosstalk" occurs at the same lysine site, we compared the lysine succinylation data here to the previous acetylation data on post-translationally modified proteins and peptides (**Figures 6** and **7**). The comparison results showed that 502 proteins overlapped (**Figure 6A**), and further enrichment analysis of KEGG pathways was performed. Of the overlapped proteins, a total of 10 KEGG pathways are enriched, of which biosynthesis of antibiotics, ribosome, and metabolic pathways are dominant (**Figure 6B**). Among the 169 specific succinylated modified proteins alone, five KEGG pathways were enriched, mainly amino acid biosynthesis, ABC transporters, and cationic antimicrobial peptide (CAMP) resistance (**Figure 6C**), while in 676 specific acetylated modified proteins, were enriched in six KEGG pathways of which metabolic pathways, biosynthesis of amino acids and pyrimidine metabolism are predominant (**Figure 6D**). Further analysis showed that DNA binding protein RpoB included 28 K_{suc} sites and 6 K_{ace} sites, while fatty acid oxidation complex subunit alpha YfcX included 2 K_{suc} sites and 17 K_{ace} sites, suggested that there is a significant difference in the

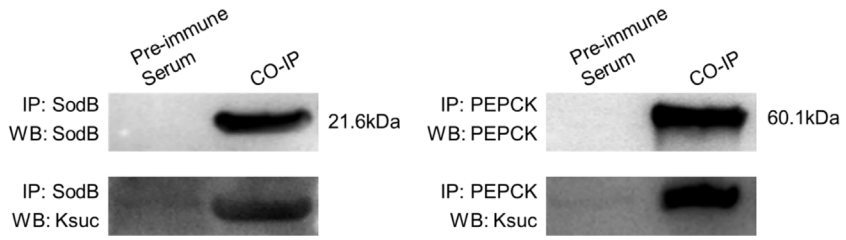

FIGURE 5 | Validation of SodB and PEPCK lysine-succinylated proteins in *V. alginolyticus* using Co-Immunoprecipitation and Western blotting. SodB and PEPCK proteins were enriched by Co-IP with specific antibodies, followed by Western blotting with SodB and PEPCK proteins specific antibodies (above), and Western blotting with anti-lysine succinylation antibodies (below).

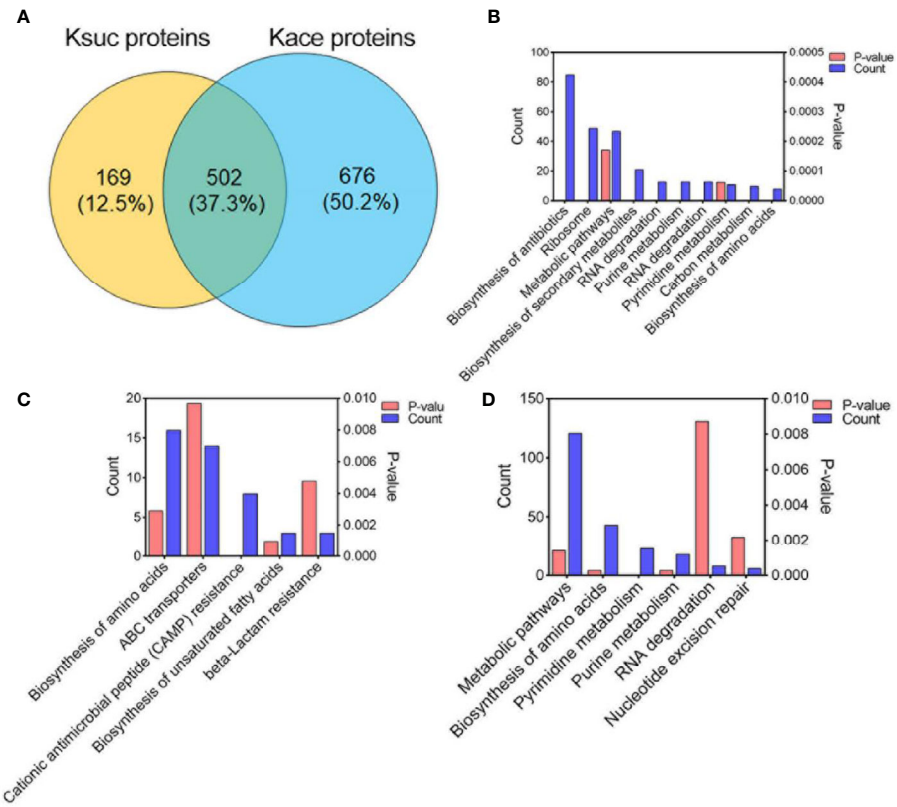

FIGURE 6 | Comparison of succinylated and acetylated proteins in *V. alginolyticus*. **(A)** Overlap between succinylated and acetylated proteins in *V. alginolyticus*. **(B–D)** KEGG pathway enrichment analysis of the overlapped proteins, specific succinylated modified proteins, and specific acetylated modified proteins.

number of acetylation and succinylation sites of the same modified protein.

At the peptide level, 1,005 peptides were overlapped, and 1,077 K_{suc}-specific peptides, and 1,878 K_{ace}-specific peptides were identified (**Figure 7**). The conserved motif analysis showed that the overlapped peptides were not enriched, but in K_{suc}-specific peptides one conserved motif was enriched in (GK_{suc} motif), and in K_{ace}-specific peptides eight conserved motifs were enriched including DK_{ace}, $LK_{ace}N(+3)$, $K_{ace}K(+4)$, $K_{ace}K(+3)$, $AK_{ace}K(+4)$, $K_{ace}L$, EK_{ace}, $EK_{ace}G(+9)$ motif, and EK_{ace} motif with the greatest enrichment.

Moreover, we illustrated the occurrence of lysine succinylation and acetylation in three central metabolic pathways: the glycolysis/gluconeogenesis, TCA cycle, and pyruvate metabolism. The results indicated that the enzymes in three pathways were acetylated (except for *frr* gene) and the majority of the enzymes were also found to be succinylated (except for *N646_2991*, *N646_2065*, *N646_3544*, *glnE*, and *oadB* genes) (**Figure 8**), our results are

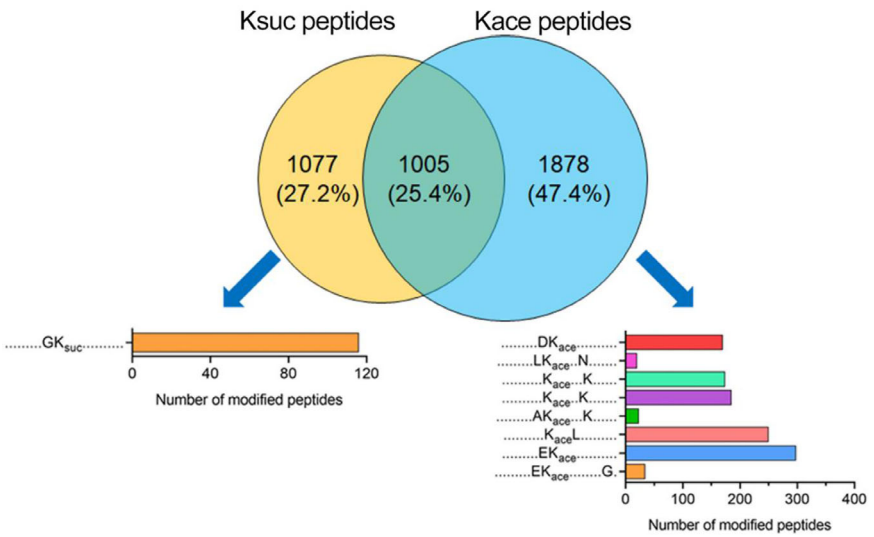

FIGURE 7 | Comparison of succinylation and acetylation peptides in *V. alginolyticus* Overlap between succinylated and acetylated peptides in *V. alginolyticus*, and motif analysis.

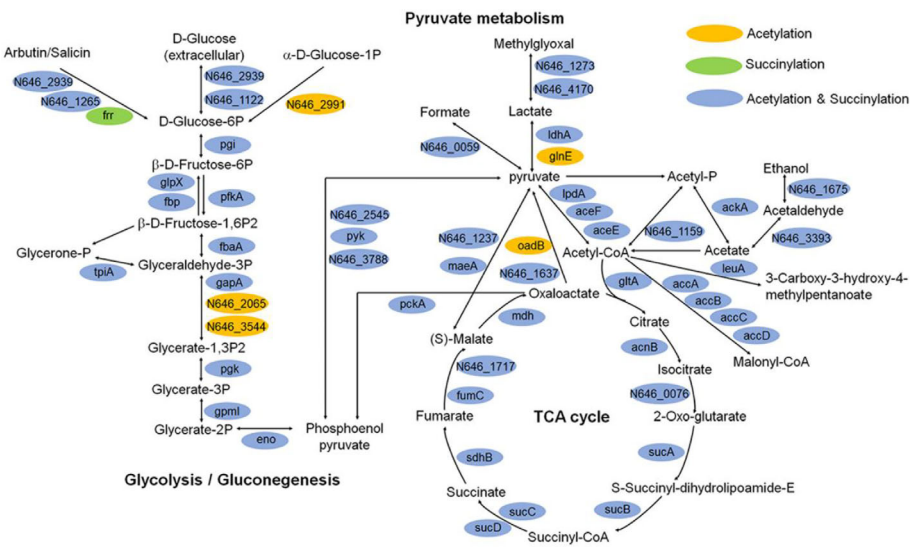

FIGURE 8 | Key enzymes with succinylation and acetylation modification in glycolysis/gluconeogenesis, TCA cycle, and pyruvate metabolism pathways.

similar with those obtained in others bacteria, such as *V. alginolyticus*, *A. hydrophila*, *Pseudomonas aeruginos*a (Pan et al., 2015; Gaviard et al., 2018; Sun et al., 2019). These results together reflect that the two types of lysine modification are highly enriched and widely overlapped in metabolism and ribosome related proteins (**Figures 6B** and **8**), suggesting that both types of modifications may play an important role in the regulation of cellular processes, especially in central metabolism and ribosome activity.

Virulence Factors of Succinylated Proteins in *V. alginolyticus*

V. alginolyticus is an important pathogen in aquaculture, which infects a variety of fish, shrimp and shellfish leading to great economic losses around the world, and also contributes to disease in humans inducing symptoms such as fever, nausea, diarrhea, and extra intestinal infections (Sasikala and Srinivasan, 2016; Yu et al., 2019). Previously, it has been reported that protein post-translational modification is closely related to

bacterial virulence, such as acetylation, succinylation, and phosphorylation (Whitmore and Lamont, 2012; Ren et al., 2017; Gaviard et al., 2019). Virulence factors (VFs) are the basis of pathogenicity of *V. alginolyticus*, so it is of great significance to study VFs. In this study, using online VFDB software analysis, we detected a total of 50 (7.45% of total K_{suc} proteins) succinylated VFs in *V. alginolyticus*, and the protein-protein interaction network among the 50 VFs proteins using online STRING database combined with Cytoscape software, showed that 40 proteins were found to interact (**Figure 9**). The results showed that VFs were enriched in the following pathways, including bacterial chemotaxis, the bacterial secretion system, TonB-dependent receptor family, and microbial metabolism in different environments, and previous reports have shown that these pathways are closely related to bacterial virulence (Wang et al., 2008; Goldberg et al., 2010; Kapitein and Mogk, 2013; Erhardt, 2016; Green and Mecsas, 2016; Guo et al., 2017).

Figure 9 showed that S-ribosylhomocystein lyase (LuxS) is a key enzyme in quorum sensing and has two Ksuc sites. Previous studies have found that this enzyme plays an important role in virulence (Coulthurst et al., 2004), and in *A. hydrophila* research it has been reported that LuxS exhibits cross-talk between lysine acetylation and succinylation, and Yao et al. research showed that the succinylation of lysines on LuxS at the K23 and K30 sites positively regulate the production of the quorum sensing autoinducer AI-2, and that these PTMs ultimately alter its competitiveness with *V. alginolyticus* (Sun et al., 2019; Yao et al., 2019). This study showed the succinylation of lysines on LuxS at the K29 and K45 sites. But whether they have the same function as LuxS in *A. hydrophila* remains to be further studied in *V. alginolyticus*.

In Gram-negative bacteria, the Sec system can transport a variety of proteins into the extracellular medium, including toxins and enzymes (Chatzi et al., 2013), which play an important role in bacterial virulence. In the Sec system SecA plays a central role in directing Sec-dependent transport, while SecE and SecY are membrane proteins that form a channel in the membrane which provides the core molecular machinery to direct secretion (Crane and Randall, 2017). Another Sec protein, YidC, is very important to *E. coli* survival and deletion of YidC will interfere with the insertion of Sec-dependent membrane proteins, thus affecting secretion processes of

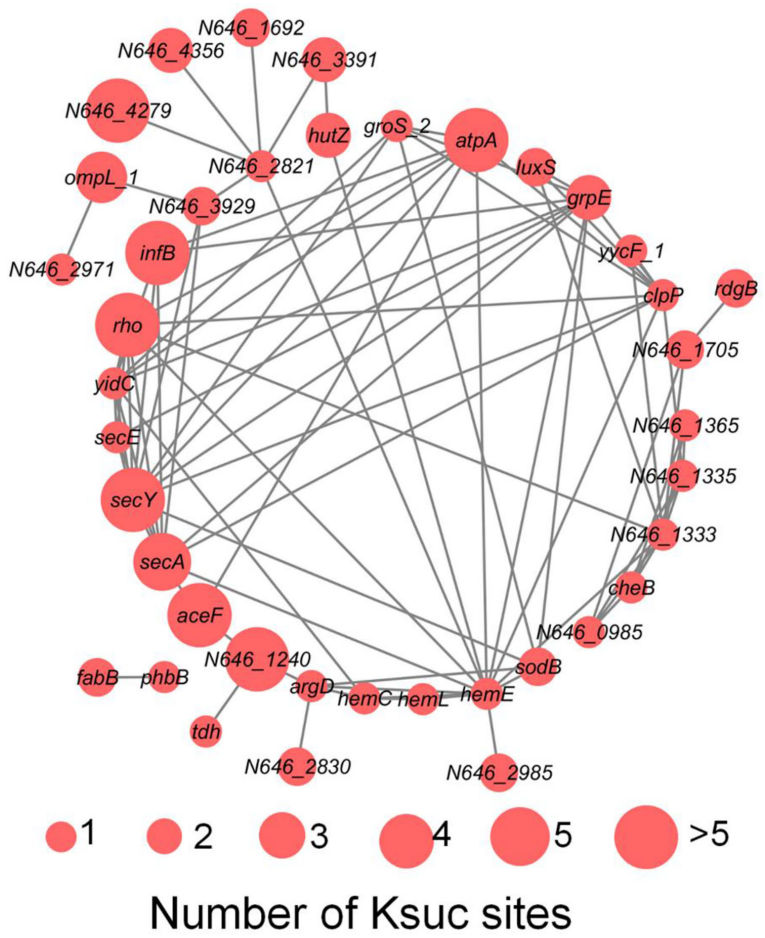

FIGURE 9 | The PPI network of succinylated virulence factors in *V. alginolyticus*. The size of the circle represents the number of Ksuc sites.

bacteria (Samuelson et al., 2000). In this study, we found that SecAEY and YidC proteins were succinylated, and SecA and SecY had five and six modification sites, respectively, indicating that succinylation modification plays a central role in the Sec system.

Other virulence factors such as *tdh*, *sodB*, *clpP* were also succinylated. *tdh* gene encodes thermostable direct hemolysin (TDH), which is a major virulence factor in *V. alginolytic*us (Avsever, 2016). Our previous research found that *sodb* and *clpp* genes are important virulence factors of *V. alginolyticus*, and deletion of those genes leads to reduction of bacterial virulence, suggesting they have potential application for the construction of live attenuated vaccines (Chen et al., 2019a; Chen et al., 2019b). Many virulence factors of *V. alginolyticus* were found to be succinylated in this study, indicating that lysine succinylation may play a crucial role in regulating the virulence of *V. alginolyticus*.

CONCLUSION

Vibrio alginolyticus is an opportunistic and halophilic Gram-negative pathogen, which impedes development of the aquaculture sector for some species of fish and affects human health. However, the intrinsic biological behavior of *V. alginolyticus* is largely unknown. Many studies have shown that succinylation of lysine within proteins is involved in the regulation of bacterial physiology and plays a major role in many biological processes. In this study we successfully identified a total of 2,082 succinylation sites matched with 671 proteins in *V. alginolyticus*. Of these 1,005 peptides and 502 proteins overlapped with acetylated proteins, indicating extensive overlap between these two PTMs, and these proteins were involved in glycolysis/gluconeogenesis, TCA cycle, and pyruvate metabolism. In conclusion, the succinylome of *V. alginolyticus* was analyzed for the first time revealing possible biological roles of lysine succinylated proteins, 7.5% of which were predicted to be virulence factors and may thus provide possible targets for the development of attenuated vaccines.

DATA AVAILABILITY STATEMENT

The mass spectrometry proteomics data have been deposited to the ProteomeXchange Consortium (http://proteomecentral.proteomexchange.org) *via* the iProX partner repository with the dataset identifier PXD023153.

AUTHOR CONTRIBUTIONS

HP and WL conceived the research project. FZ, YC, and HZ performed the experiments. WL, XL, and SR performed the data analysis. HP, WL, RH, SJM, XL and JJ interpret the data and discussed the results. WL wrote the manuscript. All authors contributed to the article and approved the submitted version.

ACKNOWLEDGMENTS

This work was sponsored by grants from Shenzhen Science and Technology Project (JCYJ20190813104207152 and JCYJ20170818111629778), NSFC projects (Nos. 32073015, 31670129, and 31802343), Southern Marine Science and Engineering Guangdong Laboratory (Zhan jiang) (No. ZJW-2019-06). The author SR thankfully acknowledges China Post-doctoral Science Foundation for the financial support to carry out the Post-doctoral research work (Grant No. 2019M662214). We also thank Novogene Co., Ltd. for the technical support.

SUPPLEMENTARY MATERIAL

The Supplementary Material for this article can be found online at: https://www.frontiersin.org/articles/10.3389/fcimb.2020.626574/full#supplementary-material

Supplementary Table 1 | The identified succinylated proteins and sites in *V. alginolyticus*.

Supplementary Table 2 | The identified succinylated peptides in *V. alginolyticus*.

REFERENCES

Avison, M. B., Bennett, P. M., Howe, R. A., and Walsh, T. R. (2002). Preliminary analysis of the genetic basis for vancomycin resistance in *Staphylococcus aureus* strain Mu50. *J. Antimicrob. Chemother.* 49, 255–260. doi: 10.1093/jac/49.2.255

Avsever, M. L. (2016). First report of *trh* positive *Vibrio alginolyticus* isolates from bivalve molluscs in Turkey. *Rev. Med. Vet.* 167, 65–70.

Cai, S. H., Wu, Z. H., Jian, J. C., and Lu, Y. S. (2007). Cloning and expression of gene encoding the thermostable direct hemolysin from *Vibrio alginolyticus* strain HY9901, the causative agent of vibriosis of crimson snapper (*Lutjanus erythopterus*). *J. Appl. Microbiol.* 103, 289–296. doi: 10.1111/j.1365-2672.2006.03250.x

Chatzi, K. E., Sardis, M. F., Karamanou, S., and Economou, A. (2013). Breaking on through to the other side: protein export through the bacterial Sec system. *Biochem. J.* 449, 25–37. doi: 10.1042/BJ20121227

Chen, Y. Y., Wu, F. L., Pang, H. Y., Tang, J. F., Cai, S., Cai, S. H., et al. (2019a). Superoxide dismutase B (*sodB*), an important virulence factor of *Vibrio alginolyticus*, contributes to antioxidative stress and its potential application for live attenuated vaccine. *Fish Shellfish Immunol.* 89, 354–360. doi: 10.1016/j.fsi.2019.03.061

Chen, Y. Y., Wu, F. L., Wang, Z. W., Tang, J. F., Cai, S. H., and Jian, J. C. (2019b). Construction and evaluation of *Vibrio alginolyticus ΔclpP* mutant, as a safe live attenuated vibriosis vaccine. *Fish Shellfish Immunol.* 98, 917–922. doi: 10.1016/j.fsi.2019.11.054

Cheng, A., Grant, C. E., Bailey, T. L., and Noble, W. S. (2017). MoMo: Discovery of post-translational modification motifs. *BioRxiv* 153882. doi: 10.1101/153882

Cheng, Z. X., Guo, C., Chen, Z. G., Yang, T. C., Zhang, J. Y., Wang, J., et al. (2019). Glycine, serine and threonine metabolism confounds efficacy of complement-mediated killing. *Nat. Commun.* 10, 3325. doi: 10.1038/s41467-019-11129-5

Colak, G., Xie, Z. Y., Zhu, A. Y., Dai, L. Z., Lu, Z. K., Zhang, Y., et al. (2013). Identification of lysine succinylation substrates and the succinylation regulatory enzyme CobB in *Escherichia coli*. *Mol. Cell. Proteomics* 12, 3509–3520. doi: 10.1074/mcp.M113.031567

Coulthurst, S. J., Kurz, C. L., and Salmond, G. P. C. (2004). *luxS* mutants of *Serratia* defective in autoinducer-2-dependent 'quorum sensing' show

strain-dependent impacts on virulence and production of carbapenem and prodigiosin. *Microbiology* 150, 1901–1910. doi: 10.1099/mic.0.26946-0

Crane, J. M., and Randall, L. L. (2017). The Sec system: protein export in *Escherichia coli*. *Ecosal Plus* 7:10. doi: 10.1128/ecosalplus.ESP-0002-2017

Dan, G., Zhang, J., Hao, Y., Xu, R. J., Zhang, Y. X., Ma, Y., et al. (2019). Alternative sigma factor RpoX is a part of RpoE regulon and plays distinct roles in stress response, motility, biofilm formation and hemolytic activities in the marine pathogen *Vibrio alginolyticus*. *Appl. Environ. Microbiol.* 85, e00234–e00219. doi: 10.1128/AEM.00234-19

Echazarreta, M. A., and Klose, K. E. (2019). *Vibrio* flagellar synthesis. *Front. Cell. Infect. Microbiol.* 9, 131. doi: 10.3389/fcimb.2019.00131

Erhardt, M. (2016). Strategies to block bacterial pathogenesis by interference with motility and chemotaxis. *Curr. Top. Microbiol. Immunol.* 398, 185–205. doi: 10.1007/82_2016_493

Feng, S. G., Jiao, K. L., Guo, H., Jiang, M. Y., Hao, J., Wang, H. Z., et al. (2017). Succinyl-proteome profiling of *Dendrobium officinale*, an important traditional Chinese orchid herb, revealed involvement of succinylation in the glycolysis pathway. *BMC Genomics* 18, 598. doi: 10.1186/s12864-017-3978-x

Ferrini, A. M., Mannoni, V., Suffredini, E., Cozzi, L., and Croci, L. (2008). Evaluation of antibacterial resistance in *Vibrio* strains isolated from imported seafood and Italian aquaculture settings. *Food Anal. Methods* 1, 164–170. doi: 10.1007/s12161-007-9011-2

Gaviard, C., Broutin, I., Cosette, P., De, E., Jouenne, T., and Hardouin, J. (2018). Lysine succinylation and acetylation in *Pseudomonas aeruginosa*. *J. Proteome Res.* 17, 2449–2459. doi: 10.1021/acs.jproteome.8b00210

Gaviard, C., Cosette, P., Jouenne, T., and Hardouin, J. (2019). LasB and CbpD virulence factors of *Pseudomonas aeruginosa* carry multiple post-translational modifications on their lysine residues. *J. Proteome Res.* 18, 923–933. doi: 10.1021/acs.jproteome.8b00556

Goldberg, M. B., Boyko, S. A., Butterton, J. R., Stoebner, J. A., and Calderwood, S. B. (2010). Characterization of a *Vibrio cholerae* virulence factor homologous to the family of TonB-dependent proteins. *Mol. Microbiol.* 6, 2407–2418. doi: 10.1111/j.1365-2958.1992.tb01415.x

Green, E. R., and Mecsas, J. (2016). Bacterial secretion systems: an overview. *Microbiol. Spectr.* 4, 213–239. doi: 10.1128/microbiolspec.VMBF-0012-2015

Guo, M. L., Huang, Z. W., and Yang, J. (2017). Is there any crosstalk between the chemotaxis and virulence induction signaling in *Agrobacterium tumefaciens*? *Biotechnol. Adv.* 35, 505–511. doi: 10.1016/j.biotechadv.2017.03.008

He, D. L., Wang, Q., Li, M., Damaris, R. N., Yi, X. L., Cheng, Z. Y., et al. (2016). Global proteome analyses of lysine acetylation and succinylation reveal the widespread involvement of both modification in metabolism in the embryo of germinating rice seed. *J. Proteome Res.* 15, 879–890. doi: 10.1021/acs.jproteome.5b00805

Hernández-Robles, M. F., lvarez-Contreras, A. K., Juárez-García, P., Natividad-Bonifacio, I., Curiel-Quesada, E., Vázquez-Salinas, C., et al. (2016). Virulence factors and antimicrobial resistance in environmental strains of *Vibrio alginolyticus*. *Int. Microbiol.* 19, 191–198. doi: 10.2436/20.1501.01.277

Horii, T., Morita, M., Muramatsu, H., Monji, A., Miyagishima, D., Kanno, T., et al. (2005). Antibiotic resistance in *Aeromonas hydrophila* and *vibrio alginolyticus* isolated from a wound infection: a case report. *J. Trauma* 58, 196–200. doi: 10.1097/01.ta.0000066381.33339.c0

Huang, L. X., Xu, W., Su, Y. Q., Zhao, L. M., and Yan, Q. P. (2018). Regulatory role of the RstB-RstA system in adhesion, biofilm production, motility, and hemolysis. *MicrobiologyOpen* 7, e00599. doi: 10.1002/mbo3.599

Jin, W. B., and Wu, F. L. (2016). Proteome-wide identification of lysine succinylation in the proteins of Tomato (*Solanum lycopersicum*). *PloS One* 11, e0147586. doi: 10.1371/journal.pone.0147586

Kapitein, N., and Mogk, A. (2013). Deadly syringes: type VI secretion system activities in pathogenicity and interbacterial competition. *Curr. Opin. Microbiol.* 16, 52–58. doi: 10.1016/j.mib.2012.11.009

Komine-Abe, A., Nagano-Shoji, M., Kubo, S., Kawasaki, H., Yoshida, M., Nishiyama, M., et al. (2017). Effect of lysine succinylation on the regulation of 2-oxoglutarate dehydrogenase inhibitor, OdhI, involved in glutamate production in *Corynebacterium glutamicum*. *Biosci. Biotechnol. Biochem.* 81, 2130–2138. doi: 10.1080/09168451.2017.1372182

Kosono, S., Tamura, M., Suzuki, S., Kawamura, Y., Yoshida, A., Nishiyama, M., et al. (2015). Changes in the acetylome and succinylome of *Bacillus subtilis* in response to carbon source. *PloS One* 10, e0131169. doi: 10.1371/journal.pone.0131169

Li, X. L., Hu, X., Wan, Y. J., Xie, G. Z., Li, X. Z., Chen, D., et al. (2014). Systematic identification of the lysine succinylation in the protozoan parasite *Toxoplasma gondii*. *J. Proteome Res.* 13, 6087–6095. doi: 10.1021/pr500992r

Nadine, P., Serge, G., and Yang, X. J. (2017). Assays for acetylation and other acylations of lysine residues. *Curr. Protoc. Protein Sci.* 87, 1–18. doi: 10.1002/cpps.26

Pan, J. Y., Chen, R., Li, C. C., Li, W. Y., and Ye, Z. C. (2015). Global analysis of protein lysine succinylation profiles and their overlap with lysine acetylation in the marine bacterium *Vibrio parahemolyticus*. *J. Proteome Res.* 14, 4309–4318. doi: 10.1021/acs.jproteome.5b00485

Pang, H. Y., Li, W. X., Zhang, W. J., Zhou, S. H., Hoare, R., Monaghan, S. J., et al. (2020). Acetylome profiling of *Vibrio alginolyticus* reveals its role in bacterial virulence. *J. Proteomics* 211, 103543. doi: 10.1016/j.jprot.2019.103543

Ren, J., Sang, Y., Lu, J., and Yao, Y. F. (2017). Protein acetylation and its role in bacterial virulence. *Trends Microbiol.* 25, 768–779. doi: 10.1016/j.tim.2017.04.001

Ribet, D., and Cossart, P. (2010). Pathogen-mediated posttranslational modifications: a re-emerging field. *Cell* 143, 694–702. doi: 10.1016/j.cell.2010.11.019

Samuelson, J. C., Chen, M. Y., Jiang, F. L., Möller, I., and Dalbey, R. E. (2000). YidC mediates membrane protein insertion in bacteria. *Nature* 406, 637–641. doi: 10.1038/35020586

Santhakumari, S., Nilofernisha, N. M., Ponraj, J. G., Pandian, S. K., and Ravi, A. V. (2017). In vitro and in vivo exploration of palmitic acid from *Synechococcus elongatus* as an antibiofilm agent on the survival of Artemia franciscana against virulent vibrios. *J. Invertebr. Pathol.* 150, 21–31. doi: 10.1016/j.jip.2017.09.001

Sasikala, D., and Srinivasan, P. (2016). Characterization of potential lytic bacteriophage against *Vibrio alginolyticus* and its therapeutic implications on biofilm dispersal. *Microb. Pathog.* 101, 24–35. doi: 10.1016/j.micpath.2016.10.017

Song, Y. X., Wang, J., Cheng, Z. Y., Gao, P., Sun, J. X., Chen, X. W., et al. (2017). Quantitative global proteome and lysine succinylome analyses provide insights into metabolic regulation and lymph node metastasis in gastric cancer. *Sci. Rep.* 7, 42053. doi: 10.1038/srep42053

Sun, L. N., Yao, Z. J., Guo, Z., Zhang, L. S., Wang, Y. Q., Mao, R. R., et al. (2019). Comprehensive analysis of the lysine acetylome in *Aeromonas hydrophila* reveals cross-talk between lysine acetylation and succinylation in LuxS. *Emerg. Microbes Infect.* 8, 1229–1239. doi: 10.1080/22221751.2019.1656549

Wang, Q. Y., Liu, Q., Cao, X. D., Yang, M. J., and Zhang, Y. X. (2008). Characterization of two TonB systems in marine fish pathogen *Vibrio alginolyticus*: their roles in iron utilization and virulence. *Arch. Microbiol.* 190, 595–603. doi: 10.1007/s00203-008-0407-1

Wang, Y. Q., Wang, X. Y., Ali, F., Li, Z. Q., Fu, Y. Y., Yang, X. J., et al. (2019). Comparative extracellular proteomics of *Aeromonas hydrophila* reveals iron-regulated secreted proteins as potential vaccine candidates. *Front. Immunol.* 10, 256. doi: 10.3389/fimmu.2019.00256

Weinert, B. T., Schölz, C., Wagner, S. A., Iesmantavicius, V., Su, D., Daniel, J. A., et al. (2013). Lysine succinylation is a frequently occurring modification in prokaryotes and eukaryotes and extensively overlaps with acetylation. *Cell Rep.* 4, 842–851. doi: 10.1016/j.celrep.2013.07.024

Whitmore, S. E., and Lamont, R. J. (2012). Tyrosine phosphorylation and bacterial virulence. *Int. J. Oral. Sci.* 4, 1–6. doi: 10.1038/ijos.2012.6

Wu, L., Gong, T., Zhou, X. D., Zeng, J. M., Huang, R. J., Wu, Y. F., et al. (2019). Global analysis of lysine succinylome in the periodontal pathogen *Porphyromonas gingivalis*. *Mol. Oral. Microbiol.* 34, 74–83. doi: 10.1111/omi.12255

Xie, L. X., Liu, W., Li, Q. M., Chen, S. D., Xu, M. M., Huang, Q. Q., et al. (2014). First succinyl-proteome profiling of extensively drug-resistant *Mycobacterium tuberculosis* revealed involvement of succinylation in cellular physiology. *J. Proteome Res.* 14, 107–109. doi: 10.1021/pr500859a

Xie, L. X., Li, J., Deng, W. Y., Yu, Z. X., Fang, W. J., Chen, M., et al. (2017). Proteomic analysis of lysine succinylation of the human pathogen *Histoplasma capsulatum*. *J. Proteomics* 154, 109–117. doi: 10.1016/j.jprot.2016.12.020

Xiong, X. P., Wang, C., Ye, M. Z., Yang, T. C., Peng, X. X., and Li, H. (2010). Differentially expressed outer membrane proteins of *Vibrio alginolyticus* in response to six types of antibiotics. *Mar. Biotechnol.* 12, 686–695. doi: 10.1007/s10126-009-9256-4

Xu, H., Chen, X. Y., Xu, X. L., Shi, R. Y., Suo, S. S., Cheng, K. Y., et al. (2016). Lysine acetylation and succinylation in HeLa cells and their essential roles in response to UV-induced stress. *Sci. Rep.* 6, 30212. doi: 10.1038/srep30212

Yang, M. K., Wang, Y., Chen, Y., Cheng, Z. Y., Gu, J., Deng, J. Y., et al. (2015). Succinylome analysis reveals the involvement of lysine succinylation in metabolism in pathogenic *Mycobacterium tuberculosis*. *Mol. Cell. Proteomics* 14, 796–811. doi: 10.1074/mcp.M114.045922

Yang, X. J., and Seto, E. (2008). Lysine acetylation: codified crosstalk with other posttranslational modifications. *Mol. Cell* 31, 449–461. doi: 10.1016/j.molcel.2008.07.002

Yao, Z. J., Guo, Z., Wang, Y. Q., Li, W. X., Fu, Y. Y., Lin, Y. X., et al. (2019). Integrated succinylome and metabolome profiling reveals crucial role of S-ribosylhomocysteine lyase in quorum sensing and metabolism of *Aeromonas hydrophila*. *Mol. Cell. Proteomics* 18, 200–215. doi: 10.1074/mcp.RA118.001035

Yu, Q., Liu, M. Z., Su, H. F., Xiao, H. H., Wu, S. T., Qin, X. L., et al. (2019). Selection and characterization of ssDNA aptamers specifically recognizing pathogenic *Vibrio alginolyticus*. *J. Fish Dis.* 42, 851–858. doi: 10.1111/jfd.12985

Zhang, Z. H., Tan, M. J., Xie, Z. Y., Dai, L. Z., Chen, Y., and Zhao, Y. M. (2011). Identification of lysine succinylation as a new post-translational modification. *Nat. Chem. Biol.* 7, 58–63. doi: 10.1038/nchembio.495

Zhang, Y. M., Wang, G. Y., Song, L. M., Mu, P., Wang, S., Liang, W. X., et al. (2017). Global analysis of protein lysine succinylation profiles in common wheat. *BMC Genomics* 18, 1–10. doi: 10.1186/s12864-017-3698-2

Zheng, H. L., He, Y., Zhou, X. W., Qian, G. Y., Lv, G. X., Shen, Y. N., et al. (2016). Systematic analysis of the lysine succinylome in *Candida albicans*. *J. Proteome Res.* 15, 3793–3801. doi: 10.1021/acs.jproteome.6b00578

Zheng, Z. W., Ye, L. W., Chan, E. W. C., and Chen, S. (2019). Identification and characterization of a conjugative bla VIM-1-bearing plasmid in *Vibrio alginolyticus* of food origin. *J. Antimicrob. Chemother.* 74, 1842–1847. doi: 10.1093/jac/dkz140

Zhou, H., Finkemeier, I., Guan, W. X., Tossounian, M., Wei, B., Young, D., et al. (2018). Oxidative stress-triggered interactions between the succinyl- and acetyl-proteomes of rice leaves. *Plant Cell Environ.* 41, 1139–1153. doi: 10.1111/pce.13100

Zhou, C. L., Dai, J. L., Lu, H. Z., Chen, Z. J., Guo, M., He, Y., et al. (2019). Succinylome analysis reveals the involvement of lysine succinylation in the extreme resistance of *Deinococcus radiodurans*. *Proteomics* 19, e1900158. doi: 10.1002/pmic.201900158

Conflict of Interest: The authors declare that the research was conducted in the absence of any commercial or financial relationships that could be construed as a potential conflict of interest.

frontiers in Cellular and Infection Microbiology

ORIGINAL RESEARCH
published: 26 February 2021
doi: 10.3389/fcimb.2021.637019

Biochemical and Virulence Characterization of *Vibrio vulnificus* Isolates From Clinical and Environmental Sources

Keri A. Lydon[1], *Thomas Kinsey*[1], *Chinh Le*[2], *Paul A. Gulig*[2] *and Jessica L. Jones*[1]*

[1] Division of Seafood Science and Technology, Gulf Coast Seafood Laboratory, U.S. Food and Drug Administration, Dauphin Island, AL, United States, [2] Department of Molecular Genetics and Microbiology, University of Florida, Gainesville, FL, United States

OPEN ACCESS

Edited by:
Lixing Huang,
Jimei University, China

Reviewed by:
Youyu Zhang,
Xiamen University, China
Wei Xu,
State Oceanic Administration, China

***Correspondence:**
Jessica L. Jones
jessica.jones@fda.hhs.gov

Specialty section:
This article was submitted to Molecular Bacterial Pathogenesis, a section of the journal Frontiers in Cellular and Infection Microbiology

Received: *02 December 2020*
Accepted: *19 January 2021*
Published: *26 February 2021*

Citation:
Lydon KA, Kinsey T, Le C, Gulig PA and Jones JL (2021) Biochemical and Virulence Characterization of Vibrio vulnificus *Isolates From Clinical and Environmental Sources. Front. Cell. Infect. Microbiol. 11:637019. doi: 10.3389/fcimb.2021.637019*

Vibrio vulnificus is a deadly human pathogen for which infections occur *via* seafood consumption (foodborne) or direct contact with wounds. Virulence is not fully characterized for this organism; however, there is evidence of biochemical and genotypic correlations with virulence potential. In this study, biochemical profiles and virulence genotype, based on 16S rRNA gene (*rrn*) and virulence correlated gene (*vcg*) types, were determined for 30 clinical and 39 oyster isolates. Oyster isolates were more biochemically diverse than the clinical isolates, with four of the 20 tests producing variable (defined as 20–80% of isolates) results. Whereas, for clinical isolates only mannitol fermentation, which has previously been associated with virulence potential, varied among the isolates. Nearly half (43%) of clinical isolates were the more virulent genotype (*rrn*B/*vcg*C); this trend was consistent when only looking at clinical isolates from blood. The majority (64%) of oyster isolates were the less virulent genotype (*rrn*A or AB/*vcg*E). These data were used to select a sub-set of 27 isolates for virulence testing with a subcutaneously inoculated, iron-dextran treated mouse model. Based on the mouse model data, 11 isolates were non-lethal, whereas 16 isolates were lethal, indicating a potential for human infection. Within the non-lethal group there were eight oyster and three clinical isolates. Six of the non-lethal isolates were the less virulent genotype (*rrn*A/*vcg*E or *rrn*AB/*vcg*E) and two were *rrn*B/*vcg*C with the remaining two of mixed genotype (*rrn*AB/*vcg*C and *rrn*B/*vcg*E). Of the lethal isolates, five were oysters and 11 were clinical. Eight of the lethal isolates were the less virulent genotype and seven the more virulent genotype, with the remaining isolate a mixed genotype (*rrn*A/*vcg*C). A discordance between virulence genotype and individual mouse virulence parameters (liver infection, skin infection, skin lesion score, and body temperature) was observed; the variable most strongly associated with mouse virulence parameters was season (warm or cold conditions at time of strain isolation), with more virulent strains isolated from cold

conditions. These results indicate that biochemical profiles and genotype are not significantly associated with virulence potential, as determined by a mouse model. However, a relationship with virulence potential and seasonality was observed.

Keywords: *Vibrio*, mouse model, mannitol, virulence, 16S rDNA, season

INTRODUCTION

Vibrio vulnificus is a gram-negative opportunistic pathogen that is naturally found in shellfish and coastal brackish waters in warmer climates (Kaspar and Tamplin, 1993; Nilsson et al., 2003). It causes gastroenteritis, wound infections, or septicemia (Blake et al., 1979; Hlady and Klontz, 1996) through two primary routes: 1) consumption of raw shellfish, primarily oysters, and 2) exposure of open wounds to *V. vulnificus* (Shapiro et al., 1998; Oliver and Kaper, 2001). This bacterium is the deadliest foodborne pathogen with a case fatality rate greater than 30% (Hlady and Klontz, 1996; Shapiro et al., 1998; Scallan et al., 2011). Moreover, individuals who are immunocompromised have the greatest risk of mortality due to increased risk of sepsis (Strom and Paranjpye, 2000; Haq and Dayal, 2005). Although this pathogen has a low rate of infection (Strom and Paranjpye, 2000), it is important to investigate methods to evaluate the virulence potential of strains due to the severity of illness and high case fatality rate. Existing strategies to evaluate and mitigate the risks associated with *V. vulnificus* focus on the total population of the pathogen. However, there is evidence that not all strains have an equal potential to cause disease in humans, and identification of reliable markers of virulent populations would permit refinement of risk assessment models and mitigation efforts.

Biotyping and genetic markers are currently used to classify the virulence potential of *V. vulnificus*. There are three biotypes, defined by biochemical profiles, associated with virulence potential based on host specificity. Biotype 1 is associated with human infections (Warner and Oliver, 2008). Biotype 2 is associated with infections in eels and occasionally in humans (Veenstra et al., 1993; Amaro and Biosca, 1996). While biotype 3 has only been associated with wound infections of fish handlers (Bisharat et al., 1999). In addition, there are genetic markers used to subtype, primarily biotype 1, *V. vulnificus* isolates, which were developed based on source of strain isolation: clinical (*i.e.*, from an ill individual) or environmental (*e.g.*, shellfish, harvest water, etc.) (Nilsson et al., 2003). Rosche et al. (2005) identified two variants of the virulence correlated gene (*vcg*) which correlated with isolation source: clinical (*vcg*C) or environmental (*vcg*E). Additionally, an evaluation of the 16S rRNA gene (*rrn*) polymorphic variants identified two types, with *rrn*A primarily associated with environmental isolates and *rrn*B associated with clinical isolates (Nilsson et al., 2003; Vickery et al., 2007). The *vcg* and *rrn* genetic markers are often complementary to one another, with *rrn*B and *vcg*C most often identified in clinical isolates, and *rrn*A and *vcg*E genotypes appearing most often in environmental isolates (Han et al., 2009). Based on these strong associations between isolate source and gene variants, the genotype *rrn*A/*vcg*E is generally assumed to be less virulent, whereas *rrn*B/*vcg*C type strains are assumed to be more virulent (Jones et al., 2013). In addition, mannitol fermentation has been associated with the *rrn*B genotype (Drake et al., 2010), indicating this as a potential biochemical marker of virulence potential.

Subtyping and genotyping assays have served as a proxy for virulence potential based on the presumption that isolates from a clinical source are likely more virulent than environmental isolates, which has been largely supported in an animal model (Starks et al., 2000; DePaola et al., 2003). A subcutaneously (s.c.) inoculated iron-dextran treated mouse model has been used to evaluate virulence potential in *V. vulnificus* (Starks et al., 2000; DePaola et al., 2003; Thiaville et al., 2011). This model has revealed systemic infection and mortality presenting more often in mice injected with clinical strains (DePaola et al., 2003), while environmental strains appear to grow slower or are more easily attenuated by the mouse host (Starks et al., 2006). Thiaville et al. (2011) was one of the first studies that measured how virulence potential, as determined by the mouse model, relates to strain genotype on a large scale; however, the strain set selected for this study was somewhat limited, with oyster isolates from warmer months underrepresented. The study identified five virulence clusters associated with differing severity on type of mouse infection. Strains that caused systemic infection (liver) following skin infection were considered potentially lethal to humans, while less virulent strains (non-lethal) caused primarily skin infections. The study concluded that while *vcg*C was associated with virulence potential, it was not predictive of virulence in biotype 1 V. *vulnificus* strains (Thiaville et al., 2011). For example, some of the most virulent strains were of the *vcg*E genotype. Mouse models are not ideal assays due to resource and time requirements, as well as the ethical considerations; however, they remain the current gold standard for evaluating *V. vulnificus* virulence (Starks et al., 2000).

Previous studies have assumed that isolate source (*i.e.*, clinical or environmental/food) is a reliable proxy for *V. vulnificus* virulence, but without specific testing they are intrinsically biased to that assumption. Investigations into the relationship of genotype and virulence potential, as measured in a mouse model, are limited by the number and diversity of the isolates examined. Most of the clinical isolates used in previous studies (Nilsson et al., 2003; DePaola et al., 2003; Vickery et al., 2007; Thiaville et al., 2011) were isolated in warm months (May–September), when most infections occur; however, the majority of environmental isolates for these studies were obtained from cooler months (October–April). Regardless, these studies indicate a relationship with (DePaola et al., 2003), but lack the predictive power to interpolate virulence potential from a common virulence genotypes (Thiaville et al., 2011). This

raises questions about the utility of these existing typing schemes. Therefore, the current study aims to further investigate the relationship of genotype and virulence potential by utilizing a geographically and seasonally diverse set of *V. vulnificus* isolates. This isolate set was examined for partial biochemical profiles (API 20E), *rrn* and *vcg* genotypes, and virulence potential as determined through the s.c. inoculated iron-dextran treated mouse model, in order to determine if an association exists between virulence potential, biochemical phenotype, genotype, isolate source, and season of isolation.

MATERIALS AND METHODS

Vibrio vulnificus Isolates Included in This Study

A total of 69 V. *vulnificus* isolates were selected for this study. All *V. vulnificus* were isolated in 2006–2007 from various parts of the United States. Of these, 30 were isolated from ill patients as part of the Cholera and Other Vibrio Illness Surveillance (COVIS) program and were contributed by the Centers for Disease Control and Prevention (**Table 1**) and 39 were isolated from retail level raw oysters [**Table 2**; (DePaola et al., 2010)]. All isolates were purified and confirmed as *V. vulnificus* by real-time PCR as previously described (Kinsey et al., 2015). Isolates were stored in TSB + 30% glycerol at −80°C.

Biochemical Characterization of Isolates

To evaluate partial biochemical profiles of the *V. vulnificus* isolates, API 20E (BioMerieux, Durham, NC) test strips were used according to the manufacturer's protocol, except that 2% NaCl was used for cell suspensions (Kaysner et al., 2004; Martinez-Urtaza et al., 2005). Oxidase tests were completed using Dry Slides (BBL, Difco, Sparks, MD). API 20E results were entered into the manufacturer's database for identification.

Determination of *vcg* and *rrn* Genotypes

Isolates were streaked from frozen stocks to Tryptic Soy Agar (TSA; Difco) to confirm purity. A single colony was transferred to Tryptic Soy Broth (TSB; Remel, Atlanta, GA) and incubated at 35 ± 2°C for 18–24 h. One ml of the overnight culture was transferred to a microfuge tube and heated at 95–100°C for 10 min to produce a crude DNA lysate, which was used as template in subsequent real-time PCR assays. Isolate genotypes were determined using qualitative real-time PCR assays as previously described for 16S rRNA (*rrn*) gene type A or B (Vickery et al., 2007) and virulence correlated gene (*vcg*) type C or E (Drake et al., 2010) on a SmartCycler II System (Cepheid, Sunnyvale, CA). Results were

TABLE 1 | Clinical *Vibrio vulnificus* isolates.

Isolate ID	Month of Isolation	Reporting Date	Reporting State	Source
CDC_K4567	Jul	2006	HI	CLINICAL; OTHER
CDC_K4574	Nov	2006	HI	BLOOD
CDC_K4633	Dec	2006	OH	BLOOD
CDC_K4712	unknown	Unknown	RI	CLINICAL; UNKNOWN
CDC_K4767	Aug	2006	VA	BLOOD
CDC_K4776	Jul	2006	AL	CLINICAL; OTHER
CDC_K5008	Apr	2007	MS	BLOOD
CDC_K5041	Apr	2007	TX	BLOOD
CDC_K5056	May	2007	TX	BLOOD
CDC_K5057	May	2007	TX	BLOOD
CDC_K5060	May	2007	GA	BLOOD
CDC_K5148	Jun	2007	MS	BLOOD
CDC_K5204-LT	Jun	2007	TX	BLOOD
CDC_K5287*	May	2007	HI	BLOOD
CDC_K5326	May	2007	VA	BLOOD
CDC_K5616	Jul	2007	NY	BLOOD
CDC_K5327	Jul	2007	VA	CLINICAL; OTHER
CDC_K5333	May	2007	TX	CLINICAL; OTHER
CDC_K5338	Aug	2007	GA	BLOOD
CDC_K5486	Jul	2007	NC	CLINICAL; OTHER
CDC_K5583	Oct	2007	GA	BLOOD
CDC_K5585	Nov	2007	GA	BLOOD
CDC_07-2405	Oct	2006	LA	STOOL
CDC_07-2418	Mar	2007	LA	BLOOD
CDC_07-2444	Sept	2007	IL	BLOOD
CDC_K4572*	Oct	2006	HI	BLOOD
CDC_K4778*	Sept	2006	AL	CLINICAL; OTHER
CDC_K5613*	Jul	2007	NY	BLOOD
CDC_K5636*	unknown	Unknown	MD	BLOOD
CDC_K5637*	Sept	2007	MD	BLOOD

*Was not identified as V. vulnificus with API 20E.

All isolates were provided by the Centers for Disease Control and Prevention. Reporting information (month/year and state reporting) was obtained from COVIS forms. The reporting state is the state from which the isolate was received and not necessarily the state from which the infection was contracted.

TABLE 2 | Oyster *Vibrio vulnificus* isolates.

Isolate ID	Month of Isolation	Date of Harvest	State of Harvest
FDA_R101-A9	Nov	2007	AL
FDA_R101-D8	Nov	2007	AL
FDA_R11-B3	Feb	2007	LA
FDA_R19-C1	Mar	2007	TX
FDA_R27-C9	Apr	2007	LA
FDA_R30-C10	Apr	2007	FL
FDA_R42-D10	May	2007	LA
FDA_R47-E7	Jun	2007	TX
FDA_R499-A8	May	2007	VA
FDA_R51-A12	Jun	2007	LA
FDA_R51-E9	Jun	2007	LA
FDA_R53-A6	Jul	2007	FL
FDA_R57-B10	Jul	2007	LA
FDA_R595-A3	Jul	2007	LA
FDA_R595-D7	Jul	2007	LA
FDA_R595-D8	Jul	2007	LA
FDA_R59-B3	Jul	2007	AL
FDA_R63-A4	Jul	2007	CT
FDA_R63-C5	Jul	2007	LA
FDA_R73-C11	Sept	2007	DE
FDA_R74-C3	Sept	2007	LA
FDA_R74-D6	Sept	2007	LA
FDA_R80-G3	Sept	2007	LA
FDA_R80-G5	Sept	2007	LA
FDA_R80-H6	Sept	2007	LA
FDA_R81-C6	Sept	2007	LA
FDA_R81-F5	Sept	2007	LA
FDA_R844-G9	Aug	2007	FL
FDA_R84-F1	Sept	2007	VA
FDA_R85-B11	Oct	2007	SC
FDA_R96-B9	Oct	2007	DE
FDA_R97-A5	Oct	2007	VA
FDA_R97-B5	Oct	2007	VA
FDA_R98-C1	Oct	2007	LA
FDA_R98-C11	Oct	2007	LA
FDA_R98-E6	Oct	2007	LA
FDA_R99-A10	Oct	2007	LA
FDA_R844-F10*	Aug	2007	FL
FDA_R60-F9*	Jul	2007	NJ

**Was not identified as V. vulnificus with API 20E.*

All isolates were obtained from retail oysters as described in DePaola et al., 2010. Harvest information was obtained from shellfish tags collected with the oyster samples.

used to define more (*rrn*B and *vcg*C) or less (*rrn*A or *rrn*AB and *vcg*E) virulent genotype categories.

Virulence Testing With Mouse Model

For mouse virulence testing, 27 isolates were selected to be representative of source and genotype combinations. Approximately 1,000 CFU of each strain was inoculated into at least two groups of five mice, as previously described (Thiaville et al., 2011). Rectal temperature was used as an indicator of illness severity and as a surrogate for death (<33°C was determined to be dead) prior to sacrifice, when animals survived. Colony forming units (CFUs) were determined by standard plate count from the skin and liver following homogenization to determine local and systemic infection, respectively. Skin lesions were scored based on the size and nature of the lesion using a scale of 1–4. The skin and liver CFU data were used to cluster strains into virulence groups as previously described (Thiaville et al., 2011): Group 1 strains caused low skin and undetectable liver (systemic) infection, Group 2 strains caused moderate skin infection with little to no liver infection, Group 3 strains caused a high skin infection but low liver infection, Group 4 strains caused high skin and moderate liver infection, and Group 5 strains caused very high skin and very high liver infection. Assuming mouse virulence translates to human infection, Group 1, 2, and 3 strains would likely not be able to cause lethal infection in humans. Group 4 and 5 strains, because they cause high skin and moderate to high liver infection, have the potential to cause lethal infection in humans.

Statistical Analyses

Data were analyzed by strain, using the mean results from all mice inoculated with that strain as the data point for each measured mouse virulence parameter to capture strain variability rather than individual mouse response. A three factor ANOVA (General Linear Model; GLM) was used to determine if interactions between source of isolation (clinical/oyster), genotype (more virulent/less virulent), or season of

isolation (warm/cool) existed. As no significant interactions were found, GLM was used to evaluate quantitative data (log CFU/g skin, log CFU/g liver, body temperature, skin lesion score, and mortality) in comparison to the fixed variables. Fisher's exact test was used to evaluate associations between isolate source, genotype, and season of isolation with biochemical reactions and lethal or non-lethal designation. Season of isolation was determined by grouping strains as either cool (October–April) or warm (May–September) seasons when *V. vulnificus* is historically less or more prevalent, respectively. Due to mixed genotype results, three isolates (FDA_R101-A9, CDC_K5148, and CDC_07-2444) were removed from statistical analyses in genotype comparisons. All statistical comparisons were conducted in JMP 13.

RESULTS

Biochemical Profiles of *Vibrio vulnificus* Isolates

API 20E identified 61 isolates as *V. vulnificus*, with the eight remaining isolates identified as *Vibrio* spp. or *Aeromonas* spp. (**Tables 1 and 2**). As API 20E may incorrectly identify *Vibrio* spp. (O'Hara et al., 2003; Sanjuan et al., 2009), PCR targeting the *vvh* gene (Kinsey et al., 2015), was used to confirm all 69 isolates as *V. vulnificus*. All *V. vulnificus* isolates (n = 69) were positive for fermentation of glucose and amygdalin and the presence of oxidase and negative for arginine dihydrolase, tryptophan deaminase, inositol fermentation, sorbitol fermentation, rhamnose fermentation, and arabinose fermentation (**Table 3**).

Additionally, some of the tests were generally positive (β-Galactosidase, lysine decarboxylase, and gelatinase), while others were generally negative (H_2S production, urease, Voges–Proskauer reaction, saccharose fermentation, and melibiose fermentation). This data may be useful in biochemical identification of *V. vulnificus*. Interestingly, there were three biochemical tests (ornithine decarboxylase, citrate utilization, and indole production) which were variable in oyster isolates, but generally present in clinical isolates, resulting in a statistically significant association between isolate source and these biochemical tests ($p < 0.04$). In this study, mannitol fermentation, which has been associated with virulent genotypes of *V. vulnificus* (Drake et al., 2010), was also significantly associated with the virulent genotypes ($p < 0.001$) here. Mannitol was the only biochemical reaction that was variable in both clinical and oyster isolates: 57% of clinical and 39% of oyster isolates were positive (**Table 3**).

Virulence Genotyping of *Vibrio vulnificus* Isolates

For virulence genotyping of the clinical isolates (n = 30), 53% were the less virulent *rrn*A or AB/*vcg*E, and 47% were the more virulent (*rrn*B/*vcg*C) genotype (**Table 4**). Additionally, two clinical isolates had mixed genotypes: CDC_K5148 (*rrn*B/*vcg*E) and CDC_07-2444 (*rrn*A/*vcg*C). Of the strains isolated from blood infections (n = 22), half were the less virulent genotype and half the more virulent genotype. In the subset (n = 8) of clinical isolates not isolated from blood, half were the less virulent genotype, three were the more virulent genotype, and one was a mixed genotype (data not shown). Oyster isolate (n = 39) genotyping identified 64% of isolates as the less virulent genotype, *rrn*A or *rrn*AB/*vcg*E, and with a mixed genotype: FDA_R101-A9 (*rrn*AB/*vcg*C) and FDA_R63-C5 (*rrn*B/*vcg*E). The remaining oyster isolates (33%) were the more virulent (*rrn*B/*vcg*C) genotype.

TABLE 3 | Biochemical properties of *V. vulnificus* isolates.

Characteristic	Test result (% of isolates) [a]	
	Clinical Isolates	Oyster Isolates
Oxidase	+ (100)	+ (100)
Amygdalin fermentation	+ (100)	+ (100)
Glucose fermentation	+ (100)	+ (100)
Lysine decarboxylase	+ (100)	+ (97)
β-Galactosidase	+ (97)	+ (97)
Gelatinase	+ (97)	+ (95)
Indole production	+ (100)	V (54)
Mannitol fermentation	V (57)	V (39)
Ornithine decarboxylase	– (97)	V (74)
Citrate utilization	– (100)	V (46)
Saccharose fermentation	– (83)	– (95)
Voges-Proskauer reaction (acetoin production)	– (100)	– (92)
H_2S production	– (100)	– (97)
Urease	– (100)	– (97)
Melibiose fermentation	– (100)	– (97)
Arginine dihydrolase	– (100)	– (100)
Tryptophan deaminase	– (100)	– (100)
Inositol fermentation	– (100)	– (100)
Sorbitol fermentation	– (100)	– (100)
Rhamnose fermentation	– (100)	– (100)
Arabinose fermentation	– (100)	– (100)

[a] *+ if >80% positive, – if >80% negative. V, variable positive percent reported.*

TABLE 4 | Genotype of *V. vulnificus* strains.

Origin		*vcg*C	*vcg*E	Total
Clinical	*rrn*A	1	15	16
	*rrn*AB	–	–	–
	*rrn*B	13	1	14
Oyster	*rrn*A	–	22	22
	*rrn*AB	–	3	3
	*rrn*B	13	1	14
	Total	28	41	69

Virulence of *Vibrio vulnificus* Isolates in the Mouse Model

None of the *V. vulnificus* isolates in this study fell into mouse virulence Group 1, the least virulent group. Six isolates (22%) were classified as Group 2 (**Table 5**), with moderate skin infection (6.3–7.7 log CFU/g) and little to no liver infection (1.4–3.3 log CFU/g): five oyster and one clinical; five *rrn*A/*vcg*E and one mixed genotype (*rrn*AB/*vcg*E). Only one of these isolates, FDA_R51-A12 (*rrn*A/*vcg*E), caused mortality and all skin lesion scores were <3. Four isolates (15%) fell into Group 3:

TABLE 5 | Mouse virulence data. Skin infection, liver infection, body temperature, and skin lesion data are provided as means of the 5–10 animals tested with each strain.

Strain	Genotype	Log_{10} Skin CFU/g	Log_{10} Liver CFU/g	Temp (°C)	Skin Lesion Score	Mortality	Virulence Group	Virulence Potential
CDC_K4574	*rrn*A/*vcg*E	6.8	1.4	38.2	2.2	0%	2	Non-lethal
FDA_R51-A12	*rrn*A/*vcg*E	7.5	3.3	34.3	2.8	7%	2	
FDA_R84-F1	*rrn*A/*vcg*E	6.3	1.5	37.5	1.2	0%	2	
FDA_R499-A8	*rrn*A/*vcg*E	7.7	1.9	37.8	1.8	0%	2	
FDA_R844-G9	*rrn*A/*vcg*E	6.3	1.7	38.1	2.2	0%	2	
FDA_R101-A9	*rrn*AB/*vcg*C	6.5	2.1	35.1	1.4	0%	2	
CDC_K5613	*rrn*B/*vcg*C	7.8	3.3	36.7	3.4	0%	3	
FDA_R73-C11	*rrn*A/*vcg*E	8.3	3.7	37.0	3.4	20%	3	
FDA_R63-A4	*rrn*B/*vcg*C	7.9	3.1	33.3	4.0	0%	3	
FDA_R63-C5	*rrn*B/*vcg*C	8.5	2.8	35.8	3.4	0%	3	
CDC_K5148	*rrn*B/*vcg*E	8.5	1.4	38.4	3.0	0%	6*	
CDC_K4767	*rrn*A/*vcg*E	7.5	5.0	32.8	3.0	30%	4	Lethal
CDC_K5008	*rrn*A/*vcg*E	7.9	4.6	31.7	4.0	60%	4	
CDC_K5326	*rrn*A/*vcg*E	7.7	4.9	31.5	4.0	40%	4	
CDC_K5583	*rrn*A/*vcg*E	8.1	4.5	33.4	4.0	20%	4	
CDC_07-2444	*rrn*A/*vcg*C	7.2	5.4	30.5	4.0	80%	4	
CDC_K4633	*rrn*B/*vcg*C	7.8	5.8	31.3	4.0	50%	4	
CDC_K4776	*rrn*B/*vcg*C	7.4	4.3	33.4	2.8	67%	4	
CDC_K5041	*rrn*B/*vcg*C	8.0	5.1	32.0	3.6	40%	4	
CDC_K5204-LT	*rrn*B/*vcg*C	8.1	4.4	31.5	3.4	50%	4	
CDC_07-2405	*rrn*B/*vcg*C	8.3	5.7	31.2	3.2	60%	4	
FDA_R19-C1	*rrn*A/*vcg*E	7.9	6.0	31.6	4.0	20%	4	
FDA_R27-C9	*rrn*A/*vcg*E	7.4	4.8	33.2	3.2	20%	4	
FDA_R98-C1	*rrn*A/*vcg*E	8.0	5.9	31.4	4.0	30%	4	
FDA_R595-D7	*rrn*AB/vcgE	8.1	5.1	32.6	3.6	10%	4	
FDA_R98-E6	*rrn*B/*vcg*C	8.0	5.4	32.2	4.0	30%	4	
CDC_K5338	*rrn*B/*vcg*C	8.5	6.7	31.6	4.0	90%	5	

**Virulence Group 6 is a novel group identified in this study and is categorized as non-lethal.*
Percent mortality is calculated based on the group of mice.

three oyster and one clinical; one *rrn*A/*vcg*E and three *rrn*B/*vcg*C. An additional clinical isolate, CDC_K5148 (*rrn*B/*vcg*E), was in its own novel classification, Group 6. However, based on its general characteristics, it is similar to Group 3, with high skin infection (7.8–8.5 log CFU/g) and low liver infection (2.8–3.7 log CFU/g for the Group 3 isolates and 1.4 log CFU/g for CDC_K5148). Only one of the Group 3 isolates, FDA_R73-C11 (*rrn*A/*vcg*E), caused mortality. All skin lesion scores were 3–4. Over half (56%) of the *V. vulnificus* isolates fell into Group 4: 5 oyster and 10 clinical; 8 *rrn*A or *rrn*AB/*vcg*E, 6 *rrn*B/*vcg*C, and 1 *rrn*A/*vcg*C. This group had high skin infection (7.2–8.3 log CFU/g) and moderate liver infection (4.4–6.0 log CFU/g). All strains caused mortality, ranging from 10% (FDA_R595-D7, *rrn*AB/vcgE) to 80% (CDC_07-2444, *rrn*A/vcgC). Skin lesion score for this group ranged from 2.8 to 4. One isolate, FDA_K5338 (*rrn*B/vcgC), was characterized as Group 5, with very high skin (8.5 log CFU/g) and very high liver (6.7 log CFU/g) infection.

Association of Mouse Virulence With Isolate Source, Virulence Genotype, and Season of Isolation

Evaluation of the association between isolate source (clinical or oyster), virulence genotype (more virulent or less virulent), and season of strain isolation (cold or warm) with mouse virulence parameters including skin infection (log CFU/g skin), liver infection (log CFU/g liver), mouse temperature (as a proxy for illness severity), and mouse mortality (percentage of mice tested that died) were examined. The majority (6 of 11) of isolates with very high skin infection (≥8 log CFU/g) in the mouse model were the more virulent genotype or were of clinical origin. Similarly, isolates with very high liver (≥5 log CFU/g) infection were the more virulent genotype (five of 10) or were of clinical origin (six of 10).

However, there were no strong statistically significant relationships ($p > 0.05$) between the virulence genotype and skin infection, liver infection, mouse temperature, or mouse mortality (**Figure 1**). However, there was a weak association with virulence genotype and skin infection ($p = 0.05$). Similarly, no statistically significant ($p > 0.05$) relationships between isolate source and skin infection, liver infection, or mouse temperature were identified. There was a strong association between isolate source and mouse mortality, with clinical isolates causing significantly more mortality than oyster isolates ($p = 0.003$). Isolate source was also weakly associated with the lethal *versus* non-lethal categorization of mouse data, with clinical isolates being significantly more lethal ($p = 0.05$) than oyster isolates.

The extrinsic factor with the strongest association to mouse virulence of *V. vulnificus* strains was season of isolation with significant associations between season of isolation and liver infection ($p = 0.04$) and mouse temperature ($p = 0.04$) identified (**Figure 2**). In both cases, isolates from the cooler season were more virulent, *i.e.*, caused higher liver infection and lower mouse body temperatures. There were no statistically significant relationships ($p > 0.05$) between season of isolation and skin infection or mouse mortality.

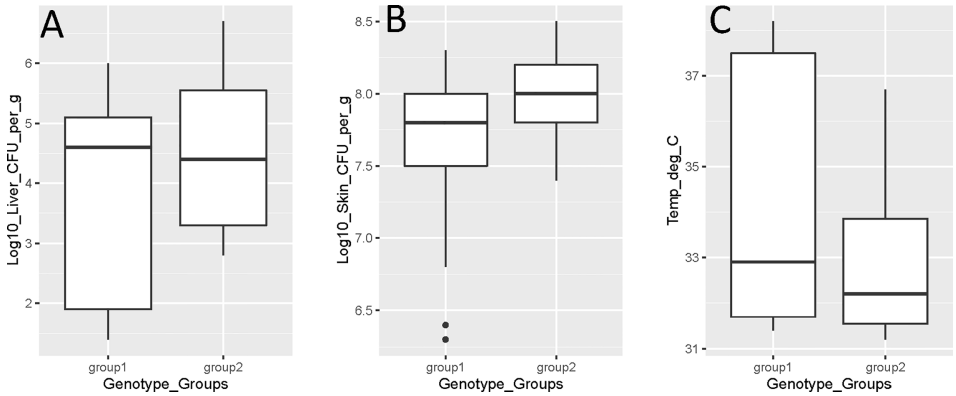

FIGURE 1 | *Vibrio vulnificus* mouse model virulence parameter data [**(A)** liver infection; **(B)** skin infection; **(C)** mouse temperature] by genotype (group 1 is *rrn*A/*vcg*E and *rrn*AB/*vcg*E; group 2 is *rrn*B/*vcg*C). Each box displays the median with the upper (25%) and lower (75%) quartiles as hinges. Whiskers represent the highest or lowest observation + 1.5*Inter quartile range. Dots represent outliers.

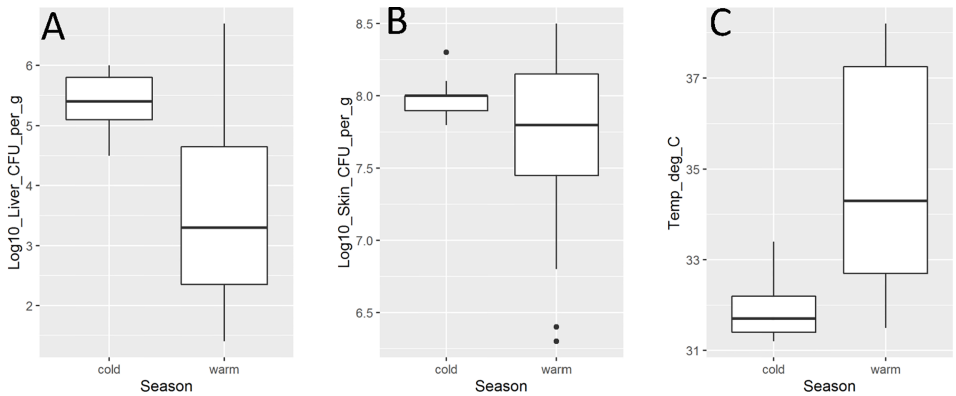

FIGURE 2 | *Vibrio vulnificus* mouse model virulence parameter data [**(A)**. liver infection; **(B)**. skin infection; **(C)**. mouse temperature] by season (cold is October–April; warm is May–September). Isolate from HI (CDC_K4574) is grouped with warm season due to lack of temperature variability in the state. Each box displays the median with the upper (25%) and lower (75%) quartiles as hinges. Whiskers represent the highest or lowest observation + 1.5*Inter quartile range. Dots represent outliers.

DISCUSSION

Biochemical Profiles of *Vibrio vulnificus* Isolates

Biochemical profiles were determined by API 20E. Only 88% of the *V. vulnificus* isolates were correctly identified, which is slightly higher than previous reports (O'Hara et al., 2003). This is likely due to the use of 2% NaCl for inoculation of the biochemical test, rather than the manufacturer's recommended 0.85%, as previously described as an improved identification method for *Vibrio* spp. from the environment (Martinez-Urtaza et al., 2005). Interestingly, a higher rate of misidentification was noted for the clinical isolates (20%), as compared to the oyster isolates (5%), which is contrary to previous findings (Martinez-Urtaza et al., 2005). Another noteworthy observation was the significantly ($p = 0.02$) lower presence of indole production in isolates from the cooler season. A higher variability in biochemical profiles was observed for the oyster isolates as compared to the clinical isolates. This difference in variability has not been noted previously, but is logical assuming environmental (oyster) isolates are under less selective pressure than clinical isolates, which need specific traits to survive in the human host.

Genotyping of *Vibrio vulnificus* Isolates

In studies establishing and investigating the utility of *V. vulnificus* genotypes for association with virulence potential (Nilsson et al., 2003; DePaola et al., 2003; Vickery et al., 2007; Thiaville et al., 2011) a similar set of isolates was used. Repeated use of this set of *V. vulnificus* isolates provided good reference for repeatability and is valuable for assay development. However, the isolate set remains limited in that clinical isolates were from the warm months (May–September) and environmental isolates were from cooler months (October–April). In contrast, this

study utilized a more balanced set of isolates collected from a range of seasonal and geographical sources. As a result, well-defined relationships between isolate origin and genotype were not clearly identified.

While the majority (64%) of oyster isolates were *rrn*A/*vcg*E, the prevalence of the *rrn*B/*vcg*C genotype (33%) was higher than a previous observation where virulent genotypes represented ~6% of isolates from the environment (Rosche et al., 2005). However, recent studies found results similar to the current work, with reports of up to 40% of *V. vulnificus* isolated from oysters having the virulent genotype (Han et al., 2009; Drake et al., 2010; Jones et al., 2013). As *V. vulnificus* that causes infection originates from the environment (where exposure occurs), one would expect a mix of genotypes and virulence potential such as observed in the current work.

Genotypes of clinical *V. vulnificus* isolates in this study were surprising, with a lower than expected prevalence of the *rrn*B/*vcg*C genotype. This holds true even when looking at the subset of clinical isolates from blood cultures and deviates from previous findings where isolates of clinical origin are nearly all *rrn*B/*vcg*C (Nilsson et al., 2003; Warner and Oliver, 2008; Drake et al., 2010). We hypothesized this discrepancy is due to seasonal and geographic variability, as our study focused on a more diverse panel compared to previous studies. This theory is supported by previous studies that observed differences in distribution of genotypes in the environment based on season and/or region (Lin and Schwarz, 2003; Warner and Oliver, 2008; Jones et al., 2013; Williams et al., 2017).

Association of Mouse Virulence With Biochemical Phenotype, Virulence Genotype, and Season of Isolation

Mouse virulence testing has previously identified non-lethal (Groups 1–3) and lethal (Groups 4–5) clusters (Thiaville et al., 2011). When using this model, with a greater sensitivity for liver infection, a novel, non-lethal cluster (Group 6) was identified. This Group caused high rates of skin infection, but low liver infection, so was classified as non-lethal. One surprising finding was that no isolates fell into virulence Group 1 (the least virulent group), even with a diversity of oyster isolates tested. Although this is different from the findings of Thiaville et al. (2011), where 16% of isolates were Group 1, the two studies are similar in that the majority of isolates were identified as Group 4 in both. Taken together, these findings suggest that the majority of *V. vulnificus* isolates can cause high skin and moderate liver infection, regardless of genotype or isolation source.

We found that lethal and non-lethal strains were only weakly correlated to clinical or oyster origin of the isolates, but strongly correlated to mouse mortality. Regardless of statistical associations, the non-lethal isolates were generally from oysters and have the less virulent genotype, as expected. Additionally, all strains that resulted in >40% mouse mortality were isolated from a clinical source, and all but one had the more virulent genotype. These observations, along with the previous data used in establishing the iron-dextran mouse model (Starks et al., 2000; DePaola et al., 2003), support the utility of this model and validity of resultant data. Interestingly, no correlation was identified between the virulence genotype of isolates and the observed mouse virulence parameters, other than skin infection. These genotypes have been reported as an indicator of severe illness potential in humans; however, the lack of correlation with mouse virulence (as a proxy for potential human infection) questions their suitability as predictors. These results are consistent with previous research demonstrating that genotypes are associated with, but do not predict, virulence in a mouse model (Thiaville et al., 2011).

Season of isolation was the factor which most correlated with virulence potential in *V. vulnificus*. Isolates from the cooler months (except the isolate from Hawaii) were lethal and were associated with higher levels of liver infection and lower body temperature. Isolates from the warmer season had mixed virulence potential; this is reflected by the wide range in liver and skin infection, as well as body temperature. Environmental drivers of *Vibrio* spp. are often attributed to two main factors, temperature and salinity, the primary differences across seasons, with higher levels generally found during the warmer season (Takemura et al., 2014; Johnson, 2015). Our results, therefore, may appear counter-intuitive, especially combined with knowledge that the majority of *V. vulnificus* infections occur during warmer months (Oliver, 2015; Centers for Disease Control and Prevention, 2017). However, this apparent discrepancy may be explained by a higher proportion of virulent *V. vulnificus* in the environment (and oysters) during the cooler season when total populations are lowest, similar to what has been observed for *V. parahaemolyticus* (Johnson et al., 2010; DePaola et al., 2010). The hypothesis that a greater proportion of the *V. vulnificus* population is virulent during the cooler season is supported by objective evidence of *V. vulnificus* infections from oyster consumption in the US (as reported to the FDA). During the cooler months (November–April), 10% of oysters have >3 log *V. vulnificus*/g compared to 34% of oysters with these high levels of *V. vulnificus* during the warm months (DePaola et al., 2010). Assuming equally virulent populations, it would be expected that there be three times more cases in the warmer months than the colder months; however, the difference is not always that large (Personal Communication (2020)), suggesting a higher proportion of disease-causing strains in the cooler season. Taken together, these data indicate an association between virulence and season; additionally, this is the first report to define this association using mouse model data.

Conclusions and Future Directions

Due to the lack of reliable markers for virulence potential, current risk evaluation and management strategies are based on total *V. vulnificus* populations. This study indicates that *vcg*C and *rrn*B, two gene variant candidates for differentiating isolate virulence, are not reliable markers of systemic virulence potential in *V. vulnificus*. It is likely that the different genotypes are reflective of a bifurcation of phylogenetic lineage (Lopez-Perez et al., 2019), rather than functional differences. This, and previous studies, demonstrated that although no reliable indicator, or set of indicators, has yet been identified, not all *V. vulnificus* isolates have the same virulence potential. In addition, we have identified a relationship between isolates from the cooler season and systemic virulence potential in *V. vulnificus*.

Using the findings of this work as a basis, future research may be directed towards identifying markers to differentiate virulence potential and to identify the driving factor(s) behind the association between season and virulence. Identification of those factors may allow focus on regulatory pathways such as long-term cold adaptation of *V. vulnificus*. Next-generation sequencing makes it is possible to discern new potential markers and pathways important to *V. vulnificus* virulence with isolate virulence known *a priori*. Previous SOLiD sequencing of four *V. vulnificus* isolates (Gulig et al., 2010), resulted in an extensive list of potential markers, likely due a lack of robust coverage of isolate genomes and small sample size. By sequencing additional well-characterized isolates on platforms with increased genome coverage, we can more readily narrow down these lists of candidate virulence genes. Identification of reliable virulence markers would allow for risk assessments and risk management approaches to be refined in order to better protect public health.

DATA AVAILABILITY STATEMENT

The original contributions presented in the study are included in the article/supplementary material. Further inquiries can be directed to the corresponding author.

ETHICS STATEMENT

The animal study was reviewed and approved by the Institutional Animal Care & Use Committee, PO Box 100142 Gainesville, Florida 32610-0142, Chair, Michael Katovich, University of Florida.

AUTHOR CONTRIBUTIONS

Designed experiment: JJ. Conducted experiments: TK, JJ, CL, and PG. Wrote paper: KL and JJ. Edited paper: TK, CL, and PG. Analysis: JJ, KL, TK, CL, and PG. All authors contributed to the article and approved the submitted version.

ACKNOWLEDGMENTS

The authors thank Dr. Cheryl Tarr, CDC for providing the clinical isolates. Huge thanks to Stuart Chirtel and John Bowers for advice on appropriate selection of statistical methods. Thank you to Ms. Lizzie Farrell, Mrs. Whitney Neil, Dr. Carolyn Simmons, and Dr. Stacey Wiggins for their comments and review of this manuscript.

REFERENCES

(2020). *RE: Personal Communication* (Melissa "Lizzie" Farrell). August 11, 2020.

Amaro, C., and Biosca, E. G. (1996). Vibrio vulnificus biotype 2, pathogenic for eels, is also an opportunistic pathogen for humans. *Appl. Environ. Microbiol.* 62, 1454–1457. doi: 10.1128/AEM.62.4.1454-1457.1996

Bisharat, N., Agmon, V., Finkelstein, R., Raz, R., Ben-Dror, G., Lerner, L., et al. (1999). Clinical, epidemiological, and microbiological features of Vibrio vulnificus biogroup 3 causing outbreaks of wound infection and bacteraemia in Israel. Israel Vibrio Study Group. *Lancet* 354, 1421–1424. doi: 10.1016/S0140-6736(99)02471-X

Blake, P. A., Merson, M. H., Weaver, R. E., Hollis, D. G., and Heublein, P. C. (1979). Disease caused by a marine Vibrio. Clinical characteristics and epidemiology. *N. Engl. J. Med.* 300, 1–5. doi: 10.1056/NEJM197901043000101

Centers for Disease Control and Prevention (2017). *Vibrio species causing vibriosis*. Available at: https://www.cdc.gov/vibrio/index.html (Accessed October 28, 2020).

DePaola, A., Nordstrom, J. L., Dalsgaard, A., Forslund, A., Oliver, J., Bates, T., et al. (2003). Analysis of Vibrio vulnificus from market oysters and septicemia cases for virulence markers. *Appl. Environ. Microbiol.* 69, 4006–4011. doi: 10.1128/AEM.69.7.4006-4011.2003

DePaola, A., Jones, J. L., Woods, J., Burkhardt, W.3rd, Calci, K. R., Krantz, J. A., et al. (2010). Bacterial and viral pathogens in live oysters: 2007 United States market survey. *Appl. Environ. Microbiol.* 76, 2754–2768. doi: 10.1128/AEM.02590-09

Drake, S. L., Whitney, B., Levine, J. F., Depaola, A., and Jaykus, L. A. (2010). Correlation of mannitol fermentation with virulence-associated genotypic characteristics in Vibrio vulnificus isolates from oysters and water samples in the Gulf of Mexico. *Foodborne Pathog. Dis.* 7, 97–101. doi: 10.1089/fpd.2009.0362

Gulig, P. A., De Crecy-Lagard, V., Wright, A. C., Walts, B., Telonis-Scott, M., and Mcintyre, L. M. (2010). SOLiD sequencing of four Vibrio vulnificus genomes enables comparative genomic analysis and identification of candidate clade-specific virulence genes. *BMC Genomics* 11, 512. doi: 10.1186/1471-2164-11-512

Han, F., Pu, S., Hou, A., and Ge, B. (2009). Characterization of clinical and environmental types of Vibrio vulnificus isolates from Louisiana oysters. *Foodborne Pathog. Dis.* 6, 1251–1258. doi: 10.1089/fpd.2009.0343

Haq, S. M., and Dayal, H. H. (2005). Chronic liver disease and consumption of raw oysters: a potentially lethal combination–a review of Vibrio vulnificus septicemia. *Am. J. Gastroenterol.* 100, 1195–1199. doi: 10.1111/j.1572-0241.2005.40814.x

Hlady, W. G., and Klontz, K. C. (1996). The epidemiology of Vibrio infections in Florida 1981-1993. *J. Infect. Dis.* 173, 1176–1183. doi: 10.1093/infdis/173.5.1176

Johnson, C. N., Flowers, A. R., Noriea, N.F.3rd, Zimmerman, A. M., Bowers, J. C., Depaola, A., et al. (2010). Relationships between environmental factors and pathogenic Vibrios in the Northern Gulf of Mexico. *Appl. Environ. Microbiol.* 76, 7076–7084. doi: 10.1128/AEM.00697-10

Johnson, C. N. (2015). Influence of Environmental Factors on Vibrio spp. in Coastal Ecosystems. *Microbiol. Spectr.* 3, VE-0008-2014. doi: 10.1128/microbiolspec.VE-0008-2014

Jones, J. L., Ludeke, C. H., Bowers, J. C., and Depaola, A. (2013). Comparison of plating media for recovery of total and virulent genotypes of Vibrio vulnificus in U.S. market oysters. *Int. J. Food Microbiol.* 167, 322–327. doi: 10.1016/j.ijfoodmicro.2013.09.017

Kaspar, C. W., and Tamplin, M. L. (1993). Effects of temperature and salinity on the survival of Vibrio vulnificus in seawater and shellfish. *Appl. Environ. Microbiol.* 59, 2425–2429. doi: 10.1128/AEM.59.8.2425-2429.1993

Kaysner, C., Depaola, A., and Jones, J. (2004). *Vibrio. Bacteriological Analytical Manual*. Available at: https://www.fda.gov/food/laboratory-methods-food/bam-chapter-9-vibrio (Accessed October 28, 2020).

Kinsey, T. P., Lydon, K. A., Bowers, J. C., and Jones, J. L. (2015). Effects of Dry Storage and Resubmersion of Oysters on Total Vibrio vulnificus and Total and Pathogenic (tdh+/trh+) Vibrio parahaemolyticus Levels. *J. Food Prot.* 78, 1574–1580. doi: 10.4315/0362-028X.JFP-15-017

Lin, M., and Schwarz, J. R. (2003). Seasonal shifts in population structure of Vibrio vulnificus in an estuarine environment as revealed by partial 16S ribosomal DNA sequencing. *FEMS Microbiol. Ecol.* 45, 23–27. doi: 10.1016/S0168-6496(03)00091-6

Lopez-Perez, M., Jayakumar, J. M., Haro-Moreno, J. M., Zaragoza-Solas, A., Reddi, G., Rodriguez-Valera, F., et al. (2019). Evolutionary Model of Cluster Divergence of the Emergent Marine Pathogen Vibrio vulnificus: From Genotype to Ecotype. *mBio* 10, e02852–18. doi: 10.1128/mBio.02852-18

Martinez-Urtaza, J., Simental, L., Velasco, D., Depaola, A., Ishibashi, M., Nakaguchi, Y., et al. (2005). Pandemic Vibrio parahaemolyticus O3:K6, Europe. *Emerg. Infect. Dis.* 11, 1319–1320. doi: 10.3201/eid1108.050322

National Shellfish Sanitation Program (Us) (2019).Guide for the control of molluscan shellfish. In: *Interstate Shellfish Sanitation Conference*. Available at: https://www.fda.gov/food/federalstate-food-programs/national-shellfish-sanitation-program-nssp (Accessed January 5, 2021).

Nilsson, W. B., Paranjype, R. N., Depaola, A., and Strom, M. S. (2003). Sequence polymorphism of the 16S rRNA gene of Vibrio vulnificus is a possible indicator of strain virulence. *J. Clin. Microbiol.* 41, 442–446. doi: 10.1128/JCM.41.1.442-446.2003

Oliver, J. D., and Kaper, J. B. (2001). "Vibrio species," in *Food microbiology: fundamentals and frontiers*, *2nd ed*. Ed. M. P. Doyle (Washington, D.C: American Society for Microbiology).

Oliver, J. D. (2015). The Biology of Vibrio vulnificus. *Microbiol. Spectr.* 3, VE-0001-2014 doi: 10.1128/microbiolspec.VE-0001-2014

O'Hara, C. M., Sowers, E. G., Bopp, C. A., Duda, S. B., and Strockbine, N. A. (2003). Accuracy of six commercially available systems for identification of members of the family vibrionaceae. *J. Clin. Microbiol.* 41, 5654–5659. doi: 10.1128/JCM.41.12.5654-5659.2003

Rosche, T. M., Yano, Y., and Oliver, J. D. (2005). A rapid and simple PCR analysis indicates there are two subgroups of Vibrio vulnificus which correlate with clinical or environmental isolation. *Microbiol. Immunol.* 49, 381–389. doi: 10.1111/j.1348-0421.2005.tb03731.x

Sanjuan, E., Fouz, B., Oliver, J. D., and Amaro, C. (2009). Evaluation of genotypic and phenotypic methods to distinguish clinical from environmental Vibrio vulnificus strains. *Appl. Environ. Microbiol.* 75, 1604–1613. doi: 10.1128/AEM.01594-08

Scallan, E., Hoekstra, R. M., Angulo, F. J., Tauxe, R. V., Widdowson, M. A., Roy, S. L., et al. (2011). Foodborne illness acquired in the United States–major pathogens. *Emerg. Infect. Dis.* 17, 7–15. doi: 10.3201/eid1701.P11101

Shapiro, R. L., Altekruse, S., Hutwagner, L., Bishop, R., Hammond, R., Wilson, S., et al. (1998). The role of Gulf Coast oysters harvested in warmer months in Vibrio vulnificus infections in the United States 1988-1996. Vibrio Working Group. *J. Infect. Dis.* 178, 752–759. doi: 10.1086/515367

Starks, A. M., Schoeb, T. R., Tamplin, M. L., Parveen, S., Doyle, T. J., Bomeisl, P. E., et al. (2000). Pathogenesis of infection by clinical and environmental strains of Vibrio vulnificus in iron-dextran-treated mice. *Infect. Immun.* 68, 5785–5793. doi: 10.1128/IAI.68.10.5785-5793.2000

Starks, A. M., Bourdage, K. L., Thiaville, P. C., and Gulig, P. A. (2006). Use of a marker plasmid to examine differential rates of growth and death between clinical and environmental strains of Vibrio vulnificus in experimentally infected mice. *Mol. Microbiol.* 61, 310–323. doi: 10.1111/j.1365-2958.2006.05227.x

Strom, M. S., and Paranjpye, R. N. (2000). Epidemiology and pathogenesis of Vibrio vulnificus. *Microbes Infect.* 2, 177–188. doi: 10.1016/S1286-4579(00)00270-7

Takemura, A. F., Chien, D. M., and Polz, M. F. (2014). Associations and dynamics of Vibrionaceae in the environment, from the genus to the population level. *Front. Microbiol.* 5, 38. doi: 10.3389/fmicb.2014.00038

Thiaville, P. C., Bourdage, K. L., Wright, A. C., Farrell-Evans, M., Garvan, C. W., and Gulig, P. A. (2011). Genotype is correlated with but does not predict virulence of Vibrio vulnificus biotype 1 in subcutaneously inoculated, iron dextran-treated mice. *Infect. Immun.* 79, 1194–1207. doi: 10.1128/IAI.01031-10

Veenstra, J., Rietra, P. J., Goudswaard, J., Kaan, J. A., Van Keulen, P. H., and Stoutenbeek, C. P. (1993). Extra-intestinal infections caused by Vibrio spp. in The Netherlands. *Ned. Tijdschr. Geneeskd.* 137, 654–657.PIMD 8469298

Vickery, M. C., Nilsson, W. B., Strom, M. S., Nordstrom, J. L., and Depaola, A. (2007). A real-time PCR assay for the rapid determination of 16S rRNA genotype in Vibrio vulnificus. *J. Microbiol. Methods* 68, 376–384. doi: 10.1016/j.mimet.2006.02.018

Warner, E., and Oliver, J. D. (2008). Population structures of two genotypes of Vibrio vulnificus in oysters (Crassostrea virginica) and seawater. *Appl. Environ. Microbiol.* 74, 80–85. doi: 10.1128/AEM.01434-07

Williams, T. C., Froelich, B. A., Phippen, B., Fowler, P., Noble, R. T., and Oliver, J. D. (2017). Different abundance and correlational patterns exist between total and presumed pathogenic Vibrio vulnificus and V. parahaemolyticus in shellfish and waters along the North Carolina coast. *FEMS Microbiol. Ecol.* 93, fix071. doi: 10.1093/femsec/fix071

Conflict of Interest: The authors declare that the research was conducted in the absence of any commercial or financial relationships that could be construed as a potential conflict of interest.

frontiers in Cellular and Infection Microbiology

ORIGINAL RESEARCH
published: 30 April 2021
doi: 10.3389/fcimb.2021.673222

TolCV1 Has Multifaceted Roles During *Vibrio vulnificus* Infection

Yue Gong[1], *Rui Hong Guo*[1], *Joon Haeng Rhee*[2] *and Young Ran Kim*[1]*

[1] College of Pharmacy and Research Institute of Drug Development, Chonnam National University, Gwangju, South Korea, [2] Clinical Vaccine R&D Center, Department of Microbiology, Combinatorial Tumor Immunotherapy MRC, Chonnam National University Medical School, Hwasun-gun, South Korea

RtxA1 is a major cytotoxin of *Vibrio vulnificus* (*V. vulnificus*) causing fatal septicemia and necrotic wound infections. Our previous work has shown that RpoS regulates the expression and secretion of *V. vulnificus* RtxA1 toxin. This study was conducted to further investigate the potential mechanisms of RpoS on RtxA1 secretion. First, *V. vulnificus* TolCV1 and TolCV2 proteins, two *Escherichia coli* TolC homologs, were measured at various time points by Western blotting. The expression of TolCV1 was increased time-dependently, whereas that of TolCV2 was decreased. Expression of both TolCV1 and TolCV2 was significantly downregulated in an *rpoS* deletion mutation. Subsequently, we explored the roles of TolCV1 and TolCV2 in *V. vulnificus* pathogenesis. Western blot analysis showed that RtxA1 toxin was exported by TolCV1, not TolCV2, which was consistent with the cytotoxicity results. Furthermore, the expression of TolCV1 and TolCV2 was increased after treatment of the host signal bile salt and the growth of *tolCV1* mutant was totally abolished in the presence of bile salt. A *tolCV1* mutation resulted in significant reduction of *V. vulnificus* induced-virulence in mice. Taken together, TolCV1 plays key roles in RtxA1 secretion, bile salt resistance, and mice lethality of *V. vulnificus*, suggesting that TolCV1 could be an attractive target for the design of new medicines to treat *V. vulnificus* infections.

Keywords: TolC, RpoS, bile salt resistance, RtxA1 secretion, *Vibrio vulnificus*

OPEN ACCESS

Edited by:
Lixing Huang,
Jimei University, China

Reviewed by:
Nam-chul Ha,
Seoul National University, South Korea
Youlu Su,
Zhongkai University of Agriculture and Engineering, China
Karla Satchell,
Northwestern University, United States

***Correspondence:**
Young Ran Kim
kimyr@jnu.ac.kr

Specialty section:
This article was submitted to Molecular Bacterial Pathogenesis, a section of the journal Frontiers in Cellular and Infection Microbiology

Received: *27 February 2021*
Accepted: *12 April 2021*
Published: *30 April 2021*

Citation:
Gong Y, Guo RH, Rhee JH and Kim YR (2021) TolCV1 Has Multifaceted Roles During Vibrio vulnificus Infection. Front. Cell. Infect. Microbiol. 11:673222. doi: 10.3389/fcimb.2021.673222

INTRODUCTION

Vibrio vulnificus (*V. vulnificus*) is a halophilic Gram-negative bacterium that causes fatal primary septicemia and necrotizing wound infections, and is commonly transmitted by seawater exposure or contaminated seafood consumption (Baker-Austin et al., 2018; Park and Lee, 2018). *V. vulnificus* infections usually occur in individuals with underlying conditions such as liver diseases, diabetes, and immune disorder (Baker-Austin et al., 2018). RtxA1, a member of multifunctional autoprocessing repeats-in-toxin (MARTX) family, is a major cytotoxin of *V. vulnificus* (Kwak et al., 2011; Roig et al., 2011). Our previous studies have demonstrated that the expression of RtxA1 is dramatically increased after the close contact of *V. vulnificus* with host cells (Kim et al., 2008), and RtxA1 toxin induces the acute cell death by forming pores in the cellular membrane (Kim et al., 2013). Additionally, the expression and secretion of RtxA1 toxin are regulated by the sigma factor RpoS (Guo et al., 2018).

V. vulnificus TolC, an outer membrane channel protein that participates in the assembly of tripartite efflux pumps, has been reported to be involved in the secretion of RtxA1 toxin (Hwang et al., 2011). In *V. vulnificus*, there are two *Escherichia coli* (*E.coli*) TolC homologs, TolCV1 and

TolCV2 (VVM0602608 and VVM0604400), showing 51.3% and 29.6% sequence identity, respectively (Lee et al., 2013). TolC is able to co-operate with several inner membrane complexes and thereby participates in the assembly of different tripartite efflux pumps, such as AcrAB-TolC (Du et al., 2014), MacAB-TolC (Du et al., 2015), EmrAB-TolC (Puértolas-Balint et al., 2020), and HlyBD-TolC (Kanonenberg et al., 2019). Some studies have demonstrated that *V. vulnificus* TolCV1 and TolCV2 can interact with *E.coli* membrane fusion protein AcrA and MacA to partially assume the efflux pump function of *E.coli* TolC (Lee et al., 2013; Lee et al., 2014b). A wide variety of substrates are directly transported across the envelope through TolC-dependent export and efflux system, which endues TolC with multiple functions and makes it to be critical for bacterial survival in the environment rich with pernicious agents or under extremal conditions (Langevin and Dunlop, 2018). Recent studies have demonstrated that AcrAB-TolC and its homologs are crucial for the drug-resistance acquisition in Gram-negative bacteria (El Meouche and Dunlop, 2018; Nolivos et al., 2019). Interestingly, *V. vulnificus* TolCV1 and TolCV2 are also associated with the efflux of diverse antibiotics (Lee et al., 2014a; Lee et al., 2015), biofilm formation (Lee et al., 2007), and iron-uptake system (Kawano et al., 2014). Several lines of evidence indicate that TolC affects virulence expression in *Vibrio cholerae*, *Francisella tularensis* and *Enterobacter cloacae* (Gil et al., 2006; Minato et al., 2011; Pérez et al., 2012) and is indispensable for bile salt resistance and colonization in *Vibrio cholerae* (Bina and Mekalanos, 2001). These fundings indicate that outer membrane TolC possesses multiple functions in various strains, which drove us to further explore more functions of TolCV1 and TolCV2 in *V. vulnificus*.

This study was conducted to further investigate the potential mechanisms of RpoS on RtxA1 secretion. First, we measured the effect of *rpoS* mutation on TolCV1 and TolCV2 expression by Western blotting. We also examined the roles of TolCV1 and TolCV2 in host factor-induced RtxA1 toxin secretion and expression, cytotoxicity to host cells, bile salt resistance and mice lethality.

MATERIALS AND METHODS

Bacterial Strains, Plasmids and Growth Conditions

The bacterial strains and plasmids used in this study are listed in **Table 1**. Bacterial strains were reserved at −80°C in growth medium with 20% (vol/vol) glycerol. Unless stated otherwise, all *V. vulnificus* strains were propagated in Luria-Bertani broth (LB broth, Difco, Becton-Dickinson, Sparks, MD, USA) at 37°C in a shaking incubator (200 rpm).

Mutant Construction and Complementation

The suicide plasmid pDM4 was used to construct an in-frame *tolCV2* deletion mutant of *V. vulnificus* MO6-24/O as described previously (Guo et al., 2020). The upstream and downstream DNA fragments of *tolCV2* were amplified by PCR from *V. vulnificus* MO6-24/O chromosomal DNA (accession number NC_014966.1) (Park et al., 2011) using the primer pairs (*tolCV2*-1: 5′-GGAATTCTCTGCTGTGAGCGTTGCGCT-3′; *tolCV2*-2: 5′-GTTGCAATAATTAACCATGCGCGCCTCCCATCATC-3′) and (*tolCV2*-3: 5′-GCATGGTTAATTATTGCAACAAACATGGCAAACG-3′; *tolCV2*-4: 5′-GCTCTAGAATATCCCGTGATCACCGG-3′), respectively. These two DNA fragments were used as templates for the second crossover PCR with *tolCV2*-1 and *tolCV2*-4 as primers. The resulting PCR products were ligated into suicide plasmid pDM4 and transformed into *E. coli* SY327*λpir* and *E. coli* SM10*λpir*, generating the pDM4::△*tolCV2*, which was conjugally transferred into MO6-24/O *via* triparental mating. The stable transconjugants were selected on TCBS agar plates with chloramphenicol and then heart infusion (HI) agar plates with 10% sucrose. The mutation was verified *via* PCR and Western blot analysis.

The complementation of *tolCV2* mutant was constructed using plasmid pLAFR3 with a primer pair (*tolCV2*-F-*EcoRI*: 5′-CGGAATTCGTCCAGACATTAAAGCCG-3′; *tolCV2*-R-*PstI*: 5′-AAAACTGCAGGTTGCAATAACGCGCTC-3′). The DNA fragment containing *tolCV2* gene and flanking DNA sequence was amplified by PCR and then cloned into pLAFR3, resulting in the pLAFR3::*tolCV2*, which was introduced into *tolCV2* mutant strain by triparental mating. Stable transconjugants were selected and confirmed by PCR and Western blot analysis.

Production of Polyclonal Anti-TolCV2 Antibody

Rabbit polyclonal anti-TolCV2 antibody was produced as described in our previous study (Guo et al., 2020). The DNA fragment encoding *tolCV2* was amplified from *V. vulnificus* MO6-24/O chromosomal DNA by PCR with the following primer pair (*tolCV2*-F-*EcoRI*: 5′-CGGAATTCATGGTTAACAAGCACCTATC-3′; *tolCV2*-R-*XhoI*: 5′-CCGCTCGAGTCATGAATGAAAAGCTCGG-3′). The resulting PCR products were then inserted into the expression vector PGEX-4T-1 (Amersham Pharmacia Biotech Inc., Piscataway, NJ) and the GST-TolCV2 fusion protein was purified by GST SpinTrap columns (GE Healthcare Life Science, Buckinghamshire, UK). The rabbit polyclonal anti-TolCV2 antibody was produced using New Zealand white rabbits, and the specificity of the polyclonal antibody against TolCV2 was confirmed by Western blotting.

Western Blotting

Single colony of *V. vulnificus* strain was inoculated into LB broth and cultured overnight at 37°C in a shaking incubator (200 rpm). The overnight cultures were diluted 200-fold with fresh LB medium and subsequently cultured at 37°C. The pellets were washed twice with DPBS (Welgene, Gyeongsan-si, Gyeongsangbuk-do, South Korea). Bacterial cells (2×10^8 CFU) resuspended in SDS-PAGE sample buffer were boiled at 100°C for 10 min and separated by 10% SDS-PAGE gels before being transferred to polyvinylidene fluoride (PVDF) membranes (Millipore, Bedford, MA, USA). The membranes were then

TABLE 1 | Bacterial strains and plasmids used in this study.

Bacterial strains or plasmids	Characteristics	Sources or references
Vibrio vulnificus		
MO6-24/O	*V. vulnificus* wild type, clinical isolate	(Reddy et al., 1992)
CMM744 (*rtxA1*-)	MO6-24/O with a deletion mutation in *rtxA1* gene	(Kim et al., 2008)
rpoS-	MO6-24/O with a deletion mutation in *rpoS* gene	(Guo et al., 2018)
tolCV1-	MO6-24/O with a deletion mutation in *tolCV1* gene	(Guo et al., 2020)
tolCV2-	MO6-24/O with a deletion mutation in *tolCV2* gene	This study
tolCV1- + pLAFR3::*tolCV1*	*tolCV1*- harbouring pLAFR3::*tolCV1*	(Guo et al., 2020)
tolCV2- + pLAFR3::*tolCV2*	*tolCV2*- harbouring pLAFR3::*tolCV2*	This study
Escherichia coli		
DH5α	F- *recA*1; restriction negative	Laboratory collection
SY327λ*pir*	(*lac pro*) *argE*(Am) *rif nalA recA*56 λ *pir* lysogen; host for π-requiring plasmids	(Miller and Mekalanos, 1988)
SM10λ*pir*	*thi thr leu tonA lacY supE recA*::RP4=-2-Tc^R : Mu λ *pir* lysogen, oriT of RP4, Km^R; Conjugal donor	(Miller and Mekalanos, 1988)
Plasmids		
pLAFR3	IncP cosmid vector, Tc^R	(Staskawicz et al., 1987)
pDM4	A suicide vector with ori *R6K sacB*, Cm^r	(Milton et al., 1996)
pRK2013	IncP, Km^R, Tra Rk2$^+$*repRK2 repE1*	(Ditta et al., 1980)

blocked with 5% skim milk in Tris-buffered saline containing 0.05% Tween 20 (TBS/T) for 2 h at room temperature and incubated with primary antibodies specific to TolCV1 (Guo et al., 2020), TolCV2 or RtxA1-D2 (Kim et al., 2013) at 4°C overnight. The membranes were rinsed with TBS/T for 1 h, incubated with horseradish peroxidase (HRP) linked anti-rabbit secondary antibody (Jackson ImmunoResearch, West Grove, PA, USA) for 1 h, and washed again with TBS/T for another 1 h. Protein bands were detected by the ECL Western blot analysis system (Advansta, Menlo Park, CA, USA). The intensity of bands was measured in arbitrary units (AU) by using ImageJ 1.50i software (National Institute of Health, USA).

Expression and Secretion of RtxA1 Toxin in HeLa Cells Infected With *V. vulnificus* Strains

HeLa cells (Korea Cell Line Bank, Seoul, Korea) were cultured in Dulbecco's modified Eagle's medium (DMEM, Welgene, Daegu, Korea) containing 10% fetal bovine serum (ThermoFisher Scientific, Waltham, MA, US). *V. vulnificus* strains from cultures grown overnight in LB broth were diluted 200-fold with 10 mL of fresh LB broth in a shaking incubator at 37°C for another 3 h. HeLa cells (5×10^5 cells/well) grown overnight in 6-well plates were washed with serum free DMEM medium before being infected with bacteria at an MOI of 20 for 120, 150, or 180 min. The supernatants (300 μL) were precipitated by the addition of 3-fold ice-cold acetone. Bacterial pellets of the supernatants and HeLa cells were lysed with the cell lysis buffer (Promega, Madison, WI, USA) containing protease inhibitor cocktail (Sigma-Aldrich, St. Louis, MO, USA) shaking on ice for 30 min and harvested by centrifugation at 13000 rpm for 10 min after scrapping. The protein concentration was quantified using the Bradford's reagent (Bio-Rad Laboratories, USA). Equal amounts of protein were separated by NuPAGE™ 3%-8% Tris-Acetate gels (Thermo Fisher Scientific, Carlsbad, CA, USA) and subsequently subjected to Western blotting using an anti-RtxA1 antibody specific to amino acid 1492-1970 (RTX-D2 domain). Western blotting was performed as described above.

LDH Assay

HeLa cells seeded into 48-well plates (5×10^4 cells/well) overnight were washed with serum-free DMEM before being infected with 3 h or 9 h cultured bacterial cells of *V. vulnificus* strains at an MOI of 20 for 120, 150, or 180 min. A CytoTox96 Non-Radioactive Cytotoxicity Assay kit (Promega, Madison, WI, USA) was used to measure the amount of lactate dehydrogenase (LDH) released in the supernatants.

The Effect of Bile Salt on TolCV1 and TolCV2 Expression

V. vulnificus wild-type grown overnight in LB broth were diluted 200-fold with fresh LB medium and then cultured with or without 0.02% bile salt at 37°C for 3 h or 9 h. Equal number of bacterial cells (2×10^8 CFU) were harvested and resolved in sample buffer for Western blotting, which was performed as described above.

Growth Determination of *V. vulnificus* Strains on TCBS Agar Plates

Thiosulphate-citrate-bile salt sucrose (TCBS) agar plate (Difco, Becton-Dickinson, Sparks, MD, USA) is usually used for the selective isolation of Vibrio species (Di Pinto et al., 2011), which contains bile salts as one of the main ingredients. To verify the growth conditions of *V. vulnificus* strains in the presence of bile salt, their overnight cultures (3 μL) were dropped on TCBS agar and then incubated at 37°C overnight.

Measurement of Growth Rates of *V. vulnificus* Strains in the Presence of Bile Salt

Overnight cultures of *V. vulnificus* strains were diluted 200-fold with fresh LB media in the presence or absence of 0.02% bile salt.

Bacterial cells were cultured in a 37°C shaking incubator and the growth was measured using a spectrophotometer at 600 nm every 2 h.

Mice Lethality Assay

Eight-week-old female ICR mice (DBL, Umsung, South Korea) were kept under specific-pathogen-free conditions. Mice were infected with *V. vulnificus* wild-type, *tolCV1* mutant, *tolCV2* mutant, or *rtxA1* mutant strains (1×10^7 CFU/mouse) through intraperitoneal (i.p.) injection. Five mice were tested for each group and infected mice were subsequently observed for 72 h. All procedures involving animals were performed in accordance with the guidelines of the Chonnam National University Animal Care and Use Committee (IACUC-YB-2020-81).

RESULTS

Effect of *rpoS* Mutation on the Expression of Outer Membrane Proteins TolCV1 and TolCV2

We previously reported that sigma factor RpoS regulates RtxA1 expression and secretion to influence *V. vulnificus* pathogenesis (Guo et al., 2018). Hence, the current study was designed to explore whether RpoS represses RtxA1 secretion associated with outer membrane proteins TolCV1 and TolCV2. First, the TolCV1 and TolCV2 expression levels were measured at various time points and results showed that the expression levels of TolCV1 were time-dependently increased, unlike those of TolCV2, which were decreased (**Figure 1A**). Subsequently, the expression levels of TolCV1 and TolCV2 were compared between *V. vulnificus* wild-type and *rpoS* mutant strains at 3 and 9 h. Results showed that both TolCV1 and TolCV2 expression levels in the *rpoS* mutant strain were significantly lower than those in the wild-type (**Figure 1B**), indicating that RpoS acts as a positive regulator in TolCV1 and TolCV2 expressions. These data suggest that RpoS plays an essential role in the time-dependent expression of the outer membrane proteins TolCV1 and TolCV2 in *V. vulnificus*.

Effect of *tolCV1* or *tolCV2* Mutation on Host Factor Induced-RtxA1 Expression and Secretion

Only when the close contact of *V. vulnificus* with host cells was allowed, the expression of RtxA1 toxin would be dramatically upregulated to induce host cell death within a short time (Kim et al., 2008). To explore if TolCV1 and TolCV2 are required for the host factor induced-RtxA1 expression and secretion, the *tolCV1* and *tolCV2* mutant strains were constructed in *V. vulnificus* MO6-24/O strain. HeLa cells were infected with either *V. vulnificus* wild-type, *rpoS* mutant, *tolCV1* mutant, *tolCV2* mutant, or *rtxA1* mutant strains at an MOI of 20 for 120, 150, or 180 min. The protein levels of RtxA1 in the supernatants and HeLa cell lysates were determined by Western blotting. Similar to our previous report (Guo et al., 2018), the *rpoS* mutation resulted in a decreased level of host factor-induced RtxA1 expression in the cell lysates (**Figure 2**). RtxA1 proteins in HeLa cell lysates was detected without differences in infection with *V. vulnificus* wild-type, *tolCV1* mutant, or *tolCV2* mutant at any time (**Figure 2**). Additionally, RtxA1 protein was completely vanished in the supernatants of *tolCV1* mutant-infected HeLa cells, suggesting that RtxA1 toxin was exported by TolCV1 only, not TolCV2. Therefore, we can draw a conclusion that TolCV1 and TolCV2 do not affect the host factor-induced RtxA1 expression and TolCV1 is responsible for RtxA1 secretion.

Effect of *tolCV1* or *tolCV2* Mutation on *V. vulnificus* Cytotoxicity to Host Cells

To determine the roles of TolCV1 and TolCV2 in *V. vulnificus* virulence, the cytotoxicity of these strains to HeLa cells was measured by LDH assay. Consistent with Western blotting results, the *rpoS* mutant strain exhibited a decreased and delayed cytotoxicity to HeLa cells (**Figure 3**). The mutation of *tolCV1* considerably decreased cell cytotoxicity of *V. vulnificus*, but that of *tolCV2* did not exhibit a significant effect (**Figure 3**), suggesting that TolCV2 was not involved in *V. vulnificus*-induced cytotoxicity to HeLa cells. In conclusion, TolCV1 affects *V. vulnificus* cytotoxicity by controlling RtxA1 secretion, which is regulated by RpoS.

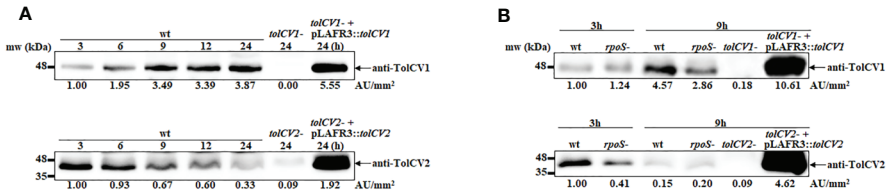

FIGURE 1 | Effect of *rpoS* mutation on the expression of outer membrane proteins TolCV1 and TolCV2. Overnight cultures of each *V. vulnificus* strains were diluted 200-fold with fresh LB broth and grown in a 37°C shaking incubator. Equivalent number of bacterial cells (2×10^8 CFU) were harvested at indicated time points followed by Western blotting with anti-TolCV1 or anti-TolCV2 primary antibodies. **(A)** Western blot analysis of *V. vulnificus* wild-type cells harvested at 3, 6, 9, 12, and 24 h cultures **(B)** Western blot analysis of *V. vulnificus* wild-type and its *rpoS* mutant cells collected at 3 h and 9 h cultures. Relative protein levels were quantified using ImageJ software. Results are representative of at least three independent experiments. Abbreviation: wt, wild-type; *tolCV1*-: *tolCV1* mutant of MO6-24/O; *tolCV1*- + pLAFR3::*tolCV1*: complementary strain of *tolCV1* mutant; *tolCV2*-: *tolCV2* mutant of MO6-24/O; *tolCV2*- + pLAFR3::*tolCV2*: complementary strain of *tolCV2* mutant; *rpoS*-: *rpoS* mutant of MO6-24/O.

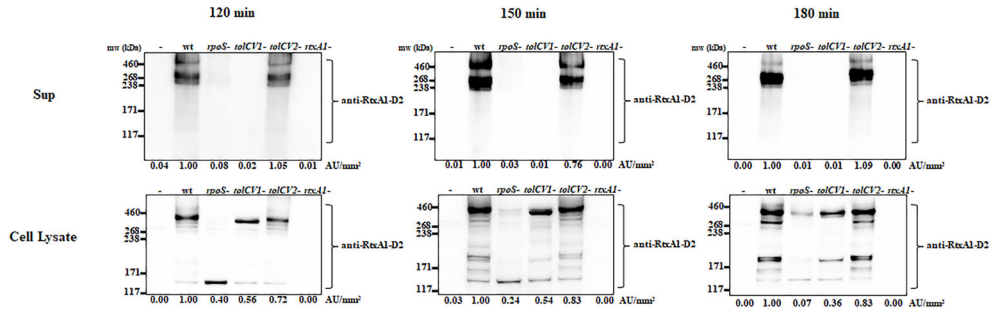

FIGURE 2 | Effect of *tolCV1* or *tolCV2* mutation on RtxA1 expression and secretion after contact with host cells. HeLa cells cultured overnight in 6-well plates (5×10^5 cells/well) were infected with either *V. vulnificus* wild-type (wt), *rpoS* mutant (*rpoS*-), *tolCV1* mutant (*tolCV1*-), *tolCV2* mutant (*tolCV2*-), or *rtxA1* mutant (*rtxA1*-) strains at an MOI of 20 for 120, 150, or 180 min. RtxA1 protein in the supernatants and cell lysates were detected by Western blot analysis with an RtxA1 antibody specific to amino acids 1492-1970 (RtxA1-D2 domain). Relative protein levels were quantified using ImageJ software. Results are representative of at least three independent experiments.

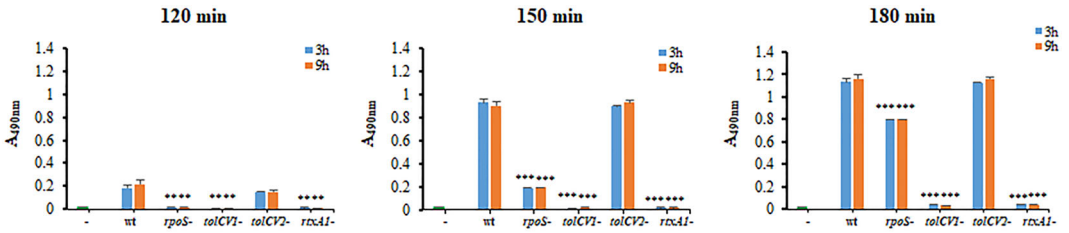

FIGURE 3 | Effect of *tolCV1* or *tolCV2* mutation on *V. vulnificus* cytotoxicity to host cells. HeLa cells cultured overnight in 48-well plates (5×10^4 cells/well) were infected with 3 h or 9 h cultured bacterial cells of *V. vulnificus* wild-type (wt), *rpoS* mutant (*rpoS*-), *tolCV1* mutant (*tolCV1*-), *tolCV2* mutant (*tolCV2*-), or *rtxA1* mutant (*rtxA1*-) strains at an MOI of 20 for 120, 150, or 180 min. The cytotoxicity of *V. vulnificus* strains was determined by measuring the amount of lactate dehydrogenase (LDH) released in the cell culture supernatants. Results are representative of at least three independent experiments. The statistical differences were analyzed by Student's t-test (*** and ** indicate $P < 0.001$ and $P < 0.01$ versus the wild-type treated group, respectively).

Effect of *tolCV1* or *tolCV2* Mutation on *V. vulnificus* Resistance to Bile Salt

To investigate the potential roles of TolCV1 and TolCV2 after bacteria enter the human body, we measured TolCV1 and TolCV2 expression levels after treatment with the host signal bile salt. The expression of TolCV1 and TolCV2 was upregulated in LB broth with 0.02% bile salt (**Figure 4A**). Consequently, *V. vulnificus* wild-type, *rpoS* mutant, *tolCV1* mutant, *tolCV2* mutant, or *rtxA1* mutant strains were cultured on TCBS agar plates to verify their growth conditions in the presence of bile salt. The *tolCV1* mutant strain showed growth defect on TCBS agar plate, which was restored by the *in trans* complementation with a plasmid-encoded wild-type allele (**Figure 4B**). Furthermore, we monitored the growth rates of the wild-type, *rpoS* mutant, *tolCV* mutant strains in LB broth containing 0.02% bile salt. Results indicated that the growth of *tolCV1* mutant was totally abolished and that of *rpoS* mutant was slightly suppressed in LB broth with 0.02% bile salt (**Figure 4C**). Based on these results, we concluded that TolCV1 is responsible for *V. vulnificus* growth in the presence of bile salt, and is crucial for *V. vulnificus* successful infection within the host.

Effect of *tolCV1* or *tolCV2* Mutation on Mice Lethality Caused by *V. vulnificus*

To further study the roles of TolC proteins *in vivo*, mice were infected with either *V. vulnificus* wild-type, *tolCV1* mutant, *tolCV2* mutant, or *rtxA1* mutant strains by intraperitoneal injection and their survival times were observed in the following 72 h. As previously reported, the mice infected with *V. vulnificus* wild-type exhibited lower activity, rapid mortality, and breathing difficultly after injection, while the *rtxA1* mutant-infected mice had improved survival rates (**Figure 5**). Moreover, the mice infected with *tolCV1* mutant performed better than mice infected with *rtxA1* mutant, showing a longer survival time and higher survival rate (**Figure 5**). In contrast, the *tolCV2* mutant-infected mice were expeditiously dead and indistinguishable from the wild-type-infected mice (**Figure 5**).

DISCUSSION

In this study, we first found that RpoS is a positive regulatory factor of TolCV1 and TolCV2 expression (**Figure 1B**) and

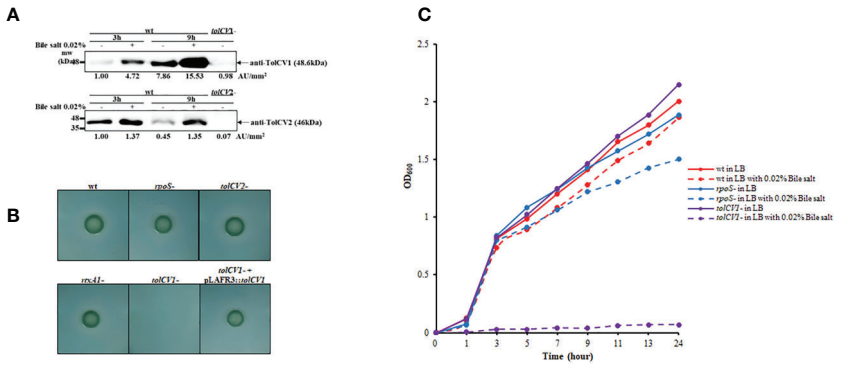

FIGURE 4 | Effect of *tolCV1* or *tolCV2* mutation on *V. vulnificus* resistance to bile salt. **(A)** *V. vulnificus* cells grown overnight in LB broth were diluted 200-fold with fresh LB medium containing 0.02% bile salt for 3 or 9 h. Equivalent number of bacterial cells (2×10^8 CFU) collected at 3 or 9 h cultures were subjected to Western blotting using anti-TolCV1 or anti-TolCV2 primary antibodies. Relative protein levels were quantified using ImageJ software. **(B)** Three microliters of overnight cultures of *V. vulnificus* strains were dropped on TCBS agar and then incubated overnight at 37°C. **(C)** Overnight cultures of *V. vulnificus* wild-type, *rpoS* mutant, or *tolCV1* mutant strains were diluted 200-fold with fresh LB media in the presence or absence of 0.02% bile salt. Bacterial cells were cultured in a shaking incubator at 37°C and the growth was measured using a spectrophotometer at 600 nm every 2 h. Results are representative of at least three independent experiments. Abbreviation: wt, wild-type; *tolCV1*-: *tolCV1* mutant of MO6-24/O; *tolCV1*- + pLAFR3::*tolCV1*: complementary strain of *tolCV1* mutant; *tolCV2*-: *tolCV2* mutant of MO6-24/O; *rpoS*-: *rpoS* mutant of MO6-24/O; *rtxA1*-: *rtxA1* mutant of MO6-24/O.

TolCV1 is responsible for exporting RtxA1 (**Figure 2**). Therefore, we concluded that the regulatory effect of RpoS on RtxA1 secretion was achieved by regulating the expression of TolCV1. In a previous report (Boardman and Satchell, 2004), it was suggested that RtxA1 was secreted by a Type I secretion system constituted by RtxB, RtxE, RtxD, and TolC in *Vibrio cholerae*. Therefore, RtxB, RtxE, RtxD may be the potential partners of TolCV1 collaboratively participated in the secretion of RtxA1 in *V. vulnificus*, which needs to be further confirmed. Additionally, the secretion of *V. vulnificus* hemolysin (VvhA) has been reported to be mediated by the Type II secretion system, and irrelevant with regard to TolC (Hwang et al., 2011). Subsequently, we explored the roles of TolCV1 and TolCV2 in *V. vulnificus* infection. The *tolCV1* mutation resulted in *V. vulnificus* growth defect in the presence of host signal bile salt (**Figures 4B**, **C**), which possibly explains why *tolCV1* mutation significantly reduced *V. vulnificus*-induced virulence in mice (**Figure 5**). RpoS is a stress sigma factor that is strongly induced during bacterial growth into stationary phase (Battesti et al., 2011). In the present study, we showed that TolCV1 expression time-dependently increased (**Figure 1A**), which may be caused by the accumulation of intracellular RpoS. This regulation presumably enables the bacteria to be more adaptive to stressful conditions in the stationary phase. In contrast, TolCV2 showed a time-dependently decreased expression trend (**Figure 1A**), suggesting that the expression of TolCV1 and TolCV2 was cooperatively regulated by several factors. A recently reported study revealed that the dead cells of bacterial swarms served as an "alarm signal" for live cells to increase their antibiotic resistance by releasing AcrA protein to bind with TolC located on the outer membrane of alive cells (Bhattacharyya et al., 2020). As the number of dead cells increased over time, we speculate that the gradually increased dead bacterial cells release some substances into the cultures that stimulate the expression of TolCV1 and TolCV2; however, this merits further research.

As previously reported, the outer membrane protein TolC affects virulence expression in *Vibrio cholerae*, *Francisella tularensis* and *Enterobacter cloacae* (Gil et al., 2006; Minato et al., 2011; Pérez et al., 2012). *V. vulnificus* TolCV1 and TolCV2 proteins display 78.65% and 44.44% sequence identity with *Vibrio cholerae* TolC, respectively. However, in *V. vulnificus*, the loss of outer membrane proteins TolCV1 and TolCV2 did not exhibit significant effect on the host factor-induced expression of RtxA1 toxin (**Figure 2**). Although Hwang et al. (Hwang et al., 2011) stated that TolC is responsible for RtxA1 secretion in *V. vulnificus*, whether TolCV1 or TolCV2 performed this task remained unclear. Here, we confirmed that RtxA1 toxin was exported by TolCV1 only, not TolCV2 (**Figure 2**). Besides, *tolCV1* and *tolCV2* mutant strains exhibited no difference with the wild-type strain in adhesion, and *tolCV1* mutation resulted in mild decreased motility of *V. vulnificus* in LB with 0.3% agar (data not shown).

V. vulnificus infections affect many people due to the intake of contaminated seafood (Chung et al., 2006). Large amounts of bile salt are distributed in the human intestinal environment, and the gastrointestinal tract is one of the most important ways for *V. vulnificus* to enter the human body. Existing evidence that TolC is indispensable for bile salt resistance and colonization in *Vibrio cholerae* (Bina and Mekalanos, 2001) encouraged us to explore the effect of TolCV1 and TolCV2 on bile salt resistance in *V. vulnificus*. The results indicated that TolCV1 is also responsible for maintaining *V. vulnificus* survival in the presence of bile salt (**Figures 4B**, **C**). Furthermore, a previous study revealed that the deletion of *rpoS* resulted in *V. vulnificus* delayed adaptation to bile salt (Chen et al., 2010), which can be explained by the downregulation of TolCV1 expression. Moreover, the mice

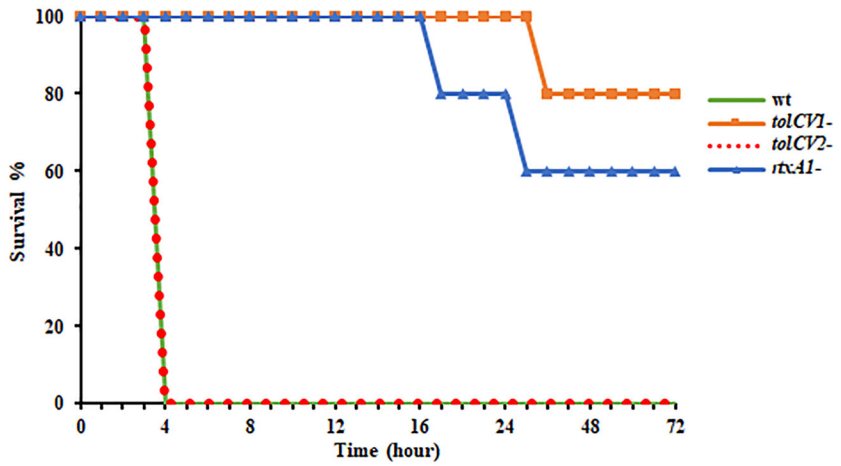

FIGURE 5 | Effect of *tolCV1* or *tolCV2* mutation on mice lethality caused by *V. vulnificus*. Eight-week-old female ICR mice were infected with *V. vulnificus* wild-type (wt), *tolCV1* mutant (*tolCV1*-), *tolCV2* mutant (*tolCV2*-), or *rtxA1* mutant (*rtxA1*-) strains (1×10^7 CFU/mouse) *via* intraperitoneal injection. Infected mice were observed for 72 h after injection and their survival times were recorded. Five mice were tested for each group.

infected with *tolCV1* mutant showed a longer survival time and higher survival rate than mice infected with *rtxA1* mutant (**Figure 5**), suggesting that TolCV1 is required for *V. vulnificus* pathogenesis and survival under *in vivo* conditions. Despite the fact that both TolCV1 and TolCV2 exhibit sequence identity in some degree to *E. coli* TolC, TolCV2 did not exhibit any comparative capacities to TolCV1. There exists an evidence that TolC is involved in the vulnibactin export of *V. vulnificus* (Kawano et al., 2014). Therefore, it is conceivable that TolCV1 and TolCV2 can also secrete other proteins or metabolites that are vital for *V. vulnificus* pathogenesis or survival. Further studies are required to comprehensively elucidate the functions of TolCV1 and TolCV2.

In the present study, we demonstrated that TolCV1 significantly influences RtxA1 secretion, bile salt resistance, and mice lethality of *V. vulnificus*. The results obtained in these experiments are encouraging, since our findings determined TolCV1 as an attractive target for developing drugs to treat *V. vulnificus* infections, which might someday lead to clinical applications.

DATA AVAILABILITY STATEMENT

Publicly available datasets were analyzed in this study. This data can be found here: https://www.ncbi.nlm.nih.gov/nuccore/NC_014966.1.

ETHICS STATEMENT

The animal study was reviewed and approved by Chonnam National University Animal Care and Use Committee (IACUC-YB-2020-81).

AUTHOR CONTRIBUTIONS

YG and RG performed the experiment and analyzed the data. YG wrote the manuscript. JR contributed to the conceptual design. YK conceived and designed the study, wrote and reviewed the manuscript. All authors contributed to the article and approved the submitted version.

FUNDING

This work was supported by a National Research Foundation of Korean (NRF) grant funded by the Korean government (Nos. 2018R1D1A3B07045194 and 2019R1A2C1005884).

ACKNOWLEDGMENTS

We would like to thank Editage (www.editage.co.kr) for English language editing.

REFERENCES

Baker-Austin, C., Oliver, J. D., Alam, M., Ali, A., Waldor, M. K., Qadri, F., et al. (2018). Vibrio Spp. Infections. *Nat. Rev. Dis. Primers.* 4, 1–19. doi: 10.1038/s41572-018-0005-8

Battesti, A., Majdalani, N., and Gottesman, S. (2011). The Rpos-Mediated General Stress Response in Escherichia Coli. *Annu. Rev. Microbiol.* 65, 189–213. doi: 10.1146/annurev-micro-090110-102946

Bhattacharyya, S., Walker, D. M., and Harshey, R. M. (2020). Dead Cells Release a 'Necrosignal'that Activates Antibiotic Survival Pathways in Bacterial Swarms. *Nat. Commun.* 11, 1–12. doi: 10.1038/s41467-020-17709-0

Bina, J. E., and Mekalanos, J. J. (2001). Vibrio Cholerae Tolc is Required for Bile Resistance and Colonization. *Infect. Immun.* 69, 4681–4685. doi: 10.1128/iai.69.7.4681-4685.2001

Boardman, B. K., and Satchell, K. J. F. (2004). Vibrio Cholerae Strains With Mutations in an Atypical Type I Secretion System Accumulate RTX Toxin

Intracellularly. *J. bacteriology.* 186, 8137–8143. doi: 10.1128/JB.186.23.8137-8143.2004

Chen, W.-L., Oliver, J. D., and Wong, H.-C. (2010). Adaptation of Vibrio Vulnificus and an Rpos Mutant to Bile Salts. *Int. J. Food Microbiol.* 140, 232–238. doi: 10.1016/j.ijfoodmicro.2010.03.027

Chung, P., Chuang, S., Tsang, T., Wai-Man, L., Yung, R., Lo, J., et al. (2006). Cutaneous Injury and Vibrio Vulnificus Infection. *Emerg. Infect. Dis.* 12, 1302. doi: 10.3201/eid1208.051495

Di Pinto, A., Terio, V., Novello, L., and Tantillo, G. (2011).). Comparison Between Thiosulphate-Citrate-Bile Salt Sucrose (TCBS) Agar and Chromagar Vibrio for Isolating Vibrio Parahaemolyticus. *Food Control.* 22, 124–127. doi: 10.1016/j.foodcont.2010.06.013

Ditta, G., Stanfield, S., Corbin, D., and Helinski, D. R. (1980). Broad Host Range DNA Cloning System for Gram-Negative Bacteria: Construction of a Gene Bank of Rhizobium Meliloti. *Proc. Natl. Acad. Sci. U. S. A.* 77, 7347–7351. doi: 10.1073/pnas.77.12.7347

Du, D., Van Veen, H. W., and Luisi, B. F. (2015). Assembly and Operation of Bacterial Tripartite Multidrug Efflux Pumps. *Trends Microbiol.* 23, 311–319. doi: 10.1016/j.tim.2015.01.010

Du, D., Wang, Z., James, N. R., Voss, J. E., Klimont, E., Ohene-Agyei, T., et al. (2014). Structure of the Acrab–Tolc Multidrug Efflux Pump. *Nature.* 509, 512–515. doi: 10.1038/nature13205

El Meouche, I., and Dunlop, M. J. (2018). Heterogeneity in Efflux Pump Expression Predisposes Antibiotic-Resistant Cells to Mutation. *Science.* 362, 686–690. doi: 10.1126/science.aar7981

Gil, H., Platz, G. J., Forestal, C. A., Monfett, M., Bakshi, C. S., Sellati, T. J., et al. (2006). Deletion of Tolc Orthologs in Francisella Tularensis Identifies Roles in Multidrug Resistance and Virulence. *Proc. Natl. Acad. Sci. U. S. A.* 103, 12897–12902. doi: 10.1073/pnas.0602582103

Guo, R. H., Gong, Y., Kim, S. Y., Rhee, J. H., and Kim, Y. R. (2020). DIDS Inhibits Vibrio Vulnificus Cytotoxicity by Interfering With Tolc-Mediated Rtxa1 Toxin Secretion. *Eur. J. Pharmacol.* 884, 173407. doi: 10.1016/j.ejphar.2020.173407

Guo, R. H., Lim, J. Y., Tra My, D. N., Jo, S. J., Park, J. U., Rhee, J. H., et al. (2018). Vibrio Vulnificus Rtxa1 Toxin Expression Upon Contact With Host Cells is Rpos-Dependent. *Front. Cell Infect. Microbiol.* 8, 70. doi: 10.3389/fcimb.2018.00070

Hwang, W., Lee, N. Y., Kim, J., Lee, M.-A., Kim, K.-S., Lee, K.-H., et al. (2011). Functional Characterization of Epsc, a Component of the Type II Secretion System, in the Pathogenicity of Vibrio Vulnificus. *Infect. Immun.* 79, 4068–4080. doi: 10.1128/IAI.05351-11

Kanonenberg, K., Smits, S. H., and Schmitt, L. (2019). Functional Reconstitution of Hlyb, a Type I Secretion ABC Transporter, in Saposin-a Nanoparticles. *Sci. Rep.* 9, 1–12. doi: 10.1038/s41598-019-44812-0

Kawano, H., Miyamoto, K., Yasunobe, M., Murata, M., Myojin, T., Tsuchiya, T., et al. (2014). The RND Protein is Involved in the Vulnibactin Export System in Vibrio Vulnificus M2799. *Microb. Pathog.* 75, 59–67. doi: 10.1016/j.micpath.2014.09.001

Kim, Y. R., Lee, S. E., Kang, I.-C., Nam, K. I., Choy, H. E., and Rhee, J. H. (2013). A Bacterial Rtx Toxin Causes Programmed Necrotic Cell Death Through Calcium-Mediated Mitochondrial Dysfunction. *J. Infect. Dis.* 207, 1406–1415. doi: 10.1093/infdis/jis746

Kim, Y. R., Lee, S. E., Kook, H., Yeom, J. A., Na, H. S., Kim, S. Y., et al. (2008). Vibrio Vulnificus RTX Toxin Kills Host Cells Only After Contact of the Bacteria With Host Cells. *Cell Microbiol.* 10, 848–862. doi: 10.1111/j.1462-5822.2007.01088.x

Kwak, J. S., Jeong, H.-G., and Satchell, K. J. (2011). Vibrio Vulnificus Rtxa1 Gene Recombination Generates Toxin Variants With Altered Potency During Intestinal Infection. *Proc. Natl. Acad. Sci.* 108, 1645–1650. doi: 10.1073/pnas.1014339108

Langevin, A. M., and Dunlop, M. J. (2018). Stress Introduction Rate Alters the Benefit of Acrab-Tolc Efflux Pumps. *J. Bacteriol.* 200, 1–11. doi: 10.1128/JB.00525-17

Lee, K.-E., Bang, J.-S., Baek, C.-H., Park, D.-K., Hwang, W., Choi, S.-H., et al. (2007). IVET-Based Identification of Virulence Factors in Vibrio Vulnificus MO6-24/O. *J. Microbiol. Biotechnol.* 17, 234–243.

Lee, M., Kim, H.-L., Song, S., Joo, M., Lee, S., Kim, D., et al. (2013). The A-Barrel Tip Region of Escherichia Coli Tolc Homologs of Vibrio Vulnificus Interacts With the Maca Protein to Form the Functional Macrolide-Specific Efflux Pump Macab-Tolc. *J. Microbiol.* 51, 154–159. doi: 10.1007/s12275-013-2699-3

Lee, S., Song, S., and Lee, K. (2014a). Functional Analysis of Tolc Homologs in Vibrio Vulnificus. *Curr. Microbiol.* 68, 729–734. doi: 10.1007/s00284-014-0537-4

Lee, S., Song, S., Lee, M., Hwang, S., Kim, J.-S., Ha, N.-C., et al. (2014b). Interaction Between the A-Barrel Tip of Vibrio Vulnificus Tolc Homologs and Acra Implies the Adapter Bridging Model. *J. Microbiol.* 52, 148–153. doi: 10.1007/s12275-014-3578-2

Lee, S., Yeom, J.-H., Seo, S., Lee, M., Kim, S., Bae, J., et al. (2015). Functional Analysis of Vibrio Vulnificus RND Efflux Pumps Homologous to Vibrio Cholerae Vexab and Vexcd, and to Escherichia Coli Acrab. *J. Microbiol.* 53, 256–261. doi: 10.1007/s12275-015-5037-0

Miller, V. L., and Mekalanos, J. J. (1988). A Novel Suicide Vector and Its Use in Construction of Insertion Mutations: Osmoregulation of Outer Membrane Proteins and Virulence Determinants in Vibrio Cholerae Requires Toxr. *J. Bacteriol.* 170, 2575–2583. doi: 10.1128/jb.170.6.2575-2583.1988

Milton, D. L., O'toole, R., Horstedt, P., and Wolf-Watz, H. (1996). Flagellin a is Essential for the Virulence of Vibrio Anguillarum. *J. Bacteriol.* 178, 1310–1319. doi: 10.1128/jb.178.5.1310-1319.1996

Minato, Y., Siefken, R. L., and Häse, C. C. (2011). Tolc Affects Virulence Gene Expression in Vibrio Cholerae. *J. Bacteriol.* 193, 5850–5852. doi: 10.1128/jb.05222-11

Nolivos, S., Cayron, J., Dedieu, A., Page, A., Delolme, F., and Lesterlin, C. (2019). Role of Acrab-Tolc Multidrug Efflux Pump in Drug-Resistance Acquisition by Plasmid Transfer. *Science.* 364, 778–782. doi: 10.1126/science.aav6390

Park, J. H., Cho, Y.-J., Chun, J., Seok, Y.-J., Lee, J. K., Kim, K.-S., et al. (2011). Complete Genome Sequence of Vibrio Vulnificus MO6-24/O. *J. Bacteriol* 193, 2062–2063. doi: 10.1128/JB.00110-11

Park, J., and Lee, C. (2018). Vibrio Vulnificus Infection. *N Engl. J. Med.* 379, 375. doi: 10.1056/NEJMicm1716464

Pérez, A., Poza, M., Fernández, A., Del Carmen Fernández, M., Mallo, S., Merino, M., et al. (2012). Involvement of the Acrab-Tolc Efflux Pump in the Resistance, Fitness, and Virulence of Enterobacter Cloacae. *Antimicrob. Agents Chemother.* 56, 2084–2090. doi: 10.1128/aac.05509-11

Puértolas-Balint, F., Warsi, O., Linkevicius, M., Tang, P.-C., and Andersson, D. I. (2020). Mutations That Increase Expression of the Emrab-Tolc Efflux Pump Confer Increased Resistance to Nitroxoline in Escherichia Coli. *J. Antimicrob. Chemother.* 75, 300–308. doi: 10.1093/jac/dkz434

Reddy, G., Hayat, U., Abeygunawardana, C., Fox, C., Wright, A., Maneval, D., et al. (1992). Purification and Determination of the Structure of Capsular Polysaccharide of Vibrio Vulnificus M06-24. *J. Bacteriol.* 174, 2620–2630. doi: 10.1128/jb.174.8.2620-2630.1992

Roig, F. J., González-Candelas, F., and Amaro, C. (2011). Domain Organization and Evolution of Multifunctional Autoprocessing Repeats-in-Toxin (MARTX) Toxin in Vibrio Vulnificus. *Appl. Environ. Microbiol.* 77, 657–668. doi: 10.1128/AEM.01806-10

Staskawicz, B., Dahlbeck, D., Keen, N., and Napoli, C. (1987). Molecular Characterization of Cloned Avirulence Genes From Race 0 and Race 1 of Pseudomonas Syringae Pv. Glycinea. *J. Bacteriol.* 169, 5789–5794. doi: 10.1128/jb.169.12.5789-5794.1987

Conflict of Interest: The authors declare that the research was conducted in the absence of any commercial or financial relationships that could be construed as a potential conflict of interest.

frontiers in Cellular and Infection Microbiology

ORIGINAL RESEARCH
published: 14 May 2021
doi: 10.3389/fcimb.2021.652957

De Novo Sequencing Provides Insights Into the Pathogenicity of Foodborne *Vibrio parahaemolyticus*

Jianfei Liu[1,2†], *Kewei Qin*[1,2†], *Chenglin Wu*[1,2], *Kaifei Fu*[1,2], *Xiaojie Yu*[1,2] *and Lijun Zhou*[1,2*]

[1] Central Laboratory, The Sixth Medical Centre, Chinese PLA (People's Liberation Army) General Hospital, Beijing, China, [2] College of Otolaryngology Head and Neck Surgery, The Sixth Medical Centre, Chinese PLA (People's Liberation Army) General Hospital, Beijing, China

Vibrio parahaemolyticus is a common pathogenic marine bacterium that causes gastrointestinal infections and other health complications, which could be life-threatening to immunocompromised patients. For the past two decades, the pathogenicity of environmental *V. parahaemolyticus* has increased greatly, and the genomic change behind this phenomenon still needs an in-depth exploration. To investigate the difference in pathogenicity at the genomic level, three strains with different hemolysin expression and biofilm formation capacity were screened out of 69 environmental *V. parahaemolyticus* strains. Subsequently, 16S rDNA analysis, *de novo* sequencing, pathogenicity test, and antibiotic resistance assays were performed. Comparative genome-scale interpretation showed that various functional region differences in pathogenicity of the selected *V. parahaemolyticus* strains were due to dissimilarities in the distribution of key genetic elements and in the secretory system compositions. Furthermore, the genomic analysis-based hypothesis of distinct pathogenic effects was verified by the survival rate of mouse models infected with different *V. parahaemolyticus* strains. Antibiotic resistance results also presented the multi-directional evolutionary potential in environmental *V. parahaemolyticus*, in agreement with the phylogenetic analysis results. Our study provides a theoretical basis for better understanding of the increasing pathogenicity of environmental *V. parahaemolyticus* at the genome level. Further, it has a key referential value for the exploration of pathogenicity and prevention of environmental *V. parahaemolyticus* in the future.

Keywords: ***Vibrio parahaemolyticus*, pathogenicity, *de novo* sequencing, virulence, mouse model**

OPEN ACCESS

Edited by:
Wenxiang Sun,
The University of Utah, United States

Reviewed by:
Graciela Castro Escarpulli,
Instituto Politécnico Nacional de México (IPN), Mexico
Vincent Tam,
Temple University, United States

***Correspondence:**
Lijun Zhou
hzzhoulj@126.com

[†]*These authors have contributed equally to this work*

Specialty section:
This article was submitted to Molecular Bacterial Pathogenesis, a section of the journal Frontiers in Cellular and Infection Microbiology

Received: *13 January 2021*
Accepted: *22 April 2021*
Published: *14 May 2021*

Citation:
Liu J, Qin K, Wu C, Fu K, Yu X and Zhou L (2021) De Novo Sequencing Provides Insights Into the Pathogenicity of Foodborne Vibrio parahaemolyticus. Front. Cell. Infect. Microbiol. 11:652957. doi: 10.3389/fcimb.2021.652957

INTRODUCTION

Vibrio parahaemolyticus is a gram-negative halophilic bacterial species, first identified in 1950 (Fujino et al., 1953). Various serotypes of *V. parahaemolyticus* have been confirmed to be opportunistically pathogenic to humans (Ueno et al., 2016), causing acute or subacute gastroenteritis accompanied with dehydration, chills, and fever, irrespective of age or gender (Yang et al., 2019b). Primary symptoms can easily progress to severe dehydration, causing shock and other concomitant complications, which can even result in the death of immunocompromised patients, if not treated in a timely manner (Shuja et al., 2014; Guillod et al., 2019). Due to its wide existence in marine and terrestrial environments (Miyamoto et al., 1962; Barker, 1974), *V. parahaemolyticus* causes foodborne diseases worldwide. It is the only

marine bacterium among the top five foodborne pathogens causing human infection (CDC, 2019). Although this bacterium was normally known to cause infections locally, since the past two decades, there have been reports of transcontinental distribution of certain *V. parahaemolyticus* strains (Miyamoto et al., 1962; Yang et al., 2019a). There has been an increase in the number of clinical cases of *V. parahaemolyticus* infection (Li et al., 2016), and sporadic or epidemic cases have been reported in some regions that were once considered unsuitable for the growth of *V. parahaemolyticus*, such as South America and Northern Europe (Martinez-Urtaza et al., 2010; Baker-Austin et al., 2013). This suggests that *V. parahaemolyticus* is continuously evolving and is developing into a more serious pathogen (Nair et al., 2007; Newton et al., 2014). However, the mechanisms of its rapid serotype conversion and pandemic evolution have not been revealed yet.

Recently, pathogenic feature changes of environmental *V. parahaemolyticus* strains suggested a high level of genetic diversity and a more rapid recombination frequency, strongly connected with highly complex and fast genomic evolution (Yang et al., 2019b), which are worthy of in-depth exploration. However, mainstream research methods, such as serotyping, multilocus sequence typing, and pulsed field gel electrophoresis, have been unable to fully explain the evolutionary attributes of environmental *V. parahaemolyticus* and the cause of its enhanced pathogenicity. Whole Genome Sequencing (WGS) technology is an emerging molecular researching method (Schürch et al., 2018), which provides a new way to study microorganisms through correlation analysis (Rossen et al., 2018), for resolving and reconstructing sample sequences and predicting detailed genomic functions by comparison to public databases. The convenience of genomic analysis by WGS technology makes it a powerful method for understanding genome properties more deeply, tracing back the phylogenetic progress, and predicting the pathogenicity of microorganisms (Ronholm et al., 2016; Gonzalez-Escalona et al., 2017). Therefore, a study on *V. parahaemolyticus* pathogenicity by WGS could provide a more comprehensive interpretation of the rapid evolutionary changes occurring in this species.

In this paper, virulence features of 69 V. *parahaemolyticus* strains derived from food products were evaluated by analyzing the hemolysin-encoding gene and differences in biofilm formation (BF), and three strains were selected for the further study. In order to interpret the difference in pathogenicity at the genomic level, *de novo* sequencing was used to understand the genetic composition and to explore the functional information. Pathogenicity *in vivo* and antibiotic resistance were also evaluated. Our study provided a more comprehensive idea for developing a better understanding of foodborne *V. parahaemolyticus* and for further interpreting the relationship between the pathogenicity and genomic changes of environmental *V. parahaemolyticus*.

MATERIALS AND METHODS

Bacteria and Growth Conditions

A total of 69 environmental strains of *V. parahaemolyticus* were used in this study (hereafter referred to as strains *Vp.* 1463–1528, *Vp.* 4213, *Vp.* 4215, and *Vp.* 11577), which were kindly provided as a gift by Prof. Shenghui Cui, who had maintained them at the National Institutes for Food and Drug Control (NIFDC) of China. Original *V. parahaemolyticus* were isolated from commercial food samples during the day of August 25, 2015, to June 1, 2016, and were land transported from Anhui, Shanxi and Fujian provinces in China, respectively. Detailed background information could be found in **Table S1**. All *V. parahaemolyticus* strains were initially maintained on 2216E agar plates (BD Biosciences, NJ, USA) at 35°C for 12 h, and routinely cultured in 2216E broth (BD Biosciences, NJ, USA) at 35°C, with shaking at 180 rpm for 12 h. Dilution or enrichment of cultured *V. parahaemolyticus* strains was performed in 3% NaCl alkaline peptone water (APW; Land Bridge Technology, Beijing, China).

Multiplex PCR Assay for *V. parahaemolyticus* Hemolysins

The culture density of all 69 V. *parahaemolyticus* strains was adjusted to 3×10^5 CFU/ml, and they were cultured in 3% NaCl APW at 35°C with shaking at 180 rpm. After culturing for 6 h, 1 ml of the cultures was centrifuged (10,000 rpm) to obtain a bacterial pellet from which genomic DNA was extracted using a DNA extraction kit (TIANGEN, Beijing, China). Concentrations of genomic DNA were measured using NanoDrop 8000 (Thermo Fisher, MA, USA).

Three pairs of primers targeting genes *tdh*, *trh*, and *tlh* were designed for PCR based on their DNA sequences (**Table S2**), using the Primer Premier 5.0 software (San Francisco, CA, USA; http://www.premierbiosoft.com/primerdesign/). Multiplex PCR amplification was optimized in a 50-μl reaction consisting of 0.5 mg purified genomic DNA, 1 μM of each primer, 25 μl of GoTaq qPCR Master Mix (Promega Corporation, WI, USA), and an appropriate volume of sterile water (Milli-Q; Merck, Darmstadt, Germany).

All multiplex PCR amplifications were performed on an ABI 2720 Thermal Cycler (Thermo Scientific, MA, USA), using the following temperature-cycling parameters: initial denaturation at 94°C for 3 min, followed by 30 cycles of amplification, with each cycle involving denaturation at 94°C for 1 min, primer annealing at 58°C for 1 min, and primer extension at 72°C for 1 min. After the amplification cycles, samples were kept at 72°C for 5 min to allow the final extension of the incompletely synthesized DNA.

Biofilm Formation Assay

The semi-quantitative adhesion test was performed for assessing biofilm formation, using the method described by Stepanovic et al., with some modifications (Stepanovic et al., 2000). In brief, cultures of all 69 V. *parahaemolyticus* strains were adjusted to 3×10^5 CFU/ml, and incubated in 96-well polystyrene microplates (Corning, NY, USA), at 35°C for 30 h. Suspended cultures were transferred to a fresh microplate to measure the CFU. The original microplate was first rinsed three times with phosphate buffered saline (PBS; Leagene, Beijing, China), followed by fixing with Bouin's fluid (Leagene, Beijing, China) for 20 min. Then the microplate was rinsed three more times with PBS, and subsequently stained with crystal violet (Leagene, Beijing,

China) for 30 min, followed by a final rinsing with PBS three times. Stained biofilm on each air-dried well was washed with crystal violet using ethanol (95%, v/v solution; Sinopharm, Beijing, China) until it was completely rinsed off. An iMark microplate reader (Bio-Rad, CA, USA) was used for measuring the absorbance at 570 nm ($OD_{570\ nm}$). The normalized BF was calculated using the following formula: normalized BF_{sample} = (original BF_{sample} − $BF_{control}$)/$\log_{(CFU/ml)}$.

Phylogenetic Analysis of *V. parahaemolyticus*

All *V. parahaemolyticus* strains were sequenced by 16S rDNA sequencing, and the general pair of primers were as follows: 27F (5′-AGAGTTTGATCCTGGCTCAG-3′) and 1492R (5′-TACG GCTACCTTGTTACGACTT-3′) (Lane, 1991). 16S rDNA sequences were assembled for phylogenetic analysis. To further determine the degree of molecular evolution, three strains, viz., *Vp.* 1474, *Vp.* 1496, and *Vp.* 1513, were selected based on the differences in the expression of hemolysin genes *tdh* and *trh*, and BF capacity. *V. probioticus* LMG 20362T, *V. rotiferianus* LMG 21460T, *V. proteolyticus* ATCC 15338T, *V. parahaemolyticus* ATCC 17802T, *V. natriegens* ATCC 14048T, *V. harveyi* NCIMB 1280T, *V. campbellii* ATCC 25920T, and *V. alginolyticus* ATCC 17749T were used as reference *Vibrio* strains for phylogenetic analysis (**Table S1**). Phylogenetic and molecular evolutionary analyses were conducted using MEGA version 6 (Pennsylvania State University, PA, USA; https://www.megasoftware.net/). The maximum likelihood tree was used for reconstructing the phylogenetic process, and detailed analyses, including phylogenetic tests on the nucleotides, were conducted using the Tamura-Nei substitution model based on a 1,000-replication bootstrap method.

De Novo Sequencing

Extraction of Genomic DNA

The strains *Vp.* 1474, *Vp.* 1496, and *Vp.* 1513 were cultured overnight in 3% NaCl APW, and genomic DNA was extracted from them using a DNA extraction kit (TIANGEN, Beijing, China). The harvested DNA was detected using agarose gel electrophoresis, and quantified using Nanodrop 8000 (Thermo Scientific, MA, USA).

Library Construction and Sequencing

Total 1 μg DNA for each of the three strains was used as input material for the DNA sample preparations. Sequencing libraries were generated using NEBNext® Ultra™ DNA Library Prep Kit for Illumina (New England BioLabs Inc., MA, USA), following the manufacturer's recommendations. Briefly, the genomic DNA was fragmented by sonication to sizes of 350 bp and 6 kb. Large DNA fragments were amplified with circularization amplification. The products were randomly disrupted into fragments of about 350 bp, and the sequences on both sides of the circularized primers were captured with probes for subsequent DNA library construction. DNA fragments were end-polished, added poly-A tail, and ligated with the full-length adaptor for further PCR amplification. At last, PCR products were purified using AMPure XP system (Beckman Coulter, CA, USA), and the insert size of libraries was analyzed for size distribution by Agilent Bioanalyzer 2100 (Agilent, CA, USA), and the libraries were quantified using real-time PCR (Roche, Basel, Switzerland).

The genomes of *Vp.* 1474, *Vp.* 1496, and *Vp.* 1513 were separately sequenced using Illumina NovaSeq PE150 (Beijing Compass Bioinformatics Technology Co., Ltd., Beijing, China). Data analyses, including genome assembly analysis, genome component prediction, gene function prediction, and comparative genomics analysis, were conducted.

Bioinformatics Analysis

The GeneMarkS software (version 4.17; Georgia Institute of Technology, GA, USA; http://exon.gatech.edu/GeneMark/genemarks.cgi) was used to predict coding genes for the sequenced genomes of *Vp.* 1474, *Vp.* 1496, and *Vp.* 1513 (Besemer et al., 2001). Based on the sequence composition, the IslandPath-DIOMB software (version 0.2; Simon Fraser University, Vancouver, Canada; http://www.pathogenomics.sfu.ca/islandpath/) was used to predict genomic islands (GIs) (Bertelli and Brinkman, 2018). Determination of GIs by detecting phylogenetic bias and mobility genes in the sequence also enabled the detection of potential horizontal gene transfers (HGT). PhiSpy software (version 3.4; Stanford University, CA, USA; https://github.com/linsalrob/PhiSpy) was used to predict prophage loci on the genome of *Vp.* 1474, *Vp.* 1496 and *Vp.* 1513 (Akhter et al., 2019). CRISPRdigger software (version 1.0; Chinese Academy of Sciences, Shenzhen, China; https://github.com/greyspring/CRISPRdigger) was used for identifying CRISPR sequences in the genome of the three selected *V. parahaemolyticus* strains (Ge et al., 2016). Predicted gene-encoding protein sequences were aligned using the Diamond software (version 2.0.1; Max Planck Institute for Developmental Biology, Tübingen, Germany, http://www.diamondsearch.org), and the gene matching e-values ≤ 1^{e-5} were screened. Based on the alignment results of each sequence, the alignment with the highest score (default identity≥ 40%, coverage≥ 40%) was selected for annotation.

Three databases, viz., Gene Ontology (GO; http://geneontology.org/), Kyoto Encyclopedia of Genes and Genomes (KEGG; https://www.genome.jp/kegg/), and Clusters of Orthologous Groups (COG; http://clovr.org/docs/clusters-of-orthologous-groups-cogs/), were used for predicting gene functions of *Vp.* 1474, *Vp.* 1496, and *Vp.* 1513. For virulence and pathogenicity analysis, Pathogen-Host Interactions database (PHI; https://www.uniprot.org/database/phi-base), Antibiotic Resistance Genes Database (ARDB; http://ardb.cbcb.umd.edu/), Comprehensive Antibiotic Research Database (CARD; https://card.mcmaster.ca/), and Virulence Factors Database (VFDB; http://www.mgc.ac.cn/VFs/) were used. Subsequently, multiple analysis tools were used to predict the gene-encoding effectors, which included the secretory protein prediction with SignalP (version 4.1; Technical University of Denmark, Copenhagen, Denmark; http://www.cbs.dtu.dk/services/SignalP/) and TMHMM software (version 2.0c; Technical University of Denmark, Copenhagen, Denmark; http://www.cbs.dtu.dk/services/TMHMM/) (Möller et al., 2001; Nielsen et al., 2019). The Type N secretion system (TNSS) proteins were screened from the TNSS-associated proteins, which were chosen and filtered

directly from multiple genomic functional databases, including Non-Redundant Protein database (NR; Li et al., 2002), Swiss-Prot database (Bairoch and Apweiler, 2000), Transporter Classification Database (TCDB; Saier et al., 2014), GO, PHI and VFDB. Type III secretion system (T3SS) effector was further predicted with EffectiveT3 software (version 1.0.1; University of Vienna, Vienna, Austria; https://effectors.csb.univie.ac.at/method/effectivet3), using the annotation results of the protein sequence function database according to the related proteins of the secretion system extracted and annotated (Jehl et al., 2011).

Genomic Visualization Analysis

The sequencing maps of the three selected strains were displayed using the Circos software (Canada's Michael Smith Genome Sciences Centre, Vancouver, Canada; http://www.circos.ca/software/) after combining the prediction results of the encoded genes (Krzywinski et al., 2009).

Survival Analysis

The three selected *V. parahaemolyticus* strains were cultured in 3% NaCl APW at 35°C, with shaking for 8 h, and the fresh culture suspensions were adjusted to OD values of 0.1, 0.2, and 0.3. The culture was centrifuged (1,680*g*, 10 min) and rinsed with sterile 9% NaCl three times, and the supernatant was discarded. The bacterial sediment was resuspended in 100 μl PBS to be made ready for intraperitoneal injection.

Eight-week-old female Balb/C mice with average weight of 18 g (17.4–18.6 g per each) were used for *in vivo* infection experiment. Survival assay contained nine groups, i.e., three selected strains with three different injection concentrations, and each test group was comprised of eight mice, allowed to feed and drink freely. The survival rate of each group was observed every hour for 12 h after *Vibrio* infection. After the 12-h acute infection period, the status of mice was observed every 12 h, and the number of deaths for each group was recorded. The experiment continued for a total of 4 days. After reaching the end of the *in vivo* experiment, the surviving mice were anesthetized excessively, and were cervical dislocated to death. The body of mice were put to harmless disposal after incineration.

All animal procedures complied with the institutional and national guidelines prescribed by the International Council for Laboratory Animal Science (ICLAS) from the Ministry of Health of the People's Republic of China. All procedures performed in this work involving animals were in accordance with the ethical standards of Animal Ethics Committee of the Sixth Medical Centre of Chinese PLA General Hospital at which the work was conducted.

Drug Sensitivity Test

A total of 22 different antimicrobial drug sensitivity test papers (OXOID, MA, USA) were used to perform the drug sensitivity tests for tetracycline (TE), cefotaxime (CTX), ceftazidime (CAZ), ciprofloxacin (CIP), levofloxacin (LEV), ofloxacin (OFX), ampicillin (AMP), amoxycillin/clavulanic acid (AMC), ampicillin/sulbactam (SAM), piperacillin (PRL), piperacillin/tazobactam (TZP), cephazolin (KZ), cefepime (FEP), cefoxitin (FOX), cefuroxime sodium (CXM), cephalothin (KF), imipenem (IPM), meropenem (MEM), amikacin (AK), gentamicin (CN), chloramphenicol (C), and sulphamethoxazole/trimethoprim (SXT). The Kirby-Bauer method, recommended by the Clinical and Laboratory Standards Institute, was used to determine the sensitivity of the 69 V. *parahaemolyticus* strains to the 22 antibiotics.

Single colonies of *V. parahaemolyticus* strains cultured on thiosulfate citrate bile salts sucrose agar culture medium (Beijing Land Bridge Technology, Beijing, China) for 18 h, were cultured in 3% NaCl APW at 35°C, with shaking for 8 h. The concentration of the culture was adjusted to 0.5 MCF with sterile physiological saline. A 90 mm Mueller-Hinton agar plate with 3% NaCl (Beijing Land Bridge Technology, Beijing, China) was streaked twice with swabs, and incubated for 20 min to affix the drug sensitivity test papers. Each plate was affixed with five different susceptibility test papers, and each antibiotic was tested in triplicate. After incubation at 35°C for 16 h, the bacteriostatic zone was measured with a Vernier caliper, and *E. coli* ATCC 25922 was used as a reference strain for quality control (**Table S1**).

Statistics

Results were analyzed using one-way analysis of variance and Dunnett's test by IBM Statistics SPSS (version 22) (IBM, NY, USA). *P* values were two-tailed, and the threshold for statistical significance was set at 0.05. Results are presented as mean ± standard error for all independent experiments at each time point. Kaplan-Meier method was used on survival analysis and Breslow test was used for statistical analyses by IBM Statistics SPSS (version 22) (IBM, NY, USA). Breslow *P* values for statistical significance was set at 0.05.

RESULTS

General Attributes of All *V. parahaemolyticus* Strains and Screening of Representative Strains

Multiplex PCR results showed that all the strains of *V. parahaemolyticus* carried the *tlh* gene, encoding thermolabile hemolysin, specifically expressed by *V. parahaemolyticus*. Multiple combination types of Thermostable direct hemolysin- (TDH-) and thermostable related hemolysin- (TRH-) encoding genes were detected, as shown in **Table 1**. Among 69 strains, four (*Vp.* 1470, *Vp.* 1474, *Vp.* 1507, and *Vp.* 4215) carried the *tdh* gene and three (*Vp.* 1511, *Vp.* 1513 and *Vp.* 4213) carried the *trh* gene. However, none of the strains carried both *tdh* and *trh* at the same time.

Among the 69 strains of foodborne *V. parahaemolyticus*, only three (*Vp.* 1474, *Vp.* 1513, and *Vp.* 11577) could form strong biofilms and three (*Vp.* 1478, *Vp.* 1479, and *Vp.* 1484) could form medium level biofilms. Fifty-six of the remaining strains formed weak biofilms, and the remaining seven (*Vp.* 1472, *Vp.* 1473, *Vp.* 1494, *Vp.* 1497, *Vp.* 1499, *Vp.* 1502, and *Vp.* 1511) were unable to form a biofilm matrix. BF of the *V. parahaemolyticus* strains had been shown in **Figure 1A**.

The 16S rDNA phylogenetic tree showed that the 69 strains of foodborne *V. parahaemolyticus* belonged to six different phylogenetic branches (**Figure 1B**). It may be assumed that during evolution, a large evolutionary lineage difference occurred

among these 69 isolates, resulting in a comparatively large difference in conserved gene sequences. Analyzing with the collaboration of the features of biofilm formation capacity and hemolysin expression, *Vp.* 1474, *Vp.* 1496, and *Vp.* 1513, each belonging to a different phylogenetic branch, were all showed significant phylogenetic differences to the reference strain *V. parahaemolyticus* ATCC 17802 (**Figure 1C**).

Therefore, *Vp.* $1474^{tdh+,trh-,BF+}$, *Vp.* $1496^{tdh-,trh-,BF-}$, and *Vp.* $1513^{tdh-,trh+,BF+}$ were selected as the representative isolates to perform the experiments in this study.

De Novo Sequencing Analysis of *V. parahaemolyticus*

Genome Assembly

Based on sequencing of small fragment library, basic genomic information such as genome size, heterozygosity and repeat rate could be obtained by 15-K-mer analysis as a rapid genome survey method. The basic evaluation of bacterial genome provided reference for the development of *de novo* sequencing strategy, and it contributed effective basis for subsequent protocol of genome assembly and annotation method of genome structure.

Based on 15-K-mer analysis, the original genome sizes of *Vp.* 1474, *Vp.* 1496, and *Vp.* 1513 were 5.34 Mb, 5.12 Mb and 5.62 Mb, respectively. After revision, the revised genome sizes of the three strains was 5.25 Mb, 5.03 Mb, and 5.53 Mb, respectively. The percentages of GC content in their genomes were 45.15%, 45.39%, and 45.28%, respectively. K-mer frequency distribution curve results of 15-K-mer analysis showed one main peak for all three strains, and the heterozygosity rates of all strains were less than 0.01%, as being 0%, 0.01% and 0.01% of *Vp.* 1474, *Vp.* 1496, and *Vp.* 1513, respectively (**Figure S1**).

Genome Component Analysis

Analysis of the total encoding-gene levels from the genomes of *Vp.* 1474, *Vp.* 1496, and *Vp.* 1513 indicated that the total length of *Vp.* 1496 was the shortest, at 4249152 bp, whereas the total length of *Vp.* 1513 was the longest, at 4909851 bp; the total length of *Vp.* 1474 was 4539612 bp. However, the average lengths of gene sequences for *Vp.* 1474, *Vp.* 1496, and *Vp.* 1513 were nearly the same, at 934 bp, 940 bp, and 939 bp, respectively. From the distribution of gene lengths of the three strains, the gene length between 400 and 500 bp had the maximum proportion (8.83%, 8.58%, and 8.42% in the genome of *Vp.* 1474, *Vp.* 1496, and *Vp.* 1513, respectively), whereas the gene length between 0 and 100 bp had the minimum proportion (0.42%, 0.40% and 0.36% in the genome of *Vp.* 1474, *Vp.* 1496, and *Vp.* 1513, respectively; **Figures 2A, E**). The greatest gene length distribution differences between *Vp.* 1474, *Vp.* 1496, and *Vp.* 1513 were 800 to 900 bp (6.28%, 5.84% and 6.43% in the genome of *Vp.* 1474, *Vp.* 1496, and *Vp.* 1513, respectively), 400 to 500 bp (8.83%, 8.58%, and 8.42% in the genome of *Vp.* 1474, *Vp.* 1496, and *Vp.* 1513, respectively), and 500 to 600 bp (6.98%, 6.61% and 6.79% in the genome of *Vp.* 1474, *Vp.* 1496, and *Vp.* 1513, respectively) in descending order, which indicated a distribution diversity in the medium-long genes (**Figures 2B, E**).

GIs contained several genomic regions, which were integrated into bacterial genome by exogenous bacteria, phages or plasmids through HGT. Various of bacterial functions could be coded by GIs, which involved in bacterial symbiosis, pathogenic mechanisms, environmental adaptability, and so on. The IslandPath-DIOMB software was used as the predicting method. By detecting DNA and RNA phylogenetically bias and mobility genes existence, such as transposases and integrases, the potential HGT and GIs of *Vp.* 1474, *Vp.* 1496, and *Vp.* 1513 were predicted. Results for prediction of the

TABLE 1 | Hemolysin features of *V. parahaemolyticus* strains.

Strain ID	*tdh*	*trh*	*tlh*	Strain ID	*tdh*	*trh*	*tlh*	Strain ID	*tdh*	*trh*	*tlh*
Vp. 1463	–	–	+	*Vp.* 1464	–	–	+	*Vp.* 1465	–	–	+
Vp. 1466	–	–	+	*Vp.* 1467	–	–	+	*Vp.* 1468	–	–	+
Vp. 1469	–	–	+	*Vp.* 1470	+	–	+	*Vp.* 1471	–	–	+
Vp. 1472	–	–	+	*Vp.* 1473	–	–	+	*Vp.* 1474	+	–	+
Vp. 1475	–	–	+	*Vp.* 1476	–	–	+	*Vp.* 1477	–	–	+
Vp. 1478	–	–	+	*Vp.* 1479	–	–	+	*Vp.* 1480	–	–	+
Vp. 1481	–	–	+	*Vp.* 1482	–	–	+	*Vp.* 1483	–	–	+
Vp. 1484	–	–	+	*Vp.* 1485	–	–	+	*Vp.* 1486	–	–	+
Vp. 1487	–	–	+	*Vp.* 1488	–	–	+	*Vp.* 1489	–	–	+
Vp. 1490	–	–	+	*Vp.* 1491	–	–	+	*Vp.* 1492	–	–	+
Vp. 1493	–	–	+	*Vp.* 1494	–	–	+	*Vp.* 1495	–	–	+
Vp. 1496	–	–	+	*Vp.* 1497	–	–	+	*Vp.* 1498	–	–	+
Vp. 1499	–	–	+	*Vp.* 1500	–	–	+	*Vp.* 1501	–	–	+
Vp. 1502	–	–	+	*Vp.* 1503	–	–	+	*Vp.* 1504	–	–	+
Vp. 1505	–	–	+	*Vp.* 1506	–	–	+	*Vp.* 1507	–	–	+
Vp. 1508	–	–	+	*Vp.* 1509	–	–	+	*Vp.* 1510	–	–	+
Vp. 1511	–	+	+	*Vp.* 1512	–	–	+	*Vp.* 1513	–	+	+
Vp. 1514	–	–	+	*Vp.* 1515	–	–	+	*Vp.* 1516	–	–	+
Vp. 1517	–	–	+	*Vp.* 1518	–	–	+	*Vp.* 1519	–	–	+
Vp. 1520	–	–	+	*Vp.* 1521	–	–	+	*Vp.* 1522	–	–	+
Vp. 1523	–	–	+	*Vp.* 1524	–	–	+	*Vp.* 1525	–	–	+
Vp. 1526	–	–	+	*Vp.* 1527	–	–	+	*Vp.* 1528	–	–	+
Vp. 4213	–	+	+	*Vp.* 4215	+	–	+	*Vp.* 11577	–	+	+

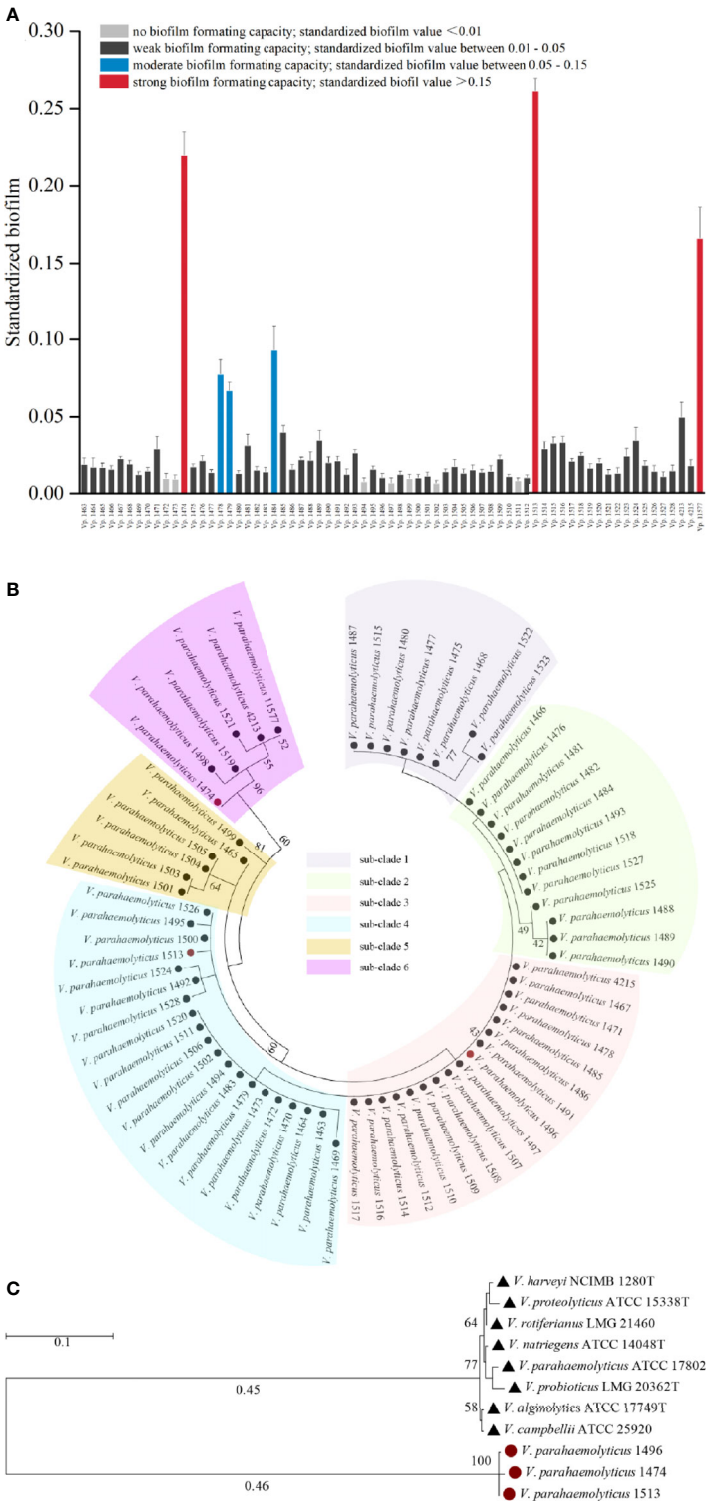

FIGURE 1 | Phylogenetic analysis and biofilm formation capacity of *V. parahaemolyticus*. **(A)** Standardized biofilms formed by 69 V. *parahaemolyticus* environmental strains. Based on the standardized biofilm values, the biofilm formation (BF) capacity of the strains was divided into four groups, viz., strong, moderate, weak, and no capacity. **(B)** Maximum likelihood tree of 69 V. *parahaemolyticus* environmental strains based on the 16S rDNA phylogenetic analysis. The bootstrap percentage value was obtained from 1000 samplings. The 69 strains were divided into 6 subclades. **(C)** Maximum likelihood tree for *V. parahaemolyticus* strains *Vp*. 1474, *Vp*. 1496, and *Vp*. 1513 based on the 16S rDNA phylogenetic analysis using type strains in *Vibrio* genus as reference. The bootstrap percentage value was obtained from 1000 samplings. Red solid circle: selected strains of *Vp*. 1474, *Vp*. 1496, and *Vp*. 1513; black solid triangle: reference *Vibrio* strains.

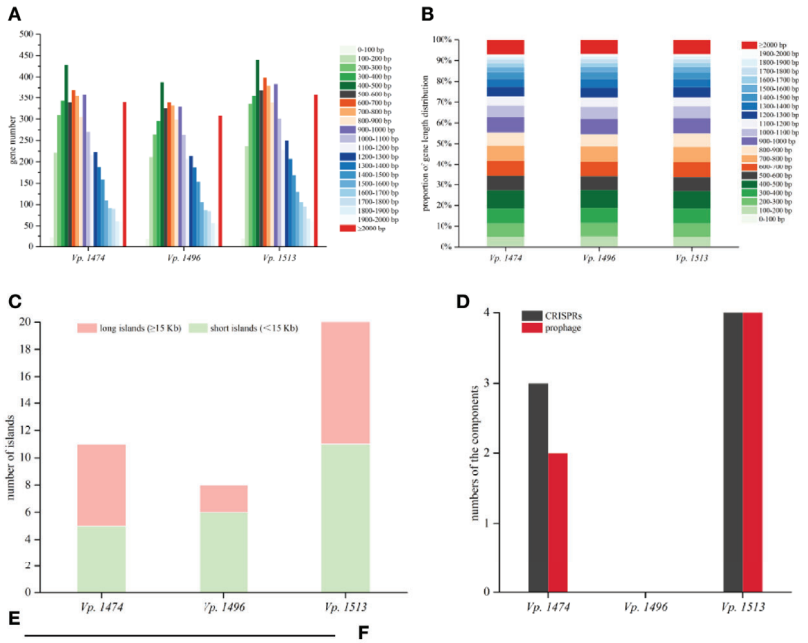

E

Numbers of the total encoding-genes, proportion of each group (%)

Gene group (bp) \ *Vp.* strain	*Vp.* 1474	*Vp.* 1496	*Vp.* 1513
0-100	21, 0.43	18, 0.40	19, 0.36
100-200	221, 4.55	211, 4.67	237, 4.53
200-300	310, 6.38	264, 5.84	336, 6.43
300-400	343, 7.06	296, 6.55	355, 6.79
400-500	429, 8.83	388, 8.58	440, 8.42
500-600	339, 6.98	325, 7.19	369, 7.06
600-700	370, 7.61	339, 7.50	398, 7.61
700-800	355, 7.31	332, 7.34	380, 7.27
800-900	305, 6.28	299, 6.61	338, 6.47
900-1000	358, 7.37	329, 7.28	384, 7.35
1000-1100	270, 5.56	263, 5.82	301, 5.76
1100-1200	216, 4.45	207, 4.587	228, 4.36
1200-1300	223, 4.59	214, 4.73	250, 4.78
1300-1400	188, 3.87	187, 4.14	207, 3.96
1400-1500	159, 3.27	153, 3.38	169, 3.23
1500-1600	110, 2.26	106, 2.34	130, 2.49
1600-1700	92, 1.89	87, 1.92	106, 2.03
1700-1800	90, 1.85	85, 1.88	95, 1.82
1800-1900	61, 1.26	57, 1.26	67, 1.28
1900-2000	59, 1.21	54, 1.19	60, 1.15
>2000	340, 7.00	308, 6.81	359, 6.87

F

Numbers of the total predicted GIs, GI proportion of each group (%)

GI group \ *Vp.* strain	*Vp.* 1474	*Vp.* 1496	*Vp.* 1513
short GIs (<15 Kb)	5, 45.45	6, 75.00	11, 55.00
long GIs (≥15 Kb)	6, 54.55	2, 25.00	9, 45.00

G

Characteristics of the predicted prophages

Vp. strain \ Description	Prophage ID	Prophage location	Start sequence base	End sequence base	Sequence length
Vp. 1474	prophage 1	scaffold 2	575928	602955	27028
	prophage 2	scaffold 1	161120	230362	69243
Vp. 1496	-	-	-	-	-
Vp. 1513	prophage 1	scaffold 13	53096	65173	12078
	prophage 2	scaffold 12	22421	37726	15306
	prophage 3	scaffold 11	31858	53992	22135
	prophage 4	scaffold 1	453313	488339	35027

H

Characteristics of the predicted CRISPRs

Vp. strain \ Description	Sequence location	Start sequence base	End sequence base	Strand property	Sequence length	Spacer sequence length	Spacer sequence number	Direct repeat sequence number
Vp. 1474	scaffold 2	28029	28537	sense	509	79	4	38
	scaffold 6	108079	108206	sense	128	72	1	28
	scaffold 6	227510	227777	sense	268	78	2	37
Vp. 1496	-	-	-	-	-	-	-	-
Vp. 1513	scaffold 3	706155	706367	sense	213	43	3	20
	scaffold 6	245444	245595	sense	152	38	2	25
	scaffold 10	18241	18799	sense	559	41	9	19
	scaffold 20	131	264	sense	134	29	2	25

FIGURE 2 | General genome components analysis of *V. parahaemolyticus* strains *Vp*. 1474, *Vp*. 1496, and *Vp*. 1513. **(A)** Statistical histogram of coding gene length distribution for the three strains. Coding gene zones were measured as 0 to 400 bp, 400 to 1,000 bp, 1,000 to 2,000 bp, and longer than 2000 bp as groups of short genes, medium long genes, long genes, and very long genes, respectively. **(B)** Percentage accumulative bar diagram of coding gene length distribution for the three strains. Coding gene zones were measured in 100 bp; 0 to 400 bp, 400 to 1,000 bp, 1,000 to 2,000 bp and longer than 2000 bp as groups of short genes, medium long genes, long genes and very long genes, respectively. **(C)** Accumulative bar diagram of genomic islands (GIs) for the three strains. GIs were divided into long islands and short islands by the length of 15 kb. **(D)** Statistical histogram of CRISPRs and prophages for the three selected strains. The component numbers of CRISPRs or prophages are shown on the Y-axis. **(E)** Statistical data of coding gene length distribution for the three strains. **(F)** Statistical data of GIs for the three strains. **(G)** Detailed characteristics of the predicted prophages for the three strains. **(H)** Detailed characteristics of the predicted CRISPRs for the three strains.

total number of GIs for the three strains showed that the differences between these three strains were in the total numbers and the lengths of GIs (**Figures 2C, F**). *Vp.* 1513 was predicted to have the largest number of GIs (n = 20), followed by *Vp.* 1474 (n = 11), and *Vp.* 1496 (n = 8). Difference in the GIs of these strains was mainly reflected in the number and proportion of long GIs (≥ 15 Kb). There were separately six (GIs001, GIs002, GIs003, GIs006, GIs008, and GIs010) and nine (GIs004, GIs006, GIs008, GIs010, GIs011, GIs012, GIs016, GIs017, and GIs018) long GIs predicted in the genome of *Vp.* 1474 and *Vp.* 1513, which was separately 54.55% and 45% of the total predicted GIs, while only two long GIs (GIs005 and GIs006) were predicted in the genome of *Vp.* 1496, which was only 25% of the total predicted GIs. Detailed gene distribution in each GI for the three *Vp*. strains were shown in **Figure S2**.

CRISPR system was proved to be a bacterial adaptive immunity system, which showed crucial effect during invasion of viruses and plasmids. After the invading process, CRISPR locus could be integrated into host genome so that it caused the adaptive immunity for host to defense against subsequent attack by the same invader (Sun et al., 2015). Further study showed that CRISPR system partially reflected bacterial evolution. Based on the nomenclature initiated and optimized by Makarova et al., the CRISPR system existed in *V. parahaemolytius* belongs to the subtype I-F, encoded by cas gene *csy3* (Makarova et al., 2011). The number of CRISPRs and prophages in the genomes of *Vp.* 1474, *Vp.* 1496, and *Vp.* 1513 showed marked differences (**Figures 2D, G, H**). The genome of *Vp.* 1496 did not present any signs of CRISPR or prophage integration, and was thus considered as the most conservative. However, the genome of *Vp.* 1513 had four CRISPRs and four prophages, which was the highest number among these strains.

Genome Function Analysis Based on Public Bioinformatics Databases

Genome Function Analysis Based on GO Database

By aligning with the GO database, more than 3000 genes were annotated in the genomes of *Vp.* 1474, *Vp.* 1496, and *Vp.* 1513. Moreover, there was a significant difference in the total annotation numbers and distributions among the three strains. For genes that annotated to the class of cellular components, *Vp.* 1513 had the greatest number of genes annotated, except for cell junction, whereas *Vp.* 1496 showed the opposite trend. *Vp.* 1474 had one gene annotated in cell junction component namely *Vp.* 1474 GM002208 that annotated with 24 GO accessions, whereas *Vp.* 1513 had one gene annotated in synapse or synapse part component namely *Vp.* 1513 GM002507 that annotated with 6 GO accessions. The components of extracellular region showed a different pattern between the three strains as compared with the trend that other components presented (**Figures 3A, D**).

For genes that annotated to the class of biological process, the total number of annotated genes was present in the same pattern as the class of cellular component. It was worth noticing that there were many more genes accounted for more proportion in the genome of *Vp.* 1513 involved in the multi-organism process (0.95% of total annotated genes) and multicellular organismal process (0.33% of total annotated genes), while *Vp.* 1496 showed the opposite trend (0.74% and 0.29% of total annotated genes, respectively). Meanwhile, the least number of genes (total number of 7288) in the genome of *Vp.* 1496 were involved in positive regulation of biological process (**Figures 3B, D**).

For genes that annotated to the class of molecular function, the total number of annotated genes in the genome of *Vp.* 1496 was the minimum among the three strains. The genes of *Vp.* 1513 were mostly found to be associated with catalytic activity, binding, and protein binding transcription factor activity, as in 41.13%, 37.17% and 1.70% of total annotated genes, respectively. On the contrary, the disadvantage of *Vp.* 1496 was mainly in the lack of genes that were involved in enzyme regulator activity (0.25% of total annotated genes; **Figures 3C, D**).

Genome Function Analysis Based on KEGG Database

By Aligning with the KEGG database, 4644, 4391, and 5017 genes were annotated in the genomes of *Vp.* 1474, *Vp.* 1496, and *Vp.* 1513, respectively. For encoding genes that participate in the pathway of cellular processes, the numbers of genes for *Vp.* 1513 annotated to cellular community, cell motility, and cell growth and death were significantly higher than that of *Vp.* 1474 and *Vp.* 1496. Considering the genome size, the proportion of the gene numbers of *Vp.* 1496 annotated to cellular community (51.98% of total annotated genes) was considerably more than that of *Vp.* 1474 (51.08% of total annotated genes) and *Vp.* 1513 (51.72% of total annotated genes). Despite of the higher gene proportion of *Vp.* 1496 annotated to transport and catabolism (5.23% of total annotated genes) than it of *Vp.* 1474 (4.86% of total annotated genes) and *Vp.* 1513 (4.89% of total annotated genes), the gene numbers for these three strains tended to be equal (**Figures 4A, G**).

For genes that are associated with the pathway of environmental information processing, there was a difference in distribution between the class of membrane transport and signal transduction. Although the genome size of *Vp.* 1496 was the least among these strains, it had more genes annotated to the membrane transport class (56.69% of total annotated genes) than *Vp.* 1474 (56.16% of total annotated genes) and more annotated to the signal transduction class (43.31% of total annotated genes) than *Vp.* 1513 (40% of total annotated genes; **Figures 4B, G**). For genes that were homologous to the cluster of genetic information processing, the gene numbers of *Vp.* 1513 were annotated the most. Note that the gene numbers of *Vp.* 1474 and *Vp.* 1513 annotated to the pathways of translation, folding, sorting, degradation, and transcription were almost equal. However, there were more genes in the *Vp.* 1513 genome participating in the pathway of replication and repair (**Figures 4C, G**). For genes that were participating in the pathway of human diseases, the main difference between the annotated genes for *Vp.* 1474, *Vp.* 1496, and *Vp.* 1513 was the number for drug resistance class, which showed a significantly lower number and a lower proportion of genes in the genome of *Vp.* 1496 (40.58% of total annotated genes**; Figures 4D, G**).

There was an abundance of genes participating in the pathway of metabolism; this number was the largest among the five clusters from the KEGG database. Among the 11 classes in this cluster, carbohydrate metabolism was the class that had

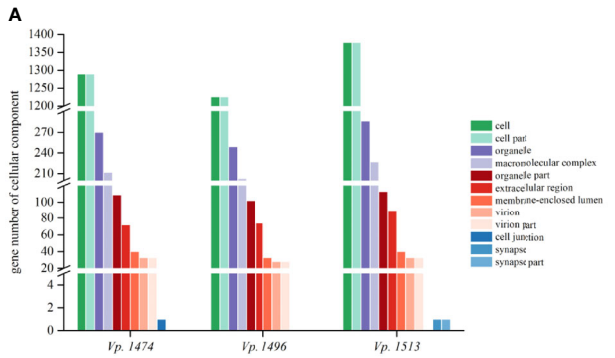

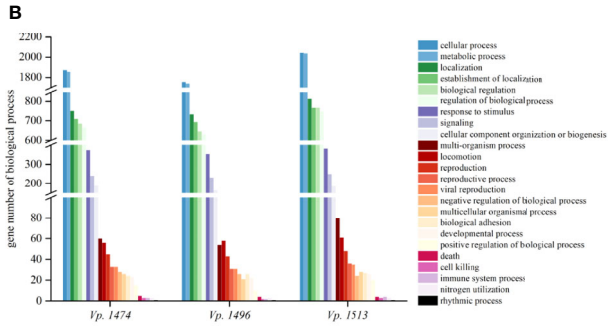

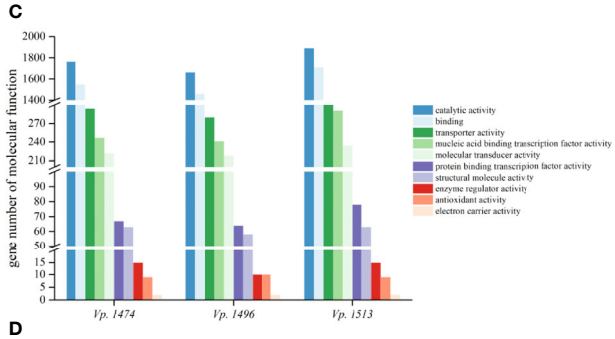

D

Numbers of the total annotated genes, gene proportion of each class (%)

Ontology	class description	*Vp.* strain	*Vp.* 1474	*Vp.* 1496	*Vp.* 1513
Cellular components	cell		1290, 38.51	1226, 38.69	1378, 38.49
	cell part		1290, 38.51	1226, 38.69	1378, 38.49
	organelle		270, 8.06	249, 7.86	286, 7.99
	macromolecular complex		212, 6.33	203, 6.41	227, 6.34
	organelle part		109, 3.25	102, 3.22	113, 3.16
	extracellular region		72, 2.15	74, 2.34	90, 2.51
	membrane-enclosed lumen		40, 1.19	33, 1.04	40, 1.12
	virion		33, 0.99	28, 0.88	33, 0.92
	virion part		33, 0.99	28, 0.88	33, 0.92
	cell junction		1, 0.03	0, 0.00	0, 0.00
	synapse		0, 0.00	0, 0.00	1, 0.03
	synapse part		0, 0.00	0, 0.00	1, 0.03
Biological process	cellular process		1874, 24.33	1756, 24.09	2043, 24.34
	metabolic process		1836, 24.09	1740, 23.87	2037, 24.27
	localization		751, 9.75	734, 10.07	813, 9.69
	establishment of localization		710, 9.22	694, 9.52	767, 9.14
	biological regulation		683, 8.89	647, 8.88	768, 9.15
	regulation of biological process		666, 8.65	632, 8.67	748, 8.91
	response to stimulus		373, 4.84	354, 4.86	382, 4.55
	signaling		241, 3.13	232, 3.18	250, 2.98
	cellular component organization or biogenesis		189, 2.45	165, 2.26	186, 2.22
	multi-organism process		60, 0.78	54, 0.74	80, 0.95
	locomotion		56, 0.73	58, 0.80	61, 0.73
Biological process	reproduction		45, 0.58	43 0.59	48, 0.57
	reproductive process		33, 0.43	31 0.43	36, 0.43
	viral reproduction		33, 0.43	31 0.43	35, 0.42
	negative regulation of biological process		28, 0.36	26 0.36	24, 0.29
	multicellular organismal process		26, 0.34	21 0.29	28, 0.33
	biological adhesion		24, 0.31	26 0.36	27, 0.32
	developmental process		23, 0.30	22 0.30	26, 0.31
	positive regulation of biological process		15, 0.19	10 0.14	20, 0.24
	death		5, 0.06	4, 0.05	4, 0.05
	cell killing		3, 0.04	2, 0.03	3, 0.04
	immune system process		3, 0.04	2, 0.03	4, 0.05
	nitrogen utilization		3, 0.04	3, 0.04	3, 0.04
	rhythmic process		1, 0.01	1, 0.01	1, 0.01
Molecular function	catalytic activity		1765, 41.69	1652, 41.49	1892, 41.13
	binding		1550, 36.61	1491, 36.47	1710, 37.17
	transporter activity		294, 6.94	280, 6.99	306, 6.65
	nucleic acid binding transcription factor activity		247, 5.83	241, 6.02	291, 6.33
	molecular transducer activity		222, 5.24	211, 5.44	234, 5.09
	protein binding transcription factor activity		67, 1.58	64 1.60	78, 1.70
	structural molecule activity		63, 1.49	58 1.45	63, 1.37
	enzyme regulator activity		15, 0.35	10 0.25	15, 0.33
	antioxidant activity		9, 0.21	10 0.25	9, 0.20
	electron carrier activity		2, 0.05	2, 0.05	2, 0.04

FIGURE 3 | Gene ontology (GO) annotation of *V. parahaemolyticus* strains *Vp*. 1474, *Vp*. 1496, and *Vp*. 1513. **(A)** Statistical histogram of gene annotation to cellular component class of the three strains. A total of 13 parts were predicted in the genome of the three strains. Gene numbers are shown on the Y-axis. **(B)** Statistical histogram of gene annotation to biological process class of the three strains. A total of 24 parts were predicted within genome genes of the three strains. Gene numbers are shown on the Y-axis. **(C)** Statistical histogram of gene annotation to molecular function class of the three strains. A total of 10 parts were predicted within genome genes of the three strains. Gene numbers are shown on the Y-axis. **(D)** Statistical data of annotated genes based on GO ontology for the three strains.

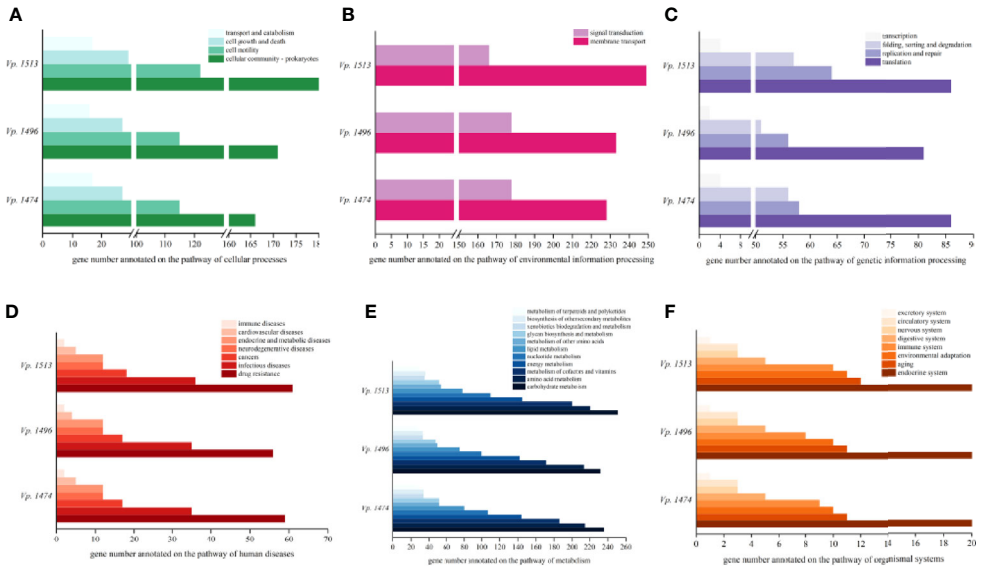

G

Numbers of the total annotated genes, gene proportion of each class (%)

Pathway annotation	class description \ *Vp.* strain	*Vp.* 1474	*Vp.* 1496	*Vp.* 1513
Cellular processes	cellular community - prokaryotes	166, 51.08	171, 51.98	180, 51.72
	cell motility	115, 35.38	115, 34.95	122, 35.06
	cell growth and death	27, 8.31	27, 8.21	29, 8.33
	transport and catabolism	17, 5.23	16, 4.86	17, 4.89
Environmental information processing	membrane transport	228, 56.16	233, 56.69	249, 60.00
	signal transduction	178, 43.84	178, 43.31	166, 40.00
genetic information processing	translation	86, 42.16	81, 42.63	86, 40.76
	replication and repair	58, 28.43	56, 29.47	64, 30.33
	folding, sorting and degradation	56, 27.45	51, 26.84	57, 27.01
	transcription	4, 1.96	2, 1.05	4, 1.90
human diseases	drug resistance	59, 41.55	56, 40.58	61, 41.78
	infectious diseases	35, 24.65	35, 25.36	36, 24.66
	cancers	17, 11.97	17, 12.32	18, 12.33
	neurodegenerative diseases	12, 8.45	12, 8.70	12, 8.22
	endocrine and metabolic diseases	12, 8.45	12, 8.70	12, 8.22
	cardiovascular diseases	5, 3.52	4, 2.90	5, 3.42
	immune diseases	2, 1.41	2, 1.45	2, 1.37

Pathway annotation	class description \ *Vp.* strain	*Vp.* 1474	*Vp.* 1496	*Vp.* 1513
metabolism	carbohydrate metabolism	236, 20.24	232, 20.64	251, 20.76
	amino acid metabolism	215, 18.44	214, 19.04	221, 18.28
	metabolism of cofactors and vitamins	186, 15.95	171, 15.21	20, 16.54
	energy metabolism	144, 12.35	142, 12.63	145, 11.99
	nucleotide metabolism	107, 9.18	100, 8.90	110, 9.10
	lipid metabolism	80, 6.86	75, 6.67	78, 6.45
	metabolism of other amino acids	51, 4.37	49, 4.36	53, 4.38
	glycan biosynthesis and metabolism	51, 4.37	47, 4.18	51, 4.22
	xenobiotics biodegradation and metabolism	34, 2.92	33, 2.94	35, 2.89
	biosynthesis of other secondary metabolites	34, 2.92	33, 2.94	36, 2.98
	metabolism of terpenoids and polyketides	28, 2.40	28, 2.49	29, 2.40
organismal systems	endocrine system	20, 32.26	20, 32.79	20, 30.77
	aging	11, 17.74	11, 18.03	12, 18.46
	environmental adaptation	10, 16.13	10, 16.39	11, 16.92
	immune system	9, 14.52	8, 13.11	10, 15.38
	digestive system	5, 8.06	5, 8.20	5, 7.69
	nervous system	3, 4.84	3, 4.92	3, 4.62
	circulatory system	3, 4.84	3, 4.92	3, 4.62
	excretory system	1, 1.61	1, 1.64	1, 1.54

FIGURE 4 | KEGG pathway annotation of *V. parahaemolyticus* strains *Vp*. 1474, *Vp*. 1496, and *Vp*. 1513. **(A)** Statistical bar diagram of genes predicted to cellular processes pathway of the three strains. A total of 4 pathways were predicted within genome genes of the three strains. Gene numbers are shown on the horizontal axis. **(B)** Statistical bar diagram of genes predicted for environmental information processing pathways in the three strains. A total of 2 pathways were predicted within genome genes of the three strains. Gene numbers are shown on the horizontal axis. **(C)** Statistical bar diagram of genes predicted for genetic information processing pathway of the three strains. A total of 4 pathways were predicted within genome genes of the three strains. Gene numbers are shown on the horizontal axis. **(D)** Statistical bar diagram of genes predicted to human diseases pathways of the three strains. A total of 7 pathways were predicted within genome genes of the three strains. Gene numbers are shown on the horizontal axis. **(E)** Statistical bar diagram of genes predicted to metabolism pathways of the three strains. A total of 11 pathways were predicted within genome genes of the three strains. Gene numbers are shown on the horizontal axis. **(F)** Statistical bar diagram of genes predicted to organismal systems pathways of the three strains. A total of 8 pathways were predicted within genome genes of the three strains. Gene numbers are shown on the horizontal axis. **(G)** Statistical data of KEGG pathway annotation for the three strains.

the highest number and the highest proportion (20.24%, 20.64% and 20.76% of total annotated genes in *Vp.* 1474, *Vp.* 1496 and *Vp.* 1513, respectively) of annotated genes. Among the three strains, *Vp.* 1513 had the most genes annotated, and *Vp.* 1496 had the least. However, in the class of metabolism of terpenoids and polyketides, the numbers of annotated genes were almost the same between these strains (**Figures 4E, G**). Similarly, there was hardly any difference in the numbers of annotated genes participating in the pathway of organismal systems (**Figures 4F, G**).

Genome Function Analysis Based on COG Database

Alignment with the COG database indicated that the numbers of annotated genes were similar to those for the GO database, at 3553, 3411, and 3857 for the genomes of *Vp*. 1474, *Vp*. 1496, and *Vp*. 1513, respectively, which meant that these three genomes have significant differences in protein-coding genes. For genes that were homologous to the cluster of cellular processing and signaling, the significant differences of protein-encoding genes were in the class of defense mechanisms and mobilome, with *Vp*. 1513 having the greatest number and proportion (10.92% and 4.41% of total annotated genes, respectively) and *Vp*. 1496 having the least (9.26% and 1.46% of total annotated genes, respectively; **Figures 5A, E**).

For genes that were homologous to the cluster of information storage and processing, the higher phylogenetic evolution level of *Vp*. 1513 was reflected in its high number and proportion of genes for replication, recombination, and repair (21.51% of total annotated genes), as well as dynamic transcription activity (43.13% of total annotated genes; **Figures 5B, E**). For genes that were homologous to the cluster of metabolism, there was no significant difference between the three strains (**Figures 5C, E**). Furthermore, there were over 550 genes with unknown functions on the basis of COG annotation results (**Figures 5D, E**).

Comparative Analysis of *V. parahaemolyticus* Virulence and Pathogenicity

T3SS prediction was performed using EffectiveT3 software, and the predicted sequences were scored and screened for the final determination of T3SS effective proteins. Although the predicted number of T3SS effective proteins for *Vp*. 1496 was the least (n=199) whereas the number of that for *Vp*. 1474 and *Vp*. 1513 were 213 and 234, respectively, their proportion compared to other proteins was not the lowest among the three selected strains, as in 4.38%, 4.40% and 4.48% of total annotated proteins, respectively (**Figures 6A, D**).

Based on the results of gene sequences, there were three common secretion systems in the genomes of *Vp*. 1474, *Vp*. 1496, and *Vp*. 1513, including Type II secretion system (T2SS), T3SS, and Type VI secretion system (T6SS), whereas only *Vp*. 1474 had the Type IV secretion system (T4SS). Three strains all presented 13 T2SS-associated proteins. However, *Vp*. 1496 presented 17 T6SS-associated proteins (41.46% of total annotated proteins), which was significantly more than the corresponding values of 10 and 9 for *Vp*. 1474 (25% of total annotated proteins) and *Vp*. 1513 (19.57% of total annotated proteins), respectively (**Figures 6B, D**). In addition to TNSS-associated proteins, secreted proteins are another important type of protein that enhance *V. parahaemolyticus* pathogenicity. It was observed that for *Vp*. 1513, the numbers of signal peptide proteins and secreted proteins were similar and less than the number of transmembrane structural proteins. However, for transmembrane structural proteins, *Vp*. 1513 was predicted to have the lowest proportion of total annotated proteins (57.33%), whereas *Vp*. 1496 was predicted to have the highest proportion (58.55%; **Figures 6C, D**). Based on the interpretation of NR and GO databases, the difference of T3SS-associated proteins among the three strains reflected on the difference of number and types of both apparatus proteins and accessory proteins such as secretion protein, membrane protein, contacting sensing protein and so on. *Vp*. 1474 had the greatest number of annotated apparatus proteins (n=4), *Vp*. 1496 had the least number (n=1), and *Vp*. 1513 had 2 apparatus proteins. Combining with the GO interpretation, *Vp*. 1496 lacked 3 apparatus proteins that might be involved in the function of ATPase activity, actin binding and proton transporting.

Based on the PHI database, the number of genes in the genomes of *Vp*. 1474, *Vp*. 1496, and *Vp*. 1513 annotated on lethal, chemistry target, and effector were the same. Associated with pathogen-host interaction, one gene existed in all three strains (*Vp*. 1474 GM000792, *Vp*. 1496 GM000568, and *Vp*. 1513 GM000720, respectively) with unclassified function, which might be identified as the similar function of gene *feoB* (PHI-base accession number 6941) that involved in the coding of ferrous iron transport protein (UniProtKB accession: A0A0F6UGK4). *Vp*. 1513 had the greatest number of genes annotated by this method, whereas *Vp*. 1496 had the least number of annotated genes. However, *Vp*. 1474 had the greatest number and the highest proportion (5.56%) of genes that were annotated in the class of increased virulence, and *Vp*. 1496 had the highest proportion of genes (2.45%) annotated in the class of lethal (**Figures 6E, G**). Based on the VFDB, *Vp*. 1513 had more genes annotated than *Vp*. 1474 and *Vp*. 1496 (**Figure 6F**), indicating a significantly higher virulence potential of this strain.

Based on the ARDB, the three strains had a slight difference in antibiotic resistance, with two to three genes responding to drug resistance. However, there were more than 170 drug resistance genes in the genomes of *Vp*. 1474, *Vp*. 1496, and *Vp*. 1513 based on the CARD. *Vp*. 1513 had the largest gene number annotated for drug resistance, whereas *Vp*. 1474 and *Vp*. 1496 had fewer, but similar number of genes annotated in that database (**Figure 6F**).

Genome-Wide Map of *V. parahaemolyticus*

Based on the assembled genome sequences of *Vp*. 1474, *Vp*. 1496, and *Vp*. 1513, the circular structures of the genomes of these three strains were displayed in a genome-wide map, with the combination of the respective prediction results of the coding genes. In the genome-wide map, relational analysis results were also displayed, including those obtained using non-coding RNA, KEGG, GO, and COG databases, which predicted the gene function annotations of *V. parahaemolyticus* (**Figure 7**).

V. parahaemolyticus Pathogenicity *In Vivo*

The theoretically predicted difference in pathogenicity for the selected strains, *Vp*. 1474, *Vp*. 1496, and *Vp*. 1513, was confirmed by the intraperitoneal infection model in mice, and the survival condition was showed as data and survival analysis in **Figure 8**. After 1 h of inoculation, the mice all showed different degrees of lethargy, inappetence, accomplishing with rough and messy hair. According to our observations, the course of disease was short after *Vp*. 1474 infection, and subjects could recover within 36 h. However, after *Vp*. 1496 infection, the course of disease was longer than that after *Vp*. 1474 infection, and subjects could return to health after 48 h. Conversely, after *Vp*. 1513 infection, the course of disease was the longest, and took a minimum of 96 h for the subjects to restore their health (**Figure 8A**).

Comparing the three chosen *V. parahaemolyticus*, the most serious acute infection induced by *Vp*. 1496 were observed within

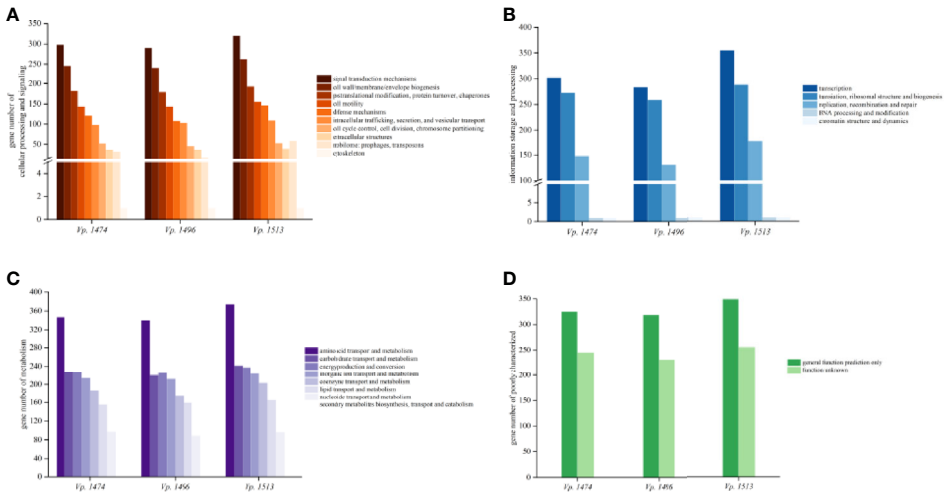

E

Numbers of the total annotated genes, gene proportion of each class (%)

Functional class	class description \ *Vp.* strain	*Vp.* 1474	*Vp.* 1496	*Vp.* 1513
cellular processing and signaling	signal transduction mechanisms	298, 24.61	290, 24.87	320, 23.93
	cell wall/membrane/ envelope biogenesis	246, 20.31	241, 20.67	262, 19.60
	postranslational modification, protein turnover, chaperones	182, 15.03	175, 15.35	193, 14.44
	cell motility	144, 11.89	144, 12.35	155, 11.59
	defense mechanisms	121, 9.99	108, 9.26	146, 10.92
	intracellular trafficking, secretion, and vesicular transport	98, 8.09	103, 8.83	109, 8.15
	cell cycle control, cell division, chromosome partitioning	52, 4.29	46,3.95	53, 3.96
	extracellular structures	37, 3.06	37,3.17	39, 2.92
	mobilome: prophages, transposons	32, 2.64	17,1.46	59, 4.41
	cytoskeleton	1, 0.08	1, 0.09	1, 0.07
information storage and processing	transcription	302, 41.66	284, 42.01	355, 43.13
	translation, ribosomal structure and biogenesis	273, 37.66	259, 38.31	289, 35.12
	replication, recombination and repair	148, 20.41	131, 19.38	177, 21.51
	RNA processing and modification	1, 0.14	1, 0.15	1, 0.12
	chromatin structure and dynamics	1, 0.14	1, 0.15	1, 0.12

Functional class	class description \ *Vp.* strain	*Vp.* 1474	*Vp.* 1496	*Vp.* 1513
metabolism	amino acid transport and metabolism	347, 22.62	340, 22.70	374, 23.06
	carbohydrate transport and metabolism	228, 14.86	220, 14.69	242, 14.92
	energy production and conversion	227, 14.80	225, 15.02	238, 14.67
	inorganic ion transport and metabolism	214, 13.95	212, 14.15	223, 13.75
	coenzyme transport and metabolism	187, 12.19	176, 11.75	203, 12.52
	lipid transport and metabolism	155, 10.10	159, 10.61	165, 10.17
	nucleotide transport and metabolism	97, 6.32	89, 5.94	96, 5.92
	secondary metabolites biosynthesis, transport and catabolism	79, 5.15	77, 5.14	81, 4.99
poorly characterized	general function prediction only	325, 57.02	319, 58.00	349, 57.78
	function unknown	245, 42.98	231, 42.00	255, 42.22

FIGURE 5 | COG function classification of *V. parahaemolyticus* strains *Vp*. 1474, *Vp*. 1496, and *Vp*. 1513. **(A)** Statistical histogram of gene classified to cellular processing and signaling cluster of the three strains. A total of 10 sub-clusters were predicted within genome genes of the three strains. Gene numbers are shown on the Y-axis. **(B)** Statistical histogram of gene classified to information storage and processing cluster of the three strains. A total of 5 sub-clusters were predicted within genome genes of the three strains. Gene numbers are shown on the Y-axis. **(C)** Statistical histogram of gene classified to metabolism cluster of the three strains. A total of 8 sub-clusters were predicted within genome genes of the three strains. Gene numbers are shown on the Y-axis. **(D)** Statistical histogram of poorly classified genes of the three strains. Only one sub-cluster was predicted to have general function, and the functions of the remaining genes were unknown. Detailed gene numbers are shown on the Y-axis. **(E)** Statistical data of annotation based on COG database for the three strains.

2 h even under a low bacterial inoculate concentration (OD=0.1; **Figure 8B**), whereas the acute infection caused by *Vp.* 1474 and *Vp.* 1513 was showed after 5 h or 6 h positively related to bacterial inoculate concentration (**Figures 8C, D**). *Vp.* 1496 had the highest fatality rate after infection, the fatality of *Vp.* 1474 was closely related to the concentration of bacteria administered, and *Vp.* 1513 had the lowest fatality.

After at least 2 d and up to 4 d of inoculation, the surviving mice gradually returned to normal posture; however, the final survival after intraperitoneal infecting by different *V. parahaemolyticus* was significantly different ($P<0.001$) based on statistical analyses despite of the inoculating concentration (**Figures 8B–D**), and final survivors after *Vp.* 1513 infection retained the most. The results of survival analysis of the mice also showed that the different *V. parahaemolyticus* strains had different pathogenic effects on infected mice, with significant differences in infection rate and mortality.

Antibiotic Resistance of *V. parahaemolyticus* Strains

In order to explore the concordance between biofilm formation capacity and the antibiotic resistance, 22 antibiotics that are frequently used clinically were tested against the 69 V. *parahaemolyticus* strains. Among the antibiotics for which

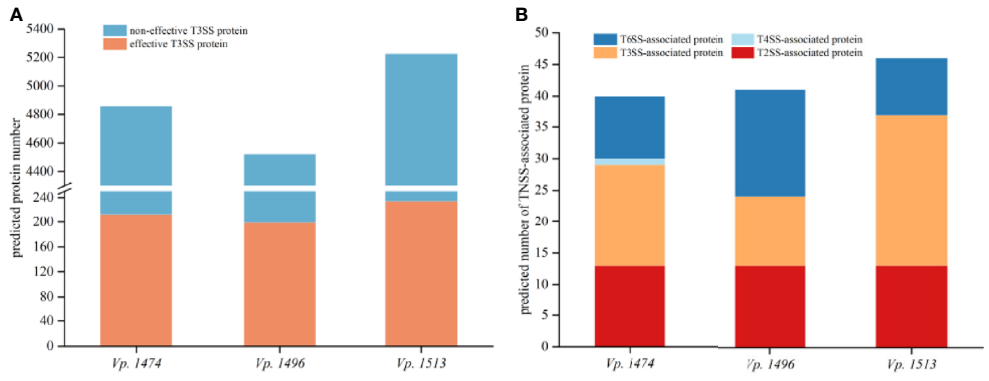

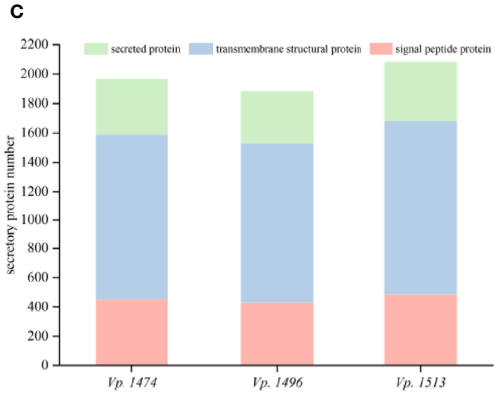

D

Numbers of predicted T3SS proteins, proportion of each group (%)

T3SS prediction \ *Vp.* strain	*Vp.* 1474	*Vp.* 1496	*Vp.* 1513
effective T3SS proteins	213, 4.38	199, 4.40	234, 4.48
non-effective T3SS proteins	4646, 95.62	4323, 95.60	4994, 95.52

Numbers of predicted secretion-associated proteins, proportion of each group (%)

TNSS prediction \ *Vp.* strain	*Vp.* 1474	*Vp.* 1496	*Vp.* 1513
T2SS-associated	13, 32.50	13, 31.71	13, 28.26
T3SS-associated	16, 40.00	11, 26.83	24, 52.17
T4SS-associated	1, 2.50	0, 0.00	0, 0.00
T6SS-associated	10, 25.00	17, 41.46	9, 19.57

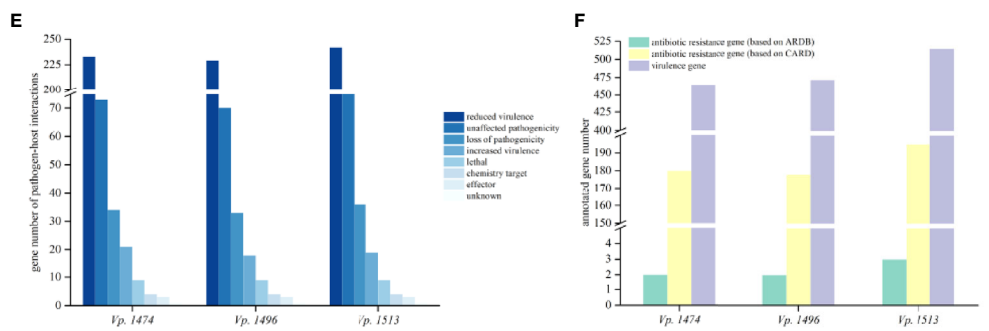

G

Numbers of annotated gene based on PHI database, proportion of each phenotype (%)

PHI phenotype \ *Vp.* strain	*Vp.* 1474	*Vp.* 1496	*Vp.* 1513	PHI phenotype \ *Vp.* strain	*Vp.* 1474	*Vp.* 1496	*Vp.* 1513
reduced virulence	233, 61.64	229, 62.40	242, 60.05	lethal	9, 2.38	9, 2.45	9, 2.23
unaffected pathogenicity	73, 19.31	70, 19.07	89, 22.08	chemistry target	4, 1.06	4, 1.09	4, 0.99
loss of pathogenicity	34, 8.99	33, 8.99	36, 8.93	effector	3, 0.79	3, 0.82	3, 0.74
increased virulence	21, 5.56	18, 4.90	19, 4.71	unknown	1, 0.26	1, 0.27	1, 0.25

FIGURE 6 | Virulence and pathogenicity analysis of *V. parahaemolyticus* strains *Vp*. 1474, *Vp*. 1496, and *Vp*. 1513. **(A)** Accumulative bar diagram of protein distribution in Type III secretion system (T3SS) of the three strains. T3SS were predicted and divided into effective and non-effective proteins, and their numbers are shown on the Y-axis. **(B)** Accumulative bar diagram of protein distribution in major Type N secretion system (TNSS) of the three strains. Four major TNSS were predicted in the three strains, viz., T2SS, T3SS, T4SS, and T6SS, and the number of TNSS-associated proteins are shown on the Y-axis. **(C)** Accumulative bar diagram of secretory proteins distribution of the three strains. Secretory proteins were divided into 3 groups, namely secreted proteins, transmembrane structural proteins, and signal peptide proteins. Numbers and detailed distribution of proteins are shown on the Y-axis. **(D)** Statistical data of predicted T3SS and other secretion-associated proteins for the three strains. **(E)** Statistical histogram of genes that are involved in pathogen-host interaction of the three strains. A total of 8 classes were predicted within genome genes of the three strains. Gene numbers are shown on the Y-axis. **(F)** Statistical histogram of genes annotated to antibiotic resistance and virulence of the three strains. Genes associated with antibiotic resistance were predicted and aligned with CARD and ARDB databases; genes annotated to virulence were predicted and aligned with VFDB database. Detailed numbers are shown on the Y-axis. **(G)** Statistical data of gene annotation based on PHI database for the three strains.

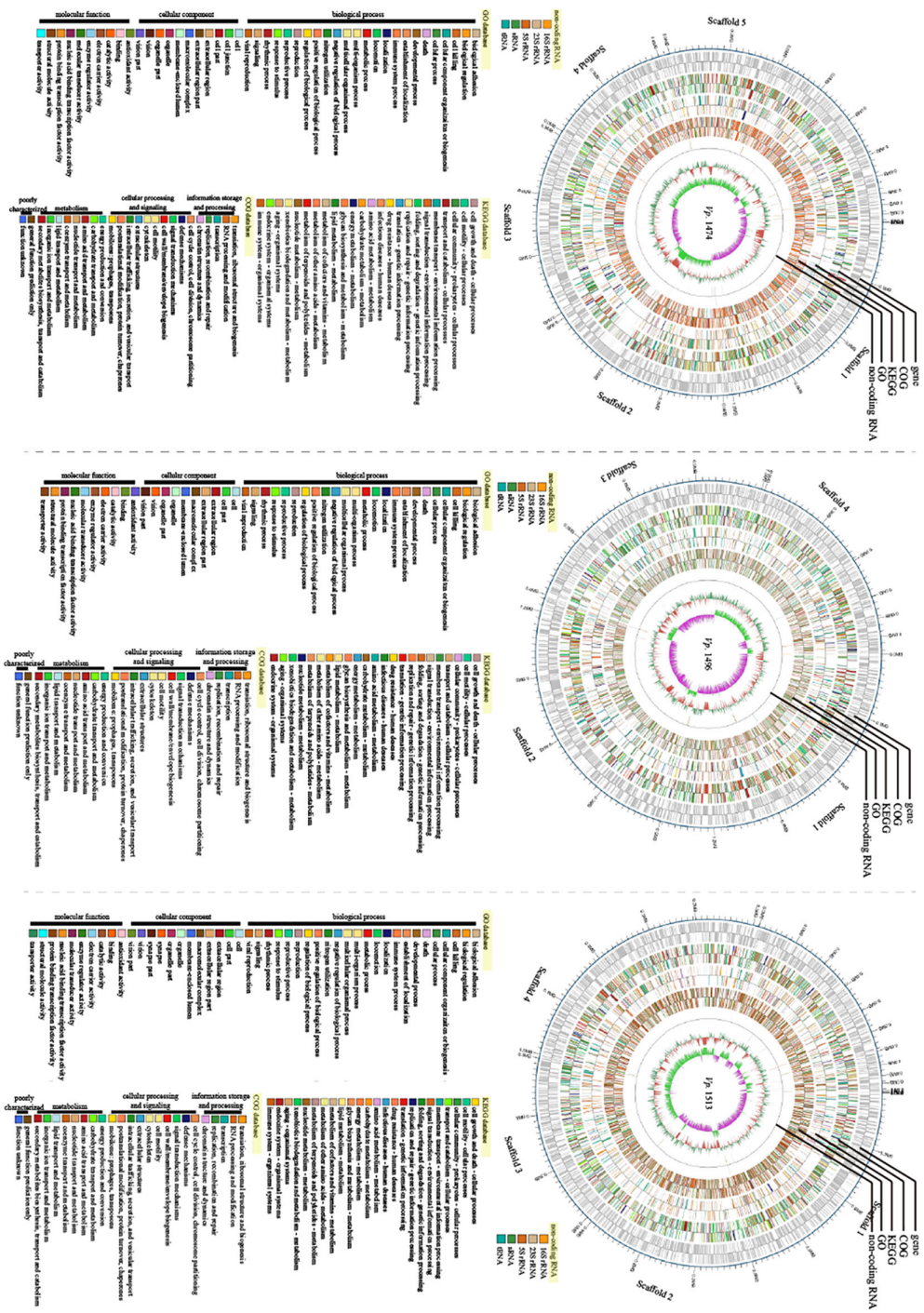

FIGURE 7 | Genomic visualization analysis of *V. parahaemolyticus* strains *Vp*. 1474, *Vp*. 1496, and *Vp*. 1513. Three genome-wide maps represented the combination of the prediction results of the coding genes. Results of gene distribution analysis, COG classification, KEGG pathway, GO annotation, and non-coding RNA are presented from the outermost to innermost rings.

resistance was tested, the 69 strains of *V. parahaemolyticus* were all sensitive to 16 antibiotics, but the zone diameter values (cm) were ambiguous for two out of 16 (data not shown). Focusing on the three selected strains, *Vp.* 1496 was significantly resistant to PRL (mean zone diameter value=0.05 cm), *Vp.* 1474 was resistant to KF (mean zone diameter value=1.4 cm) and was intermediately sensitive to KZ (mean zone diameter value=1.7 cm), and *Vp.* 1513 was sensitive to PRL, KF, and KZ (**Figure 9A**).

A

Surviving data of mice after *V. parahaemolyticus* intraperitoneal infection surveilled within 168 h

Time (h)	Inoculating strain (*Vp.*)	1474			1496			1513		
	Inoculating concentration (OD)	0.1	0.2	0.3	0.1	0.2	0.3	0.1	0.2	0.3
0	Surviving number (n)	8	8	8	8	8	8	8	8	8
1		8	8	8	8	8	8	8	8	8
2		8	8	8	8	8	8	8	8	8
3		8	8	8	5	4	5	8	8	8
4		8	8	8	0	2	3	8	8	8
5		8	7	5	0	2	0	8	8	8
6		7	4	1	0	1	0	8	8	8
7		6	3	1	0	1	0	8	8	8
8		6	1	1	0	1	0	8	8	8
9		6	1	1	0	1	0	8	8	8
10		6	1	1	0	1	0	8	8	8
11		5	1	1	0	1	0	8	8	8
12		2	0	1	0	1	0	8	4	8
24		1	0	1	0	1	0	8	4	6
48		1	0	1	0	1	0	8	4	6
72		1	0	1	0	1	0	8	4	6
96		1	0	1	0	1	0	8	4	6
120		1	0	1	0	1	0	8	4	6
144		1	0	1	0	1	0	8	4	6
168		1	0	1	0	1	0	8	4	6

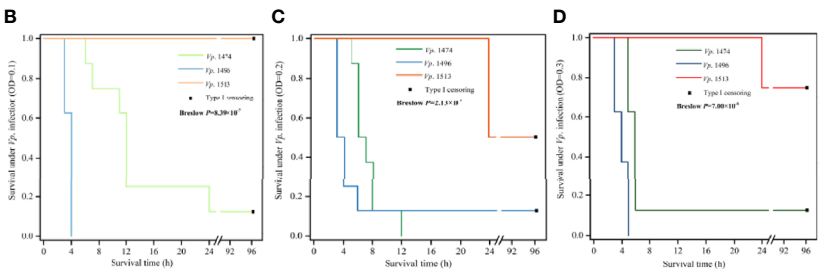

FIGURE 8 | *V. parahaemolyticus in vivo* infection and data statistics. **(A)** Operation of *in vivo* infection and data presentation. Suspension cultures of the selected strains, viz., *Vp*. 1474, *Vp*. 1496, and *Vp*. 1513, were adjusted to optical densities (OD) of 0.1, 0.2, and 0.3, and intraperitoneally injected into each group (9 groups, 8 mice per group). **(B)** Survival analysis of mice infected with *V. parahaemolyticus* under low concentration of injection (OD=0.1). **(C)** Survival analysis of mice infected with *V. parahaemolyticus* under moderate concentration of injection (OD=0.2). **(D)** Survival analysis of mice infected with *V. parahaemolyticus* under high concentration of injection (OD=0.3). Grey patch: the surviving mice that were observed in a poor living condition. The survival rate was updated every hour in acute infection period (≤12 h), and subsequently updated every 12 h in infection recovery period. The experiment continued for 4 days.

According to the zone diameter values, although the definition of drug resistance feature was different between KF and KZ resistance in *Vp*. 1474, the zone diameters were only marginally different (**Figure 9B**). It was worth noting that all 69 strains were resistant to AMP. Results indicated that the nature of drug resistance did not differ significantly amongst the different environmental strains of *V. parahaemolyticus*, and certain strains had gradually developed multi-antibiotic resistance potential.

DISCUSSION

Due to the increasing global incidence of foodborne gastroenteritis caused by *V. parahaemolyticus* (Rezny and Evans, 2020), it is imperative to reevaluate the pathogenicity of this bacteria using modern tools. WGS has played an important role in analyzing the evolution of *V. parahaemolyticus* and revealing the mechanism of their rapid serotype conversion (Han et al., 2019). However, the uncertainty of pathogenic difference on *V. parahaemolyticus*

remains the difficulty providing complication to its virulence and pathogenic prediction, which reflects in the different isolating sources, geographic positions and infecting concentration correlation. Therefore, this study focused on the interpretation on the genome differences of three environmental *V. parahaemolyticus* namely *Vp*. 1474, *Vp*. 1496, and *Vp*. 1513. Results obtained by this study could provide the possible explanation to the pathogenic and virulent difference in environmental isolates.

Genome Component Analysis for CRISPR, Prophage, and GIs

According to the *de novo* sequencing results in our study, there was a significant difference in the number of genes with different lengths in the genomes of *Vp*. 1474, *Vp*. 1496, and *Vp*. 1513, which indicated the existence of distinct evolutionary trajectories for the three *V. parahaemolyticus* strains. Compared to *Vp*. 1496, there was a higher number of long genes in the genome of *Vp*. 1513, indicating its significant evolutionary advantages.

CRISPR

CRISPR is a part of the prokaryotic adaptive immune system, which evolves when bacteria defend themselves against exogenous DNA, such as during phage attacks (Labrie et al., 2010). It consists of direct repeat, leader sequence, spacer sequence, and CRISPR associated (Cas) protein (Wright et al., 2016). The rapid evolution of bacteria depends on the insertion of exogenous spacer sequences into the genome to increase the chances of survival (Barrangou et al., 2007). Analyzing the genes annotated to CRISPR elements of the selected strains revealed that *Vp*. 1513 had the most CRISPR elements, whereas *Vp*. 1496 did not show any genes annotated to CRISPR elements integrated in its genome. The difference of CRISPR number in the genomes of *V. parahaemolyticus* environmental isolates might relate to genus specificity and *V. parahaemolyticus* source (Skovgaard et al., 2001). Based on the phylogenetic results showed in **Figure 1B**, *Vp*. 1513 underwent a higher level of genetic variation than that of *Vp*. 1496, and proceeded a longer evolutionary process, therefore the integration of a higher number of CRISPR elements might be due to phage attacks improved its resistance against viruses. In addition, studies confirmed that CRISPR was involved in biological behaviors of bacteria such as biofilm formation and swarming motility, besides self-defense (Zegans et al., 2009). The presence of a higher number of CRISPR elements might explain why *Vp*. 1513 had stronger biofilm formation capacity than other tested *V. parahaemolyticus* strains.

Prophage

Prophages integrate into the genome of bacterial hosts and pass along with bacterial proliferation, the feature which determines HGT. Thus, prophages often have an important effect on the pathogenicity of bacteria (Zrelovs et al., 2020). Takashi et al. reported a negative correlation between the number of prophages and CRISPRs in *Streptococcus pyogenes*, indicating that CRISPR integration could limit the insertion of prophage (Nozawa et al., 2011). Comparative genomic research showed that pathogenic *V. parahaemolyticus* could promote the insertion of prophage when lacking CRISPR (Yu et al., 2020).

Results of analysis for prophage genes in the genomes of *Vp*. 1474, *Vp*. 1496, and *Vp*. 1513 indicated that *Vp*. 1513 had the highest number of prophage genes, while *Vp*. 1496 had none. This phenomenon was inconsistent with the reports in literature. The difference between our research and previous literature might be explained by the concept that multiple survival advantages provided by lysogenic infection by prophage in *V. parahaemolyticus* could enable the survival of bacteria in an adverse environment (Wang et al., 2010).

GIs

GIs expand gene diversity through autologous transfer and loss of genetic information and participate in the genetic evolution of a microorganism. Notably, GIs arising due to HGT were a major reason for the evolution of novel pathogenic *Vibrio* strains (Hazen et al., 2010; Deng et al., 2019). GIs in the genome of *V. parahaemolyticus* are referred to as *Vibrio* pathogenicity islands for encoding virus factors and are a major reason for the evolution of novel pathogenic *V. parahaemolyticus* strains (Hacker and Carniel, 2001).

In this study, two out of three environmental isolates of *V. parahaemolyticus* had GIs in their genomes, confirming the phenomenon of HGT present in the selected *V. parahaemolyticus*. It could actuate *V. parahaemolyticus* environmental isolates to evolve towards pandemic strains by enhancing the differences of GIs and other mobile elements in the genome (Chen et al., 2011), and subsequently enhance the virulence potential by increasing the adaption of environmental isolates to marine environment (Baker-Austin et al., 2017), and finally acquiring the capacity to infect humans. The above-mentioned evidence indicated that *V. parahaemolyticus* might had upgraded their pathogenicity potential. However, it is difficult to explain this phenomenon only based on SNP and HGT analysis. Therefore, it needs to be compared on the whole genome level while retrospecting the evolution of *V. parahaemolyticus* to assess the extent and type of changes (Loyola et al., 2016).

Genome Function Analysis Based on Public Bioinformatics Databases

In our study, research focusing on the genomes of *Vp*. 1474, *Vp*. 1496, and *Vp*. 1513 was performed through annotation using a combination of databases. According to our results, there were distinct differences in the functional annotations of biological process (GO database), organismal systems (KEGG database), and information storage and processing (COG database).

Based on the interpretation of GO database, *Vp*. 1496 lacked genes that was involved in the construction of membrane and synaptic transmission, as the performance of gene GM002208 in *Vp*. 1474 genome or gene GM002507 in *Vp*. 1513 genome. Existing in a type of septin-associated protein, *Vp*. 1474 GM002208 formed as a ring-shaped structure and involved in the formation of BLOC-1 complex, so that bacterial cells could adhere and then provide a discrete opening to eukaryotic cell of hosts by joining the nuclear membranes as a transport vesicle. *Vp*. 1474 GM002208 could be

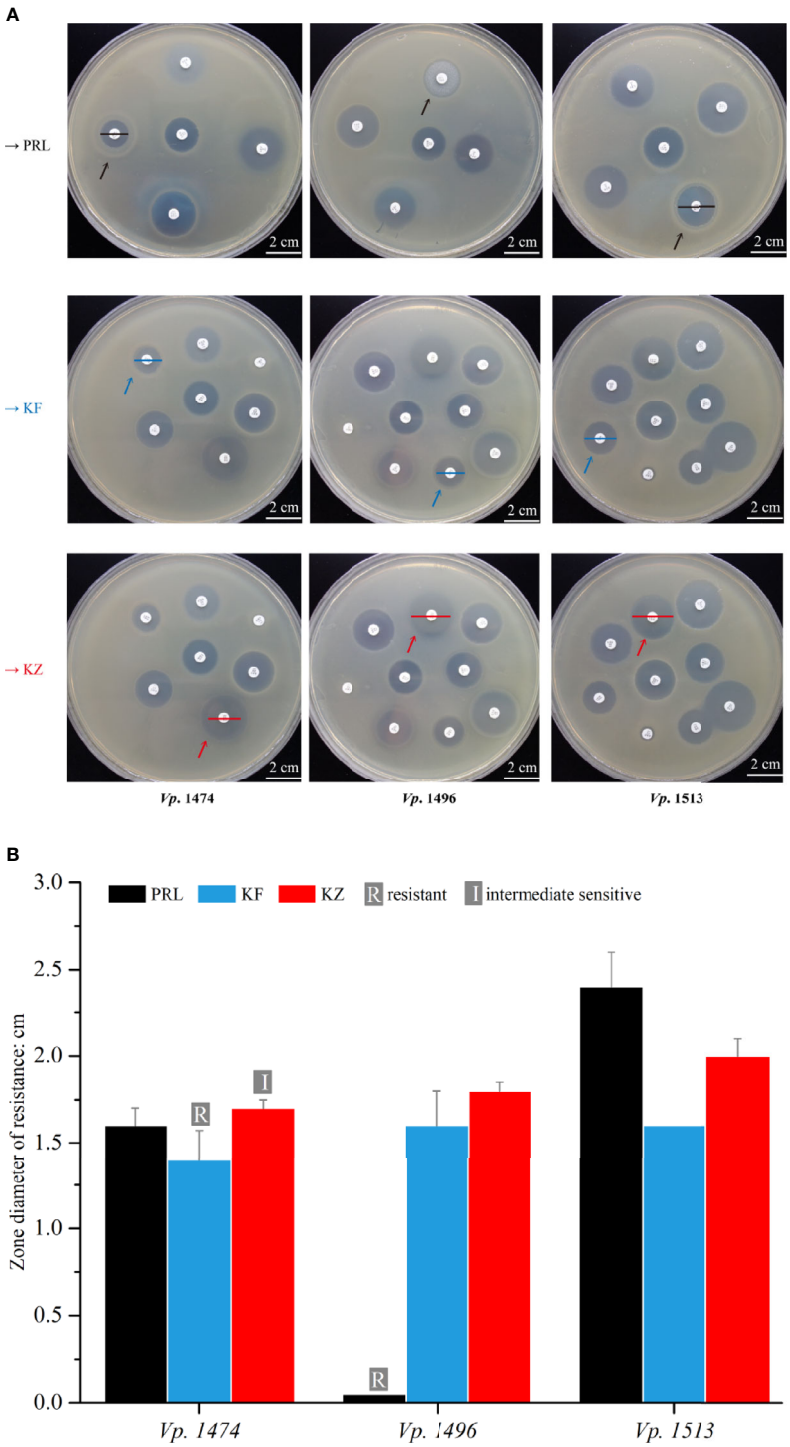

FIGURE 9 | Antibiotic resistance analysis of mice infected by *V. parahaemolyticus* strains *Vp.* 1474, *Vp.* 1496, and *Vp.* 1513. **(A)** Representative results of antimicrobial susceptibility test using Kirby-Bauer method. Black arrow: paper position of piperacillin (PRL) on the representative plates; blue arrow: paper position of cephalothin (KF) on the representative plates; red arrow: paper position of cephazolin (KZ) on the representative plates; black line: zone diameter of *V. parahaemolyticus* strains resistant to PRL; blue line: zone diameter of *V. parahaemolyticus* strains resistant to KF; red line: zone diameter of *V. parahaemolyticus* strains resistant to KZ. **(B)** Statistical histogram of antibiotic resistance to PRL, KF, and KZ for the three strains. For PRL, the zone diameters for resistant, intermediately sensitive, and sensitive are ≤1.7 cm, 1.8 to 2.0 cm, and ≥2.1 cm, respectively; for KF and KZ, the zone diameters for resistant, intermediately sensitive, and sensitive are ≤1.4 cm, 1.5 to 1.7 cm, and ≥1.8 cm, respectively.

built and secreted as a transport vesicle in Golgi to perform the function of tyrosine kinase and transporter activity, involving in lipid and DNA binding, transcription elongation regulation, protein phosphorylation and metabolic processes. *Vp*. 1513 GM002507 encoded a part of postsynaptic membrane. Through the binding of zinc ion and acetylcholine receptor, *Vp*. 1513 GM002507 involved in synaptic transmission.

Annotating to subclass of multi-organism and multicellular organismal processes, *Vp*. 1496 showed a serious lack of genetic constitution compared to *Vp*. 1513 both in gene number and gene proportion, which presented a less of its genome in these functions. In addition, the genome of *Vp*. 1496 lacked genes that were related to interaction between bacteria and host, which was reflected by the significant decrease of enzyme numbers that regulated this function. The reason for this may be the reduced protein transcriptional activity, which was in accordance with the lack of genes that involved in transportation and synaptic transmission by the explanation of GO database.

Gene numbers annotated to the drug resistance subclass for the class of human disease in the KEGG database were distinct, possibly accounting for the large differences in antibiotic resistance among the three strains, especially for piperacillin. According to the gene distribution for the class of genetic information processing and cellular processes in KEGG database, gene numbers of *Vp*. 1513 that annotated to subclass of replication and repair, cellular community—prokaryotes, and cell motility were significantly more than that of *Vp*. 1474 and *Vp*. 1496. This indicated that the mechanisms of cell proliferation and repairing in *Vp*. 1513 were more complicated, resulting in enhanced bacterial communication and cell motility, which could help *Vp*. 1513 to escape from surrounding adverse environment and seek more advantageous environments for colonization, ultimately increasing its chances of survival. On the contrary, the evolutionary process of *Vp*. 1496 was more conservative, and there was a lack of interconnection and coordinated communication between bacterial populations, resulting in the lack of adaptability to harsh environments.

Nevertheless, the virulence of *Vp*. 1496 was significantly increased based on the *in vivo* infection results. According to the results interpretation on GO and KEGG databases, a significant larger number and proportion of genes of the genome of *Vp*. 1496 was annotated and classified in subclasses of locomotion (58, 0.80% in the genome) and biological adhesion (26, 0.36% in the genome) than those in genome of *Vp*. 1474 and *Vp*. 1513, in addition with more proteins involved in the signal pathways of prokaryotic cellular community and digestive system. These results revealed that the increased virulence of *Vp*. 1496 possibly depended on the precursor process of quorum communication-derived cell adhesion, which regulated the movement of bacterial cells and their adherence towards suitable hosts and suitable proliferating environment such as digestive system.

V. parahaemolyticus Pathogenicity (TDH or TRH/TNSS)

Previous studies confirmed that various biological processes play significant roles in the pathogenicity of *V. parahaemolyticus*, such as hemolysis. TDH and TRH are two major hemolysins involved in *V. parahaemolyticus* pathogenicity, due to their distinct cell cytotoxicity and hemocytocatheresis (Cai and Zhang, 2018). The analysis of the expression of hemolysin genes is an important approach for understanding the pathogenicity of *V. parahaemolyticus*.

Considering that the genome of foodborne *V. parahaemolyticus* strains contained various functional regions with rich diversity, the differences in pathogenicity may have resulted from the distinction in the distribution of key genetic elements and differences in the secretory system compositions.

TDH or TRH

Compared with environmental isolates, clinical isolates of *V. parahaemolyticus* usually carry virulence factors, such as TDH or TRH (Nair et al., 2007), which may increase the toxicity of *V. parahaemolyticus* carrying both TDH and TRH (Martinez-Urtaza et al., 2017). Although, most *V. parahaemolyticus* are non-pathogenic isolates (Nair et al., 2007), even non-toxic *V. parahaemolyticus* can cause acute gastroenteritis (Ottaviani et al., 2012). Clinical isolates lacking TDH and TRH, such as the *V. parahaemolyticus* ST674 strain (Xu et al., 2017), have also been reported to have cytotoxicity independent of the TDH or TRH production (Lynch et al., 2005), indicating that non-toxic *V. parahaemolyticus* might also possess novel virulence mechanisms (Kamruzzaman et al., 2008). Previous studies could explain the results of mice infection model in our study. In our research, although the expression of TDH or TRH was detected in various strains, none of the 69 strains expressed TDH and TRH at the same time, indicating that *V. parahaemolyticus* environmental isolates expressed hemolysin at a low level, with a much lower level of expression of multiple hemolysins in the population. This conclusion was coincident with the previous study (Jiang et al., 2019), which might be a key trend of the distribution of hemolysin from *V. parahaemolyticus* environmental isolates. Results of pathogenicity experiments for *Vp*. 1474, *Vp*. 1496, and *Vp*. 1513, which were selected on the basis of differences in hemolysin expression and biofilm formation, showed a significant difference in the pathogenicity of the three strains in mice, with a marked distinction regarding the fatality and lethal time, with *Vp*. $1496^{tdh-,trh-}$ being the most lethal. Considerable differences in the pathogenicity of *V. parahaemolyticus* environmental isolates indicated their strong environmental and host adaptability (Liu et al., 2016), which may be one of the major reasons behind their distribution worldwide (Lovell, 2017).

TNSS

TNSS is involved in multiple pathogenic mechanisms during *V. parahaemolyticus* infection. The T3SS1 gene cluster is related to cytotoxic activity and is commonly found in *V. parahaemolyticus*; the T3SS2 gene cluster is mainly found in clinical isolates and is associated with intestinal toxicity (Ham and Orth, 2012). Another secretory system found in *V. parahaemolyticus*, T6SS, is also responsible for the pathogenicity of this species. T6SS is divided into two types, T6SS1 and T6SS2. T6SS1, mainly found in clinical isolates, improves adhesion to hosts (Yu et al., 2012). Recently, a

large and broad population study of *V. parahaemolyticus* by Yang and Pei et al. also referred that T6SS was differentiated between sampling groups, which could be involved in environment fitness difference of this species, and it was noteworthy (Yang et al., 2019a).

In our study, the results of *V. parahaemolyticus in vivo* infection showed a significant difference of pathogenicity between the three selected strains, with *Vp*. 1496 being the most pathogenic. Combined with the results of genes annotated to T3SS, there was a lack of difference in T3SS prediction in the three strains, which partially indicated that the pathogenic properties of *Vp*. 1496 might not be developed from the T3SS. Conversely, the marked increase in the number of T6SS-associated protein in *Vp*. 1496 suggests that the pathogenic properties of this strain were most likely enhanced by T6SS-associated mechanisms. Previous literature showed that T6SS might be related to environmental fitness, but not to pathogenicity of foodborne *V. parahaemolyticus* due to its high frequency of distribution (Yang et al., 2019b). However, based on our research, it may be stated that T6SS in foodborne *V. parahaemolyticus* requires further surveillance, for its possible role in *V. parahaemolyticus* infection.

Antibiotic Resistance of *V. parahaemolyticus*

The other significant biological process in the pathogenicity of *V. parahaemolyticus* lies in cell adhesion and secretion systems. Biofilm formation is the external manifestation of bacterial adhesion ability, which directly affects the antibiotic resistance of bacteria (Carniello et al., 2018). In *Vibrio*, the biofilm formation capacity not only positively reflects colonization stability in the host, but is also closely related to the course of disease after *Vibrio* infection (Khan et al., 2020).

Based on the conclusions drawn from different studies, the drug resistance of *V. parahaemolyticus* is divergent. The antibiotic resistances of strains collected from different locations in the world, and from different sources (clinical isolates and environmental isolates) show a complicated trend (WHO, 2014). However, it must be noted that previous studies on antibiotic resistance of *V. parahaemolyticus* have not been documented as extensively as those for other common foodborne bacteria (Elmahdi et al., 2016).

Based on *de novo* sequencing, the potential antibiotic resistance features of the three tested *V. parahaemolyticus* strains could partially be reflected by ARDB result interpretation, which all showed multiple antibiotic relevant genes annotated to tigecycline (TGC), streptomycin (SM), kanamycin (KAR), CIP, norfloxacin (NFX), and TE. However, some of the antibiotics were not commonly used clinically. Therefore, drug sensitivity test was performed in addition to verify the clinical antibiotic resistance of environmental *V. parahaemolyticus* strains. The antibiotic tests showed different results from those reported in previous studies. The resistance of *V. parahaemolyticus* environmental isolates to AMP was fully confirmed and is consistent with findings of previous studies (Han et al., 2017; Jiang et al., 2019). However, the resistance of *V. parahaemolyticus* environmental isolates to quinolones and cephalosporins, especially to CAZ and CIP, which was confirmed by Lopatek et al. (Lopatek et al., 2018), could not be established by this method. Further, the resistance of *V. parahaemolyticus* environmental isolates to aminoglycosides and TE could not be verified because of the insufficient sample size by this method, while the resistance to TE could be confirmed by ARDB interpretation. The results also suggest that β-lactam antibiotics need to be selected carefully when treating *V. parahaemolyticus* infections, because some of the selected strains were resistant to such antibiotics, including cephalosporin, PRL, KF, and KZ. Finally, the biofilm formation capacity of *V. parahaemolyticus* environmental isolates were weak, and there appeared to be no significant correlation between their biofilm formation and antibiotic resistance.

According to two methods referring to genomics and clinical detection, *V. parahaemolyticus* environmental isolates showed a complicated antibiotic resistance potential. The results suggested that the antibiotic resistance of environmental *V. parahaemolyticus* might be regulated by various mechanisms, and the resistance prediction based on genomics needed to be verified by clinical detection. Similarly, clinical medication when treating *V. parahaemolyticus* infection should be combined with genomic sequencing indication, which need to be studied further.

CONCLUSION

Our study analyzed the genetic distribution, genetic elements, and pathogenicity of environmental *V. parahaemolyticus* strains using the WGS method. Our analyses revealed that the difference in pathogenicity of environmental *V. parahaemolyticus* strains resulted from the combination of HGT level, distribution of pathogenic elements, and the nature of the secretory system. Thus, further research on the genome differences between environmental and clinical *V. parahaemolyticus* is necessary for developing a better understanding of these pathogenic bacteria.

DATA AVAILABILITY STATEMENT

The original contributions presented in the study are publicly available. This data can be found here: NCBI repository, accession number: PRJNA722971 (https://www.ncbi.nlm.nih.gov/bioproject/PRJNA722971).

ETHICS STATEMENT

The animal study was reviewed and approved by Animal Ethics Committee of the Sixth Medical Centre of Chinese PLA General Hospital.

AUTHOR CONTRIBUTIONS

LZ conceived this study. JL and KQ designed the research. JL, KQ, and CW performed the experiments. KF and XY analyzed experimental data. JL, KQ, CW, and LZ wrote the paper. JL and

KQ contributed equally to this work. All authors contributed to the article and approved the submitted version.

FUNDING

This work was supported by the Medical and Health key Project under grant no. 14J004; the Innovation Project of General Hospital under grant no. CX19027; the Innovation Incubation Fund of the Navy General Hospital under grant no. CXPY201822 and CXPY201824; and the Beijing Municipal Natural Science Foundation under grant no. 7204314.

ACKNOWLEDGMENTS

We thank Dr. Shenghui Cui for the generous gift of *V. parahaemolyticus* environmental strains and for the help in their preparation.

SUPPLEMENTARY MATERIAL

The Supplementary Material for this article can be found online at: https://www.frontiersin.org/articles/10.3389/fcimb.2021.652957/full#supplementary-material

REFERENCES

Akhter, S., McNair, K., and Decewicz, P. (2019). "PhiSpy". *3.4 ed* (Cambridge, Massachusetts, United States: Massachusetts Institute of Technology).

Centers for Disease Control and Prevention (CDC) (2019). Surveillance for Foodborne Disease Outbreaks, United States. Annual Report. (2017). (Atlanta, Georgia: U.S. Department of Health and Human Services), 3–10.

Bairoch, A., and Apweiler, R. (2000). The SWISS-PROT Protein Sequence Database and its Supplement TrEMBL in 2000. *Nucleic Acids Res.* 28 (1), 45–48. doi: 10.1093/nar/28.1.45

Baker-Austin, C., Trinanes, J. A., Taylor, N. G. H., Hartnell, R., Siitonen, A., and Martinez-Urtaza, J. (2013). Emerging Vibrio risk at high latitudes in response to ocean warming. *Nat. Clim. Chang.* 31 (1), 73–77. doi: 10.1038/nclimate1628

Baker-Austin, C., Trinanes, J., Gonzalez-Escalona, N., and Martinez-Urtaza, J. (2017). Non-Cholera Vibrios: The Microbial Barometer of Climate Change. *Trends Microbiol.* 25 (1), 76–84. doi: 10.1016/j.tim.2016.09.008

Barker, W. H. J. (1974). *International Symposium on Vibrio Parahaemolyticus*. Eds. T. Fujino, G. Sakaguchi, R. Sakazaki and Y. Takeda (Tokyo: Saikon Publishing Co., Ltd), 47–52.

Barrangou, R., Fremaux, C., Deveau, H., Richards, M., Boyaval, P., Moineau, S., et al. (2007). CRISPR Provides Acquired Resistance Against Viruses in Prokaryotes. *Science* 315 (5819), 1709–1712. doi: 10.1126/science.1138140

Bertelli, C., and Brinkman, F. S. L. (2018). Improved Genomic Island Predictions With Islandpath-DIMOB. *Bioinformatics* 34 (13), 2161–2167. doi: 10.1093/bioinformatics/bty095

Besemer, J., Lomsadze, A., and Borodovsky, M. (2001). GeneMarkS: A Self-Training Method for Prediction of Gene Starts in Microbial Genomes. Implications for Finding Sequence Motifs in Regulatory Regions. *Nucleic Acids Res.* 29 (12), 2607–2618. doi: 10.1093/nar/29.12.2607

Cai, Q., and Zhang, Y. (2018). Structure, Function and Regulation of the Thermostable Direct Hemolysin (TDH) in Pandemic Vibrio Parahaemolyticus. *Microb. Pathog.* 123, 242–245. doi: 10.1016/j.micpath.2018.07.021

Carniello, V., Peterson, B. W., van der Mei, H. C., and Busscher, H. J. (2018). Physico-Chemistry From Initial Bacterial Adhesion to Surface-Programmed Biofilm Growth. *Adv. Colloid Interface Sci.* 261, 1–14. doi: 10.1016/j.cis.2018.10.005

Chen, Y., Stine, O. C., Badger, J. H., Gil, A. I., Nair, G. B., Nishibuchi, M., et al. (2011). Comparative Genomic Analysis of Vibrio Parahaemolyticus: Serotype Conversion and Virulence. *BMC Genomics* 12, 294. doi: 10.1186/1471-2164-12-294

Deng, Y., Xu, H., Su, Y., Liu, S., Xu, L., Guo, Z., et al. (2019). Horizontal Gene Transfer Contributes to Virulence and Antibiotic Resistance of Vibrio Harveyi 345 Based on Complete Genome Sequence Analysis. *BMC Genomics* 20 (1), 761. doi: 10.1186/s12864-019-6137-8

Elmahdi, S., DaSilva, L. V., and Parveen, S. (2016). Antibiotic Resistance of Vibrio Parahaemolyticus and Vibrio Vulnificus in Various Countries: A Review. *Food Microbiol.* 57, 128–134. doi: 10.1016/j.fm.2016.02.008

Fujino, T., Okuno, Y., Nakada, D., Aoyama, A., Fukai, K., Mukai, T., et al. (1953). On the Bacteriological Examination of Shirasu Food Poisoning. *Med. J. Osaka Univ.* 4, 299–304.

Ge, R., Mai, G., Wang, P., Zhou, M., Luo, Y., Cai, Y., et al. (2016). Crisprdigger: Detecting CRISPRs With Better Direct Repeat Annotations. *Sci. Rep.* 6 (1), 32942. doi: 10.1038/srep32942

Gonzalez-Escalona, N., Jolley, K. A., Reed, E., and Martinez-Urtaza, J. (2017). Defining a Core Genome Multilocus Sequence Typing Scheme for the Global Epidemiology of Vibrio Parahaemolyticus. *J. Clin. Microbiol.* 55 (6), 1682–1697. doi: 10.1128/jcm.00227-17

Guillod, C., Ghitti, F., and Mainetti, C. (2019). Vibrio Parahaemolyticus Induced Cellulitis and Septic Shock After a Sea Beach Holiday in a Patient With Leg Ulcers. *Case Rep. Dermatol.* 11 (1), 94–100. doi: 10.1159/000499478

Hacker, J., and Carniel, E. (2001). Ecological Fitness, Genomic Islands and Bacterial Pathogenicity. A Darwinian View of the Evolution of Microbes. *EMBO Rep.* 2 (5), 376–381. doi: 10.1093/embo-reports/kve097

Ham, H., and Orth, K. (2012). The Role of Type III Secretion System 2 in Vibrio Parahaemolyticus Pathogenicity. *J. Microbiol.* 50 (5), 719–725. doi: 10.1007/s12275-012-2550-2

Han, D., Yu, F., Chen, X., Zhang, R., and Li, J. (2019). Challenges in Vibrio Parahaemolyticus Infections Caused by the Pandemic Clone. *Future Microbiol.* 14, 437–450. doi: 10.2217/fmb-2018-0308

Han, D., Yu, F., Tang, H., Ren, C., Wu, C., Zhang, P., et al. (2017). Spreading of Pandemic Vibrio Parahaemolyticus O3:K6 and Its Serovariants: A Re-Analysis of Strains Isolated From Multiple Studies. *Front. Cell Infect. Microbiol.* 7, 188. doi: 10.3389/fcimb.2017.00188

Hazen, T. H., Pan, L., Gu, J. D., and Sobecky, P. A. (2010). The Contribution of Mobile Genetic Elements to the Evolution and Ecology of Vibrios. *FEMS Microbiol. Ecol.* 74 (3), 485–499. doi: 10.1111/j.1574-6941.2010.00937.x

Jehl, M. A., Arnold, R., and Rattei, T. (2011). Effective–a Database of Predicted Secreted Bacterial Proteins. *Nucleic Acids Res.* 39 (Database issue), D591–D595. doi: 10.1093/nar/gkq1154

Jiang, Y., Chu, Y., Xie, G., Li, F., Wang, L., Huang, J., et al. (2019). Antimicrobial Resistance, Virulence and Genetic Relationship of Vibrio Parahaemolyticus in Seafood From Coasts of Bohai Sea and Yellow Sea, China. *Int. J. Food Microbiol.* 290, 116–124. doi: 10.1016/j.ijfoodmicro.2018.10.005

Kamruzzaman, M., Bhoopong, P., Vuddhakul, V., and Nishibuchi, M. (2008). Detection of a Functional Insertion Sequence Responsible for Deletion of the Thermostable Direct Hemolysin Gene (Tdh) in Vibrio Parahaemolyticus. *Gene* 421 (1-2), 67–73. doi: 10.1016/j.gene.2008.06.009

Khan, F., Tabassum, N., Anand, R., and Kim, Y. M. (2020). Motility of Vibrio Spp.: Regulation and Controlling Strategies. *Appl. Microbiol. Biotechnol.* 104 (19), 8187–8208. doi: 10.1007/s00253-020-10794-7

Krzywinski, M. I., Schein, J. E., Birol, I., Connors, J., Gascoyne, R., Horsman, D., et al. (2009). Circos: An Information Aesthetic for Comparative Genomics. *Genome Res.* 19 (9), 1639–1645. doi: 10.1101/gr.092759.109

Labrie, S. J., Samson, J. E., and Moineau, S. (2010). Bacteriophage Resistance Mechanisms. *Nat. Rev. Microbiol.* 8 (5), 317–327. doi: 10.1038/nrmicro2315

Lane, D. J. (1991). *16s/23s rRNA Sequencing. In Nucleic Acid Techniques in Bacterial Systematics* (London: Wiley).

Li, W., Jaroszewski, L., and Godzik, A. (2002). Tolerating Some Redundancy Significantly Speeds Up Clustering of Large Protein Databases. *Bioinformatics* 18 (1), 77–82. doi: 10.1093/bioinformatics/18.1.77

Liu, B., Liu, H., Pan, Y., Xie, J., and Zhao, Y. (2016). Comparison of the Effects of Environmental Parameters on the Growth Variability of Vibrio Parahaemolyticus Coupled With Strain Sources and Genotypes Analyses. *Front. Microbiol.* 7, 994. doi: 10.3389/fmicb.2016.00994

Li, J., Xue, F., Yang, Z., Zhang, X., Zeng, D., Chao, G., et al. (2016). Vibrio Parahaemolyticus Strains of Pandemic Serotypes Identified From Clinical and Environmental Samples From Jiangsu, China. *Front. Microbiol.* 7, 787. doi: 10.3389/fmicb.2016.00787

Lopatek, M., Wieczorek, K., and Osek, J. (2018). Antimicrobial Resistance, Virulence Factors, and Genetic Profiles of Vibrio Parahaemolyticus From Seafood. *Appl. Environ. Microbiol.* 84 (16), e00537–18. doi: 10.1128/AEM.00537-18

Lovell, C. R. (2017). Ecological Fitness and Virulence Features of Vibrio Parahaemolyticus in Estuarine Environments. *Appl. Microbiol. Biotechnol.* 101 (5), 1781–1794. doi: 10.1007/s00253-017-8096-9

Loyola, D., Yañez, C., Plaza, N., Garcia, K., and Espejo, R. T. (2016). Genealogy of the Genome Components in the Highly Homogeneous Pandemic Vibrio Parahaemolyticus Population. *J. Phylogenet. Evol. Biol.* 4 (2), 1000165. doi: 10.4172/2329-9002.1000165

Lynch, T., Livingstone, S., Buenaventura, E., Lutter, E., Fedwick, J., Buret, A. G., et al. (2005). Vibrio Parahaemolyticus Disruption of Epithelial Cell Tight Junctions Occurs Independently of Toxin Production. *Infect. Immun.* 73 (3), 1275–1283. doi: 10.1128/IAI.73.3.1275-1283.2005

Makarova, K. S., Haft, D. H., Barrangou, R., Brouns, S. J., Charpentier, E., Horvath, P., et al. (2011). Evolution and Classification of the CRISPR-Cas Systems. *Nat. Rev. Microbiol.* 9 (6), 467–477. doi: 10.1038/nrmicro2577

Martinez-Urtaza, J., Bowers, J. C., Trinanes, J., and DePaola, A. (2010). Climate Anomalies and the Increasing Risk of Vibrio Parahaemolyticus and Vibrio Vulnificus Illnesses. *Food Res. Int.* 43 (7), 1780–1790. doi: 10.1016/j.foodres.2010.04.001

Martinez-Urtaza, J., van Aerle, R., Abanto, M., Haendiges, J., Myers, R. A., Trinanes, J., et al. (2017). Genomic Variation and Evolution of ST36 Over the Course of a Transcontinental Epidemic Expansion. *mBio*. 8 (6), e01425–01417. doi: 10.1128/mBio.01425-17

Miyamoto, Y., Nakamura, K., and Takizawa, K. (1962). Seasonal Distribution of Oceanomonas Spp., Halophilic Bacteria, in the Coastal Sea: its Significance in Epidemiology and Marine Industry. *Microbiol. Immunol.* 6 (2-4), 141–158. doi: 10.1111/j.1348-0421.1962.tb00231.x

Möller, S., Croning, M. D., and Apweiler, R. (2001). Evaluation of Methods for the Prediction of Membrane Spanning Regions. *Bioinf. (Oxford England)* 17 (7), 646–653. doi: 10.1093/bioinformatics/17.7.646

Nair, G. B., Ramamurthy, T., Bhattacharya, S. K., Dutta, B., Takeda, Y., and Sack, D. A. (2007). Global Dissemination of Vibrio Parahaemolyticus Serotype O3: K6 and its Serovariants. *Clin. Microbiol. Rev.* 20 (1), 39–48. doi: 10.1128/cmr.00025-06

Newton, A. E., Garrett, N., Stroika, S. G., Halpin, J. L., Turnsek, M., and Mody, R. K. (2014). Increase in Vibrio Parahaemolyticus Infections Associated With Consumption of Atlantic Coast Shellfish–2013. *Morb. Mortal. Wkly. Rep.* 63 (15), 335–336.

Nielsen, H., Tsirigos, K. D., Brunak, S., and Heijne, G. V. (2019). A Brief History of Protein Sorting Prediction. *Protein J.* 38 (3), 200–216. doi: 10.1007/s10930-019-09838-3

Nozawa, T., Furukawa, N., Aikawa, C., Watanabe, T., Haobam, B., Kurokawa, K., et al. (2011). CRISPR Inhibition of Prophage Acquisition in Streptococcus Pyogenes. *PLoS One* 6 (5), e19543. doi: 10.1371/journal.pone.0019543

Ottaviani, D., Leoni, F., Serra, R., Serracca, L., Decastelli, L., Rocchegiani, E., et al. (2012). Nontoxigenic Vibrio Parahaemolyticus Strains Causing Acute Gastroenteritis. *J. Clin. Microbiol.* 50 (12), 4141–4143. doi: 10.1128/jcm.01993-12

Rezny, B. R., and Evans, D. S. (2020). "Vibrio Parahaemolyticus," in *Statpearls* (Treasure Island (FL: StatPearls Publishing Copyright © 2020, StatPearls Publishing LLC).

Ronholm, J., Nasheri, N., Petronella, N., and Pagotto, F. (2016). Navigating Microbiological Food Safety in the Era of Whole-Genome Sequencing. *Clin. Microbiol. Rev.* 29 (4), 837–857. doi: 10.1128/CMR.00056-16

Rossen, J. W. A., Friedrich, A. W., and Moran-Gilad, J. (2018). Practical Issues in Implementing Whole-Genome-Sequencing in Routine Diagnostic Microbiology. *Clin. Microbiol. Infect.* 24 (4), 355–360. doi: 10.1016/j.cmi.2017.11.001

Saier, M. H.Jr., Reddy, V. S., Tamang, D. G., and Västermark, A. (2014). The Transporter Classification Database. *Nucleic Acids Res.* 42 (Database Issue), D251–D258. doi: 10.1093/nar/gkt1097

Schürch, A. C., Arredondo-Alonso, S., Willems, R. J. L., and Goering, R. V. (2018). Whole Genome Sequencing Options for Bacterial Strain Typing and Epidemiologic Analysis Based on Single Nucleotide Polymorphism Versus Gene-by-Gene-Based Approaches. *Clin. Microbiol. Infect.* 24 (4), 350–354. doi: 10.1016/j.cmi.2017.12.016

Shuja, A., Dickstein, A., and Lee, H. M. (2014). Vibrio Parahaemolyticus: A Rare Cause of Chronic Diarrhea in a Heart Transplant Patient. *ACG Case Rep. J.* 1 (4), 202–203. doi: 10.14309/crj.2014.52

Skovgaard, M., Jensen, L. J., Brunak, S., Ussery, D., and Krogh, A. (2001). On the Total Number of Genes and Their Length Distribution in Complete Microbial Genomes. *Trends Genet.* 17 (8), 425–428. doi: 10.1016/s0168-9525(01)02372-1

Stepanovic, S., Vukovic, D., Dakic, I., Savic, B., and Svabic-Vlahovic, M. (2000). A Modified Microtiter-Plate Test for Quantification of Staphylococcal Biofilm Formation. *J. Microbiol. Methods* 40 (2), 175–179. doi: 10.1016/s0167-7012(00)00122-6

Sun, H., Li, Y., Shi, X., Lin, Y., Qiu, Y., Zhang, J., et al. (2015). Association of CRISPR/Cas Evolution With *Vibrio Parahaemolyticus* Virulence Factors and Genotypes. *Foodborne Pathog. Dis.* 12 (1), 68–73. doi: 10.1089/fpd.2014.1792

Ueno, H., Tomari, K., Kikuchi, K., Kobori, S., and Miyazaki, M. (2016). The First Report of Vibrio Parahaemolyticus Strain O10:K60 in Japan, a New Combination of O and K Serotypes Isolated From a Patient With Gastroenteritis. *Jpn. J. Infect. Dis.* 69 (1), 28–32. doi: 10.7883/yoken.JJID.2014.538

Wang, X., Kim, Y., Ma, Q., Hong, S. H., Pokusaeva, K., Sturino, J. M., et al. (2010). Cryptic Prophages Help Bacteria Cope With Adverse Environments. *Nat. Commun.* 1, 147. doi: 10.1038/ncomms1146

WHO (2014). *"Antimicrobial Resistance: Global Report on Surveillance 2014". April, 2014 ed* (Geneva, Switzerland: World Health Organization).

Wright, A. V., Nuñez, J. K., and Doudna, J. A. (2016). Biology and Applications of CRISPR Systems: Harnessing Nature's Toolbox for Genome Engineering. *Cell* 164 (1-2), 29–44. doi: 10.1016/j.cell.2015.12.035

Xu, F., Gonzalez-Escalona, N., Drees, K. P., Sebra, R. P., Cooper, V. S., Jones, S. H., et al. (2017). Parallel Evolution of Two Clades of an Atlantic-Endemic Pathogenic Lineage of Vibrio Parahaemolyticus by Independent Acquisition of Related Pathogenicity Islands. *Appl. Environ. Microbiol.* 83 (18), e01168–17. doi: 10.1128/AEM.01168-17

Yang, C., Pei, X., Wu, Y., Yan, L., Yan, Y., Song, Y., et al. (2019a). Recent Mixing of Vibrio Parahaemolyticus Populations. *Isme J.* 13 (10), 2578–2588. doi: 10.1038/s41396-019-0461-5

Yang, C., Zhang, X., Fan, H., Li, Y., Hu, Q., Yang, R., et al. (2019b). Genetic Diversity, Virulence Factors and Farm-to-Table Spread Pattern of Vibrio Parahaemolyticus Food-Associated Isolates. *Food Microbiol.* 84, 103270. doi: 10.1016/j.fm.2019.103270

Yu, L. H., Teh, C. S. J., Yap, K. P., Ung, E. H., and Thong, K. L. (2020). Comparative Genomic Provides Insight Into the Virulence and Genetic Diversity of Vibrio Parahaemolyticus Associated With Shrimp Acute Hepatopancreatic Necrosis Disease. *Infect. Genet. Evol.* 83, 104347. doi: 10.1016/j.meegid.2020.104347

Yu, Y., Yang, H., Li, J., Zhang, P., Wu, B., Zhu, B., et al. (2012). Putative Type VI Secretion Systems of Vibrio Parahaemolyticus Contribute to Adhesion to Cultured Cell Monolayers. *Arch. Microbiol.* 194 (10), 827–835. doi: 10.1007/s00203-012-0816-z

Zegans, M. E., Wagner, J. C., Cady, K. C., Murphy, D. M., Hammond, J. H., and O'Toole, G. A. (2009). Interaction Between Bacteriophage DMS3 and Host CRISPR Region Inhibits Group Behaviors of Pseudomonas Aeruginosa. *J. Bacteriol.* 191 (1), 210–219. doi: 10.1128/JB.00797-08

Zrelovs, N., Dislers, A., and Kazaks, A. (2020). Novel Erwinia Persicina Infecting Phage Midgardsormr38 Within the Context of Temperate Erwinia Phages. *Front. Microbiol.* 11, 1245. doi: 10.3389/fmicb.2020.01245

Conflict of Interest: The authors declare that the research was conducted in the absence of any commercial or financial relationships that could be construed as a potential conflict of interest.

Advantages of publishing in Frontiers

OPEN ACCESS
Articles are free to read for greatest visibility and readership

FAST PUBLICATION
Around 90 days from submission to decision

HIGH QUALITY PEER-REVIEW
Rigorous, collaborative, and constructive peer-review

TRANSPARENT PEER-REVIEW
Editors and reviewers acknowledged by name on published articles

Frontiers
Avenue du Tribunal-Fédéral 34
1005 Lausanne | Switzerland

Visit us: www.frontiersin.org
Contact us: frontiersin.org/about/contact

REPRODUCIBILITY OF RESEARCH
Support open data and methods to enhance research reproducibility

DIGITAL PUBLISHING
Articles designed for optimal readership across devices

FOLLOW US
@frontiersin

IMPACT METRICS
Advanced article metrics track visibility across digital media

EXTENSIVE PROMOTION
Marketing and promotion of impactful research

LOOP RESEARCH NETWORK
Our network increases your article's readership